IDENTIFICATION OF THE HYDRODYNAMIC MODEL OF AN UNDERWATER ROBOTIC VEHICLE HEAVING AND PITCHING NEAR THE SEA SURFACE USING ITS MEASURED RESPONSE

AYMAN B. MAHFOUZ

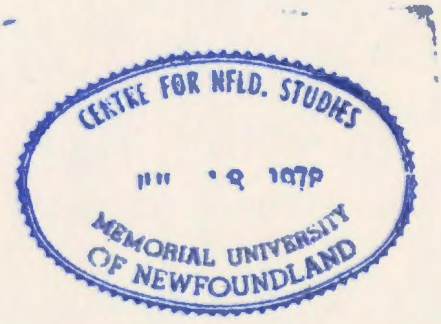
CENTRE FOR NFLD. STUDIES
MEMORIAL UNIVERSITY
OF NEWFOUNDLAND

INFORMATION TO USERS

This manuscript has been reproduced from the microfilm master. UMI films the text directly from the original or copy submitted. Thus, some thesis and dissertation copies are in typewriter face, while others may be from any type of computer printer.

The quality of this reproduction is dependent upon the quality of the copy submitted. Broken or indistinct print, colored or poor quality illustrations and photographs, print bleedthrough, substandard margins, and improper alignment can adversely affect reproduction.

In the unlikely event that the author did not send UMI a complete manuscript and there are missing pages, these will be noted. Also, if unauthorized copyright material had to be removed, a note will indicate the deletion.

Oversize materials (e.g., maps, drawings, charts) are reproduced by sectioning the original, beginning at the upper left-hand corner and continuing from left to right in equal sections with small overlaps.

Photographs included in the original manuscript have been reproduced xerographically in this copy. Higher quality 6" x 9" black and white photographic prints are available for any photographs or illustrations appearing in this copy for an additional charge. Contact UMI directly to order.

ProQuest Information and Learning
300 North Zeeb Road, Ann Arbor, MI 48106-1346 USA
800-521-0600

Identification of the Hydrodynamic Model of an Underwater Robotic Vehicle Heaving and Pitching Near the Sea Surface Using Its Measured Response

by

©Ayman B. Mahfouz, B.Sc., M.Sc.

A thesis submitted to the School of Graduate Studies
in conformity with the requirements for the
Degree of Doctor of Philosophy

Faculty of Engineering and Applied Science
Memorial University of Newfoundland
January 2001

St. John's **Newfoundland** **Canada**

Abstract

An accurate estimation of the hydrodynamic parameters for Underwater Robotic Vehicles (URV) is a top priority for the designing of the control strategies for such vehicles. The identification of these parameters constitutes a main difficulty in the development of a URV. Several methods have been developed to estimate such parameters. These methods include: strip theory, slender body theory, semi-empirical approaches, and parametric identification. Most of these methods have many assumptions and drawbacks that restrict their applicability.

I am mainly concerned with the parametric identification. One of the advantages of parametric identification is that if it can be done in real time then one can have a tool for updating the dynamic model as the vehicle moves through the water. Responses obtained using this model will be realistic and increase the chances of having better control of the vehicle.

In this dissertation, I develop a new robust technique for the identification of the damping, restoring, and coupling parameters in the equations describing the coupled heave and pitch motions for an URV sailing near the water surface in random waves. The developed technique is called *RDLRNNT*, which is a combination of the random decrement technique, multi-linear regression algorithm, and a neural networks technique. *RDLRNNT* requires only the measured coupled heave and pitch responses for the URV in random waves and does not require a prior knowledge of the wave excitation. The developed technique would be particularly useful in identifying the parameters for both moderately and lightly damped motions under the action of unknown wave excitations affected by a realistic sea.

Numerically generated data for the coupled heave and pitch motion of an URV are used initially to test the accuracy of the technique for both different levels of damping and a wide range of damped natural frequencies in heave and pitch motions. Moreover, several case studies are further investigated to test the dependency of the developed technique on the wave excitation forms. Two different excitations are investigated: a wide-band and a narrow-band form.

Experimental data are also used to validate the identification technique for different functions of wave excitations and different towing speeds. Three main experimental variables are further investigated: the significant wave height (H_S), the wave modal frequency (Ω), and the towing speed (U).

Acknowledgments

First of all, I am thankful to The Almighty God (Allah), Who in His infinite mercy has helped me to make this possible.

I also owe a lot to my family, especially my mother and father for their continuous support, prayers, and great sacrifices that were the major factors in achieving this work. I would like to thank my wife for her support, encouragement and great sacrifices in this work. Also, I appreciate her patience since the course of this work. Really, I present my apologies and asking for her forgiveness. I like to thank my brother Mr. Mohamed Mahfouz (*Abu-Qir Fertilization Co., Alexandria, Egypt*) and my sister Dr. Nadia Mahfouz (*Professor, Tanta University, Egypt*) for their continuous help and encouragement. I also like to thank my brothers Talat and Nabil for their help and encouragement.

I like to express my sincere thanks and my deepest gratitude to my supervisor Dr. M. R. Haddara for his supervision, guidance, support, encouragement and cooperation in the course of this work. I am absolutely sure that without his guidance in this work, I might be lost. I also do not forget the support and help of my supervisory committee Dr. M. Hinchey and Dr. C. Williams.

I am grateful to my course instructors Dr. R. Seshadri, Dr. A., Swamidas, Dr. M. Booton, Dr. M. Hinchey, and Dr. S. O' Young. I like to express my deepest gratitude to Dr. A. Swamidas for his help and constructive discussions.

I like to thank the Canadian International Development Agency (*CIDA*) and the School of Graduate Studies at Memorial University of Newfoundland (*MUN*) for their financial support they provided during my Ph.D. program in a cooperation program

(*CIDA-MUN* Marine- Scholarship). I like to thank Dr. Anthony Dickinson (Director, *CIDA*) and Miss Colleen Clark (International Projects Administrator, *CIDA*) for their supports and encouragements.

Special thanks are due to Andrew Kuczora and Darrell Sparkes who cooperated in carrying out the experimental work for this dissertation at Memorial University towing tank.

I also do not forget the first support and encouragement from my home department (*Naval Architecture & Marine Engineering*, Alexandria University, Egypt) especially Dr. M. Shama, Dr. A. Sabit, Dr. M. Salm, Dr. Y. Welaya, Dr. A. Elbadan, Dr. M. El-Gammal, Dr. A. Iraqi, Dr. H. Leheta, and A. Banawan.

I like to express my deepest gratitude to the external examiner for my M.Sc. thesis, Dr. Adil Elbatouti (*General Manger, American Bureau of Shipping* [*ABS*], *Alexandria, Egypt*) for his recommendation to pursue my Ph.D. at Memorial University under supervision of Dr. M. R. Haddara.

I like to express my gratitude to my fellow graduate students at Memorial University for their support and encouragement.

Finally, I like to thank both the Canadian and the Egyptian Governments for giving me the opportunity to pursue this work at Memorial University of Newfoundland.

Contents

List of Figures

List of Tables

Notation and List of Abbreviations

ω_e	: Encounter wave frequency
ω_n	: Cutoff frequency (butter- filter)
ω_i	: i^{th} frequency
Ω	: Wave modal frequency
$H_1(R_{21}, \dot{R}_{21})$	: Coupling function for heave motion (auto- and cross-correlation)
$G_1(\mu_2, \dot{\mu}_2)$	: Coupling function for heave motion (random decrement)
$H_2(R_{11}, \dot{R}_{11})$	: Coupling function for pitch motion (auto- and cross-correlation)
$G_2(\mu_1, \dot{\mu}_1)$	: Coupling function for pitch motion (random decrement)
< > or E [.]	: Ensemble average
δ (t)	: Dirac delta function
ζ	: Damping ration
ν	: Phase angle for exciting moment
δ	: Phase angle for regular heave motion
ε	: Phase angle for regular pitch motion
σ	: Phase angle for the exciting force
Θ	: Pitch motion response
ρ	: Water density
∇	: Volume of submerged body of the vehicle
τ	: Time lag
$\Delta\omega$	: Frequency increment
ζ_a	: Regular wave amplitude
ϕ_i	: Phase angle of wave amplitude i
β_j	: Synaptic weight of neuron j in the hidden layer
μ_{km}	: Input motion vector to the neural network
μ_{kn}	: Calculated motion vector using the neural network
θ_o	: Regular pitch motion amplitude
ζ_w	: Depression of the regular wave surface

π : Constant equal to 3.141593

μ_i : Ensemble average of y_i, i = 1,..,4

$\overline{F}$: Sinusoidal wave excitation force

$\overline{M}$: Sinusoidal wave excitation moment

2D : Two-Dimensional flow

3D : Three-Dimensional flow

a_{33} : Added mass for heave motion

a_{55} : Added mass moment of inertia for pitch motion

a_{35}, b_{35}, c_{35} : Coupling parameter for heave motion

a_{53}, b_{53}, c_{53} : Coupling parameter for pitch motion

A_H : Water plane area for the hydrofoil connection

a_{hi} : Sinusoidal heaving force amplitude i^{th}

ALF : Adaptive Lainiotis Filter

AP : After Perpendicular (Station # 81)

a_{pi} : Sinusoidal pitching moment amplitude i^{th}

AUVs : Autonomous Underwater Vehicles

b_{33} : Damping parameter for heave motion

b_{55} : Damping parameter for pitch motion

BM : Metacentric radius

c_{33} : Restoring parameter for heave motion

c_{55} : Restoring parameter for pitch motion

CFD : Computational Fluid Dynamics

CIDA : Canadian International Development Agency

DOLPHIN : Deep Ocean Logging Platform with Hydrographic Instrumentation for Navigation

DSVs : Deep Submersible Vehicles

f : Sigmoidal function or Squashing function

F(t) : Exciting wave force

FFT : Fast Fourier Transform algorithm

FLOW-3D : CFD software program

FNNs : Feedforward Neural Networks

FP	: Forward Perpendicular (Station # 0)
g	: Acceleration of gravity
GENESIS	: Genetic algorithm computer program
GM	: Metacentric height
GZ-Θ	: Statically stability curve
I	: Mass moment of inertia of the model
I_L	: Longitudinal second moment of the hydrofoil area about its center
IMD	: Institute for Marine Dynamics
ITTC	: International Towing Tank Conference
JONSWAP	: Joint North Sea Wave Project
k	: Wave number
KB	: Vertical center of buoyancy of the model
KG	: Vertical center of gravity of the model
L	: Lever
LCB	: Longitudinal center of buoyancy of the model
LCG	: Longitudinal center of gravity of the model
m	: Mass of the model
M(t)	: Exciting wave moment
MDTF	: Marine Dynamic Test Facility
M_i	: Mass component i^{th}
MUN	: Memorial University of Newfoundland
n	: Number of neurons in the hidden layer of the neural network
NNT	: Neural Networks Technique
N_P	: Number of points
NSERC	: Natural Sciences and Engineering Research Council of Canada
PMM	: Planner Motion Mechanism
P-Value	: Probability of getting the regression mapping model
R	: Distance from the center of gravity and the pitching pivot of the dynamometer flange
$R(\tau)$	: Auto-correlation function
RDLRNNT	: Random Decrement, Linear Regression, and Neural Network Technique

R_{ij} : Auto-correlation functions ($i = j$)

: Cross-correlation functions ($i \neq j$)

RNNs : Recurrent Neural Networks

ROVs : Remotely Operated Vehicles

R-sq : Coefficient of determination

$S_h(\omega_i)$: Narrow-band spectrum for heaving force at frequency, ω_i

SM : Simpson's Multiplier

$S_p(\omega_i)$: Narrow-band spectrum for pitching moment at frequency, ω_i

SPI : Standard Parametric Identification Technique

t : Time

URV-Motion : Developed computer program for regular heave and pitch motions

URV : Underwater Robotic Vehicles

VIF : Variance Inflation Factor

W_i : Weight component i^{th}

W_{ij} : Synaptic weight of neuron i^{th} in the input layer to the j^{th} neuron in the hidden layer

X_H : Center of the water plane area for the hydrofoil connection

X_i : Longitudinal center of buoyancy or gravity of component i^{th}

X_n : Input vector to the input layer of the neural network

y_i : The displacement and the velocity of the heave and the pitch motions ($i = 1,\ldots,4$), respectively

Y_i : Vertical center of buoyancy or gravity of component i^{th}

Y_U : Half breadth of the NACA 0024 section

Z : Heave motion response

Z_O : Heave trigger value

Chapter 1
Introduction

1.1 Objectives

The main objective of this work is to develop a robust technique for the identification of the damping, restoring, and coupling parameters in the equations describing the coupled heave and pitch motions for an Underwater Robotic Vehicle (URV) sailing near the sea surface in random waves.

The technique should be able to deal with situations where the level of damping is high and where the wave spectrum can no longer be considered white noise. A long-term objective is to develop this technique into a tool for continuous monitoring of the URV's motion and stability. The tool will be helpful in raising the level of reliability of the URV. It will also provide full-scale data, which can be used to improve the design procedure for such vehicles. The technique developed in this work can also be used for the analysis of towing tank data.

1.2 Methodology

A robust identification technique called "*RDLRNNT*" has been developed in this work to identify the parameters in the equations describing the coupled heave and pitch motions for an URV sailing near the sea surface in random waves. The technique is based on the use of a combination of a random decrement technique, a multi-linear regression

algorithm and a neural networks technique. The present technique uses only the measured heave and pitch motion responses at sea without a prior knowledge of the wave excitation.

The identification procedure consists of three steps. In the first step I derive the random decrement equations. The derivation is based on a mathematical model describing the coupled heave and pitch motions for an URV sailing near the sea surface in random waves. In the second step a multi-linear regression algorithm is applied to the random decrement equations to identify the damping and the restoring parameters. In the third step a neural networks technique is used to identify the coupling functions for the heave and pitch motions.

The neural networks technique is based on the minimization of the error between a target function and the network's output. In the problem at hand, it is difficult to determine the target function. Substituting the network's output back into the differential equations and integrating these equations to obtain the heave and pitch displacements have remedied this situation. The obtained heave and pitch displacements are then used as network outputs and the error is calculated between these outputs and the measured heave and pitch displacements.

1.3 Thesis Organization

The thesis is divided into four parts. In the first part, which can be found in Chapter 2, I provide a literature survey in two main areas: dynamics of the underwater robotic vehicles and identification techniques. The survey sheds light on different methods used

in the identification of the hydrodynamic parameters for ships and underwater robotic vehicles. In addition, the survey covered the most recent methods in the identification of the hydrodynamic forces: parametric identification and neural networks. In the survey, I describe the advantages and disadvantages as well as the limitations of each method.

In the second part, which can be found in Chapters 3 and 4, a mathematical model that describes the coupled heave and pitch motions for an URV sailing near the sea surface in random waves, is formulated using rigid body dynamics and Newton's laws of motion. In addition, the random decrement equations as well as the auto- and cross-correlation functions for the coupled heave and pitch motions for an URV are derived. I briefly introduce the new developed identification technique, *RDLRNNT*. In this part, the developed technique is based on a combination of the random decrement technique or auto- and cross-correlation functions, a multi-linear regression algorithm, and a neural networks technique. These techniques are briefly introduced in this part.

In the third part, which can be found in Chapter 5, I introduce a procedure for the validation of the model using both numerically generated data and experimental data. In addition, the main features of the designed URV-model as well as the associated calculations: weight, buoyancy, ballast, and stability are presented. Moreover, I investigate the use of strip theory in the prediction of the coupled heave and pitch motions for a harmonic excitation.

I introduce briefly the preparation of the URV-model for carrying out the experimental work. Two main categories of experiments are carried out in this work: calm water experiments and random wave experiments. The first category was needed to measure the free decay coupled heave and pitch motions for the URV-model, while the

second one was important to validate the utility of the developed technique in the identification of the hydrodynamic parameters in the equations describing the coupled heave and pitch motions for an URV sailing near the sea surface in random waves.

In the fourth part, which can be found in Chapter 6, I generate random data for the coupled heave and pitch motions using the mathematical model. The random data were generated for both wide-band and narrow-band excitations. In this part, I investigate the effect of using a band-pass filter centered around the damped natural frequencies for heave and pitch motions, on the identified parameters. Furthermore, I present the numerical simulation results for random motions taking into account the variation of both the damping levels and different values of damped natural frequencies for heave and pitch motions.

Furthermore, I present the experimental results for random motions taking into account the variation of towing speed, and both the significant wave height and the modal frequency of the wave excitations. I finally conclude our work in Chapter 7 and give some directions for the future open problems in the area.

1.4 Scope of Research

The dissertation focuses on the development of a reliable and robust technique for the identification of the parameters in the equations describing the coupled heave and pitch motions for an URV sailing near the sea surface in random waves. The developed technique depends only on the measured responses of the URV and does not require a prior knowledge of the wave excitation.

The developed technique has been validated using both numerically generated data as well as experimental data. Numerical data for random motions have been generated taking into account the variation of both the damping levels in heave and pitch motions, and different values for the damped natural frequencies. Both the effects of wide-band and narrow-band excitations on the identified parameters are investigated using the developed technique. In addition, the effect of using a band-pass filter centered near the damped natural frequencies for heave and pitch motions on the identified parameters is investigated.

An experimental program was designed and conducted at the towing tank at Memorial University. The main objective for carrying out the experimental program is to measure the coupled heave and pitch motions for the URV corresponding to different random wave excitations. Three main parameters are varied in the experimental program: the significant wave height, H_S, the wave modal frequency, Ω, and the towing speed, U.

Computer programs for calculating the random decrement signatures, the auto- and cross-correlation functions using both numerically generated random data and the measured random data for the coupled heave and pitch motions for the URV were developed.

Chapter 2
Literature Review

2.1 Introduction

The ocean is an important source of resources such as fish, minerals, natural gas, and oil. A huge effort has been made to utilize and to protect these resources since they can contribute significantly to the development of our lives. The first step towards the ocean exploration was the use of diving suits and manned submersibles. Since the appearance of their limitations, various forms of unmanned remotely controlled vehicles were developed.

Several studies have been carried out to develop vehicles that can be used in ocean exploration. These studies have been under way for several decades. They were mainly directed to military tasks and scientific research. In the 1960s and 1970s, two main types of vehicles were developed: deep submersible vehicles (DSVs) and underwater robotic vehicles (URVs) [1,2].

It is essential that the DSVs be large enough to accommodate several persons, such as a pilot and observers. These vehicles are classified as human occupied vehicles. Therefore, these vehicles are more difficult to handle at sea and more difficult to position in restricted work areas. Most DSVs require the presence of a mother ship to provide the supervision support for the vehicle and personnel.

URVs include the whole range of unmanned underwater vehicles from remotely operated vehicles (ROVs) to autonomous underwater vehicles (AUVs) [3]. These

vehicles are classified as unoccupied vehicles. ROVs provide greater endurance and larger range than DSVs at a lower cost. In addition, ROVs can operate in hazardous environments and provide on-line real time observation. This is because life-safety support is not necessary for ROVs. Thus, ROVs have replaced DSVs in most commercial applications.

ROVs were originally developed for military applications. In the early 1970s, the offshore oil industry needed such vehicles to construct and to maintain underwater structures [1]. ROVs technology was further developed to meet such needs by private firms. They are the most common type of underwater vehicles. Because of user familiarity and extensive proven capabilities for such vehicles, they are widely used.

Using a tether (umbilical cable), an ROV is usually connected to a mother ship. The tether carries power and control signals from the mother ship, and transmits the feedback-measured data from the vehicle. In general, ROVs have been classified into three main types depending on the type of mission: small, light and medium-weight, and large-work class ROVs [1]. The tether constrains the vehicle in many ways. Therefore, the use of ROVs is restricted by tether drag and the stability of ROVs can be affected by the surface waves. Due to the tether's limitation, unmanned autonomous underwater vehicles (AUVs) have been created as an alternative exploration and work platform.

AUVs have potential advantages over ROVs and DSVs because they are free from tethers and human occupants. Therefore, the vehicle is free to roam widely in the ocean. Furthermore, they can be used in hazardous environments such as a toxic area, or in radioactive material areas, or in poor weather conditions. Humans cannot reach these

environments. In addition, these vehicles are suitable for repetitive and long time missions instead of using surface platforms.

The development of these vehicles has been under way for several decades and was mainly funded by the military. The development of these vehicles was slower than ROVs, because there was no experience with such vehicles in the commercial sector [1]. The currently existing AUVs are restricted with limited decision-making capability and endurance. AUVs are still in their developing phase. There is a lack of operational experience with these vehicles in the open ocean. This marks them as an immature technology with very important potential for the future.

The last three decades saw a rapid growth in the development and use of the URVs. The early use of these vehicles was limited to military applications. However, the use has spread recently to all types of industrial activities. Foremost, among these activities is the use in offshore oil and gas applications. The success of an URV in achieving its mission depends largely on the sophistication of the control strategies used in controlling the motion of the vehicle and the ability of the vehicle to perform required maneuvers. Accurate dynamic modeling is a prerequisite for designing effective control strategies [3,4,5,6].

The dynamic behavior of a URV is based on the hydrodynamic forces and moments that represent the main difficulty in the modeling of the URVs. However, the high performance of URVs cannot be achieved without resolving this difficulty. In addition, the dynamics of these vehicles are strongly coupled due to the comparable velocities along the three axes of the motion. Moreover, the added mass values and the location of the centers of gravity and buoyancy suffer large variation because of large

changes in the load of the vehicle during its mission. Finally, underwater currents have significant effects on the performance of the URVs.

Different types of external forces and moments are exerted on the vehicle body during its mission. These are hydrodynamic forces, weight and buoyancy forces, and current forces. Likewise, the advancing motion of the URV in water causes two major effects: accelerating the layer of the water surrounding the vehicle and introducing drag forces due to the effects of viscosity.

The equations of motion describing the motion of the URV can be formulated using rigid body dynamics and Newton's laws of motion. The hydrodynamic parameters of the vehicles are important components of the model. Several methods have been used to define and calculate these parameters. These include: strip theory, slender-body theory, a semi-empirical approach and most recently, parametric identification. I am mainly concerned with last approach.

The most recent approach to estimate the hydrodynamic parameters for a particular vehicle is the parametric identification technique. The relationship between the inputs and the outputs is assumed based on the nature of the dynamic system. This relationship is known as a mathematical model. The unknown parameters in that model are determined by minimizing the mean square of the error function, which is the difference between the output of the mathematical model and the measured output of the dynamic system.

One of the advantages of parametric identification is that if it can be done in real time then one can have a tool for updating the dynamic model as the vehicle moves

through the water. Responses obtained using this model will be realistic and increase the chances of having better control of the vehicle.

One main drawback for the classical identification techniques is that they require knowledge of the input and the output to the system. In case of a ship at sea, input measurements are difficult to carry out. A technique that depends on the knowledge of the output only is desirable in this case.

Some parametric identification techniques have been used successfully in the area of ship motion such as equivalent linearization technique, auto-correlation function, random decrement technique, and neural networks technique [7,8,9,10].

In general, the hydrodynamic parameters of the URV are functions of forward speed and frequency. A method, which could estimate these parameters in real time and feed them into the dynamic model to update the vehicle state variables continuously with time, is desirable. Such a method would have to rely only on the measured response of the vehicle because it is difficult to get information about the environmental conditions while the vehicle is moving. A method that is based on the random decrement concept seems to be most suitable for such problems.

The method for obtaining the random decrement signature applies an averaging technique that has been used successfully in the on-line failure detection and damping identification for linear systems [11,12]. Statistical properties obtained indicate that this signature is stable in form and scale. This marks it as a reliable method with very important potential in damping identification.

The random decrement signature is the ensemble average of a large number of segments of the response of a system. Each segment must start with the same initial

conditions. The random decrement is based on the fact that when the general response of a single-degree-of-freedom system is averaged, the contribution of its steady state component to the expected value of the response vanishes when the excitation function is a Gaussain white noise random process. Then, the expected value of the random response is represented only by the contribution of its transient component caused by the initial conditions [13,14].

In other words, when a Gaussain white noise random process excites a single-degree-of-freedom system, the random decrement signature is identical in form to its free response and its auto-correlation function in the case of lightly damped motions. However, for nonlinear and multiple-degree-of-freedom systems in heavily damped motions which are excited by other excitations, it differs. Moreover, the obtained signatures for the systems are influenced by the excitations and this must be taken into account in the interpretation [12].

The method has been developed in connection with the identification of the rolling motion of a ship [14]. It is based on calculating the random decrement signature from the random response. It was shown that the random decrement signature agrees well with both the auto-correlation function and the free decay roll response. The method was extended to the case of the coupled sway and yaw motions for a ship [13] and to the case of two-degrees-of-freedom systems [15].

Coupled heave and pitch motions for semi-submersible rigid bodies have been studied in several research studies [6,10,16,17,18]. The main parameters of the coupled heave and pitch motion equations are: the virtual mass of the body and its virtual moment of inertia, heave and pitch damping parameters, heave and pitch restoring parameters, the

exciting wave force and moment, and the coupling parameters. Fourteen unknown parameters in these equations are to be determined. The coupled heave and pitch equations can be normalized with respect to the total virtual mass and the virtual moment of inertia of the body, respectively. In this case I am left with only twelve quantities to determine.

The case of the coupled heave and pitch motions [15] showed that the random decrement signatures and the components of the correlation matrix satisfy the same equations describing the free decay motion of a heaving and pitching floating body. It has also been shown that both the correlation functions and the random decrement signatures yield good results for systems, which have weak damping. When damping is low, the random decrement signatures and the correlation functions provide good representation of the free decay motion of the system. However, for highly damped systems this ceases to be the case. High damping causes the transient solution to die very quickly and the random decrement signatures and the correlation functions become affected by the external excitation.

A modification of the above mentioned approach has been developed. The results of the new technique are presented. This new approach enables us to use the random decrement signatures or the correlation functions to represent the free decay coupled heave and pitch motions of a moderately damped semi-submersible vehicle. The modified approach is used to show that the free decay coupled heave and pitch motions for an URV can be determined using its measured stationary random response.

The spectral densities of the coupled heave and pitch motions of a URV/ship floating near the water surface in random waves are characterized by well separated

multiple peaks. One peak is usually centered around the natural frequency while the other is usually centered around the wave modal frequency. With the present state of knowledge in the area of ship motion, one can get rough estimates for the natural frequencies for heave and pitch motions. One can then use a band-pass filter centered around the estimated natural frequency to get a signal which is composed mainly of the transient response of the floating vehicle. The correlation functions and/or the random decrement signatures can be then calculated using this filtered signal.

A robust technique has been developed in this dissertation to identify the damping, the restoring, and the coupling parameters in the equations describing the coupled heave and pitch motion for an URV working near the sea surface in random waves using only its measured random responses without a prior knowledge of the wave excitation. This has been achieved using a combination of the random decrement technique, a multiple-linear regression algorithm and a neural networks technique in one technique, which I called as "*RDLRNNT*".

In this chapter, I am going to present the literature survey for this work. This survey has been conducted and classified into two main tasks: dynamics of the URVs, and identification techniques. These tasks will be discussed in the following sections.

2.2 Dynamics of Underwater Robotic Vehicles

During the last three decades, the use of URVs has rapidly increased in different areas. This is because the use of URVs is no longer limited to the military field only. Reliability of operation for these vehicles has become an important factor in their development

because they work in a hostile ocean environment, which is unrestricted and unpredictable. Many problems have restricted the development of these vehicles such as maneuverability, and control strategies. This is due to the fact that the dynamic behavior of the URV is highly nonlinear and strongly coupled [3,4,5,6].

The advancing motion of the URV in water causes two major effects: accelerating the layer of the water surrounding the vehicle and introducing drag forces due to the effects of viscosity. The mass of the layer of the surrounding water that has been accelerated by the vehicle motion is known as the added mass. Added mass parameters are proportionality constants that relate each of the linear and angular accelerations to each hydrodynamic force and moment they generate [4]. Thus, the effective mass of the vehicle and its moment of inertia should be calculated based on the added mass terms. The effect of the added mass terms will be significant in the case of high acceleration motion.

Another result from the motion of the URV in the water is drag force, which results from the friction between the URV body and the surrounding water particles. This force is proportional to the square of the corresponding relative motion [4]. Forces and moments resulting from thruster dynamics, weight and buoyancy should be defined at the local coordinate systems. All of the mentioned forces should be included in the equations that describe the motion of the URV.

Three approaches have been used to study the motion of URVs: theoretical investigations, model experiments, and full-scale measurements. Theoretical developments in the area of URVs motion may be largely divided into two main categories: analytical and empirical methods [16].

The methods in the first category focus on finding numerical solutions to problems, which deal with linear and nonlinear, two-dimensional (2D) and three-dimensional (3D) surface flow around a floating body. Some of these methods used include strip theory, slender-body theory, and panel source method.

Strip theory allows for good estimates of the vertical motions of conventional ships. It has proven more than satisfactory for the calculation of some ship motions [19]. Korvin Kroukovesky and Jacobs originally developed strip theory to calculate the coupled heave and pitch motions for a ship [17]. This theory considers the floating/submerged body as a cylinder having a series of transverse strips. Each strip is assumed to be a part of infinite cylinder having a 2D flow. This assumption reduces the problem from a 3D flow problem to a 2D. The response of each strip is easily calculated. The total response of the floating/submerged body is found by integrating the component reactions of all strips along the length of body. This method reduces the 3D flow problem to a 2D one with specific assumptions. One of these assumptions is zero-interaction between the flows at adjacent sections. However, there is a significant difference between 2D and 3D flows. The assumption restricts the applicability of the strip theory. Moreover, the strip theory is still in a state of refinement due to the complexities of free surface effects. In fact, the practical limits of this method are poorly known [20].

Slender-body theory is another method that could be utilized to solve the 3D-flow problem around floating/submerged bodies [21]. It is used in the calculation of resistance and hydrodynamic forces of ships. The vehicle's beam and the draft are small compared to the length of the vehicle. The fluid actions are described by the unified slender-body theory presented by Newman in 1978 [22]. The comparison between the experiments and

the slender-body theory is difficult because the theory neglects the effects of control surfaces, propellers, and other appendages in the model, whereas experiments are usually conducted using full-form models with all appendages [7]. Moreover, the applications of slender-body theory are limited in ocean engineering. The URV may have many manipulators, links, fins, and thrusters. Therefore, this method will not be suitable for the calculation of the hydrodynamic forces for such vehicles.

A panel source method is based on the approximation of the velocity potential flow of the submerged vehicle in waves. This approximation is obtained by distributing sources and normal dipoles on the submerged surface of the vehicle. An integral equation for the strength of these singularities is derived from the corresponding boundary conditions [19,20]. This method is suitable for the complicated structure shapes. However, it is considered to be a highly time-consuming method, where its accuracy is proportional to the square of the number of panels.

The basic assumption underlying the second category is that the Froude-Kirylov hypothesis is valid [5,6,8]. According to this hypothesis, one can decompose the forces acting on an URV advancing in waves into two types of forces: hydrodynamic forces and exciting forces. The equations of motion have been obtained using Newton's law of motion while considering the effect of the underwater currents, torques, and cable traction only in the case of ROVs [6].

Hydrodynamic forces are produced as a result of the oscillations of the URV about a stationary or steadily advancing mean position below the calm free surface. Exciting forces are produced as a result of the pressure distribution in waves assuming that URV is fixed at the mean position. The analysis is carried further by assuming that

the hydrodynamic forces are functions of the accelerations, velocities, and displacements of the URV. Thus, the Taylor or McLaurin expansions of these variables are used to express these forces mathematically. The parameters of the different acceleration, velocity, and displacement terms are generally called added masses, damping parameters, and hydrostatic spring parameters, respectively. Different methods exist in the literature for the determination of these parameters [9]. The hydrostatic parameters are easily calculated by theory; however, the added masses and damping parameters are extremely difficult to calculate especially for large amplitudes and coupled motions.

Abkowitz (1964) replaced the hydrodynamic forces and moments by their Taylor expansions [10] and Baiardi et al., approximated these forces and moments for low velocity motion by using McLaurin expansions [9]. Since, the use of Taylor or McLaurin expansions is limited only for the analytical functions, the hydrodynamic forces and moments are assumed to be of this nature at least for the linear term and third order term [10].

However, truncation of the higher order terms from these expansions diminishes the accuracy of the estimated values. In addition, the number of the parameters to be identified is large, which means a large time-consuming calculation procedure.

Yuh and Choi et al. have developed a mathematical model describing the dynamics of the URV [4,5,23]. In this model, all the nonlinear dynamic terms with velocity terms, terms associated with forces and moments exerted on the vehicle by fluid motion, drag forces and torque are included in one matrix. The inertia matrix includes the mass of rigid body plus the added mass and added inertia associated with the motion of rigid body in the fluid. There are two force vectors, one for gravity and buoyancy forces,

and the other represents the forces and torque generated by thruster forces. Unfortunately, there are poorly known hydrodynamic parameters among the parameters of the dynamic model. Therefore, a conventional control scheme cannot guarantee high performance in URVs motion control.

When one or more manipulators are attached to the vehicle, it becomes a multiple-body system. In this case, a significant effect on the global motion of the vehicle will be introduced. Consequently, the dynamic modeling of such vehicles will be very complicated [3]. Uncertainty involved in the evaluation of the hydrodynamic parameters of URVs usually introduces the significant error in the final prediction results.

A semi-empirical approach is based on the derivation of empirical models (relationships) for the hydrodynamic parameters of a tested-vehicle as functions of its attitude and motion. These models can be obtained using a multiple-linear regression algorithm for the measured values of these parameters corresponding to particular motions for such a vehicle. The measured values for these parameters can be determined using a forced/captive model experiments for a particular vehicle such as planar motion mechanism (PMM), rotating arm technique, and marine dynamic test facility (MDTF).

Nahon [16] used well-known empirical hydrodynamic relations, which use the geometrical shape of the vehicle to calculate the hydrodynamic parameters for streamlined underwater vehicles. The vehicle's body has been decomposed into its basic elements: hull, individual control surfaces, and propulsion system. Each element is modeled using well-known empirical hydrodynamic relations. The total hydrodynamic forces and moments are then considered as a summation of the element effects with some corrections. The approach is valid only for streamlined underwater vehicles; however,

most of the working underwater vehicles have some complicated geometry. However, the correction factors that have been used as a result of the interference effects between different elements constituting the streamlined vehicle are difficult to obtain accurately.

The idea of a numerical wave tank (computer codes) is currently being developed. Great progress is being achieved in this area of research, but the complexity of involved phenomena and the high degree of nonlinearly still constitute the main difficulty. Also, many difficulties remain in order to obtain practical tools to solve the URV design problems. In addition, numerical wave tank predictions do not indicate that Computational Fluid Dynamics (CFD) is actually replacing the physical towing tank. One of the computer codes which has been used in the simulation of offshore structures is FLOW-3D.

Model experiments have been used extensively in applied sciences and engineering to provide a practical tool for validating the theoretical prediction of the behavior of the floating/submerged vehicles in a realistic sea. In addition, they are used to study new hull shapes and wave loads that a floating/submerged body will encounter for its optimum design. Model test results suffer from scale effects, which may be of great importance especially in cases where viscosity plays a major role [17].

Full-scale tests are performed in limited cases due to the expense involved. Their use is usually limited to the conditions under which the tests have been carried out. Thus, the results of these tests do not provide excitation independent transfer functions, which can be used later for calculating a vehicle's response to different excitations [17].

Currently, an important desire exists for research to develop a practical and reliable tool for the prediction of the URVs response in realistic seas without the drawbacks of the traditional methods. This desire is the focus of this dissertation.

2.3 Identification Techniques

The existing techniques for the determination of the hydrodynamic parameters of URVs are theoretical predictions, water tunnel and towing tank tests, and trial and error adjustment of model parameters. These techniques have drawbacks such as high cost, are time-consuming, and do not provide any mathematically defined optimum.

In the last two decades, several studies have been conducted in the area of the identification techniques. Recently, system identification techniques have been applied to identify the hydrodynamic parameters included in the dynamic model describing the motion of the URV. The dynamic model is traditionally formulated using rigid body dynamics and Newton's law of motion.

Parametric identification techniques have been used instead of the traditional methods to overcome the drawbacks from using them [18]. Many parameter identification techniques have been developed, of which most involve a minimized measure of the mean square error between the output of the predicted model and that from the measured data.

Abkowitz [24] used a Kalman Filter approach to identify the hydrodynamic parameters in the maneuvering equations of the ship. Roberts et al. [25] developed a method for the prediction of the hydrodynamic parameters of a single-degree-of-freedom rolling equation from roll measurements in realistic sea. This method assumes the

property of the energy envelope process associated with the roll motion is a Markov process. Healey [26] applied both Batch Least Squares and Kalman Filters for system parameter identification to the experimental maneuvering responses of AUV to detect a change in AUV performance.

Roberts et al. [27] initiated an approach, based on the use of a combination of the Markov process theory and the statistical linearization technique. Roberts' approach does not require prior knowledge of the excitation data. It requires long records of data and the results are not always unique because of the large number of parameters to be determined.

The development of a robust identification technique, which uses the measured response at sea, does not require prior knowledge of wave excitation and deals only with a few unknown parameters, seems to be in order. Haddara [14] used the Markov process theory to extend the random decrement technique to the case of nonlinear roll motion. This technique is based on calculating the random decrement signature from the random response. It was shown that the random decrement signature agrees well with both the auto-correlation function and the free decay roll [14]. The random decrement signature can then be used to identify the parameters in the equation of motion without a need to know the input to the system.

Originally, Cole [11,12] developed the random decrement technique empirically in 1968. The basic assumption underlying this method is that one can obtain the free response of a linear system excited by a zero mean, stationary, white, Gaussian random process by ensemble averaging of the selected segments of the system response. These segments are selected such that they all start with the same initial conditions

(displacement and velocity values). This value is then considered to be an initial condition for the free response. The random decrement signature has been used as an identification technique in the aerospace industry such as aircraft structures since 1968. It has been used successfully for the damping identification of linear structures. The random decrement signature has been also considered as the main basis of "Ibrahim Time Domain Model Vibration Testing Technique"[28].

During that time, a mathematical basis of random decrement signature did not exist to determine the accuracy of that technique in the estimation of damping ratio of a dynamic system. Vandiver et al. [29] developed a mathematical basis for the random decrement technique, and provided the relationship between the random decrement signature of a random process and its auto-correlation function. This relationship is for a linear time invariant system excited by a zero-mean, stationary, Gaussian white random process, in which the random decrement signature of the response is proportional to its auto-correlation function. Fortunately, most applications of the random decrement technique have been restricted with the assumption that the excitation was sufficiently broadband (Gaussian white noise random process).

The random decrement technique has successfully extended to nonlinear dynamic systems, by Haddara [14]. The equations governing the random decrement signature for ship rolling motion in a random sea have been derived. These equations are used to identify the nonlinear rolling damping. This technique when combined with Standard Parametric Identification techniques (SPI) yields values for damping and restoring parameters without prior knowledge of the excitation. Haddara et al. [30] has conducted the identification of the parameters successfully and the method was tested using

simulations, model tests, and full-scale results. The method was shown to be successful and is used by a local company as the basis for design and production of stability continuous monitoring systems [31].

Haddara [32] has combined the random decrement technique and neural networks technique, as an identification technique of stability parameters in a random sea. C. Y. Liaw et al. [33] has applied the Genetic algorithm in the parametric identification of nonlinear-coupled roll and heave motions. In this algorithm, one can start the identification process with a population of a random set of parameters, or genes. Each set of these parameters is coded into binary digits, the chromosomes. Genetic algorithm can then manipulate chromosomes in order to find the fittest set of parameters with respect to the target function (free decay record). Any available Genetic algorithm computer program, for example GENESIS, can be used. This algorithm needs only a feedback from the searching space to be consistent, so that the solution yields better evaluations.

Haddara et al. [15] derived random decrement equations that describe the coupled heave-pitch motions for a ship sailing in random waves. It has been shown in that work that the random decrement signatures and the components of the correlation matrix satisfy the same equations describing the free decay motions of heaving and pitching for a ship. It has also been shown that both the correlation functions and the random decrement signatures yield good results for systems, which have weak damping. When the damping is low, the random decrement signature and the correlation function provides good representation of the free decay motion of the system. However, for highly damped systems this ceases to be the case. High damping causes the transient solution to

die very quickly and the random decrement signatures and the correlation functions become affected by the external excitation.

Multiple-linear regression algorithms may be used to estimate the parameters in a linear mathematical model; however, for a nonlinear and coupled model with a large number of independent variables (regressors), the accuracy of the algorithm decreases. One of the limitations of using a multiple-regression algorithm is that there is no control over the values that the method allocates to the different parameters in the model. For a multiple-parameter model, there is some sort of "energy sharing" between the different parameters. This sometimes results in a phenomena where an estimated value of a parameter is larger than it should be, while the estimated value of another parameter decreases to compensate for the increase in the value of the first parameter.

The most recent technique in the area of the parametric identification is the use of an artificial neural network. In general, research on artificial neural network models has a long history. Development of detailed mathematical models began more than 50 years ago [34]. Neural networks try to mimic biological networks [35]. The present artificial neural networks are considered much simpler compared to the biological networks especially in the number of neurons, size, and construction complexity [36].

Current interest in the field of neural networks is due to the vast development of new network topologies and algorithms. Due to the rapid growth in the range of alternative neural network systems, it is necessary that these systems be classified. This classification is based on four characteristics: data format, mode of operation, principal connection shape, and training process [36]. The network topology, neuron characteristics, and training algorithms specify neural network systems [37]. Artificial

neural networks have been proven to be more successful as a robust tool for identification of discrete nonlinear control systems than conventional statistical techniques. This is because there are many more processing nodes, each with primary local connections.

In an artificial neural network, the outputs can be fed back to the input layer to adapt its weights by using learning algorithms. However, the main current concern area in neural networks is to improve the training algorithms. Since the conventional techniques typically process all training data simultaneously before being used with new data, strong assumptions have been made concerning underlying distributions of the input elements [34]. On the contrary, these assumptions do not exist in the neural networks. This is because neural networks have a large number of simple processing elements operating in parallel [34].

Currently, neural networks are used in almost all branches of engineering. For example, in mechanical engineering, neural networks are used in the modeling of dynamic systems for both design and control strategies. The use of the conventional controllers has been restricted by the difficulties in the modeling of URV and the hazardous environment of the ocean. Moreover, the technology for land vehicles cannot be easily applied to URVs because the nature of the ocean environment is much more complicated than the land environment [38]. Therefore, researchers are trying to develop an intelligent control strategy for effective operation of URVs.

The emergence of neural networks as an effective learning system for a wide variety of applications has resulted in the use of these networks as learning controllers for dynamic systems. One of the most important advantages of using neural networks for

control applications is that the dynamics of URVs need not be completely known as a prior condition for controller design.

Masri et al. [37] used a neural network in the identification of a nonlinearity in a single-degree-of-freedom dynamic system. However, Haddara et al. [15,39] used neural networks techniques successfully in the identification of the hydrodynamic parameters in the equations describing the coupled sway and yaw motions for a ship. In addition, Haddara suggested a method, which is used as a part of continuous monitoring system to provide information about instantaneous values of ship stability. This method has been made by using the neural network technique to identify stability parameters [32].

Lainiotis et al. [40] has developed a comparison between the Kalman Filter estimator and the neural network one. The conclusion from this comparison is that the neural network estimator requires only very little information about the dynamics of the system compared to that required by the Kalman Filter estimator. Nevertheless, the performance of the conventional statistical techniques depends basically on the information about the possible variations of the unknown parameters. The prediction of the ship position by using a neural network estimator is much better than that obtained by using a Kalman Filter estimator in cases where the underlying statistics and dynamics of the system are not completely known to the estimator.

In order to compare the Adaptive Lainiotis Filter (ALF) and adaptive neural network estimator, three experiments in the ship position estimation were developed by Lainiotis et al. [41]. In the first experiment, it is supposed that the dynamic model of the system is partially known. In the second experiment, it is supposed that there is a different uncertainty scenario for the model. The result of the comparison from these

experiments is that both ALF and neural network estimators identify the actual model very well. It must be emphasized that the neural network estimator does not require any statistical or deterministic information about the inputs to the model. In the third experiment, there is a more difficult uncertainty scenario. It has been found from this experiment that the adaptive neural network estimator provides a very reliable solution to the problem of ship motion estimation. This is because it provides accurate and consistent results despite the minimum information about the nature of the dynamic systems.

The identification of the nonlinear dynamic systems has been done using two popular types of artificial neural networks. These types are feedforward neural networks (FNNs) and recurrent neural networks (RNNs). Recurrent neural networks are the networks with internal or external feedback in which the past system outputs are replaced by the past outputs of the network, while in FNNs, past system inputs and outputs are used as neural network inputs. Any dynamic system can be modeled using FNNs with at least one hidden layer to any level of accuracy [42].

However, Flood et al. [36] suggested that FNNs with at least two hidden layers would provide a greater flexibility in the modeling of any dynamic system. In the mean time Haddara et al. [13,15,35,39] obtained good results by using FNNs with one hidden layer in the modeling of dynamic systems. It is concluded that FNNs with one hidden layer is more efficent to model most dynamic systems.

In conclusion, neural networks should be regarded as a complement part to conventional computing techniques. A neural network model reflects only the input-output behavior of a dynamic system without regard to an internal physical mechanism that reproduces the outputs. The artificial neural network approach does not require any

assumptions about the internal structure of the system to be made [36]. The operating mechanism of the neural network can be easily understood by knowing the main concepts, construction elements and their functions in the network, and how these elements work simultaneously in the network.

From this review, it is obvious that during the last two decades, researchers have used the random decrement technique several times. In this dissertation, I am going to combine the classical identification techniques with the neural networks technique.

Chapter 3

Mathematical Formulation

3.1 Equations of Motion

In order to measure the coupled heave and pitch motions for an URV-model using the available dynamometer in the wave tank at Memorial University, a connection was made between the main body of the model and the dynamometer flange. This connection has a hydrofoil cross-section of area as shown in Figure (3.1).

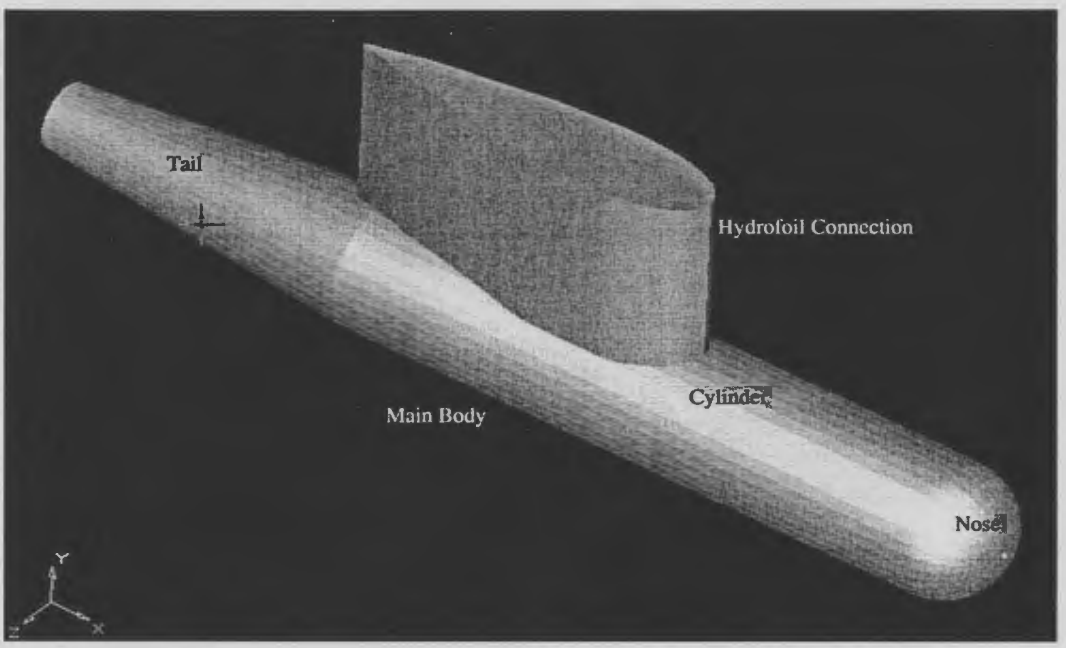

Figure 3.1 URV-Model Drawing

The connection also provided a watertight environment for the transducers, which are used for measuring the coupled heave and pitch motions. The main body of the URV and

the hydrofoil part are designed to constitute one neutrally buoyant body taking into account the effect of the weight of the dynamometer flange.

The dynamics of the URV-model in this case should take into account the effects arising from both the hydrofoil connection and the dynamometer. The equations of motion in this case are similar to those describing the motion of vehicles floating at the surface. The neutrally buoyant body in this case is considered as a semi-submersible vehicle. The equations of motion describing the coupled heave and pitch motions for that body, are given as [43]:

$$(m + a_{33})\ddot{Z} + b_{33}\dot{Z} + c_{33}Z + a_{35}\ddot{\Theta} + b_{35}\dot{\Theta} + c_{35}\Theta = F(t) \tag{3.1}$$

$$(I_{yy} + a_{55})\ddot{\Theta} + b_{55}\dot{\Theta} + c_{55}\Theta + a_{53}\ddot{Z} + b_{53}\dot{Z} + c_{53}Z = M(t) \tag{3.2}$$

where Z and Θ are the heave displacement and the pitch angle, respectively. A dot over the variable indicates differentiation with respect to time; I_{yy} and m are the mass moment of inertia for the neutrally buoyant body and its mass, respectively; a_{33} and a_{55} are the added mass for heaving and the added mass moment of inertia for pitching, respectively; b_{33} and b_{55} are the damping parameters for heaving and pitching, respectively; c_{33} and c_{55} are the restoring force parameters for heaving and pitching, respectively; a_{35}, b_{35}, c_{35}, a_{53}, b_{53}, and c_{53} are coupling parameters. F(t) and M(t) are the wave exciting force and moment, respectively. In the derivation of equation (3.2), I have ignored second order terms similar to $R.\dot{\Theta}.\dot{Z}$, for small heave and pitch motion.

These equations are written with reference to a right-hand system of coordinate axes having its origin at the center of gravity of the URV and its x-axis in the longitudinal plane of symmetry of the URV with its positive direction pointing forward, as shown in Figure (3.2).

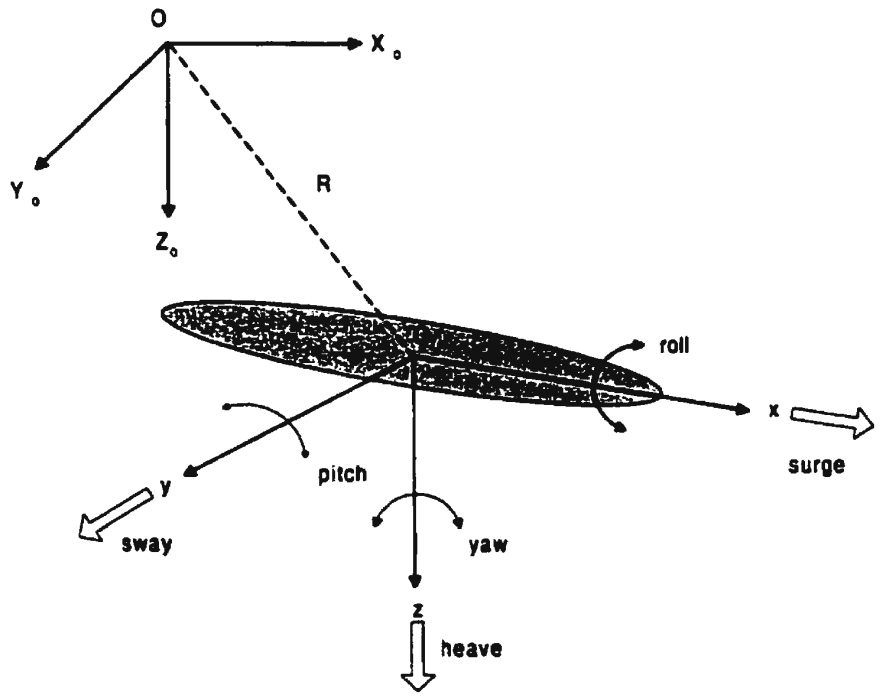

Figure 3.2 Vertical plane motion of a URV with respect to earth axes

where R is the distance between the center of gravity of the model and the pitching pivot of the dynamometer flange. This distance is 0.41 m.

Normalizing equations (3.1) and (3.2) with respect to the total virtual mass and total virtual mass moment of inertia of the neutral buoyant body, respectively and using the following change of variables:

$$Y(t) = \begin{bmatrix} y_1 \\ y_2 \\ y_3 \\ y_4 \end{bmatrix} = \begin{bmatrix} Z \\ \Theta \\ \dot{Z} \\ \dot{\Theta} \end{bmatrix} \tag{3.3}$$

equations (3.1) and (3.2) can be easily replaced by the following set of four first order differential equations [15]:

$$\dot{Y}(t) = D\,Y(t) + K(t) \tag{3.4}$$

where

$$D = \begin{bmatrix} 0 & 0 & 1 & 0 \\ 0 & 0 & 0 & 1 \\ -d_{31} & -d_{32} & -d_{33} & -d_{34} \\ -d_{41} & -d_{42} & -d_{43} & -d_{44} \end{bmatrix}, \quad K(t) = \begin{bmatrix} 0 \\ 0 \\ F_t(t) \\ M_t(t) \end{bmatrix}, \quad \begin{aligned} F_t(t) &= -\varepsilon_1 F(t) - \varepsilon_2 M(t) \\ M_t(t) &= -\sigma_1 F(t) - \sigma_2 M(t) \end{aligned} \tag{3.5}$$

where d_{33} and d_{31} are the damping force and the restoring force parameters for heave motion, respectively; d_{44} and d_{42} are the damping moment and restoring moment parameters for pitch motion, respectively; d_{32}, d_{34} and d_{41}, d_{43} are the coupling parameters for heave and pitch equations, respectively; ε_1, ε_2, σ_1, and σ_2 are constants. Detailed expressions for these parameters are given in Appendix A.

The excitation vector, K(t) is assumed to be a Gaussain white noise random process whose components satisfy the following conditions [15]:

$$\begin{aligned} &E[k_i(t)] = 0 \\ &E[k_i(t)\ k_i(t+\tau)] = \psi_i\,\delta(\tau) \qquad i = 1,4 \\ &E[k_i(t)\ k_j(t+\tau)] = 0 \qquad (i \neq j) \end{aligned} \tag{3.6}$$

where ψ_i , i =1,....,4, are the elements of the covariance matrix of the excitation vector, K(t). δ and τ are the Dirac delta function and time lag, respectively. E [.] denotes the ensemble average of a variable.

3.2 Conditional Probability Equation

Assuming that the random process Y(t) is a Markov process, a Fokker-Planck equation can be used to describe the conditional probability density function, $P(Y,t|Y_O)$ for the random process, Y(t) [14]:

$$\frac{\partial P}{\partial t} = -\sum_{i=1}^{2}[\frac{\partial}{\partial y_i}(y_{i+2}\ P)] - \sum_{i=3}^{4}(\frac{\partial}{\partial y_i}[\sum_{j=1}^{4}(d_{ij}\, y_j)\ P]) + \frac{1}{2}\sum_{i=3}^{4}[\frac{\partial^2}{\partial y_i^{\ 2}}(\Psi_i\ P)] \qquad (3.7)$$

The solution of equation (3.7) subject to the initial condition

$$Lim_{t\to 0}\ P(Y,t\,|\,Y_O) = \prod_{i=1}^{4}\ \delta(y_i - y_{iO})$$

yields the conditional probability density function which describes the Markov process, Y(t) completely. Here y_{iO}, i =1,..,4 are the initial conditions for the heave and pitch displacements and heave and pitch rates.

3.3 Random Decrement Equations

A mathematical model that describes the coupled heave and pitch motions for a URV is formulated above. The next step is to use the concept of the random decrement to get rid of the explicit dependence of the force vector on time. This is accomplished by assuming

that the process, Y(t) is a multi-dimensional Markov process. Next I use the Fokker-Planck equation to derive the equations, which describe the propagation of the response ensemble average vector as a function of time as well as the auto- and cross-correlation functions.

The derivation of the propagation of the conditional mean values corresponding to the coupled heave and pitch motions given by equations (3.1) and (3.2) is based on the Fokker-Planck equation (3.7). Multiplying equation (3.7) by the variables y_i , i =1,..,4 each one at a time and integrating the whole equation over the range of the four variables, the equations describing the propagation of the conditional expected values of $y_i(t)$, i =1,..., 4 can be obtained as

$$\dot{\mu}_1 = \mu_3 \tag{3.8}$$

$$\dot{\mu}_2 = \mu_4 \tag{3.9}$$

$$\dot{\mu}_3 = -\sum_1^4 d_{3j}\mu_j \tag{3.10}$$

$$\dot{\mu}_4 = -\sum_1^4 d_{4j}\mu_j \tag{3.11}$$

where

$$\mu_i = \int_{-\infty}^{\infty}\int\int\int y_i\, P(Y,t \mid Y_O)\, dy_1\, dy_2\, dy_3\, dy_4 \quad i = 1,\ldots,4$$

Equations (3.8) to (3.11) can be written in a matrix form as

$$\dot{M} = D\,M \tag{3.12}$$

where

$$M = [\mu_1\ \mu_2\ \mu_3\ \mu_4]^T$$

The random decrement signatures for the coupled heave and pitch motions are calculated based on the procedure given in [15]. In this procedure, one of the two-degrees-of-freedom is chosen as a reference. In this work, the heave motion is chosen as the reference motion.

The random decrement signatures for heave and pitch motions are calculated from the numerically generated random data as well as from the measured motion responses by dividing the response into a number of overlapping segments with equal length of time. The segments are chosen in such a way that each segment start with the same initial heave displacement, Z_O and heave velocity. Half of these segments start with positive velocity (slope) and the other half start with a negative velocity. The random decrement signatures for heave and pitch motions, μ_1 and μ_2 are calculated as

$$\mu_1(\tau) = \frac{1}{2N_P}\left[\sum_{i=1}^{N_P} Z_1(t_i+\tau) + \sum_{j=1}^{N_P} Z_2(t_j+\tau)\right] \tag{3.13}$$

$$\mu_2(\tau) = \frac{1}{2N_P}\left[\sum_{i=1}^{N_P} \Theta_1(t_i+\tau) + \sum_{j=1}^{N_P} \Theta_2(t_j+\tau)\right] \tag{3.14}$$

where

$t = t_i$ at $Z_1(t) = Z_O$ and $\dot{Z}_1(t) \rangle 0$

$t = t_j$ at $Z_2(t) = Z_O$ and $\dot{Z}_2(t) \langle 0$

The derivatives on the left hand side of equations (3.8), (3.9), (3.10), and (3.11) are calculated using numerical differentiation.

3.4 Auto-and Cross-correlation Equations

The derivation of the auto– and cross–correlation equations corresponding to the two-degrees-of-freedom system given by equations (3.1) and (3.2) is based on the Fokker–Planck equation (3.7). The latter equation is to be multiplied by $y_i(t)$ $y_j(t+\tau)$ $P_s(Y)$, i =1,..,4 and j =1,..,4, each in time and integrating the whole equations over the range of the two variables. $P_s(Y)$ is the steady state probability function and it is independent of time and the initial condition Y_O. The following equations are obtained:

$$\dot{R}_{ij}(\tau) = R_{i+2\,j}(\tau) \qquad i = 1,2\ ,\ j = 1,\ldots,4 \tag{3.15}$$

$$\dot{R}_{ij}(\tau) = -\sum_{k=1}^{4} d_{ik}\ R_{kj}(\tau) \qquad i = 3,4\ ,\ j = 1,\ldots,4 \tag{3.16}$$

where

$$R_{ij}(\tau) = \int_{-\infty}^{\infty}\int\int\int\int\ y_i(t)\, y_j(t+\tau)\, P_s(Y)\, dy_1\, dy_2\, dy_3\, dy_4 \qquad i\ ,\ j = 1,\ldots,4$$

Equations (3.15) and (3.16) have four sets (j = 1,..,4) of first order differential equations. I consider here only one set of these equations (j =1) in order to show that the auto- and cross-correlation functions are similar to those that describe the free-coupled heave and pitch motions for an URV.

$$\dot{R}_{11} = R_{31} \tag{3.17}$$

$$\dot{R}_{21} = R_{41} \tag{3.18}$$

$$\dot{R}_{31} = -\sum_{k=1}^{4} d_{3k}\, R_{k1} \tag{3.19}$$

$$\dot{R}_{41} = -\sum_{k=1}^{4} d_{4k}\, R_{k1} \tag{3.20}$$

Equations (3.17) to (3.20) can be written in a matrix form as

$$\dot{R}_C = D\, R_C \tag{3.21}$$

where

$$R_C = [R_{11}\ R_{21}\ R_{31}\ R_{41}]^T$$

The auto- and cross-correlation functions are calculated from the random motion responses for the heave and pitch motions using the following expression:

$$R_{ik}(\tau) = \frac{1}{(N_p - \tau)} \sum_{j=1}^{N_p - \tau} y_i(j)\ y_k(j+\tau) \tag{3.22}$$

where N_p and τ are the total number of points in the both heaving and pitching responses, and the time lag, respectively. The derivatives on the left hand side of equations (3.17), (3.18), (3.19), and (3.20) are calculated using numerical differentiation.

Chapter 4

The Identification Technique

4.1 Introduction

The main objective of this work is to develop a new procedure for the identification of the parameters in the mathematical model describing the coupled heave and pitch motions for an URV sailing near the sea surface in random waves using only its measured responses.

In this chapter, I introduce the developed technique "*RDLRNNT*". This technique is based on the use of both multi-linear regression and neural networks algorithms.

4.2 Identification Technique "*RDLRNNT*"

Combining the random decrement equations (3.8), (3.9), (3.10) and (3.11), one can get the following equations:

$$\ddot{\mu}_1 + d_{33}\dot{\mu}_1 + d_{31}\mu_1 + G_1(\mu_2, \dot{\mu}_2) = 0 \tag{4.1}$$

$$\ddot{\mu}_2 + d_{44}\dot{\mu}_2 + d_{42}\mu_2 + G_2(\mu_1, \dot{\mu}_1) = 0 \tag{4.2}$$

where

$$G_1(\mu_2, \dot{\mu}_2) = d_{32}\mu_2 + d_{34}\dot{\mu}_2 \tag{4.3}$$

$$G_2(\mu_1, \dot{\mu}_1) = d_{41}\mu_1 + d_{43}\dot{\mu}_1 \tag{4.4}$$

This form shows that the average motion of the URV at sea is an oscillatory motion, with some damped natural frequency. It is shown in equations (4.1) and (4.2) that the random decrement signatures of the heave and pitch responses, μ_1 and μ_2, respectively satisfy the homogenous-coupled heave and pitch differential equations.

Similarly, combining the auto- and cross-correlation equations (3.17), (3.18), (3.19) and (3.20), one can get the following equations:

$$\ddot{R}_{11} + d_{33}\ \dot{R}_{11} + d_{31}R_{11} + H_1(R_{21}, \dot{R}_{21}) = 0 \tag{4.5}$$

$$\ddot{R}_{21} + d_{44}\ \dot{R}_{21} + d_{42}R_{21} + H_2(R_{11}, \dot{R}_{11}) = 0 \tag{4.6}$$

where

$$H_1(R_{21}, \dot{R}_{21}) = d_{32}R_{21} + d_{34}\dot{R}_{21} \tag{4.7}$$

$$H_2(R_{11}, \dot{R}_{11}) = d_{41}R_{11} + d_{43}\dot{R}_{11} \tag{4.8}$$

Similarly, as in the random decrement equations, the auto- and cross-correlation functions for the heave and pitch responses satisfy the homogenous-coupled heave and pitch differential equations as shown in equations (4.5) and (4.6).

The damping and the restoring parameters in the above equations are identified using a multi-linear regression algorithm, while the coupling parameters are identified using a neural networks technique. Once the parameters in these equations have been identified, a heave-pitch motions model for the vehicle has been obtained. The success of this model depends on the accurate estimation of the motion.

The dynamic model is independent of the wave excitation. It can be used to predict the motion to any form of excitation. A flowchart for the developed technique is presented in Figure (4.1).

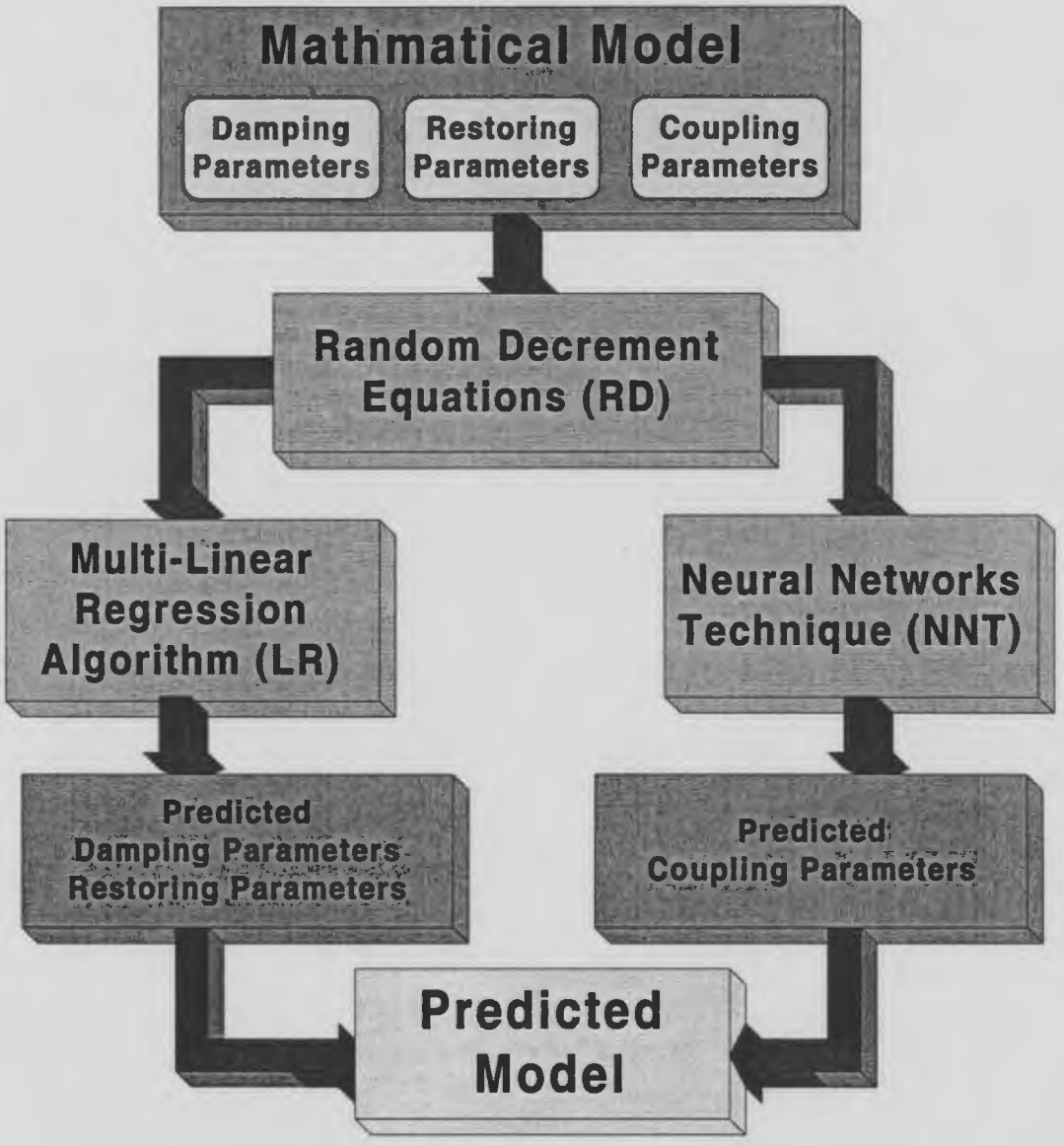

Figure 4.1 Developed identification technique " *RDLRNNT*"

4.3 Multi-Linear Regression Algorithm

An iterative technique is used to identify the values of the damping, restoring, and coupling parameters for an URV using equations (3.10), (3.11), (4.1), and (4.2) corresponding to the derived random decrement equations as well as using equations (3.19), (3.20), (4.5), and (4.6) corresponding to the derived auto- and cross-correlation functions. This technique is based on the use of multi-linear regression algorithm. Three statistical indices are used to ascertain the suitability of the regression model. These are the *P-value*, the *R-sq*, and the *Variance Inflation Factor* (*VIF*). The following criteria are selected and should be satisfied by a model in order that the model is accepted: a *P-value* < 0.05, an *R-sq* ≥ 0.85 and a *VIF* < 10. These criteria are in agreement with criteria used in similar research [44,45,46,47].

First, the following two equations are used to determine estimates of the damping and restoring parameters for the coupled heave and pitch motions using the random decrement equations:

$$\dot{\mu}_3 = -d_{33}\mu_3 - d_{31}\mu_1 \tag{4.9}$$

$$\dot{\mu}_4 = -d_{44}\mu_4 - d_{42}\mu_2 \tag{4.10}$$

Alternatively, the auto- and cross-correlation functions can also be used to determine the damping and restoring parameters using the following equations:

$$\dot{R}_{31} = -d_{33}\dot{R}_{11} - d_{31}R_{11} \tag{4.11}$$

$$\dot{R}_{41} = -d_{44}\dot{R}_{21} - d_{42}R_{21} \tag{4.12}$$

The parameters identified using equations, (4.9) and (4.10) should equal those identified using equations, (4.11) and (4.12). The derivatives on the left hand side of equations (4.9), and (4.10) or equations (4.11) and (4.12), are calculated using numerical differentiation.

Values for the identified parameters d_{31}, d_{33}, d_{42}, and d_{44} are obtained from either equations (4.9) and (4.10) or equations (4.11) and (4.12). These values are then substituted back in equations (4.1) and (4.2) or equations (4.5) and (4.6). Having determined the values of d_{31}, d_{33}, d_{42}, and d_{44}, equations (4.1) and (4.2) or equations (4.5) and (4.6) will have two more unknown functions, $G_1(\mu_2, \dot{\mu}_2)$ and $G_2(\mu_1, \dot{\mu}_1)$ or $H_1(R_{21}, \dot{R}_{21})$ and $H_2(R_{11}, \dot{R}_{11})$, to be determined, respectively. These functions are then identified using a neural networks technique as described in the following section.

4.4 Neural Networks Technique

The concept behind developing artificial neural networks is to try to mimic the work of biological networks [35]. Lately, neural networks become much simpler in size, number of neurons and complexity of construction when compared with actual biological networks [36]. Artificial neural networks have been used successfully in function approximation and parametric identification [15].

The coupling parameters in the equations describing the coupled heave and pitch motions for an URV sailing near the sea surface in random waves are lumped in the two

functions $G_1(\mu_2,\dot{\mu}_2)$ and $G_2(\mu_1,\dot{\mu}_1)$ or $H_1(R_{21},\dot{R}_{21})$ and $H_2(R_{11},\dot{R}_{11})$, as shown in equations (4.1) and (4.2) or equations (4.5) and (4.6), respectively. Continuous records of the measured coupled heave and pitch responses are used with equations (4.1) and (4.2) to identify the lumped functions using a neural networks technique.

Two single hidden layer feedforward neural networks as shown in Figure (4.2), are used to identify the lumped function, $G_1(\mu_2,\dot{\mu}_2)$ or $H_1(R_{21},\dot{R}_{21})$. The input to each network is a vector consisting the random decrement signatures for the measured coupled heave and pitch motion responses and their derivatives with respect to time, and a bias. The hidden layer consists of several neurons. In this work, 11 neurons give a sufficient accuracy in the identification parameters. The output layer consists of one neuron, which yields the values of the identified lumped function, $G_1(\mu_2,\dot{\mu}_2)$ or $H_1(R_{21},\dot{R}_{21})$ [15].

The input to the j^{th} neuron in the hidden layer is the weighted sum of the inputs to the network. This relationship is given as

$$A_j = \sum_{i=1}^{5} w_{ij} \times \mu_i \qquad j = 1,..,11 \tag{4.13}$$

where w_{ij} is the synaptic weight of the i^{th} neuron in the input layer to the j^{th} neuron in the hidden layer; μ_5 is the bias and is equal to 1.0. The function A_j is acted upon by a sigmoidal function f, as follows:

$$f(A_j) = \frac{1}{1+e^{-(A_j)}} \tag{4.14}$$

The lumped function, $G_1(\mu_2,\dot{\mu}_2)$ or $H_1(R_{21},\dot{R}_{21})$ is obtained as the weighted sum of the outputs of the hidden layer neurons expressed as

$$G_1(\mu_2,\dot{\mu}_2) = \sum_{i=1}^{12} \beta_j \times f(A_j) \tag{4.15}$$

where β_j is the synaptic weight of neuron j^{th} in the hidden layer and $A_{12}=1$.

Using an arbitrary starting set of weights, an initial value of the lumped function is obtained. The obtained value of that function is substituted back into equation (4.1) or equation (4.5), and the equation is integrated numerically using the Runge–Kutta algorithm. The calculated heave response, μ_{kn} obtained from the integration is compared to the input heave response to the network, μ_{im}. Here, i is the number of the inputs to the neural network, k; m and n refer to the measured response and the obtained response using the network, respectively. The difference between these two responses is the error. The synaptic weights w_{ij} and β_j are then updated and the process is repeated in an iterative fashion until the error in the response is minimized. A simple flowchart for the neural network technique is shown in Figure (4.3).

Similarly, the pitch lumped function, $G_2(\mu_1, \dot{\mu}_1)$ or $H_2(R_{11}, \dot{R}_{11})$ can be identified using a similar but independent neural network. Then, the coupling parameters d_{32}, d_{34}, d_{41}, and d_{43} are identified using a multi-linear regression algorithm for equations (4.3) and (4.4) or equations (4.7) and (4.8).

The reason for using a combination of multi-linear regression and neural networks is to have a more efficient identification technique. Using a multi-linear regression algorithm alone, produces unreliable estimates for the individual parameters which constitute the model. This has been observed by other researches [47] especially when the number of the parameters to be identified is large. In this case, although the whole identified model produces good estimates for the response, the individual values of the parameters may not be accurate. This happens because of the interaction that occurs between these parameters.

Using neural networks alone produces a reliable model because only one function is being identified. However, the iterations needed to optimize the solution require a huge amount of computer time. For these reasons, it has been found optimum to use a hybrid model, which combines the use of multi-linear regression, and neural networks.

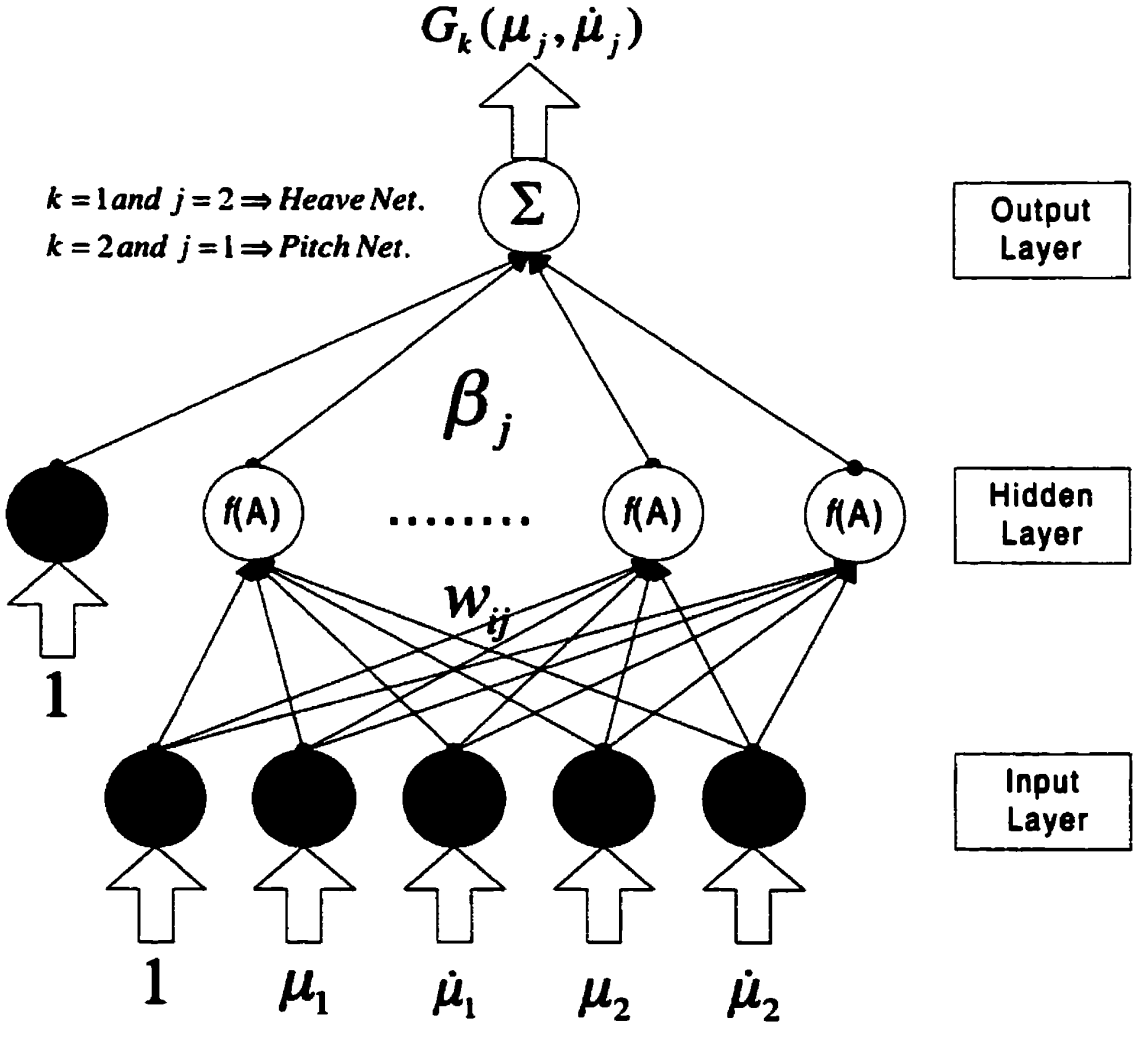

Figure 4.2 Feedforward neural networks

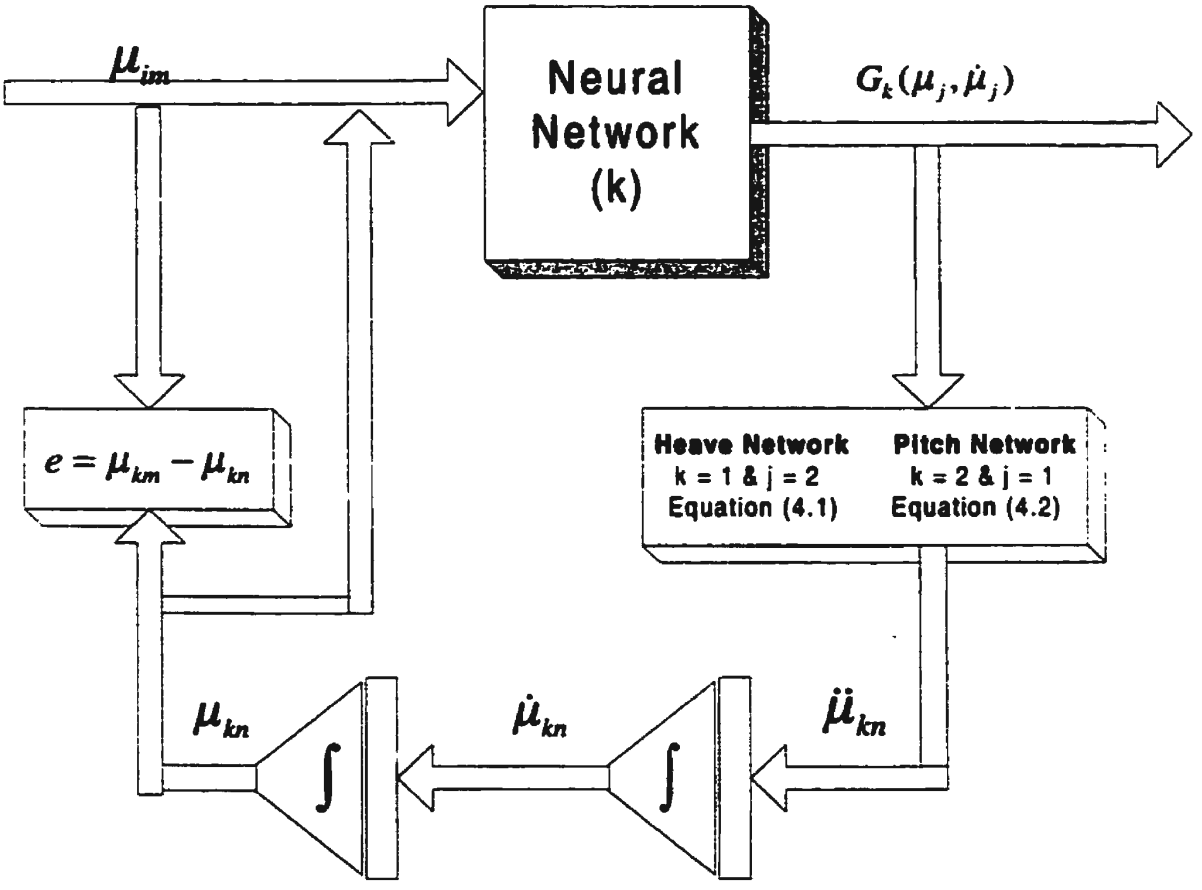

Figure 4.3 Neural networks technique

Chapter 5
Model Validation

5.1 Numerically Generated Data

A numerical simulation procedure is an important stage in the development of a new prediction method. Carrying out a numerical simulation can provide a clear understanding about the relationship between the input and the output of a dynamic system. Three main objectives are desired from conducting a numerical simulation in this work. First, checking the accuracy of the proposed method using a direct comparison between the actual values of the parameters and the predicted ones. Second, a series of complete numerical experiments can be conducted under controlled input environment. Finally, the estimated cost for a numerical simulation is much less than carrying out real experiments especially in the developing stage of a new method.

The description and the main features of the designed URV-model, and the associated different calculations are presented in Appendix B. The calculations for the hydrodynamic parameters, the wave exciting force and moment using a 2D-strip theory are presented in Appendix C. The main objective behind the use of the strip theory in the designed stage of the URV-model is to ascertain the suitability of the available dynamometer for measuring the coupled heave and pitch motions for such model. I generate the numerical data for random motions taking into account the variation of both the damping levels in heave and pitch motions, and different values for the damped natural frequencies.

Both the effects of wide-band and narrow-band excitations on the identified parameters are investigated using the developed technique. In addition, the effect of using a band-pass filter centered near the damped natural frequencies for heave and pitch motions on the identified parameters is investigated.

5.1.1 Case Studies

Several case studies have been investigated in this work. Numerical random data for the case studies are generated for the coupled heave and pitch motions for an URV sailing near the water surface in random waves using a mathematical model given as

$$\ddot{Z} + d_{33}\dot{Z} + d_{31}Z + d_{34}\dot{\Theta} + d_{32}\Theta = F_t(t) \tag{5.1}$$

$$\ddot{\Theta} + d_{42}\dot{\Theta} + d_{44}\Theta + d_{43}\dot{Z} + d_{41}Z = M_t(t) \tag{5.2}$$

where $F_t(t)$ and $M_t(t)$ are the normalized wave excitation force and moment.

Several spectra have been used in the description of the ocean waves. These spectra are classified into two main categories: wide-band spectra and narrow-band spectra. The wide-band spectra are such as ITTC, Bretschneider and Pierson-Moskowitz while the narrow-band spectra are such as JONSWAP. The Joint North Sea Wave Project team has derived the JONSWAP spectrum. This spectrum is an extension of the Pierson-Moskowitz spectrum to account for a much sharper spectral peak [48].

Numerical random data for the coupled heave and pitch motions for the URV have been generated for both wide-band and narrow-band excitations. The main

objectives for generating such data are to ascertain the suitability of the developed technique in different forms of excitation and to test its dependency on the excitation form. A JONSWAP wave spectrum is used as a narrow-band spectrum.

5.1.2 Wide-Band Excitations

A wide-band excitation is a stationary random process whose spectral density function has significant values over a band of frequencies, which is approximately the same order of magnitude as the band center frequency [49].

As shown in equations (5.3) and (5.4), the normalized wave exciting force and moment, $F_t(t)$ and $M_t(t)$, respectively, are composed of 70 sinusoidal components of constant amplitude of 0.07 m/sec^2 and 0.15 rad/sec^2, respectively. The phase angle, ϕ_i between these components, is taken as a random variable uniformly distributed between 0 and 2π. The frequency band for the excitation is taken between 2.0 and 5.0 rad/sec.

$$F_t(t) = \sum_{i=1}^{70} 0.07 \sin(\omega_i t + \phi_i) \tag{5.3}$$

$$M_t(t) = \sum_{i=1}^{70} 0.15 \sin(\omega_i t + \phi_i) \tag{5.4}$$

Numerically generated data for the coupled heave and pitch motions are obtained by integrating equations (5.1) and (5.2). The numerical integration of these equations has been conducted using the Runge-Kutta algorithm. A MATLAB program has been developed. Details of the program called "*D.E. SOLVER*" are given in Appendix F. The values of the damping, restoring, and coupling parameters in equations (5.3) and (5.4) used are given in Tables (5.1) and (5.2).

Ten case studies are used in this section to test the validity of the proposed identification technique. The purpose of the case studies is to investigate the effect of the different levels of damping and different values of the damped natural frequency on the ability of the random decrement signatures to represent the URV's free decay coupled heave and pitch motion. The first six cases are used to validate the technique for different levels of damping, while the last four cases are used to validate the technique for different values of the damped natural frequencies in the coupled heave and pitch motions. The identified parameters for these case studies are shown in Tables (5.1) and (5.2). Tables (5.3) and (5.4) show the error percentages for the identified parameters using the developed technique.

Table 5.1 Comparison between the actual and the predicted parameters from the numerically generated data for heave motion (Wide-band)

Case #	Heave Motion							
	Actual				Prediction			
	d_{31}	d_{32}	d_{33}	d_{34}	d_{31}	d_{32}	d_{33}	d_{34}
1	19.8356	0.0149	0.2500	0.0190	19.9301	0.0313	0.1492	0.0075
2	19.8356	0.0149	0.3500	0.0190	19.9418	-0.0034	0.3887	-0.0027
3	19.8356	0.0149	0.5500	0.0190	20.1730	0.0027	0.5656	-0.0004
4	19.8356	0.0149	0.7500	0.0190	20.1291	0.0666	0.6926	0.0227
5	19.8356	0.0149	1.5000	0.0190	19.2921	0.2159	1.4809	-0.0525
6	19.8356	0.0149	2.0000	0.0190	20.0685	0.6335	1.6432	0.1669
7	10.0000	0.0056	0.2500	0.0016	9.9263	-0.0016	0.2641	-0.0014
8	6.0000	0.0056	0.2500	0.0016	5.9142	0.0319	0.2283	-0.0084
9	5.0000	0.0056	0.3000	0.0016	4.8842	0.0308	0.2822	-0.0368
10	3.0000	0.0056	0.3000	0.0016	2.9938	-0.0073	0.2710	0.0069

Table 5.2 Comparison between the actual and the predicted parameters from the numerical generated data for pitch motion (Wide-band)

Case #	Pitch Motion							
	Actual				Prediction			
	d_{41}	d_{42}	d_{43}	d_{44}	d_{41}	d_{42}	d_{43}	d_{44}
1	0.0015	19.4143	0.0738	0.2900	0.1253	19.6725	0.0176	0.1863
2	0.0015	19.4143	0.0738	0.4000	-0.0086	19.5206	-0.0042	0.4554
3	0.0015	19.4143	0.0738	0.6000	-0.0056	19.7674	-0.0078	0.6352
4	0.0015	19.4143	0.0738	0.8000	0.2997	19.7508	0.0857	0.7545
5	0.0015	19.4143	0.0738	2.0000	0.5654	18.7744	-0.2089	1.9202
6	0.0015	19.4143	0.0738	2.5000	2.1374	19.3307	0.5415	1.8572
7	0.0105	9.0000	0.0738	0.2000	-0.0310	9.0040	-0.0127	0.1725
8	0.0105	4.0000	0.0738	0.2000	0.0776	4.0784	-0.0308	0.1749
9	0.0105	3.5000	0.0738	0.1500	0.0040	3.6261	-0.0001	0.1479
10	0.0105	1.5000	0.0738	0.1500	-0.0022	1.4306	-0.0153	0.1449

Table 5.3 Error percentages for heave parameters (Wide-band)

Case #	Heave Motion			
	d_{31}	d_{32}	d_{33}	d_{34}
1	0.48	110	40.00	60
2	0.54	77	11.00	0.04
3	1.70	82	2.80	102
4	1.48	347	7.60	80
5	2.74	1349	1.30	376
6	1.17	4151	17.80	778
7	0.74	128	5.60	187
8	1.43	470	8.70	625
9	2.32	450	6.00	3487
10	0.20	230	9.60	331

Table 5.4 Error percentages for pitch parameters (Wide-band)

Case #	Pitch Motion			
	d_{41}	d_{42}	d_{43}	d_{44}
1	8253	1.33	76	35.70
2	6733	0.55	106	13.80
3	473	1.82	111	5.80
4	19880	1.85	16	5.70
5	37593	3.29	383	4.00
6	142393	0.43	634	25.70
7	395	0.04	117	13.75
8	639	1.96	142	12.50
9	62	3.60	1	1.40
10	121	4.60	120	3.40

5.1.3 Narrow-Band Excitations

A narrow-band excitation is a stationary process whose spectral density function has significant values only for a band of frequencies whose width is small compared to the magnitude of the center frequency of the process [49]. The most recent wave spectrum to describe ocean waves is the JONSWAP spectrum. The narrow-band heave force and pitch moment excitations for the mathematical model are expressed by

$$F_t(t) = \sum_{i=1}^{70} a_{hi} \sin(\omega_i t + \phi_i) \tag{5.5}$$

$$M_t(t) = \sum_{i=1}^{70} a_{pi} \sin(\omega_i t + \phi_i) \tag{5.6}$$

where

$$a_{hi} = \sqrt{2 S_h(\omega_i)\, \Delta\omega} \tag{5.7}$$

$$a_{pi} = \sqrt{2 S_p(\omega_i)\, \Delta\omega} \tag{5.8}$$

where a_{hi} and a_{pi} are the individual sinusoidal heave force and pitch moment amplitudes, respectively; $S_h(\omega_i)$ and $S_p(\omega_i)$ are the heaving force and the pitching moment power spectral density functions at of frequency of ω_i, respectively; $\Delta\omega$ is the frequency increment.

The phase difference between heave and a pitch motion was taken as a uniformly distributed random number between 0 and 2π. The frequency increment and the range to generate the JONSWAP wave excitations were taken as 0.0285 Hz and 2.0 Hz, respectively.

Numerically generated random data for the coupled heave and pitch motions corresponding to a narrow-band excitations are obtained using the numerical integration of equations (5.1) and (5.2). The numerical integration of these equations has been conducted using a Runge-Kutta algorithm.

Six case studies are used in this section to ascertain the validity of the proposed identification technique for a narrow-band wave excitation as shown in Tables (5.5) and (5.6). The purpose of using the case studies is to investigate the effect of different levels of damping and different values of the damped natural frequency on the ability of the random decrement signatures to represent the URV's free decay coupled heave and pitch motion. The first three cases are used to validate the technique for different levels of damping, while the others are used to validate the technique for different values for the

damped natural frequencies in the coupled heave and pitch motions. The values of the predicted damping, restoring, and coupling parameters corresponding to each case are given in Tables (5.5) and (5.6). Table (5.7) shows the natural and the modal frequencies for the six case studies. Tables (5.8) and (5.9) show the error percentages for the identified parameters using the developed technique.

Table 5.5 Comparison between the actual and the predicted parameters from the numerically generated data for heave motion (Narrow-band)

Case #	Heave Motion							
	Actual				Prediction			
	d_{31}	d_{32}	d_{33}	d_{34}	d_{31}	d_{32}	d_{33}	d_{34}
1'	19.8356	0.0149	0.2500	0.0190	19.8064	0.0012	0.2382	0.0009
2'	19.8356	0.0149	0.3500	0.0190	19.9034	0.0290	0.3005	0.0086
3'	19.8356	0.0149	0.5500	0.0190	20.3730	0.0252	0.4979	-0.0128
7'	10.0000	0.0056	0.2500	0.0016	9.9871	-0.0001	0.2674	0.0018
8'	6.0000	0.0056	0.2500	0.0016	5.9113	0.0266	0.2341	0.0121
9'	5.0000	0.0056	0.3000	0.0016	4.8630	0.0971	0.3141	-0.0009

Table 5.6 Comparison between the actual and the predicted parameters from the numerically generated data for pitch motion (Narrow-band)

Case #	Pitch Motion							
	Actual				Prediction			
	d_{41}	d_{42}	d_{43}	d_{44}	d_{41}	d_{42}	d_{43}	d_{44}
1'	0.0015	19.4143	0.0738	0.2900	0.0038	19.4023	0.0014	0.2835
2'	0.0015	19.4143	0.0738	0.4000	0.0610	19.5408	0.0131	0.3499
3'	0.0015	19.4143	0.0738	0.6000	0.0338	20.0447	-0.0221	0.5819
7'	0.0105	9.0000	0.0738	0.2000	0.0002	9.0670	0.0003	0.1931
8'	0.0105	5.0000	0.0738	0.2000	0.1079	4.8935	0.0238	0.1973
9'	0.0105	3.5000	0.0738	0.1500	0.1360	3.5204	-0.0370	0.2120

Table 5.7 Damped natural frequencies for heave and pitch motions and the excitation modal frequency

Case #	Heave Frequency (Hz)	Pitch Frequency (Hz)	Modal Frequency (Hz)
1'	0.7080	0.7010	0.5000
2'	0.7080	0.7010	0.5000
3'	0.7080	0.7010	0.5000
7'	0.5030	0.4770	0.5000
8'	0.3890	0.3560	0.5000
9'	0.3560	0.2970	0.5000

Table 5.8 Error percentages for heave parameters (Narrow-band)

Case #	Heave Motion			
	d_{31}	d_{32}	d_{33}	d_{34}
1'	0.15	92	4.72	95
2'	0.34	94.6	14	55
3'	2.71	69.1	9.5	167
7'	0.13	102	6.96	12
8'	1.5	375	6.36	656
9'	2.74	1634	4.7	156

Table 5.9 Error percentages for pitch parameters (Narrow-band)

Case #	Pitch Motion			
	d_{41}	d_{42}	d_{43}	d_{44}
1'	153	0.06	98	2.24
2'	3966	0.65	82	12.50
3'	2153	3.25	130	3.00
7'	98	0.74	100	3.45
8'	927	2.13	68	1.35
9'	1195	0.58	150	41.00

Investigating the effect of using a band-pass filter centered around the estimated natural frequencies for heave and pitch motions on the identified parameters using the developed technique has been carried out using the previous six case studies. The values of the predicted damping, restoring, and coupling parameters corresponding to each case are given in Tables (5.10) and (5.11). Tables (5.12) and (5.13) show the error percentages for the identified parameters using the developed technique.

Table 5.10 Comparison between the actual and the predicted parameters from the numerically generated data for heave motion with filtering

Case #	Heave Motion							
	Actual				Prediction			
	d_{31}	d_{32}	d_{33}	d_{34}	d_{31}	d_{32}	d_{33}	d_{34}
1'	19.8356	0.0149	0.2500	0.0190	19.6716	0.0019	0.1715	0.0009
2'	19.8356	0.0149	0.3500	0.0190	19.6308	0.0068	0.3262	0.0056
3'	19.8356	0.0149	0.5500	0.0190	19.7629	0.0054	0.4142	0.0050
7'	10.0000	0.0056	0.2500	0.0016	9.9665	-0.0005	0.2436	0.0012
8'	6.0000	0.0056	0.2500	0.0016	5.9372	-0.0037	0.2513	0.0025
9'	5.0000	0.0056	0.3000	0.0016	4.8002	0.00074	0.2651	0.00051

Table 5.11 Comparison between the actual and the predicted parameters from the numerical generated data for pitch motion with filtering

Case #	Pitch Motion							
	Actual				Prediction			
	d_{41}	d_{42}	d_{43}	d_{44}	d_{41}	d_{42}	d_{43}	d_{44}
1'	0.0015	19.4143	0.0738	0.2900	0.0053	19.3539	0.0014	0.2024
2'	0.0015	19.4143	0.0738	0.4000	0.0208	19.1831	0.0090	0.3689
3'	0.0015	19.4143	0.0738	0.6000	0.0162	19.3893	0.0088	0.4577
7'	0.0105	9.0000	0.0738	0.2000	0.0008	9.0534	0.0024	0.1741
8'	0.0105	5.0000	0.0738	0.2000	0.0043	4.9934	0.0052	0.1714
9'	0.0105	3.5000	0.0738	0.1500	-0.0004	3.4647	-0.0053	0.1371

Table 5.12 Error percentages for heave parameters with filtering (Narrow-band)

Case #	Heave Motion			
	d_{31}	d_{32}	d_{33}	d_{34}
1'	0.82	87	31.40	95
2'	1.00	54	6.80	70
3'	0.37	64	25.00	74
7'	0.34	108	2.60	94
8'	0.30	166	0.52	87
9'	4.00	86	11.63	97

Table 5.13 Error percentages for pitch parameters with filtering (Narrow-band)

Case #	Pitch Motion			
	d_{41}	d_{42}	d_{43}	d_{44}
1'	253	0.30	98	30
2'	1287	1.20	88	8
3'	980	0.13	88	24
7'	92	1.00	97	13
8'	59	0.13	93	14
9'	104	1.00	104	9

5.2 Experimental Data

The experimental program for this research is important to validate the developed identification technique, *RDLRNNT*. A model of an URV has been designed and built for the purpose of this work. In this chapter, I describe the preparation of the URV-model for carrying out the designed experimental program. Preparatory experiments were conducted to adjust and estimate the longitudinal metacentric height and the natural frequencies for heave and pitch. In the following sections, I outline briefly the different aspects of the experimental program.

In the derivation of the random decrement equations for the mathematical model for the coupled heave and pitch motions for a URV, the wave excitation has been assumed Gaussian white noise random process. This is an ideal process that cannot be generated in the towing tank. Only a narrow-band wave excitation process (JONSWAP) has been used in the experimental work.

The suitability of the developed technique has been tested for both narrow-band and wide-band wave excitations using numerically generated random data for the coupled heave and pitch motions. The obtained results show that the developed technique is independent of the wave excitation. The identified parameters from the experimentally measured random data for a narrow-band wave excitation estimate the coupled heave and pitch motions with reasonable accuracy.

5.2.1 URV-Model Preparation

The main body of the URV-model has been built from aluminum alloy in a local company in St. John's. This body consists of three main parts: a hemispherical nose, a cylindrical tube, and a conical tail. A hydrofoil connection has been built from a *Styrofoam* material at Memorial University in order to house the dynamometer flange as shown in Figure (5.1). The model was ballasted as shown in Figure (5.2).

An inclining experiment was conducted in the deep tank at Memorial University. The deep tank has dimensions of 3.65 m ×3.65 m × 3.65 m with a water depth of 3.35 m. The main objective of this experiment is to determine the value of the longitudinal metacentric height GM_L as shown in Figure (5.3). The trim angle corresponding to each movement is recorded. The corresponding trimming and righting moments are calculated. Using a linear regression algorithm, the value of GM_L is determined as +0.0481 m.

Knowing the values of the KB and the BM_L as calculated in Appendix B, the value of the KG is determined as 0.1494 m from the base line of the model. Furthermore, the heave and pitch natural periods are determined. This was conducted by causing the

model initial displacements from its equilibrium position in both heave and pitch directions and release it to oscillate freely in calm water. Several periods for heave and pitch motions are recorded. The averages of these periods are calculated as 2.82 sec and 6.1 sec for heave and pitch motions, respectively.

Another experiment has been carried out to determine the value of the KG. In addition, the moments of inertia about the transverse and longitudinal axes of the model passing through the center of gravity are determined. This has been conducted using a frame-table at Memorial University. The frame-table consists of two main frames: a fixed frame to the ground and the other is pivoted on the fixed one as shown in Figure (5.4). The value of the KG is determined as 0.1465 m from the base line of the model, which is close to that obtained from the inclining experiment. The moments of inertia about the transverse and the longitudinal axes of the model are determined as 24.8 kg-m^2 and 7.34 kg-m^2, respectively.

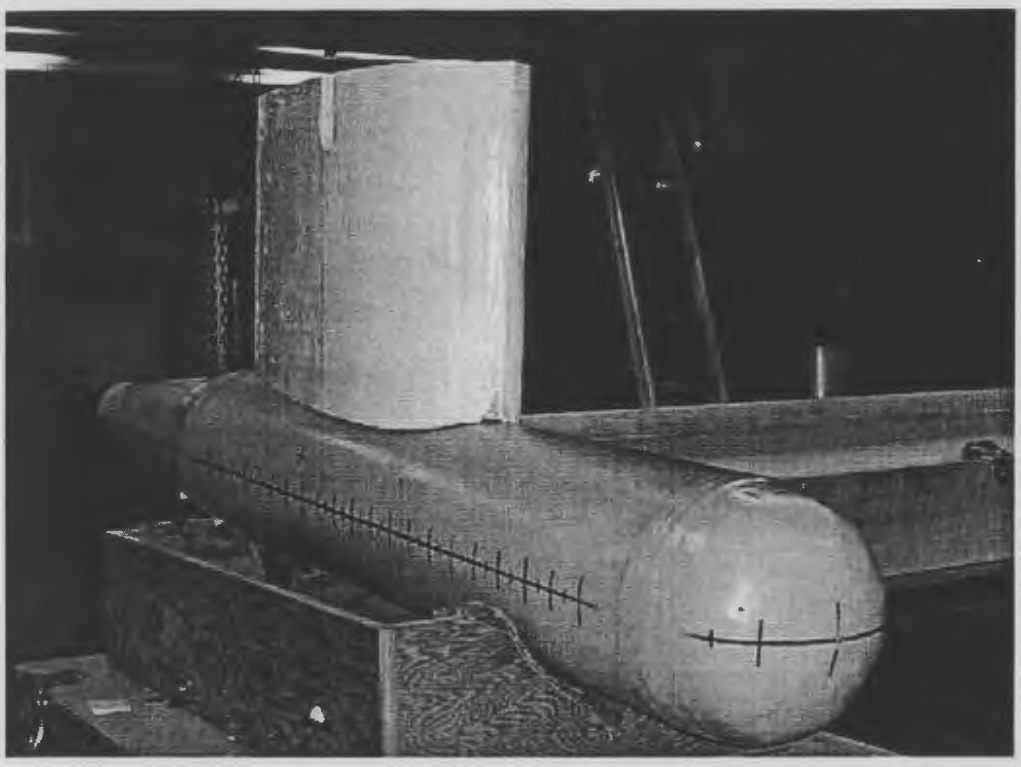

Figure 5.1 URV-Model

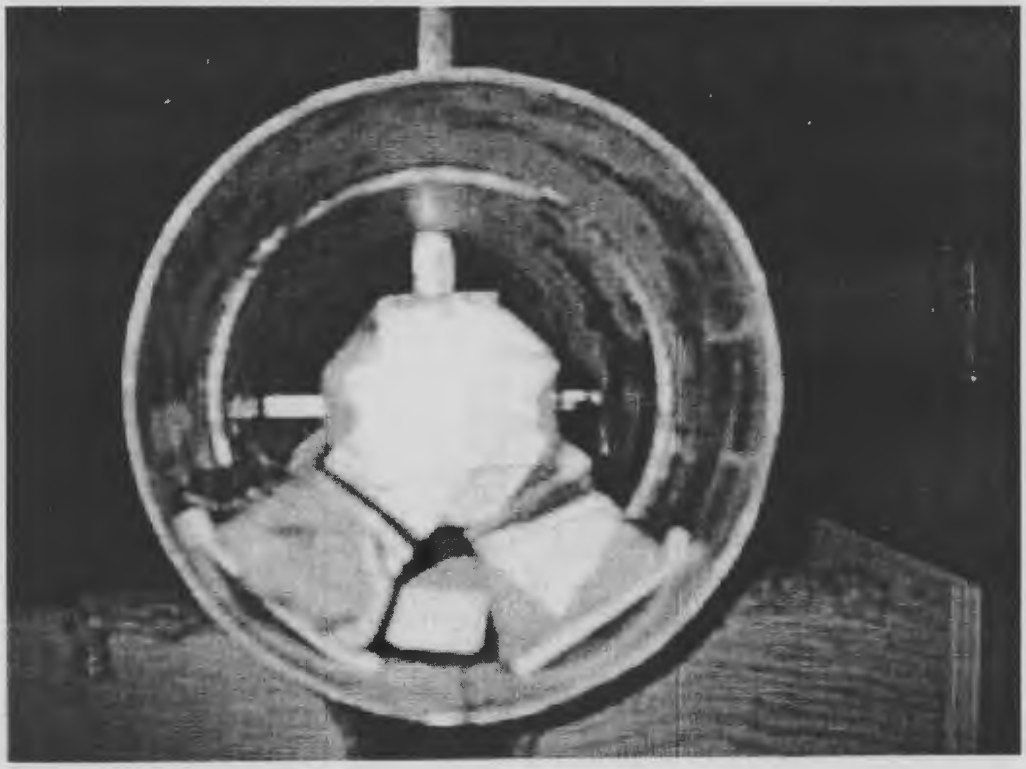

Figure 5.2 Ballasting of the URV-Model

Figure 5.3 Inclining experiment setup in the deep tank

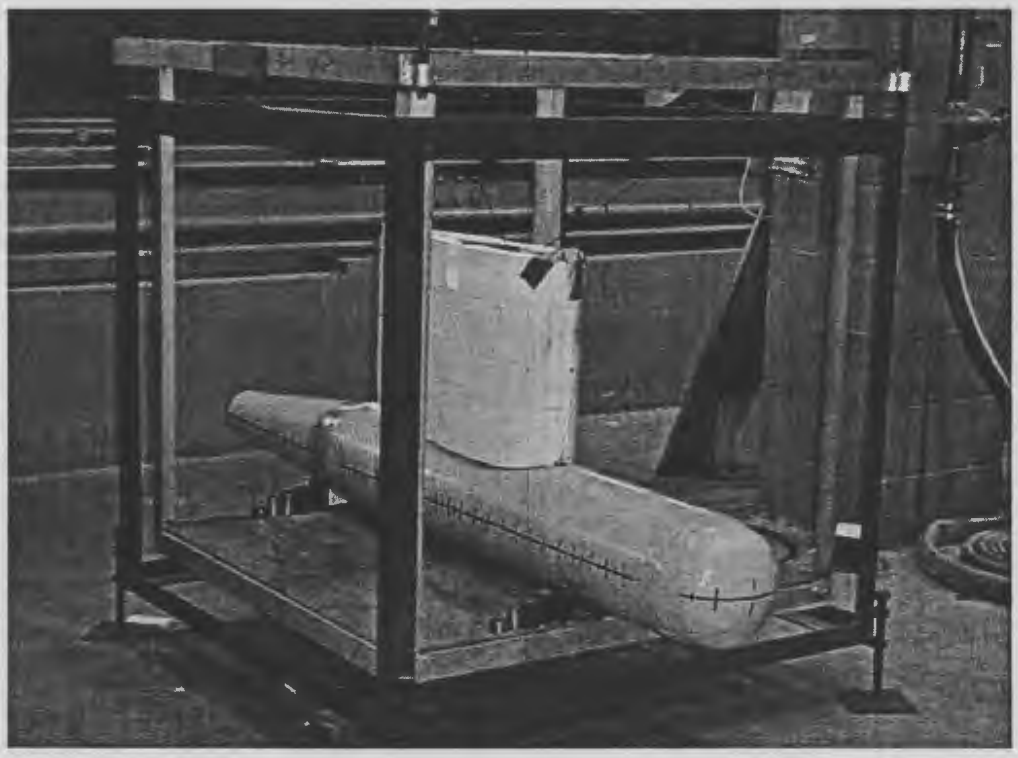

Figure 5.4 Setup of the URV-Model on the frame-table for pitching

5.2.2 Experimental Setup

The URV-model that was used in the experimental work for this research is shown in Figure (5.1). It consists of four parts: a hemispherical nose of dimension 0.254 m diameter, a cylindrical hull of dimensions 0.254 m diameter × 1.225 m length, conical tail of dimensions 0.675 m length × 0.12 m diameter × 0.254 m diameter, and a hydrofoil connection of NACA0024 section × 0.75 m cord × 0.35 m height. The main hull of the model is made of aluminum alloy and the hydrofoil connection is made of *Styrofoam* material. The total mass of the model including the ballast weights is 104 kg.

The experimental data was obtained by testing the URV-model in the towing tank of Memorial University. The towing tank is approximately 58 m × 4.5 m × 3 m. A hydraulically operated, piston-type wavemaker made of aluminum with a watertight Teflon seal around its periphery is located at one end. An upright wave absorber is located at the other end. This construction is intended to absorb and dissipate the energy contained in the incident wave and maintain a minimum reflection coefficient.

A towing carriage is installed on the rails of the tank, which is used in towing the URV-model with fixed forward speed. The carriage can attain a maximum speed of 5 m/sec. The model is attached to the dynamometer that can measure the coupled heave and pitch motions within 0.40 m for heave displacement and $\pm 30^{\circ}$ for pitch.

The URV-model is attached to the dynamometer flange such that heave and pitch are allowed while other motions are constrained see Figure (5.5). A dynamometer that measures the coupled heave and pitch motions for the URV-model is shown in Figure (5.6). The attachment of the URV-model with the vertical dynamometer flange is shown in Figure (5.7) and Figure (5.8). A capacitance-type wave probe used to monitor the time

history of the wave profile as shown in Figure (5.9). Data from accelerometers, inclinometers and wave probes are digitized with a 16-channel Keithley System 500 analog to digital converter and microcomputer.

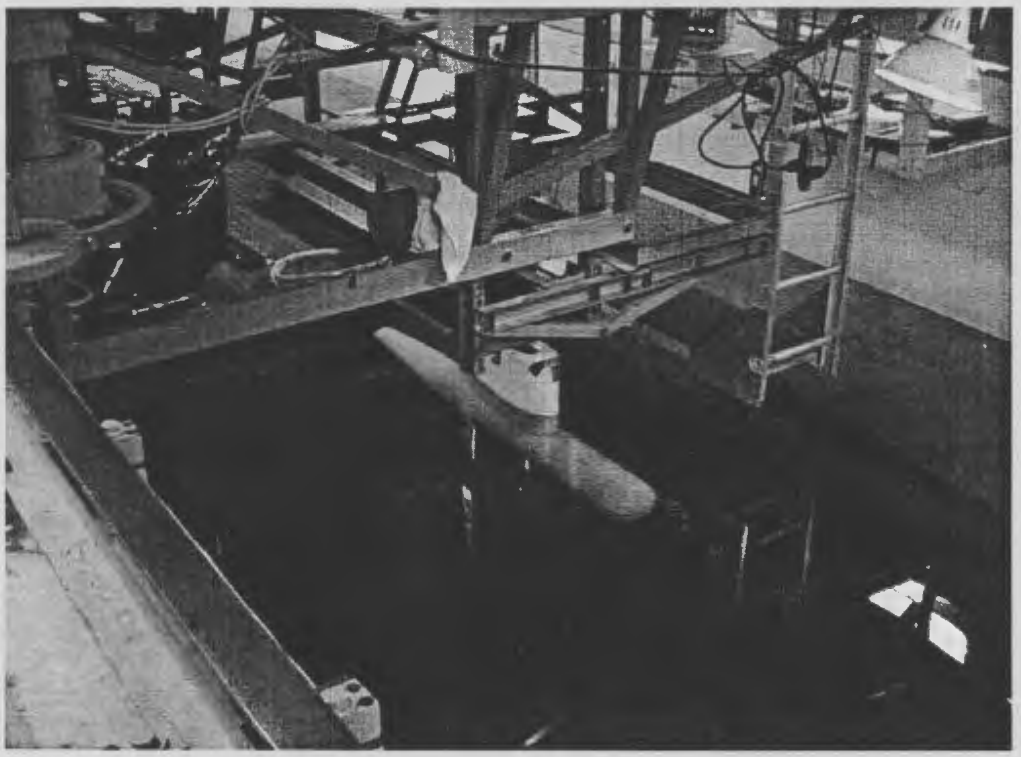

Figure 5.5 Experimental setup for the URV-Model in the towing tank

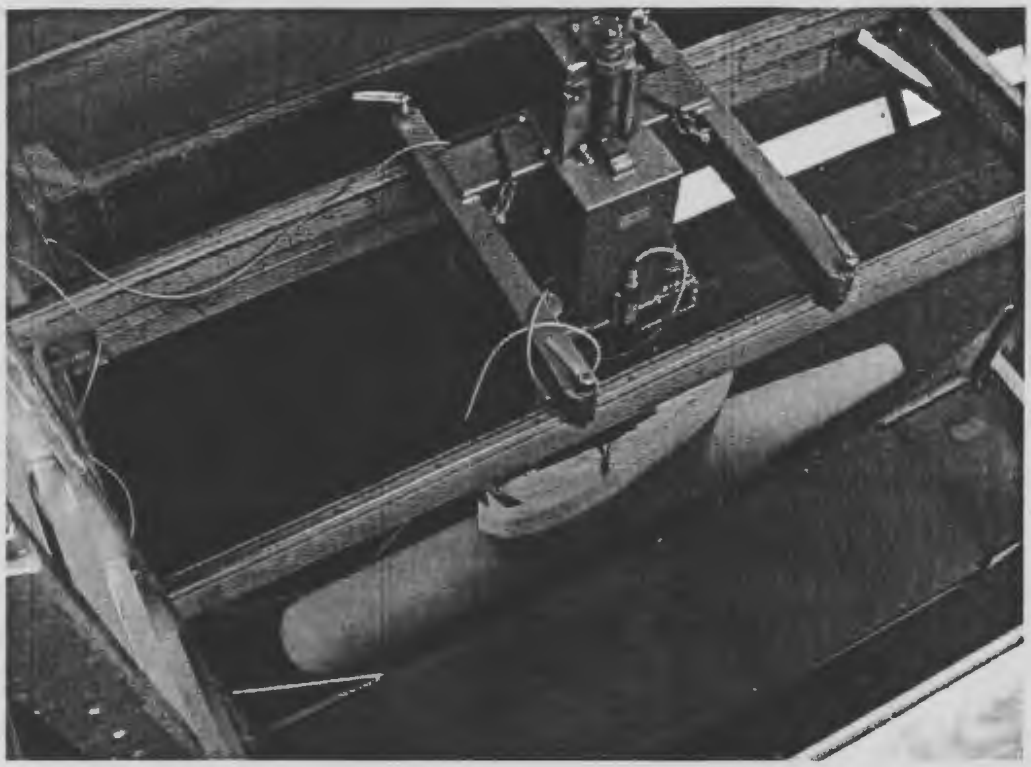

Figure 5.6 Dynamometer for measuring the motions of URV-Model

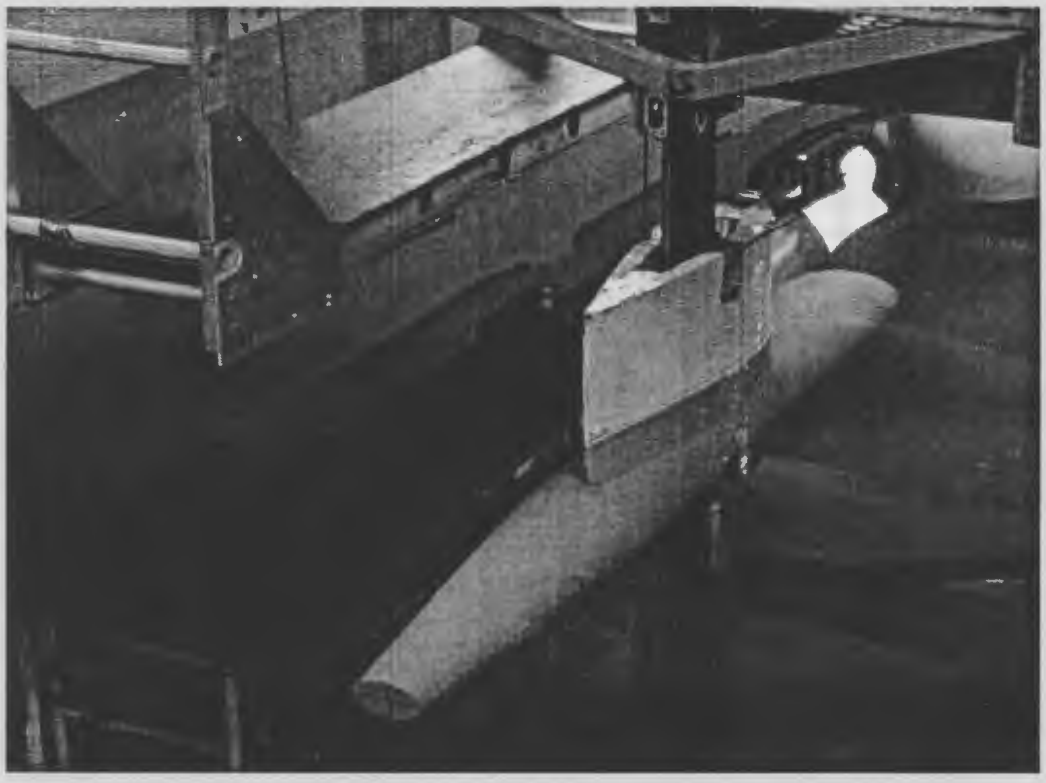

Figure 5.7 Dynamometer flange with the URV-Model

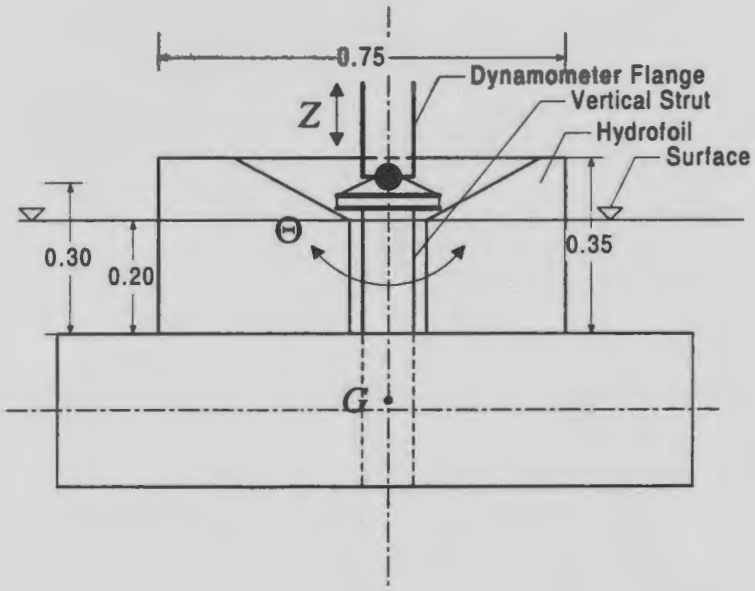

Figure 5.8 Sketch of the dynamometer flange with the URV-Model

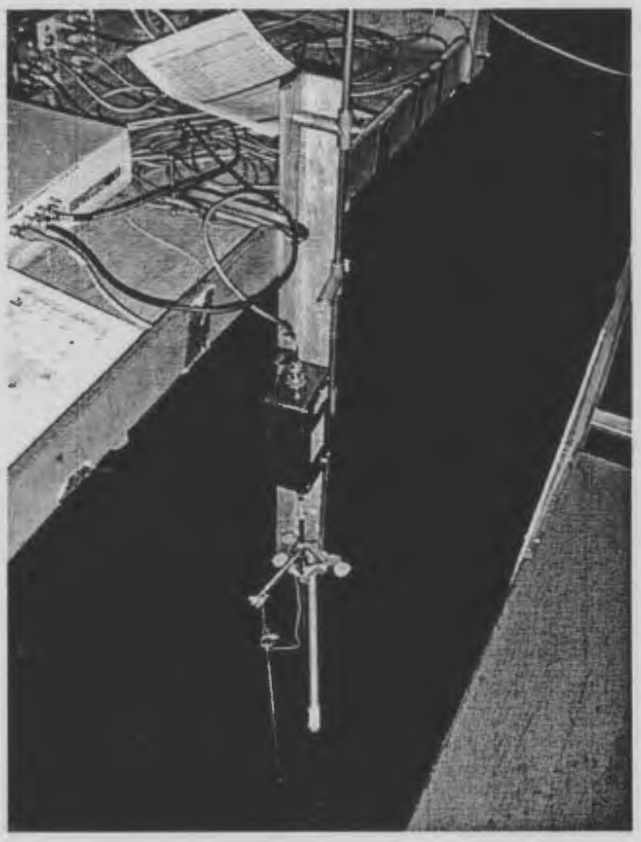

Figure 5.9 Capacitance wave probe

5.2.3 Experimental Procedure

Two main experiments carried out at the towing tank: calm water experiments and random wave experiments. The main objective for the calm water experiments to measure the free decay coupled heave and pitch motions, while the main objective for carrying out the random wave experiments to measure the random motion responses for the coupled heave and pitch motions when the URV-model excited using random waves. These measurements are needed to validate the identification technique.

5.2.3.1 Calm Water Experiments

The URV-model attached to the dynamometer as shown in Figure (5.5). The carriage was located at the mid length of the towing tank in a stationary case state. Calm water experiments have been carried out in this situation to measure the free decay coupled heave and pitch motion responses for the URV-model. This has been conducted by giving the model an initial heave displacement and pitch angle. After the model initially inclined, it is then released and the free motion responses measured. The measured free decay coupled heave and pitch motion responses are shown in Figures (5.10) and (5.11), respectively. The random and free motion responses measured using the available data acquisition system at the wave tank.

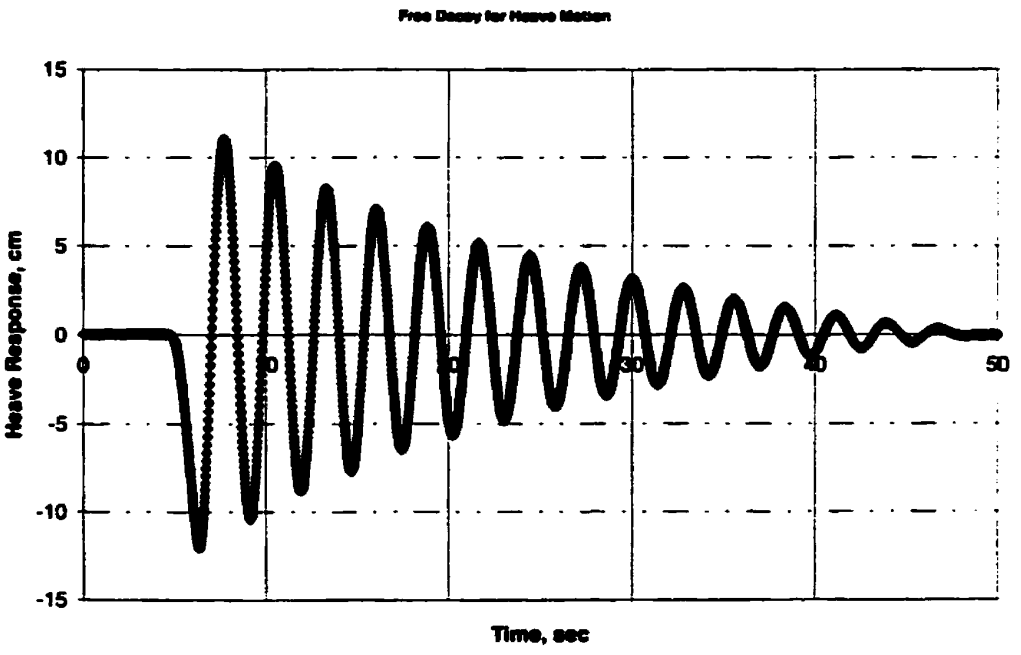

Figure 5.10 Free decay heave motion response

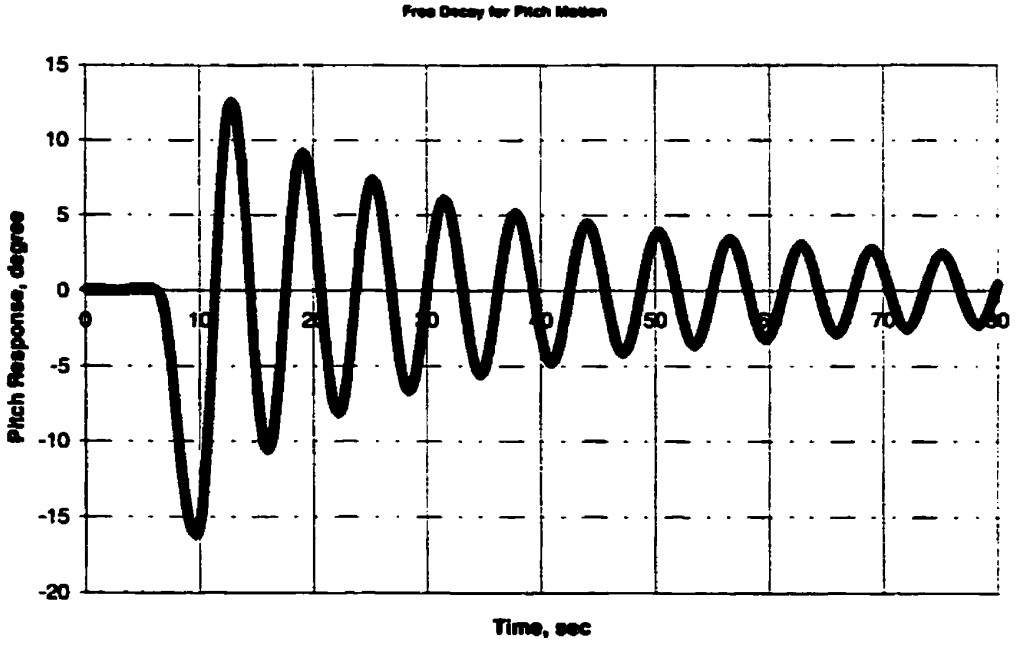

Figure 5.11 Free decay pitch motion response

5.2.3.2 Random Wave Experiments

The developed technique for the identification of the parameters in the equations describing the coupled heave and pitch motions for an URV sailing near the water surface in random waves, requires only the measured responses at seas. Therefore, JONSWAP wave spectra with different significant wave heights and different wave modal frequencies were used to excite the model in the tank. Three main groups were generated to validate the proposed identification technique.

Tests were conducted with the model attached to the dynamometer's flange. Each JONSWAP spectrum in these groups has been generated for the stationary state case as well as for two forward towing speeds: 0.1 m/sec and 0.2 m/sec. Since the length of the wave tank is small compared to the required length of the collected data (400 sec with sampling rate of 20 Hz), a complete experimental run was conducted in two parts of 200 sec long each for case when the model was towed with a speed of 0.1 m/sec and four parts of 100 sec long each when the towing speed of 0.2 m/sec.

5.2.4 Experimental Program

The experimental program was designed to investigate the effects of different wave excitations and different towing speeds on the identification of the parameters in the motion equations. The JONSWAP wave spectrum was used in this work as a wave excitation source for the URV-model. The spectrum has two main characteristic parameters: significant wave height, H_S and wave modal frequency (wave peak

frequency), Ω. JONSWAP wave spectra with different significant wave heights and different wave modal frequencies were used to excite the model in the towing tank.

The experimental program was been divided into three main groups as shown in Appendix L in Tables (L.1), (L.2), and (L.3). Each group has nine complete runs in which each run may have sub-runs based on the required total time for collecting data and both the length of the towing tank and the forward towing speed. These runs have been tested for three different JONSWAP spectra having constant significant wave heights: 0.07 m, 0.10 m, and 0.15 m, and different wave modal frequencies: 0.5 Hz, 0.6 Hz, and 0.7 Hz. Since the pitch pivot was not located at the center of gravity of the model, the ranges of the experimental variables were taken small. This was considered in the experimental work to avoid the effect of the dynamometer flange. Therefore, each wave spectrum has been generated for the stationary state case as well as for two forward towing speeds: 0.1 m/sec and 0.2 m/sec.

It is obvious in Table (L.3) that a significant wave height of 0.13 m is used instead of 0.15 m for runs: 21-0, 26-01, and 27-02. The main reason for this is that when I tried to generate a JONSWAP spectrum corresponding to a significant wave height of 0.15 m and a wave modal frequency of 0.7 Hz, the wavemaker shut itself down several times. I realized that the significant wave height of 0.15 m couldn't be obtained with a frequency of 0.7 Hz, which is reasonably high. Therefore, I tried to generate a JONSWAP spectrum for another significant wave height of 0.13 m with the same modal frequency, and I succeeded.

In order to carry out the experimental program for this work, three persons are needed. The first one should stay in the control room where an electronic control for the

waveboard is provided through an MTS closed-loop, servo-controlled system with error detection and compensation implemented through LVDT feedback loop. The second one is a person who controls the towing carriage. Finally, the third one is a person who controls the data acquisition system through a microcomputer which available on the towing carriage.

Chapter 6

Results and Discussions

6.1 Numerical Results

Numerical random data for the coupled heave and pitch motions for an URV sailing near the water surface in random waves have been generated for both wide-band excitation and narrow-band excitation data. The data have been analyzed using the developed identification technique, RDLRNNT. Numerically generated data for the coupled heave and pitch motion of an URV are used initially to test the accuracy of the technique. Moreover, the effect of using a band-pass filter for the data on the identified parameters is further investigated.

6.1.1 Wide-Band Excitations

Numerically generated data for the coupled heave and pitch motions are obtained using numerical integration of equations (5.1) and (5.2) using wide-band excitations given as in equations (5.3) and (5.4).

Ten case studies were investigated and are presented in this section. The values of the actual damping, restoring, and coupling parameters in equations (5.1) and (5.2) used in the case studies are given in Tables (5.1) and (5.2). The first six cases are used to validate the technique for different levels of damping, while the last four cases are used to validate the technique for different values of the damped natural frequencies in the

coupled heave and pitch motions. The values of the predicted damping, restoring, and coupling parameters corresponding to each case are given in Tables (5.1) and (5.2).

The coupling functions for heave and pitch motions, $G_1(\mu_2, \dot{\mu}_2)$ and $G_2(\mu_1, \dot{\mu}_1)$ are identified using the neural networks technique given in Chapter (4). Figures (6.1) and (6.2) show the predicted functions $G_1(\mu_2, \dot{\mu}_2)$ and $G_2(\mu_1, \dot{\mu}_1)$ for Case (1) as functions of the average values of heave and pitch responses. The outputs of the neural networks for heave and pitch motions are shown in Figures (6.3) and (6.4), respectively. These figures show that the predicted heave and pitch motion responses using the neural networks are identical with the target inputs to the networks. This has been obtained by minimizing the mean square error between the simulated response and the calculated response using the neural networks algorithm.

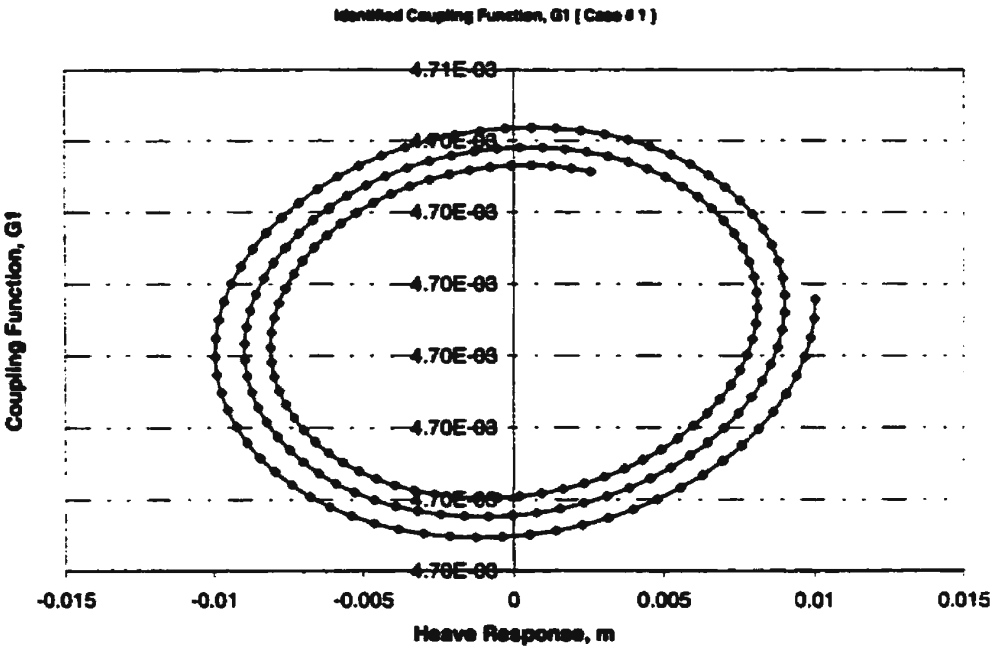

Figure 6.1 Identified coupling function for heave motion [Case # 1]

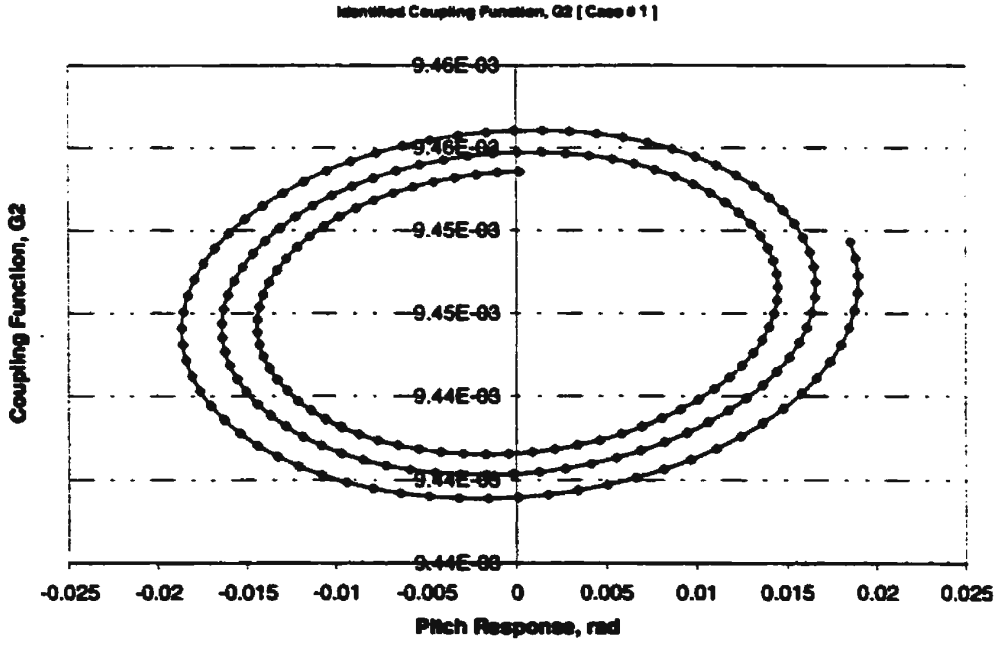

Figure 6.2 Identified coupling function for pitch motion [Case # 1]

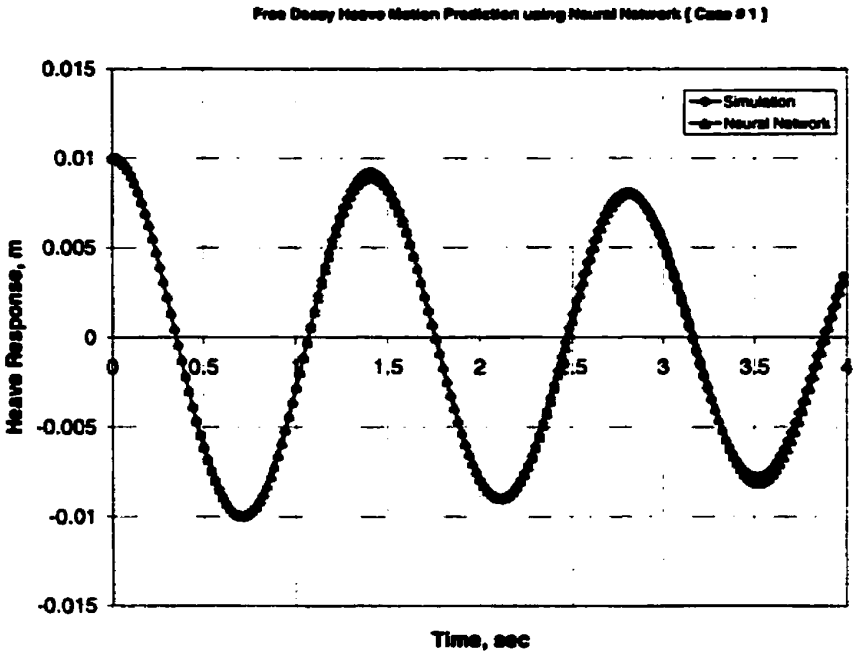

Figure 6.3 Output of the neural network for heave motion [Case # 1]

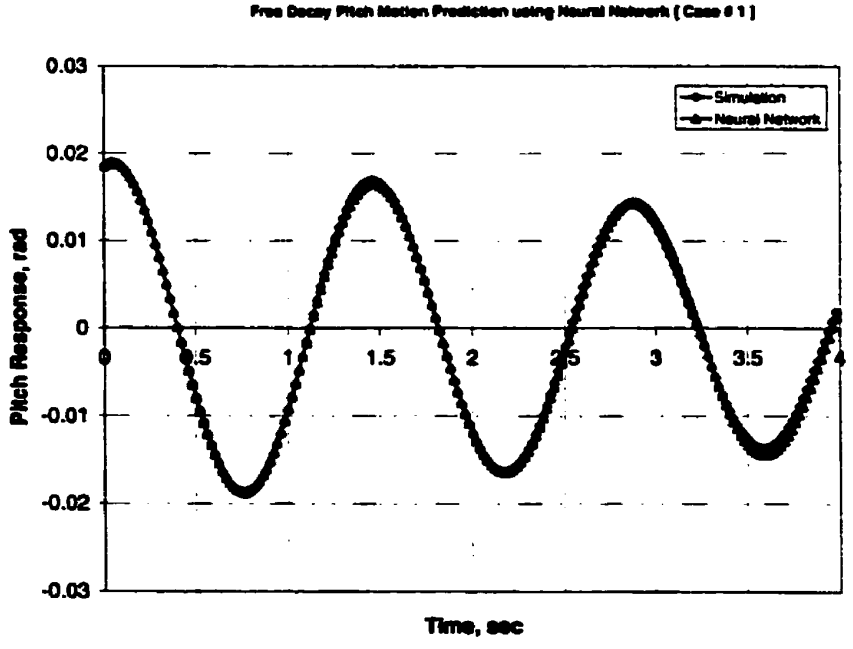

Figure 6.4 Output of the neural network for pitch motion [Case # 1]

6.1.1.1 Effect of the Damping Level

The damping parameter of a dynamic system is an important parameter that characterizes the behavior of the system. The damping of an URV results from the friction between its surface and the surrounding water particles. This type of damping is called friction damping.

With the present state of knowledge in the area of URV/ship motions, no analytical method is available for the determination of the heave and pitch damping parameters for a floating vehicle sailing near the surface in random waves. Therefore, there is an essential need to develop a practical and reliable technique that can identify such parameter. Such a technique has been developed in this work and is dependent only on the measured response at sea. In order to test the validity of the proposed technique, random data have been generated numerically. The data were generated for a wide range of damping levels in the heave and pitch equations. These cases are represented by Case studies (1) to (6).

The power spectral density functions corresponding to the random time series for the heave and pitch motions are calculated for the six case studies as shown in Figures (6.5) to (6.16). It is obvious from these figures that multiple peaks characterize the power spectral density functions. In addition, the maximum energy content in the motion spectra are distributed closely around the damped natural frequencies for heave and pitch motions.

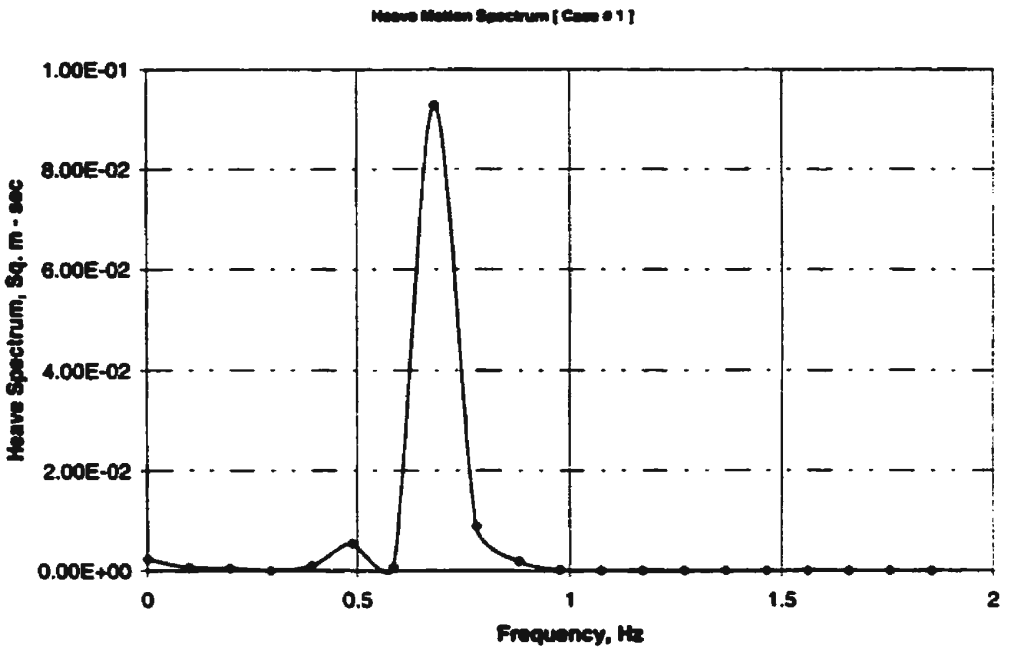

Figure 6.5 Power spectral density function for heave motion [Case # 1]

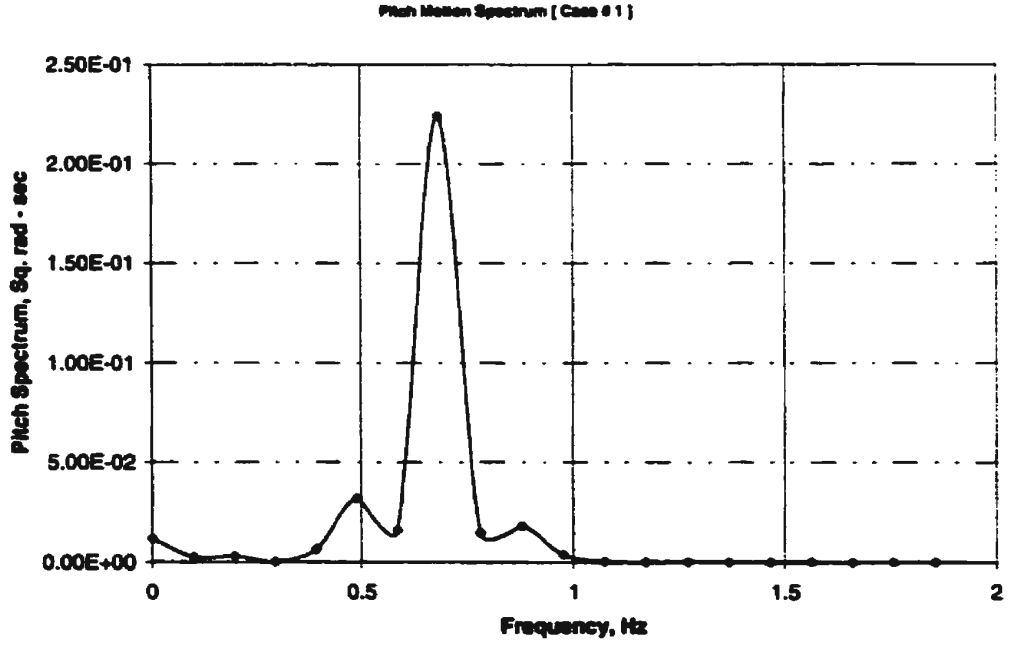

Figure 6.6 Power spectral density function for pitch motion [Case # 1]

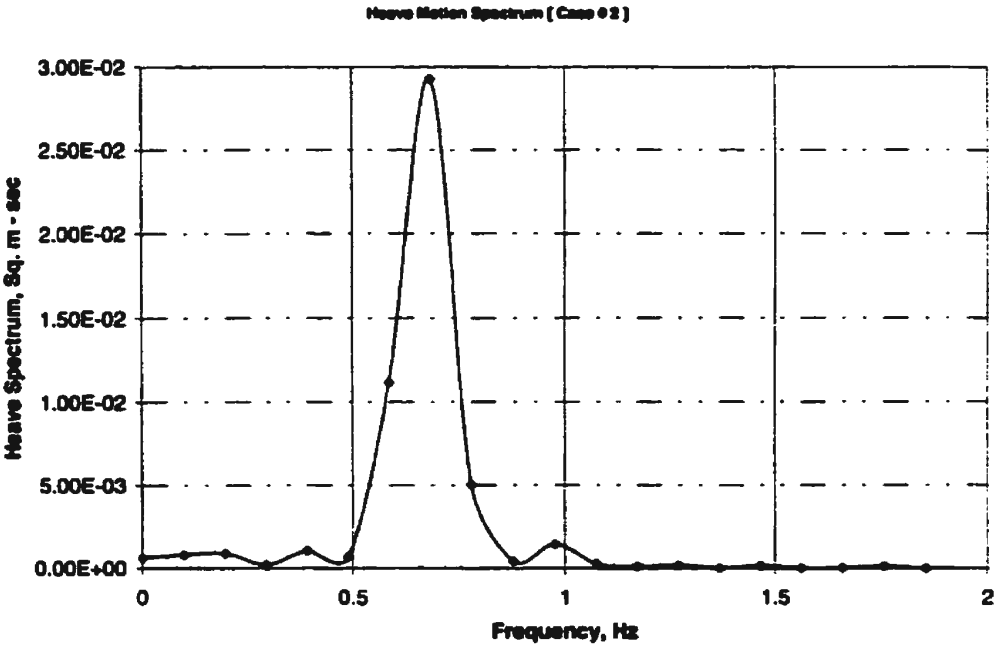

Figure 6.7 Power spectral density function for heave motion [Case # 2]

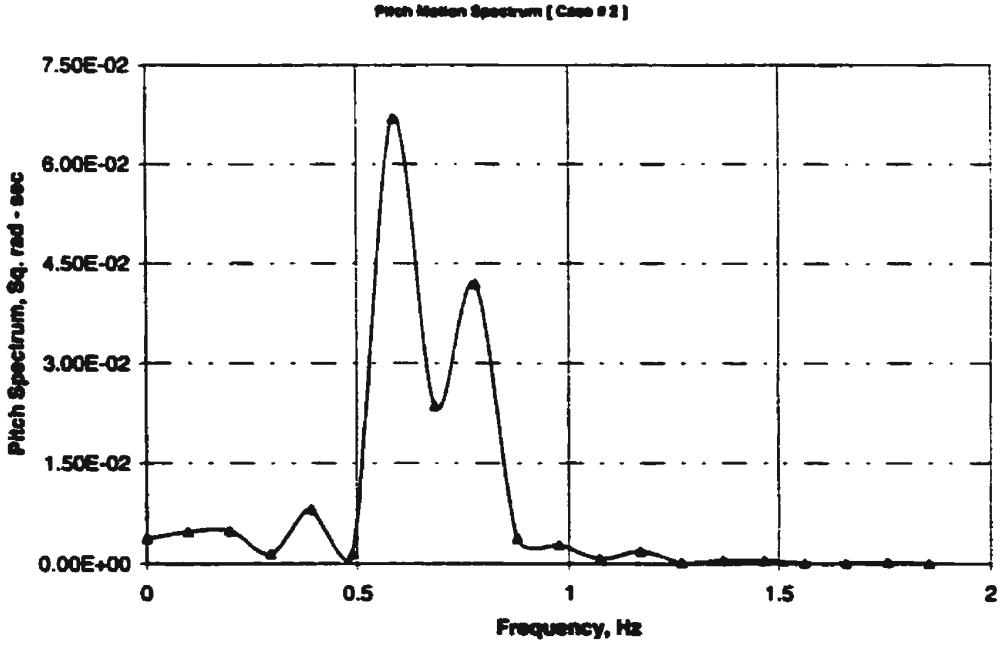

Figure 6.8 Power spectral density function for pitch motion [Case # 2]

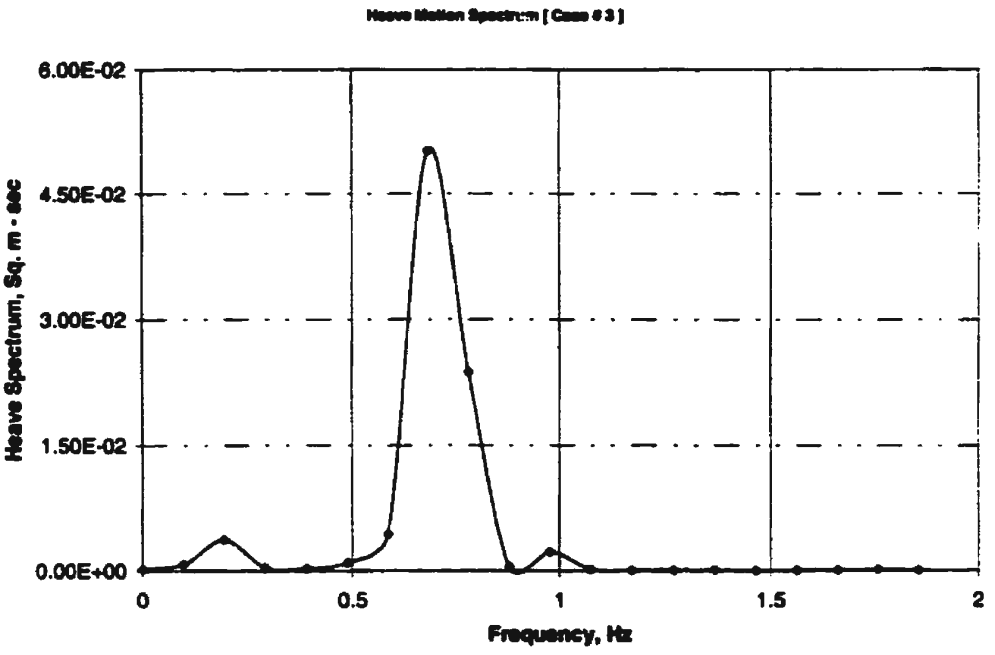

Figure 6.9 Power spectral density function for heave motion [Case # 3]

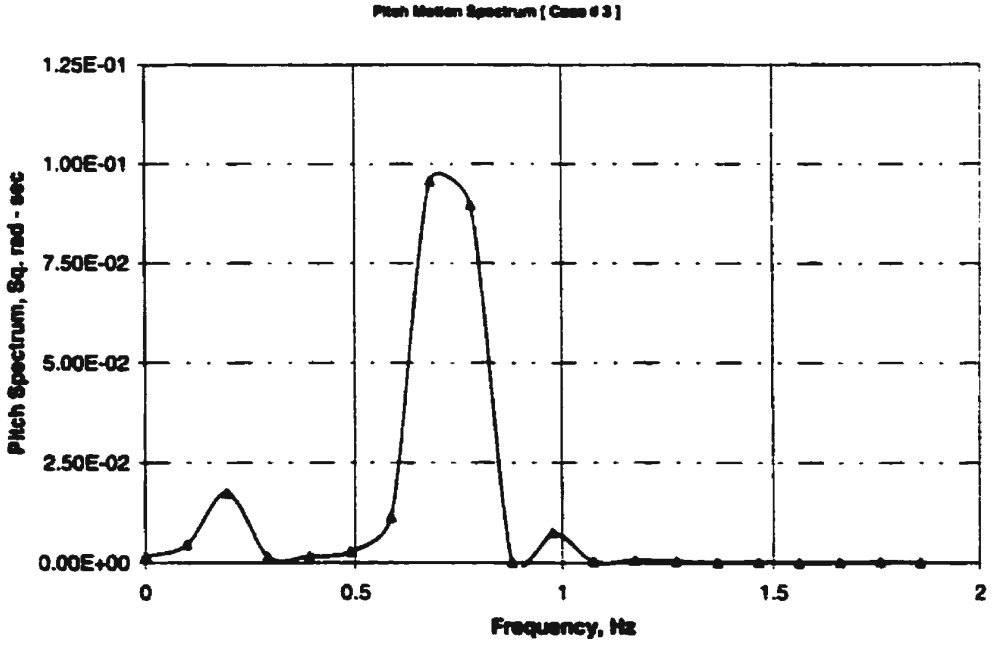

Figure 6.10 Power spectral density function for pitch motion [Case # 3]

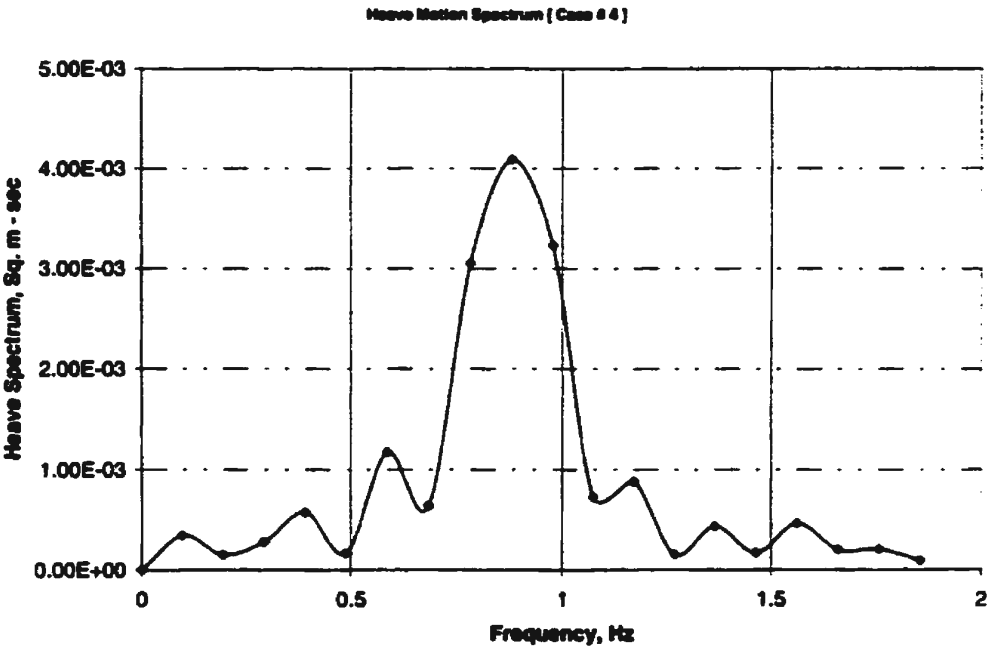

Figure 6.11 Power spectral density function for heave motion [Case # 4]

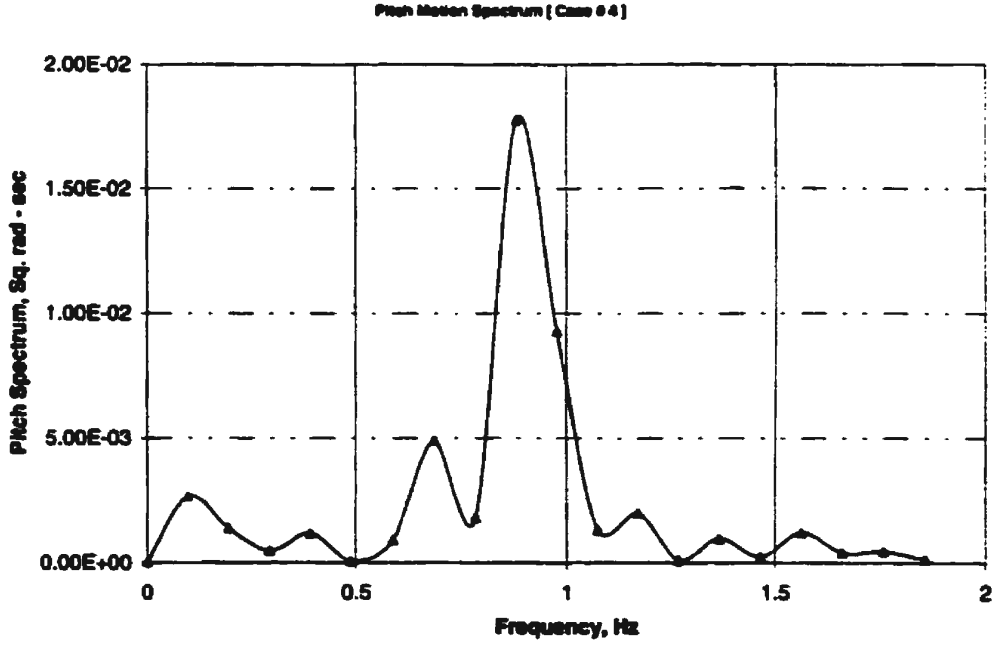

Figure 6.12 Power spectral density function for pitch motion [Case # 4]

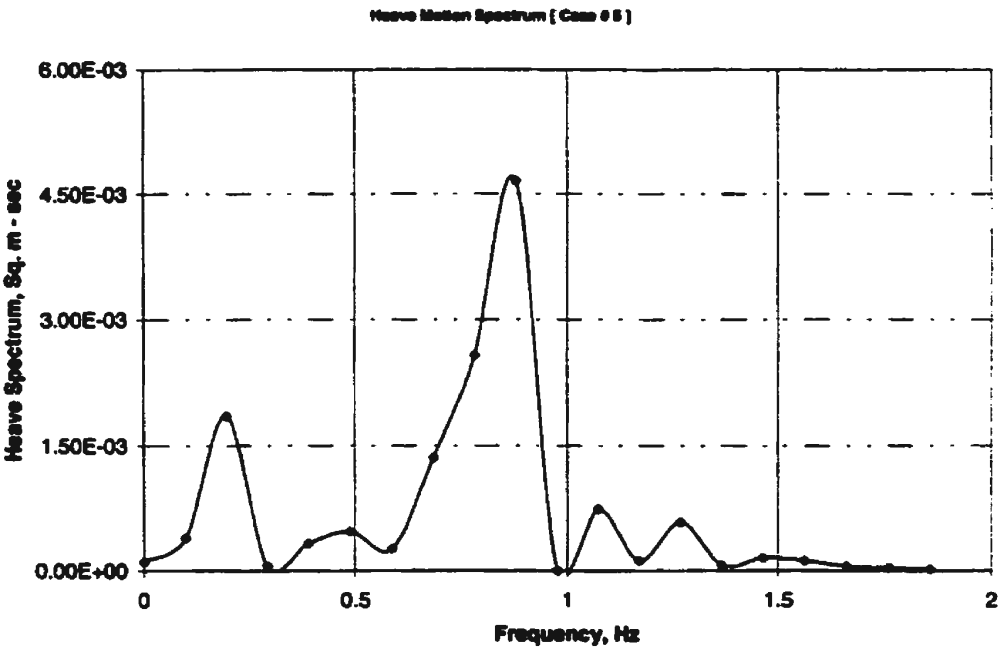

Figure 6.13 Power spectral density function for heave motion [Case # 5]

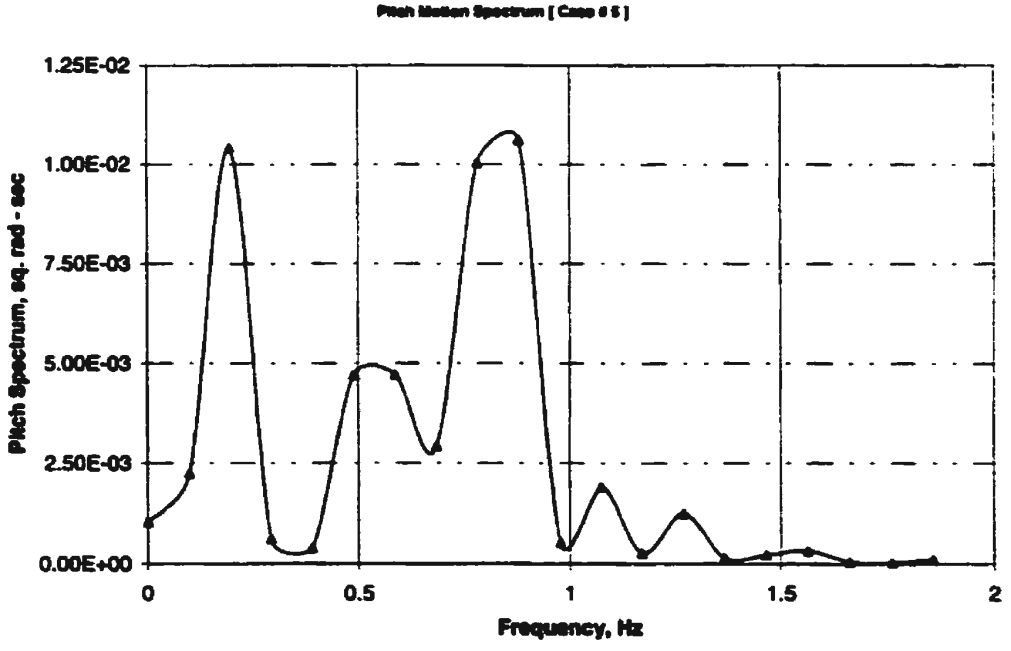

Figure 6.14 Power spectral density function for pitch motion [Case # 5]

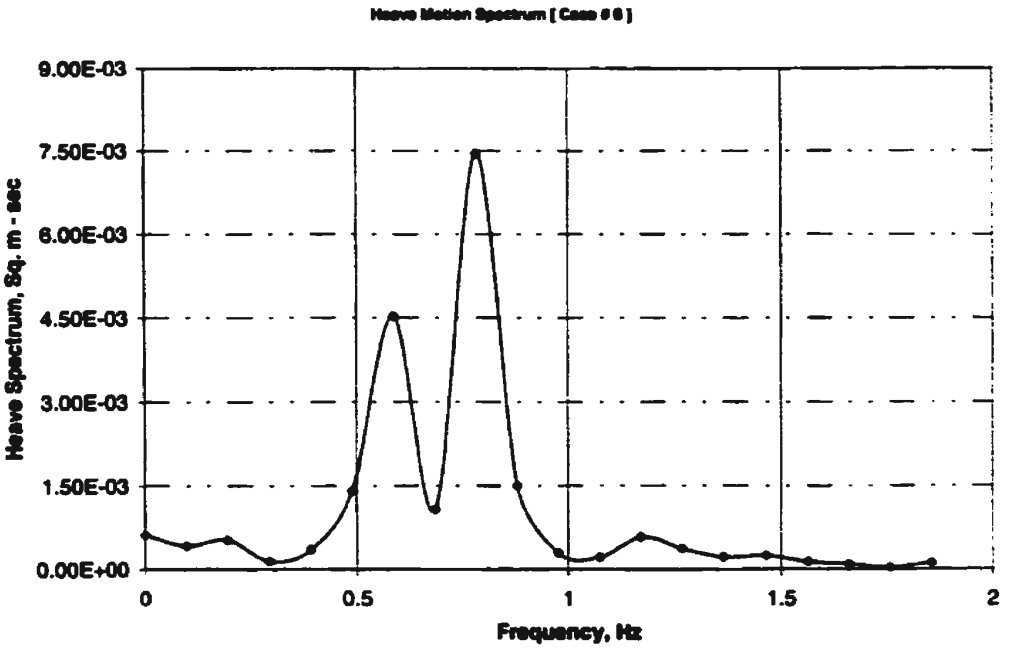

Figure 6.15 Power spectral density function for heave motion [Case # 6]

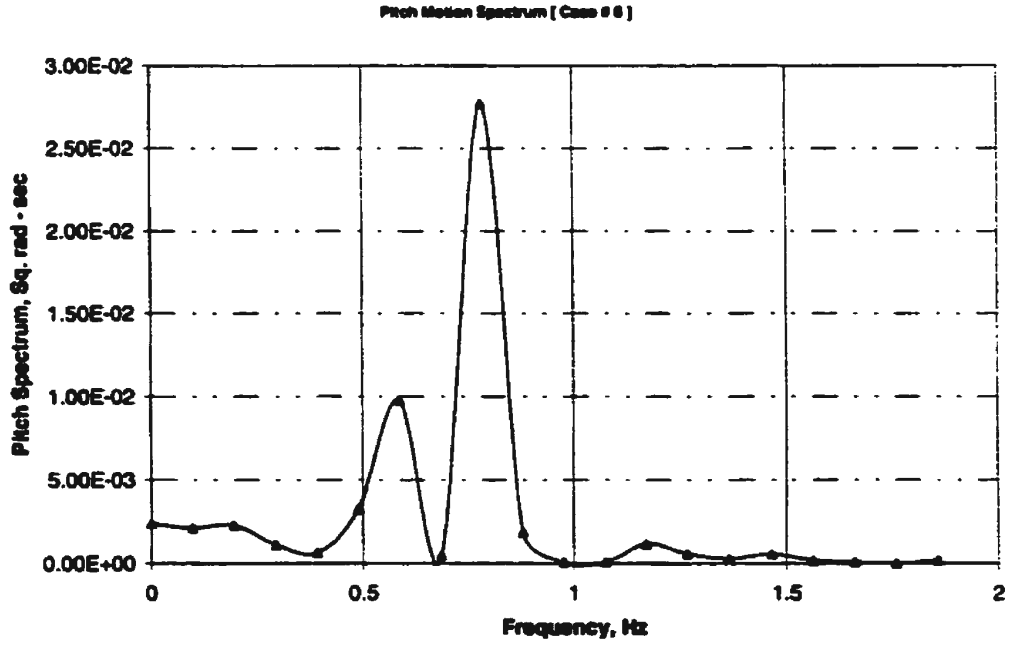

Figure 6.16 Power spectral density function for pitch motion [Case # 6]

Both the random decrement signatures and the auto-correlation functions have been calculated using numerically generated random data for the coupled heave and pitch motions using a MATLAB program called "*RD&AC_sim*", see Appendix G.

The random decrement signatures are compared with the predicted free responses using equations (5.1) and (5.2) for each case. The comparison is shown in Figures (H.1) to (H.12) for the six case studies as given in Appendix H. An example of the results is shown in Figures (6.17) to (6.20) for Cases (1) and (2).

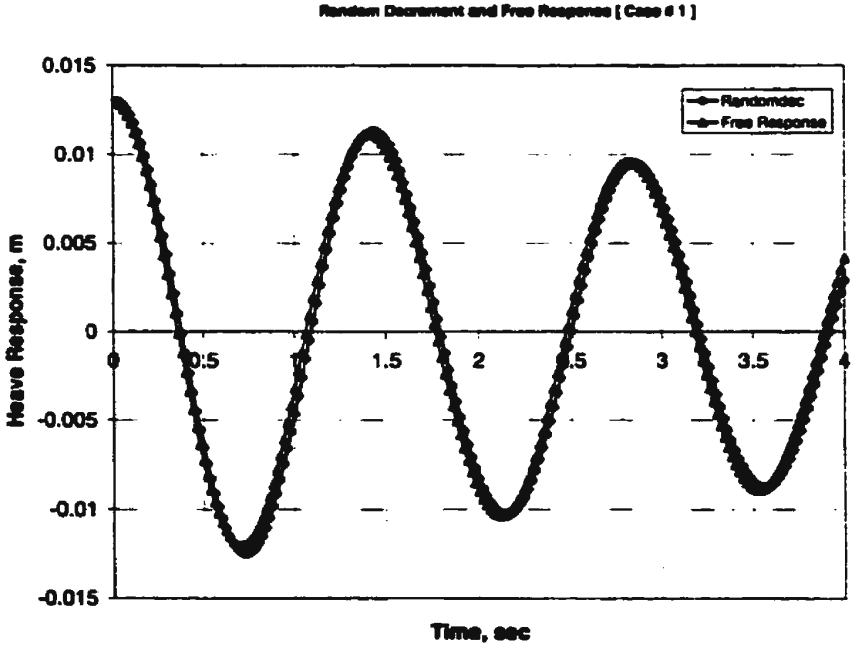

Figure 6.17 Comparison between the random decrement signature and the free response for heave motion [Case # 1]

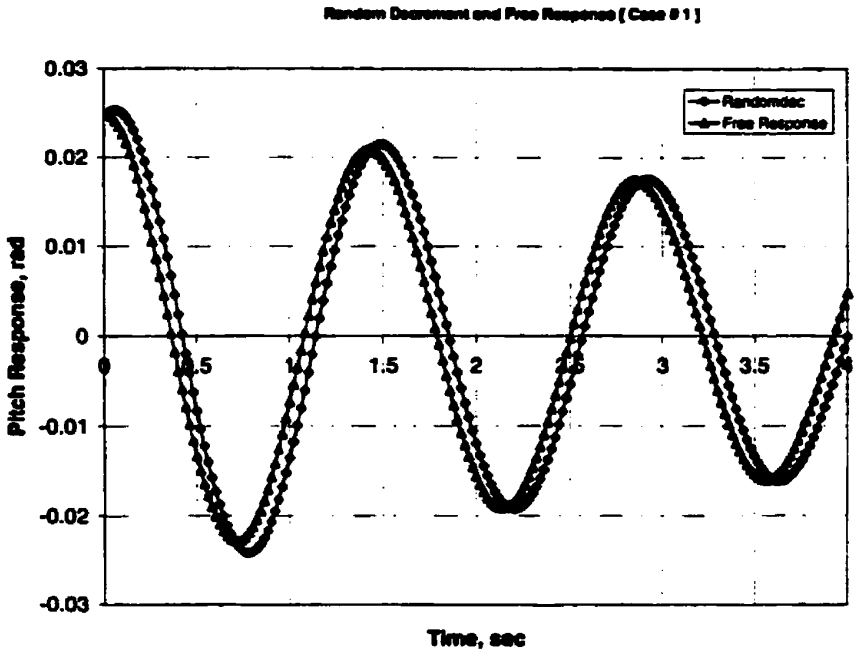

Figure 6.18 Comparison between the random decrement signature and the free response for pitch motion [Case # 1]

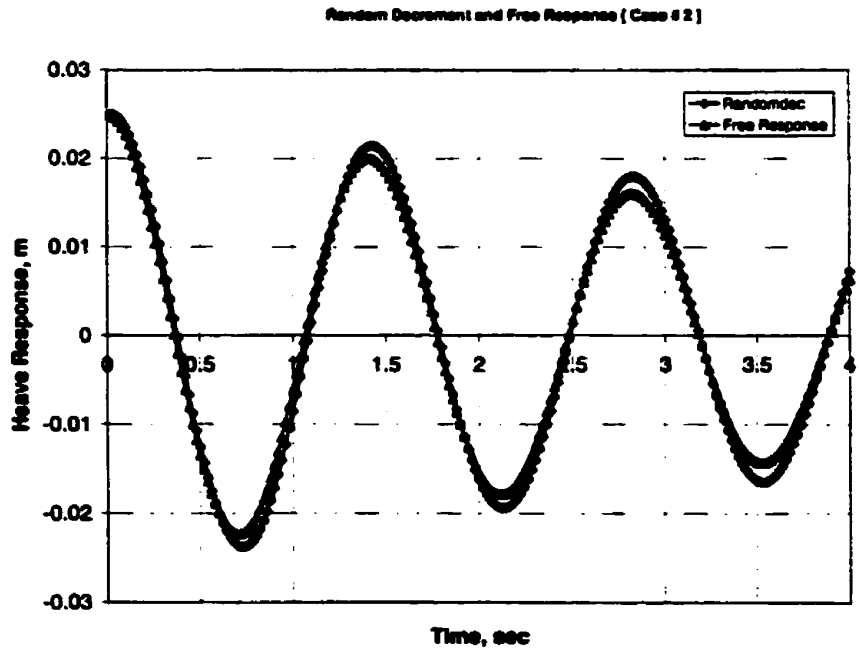

Figure 6.19 Comparison between the random decrement signature and the free response for heave motion [Case # 2]

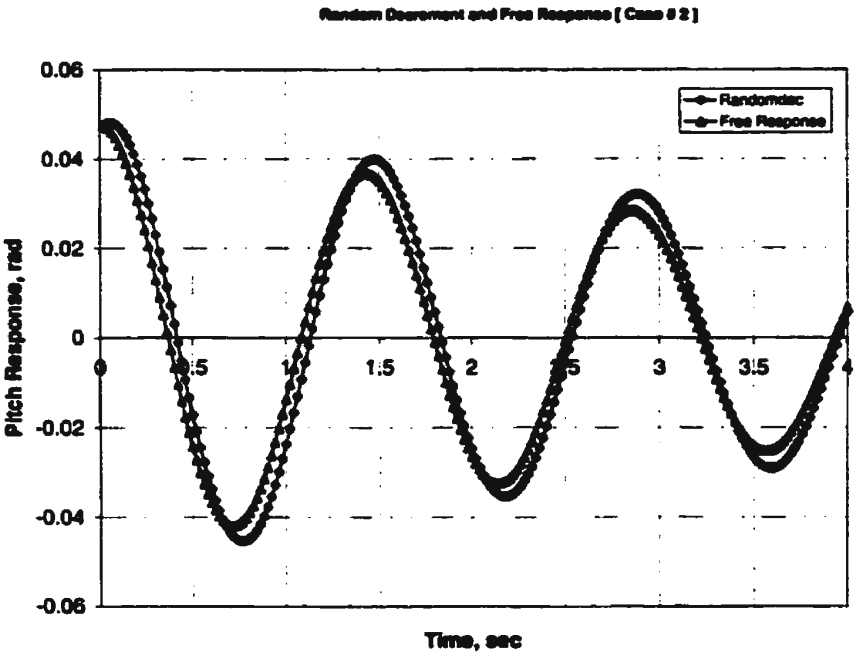

Figure 6.20 Comparison between the random decrement signature and the free response for pitch motion [Case # 2]

As the damping increases, the agreement between the random decrement and the free response deteriorates as shown in Figures (H.9) and (H.10), and Figures (H.11) and (H.12) for Cases (5) and (6), respectively. The reason behind this can be observed from the shape of the power spectral density of Case (6), Figures (6.15) and (6.16). These graphs show that the peak around the natural frequency becomes less pronounced than in Cases (1) to (4). The number of segments that can be used to construct the random decrement becomes small. This will cause the random decrement to be less representatives of the free motion.

Another comparison has been conducted between the random decrement and the auto-correlation functions for the heave and pitch motions. The comparison is shown in Figures (I.1) to (I.12) for the six case studies as given in Appendix I. An example of the results is shown in Figures (6.21) to (6.24) for Cases (1) and (2).

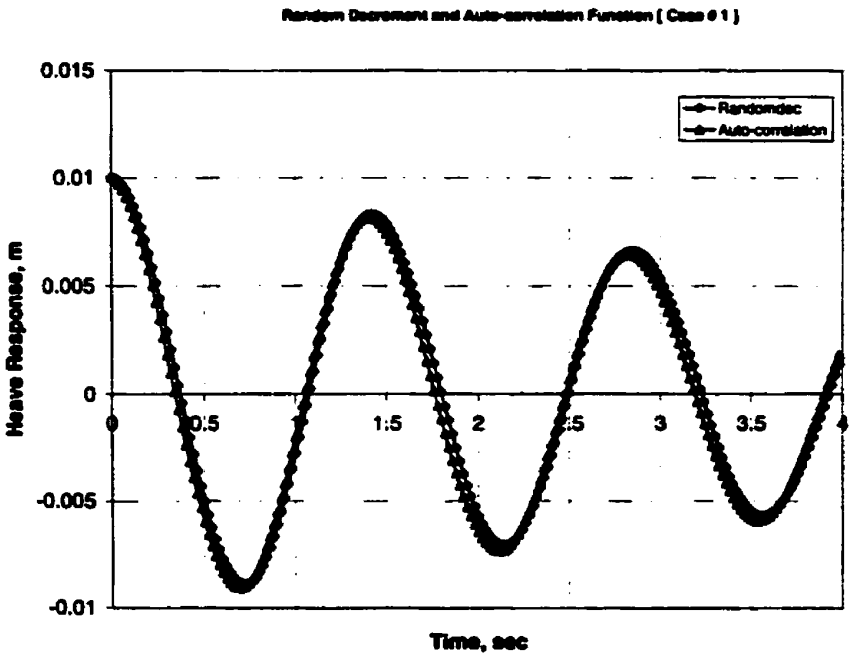

Figure 6.21 Comparison between the random decrement signature and the auto-correlation function for heave motion [Case # 1]

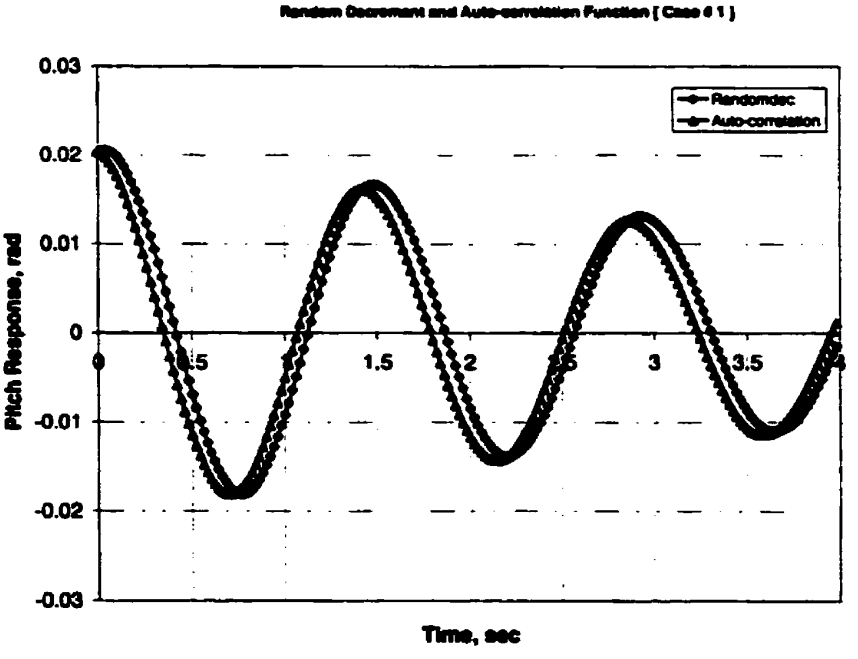

Figure 6.22 Comparison between the random decrement signature and the auto-correlation function for pitch motion [Case # 1]

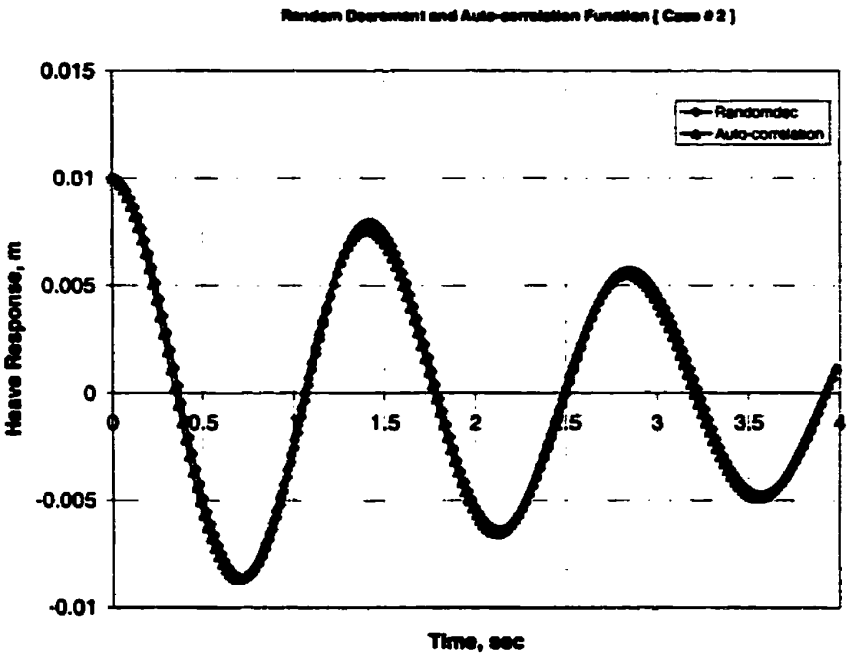

Figure 6.23 Comparison between the random decrement signature and the auto-correlation function for heave motion [Case # 2]

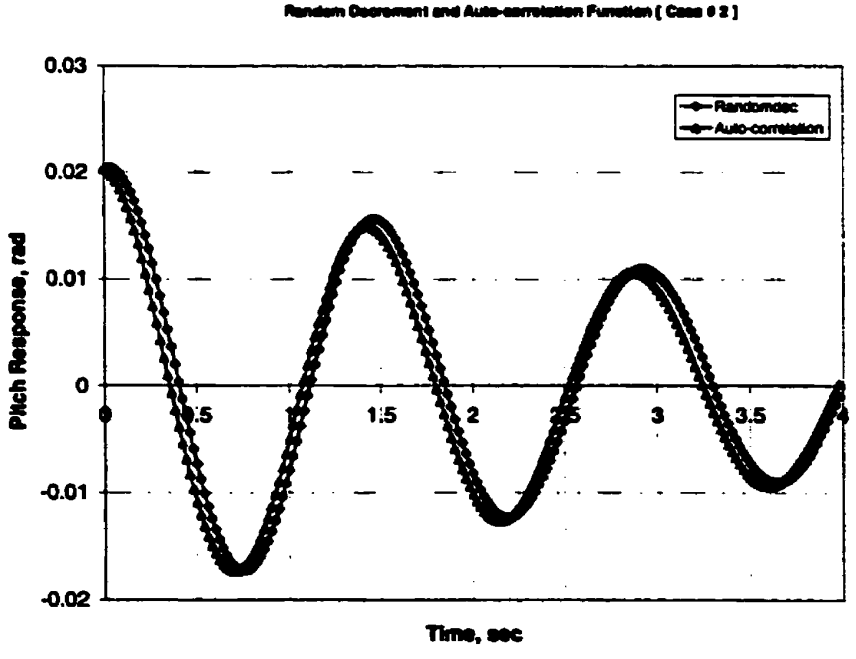

Figure 6.24 Comparison between the random decrement signature and the auto-correlation function for pitch motion [Case # 2]

Similarly, as the damping increases, the agreement between the random decrement signature and the auto-correlation function deteriorates. This result is obvious as shown in Figures (I.9) and (I.10), and Figures (I.11) and (I.12) for Cases: (5) and (6), respectively.

I can conclude from the previous comparisons that as damping increases, the agreement between the random decrement signature and the free response, and that between the random decrement signature and the auto-correlation function, deteriorates. However, for moderately damped motions, excellent agreement has been obtained as shown in Cases (1) to (4).

6.1.1.2 Effect of the Damped Natural Frequency

The last four Case studies: (7) to (10), have been considered in this work to test the validity of the developed identification technique for different values of the damped natural frequencies in the equations describing the coupled heave and pitch motions for a URV.

The power spectral density functions corresponding to the random time series for heave and pitch motions are calculated for the case studies as shown in Figures (6.25) to (6.32). Again, it is shown in these figures that multiple peaks characterize the power spectral density functions. In addition, the maximum energy contents in the motion spectra are distributed closely around the damped natural frequencies.

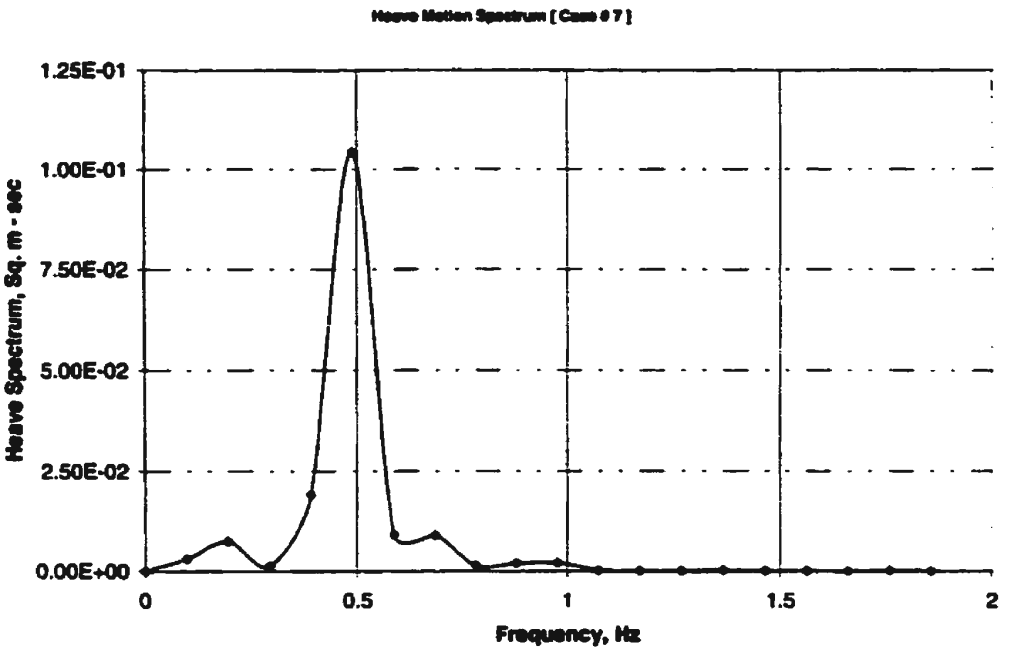

Figure 6.25 Power spectral density function for heave motion [Case # 7]

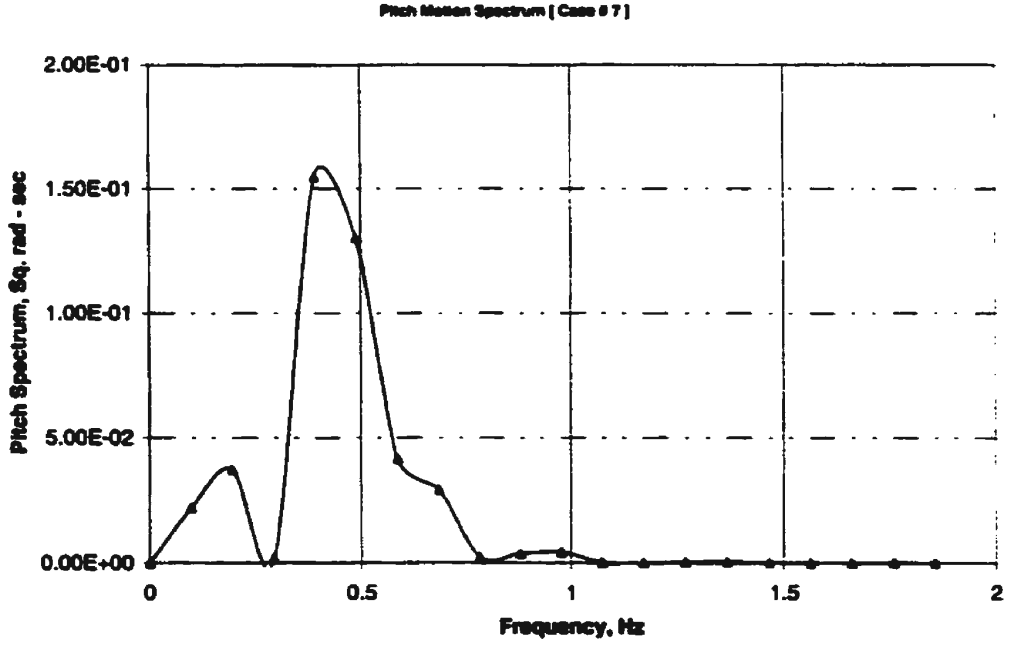

Figure 6.26 Power spectral density function for pitch motion [Case # 7]

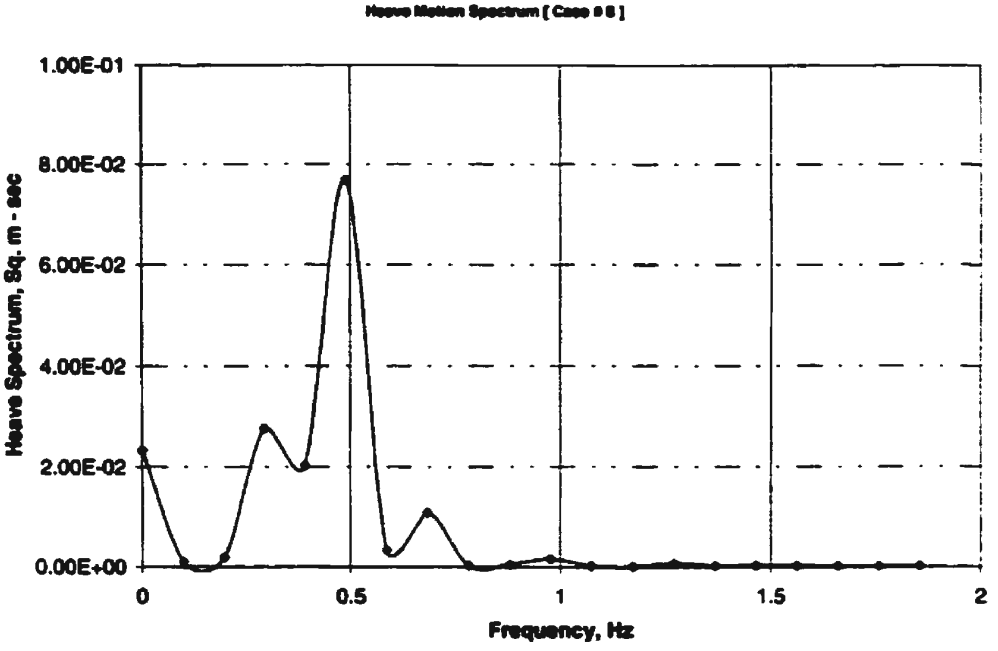

Figure 6.27 Power spectral density function for heave motion [Case # 8]

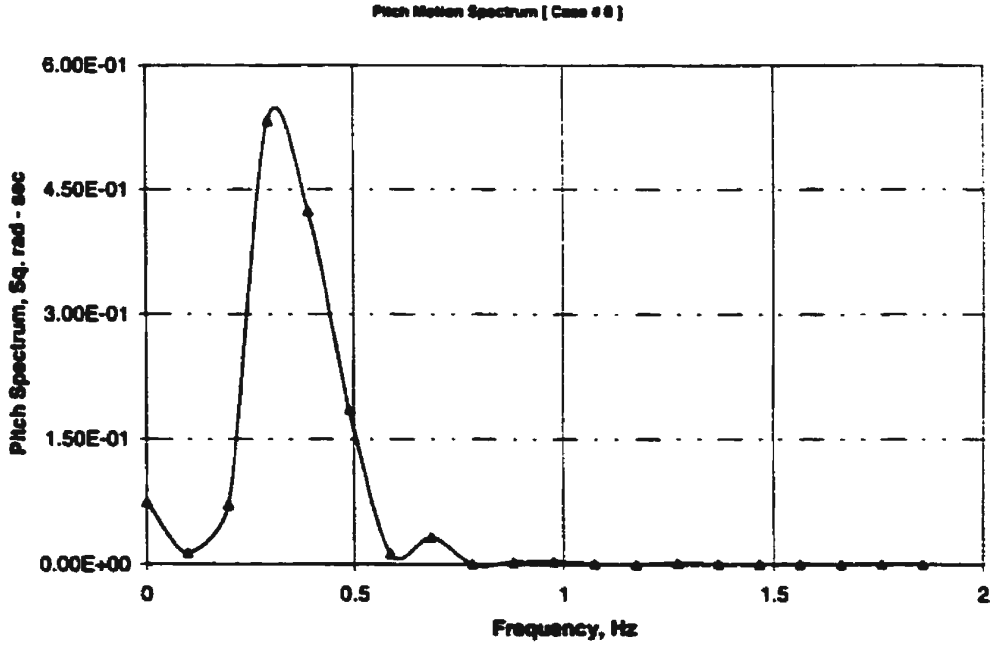

Figure 6.28 Power spectral density function for pitch motion [Case # 8]

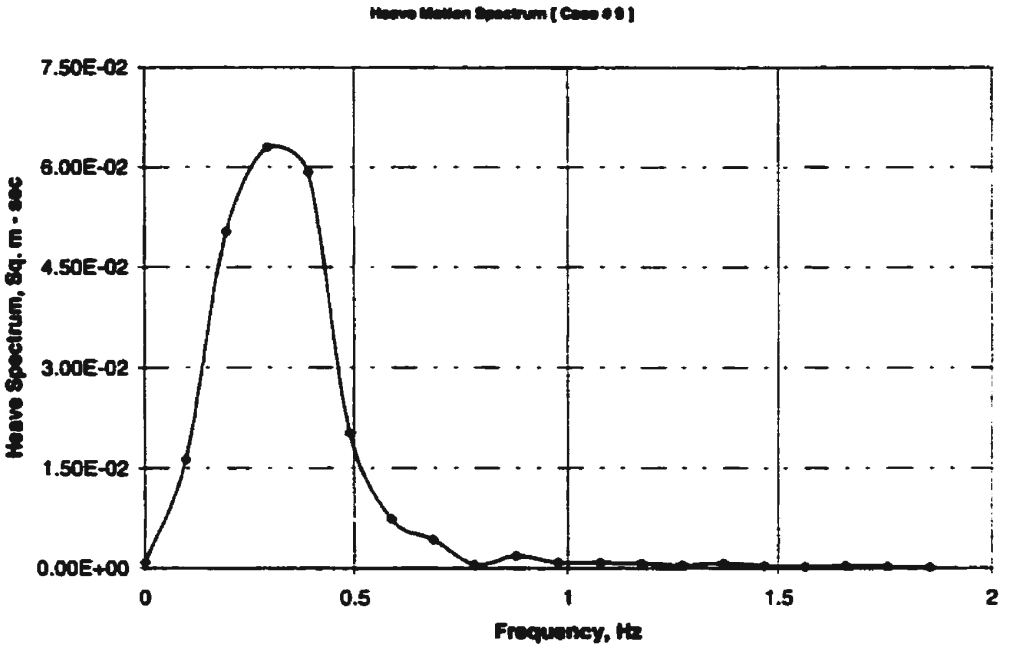

Figure 6.29 Power spectral density function for heave motion [Case # 9]

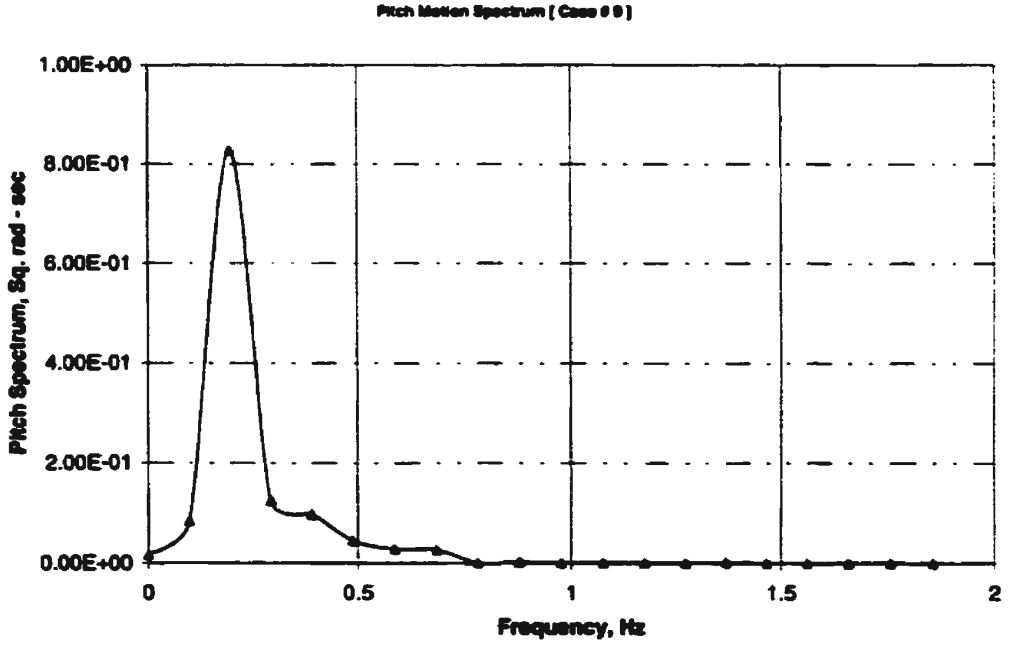

Figure 6.30 Power spectral density function for pitch motion [Case # 9]

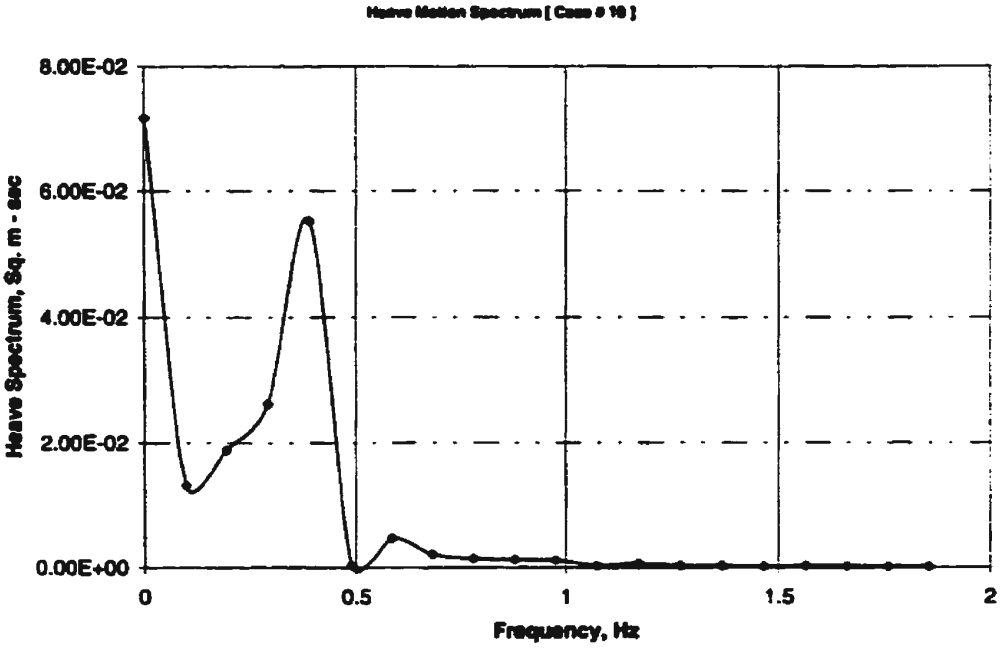

Figure 6.31 Power spectral density function for heave motion [Case # 10]

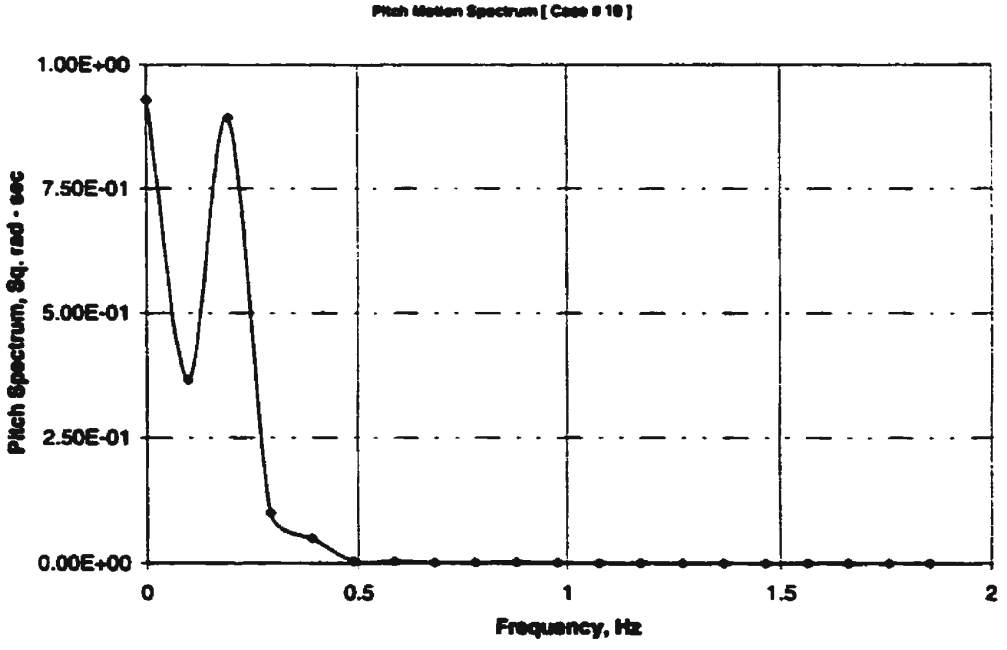

Figure 6.32 Power spectral density function for pitch motion [Case # 10]

The random decrement signatures are compared with the predicted free responses for each case study. The comparison is shown in Figures (H.13) to (H.20) for the four cases as given in Appendix H. An example of the results is shown in Figures (6.33) to (6.36) for Cases (7) and (8).

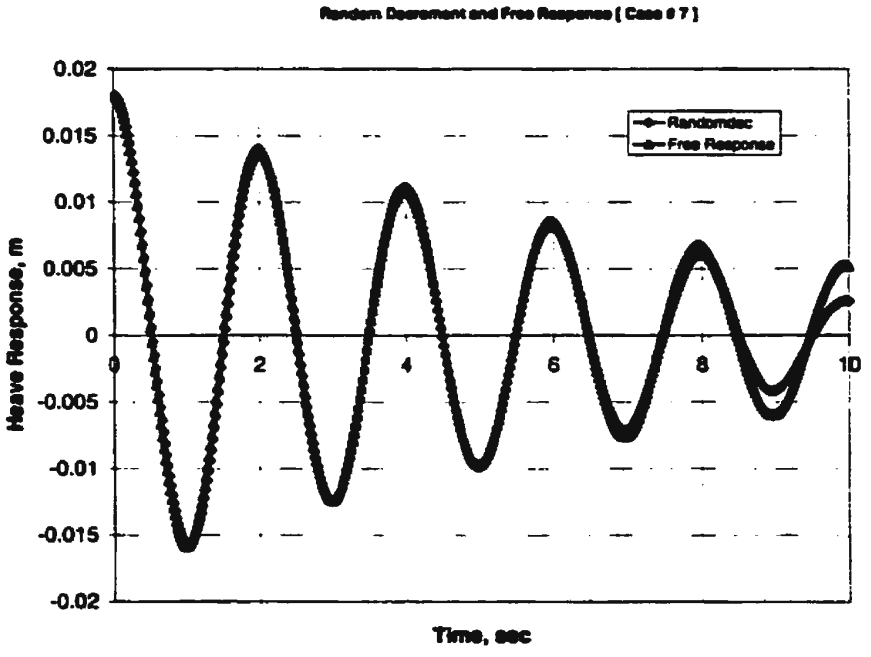

Figure 6.33 Comparison between the random decrement signature and the free response for heave motion [Case # 7]

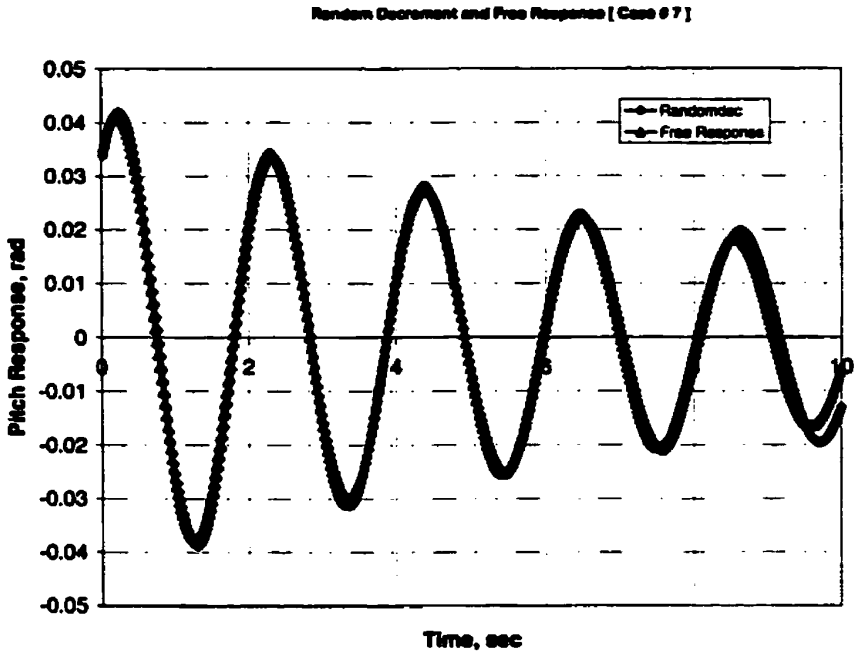

Figure 6.34 Comparison between the random decrement signature and the free response for pitch motion [Case # 7]

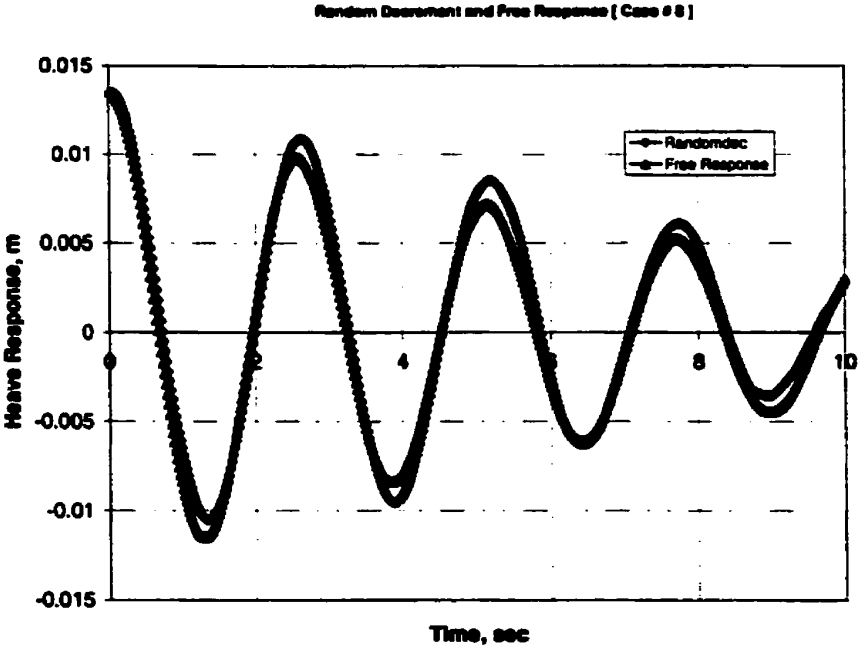

Figure 6.35 Comparison between the random decrement signature and the free response for heave motion [Case # 8]

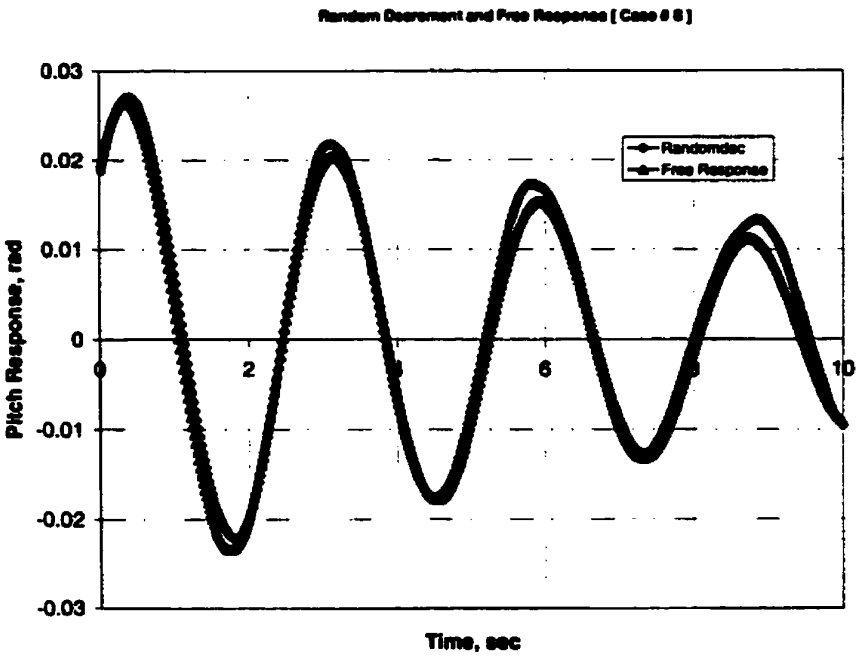

Figure 6.36 Comparison between the random decrement signature and the free response for pitch motion [Case # 8]

As the difference between the exciting frequency and the natural frequency increases, the agreement between the random decrement signature and the free response deteriorates. This result is clear in Figures (H.19) and (H.20) for Case (10). At resonance, the dynamic system vibrates at its own natural frequency. This will produce a better random decrement, since the energy around the natural frequency will be large. The random response will yield a large number of segments that can be used to construct the random decrement signature.

Similarly, a comparison between the random decrement signatures and the auto-correlation functions for the heave and pitch motions, has been conducted. The comparison is shown in Figures (I.13) to (I.20) as given in Appendix I. An example of the results is shown in Figures (6.37) to (6.40) for Cases (7) and (8).

Again, as the difference between the exciting frequency and the natural frequency increases, the agreement between the random decrement signature and the auto-correlation function deteriorates as shown in the figures corresponding to the pitch motion. The discrepancies in these figures show that the auto-correlation function ceases to represent the random decrement signature.

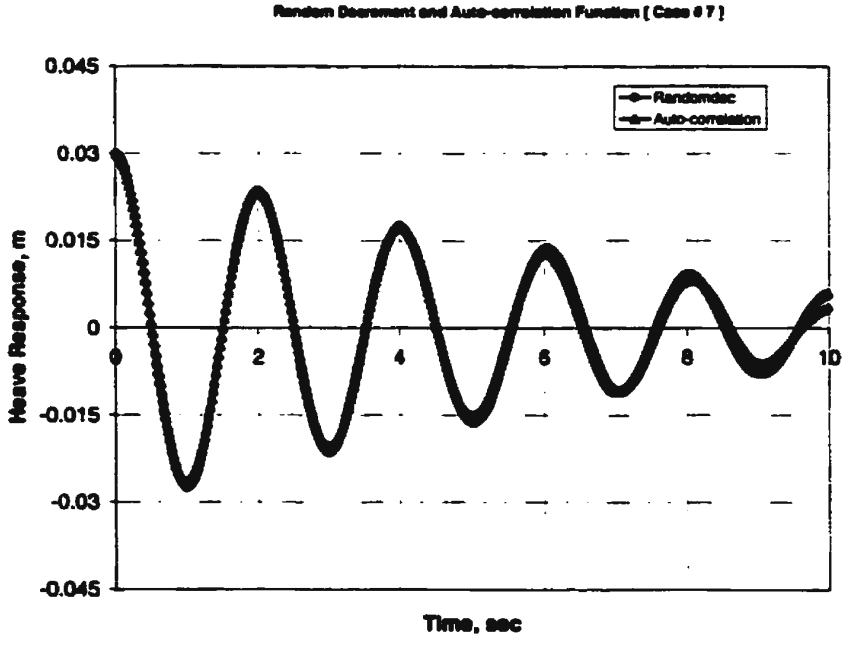

Figure 6.37 Comparison between the random decrement signature and the auto-correlation function for heave motion [Case # 7]

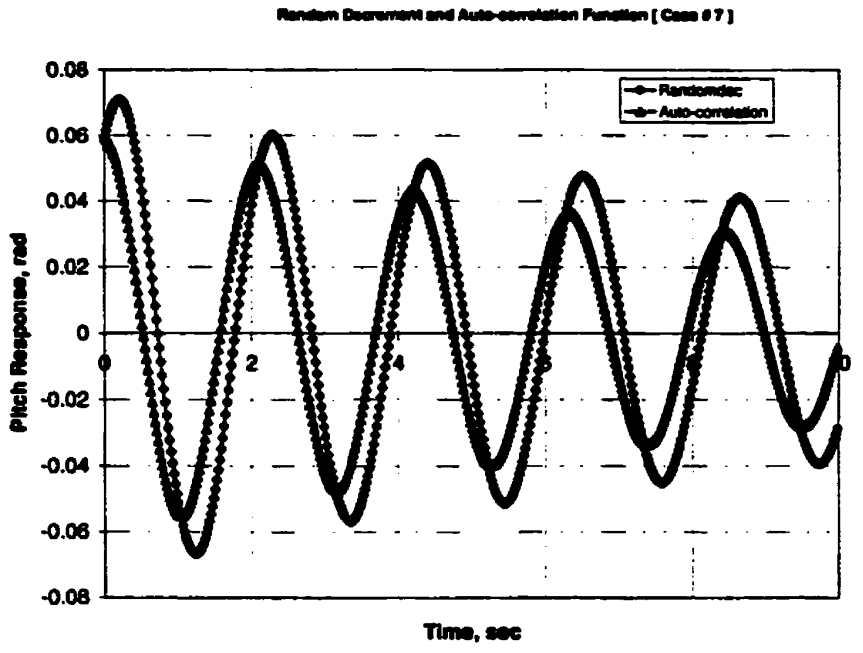

Figure 6.38 Comparison between the random decrement signature and the auto-correlation function for pitch motion [Case # 7]

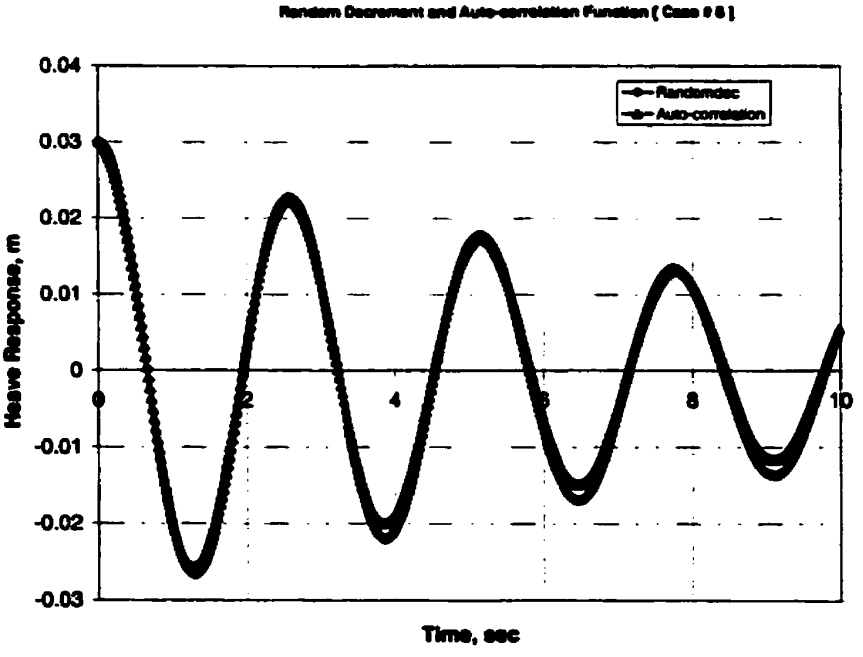

Figure 6.39 Comparison between the random decrement signature and the auto-correlation function for heave motion [Case # 8]

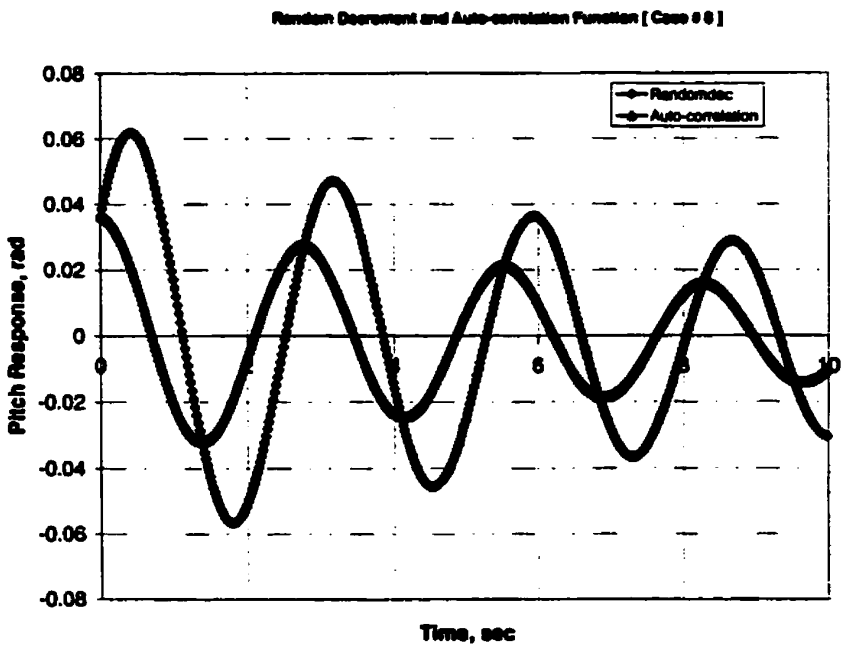

Figure 6.40 Comparison between the random decrement signature and the auto-correlation function for pitch motion [Case # 8]

I can conclude from the previous comparisons that both the random decrement signature and the auto-correlation function describe the free motion of the vehicle for lightly and moderately damped motions. For heavily damped motions, the use of the random decrement signature to represent the free motion is better than the use of the auto-correlation function. This result is clearly obvious from the comparison of Figures (6.33) to (6.36) and Figures (6.37) to (6.40).

6.1.1.3 Motion Prediction

A comparison between the parameters used in the actual model and the predicted parameters for the ten case studies is shown in Tables (5.1) and (5.2). It is obvious from

these tables that the predicted damping and restoring parameters, d_{31}, d_{33}, d_{42}, and d_{44} for the heave and pitch motions are in close agreement with the actual values used in the generation of the numerical random motion responses. The agreement between the actual and the predicted values for the coupling parameters, d_{32}, d_{34}, d_{41}, and d_{43} is poor.

However, the criterion should be the quality of motion predictions that the model is able to achieve. The predicted model was then used to generate the free and regular coupled heave and pitch motion responses using equations (5.1) and (5.2). The free motion responses have been obtained by replacing the R.H.S. of equations (5.1) and (5.2) with zeros while, the regular motion responses have been obtained using an excitation of the form

$$F_t(t) = 0.2 \sin (2.5\, t + \pi) \tag{6.1}$$

$$M_t(t) = 0.25 \sin (2.5\, t + \pi) \tag{6.2}$$

A comparison of the motion predictions using the actual and the predicted models for the ten cases has been conducted. The comparison between the actual and the predicted free motion responses is shown in Figures (J.1) and (J.20) as presented in Appendix J.

Figures (J.1) to (J.12) show the comparison between the predicted and the actual coupled free heave and pitch responses corresponding to Case studies: (1) to (6). It is shown in these figures that the agreement between the actual and the predicted responses is excellent. In general, the agreement between the predicted and the actual free heave responses, is better than that obtained for the predicted free pitch responses.

Figures (6.41) and (6.44) show the predicted and the actual free responses for heave and pitch, respectively corresponding to Cases (1) and (2). In these figures there are some disagreements between the responses for the last cycle in the signatures.

As the damping level increases, the agreement between the actual and the predicted free responses is still acceptable even with heavily damped cases such as Case (6). This result shows that an accurate free motion prediction can be obtained using the developed identification technique, RDLRNNT.

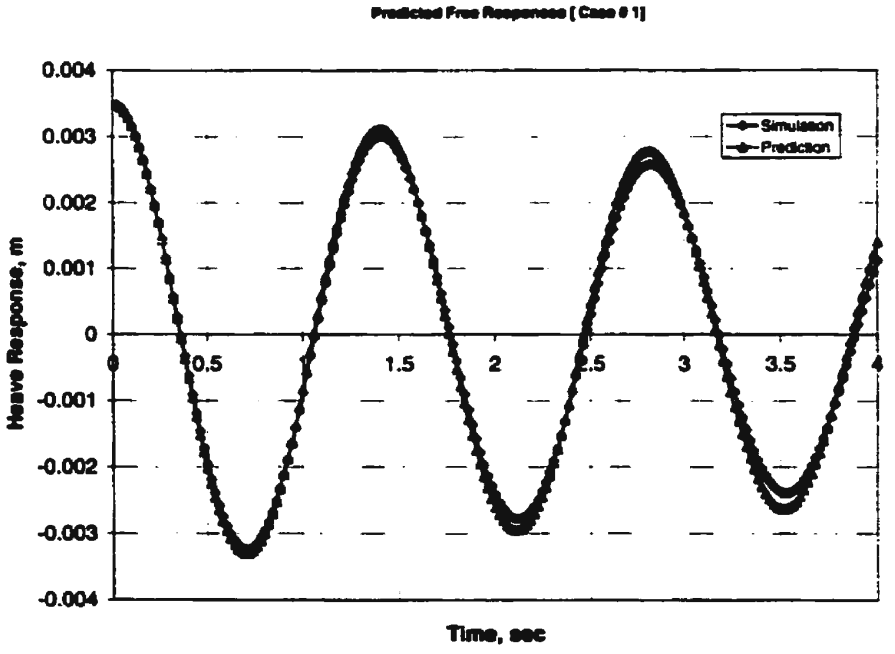

Figure 6.41 Comparison between the simulated and the predicted free responses for heave motion [Case # 1]

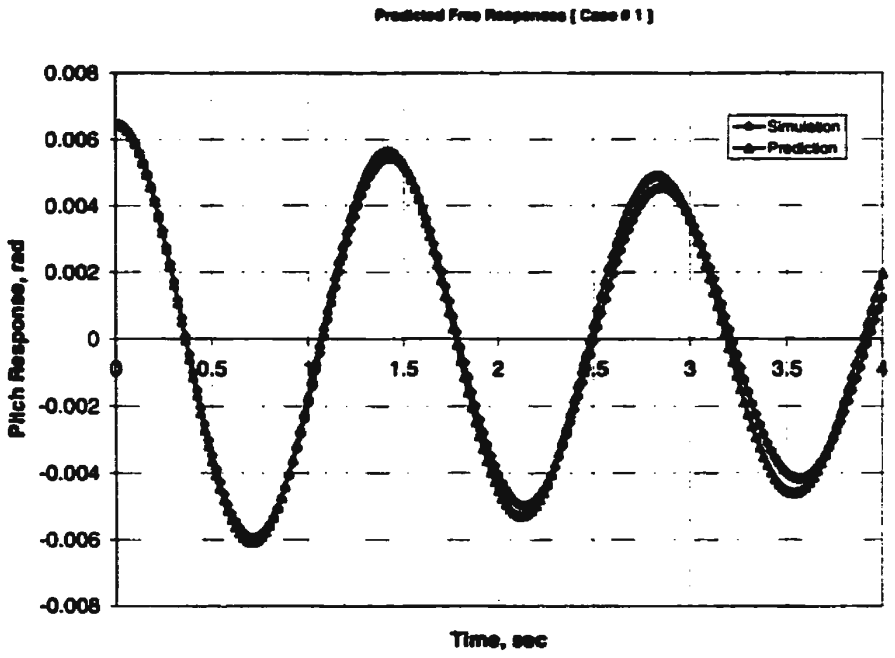

Figure 6.42 Comparison between the simulated and the predicted free responses for pitch motion [Case # 1]

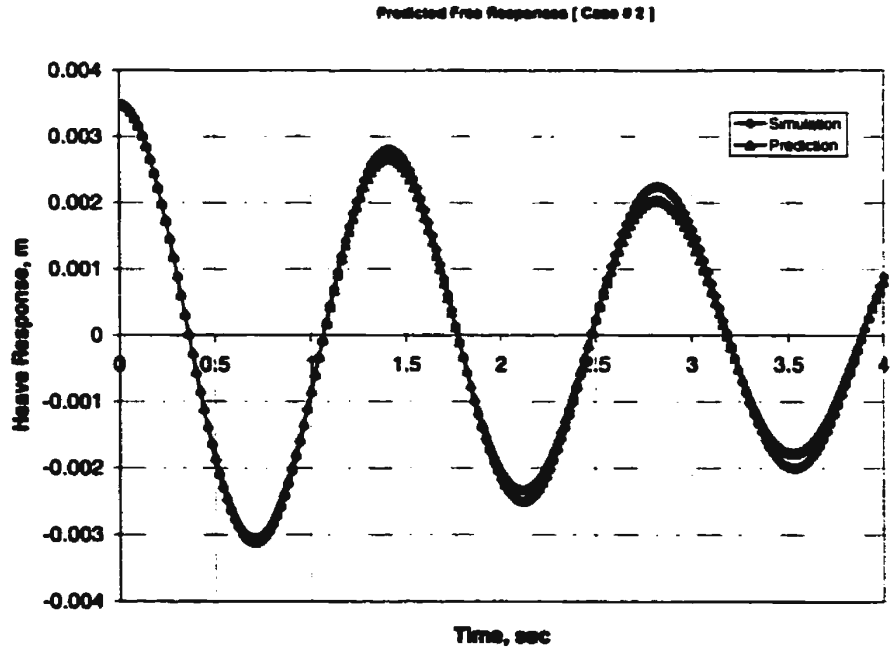

Figure 6.43 Comparison between the simulated and the predicted free responses for heave motion [Case # 2]

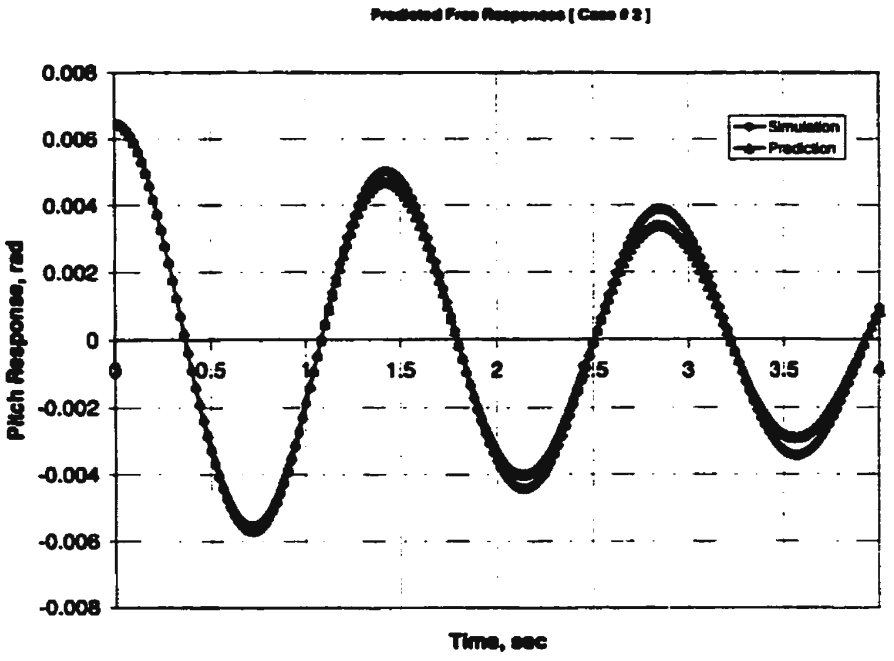

Figure 6.44 Comparison between the simulated and the predicted free responses for pitch motion [Case # 2]

The disagreement in Case (6) is mainly due to the high level of damping used in this case. This does not pose a major problem in the case of underwater vehicles. It is clear from results of the case studies that the measured damping parameters are smaller than those for which the random decrement ceases to be representative of the free motion of the vehicle.

Figures (J.13) to (J.20) show the comparisons between the predicted and the actual coupled free heave and pitch responses corresponding to Case studies (7) to (10). An example of the results is shown in Figures (6.45) to (6.48) for Cases (7) and (8). It is clear that the agreement between the predicted and the actual free coupled heave and pitch responses is excellent for Case (7) as shown in Figures (J.13) and (J.14).

As the difference between the exciting frequency and the natural frequency increases, the agreement deteriorates as shown in Figures (J.15) to (J.20). In addition, the

agreement for the predicted free heave responses is better than that obtained for the pitch responses. Moreover, the agreement for low damped natural frequencies is poor as shown in Figures (J.19) and (J.20) for Case (10).

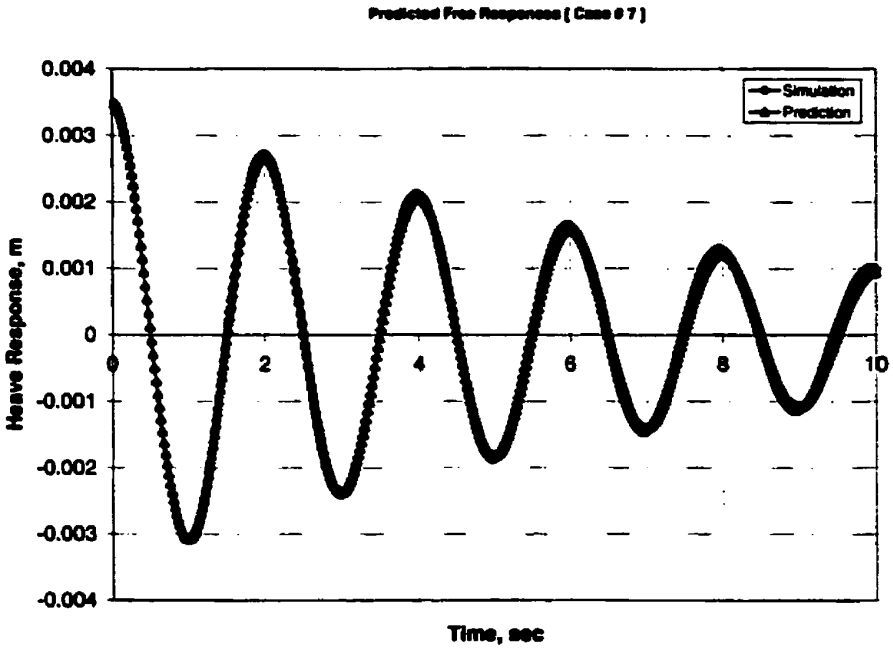

Figure 6.45 Comparison between the simulated and the predicted free responses for heave motion [Case # 7]

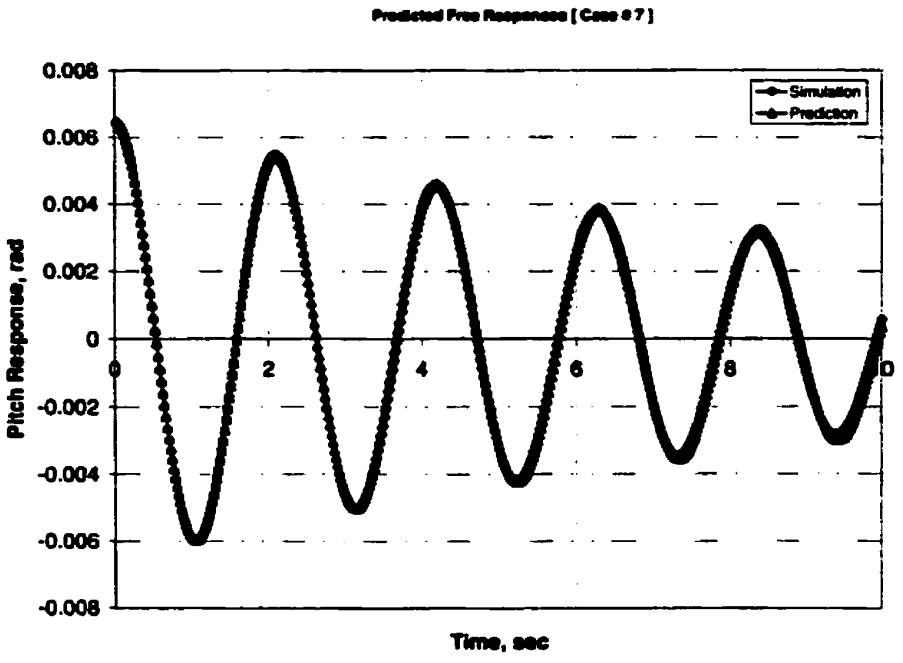

Figure 6.46 Comparison between the simulated and the predicted free responses for pitch motion [Case # 7]

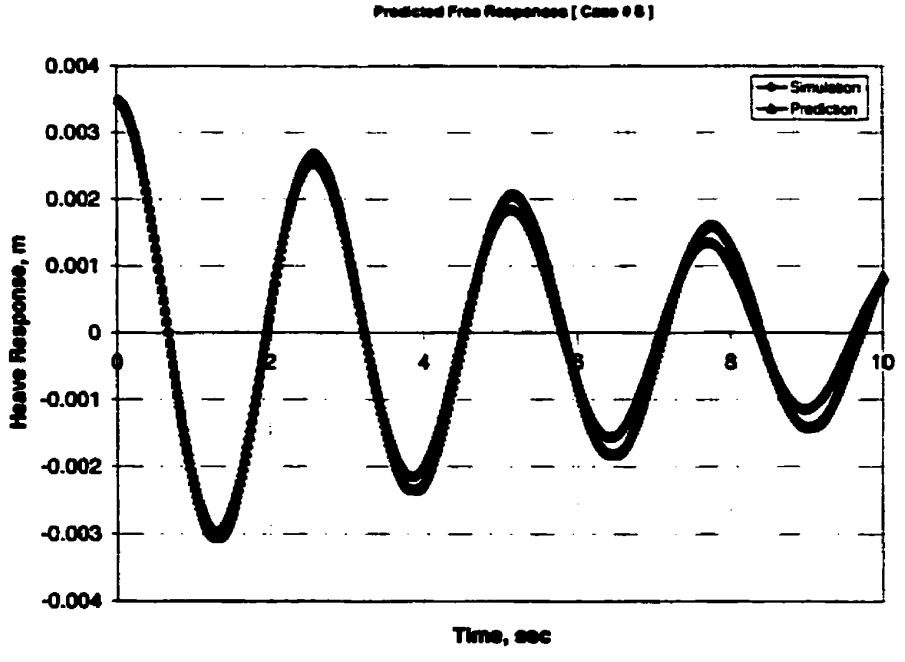

Figure 6.47 Comparison between the simulated and the predicted free responses for heave motion [Case # 8]

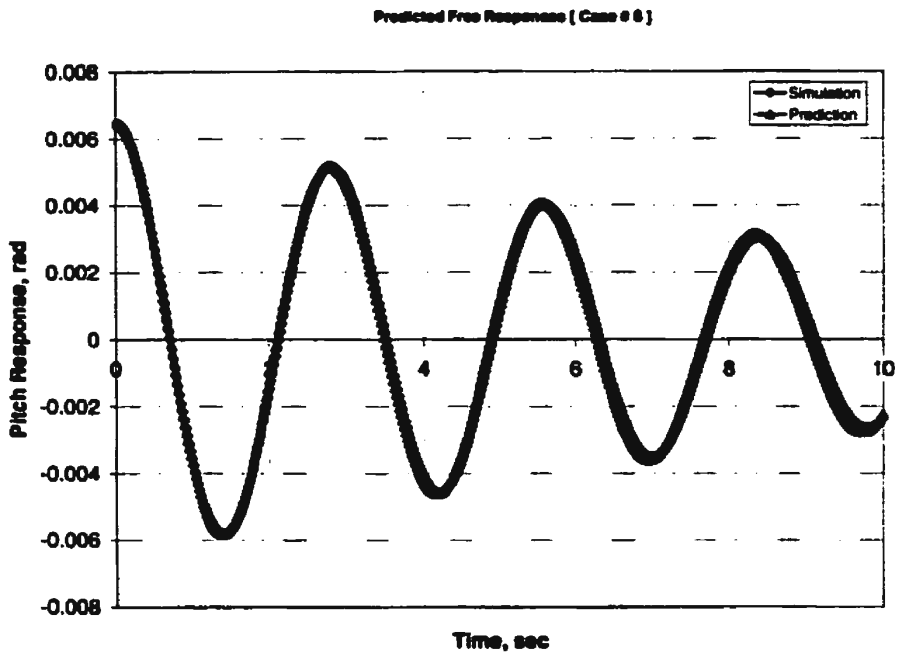

Figure 6.48 Comparison between the simulated and the predicted free responses for pitch motion [Case # 8]

It is clear from these results that the agreement between the actual and the predicted values for the damping and the restoring parameters is excellent. The agreement is not as good for the coupling parameters. However, the criterion should be whether the model yields accurate motion predictions. The predicted model was then used to generate the regular coupled heave and pitch motion responses. Results for the comparison of the predicted and the actual regular responses for the ten case studies are shown in Figures (K.1) to (K.20) as presented in Appendix K. An example of the results is shown in Figures (6.49) to (6.52) for Cases (1) and (2).

The agreement between the actual and the predicted regular responses is excellent for all case studies except for Cases (6) and (10), which represent a heavily damped system and a case in which the natural frequency is much smaller than the exciting

frequency, respectively. This was expected since the agreement between the random decrement and the free motion is poor in these two cases. In addition, the agreement between the random decrement signature and the auto-correlation function is not good. Good agreement between the actual and the predicted regular responses for all case studies (lightly and moderately damped levels) except in Cases (6) and (10). Table (6.1) shows the error percentages for the predicted heave and pitch motion amplitudes. It is obvious in the previous table that the coupled heave and pitch motions can be predicted accurately using the developed technique with 10% error percentage. This result shows the utility of the developed technique in the identification of the hydrodynamic parameters in the equations describing the coupled heave and pitch motion for an URV sailing near the sea surface in random seas.

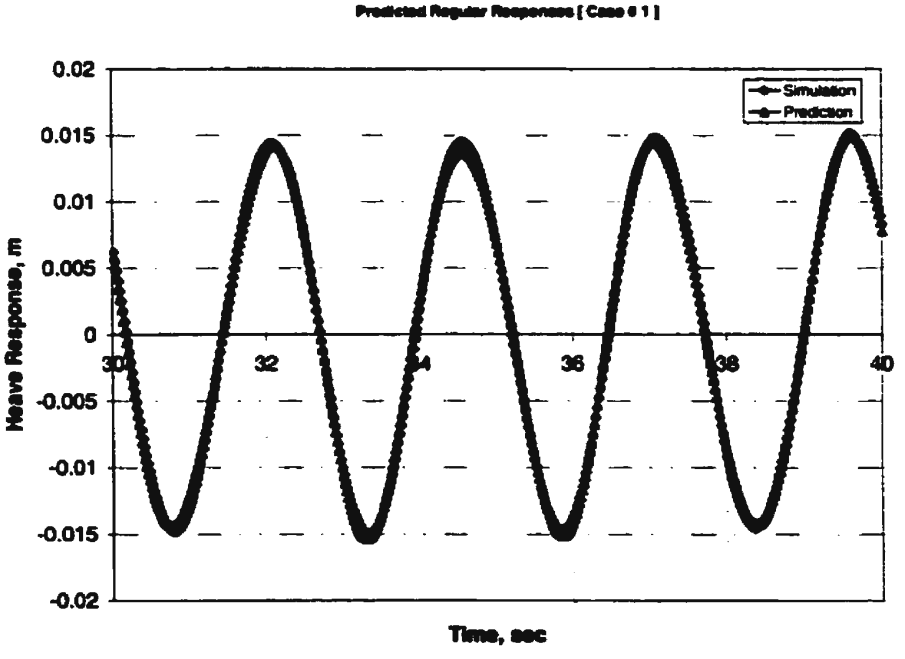

Figure 6.49 Comparison between the simulated and the predicted regular responses for heave motion [Case # 1]

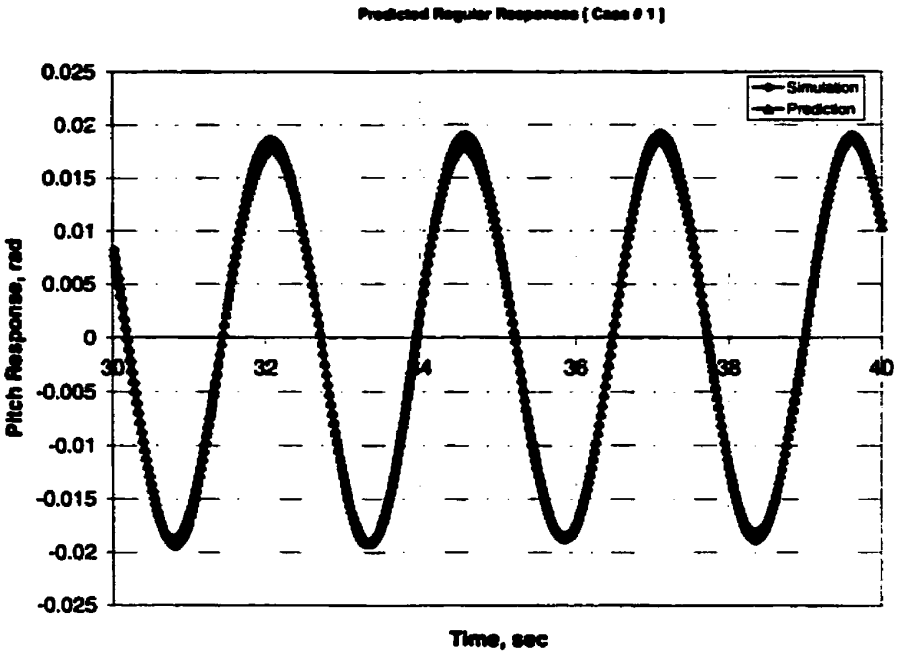

Figure 6.50 Comparison between the simulated and the predicted regular responses for pitch motion [Case # 1]

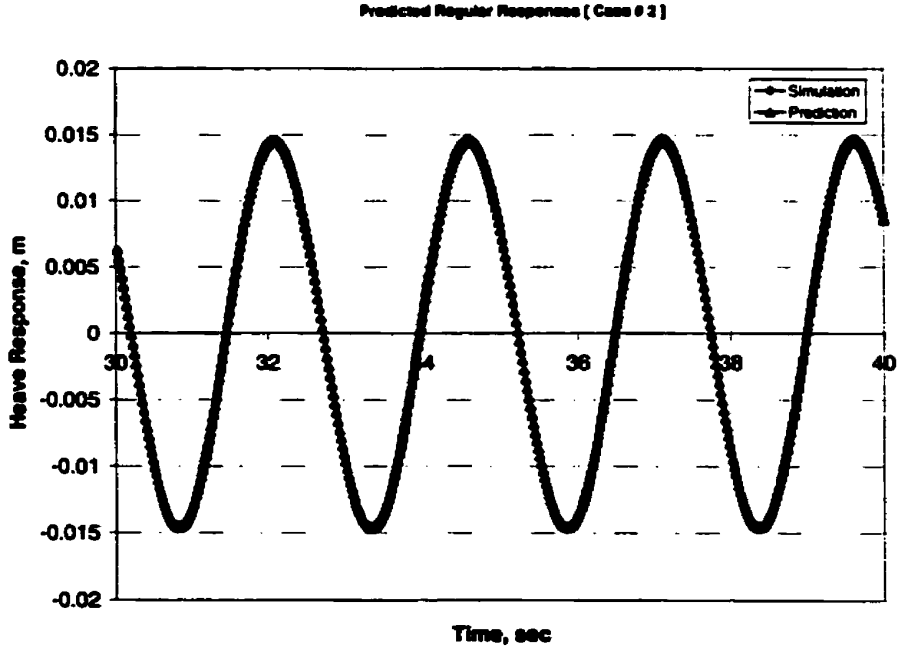

Figure 6.51 Comparison between the simulated and the predicted regular responses for heave motion [Case # 2]

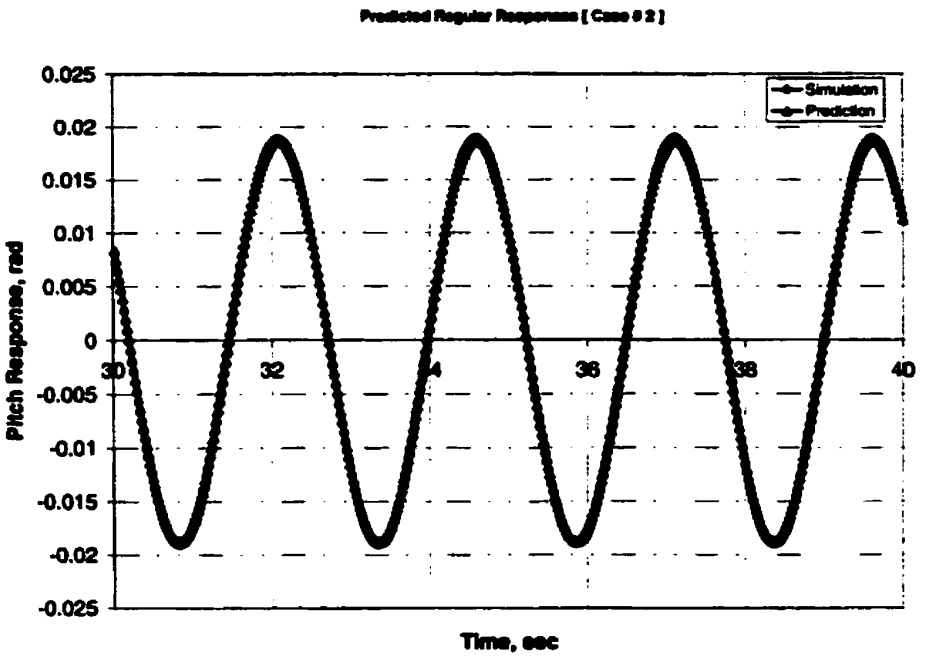

Figure 6.52 Comparison between the simulated and the predicted regular responses for pitch motion [Case # 2]

Table 6.1 Error percentages for the motion amplitudes

Case #	Heave Motion	Pitch Motion
1	4.80	5.30
2	0	0
3	2.70	2.60
4	2.00	4.80
5	2.10	2.30
6	7.30	9.30
7	0.95	0
8	7.80	0
9	3.60	6.80
10	0.85	9.20

6.1.2 Narrow-Band Excitations

Numerically generated random data for the coupled heave and pitch motions corresponding to narrow-band excitations are obtained using numerical integration for equations (5.1) and (5.2). The numerical integration of these equations has been done using a Runge-Kutta algorithm.

Case studies (1') to (6') are used in this section to ascertain the validity of the proposed identification technique for a narrow-band wave excitation. It has also been noticed that a good agreement between the random decrement signature and the free response is obtained when the natural frequency is near the wave modal frequency. In this case, the transient solution is strong. This result is clearly obvious in Figures (6.77) and (6.78) for Case (7').

The values of the predicted damping, restoring, and coupling parameters for Case (7') are very close to the actual values as shown in Tables (5.5) and (5.6). Similar agreement has been obtained between the actual free response and the predicted response using the developed technique as shown in Figures (6.95) and (6.96) for Case (7'). This result was expected since the damped natural frequency is close to the modal frequency of the excitation. In addition, the maximum energy content is distributed around the natural frequency. This result explains the appearance of the disagreement in other cases where the modal frequency is far from the natural frequency.

6.1.2.1 Effect of the Damping Level

It is obvious from Tables (5.5) and (5.6) that the first three Case studies: (1') to (3') were chosen similar to the first three cases in section (6.1.1). The main objective behind this is to test the effect of the identification technique on the form of the excitation. Numerically generated random data for coupled heave and pitch motions are obtained using the actual values of the parameters given in Tables (5.5) and (5.6).

The power spectral density functions for the heave and pitch motions are calculated for each case study as shown in Figures (6.53) to (6.58). Again, it can be seen from these figures that multiple peaks characterize the power spectral density functions. Two main peaks are significant: the first peak corresponds to the damped natural frequency, while the second corresponds to the modal frequency of the excitation. Moreover, the maximum energy contents in the motion spectra are distributed closely around the damped natural frequencies for heave and pitch motions.

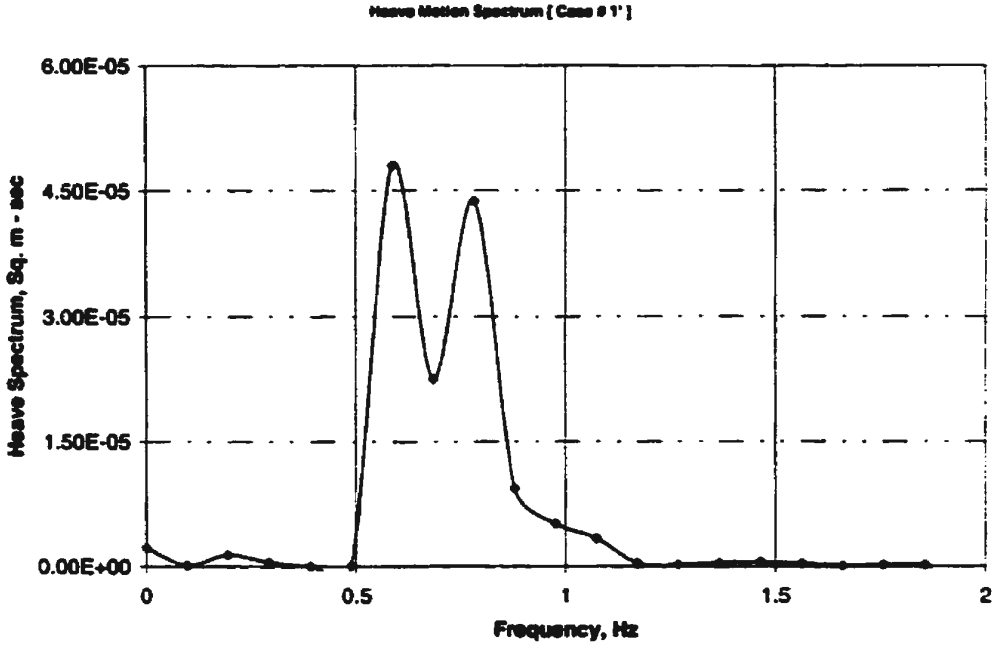

Figure 6.53 Power spectral density function for heave motion [Case # 1']

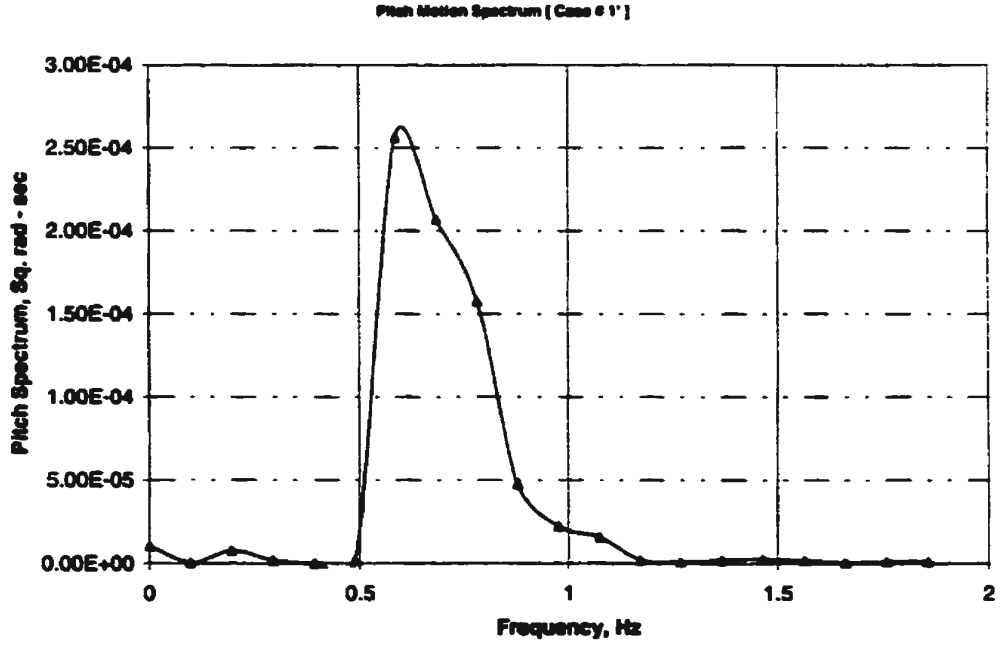

Figure 6.54 Power spectral density function for pitch motion [Case # 1']

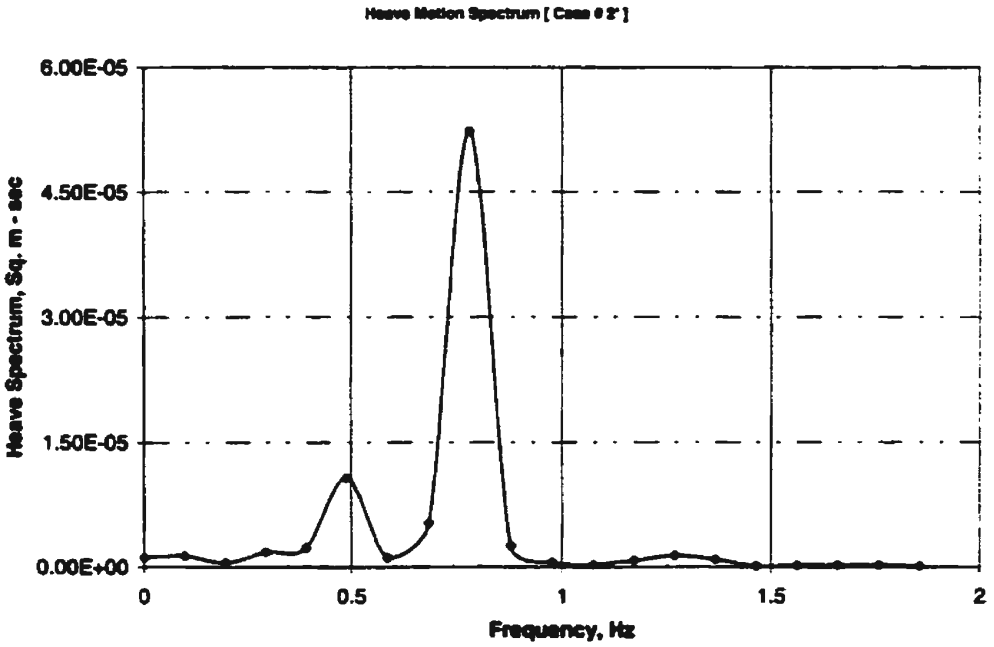

Figure 6.55 Power spectral density function for heave motion [Case # 2']

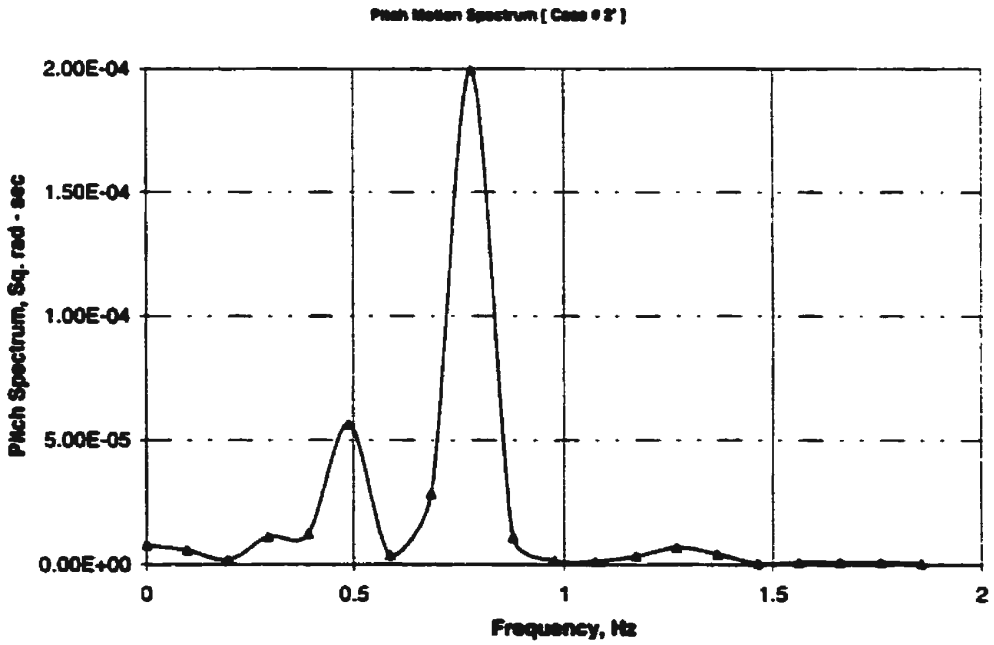

Figure 6.56 Power spectral density function for pitch motion [Case # 2']

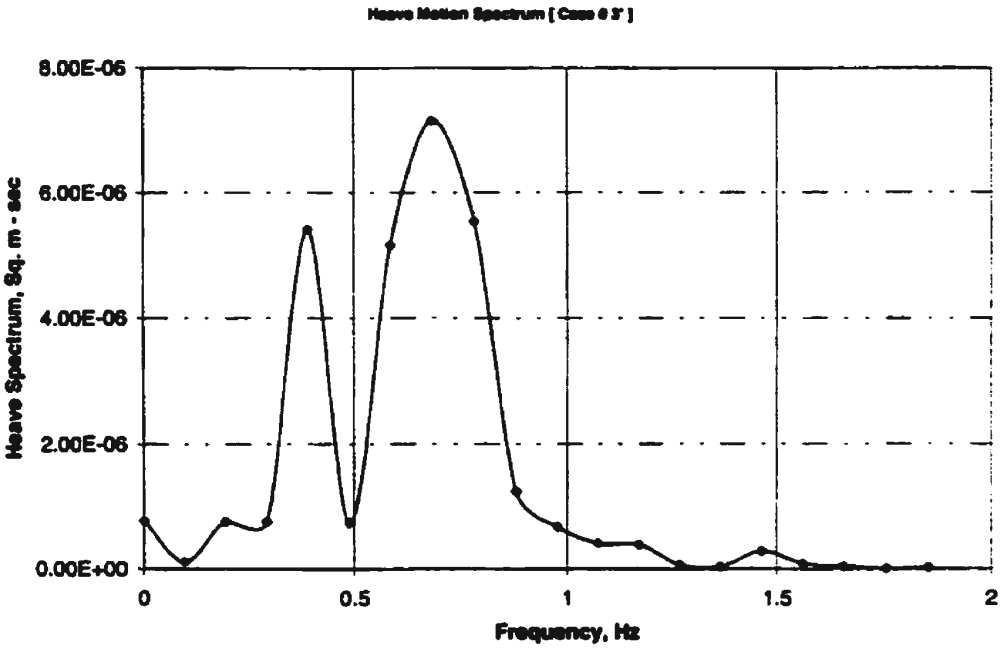

Figure 6.57 Power spectral density function for heave motion [Case # 3']

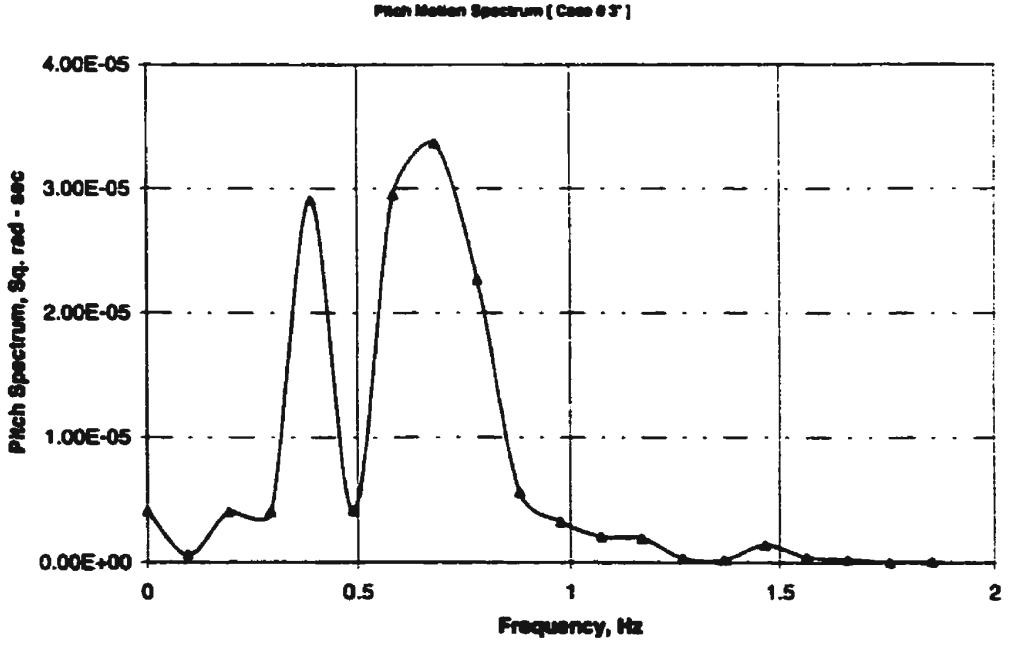

Figure 6.58 Power spectral density function for pitch motion [Case # 3']

The random decrement signatures have been obtained from the numerically generated random data for the coupled heave and pitch motions corresponding to the three case studies. In each case, a comparison between the random decrement and the free response has been made as shown in Figures (6.59) to (6.64). The main objective of this study is to investigate the utility of the developed technique for a wide range of damping levels for the coupled heave and pitch motions.

As the damping level increases, the agreement between the obtained random decrement signature and the free motion response deteriorates as seen in Figures (6.63) and (6.64) for Case (3').

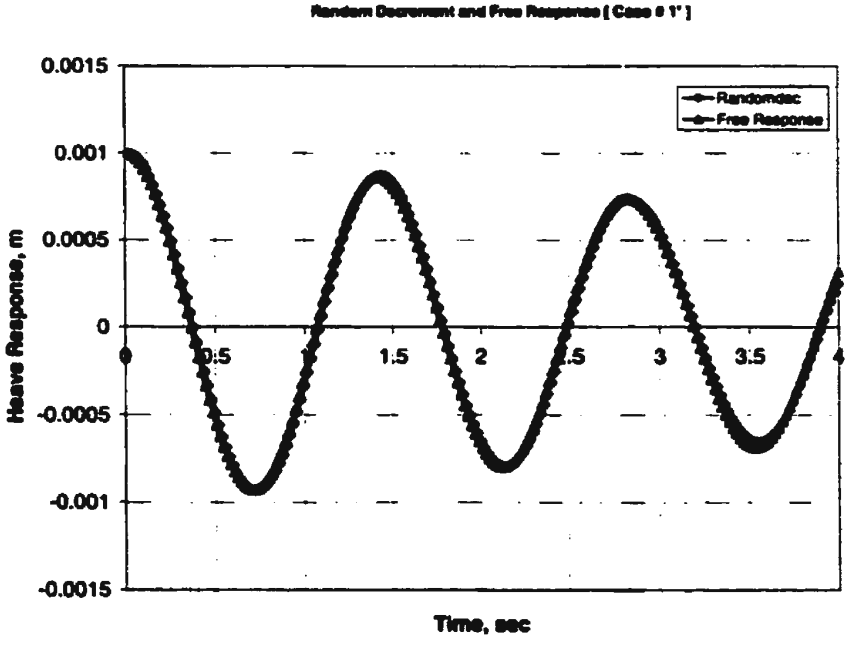

Figure 6.59 Comparison between the random decrement signature and the free response for heave motion [Case # 1']

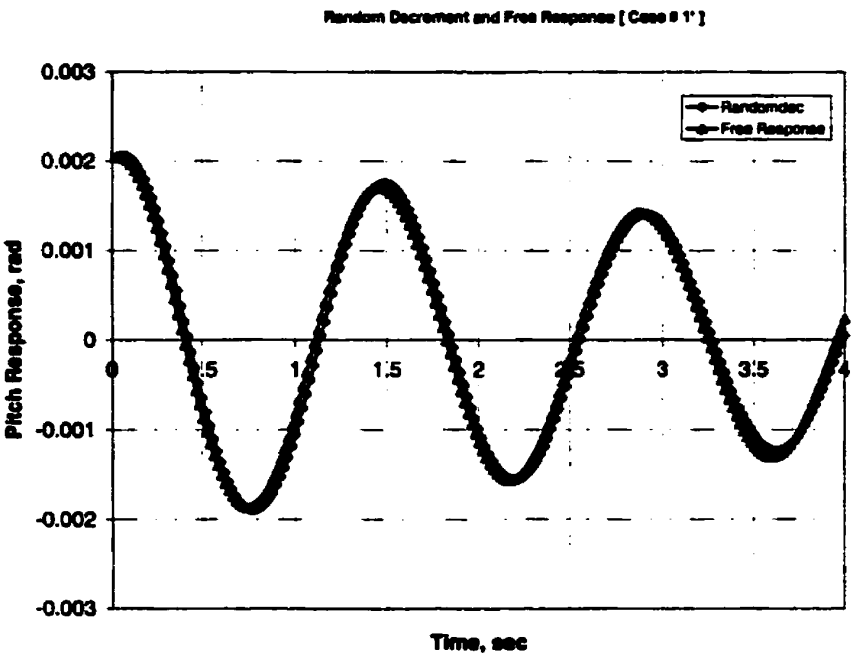

Figure 6.60 Comparison between the random decrement signature and the free response for pitch motion [Case # 1']

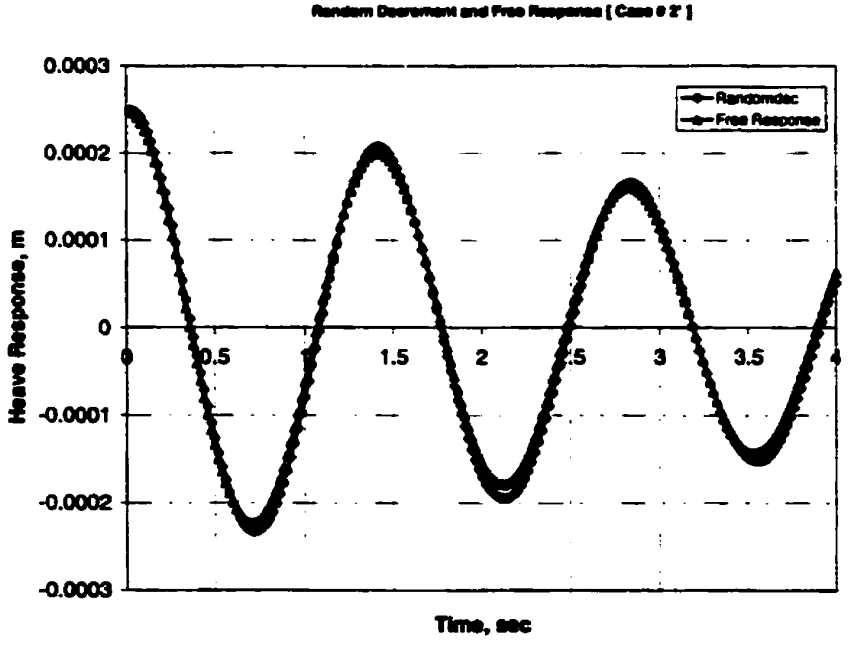

Figure 6.61 Comparison between the random decrement signature and the free response for heave motion [Case # 2']

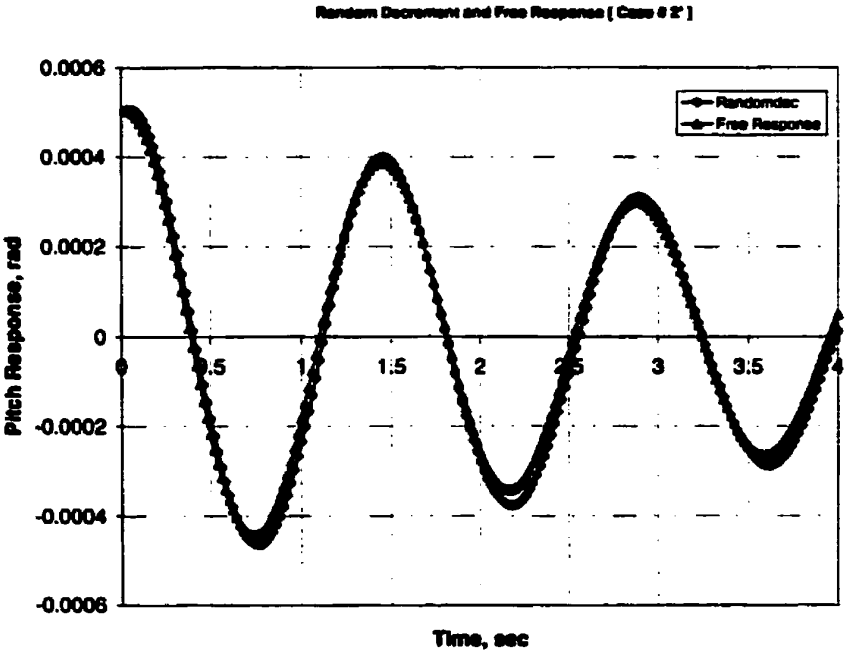

Figure 6.62 Comparison between the random decrement signature and the free response for pitch motion [Case # 2']

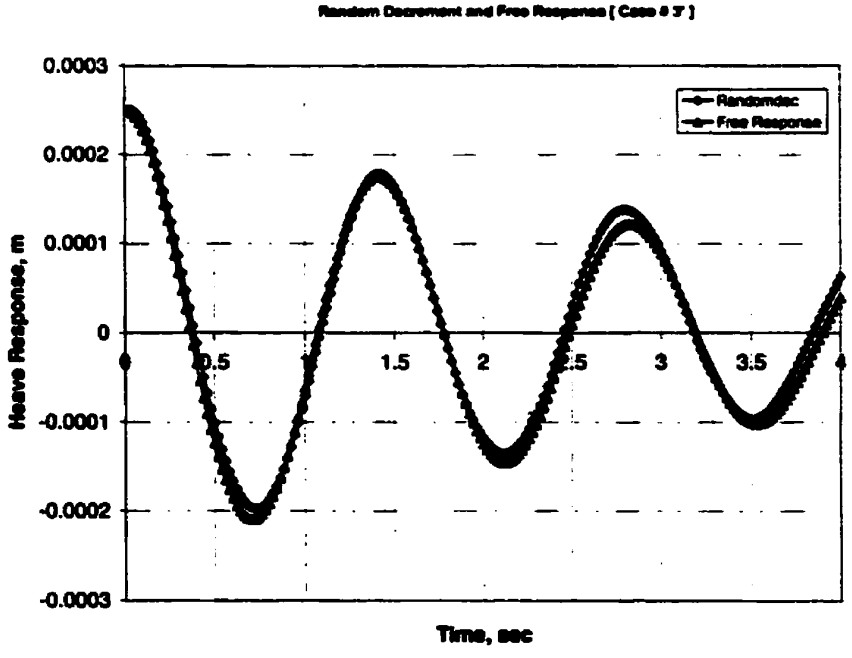

Figure 6.63 Comparison between the random decrement signature and the free response for heave motion [Case # 3']

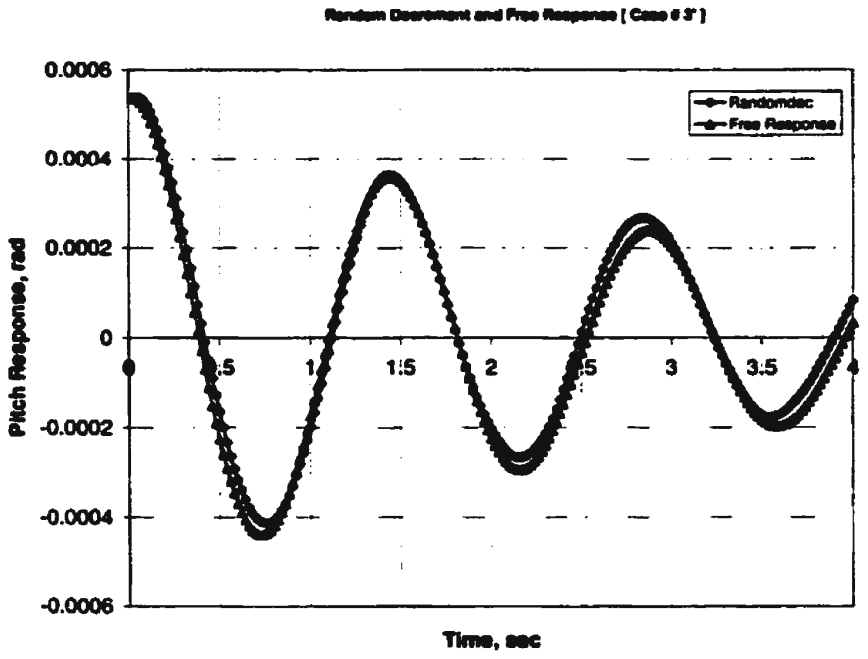

Figure 6.64 Comparison between the random decrement signature and the free response for pitch motion [Case # 3']

Another comparison has been made between the random decrement signatures and the auto-correlation functions for the heave and pitch motions. The comparison is shown in Figures (6.65) to (6.70). Similarly, as the damping increases, the agreement between the random decrement signature and the auto-correlation function deteriorates. This result can be seen from Figures (6.69) and (6.70) for Case (3').

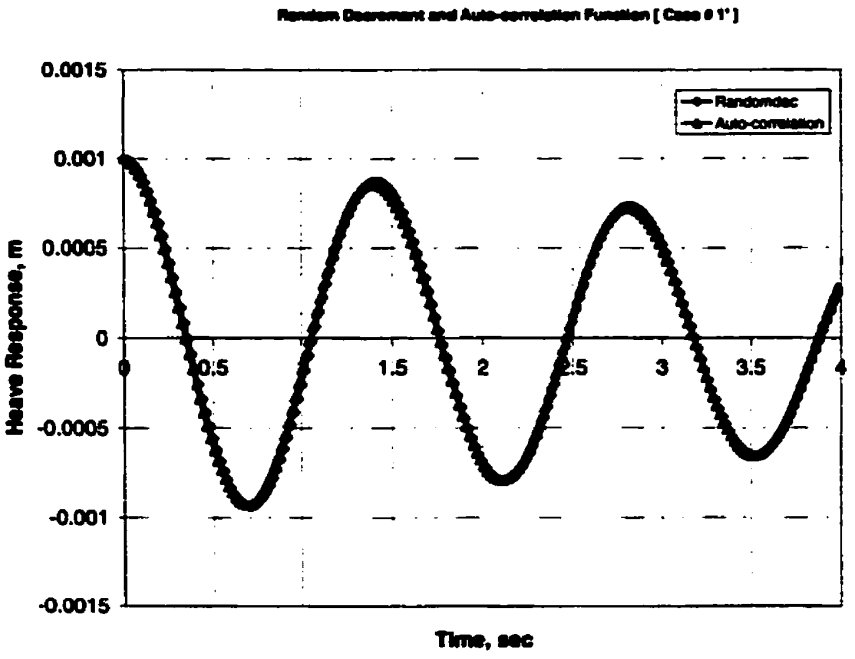

Figure 6.65 Comparison between the random decrement signature and the auto-correlation function for heave motion [Case # 1']

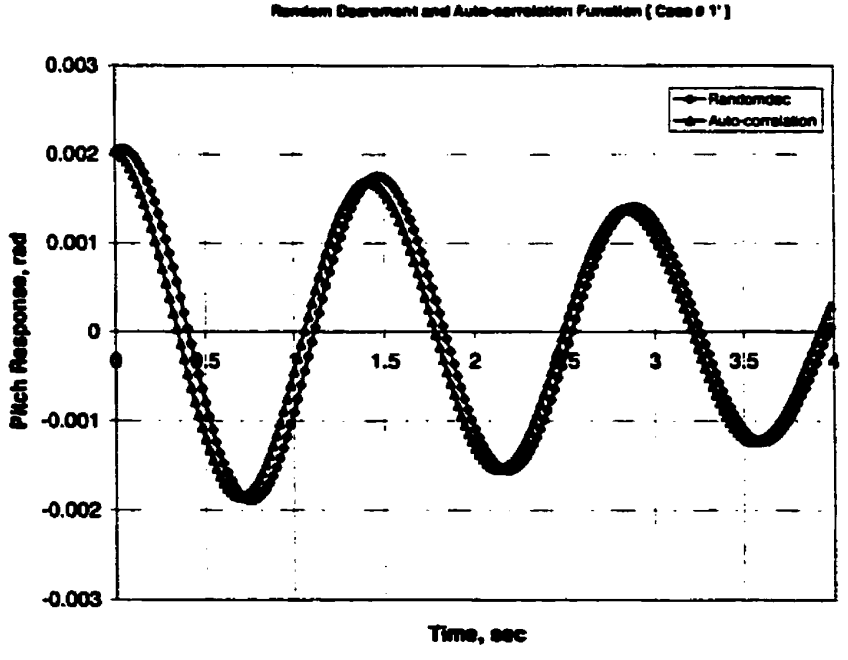

Figure 6.66 Comparison between the random decrement signature and the auto-correlation function for pitch motion [Case # 1']

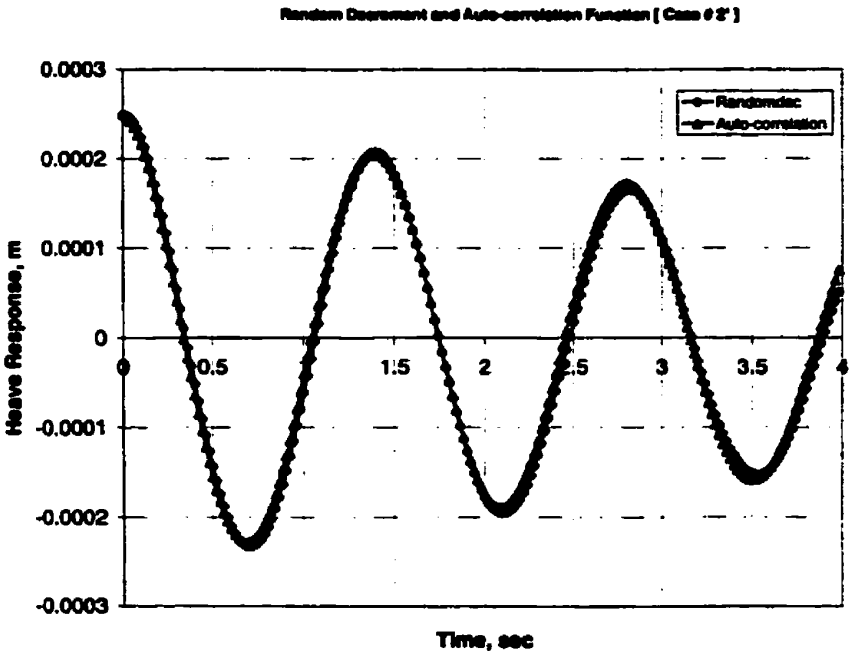

Figure 6.67 Comparison between the random decrement signature and the auto-correlation function for heave motion [Case # 2']

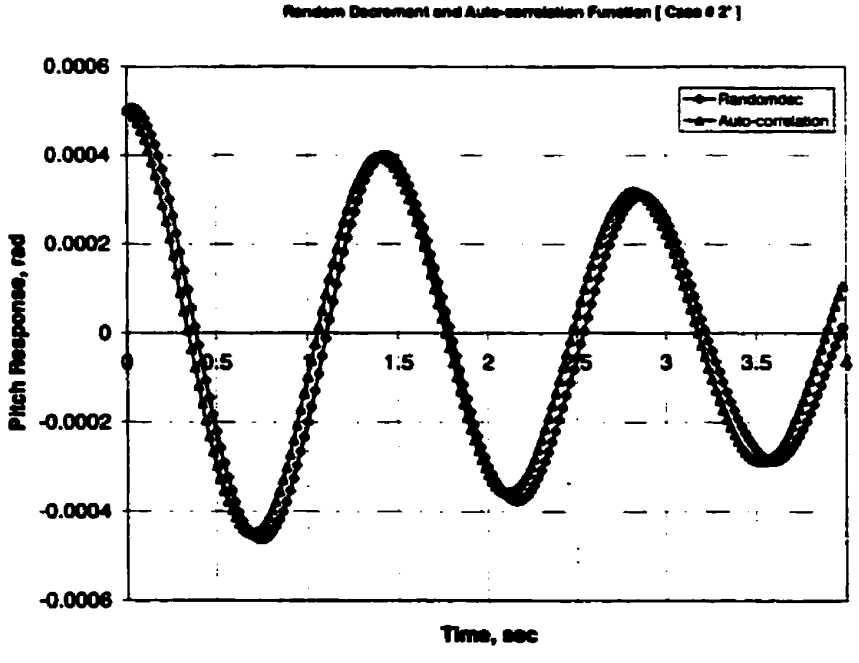

Figure 6.68 Comparison between the random decrement signature and the auto-correlation function for pitch motion [Case # 2']

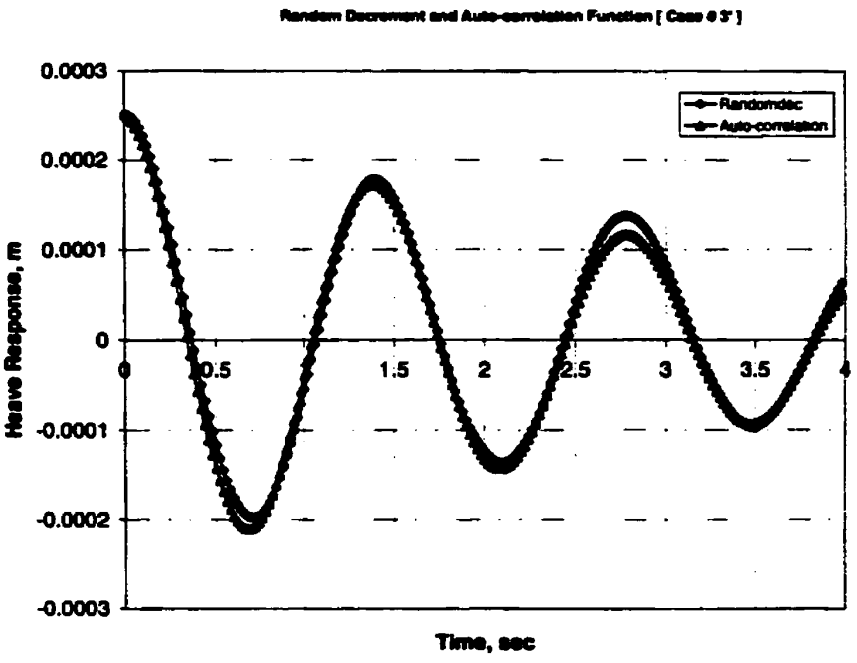

Figure 6.69 Comparison between the random decrement signature and the auto-correlation function for heave motion [Case # 3']

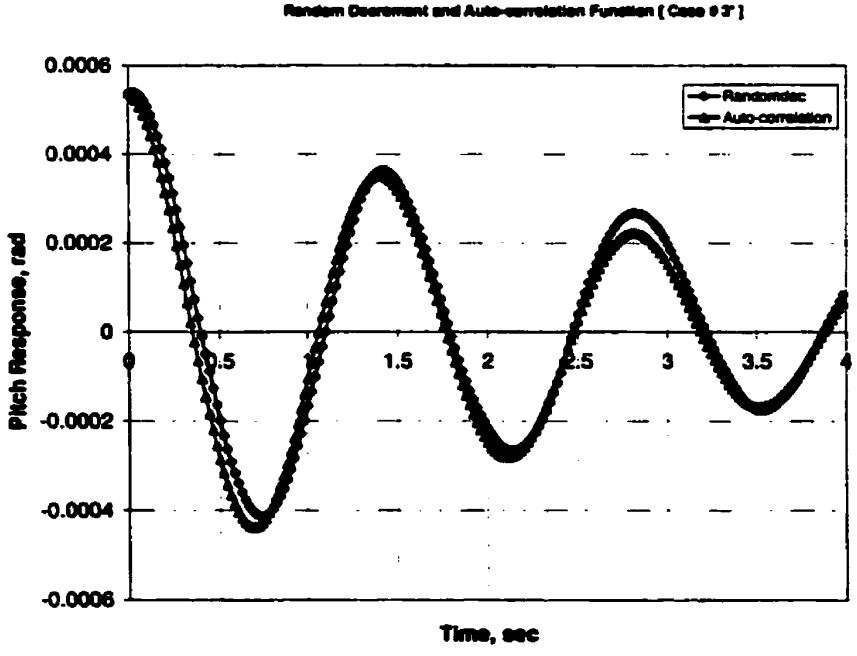

Figure 6.70 Comparison between the random decrement signature and the auto-correlation function for pitch motion [Case # 3']

6.1.2.2 Effect of the Damped Natural Frequency

The last three cases in Tables (5.5) and (5.6): (7') to (9') are chosen similar to Cases: (7) to (9) in section (6.1.1). The main objective of this part of the study is to test the dependency of the identification technique on the excitation forms. Numerical random data for coupled heave and pitch motions are generated using the actual values of the parameters for Cases: (7') to (9') as given in Tables (5.5) and (5.6).

The power spectral density functions corresponding to the random time series for the coupled heave and pitch motions are calculated for each case study as shown in Figures (6.71) to (6.76). It can be seen from these figures that well-separated peaks characterize the power spectral density functions. It is clear in these figures that the maximum energy content in the heave and pitch motion spectra are distributed around the damped natural frequencies in heave and pitch.

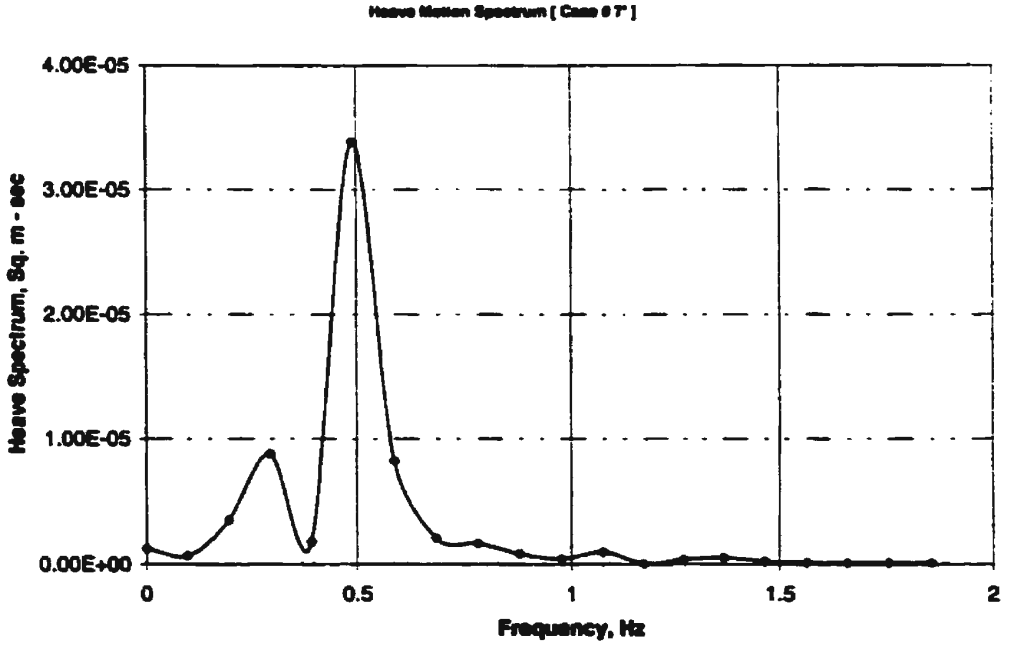

Figure 6.71 Power spectral density function for heave motion [Case # 7']

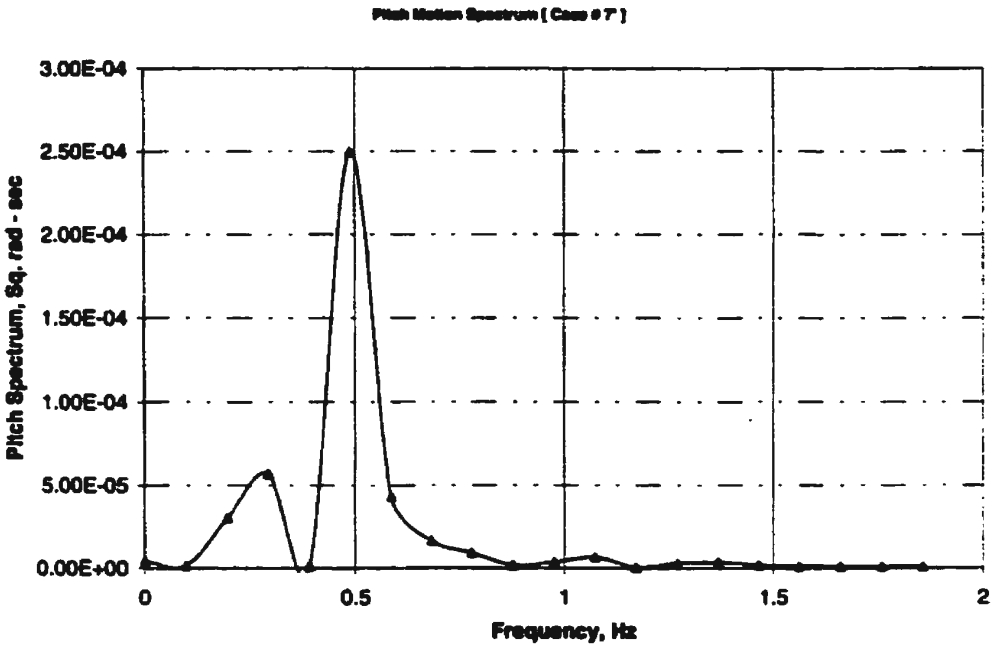

Figure 6.72 Power spectral density function for pitch motion [Case # 7']

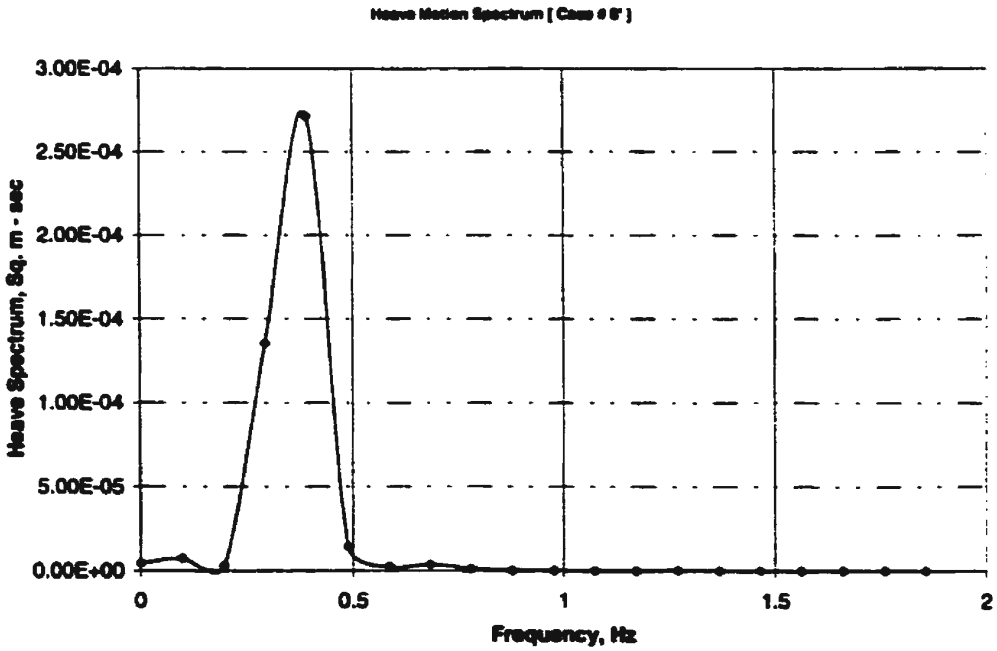

Figure 6.73 Power spectral density function for heave motion [Case # 8']

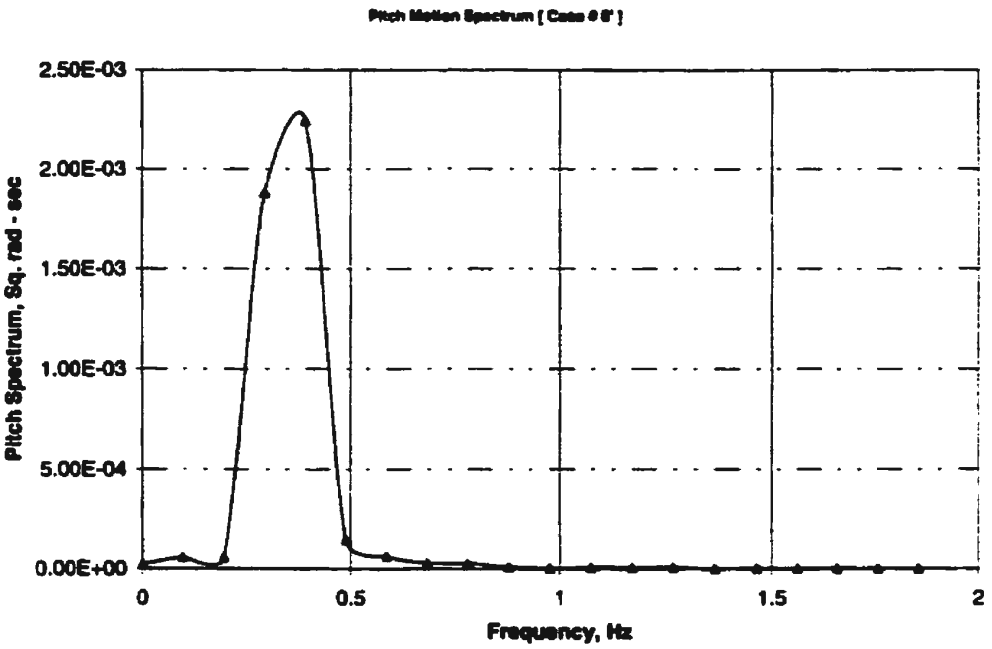

Figure 6.74 Power spectral density function for pitch motion [Case # 8']

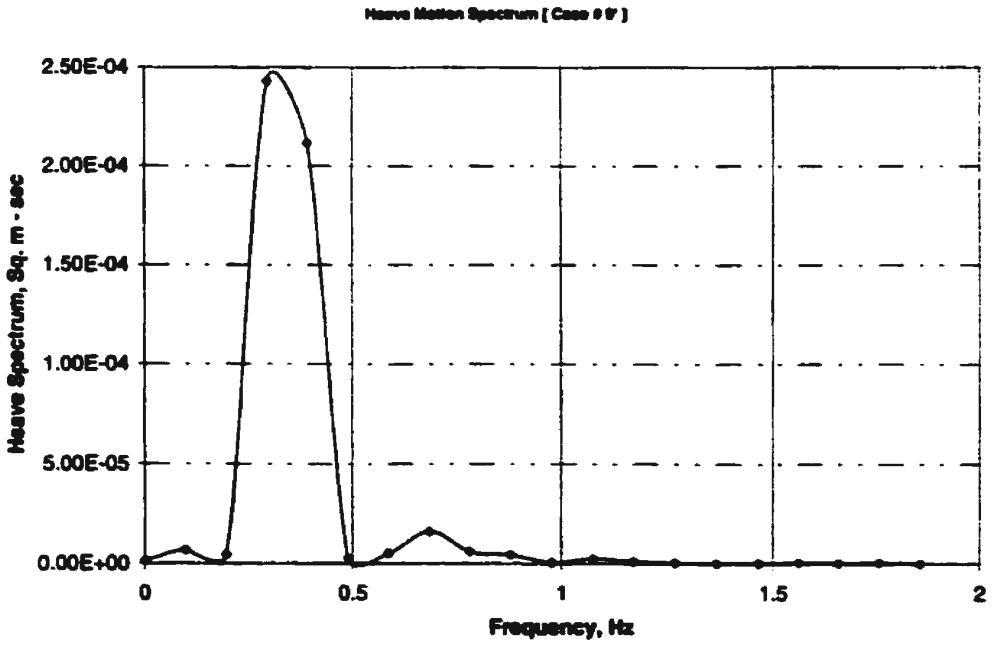

Figure 6.75 Power spectral density function for heave motion [Case # 9']

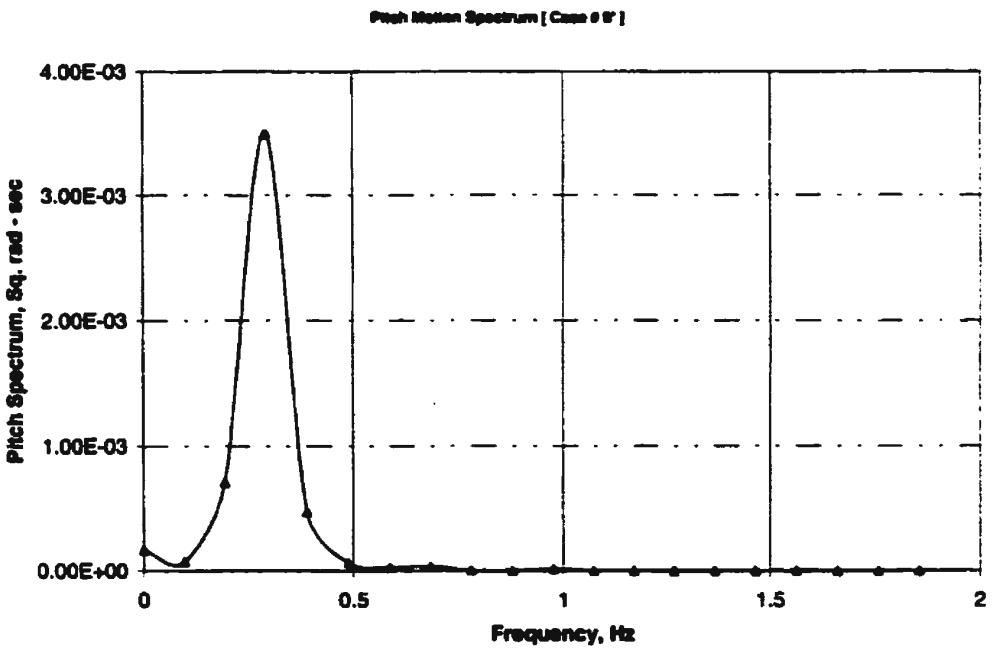

Figure 6.76 Power spectral density function for pitch motion [Case # 9']

A comparison between the random decrement and the free response has been made as shown in Figures (6.77) to (6.82). The main objective of studying these cases is to validate the developed technique for different values of the damped natural frequency. As the difference between the exciting frequency and the damped natural frequency increases, the agreement between the random decrement signature and the predicted free response deteriorates. The disagreement appears in the comparison for the pitch motion for Case (8') and become significant in both heave and pitch motions for Case (9') as shown in Figure (6.80) and Figures (6.81) and (6.82), respectively.

From the above discussion it can seen that the agreement as the damping level increases and that as the difference between the exciting frequency and the natural frequency increases, that the accuracy of using the developed technique in the identification of the parameters decreases.

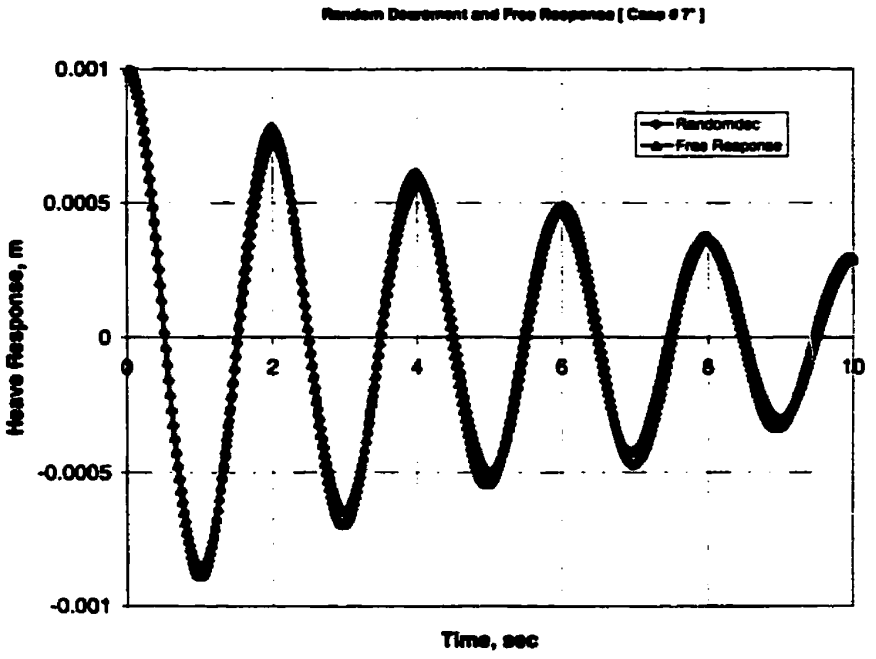

Figure 6.77 Comparison between the random decrement signature and the free response for heave motion [Case # 7']

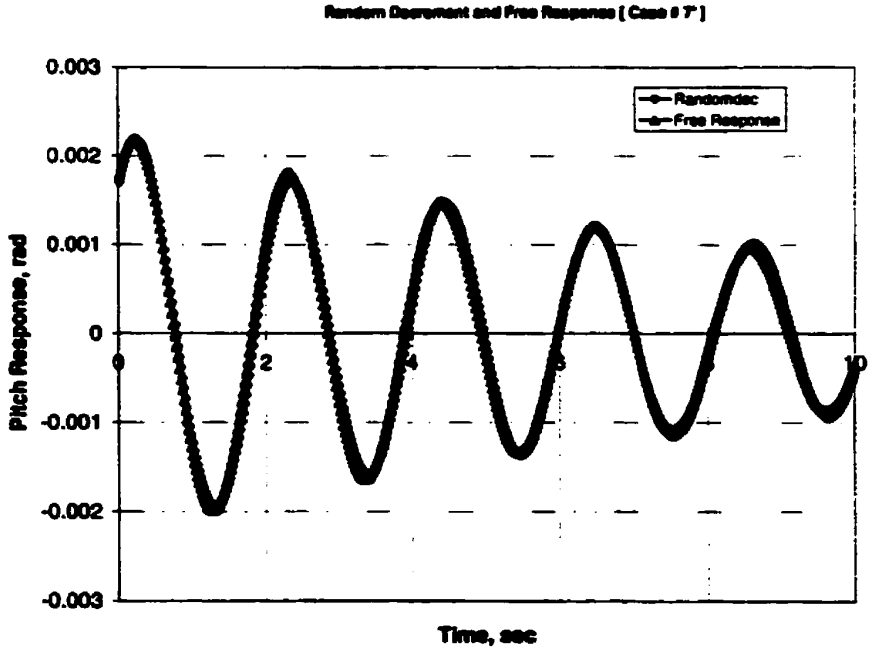

Figure 6.78 Comparison between the random decrement signature and the free response for pitch motion [Case # 7']

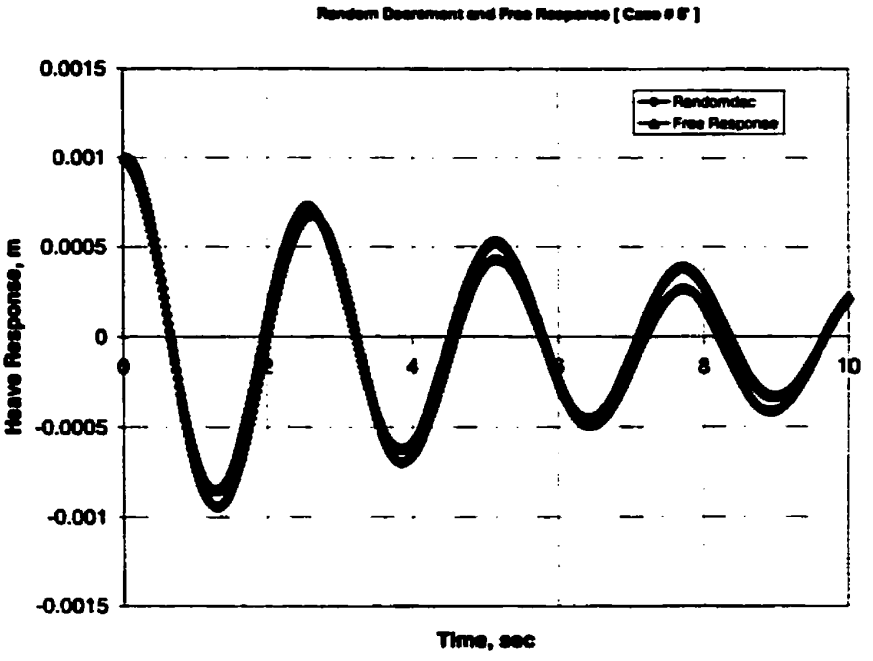

Figure 6.79 Comparison between the random decrement signature and the free response for heave motion [Case # 8']

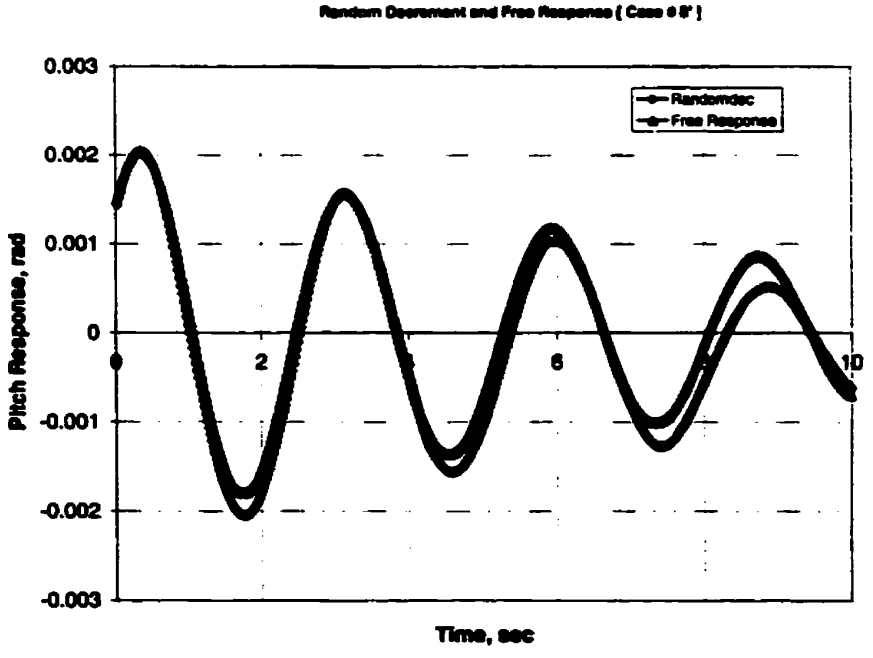

Figure 6.80 Comparison between the random decrement signature and the free response for pitch motion [Case # 8']

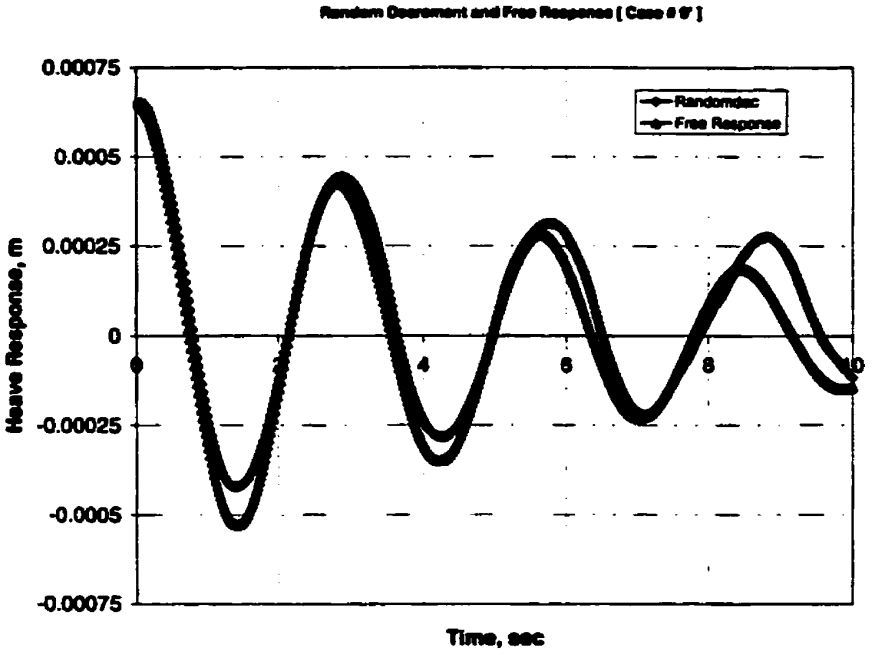

Figure 6.81 Comparison between the random decrement signature and the free response for heave motion [Case # 9']

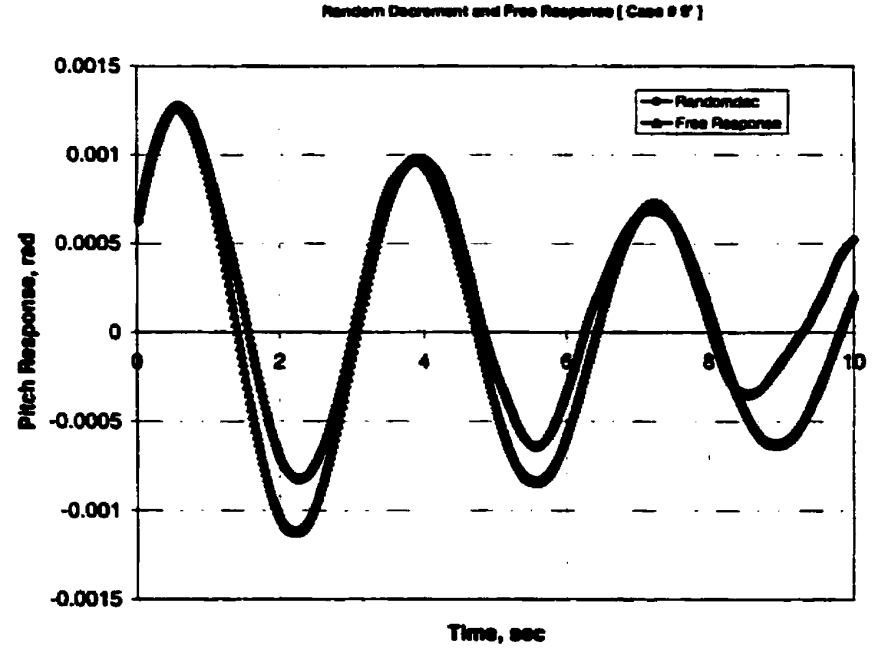

Figure 6.82 Comparison between the random decrement signature and the free response for pitch motion [Case # 9']

Also, a comparison between the random decrement signatures and the auto-correlation functions for the heave and pitch motions, has been made. The comparison is shown in Figures (6.83) to (6.88). As the damping increases, the agreement between the random decrement signature and the auto-correlation function deteriorates. This result is seen from Figures (6.84), (6.86), and (6.88) for pitch motion. The agreement is not as good for Case (9'), where the damped natural frequency is very low.

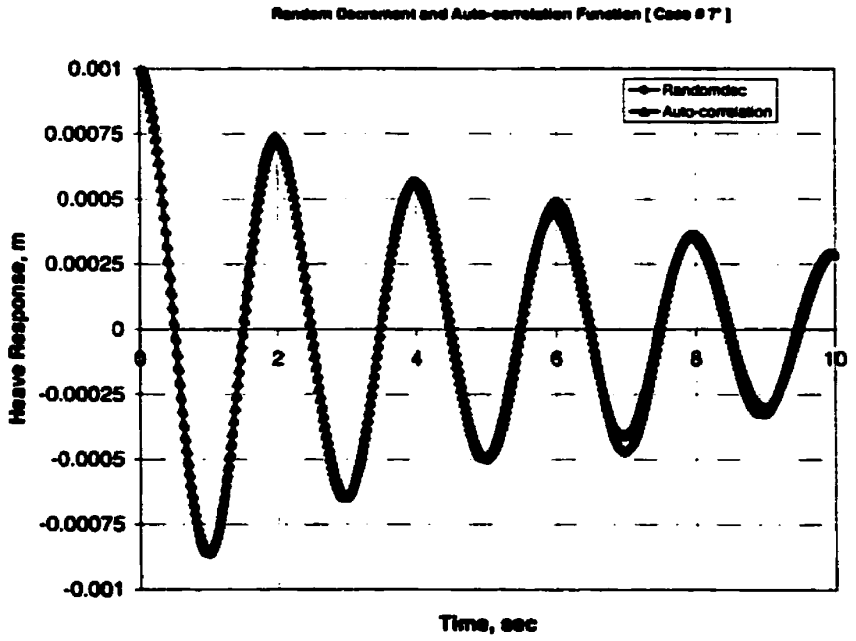

Figure 6.83 Comparison between the random decrement signature and the auto-correlation function for heave motion [Case # 7']

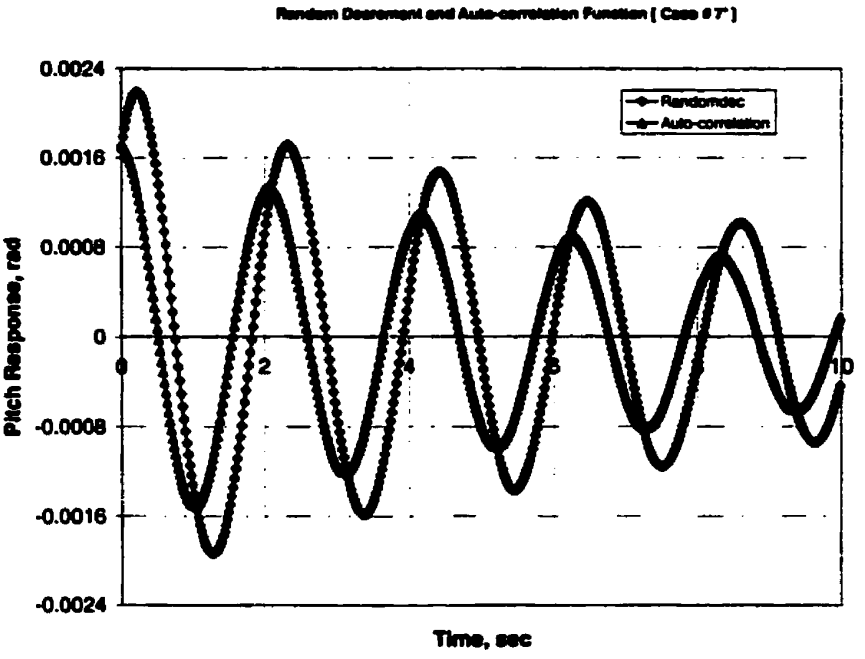

Figure 6.84 Comparison between the random decrement signature and the auto-correlation function for pitch motion [Case # 7']

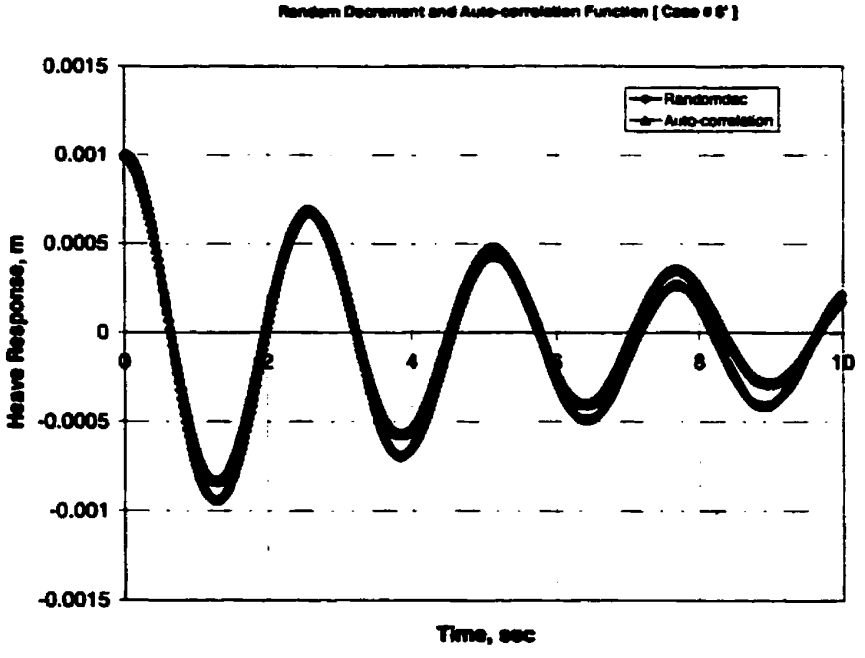

Figure 6.85 Comparison between the random decrement signature and the auto-correlation function for heave motion [Case # 8']

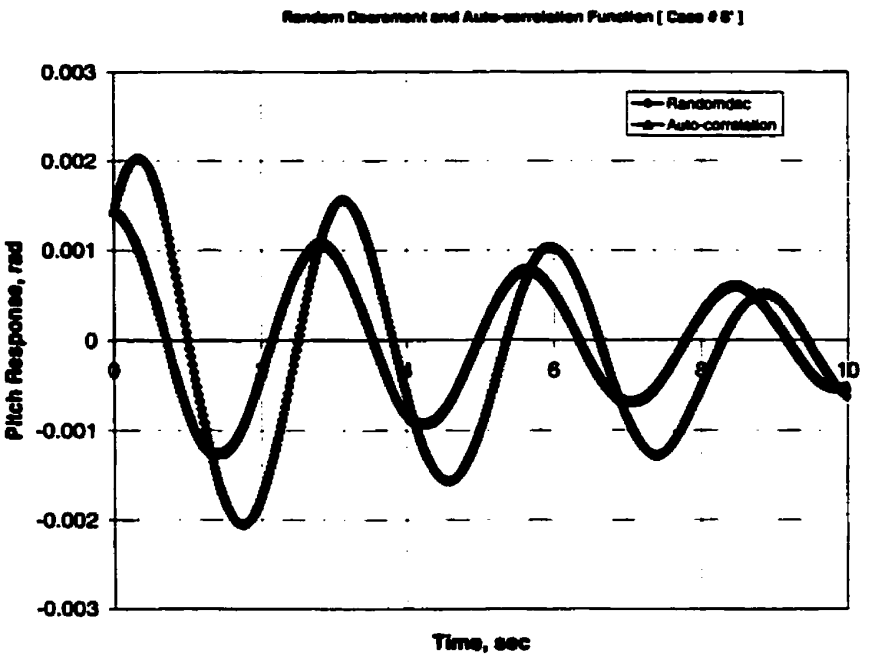

Figure 6.86 Comparison between the random decrement signature and the auto-correlation function for pitch motion [Case # 8']

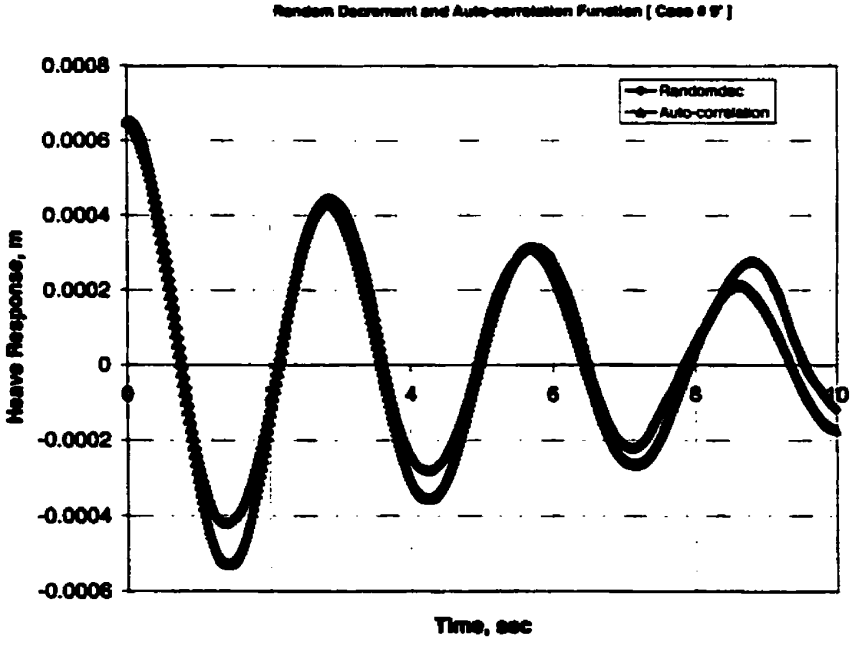

Figure 6.87 Comparison between the random decrement signature and the auto-correlation function for heave motion [Case # 9']

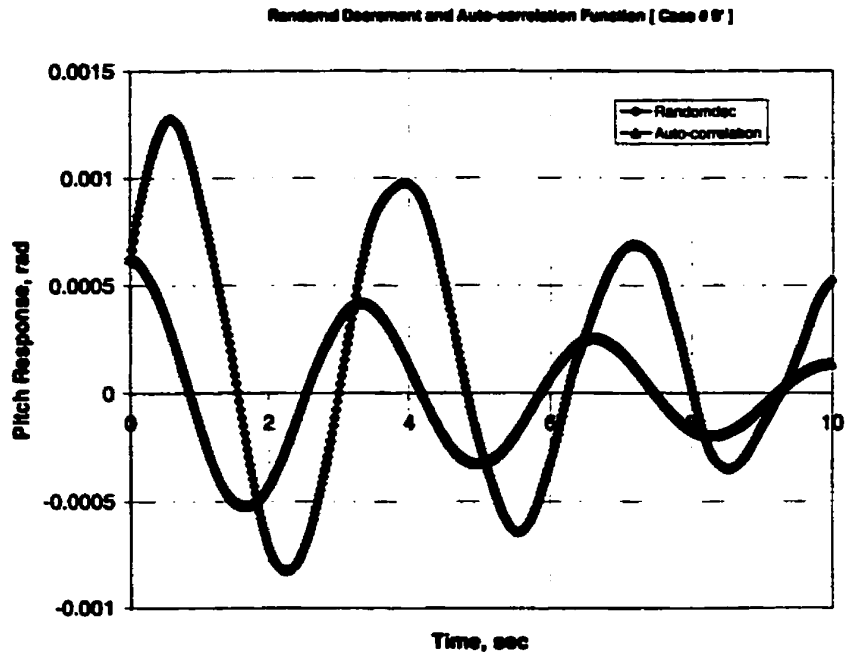

Figure 6.88 Comparison between the random decrement signature and the auto-correlation function for pitch motion [Case # 9']

6.1.2.3 Motion Prediction

Since there is some disagreements between the random decrement signature and the free response, and also between the random decrement signature and the auto-correlation function, the actual model and the predicted one in Tables (5.5) and (5.6) are substituted back in equations (5.1) and (5.2) to generate motion predictions. A comparison between the actual and the predicted free response is conducted. Results for this comparison are shown in Figures (6.89) to (6.94), and Figures (6.95) to (6.100) for Cases (1') to (3') and Cases (7') to (9'), respectively.

Although the damping level increases, the agreement between the actual and the predicted free responses is still excellent as shown in Figures (6.93) and (6.94) for Case

(3'). As the difference between the exciting frequency and the natural frequency increases, the agreement between the predicted free responses deteriorates as shown in Figures (6.99) and (6.100) for Case (9').

I can conclude from the above discussion that the accuracy of using the developed technique in the identification of the parameters in the equations describing the coupled heave and pitch motions for an URV is affected significantly with the increase in the difference between the exciting frequency and the natural frequency.

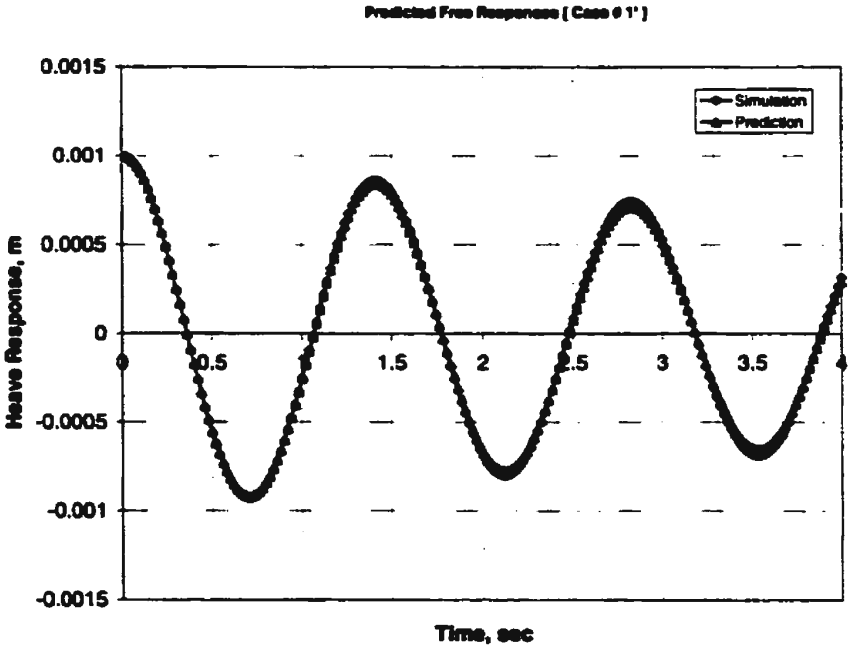

Figure 6.89 Comparison between the simulated and the predicted free responses for heave motion [Case # 1']

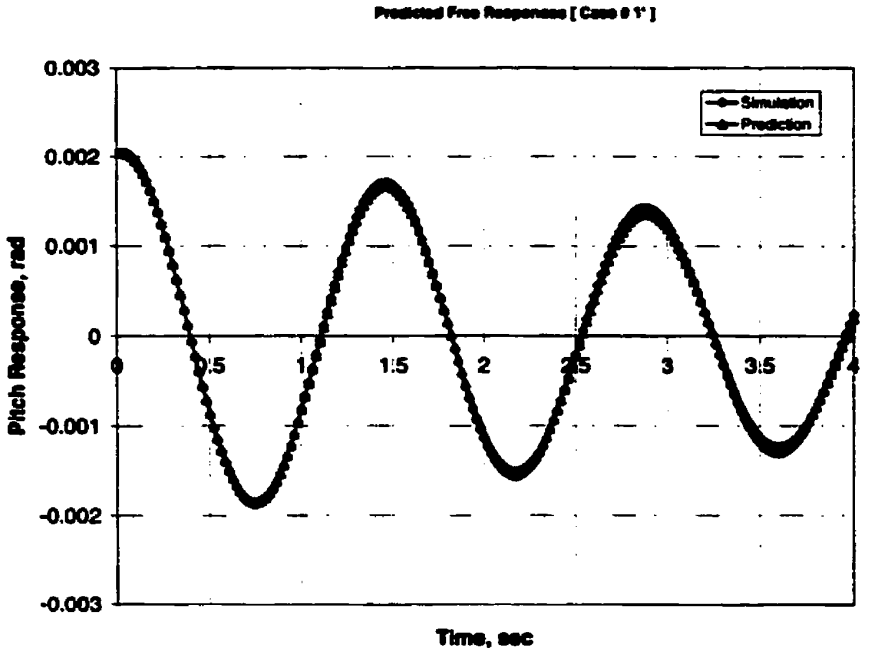

Figure 6.90 Comparison between the simulated and the predicted free responses for pitch motion [Case # 1']

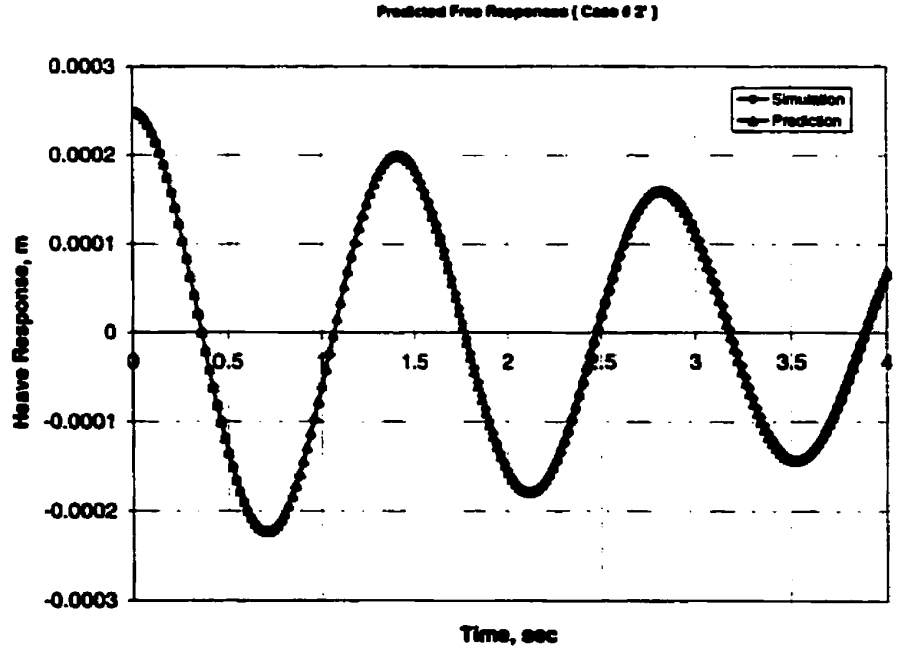

Figure 6.91 Comparison between the simulated and the predicted free responses for heave motion [Case # 2']

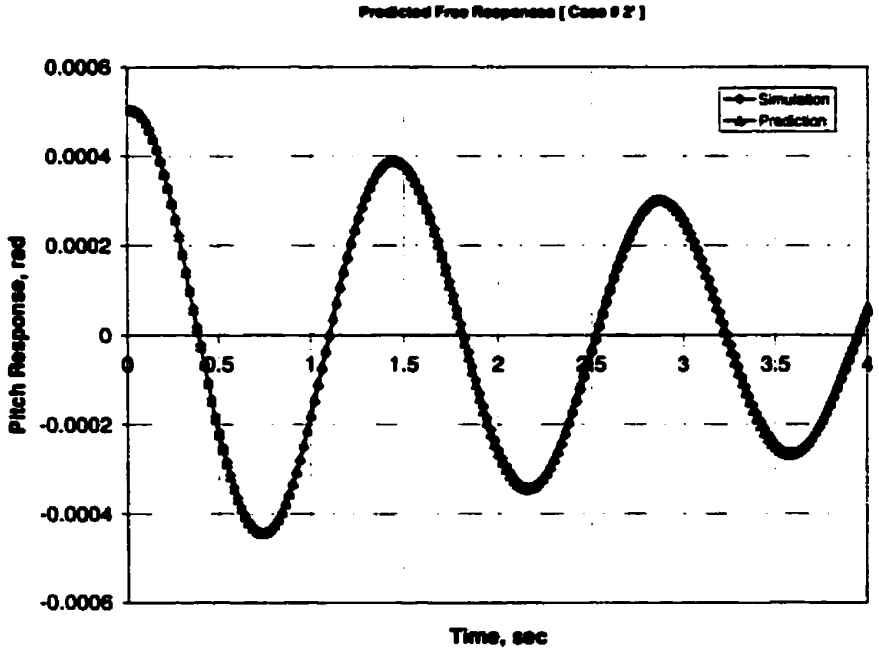

Figure 6.92 Comparison between the simulated and the predicted free responses for pitch motion [Case # 2']

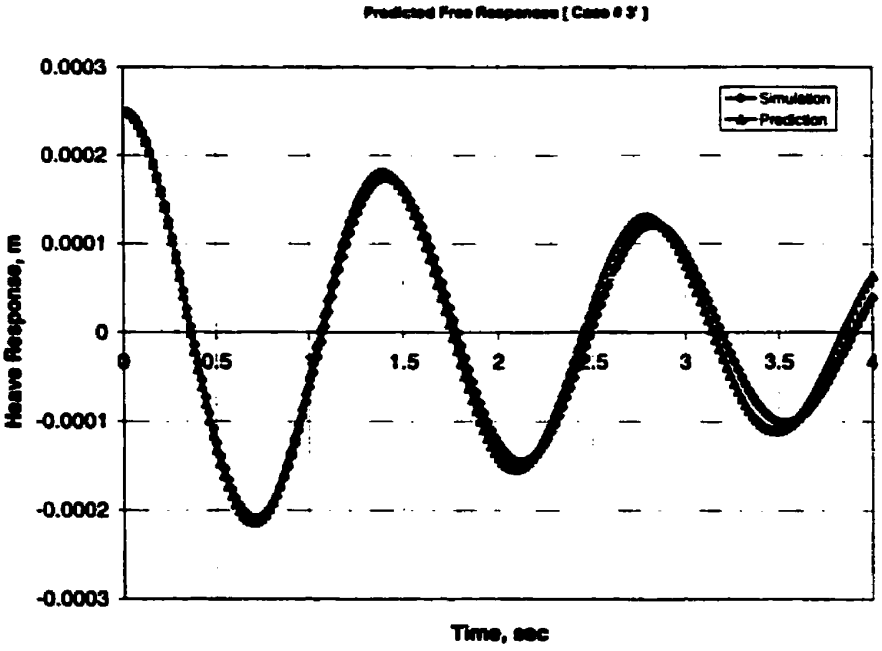

Figure 6.93 Comparison between the simulated and the predicted free responses for heave motion [Case # 3']

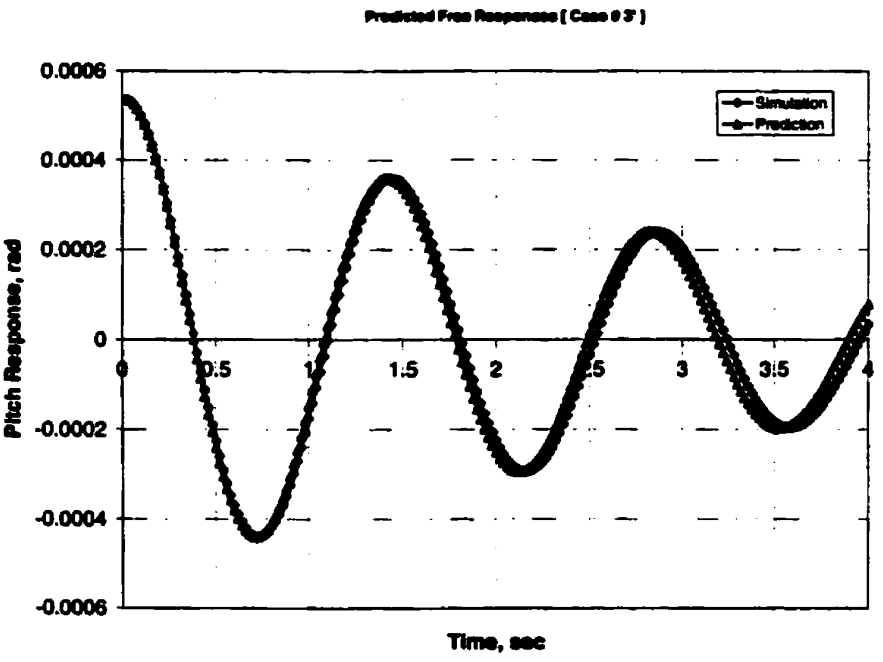

Figure 6.94 Comparison between the simulated and the predicted free responses for pitch motion [Case # 3']

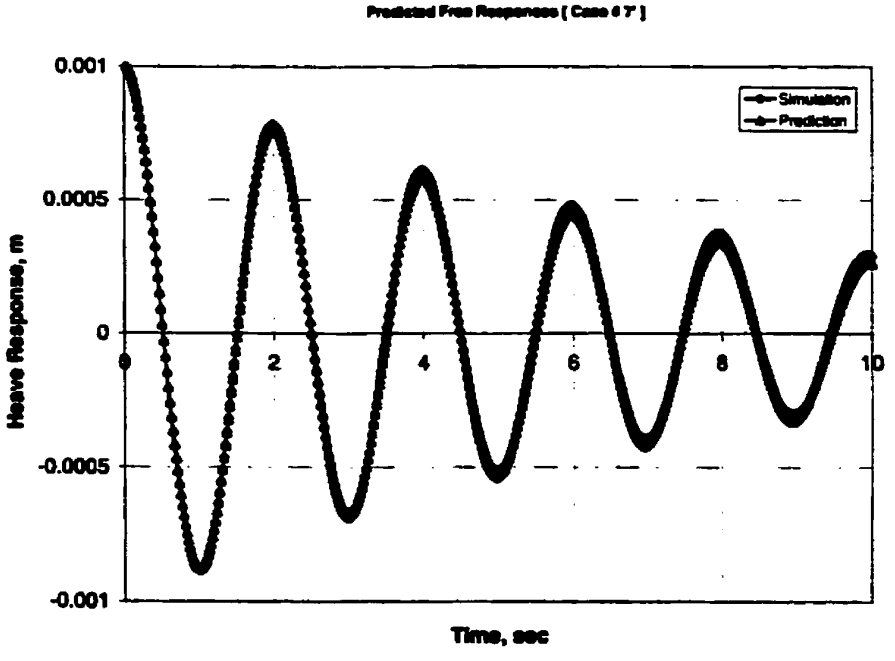

Figure 6.95 Comparison between the simulated and the predicted free responses for heave motion [Case # 7']

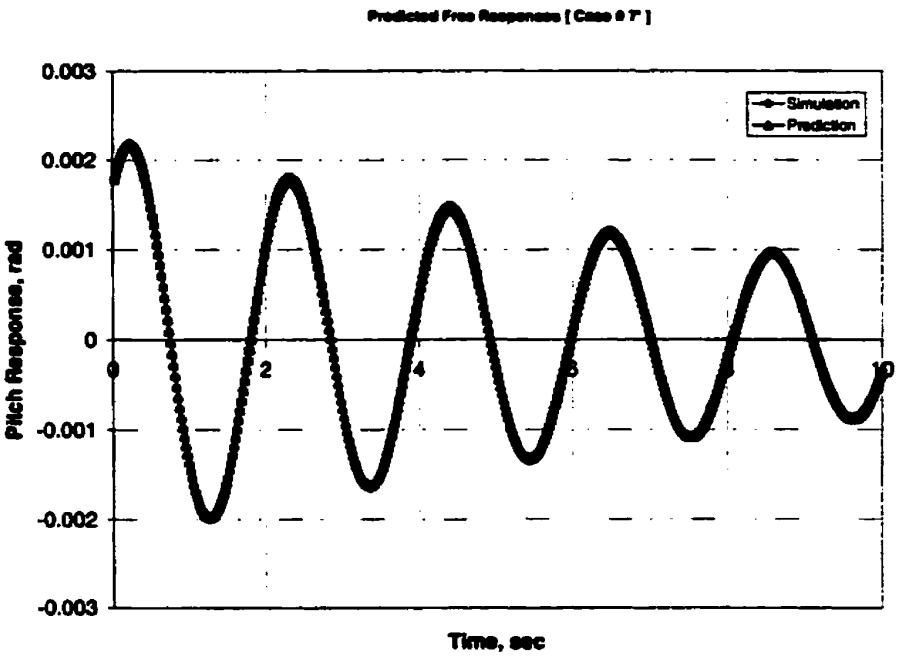

Figure 6.96 Comparison between the simulated and the predicted free responses for pitch motion [Case # 7']

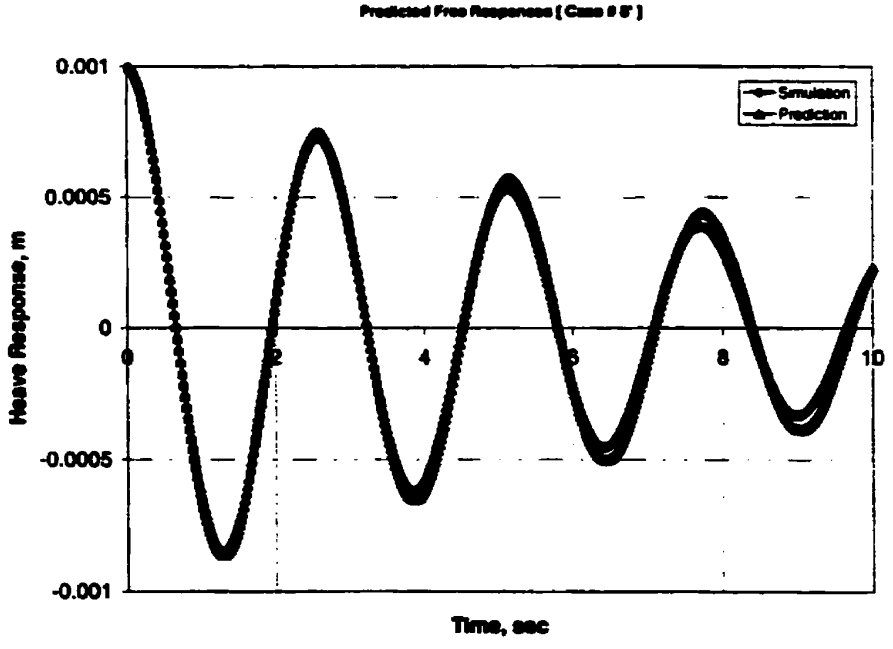

Figure 6.97 Comparison between the simulated and the predicted free responses for heave motion [Case # 8']

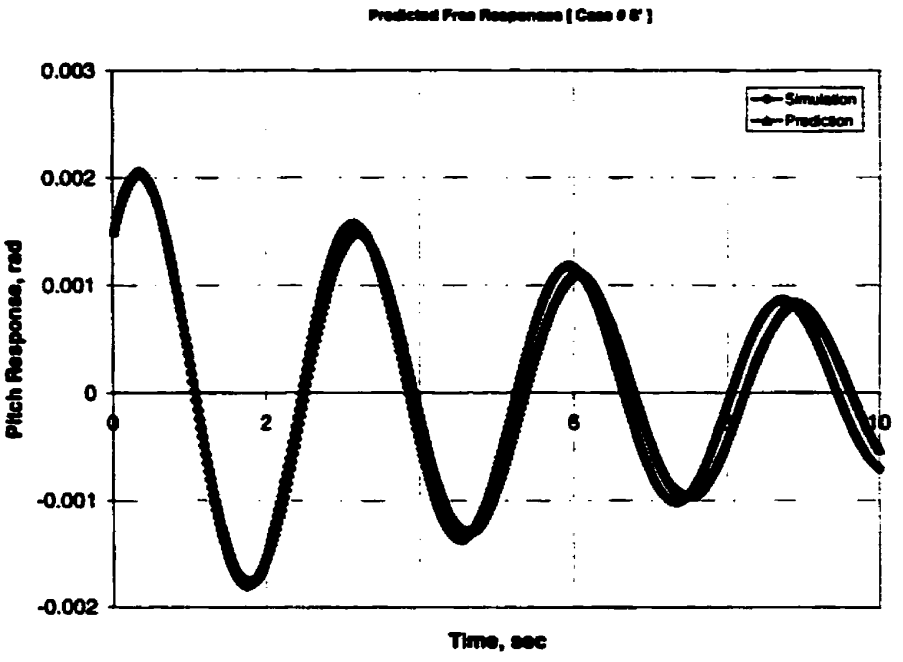

Figure 6.98 Comparison between the simulated and the predicted free responses for pitch motion [Case # 8']

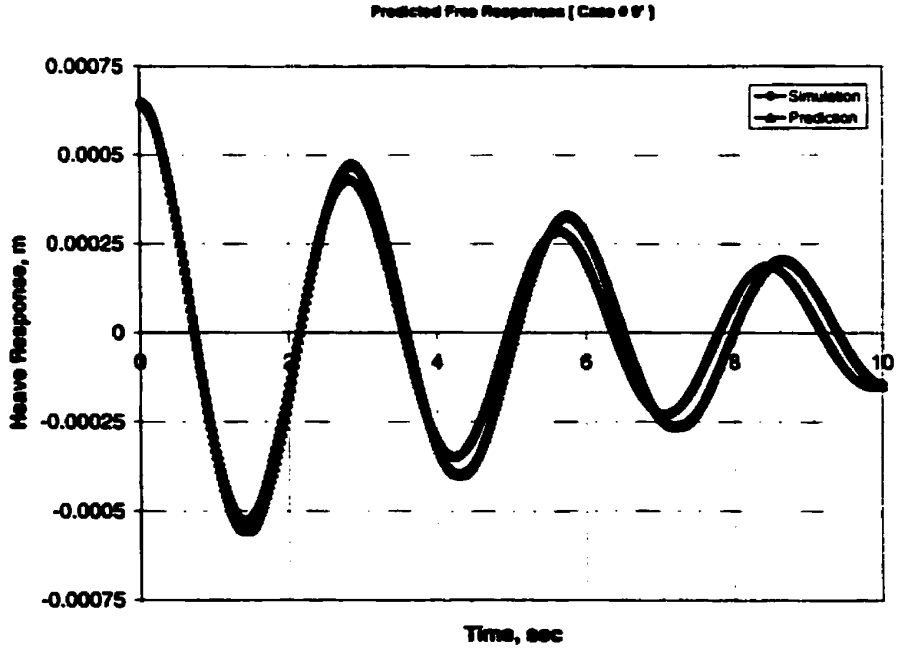

Figure 6.99 Comparison between the simulated and the predicted free responses for heave motion [Case # 9']

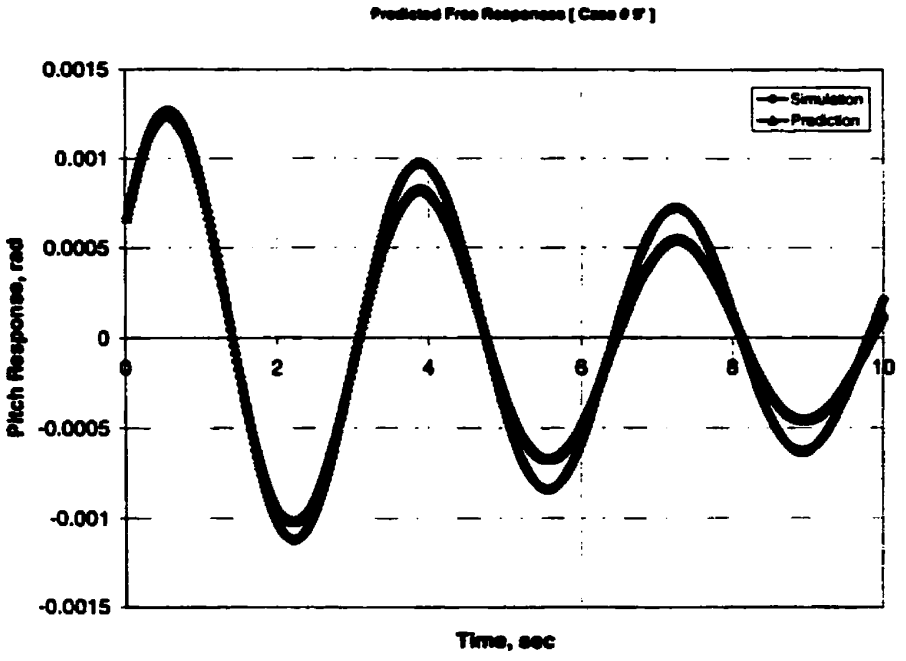

Figure 6.100 Comparison between the simulated and the predicted free responses for pitch motion [Case # 9']

6.1.2.4 Filtered Data

It is obvious in the previous discussion that some discrepancies appeared in the obtained agreement for the motion predictions for both heavily damped motions and when the difference between the exciting frequency and the damped natural frequency is large. Therefore, it was suggested that I use a one-dimensional digital band-pass filter centered around the estimated natural frequencies for heave and pitch motions to get signals which were composed mainly of the transient responses of the floating vehicle. The filter has two main characterized vectors coefficients: A and B as given below:

$$Y = FILTER\,(B, A, X) \tag{6.3}$$

where X and Y are the original data vector and its filtered data vector, respectively. The values of the vectors A and B characterize the type of the filter and are known as the filter coefficients. These values are designed using a MATLAB Toolbox function called *butter* as follow:

$$[B, A] = butter(n, \omega_n) \tag{6.4}$$

where n and ω_n are the order of the filter and the cutoff frequency, respectively. The cutoff frequency is that frequency where the magnitude response of the filter is $\sqrt{1/2}$. In the band-pass filter the cutoff frequency is given by:

$$\omega_n = [\omega_1 \ \ \omega_2] \quad \text{and} \quad \omega_1 < \omega_n < \omega_2 \tag{6.5}$$

The *butter* function designs an n^{th} order digital band-pass Butterworth filter and returns the filter coefficients in length 2n vectors B and A. The upper and lower frequencies of the filters were determined from the shapes of the power spectral density functions for the coupled heave and pitch motion spectra.

The comparison between the parameters used in the actual model and the predicted parameters for the previous six case studies is shown in Tables (5.10) and (5.11). The comparison of these tables with Tables (5.5) and (5.6) shows the effect of using a band-pass filter on the parameters identified using the developed technique. The identified damping and restoring parameters from the filtered data are better than those obtained without filtering. I chose Cases (2') and (8') to discuss the results obtained using

the band-pass filter. Cases (2') and (8') represent a case of moderate damped motion and a case of low damped natural frequency motion, respectively.

Results for the comparison between the random decrement signature and the predicted free response is shown in Figures (6.101) to (6.104). The agreement between the responses is better than that obtained without filtering.

The comparison between the random decrement signature and the auto-correlation function is shown in Figures (6.105) to (6.108). It is obvious that the agreement between the random decrement and the auto-correlation function for the heave motion is better than that obtained for the pitch motion for Case (8'). This is because the damped natural frequency for pitch motion is relatively small compared to that for the heave frequency. This agreement is better also than that obtained without filtering.

The actual model as well as the predicted one are used to generate the motion predictions using equations (5.1) and (5.2). The comparison between the actual free response and the predicted one is conducted and is shown in Figures (6.109) to (6.112).

The agreement between the predicted free responses for Case (2') is excellent. The comparison for Case (8') is good. This is because the damped natural frequencies for Case (2') are higher than that used in Case (8'). Even in Case (8') itself, the agreement of the comparison for the heave motion is better than that obtained for the pitch motion since the damped natural frequency for the pitch motion is smaller than that for the heave motion. This result shows that the use of band-pass filter is more effective when the difference between the exciting frequency and the damped natural frequency is large.

Despite these conclusions, the agreement obtained here with filtering around the damped natural frequencies for heave and pitch motions, is better than that obtained

without filtering. It is clear from the above results that the use of a band-pass filter for the coupled heave and pitch responses is important in the identification of the hydrodynamic parameters. Therefore, I recommend the use of this filter for the measured data.

Moreover, it is obvious from Tables (5.3), (5.4), (5.8), (5.9), (5.12) and (5.13) that the error percentages for the coupling parameters are larger than correspond to the damping and restoring parameters. This result has been obtained directly from the visual comparison between the actual and the identified parameters. It seems that the coupling parameters are unimportant in this case since they did not change the solution. In general application, the identification technique has been developed for cases where the coupling parameters are important.

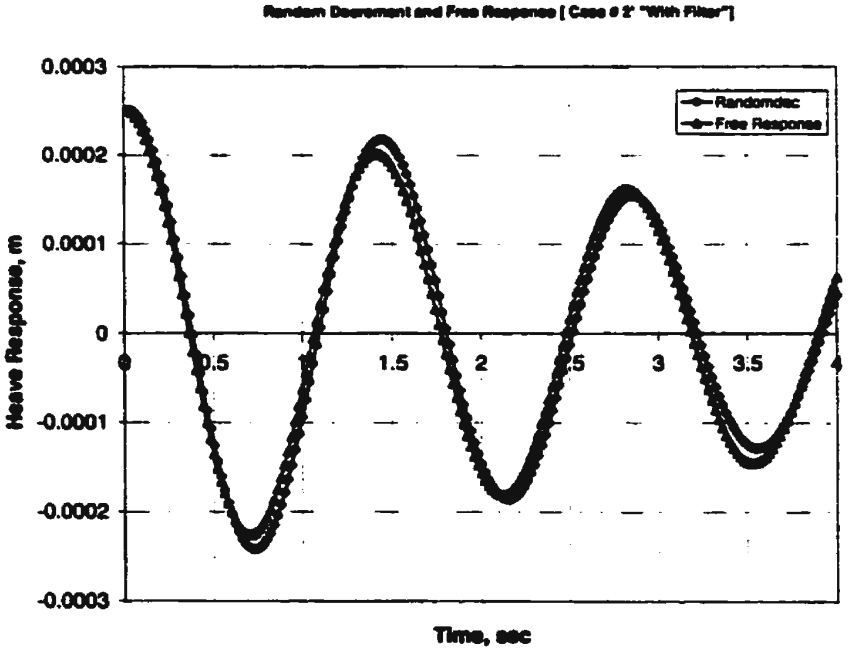

Figure 6.101 Comparison between the random decrement signature and the free response for heave motion [Case # 2']

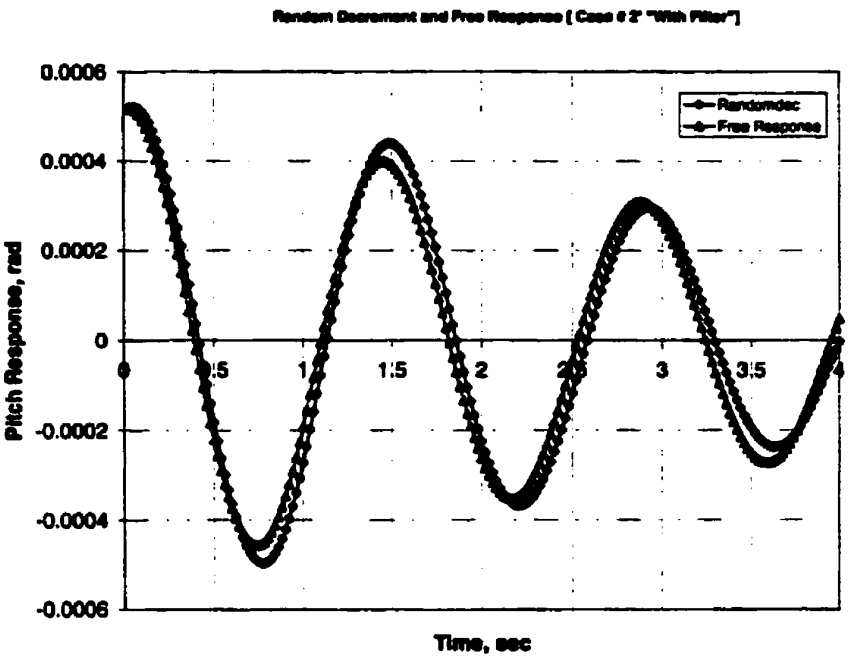

Figure 6.102 Comparison between the random decrement signature and the free response for pitch motion [Case # 2']

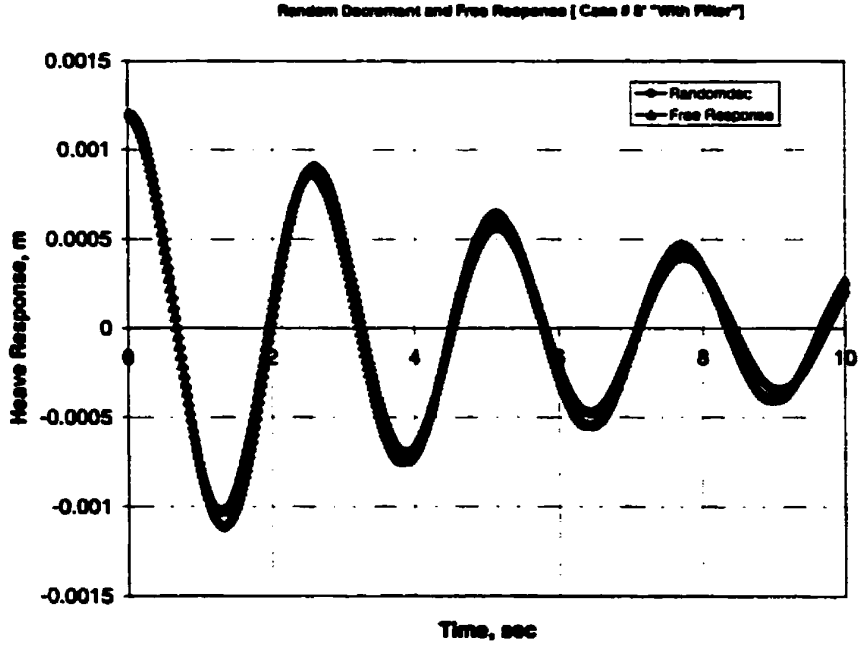

Figure 6.103 Comparison between the random decrement signature and the free response for heave motion [Case # 8']

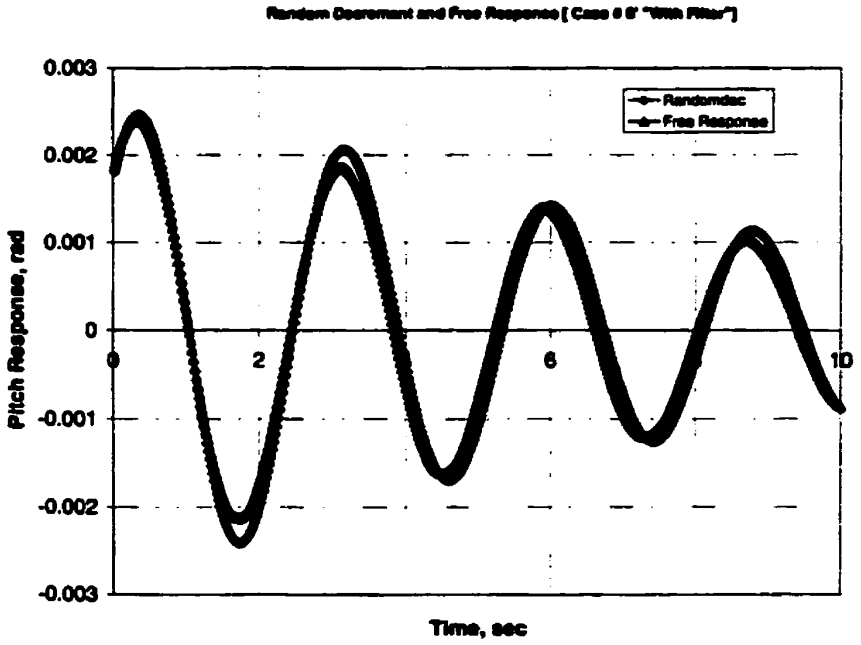

Figure 6.104 Comparison between the random decrement signature and the free response for pitch motion [Case # 8']

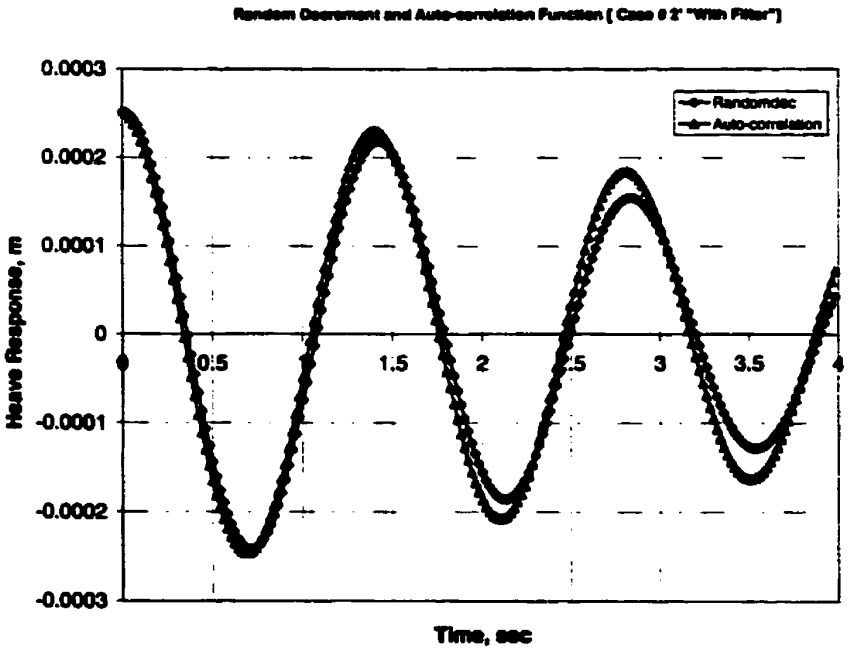

Figure 6.105 Comparison between the random decrement signature and the auto-correlation function for heave motion [Case # 2']

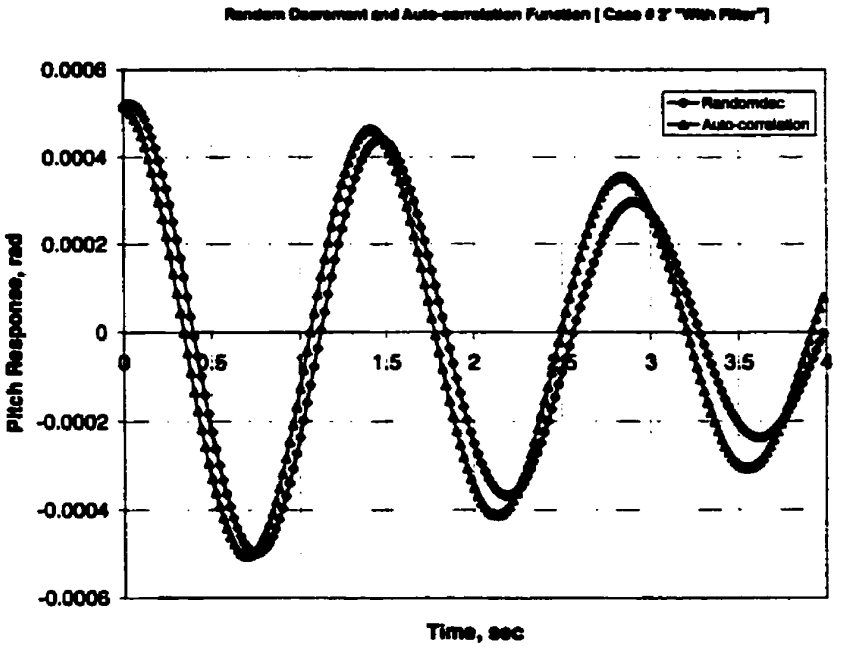

Figure 6.106 Comparison between the random decrement signature and the auto-correlation function for pitch motion [Case # 2']

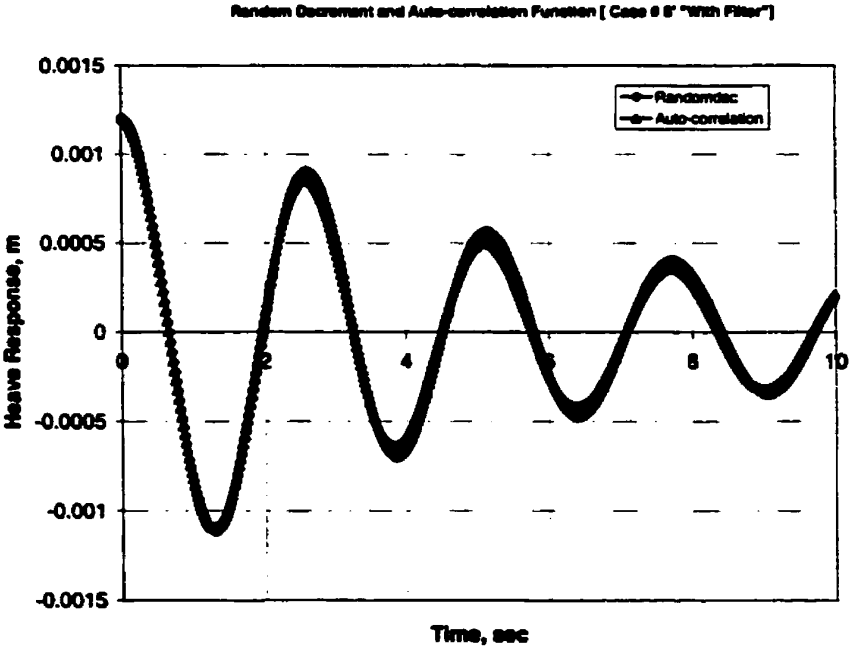

Figure 6.107 Comparison between the random decrement signature and the auto-correlation function for heave motion [Case # 8']

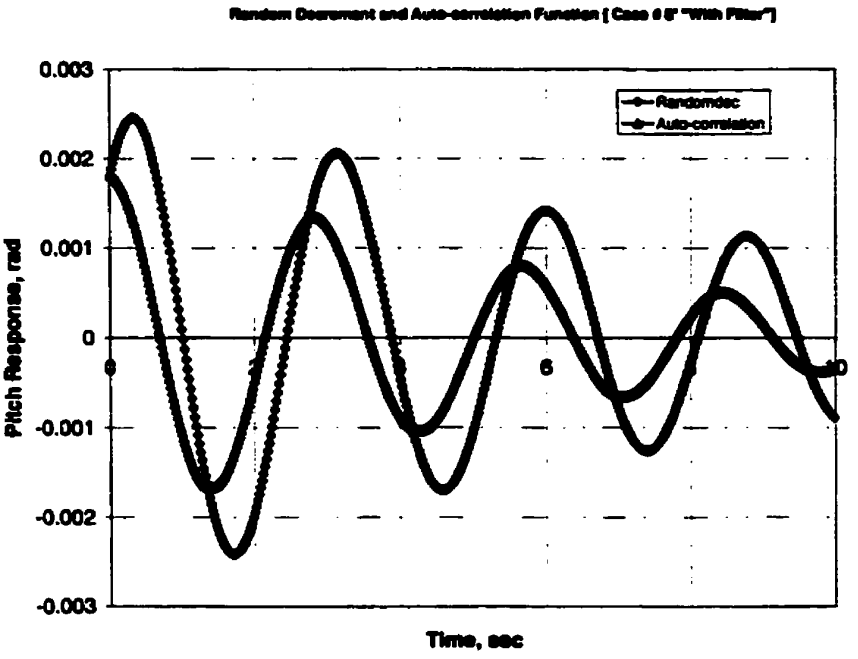

Figure 6.108 Comparison between the random decrement signature and the auto-correlation function for pitch motion [Case # 8']

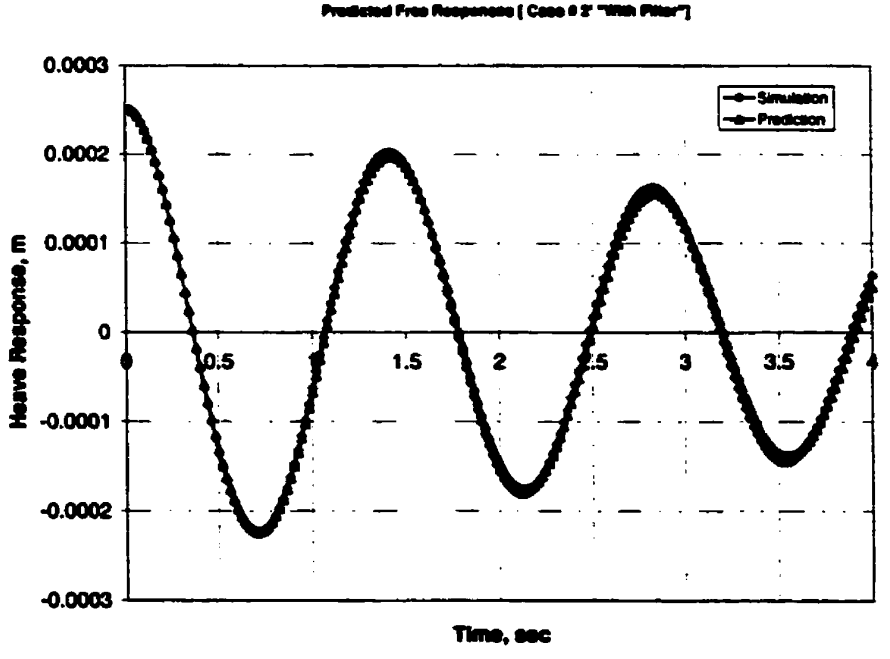

Figure 6.109 Comparison between the simulated and the predicted free responses for heave motion [Case # 2']

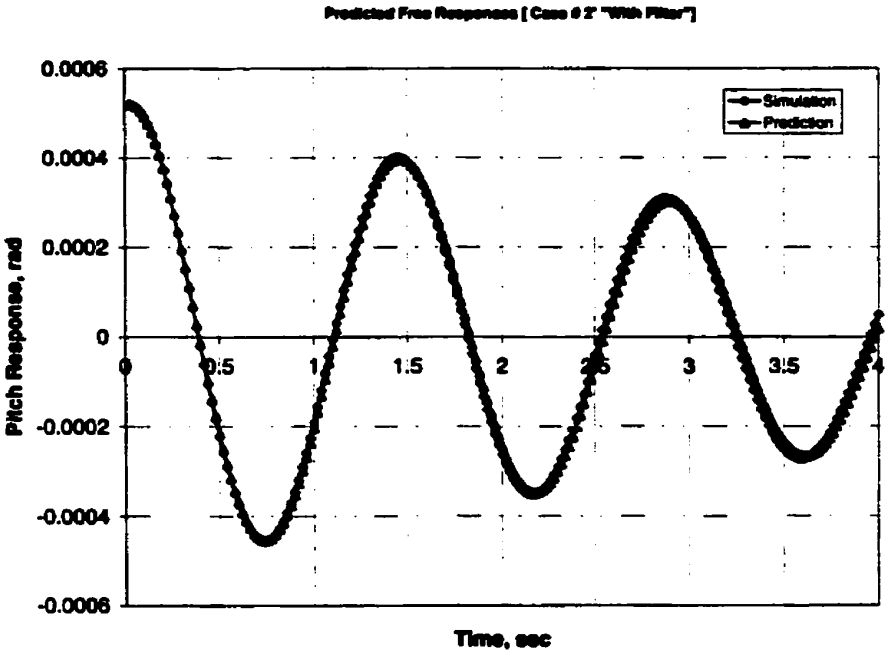

Figure 6.110 Comparison between the simulated and the predicted free responses for pitch motion [Case # 2']

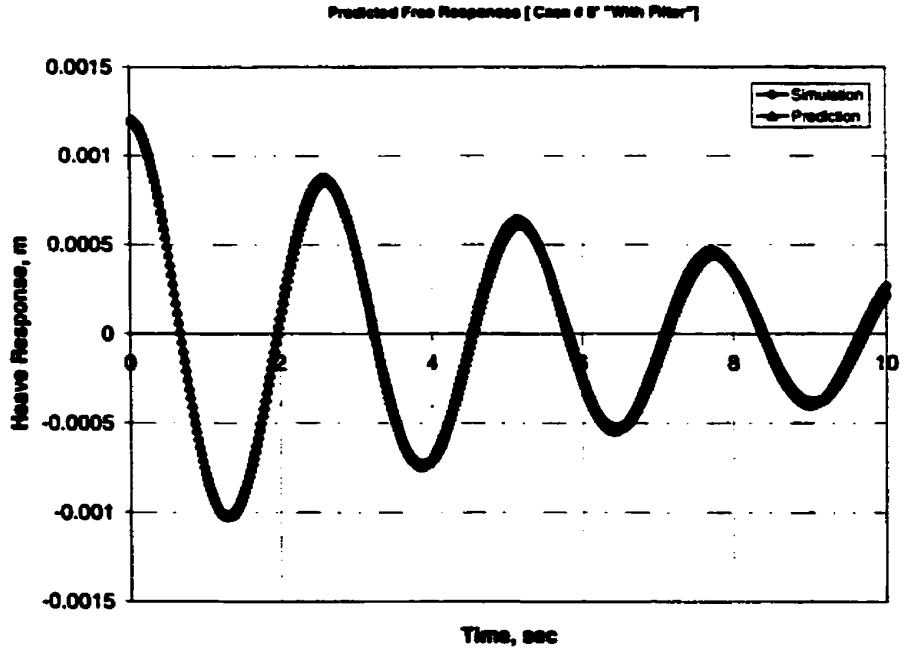

Figure 6.111 Comparison between the simulated and the predicted free responses for heave motion [Case # 8']

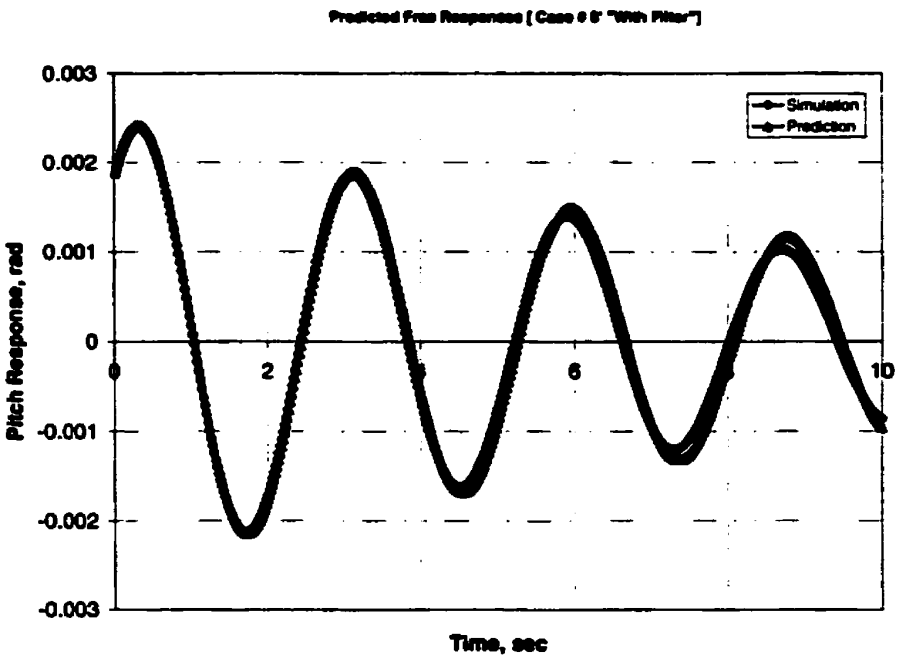

Figure 6.112 Comparison between the simulated and the predicted free responses for pitch motion [Case # 8']

6.2 Experimental Results

The experimental program was conducted using the model in the towing tank. Four measurements were collected for each individual run: towing speed, wave height, and the coupled heave and pitch random motion responses. Wave height represents the input to the URV-model, while the coupled heave and pitch motions represent the output.

The power spectral density functions for the wave height and the coupled heave and pitch time series for each run have been obtained using the Fast Fourier Transform (FFT) algorithm. Results for the wave and the motion power spectral density functions for the experimental program are presented in Appendix M, and Appendix N and Appendix O, respectively. The main objective for calculating the power spectral density functions for the input and the output time-series is to look at the energy distribution. In

addition, the power spectral density functions for the wave excitation (input) and the coupled heave and pitch motion spectra (outputs) are needed in the determination of the correlation between the wave modal frequency and the damped natural frequencies for heave and pitch motions.

The maximum energy content in the coupled heave and pitch motion spectra are distributed closely around the wave modal frequency of the excitation as shown in Appendix N and Appendix O. It is clear from Appendices N and O that multiple peaks characterize the motion power spectral density functions. In order to investigate the utility of the power spectral density functions, two experimental runs, 5-02 and 19-0, are considered. The power spectral density functions for the time series corresponding to the two runs are obtained as shown in Figures (6.113) to (6.118).

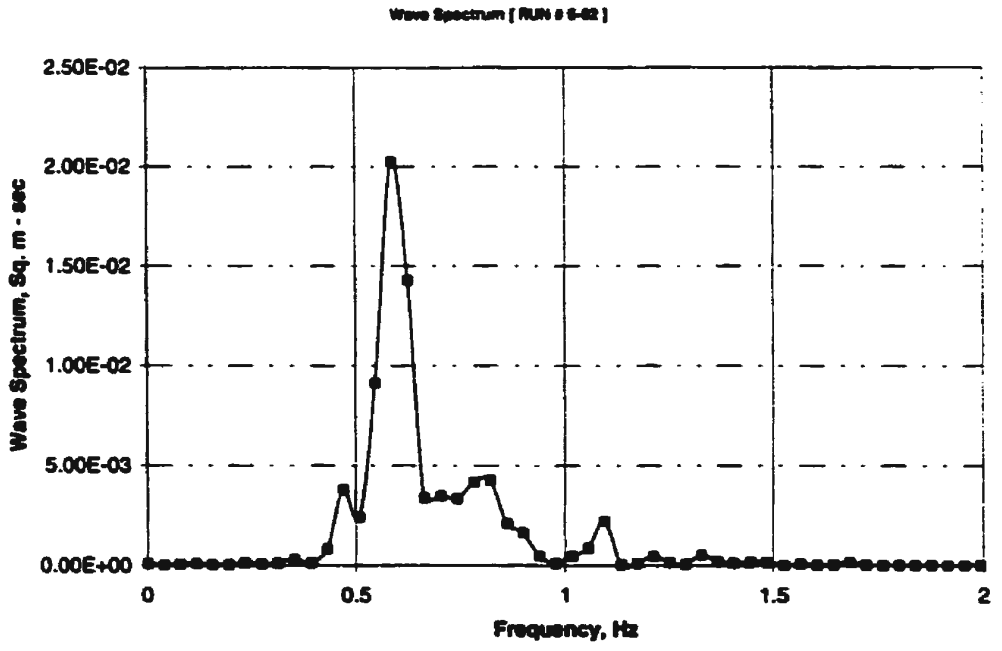

Figure 6.113 Wave power spectral density function [Run # 5-02]

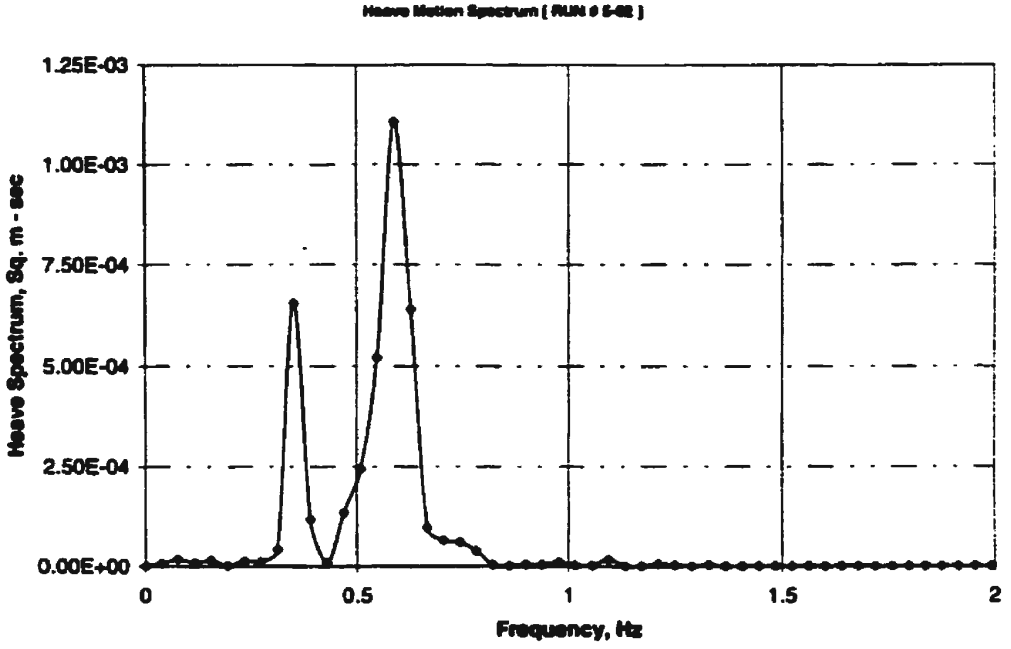

Figure 6.114 Heave power spectral density function [Run # 5-02]

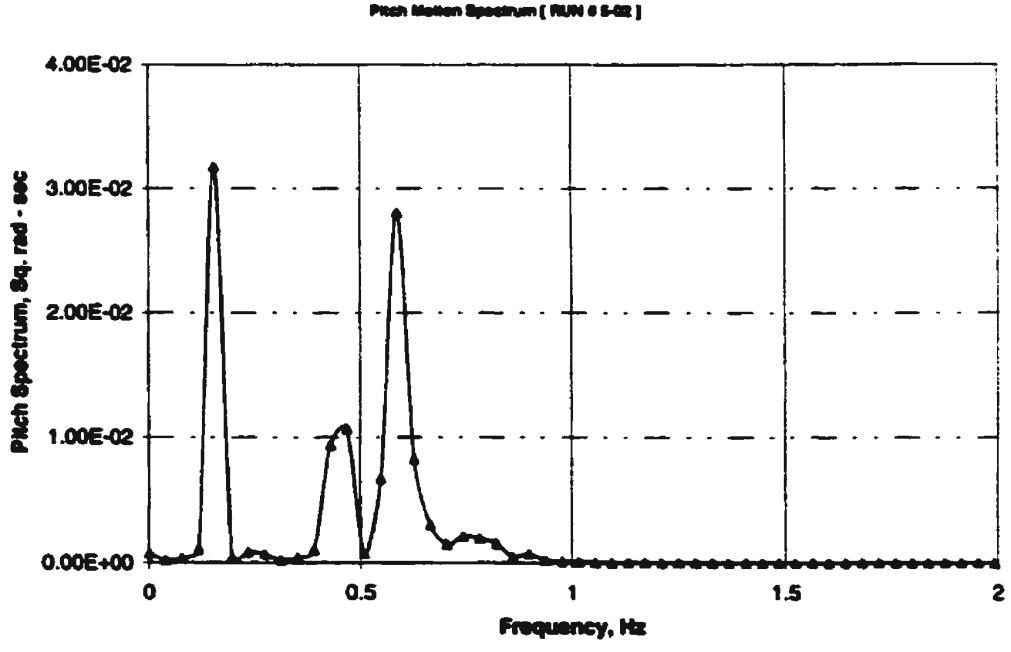

Figure 6.115 Pitch power spectral density function [Run # 5-02]

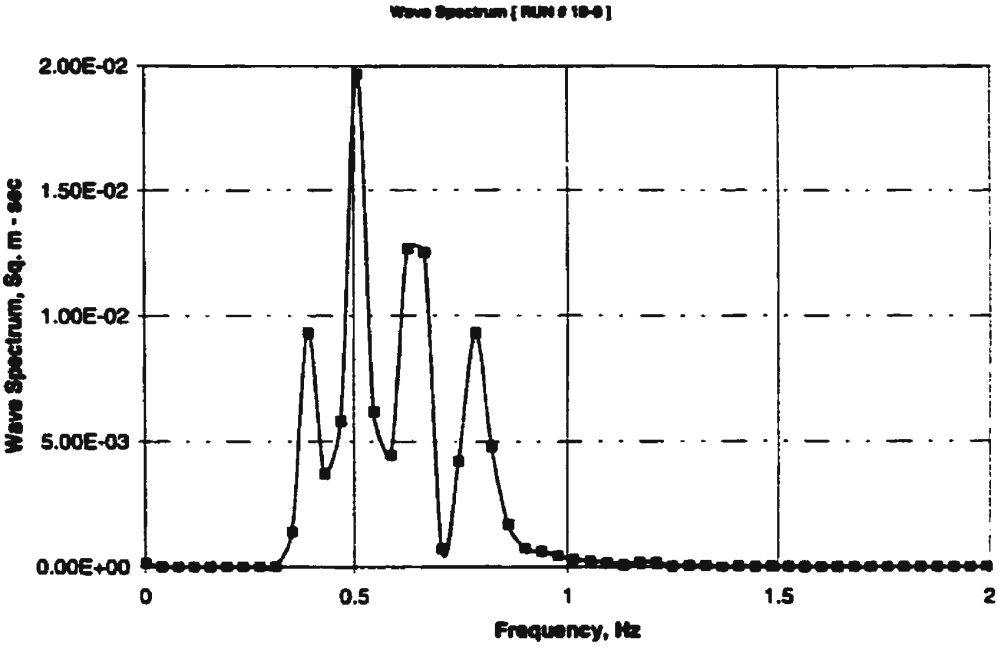

Figure 6.116 Wave power spectral density function [Run # 19-0]

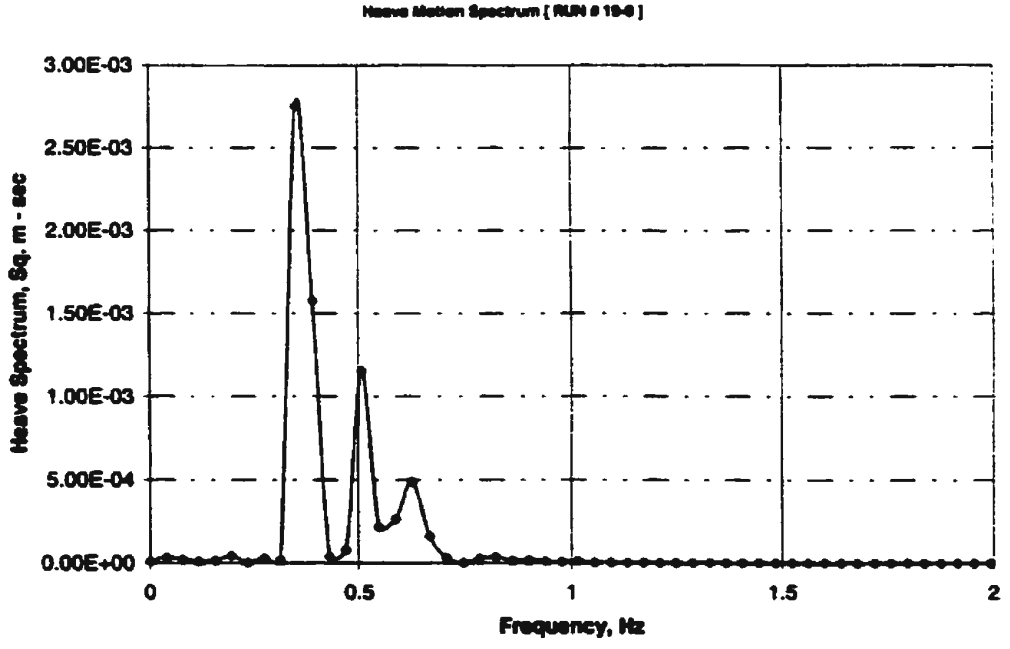

Figure 6.117 Heave power spectral density function [Run # 19-0]

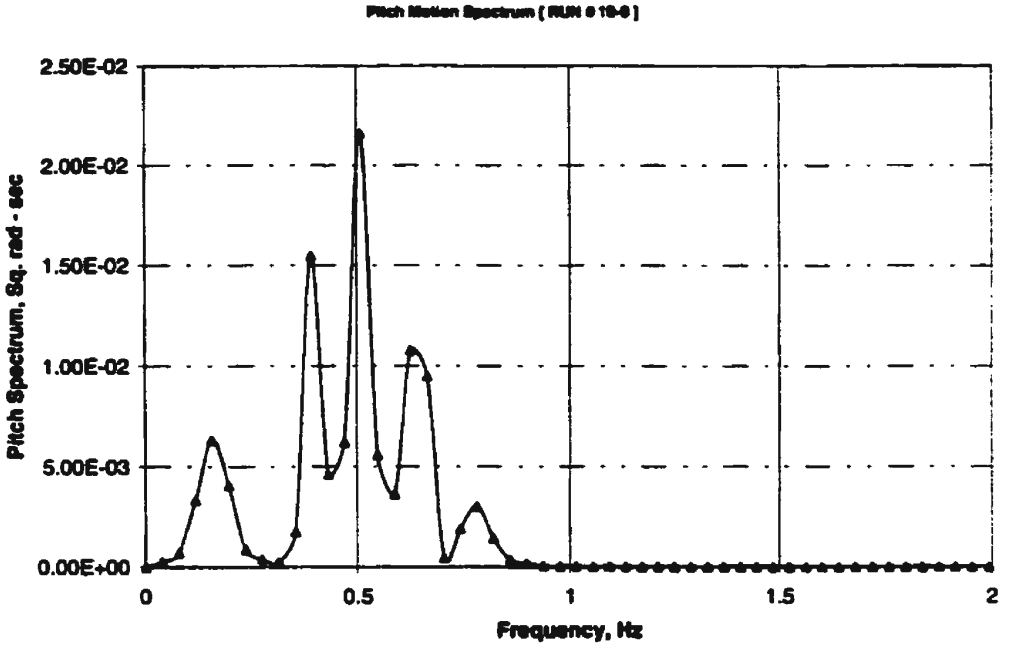

Figure 6.118 Pitch power spectral density function [Run # 19-0]

Two main peaks are significant in the motion spectra: one corresponds to the damped natural frequency while the other corresponds to the modal frequency of the wave excitation. In addition, Figures (6.115) and (6.118) have another peak characterizes the pitch motion spectra. This peak corresponds to the damped natural frequency for heave motion and is located between the previous two peaks. This shows the coupling between the heave and pitch motions in the experimentally measured data.

It is obvious from Figures (6.113) to (6.118) that the maximum energy content in these spectra is distributed around the modal frequency of the wave excitation. In order to obtain a random decrement signature that resembles the free response of the system, the motion response is filtered around the natural frequency of the URV.

Using a band-pass filter centered around the damped natural frequency, one can get a signal, which is composed of the transient response of the floating URV. Then, the

random decrement signature is calculated using the filtered signal for the coupled heave and pitch motions.

Using the filtered random response, the damping, the restoring and the coupling parameters in the equations describing the coupled heave and pitch motions for an URV are identified using the technique developed in this work. The technique has been applied to the runs given in Table (6.2). The predicted parameters for these runs are shown in Tables (6.3) and (6.4). The predicted parameters are substituted back in equations (5.1) and (5.2) and the equations are integrated numerically using the Runge-Kutta algorithm to generate the predicted free response.

Table 6.2 Experimental Parameters

RUN #	Experimental Parameters		
	Towing Speed	JONSWAP Wave Excitation	
	U (m/sec)	H_S (m)	Ω (Hz)
1-0	0	0.07	0.5
5-02	0.20	0.07	0.5
9-02	0.20	0.07	0.7
10-0	0	0.10	0.5
12-0	0	0.10	0.7
13-01	0.10	0.10	0.5
16-02	0.20	0.10	0.6
18-02	0.20	0.10	0.7
19-0	0	0.15	0.5
21-0	0	0.13	0.7
22-01	0.10	0.15	0.5

Table 6.3 The predicted parameters from the experimental data for heave motion

RUN #	Heave Motion			
	Predicted Parameters			
	d_{31}	d_{32}	d_{33}	d_{34}
1-0	5.10570	0.12170	0.07900	0.12130
5-02	4.93470	0.02520	0.08530	-0.02370
9-02	4.83660	-0.00660	0.08490	-0.03510
10-0	5.24100	0.08650	0.08450	-0.03150
12-0	4.85530	0.01560	0.09360	0.08420
13-01	5.07070	0.04360	0.07930	0.15750
16-02	4.92830	-0.08250	0.10850	0.32640
18-02	4.79630	0.00110	0.11970	0.00580
19-0	5.15560	0.00270	0.10830	0.00690
21-0	5.05250	0.00430	0.11450	0.04500
22-01	5.19690	-0.00470	0.10400	0.03580

Table 6.4 The predicted parameters from the experimental data for pitch motion

RUN #	Pitch Motion			
	Predicted Parameters			
	d_{41}	d_{42}	d_{43}	d_{44}
1-0	0.00170	1.10860	0.00360	0.06860
5-02	-0.00013	0.99840	-0.00084	0.07820
9-02	-0.00100	1.00390	0.02150	0.07090
10-0	0.00064	1.03330	0.00086	0.06560
12-0	0.00010	0.98880	0.00230	0.03870
13-01	-0.00190	1.03900	-0.00470	0.04500
16-02	0.00030	1.02930	0.01020	0.04530
18-02	0.00210	0.98700	-0.01730	0.05680
19-0	-0.00010	1.12410	-0.00017	0.05280
21-0	0.00001	1.16390	0.00009	0.05810
22-01	-0.00100	0.96810	-0.00190	0.04010

The comparison between the obtained random decrement signature and the measured free motion response for those runs is shown in Figures (6.119) to (6.140). It is obvious from these figures that the agreement between the random decrement signatures and the measured free responses for heave and pitch motions is good especially for the first cycle of the signatures.

The agreement for the heave motion is better than that obtained for the pitch motion. The results for the pitch motion seem to suffer a phase shift. In this case, the pitch damped natural frequency for the URV model is very small compared to the heave one. Moreover, the difference between the damped natural frequency for heave and the exciting frequency is smaller than the difference between the damped natural frequency for pitch and the exciting frequency. Therefore, the obtained agreement for the heave motion is better than that obtained for the pitch motion.

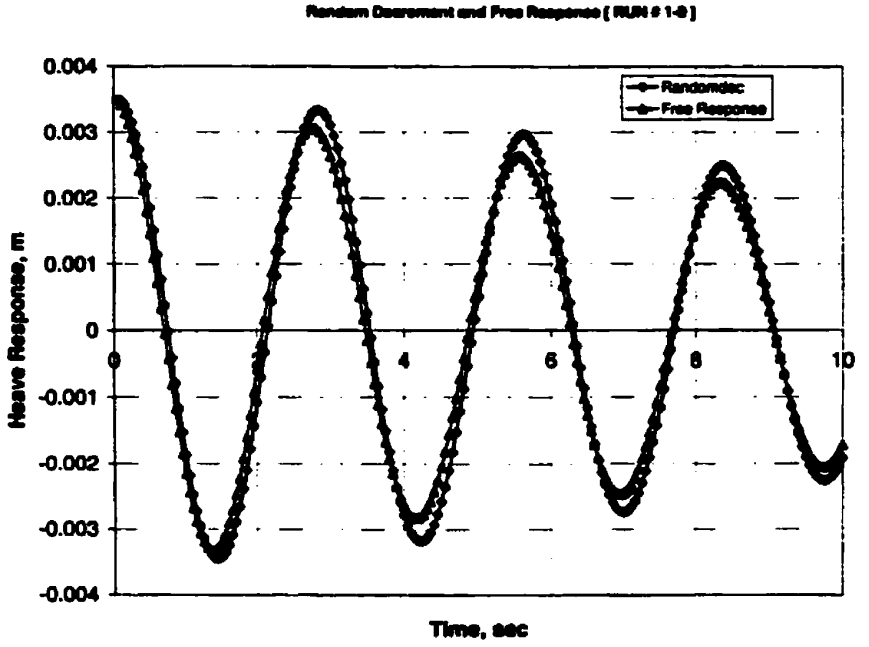

Figure 6.119 Comparison between the random decrement and the measured free response for heave motion [Run # 1-0]

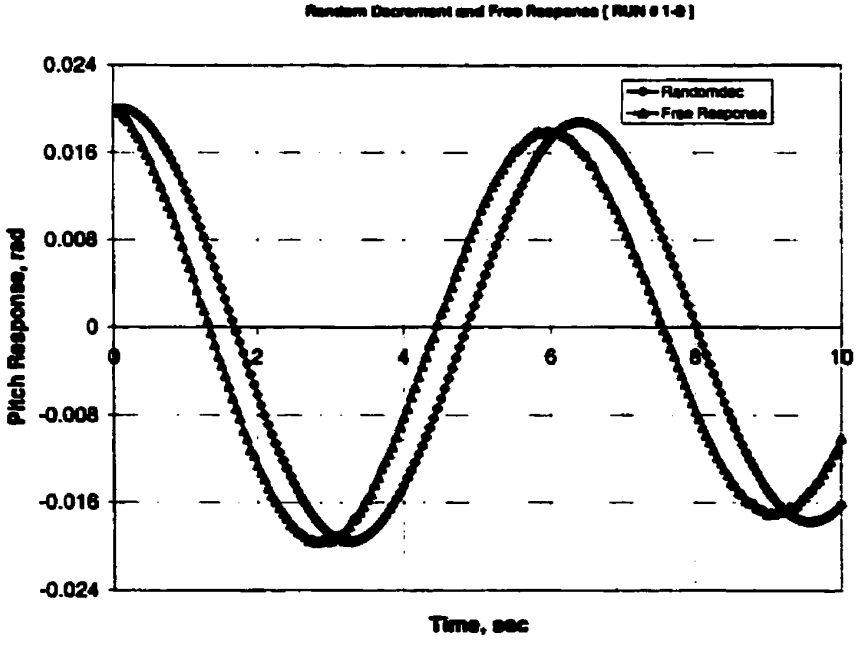

Figure 6.120 Comparison between the random decrement and the measured free response for pitch motion [Run # 1-0]

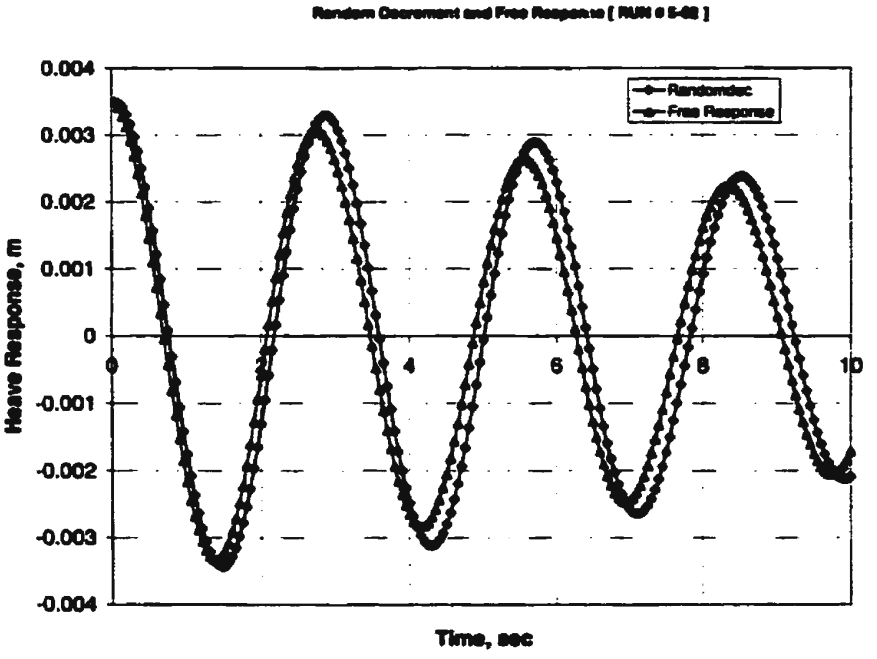

Figure 6.121 Comparison between the random decrement and the measured free response for heave motion [Run # 5-02]

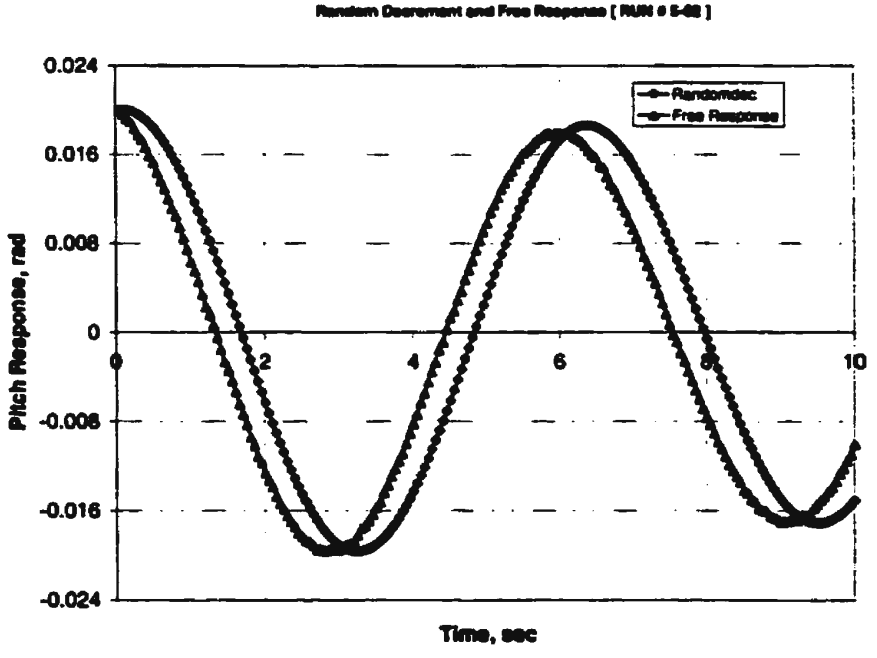

Figure 6.122 Comparison between the random decrement and the measured free response for pitch motion [Run # 5-02]

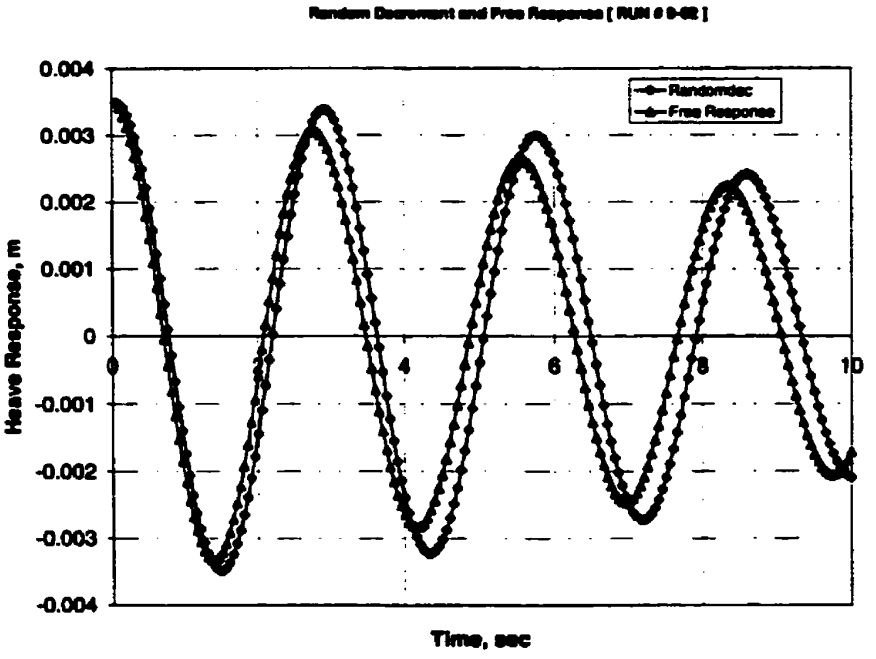

Figure 6.123 Comparison between the random decrement and the measured free response for heave motion [Run # 9-02]

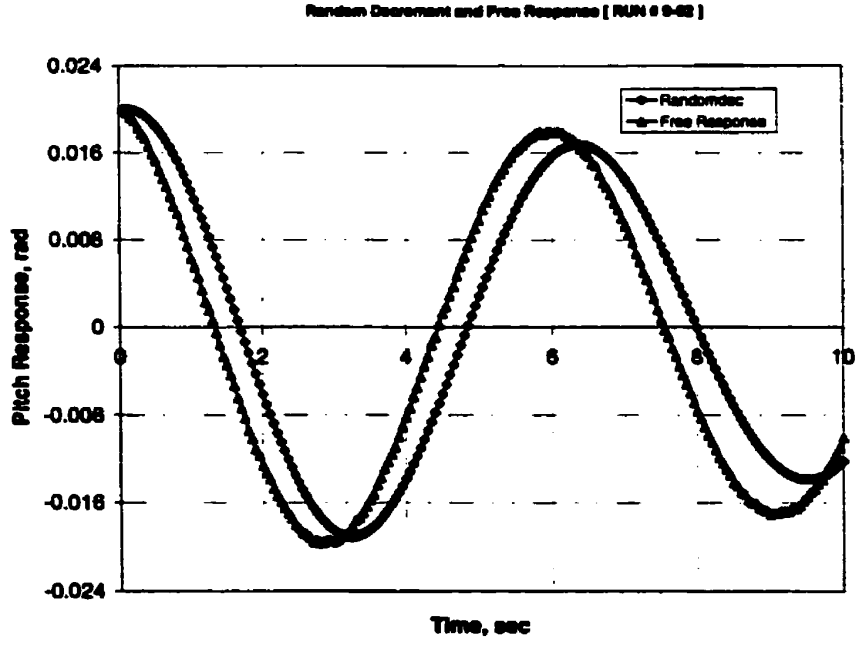

Figure 6.124 Comparison between the random decrement and the measured free response for pitch motion [Run # 9-02]

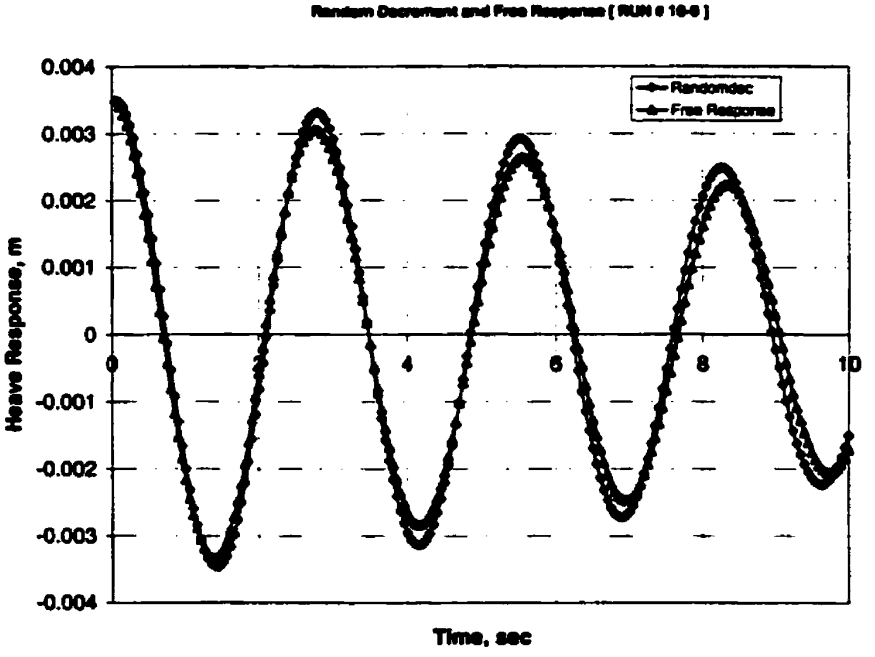

Figure 6.125 Comparison between the random decrement and the measured free response for heave motion [Run # 10-0]

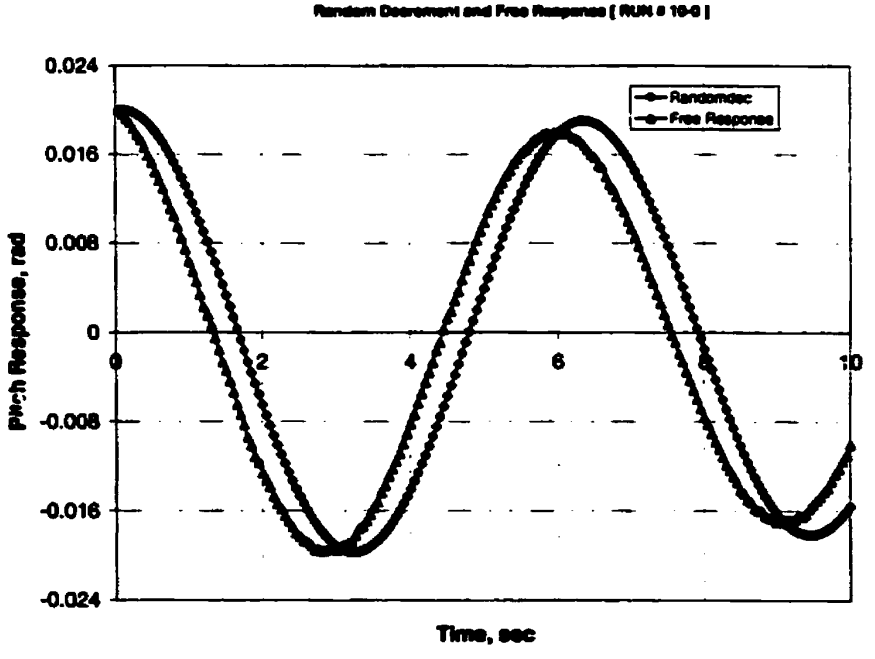

Figure 6.126 Comparison between the random decrement and the measured free response for pitch motion [Run # 10-0]

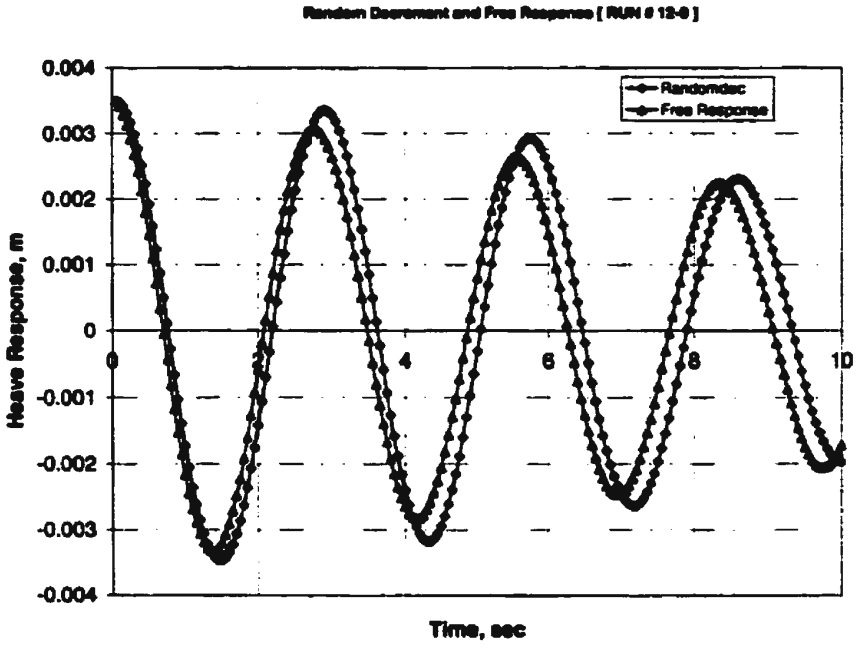

Figure 6.127 Comparison between the random decrement and the measured free response for heave motion [Run # 12-0]

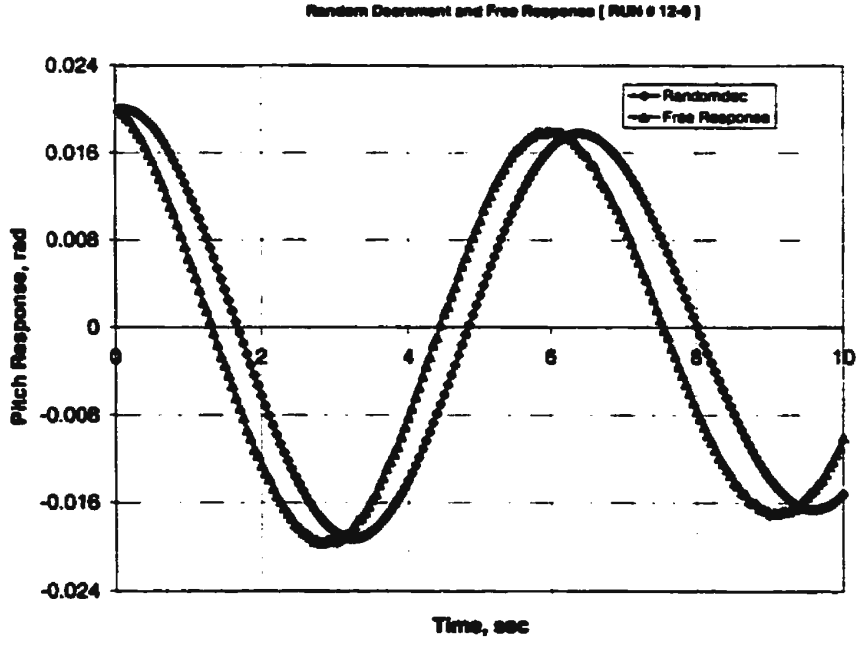

Figure 6.128 Comparison between the random decrement and the measured free response for pitch motion [Run # 12-0]

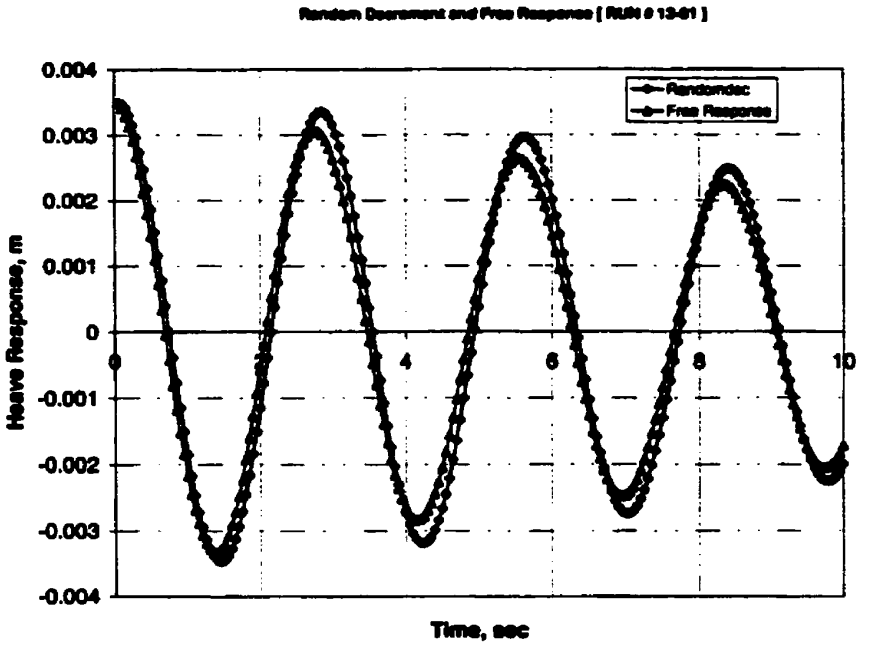

Figure 6.129 Comparison between the random decrement and the measured free response for heave motion [Run # 13-01]

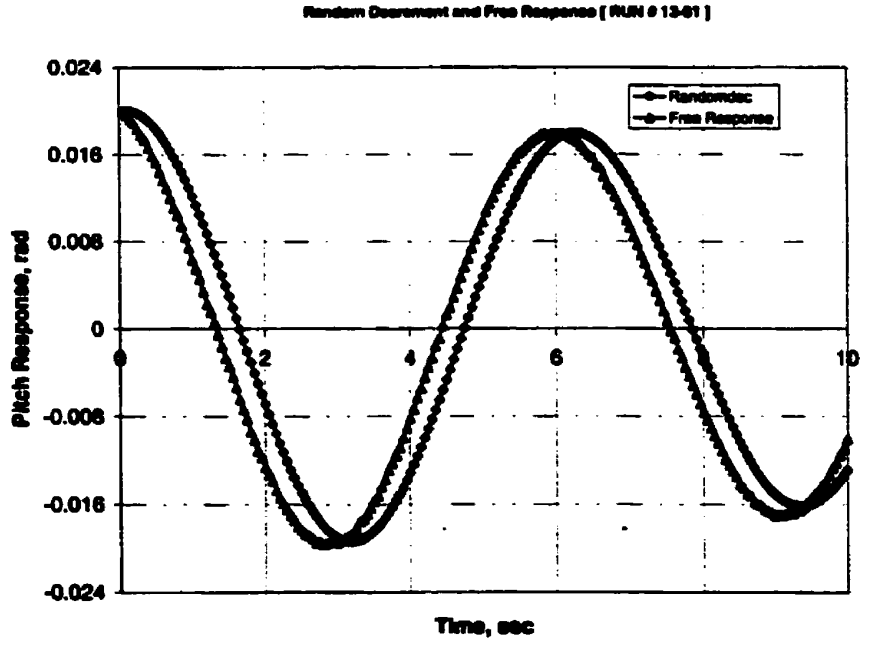

Figure 6.130 Comparison between the random decrement and the measured free response for pitch motion [Run # 13-01]

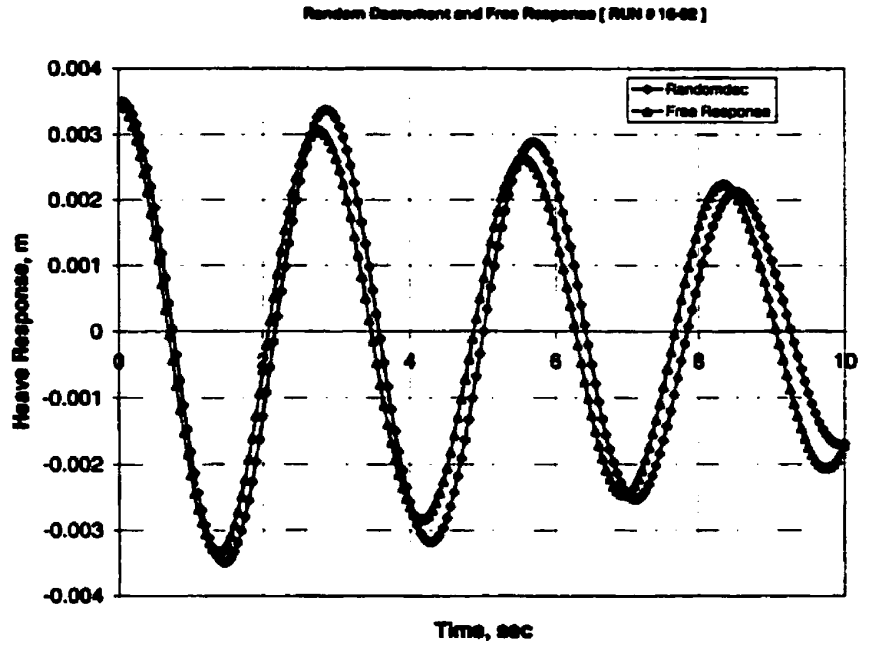

Figure 6.131 Comparison between the random decrement and the measured free response for heave motion [Run # 16-02]

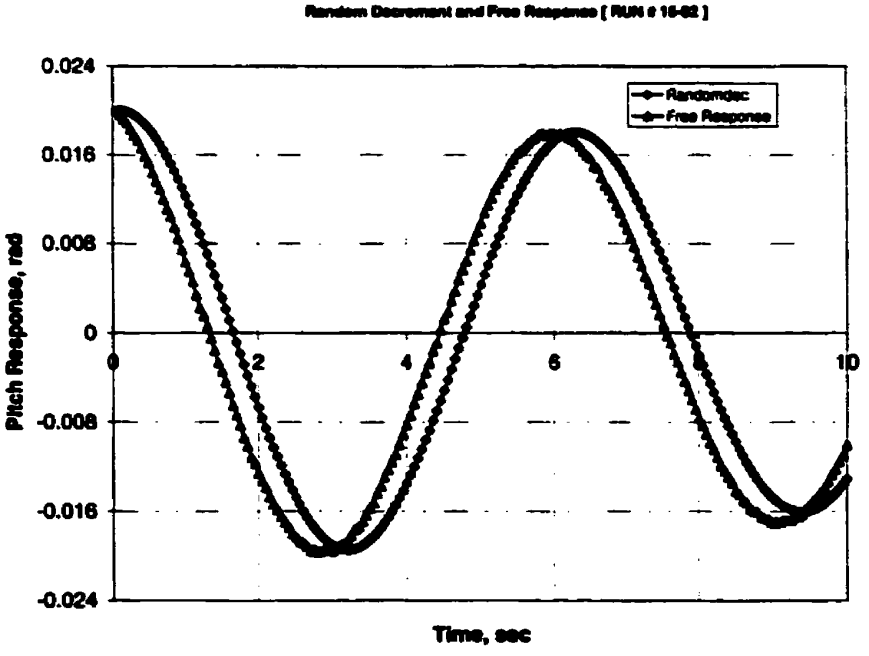

Figure 6.132 Comparison between the random decrement and the measured free response for pitch motion [Run # 16-02]

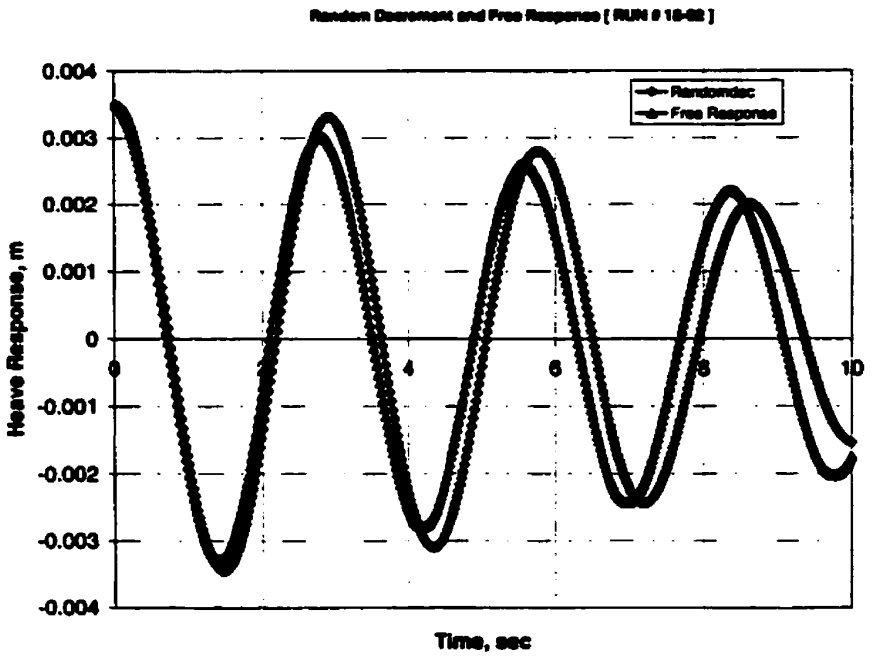

Figure 6.133 Comparison between the random decrement and the measured free response for heave motion [Run # 18-02]

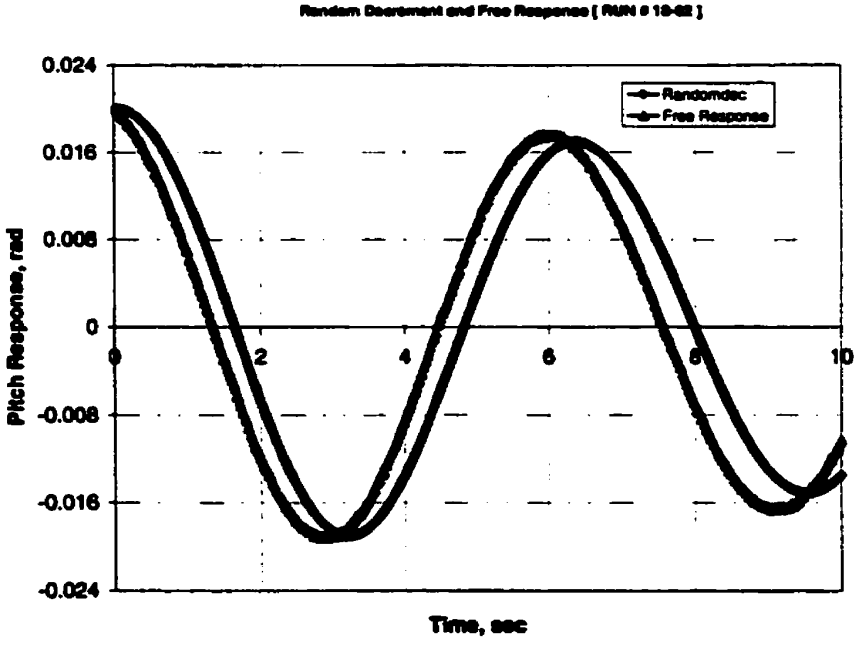

Figure 6.134 Comparison between the random decrement and the measured free response for pitch motion [Run # 18-02]

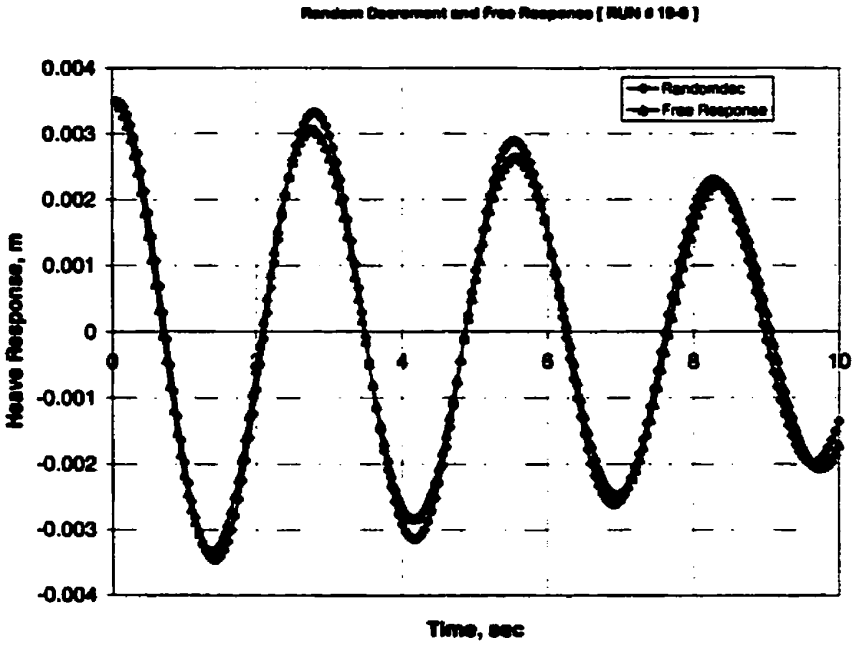

Figure 6.135 Comparison between the random decrement and the measured free response for heave motion [Run # 19-0]

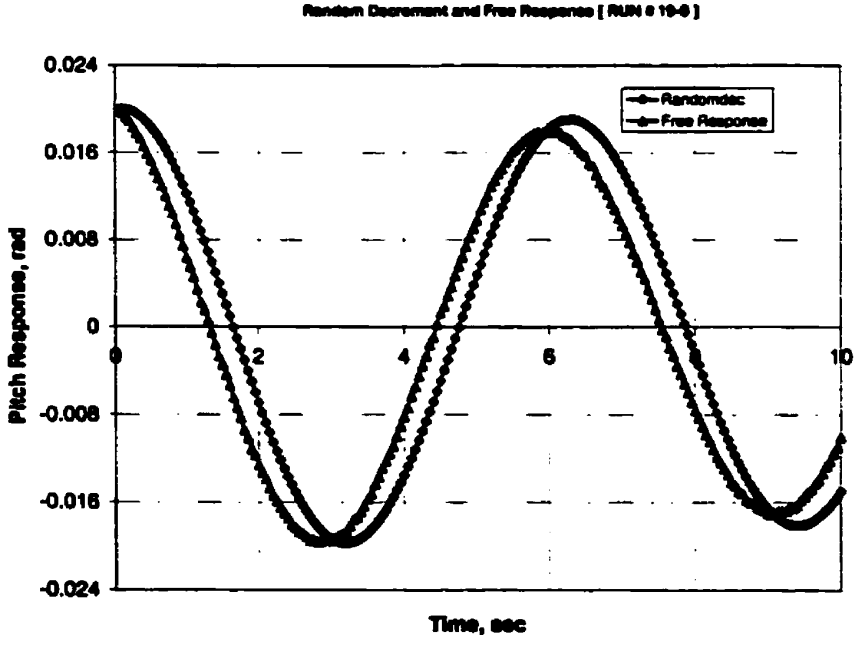

Figure 6.136 Comparison between the random decrement and the measured free response for pitch motion [Run # 19-0]

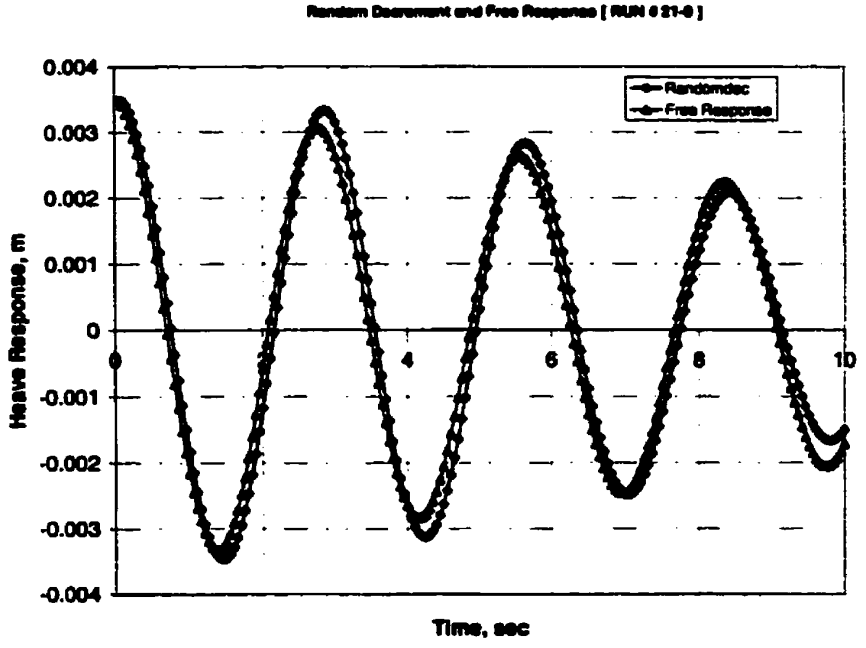

Figure 6.137 Comparison between the random decrement and the measured free response for heave motion [Run # 21-0]

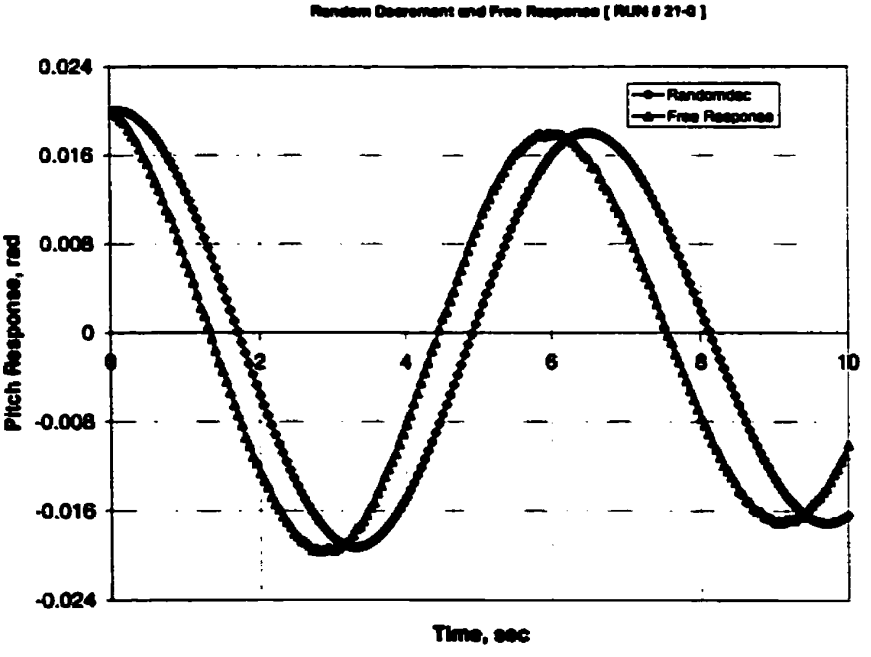

Figure 6.138 Comparison between the random decrement and the measured free response for pitch motion [Run #21-0]

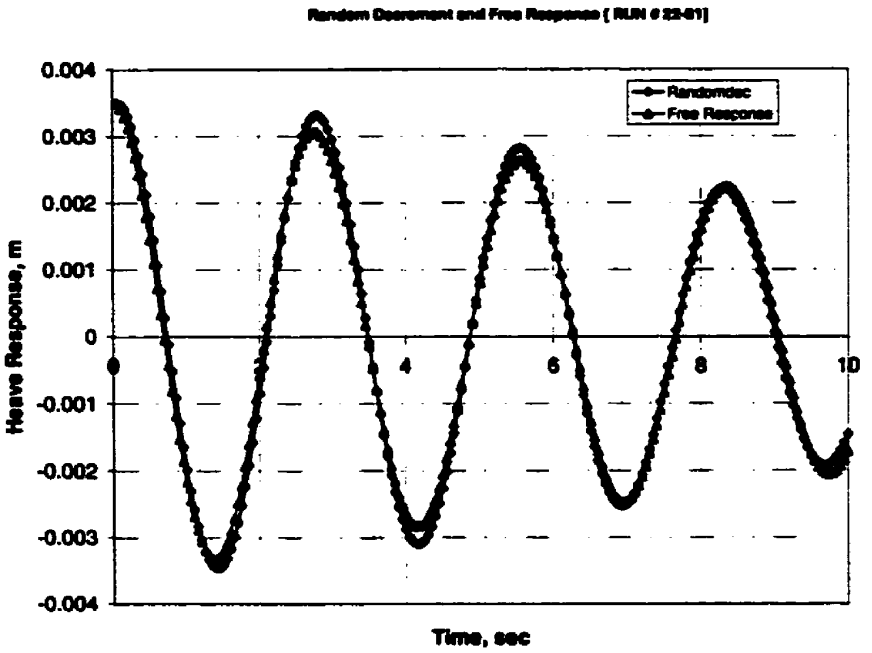

Figure 6.139 Comparison between the random decrement and the measured free response for heave motion [Run # 22-01]

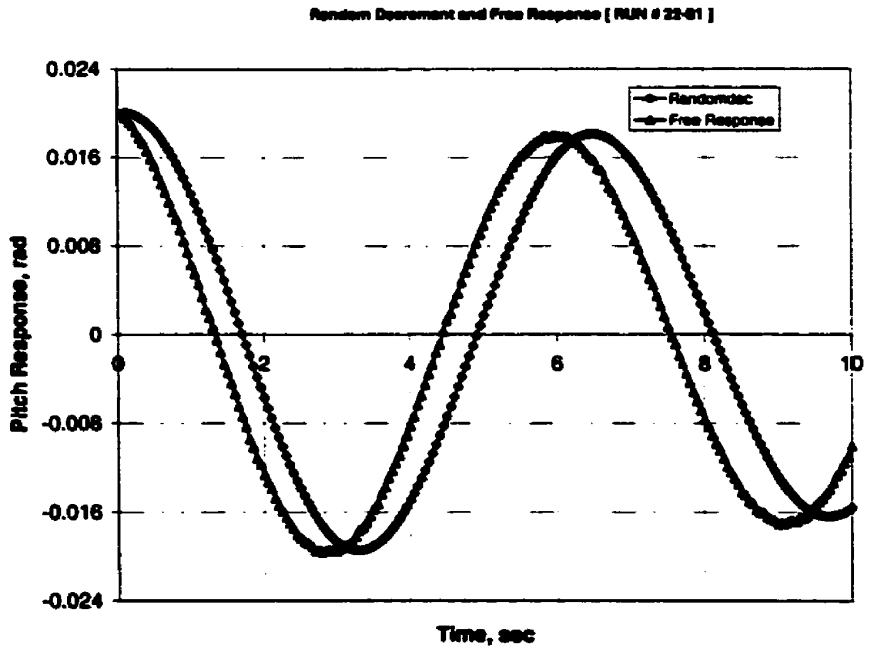

Figure 6.140 Comparison between the random decrement and the measured free response for pitch motion [Run # 22-01]

The previous figures show that the random decrement signature obtained from the filtered response agrees well with the measured free motion response for the coupled heave and pitch motions. This result emphasizes that the random decrement signature obtained from the filtered signal represents the free motion of an URV.

The values of the identified damping, restoring, and coupling parameters for the experimental runs given in Table (6.2), are obtained using the developed technique. These parameters are given in Tables (6.3) and (6.4) for the heave and pitch motions, respectively. The values of the damping and restoring parameters d_{31} and d_{33}, and d_{42} and d_{44} determined from the different runs are nearly the same, within the expected experimental error.

The agreement for the coupling parameters d_{32} and d_{34}, and d_{41} and d_{43} is not as good. However, the criterion should be whether the identified model yields an accurate motion prediction. Therefore, the identified models were used to generate predictions of the free motion using equations (5.1) and (5.2). The predicted free motion responses have been obtained by setting the normalized excitation force and moment functions, $F_i(t)$ and $M_i(t)$ to zero.

The comparison between the free responses obtained using the proposed identification technique and the measured free responses for heave and pitch motions is shown in Figures (6.141) to (6.163). The agreement between the predicted free response and the measured response is excellent for the heave motion. The agreement for the pitch prediction is excellent except for a phase between the two responses. It should be noted that, in spite of the phase shift in the predicted pitch response, the prediction gives the amplitude and the frequency with reasonable accuracy.

The agreement in the previous figures shows that the identification technique suggested in this work can be used to identify the parameters in the equations describing the coupled heave and pitch motions for an URV sailing near the water surface in random waves using only the measured responses at sea.

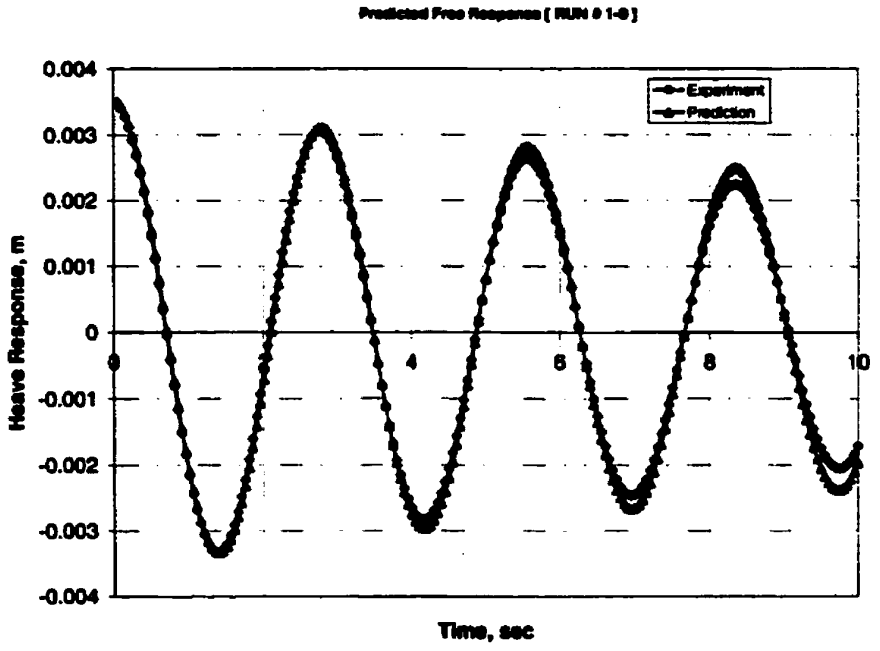

Figure 6.141 Comparison between the measured and the predicted free responses for heave motion [Run # 1-0]

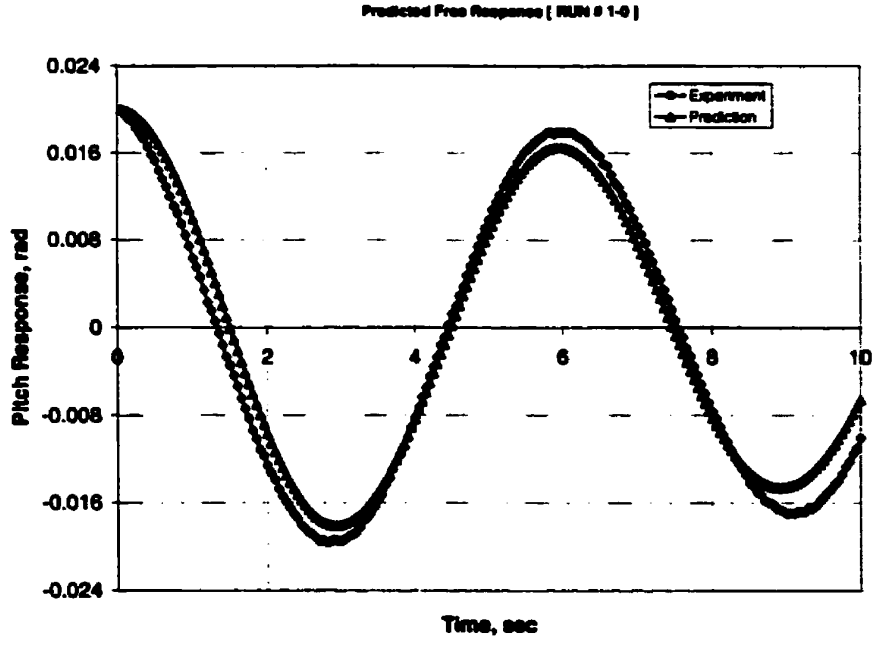

Figure 6.142 Comparison between the measured and the predicted free responses for pitch motion [Run # 1-0]

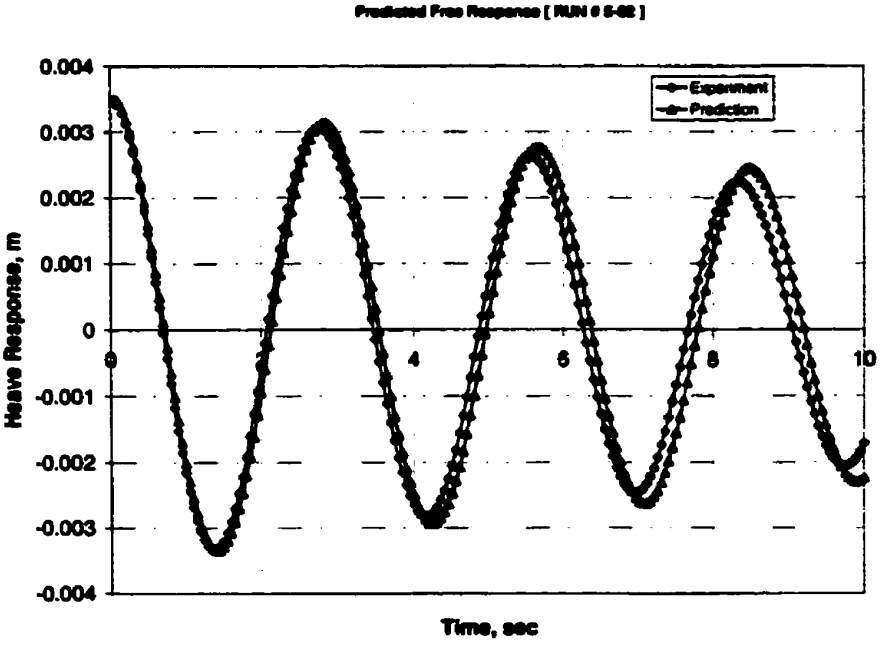

Figure 6.143 Comparison between the measured and the predicted free responses for heave motion [Run # 5-02]

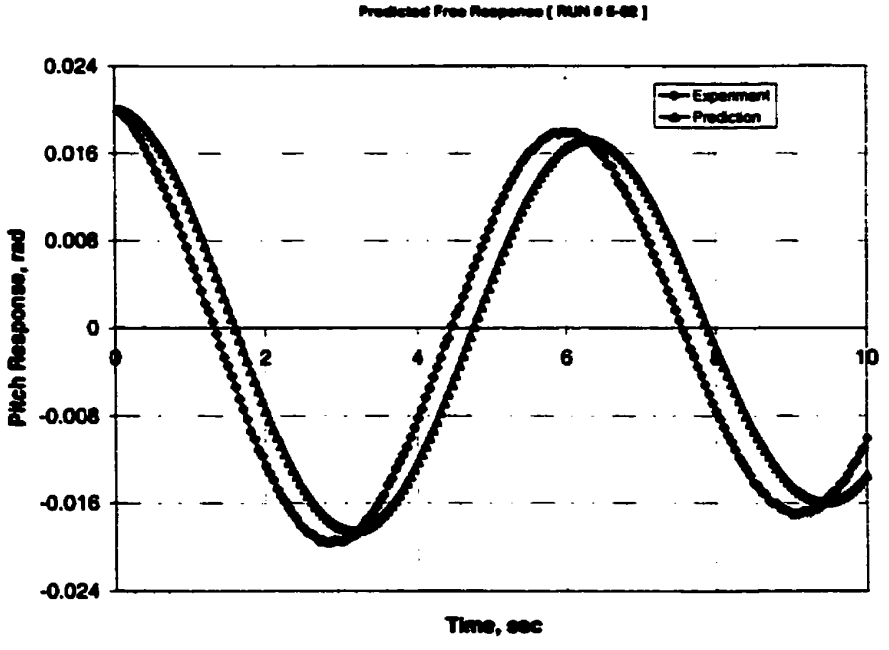

Figure 6.144 Comparison between the measured and the predicted free responses for pitch motion [Run # 5-02]

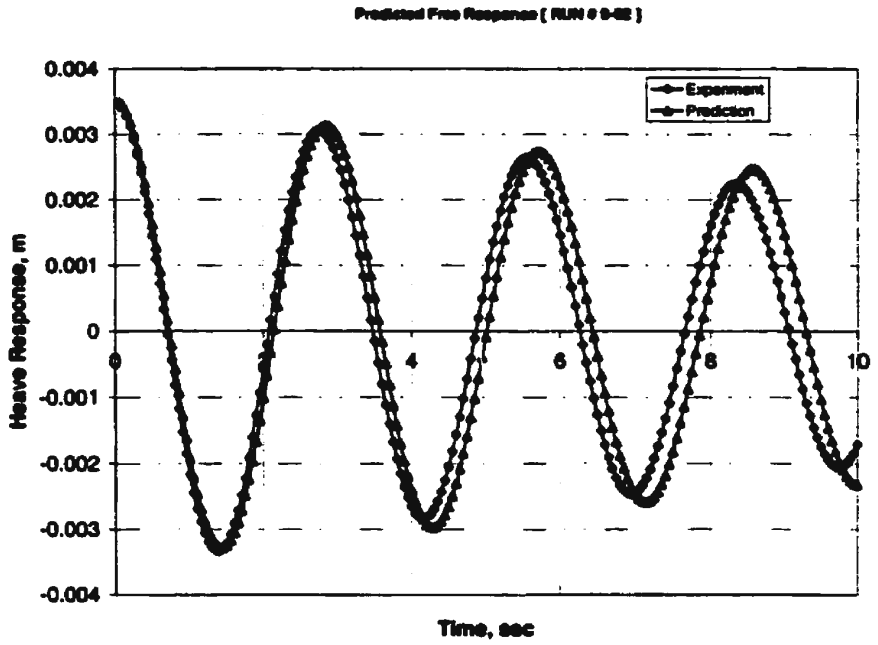

Figure 6.145 Comparison between the measured and the predicted free responses for heave motion [Run # 9-02]

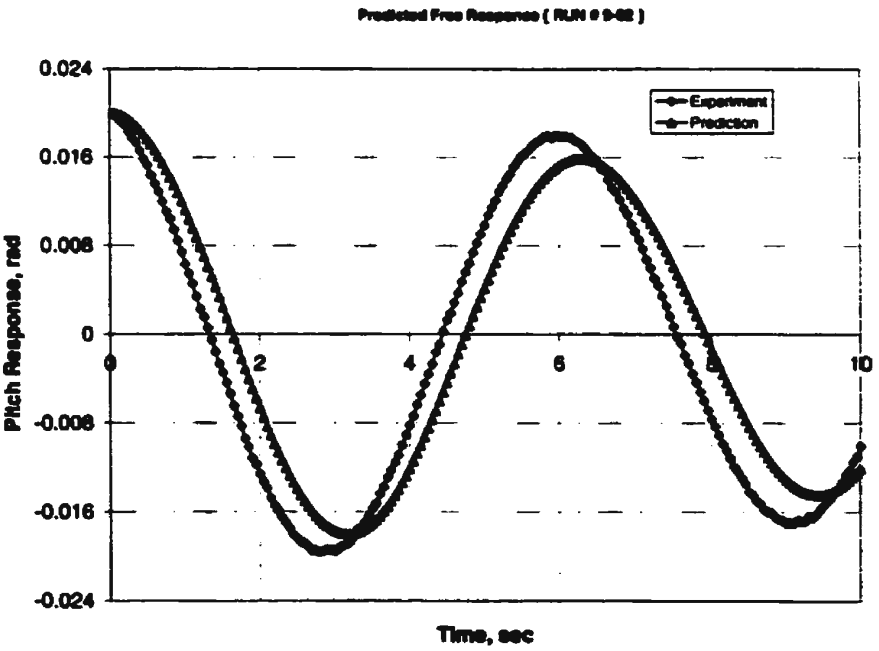

Figure 6.146 Comparison between the measured and the predicted free responses for pitch motion [Run # 9-02]

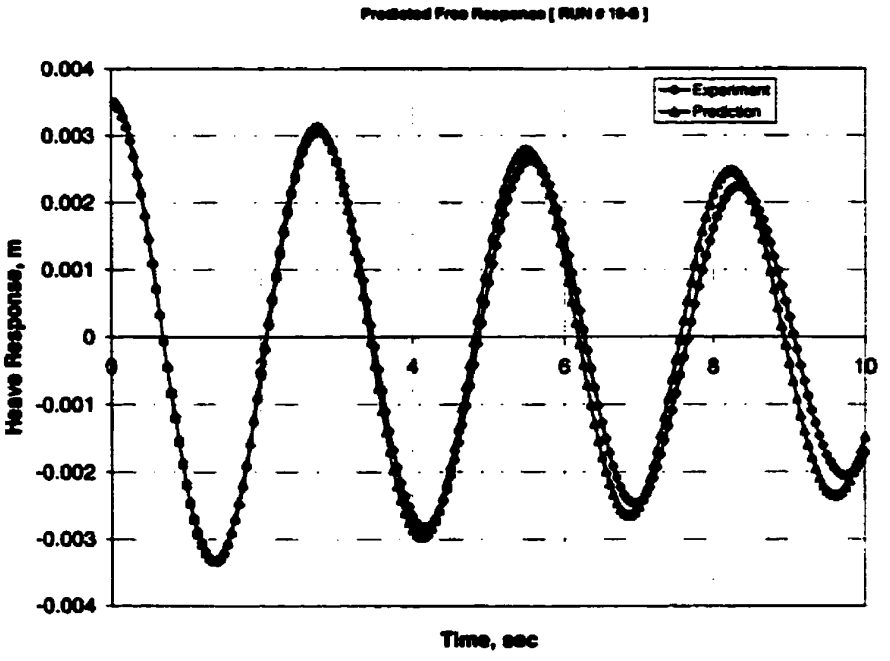

Figure 6.147 Comparison between the measured and the predicted free responses for heave motion [Run # 10-0]

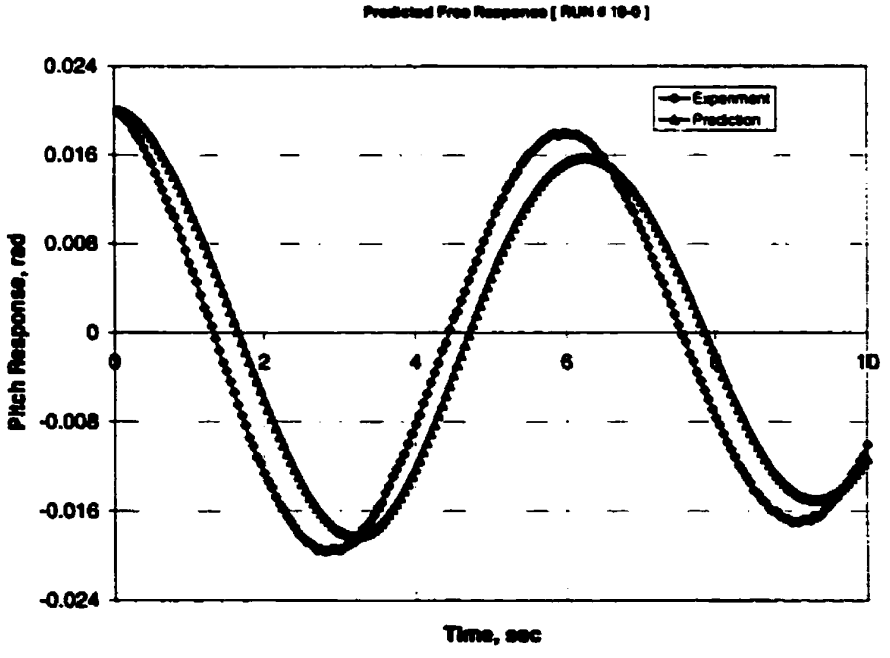

Figure 6.148 Comparison between the measured and the predicted free responses for pitch motion [Run # 10-0]

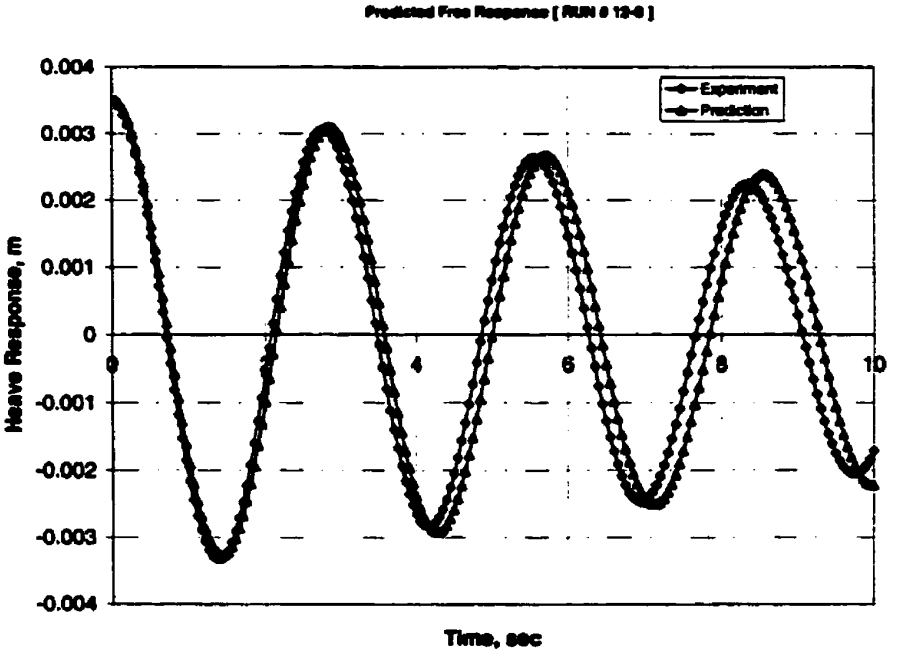

Figure 6.149 Comparison between the measured and the predicted free responses for heave motion [Run # 12-0]

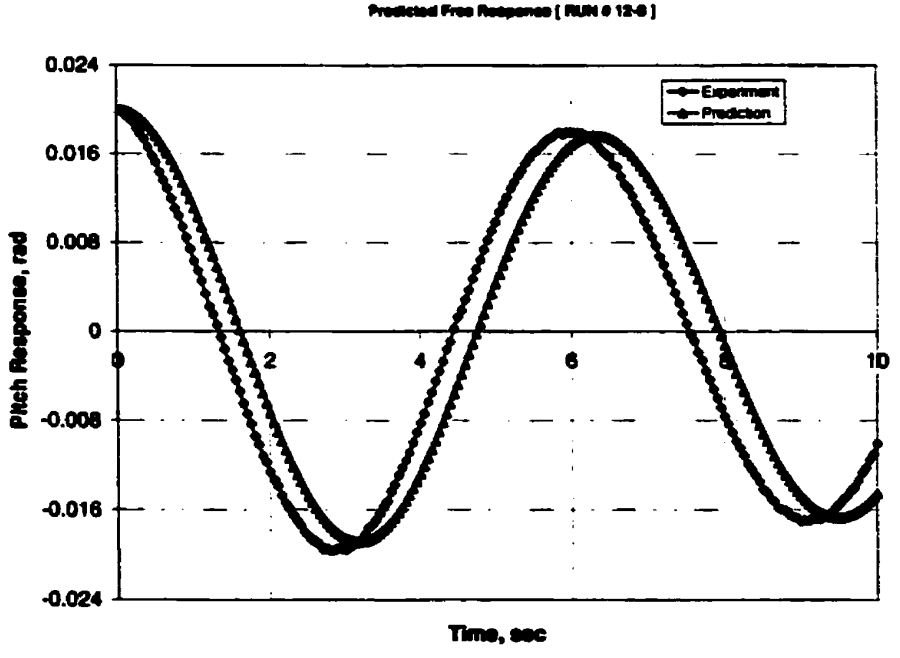

Figure 6.150 Comparison between the measured and the predicted free responses for pitch motion [Run # 12-0]

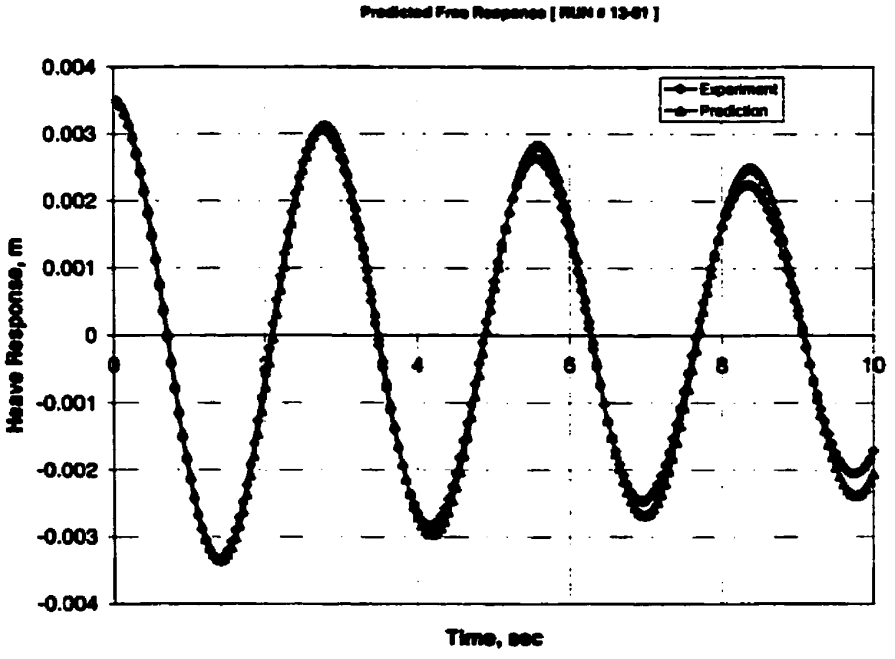

Figure 6.151 Comparison between the measured and the predicted free responses for heave motion [Run # 13-01]

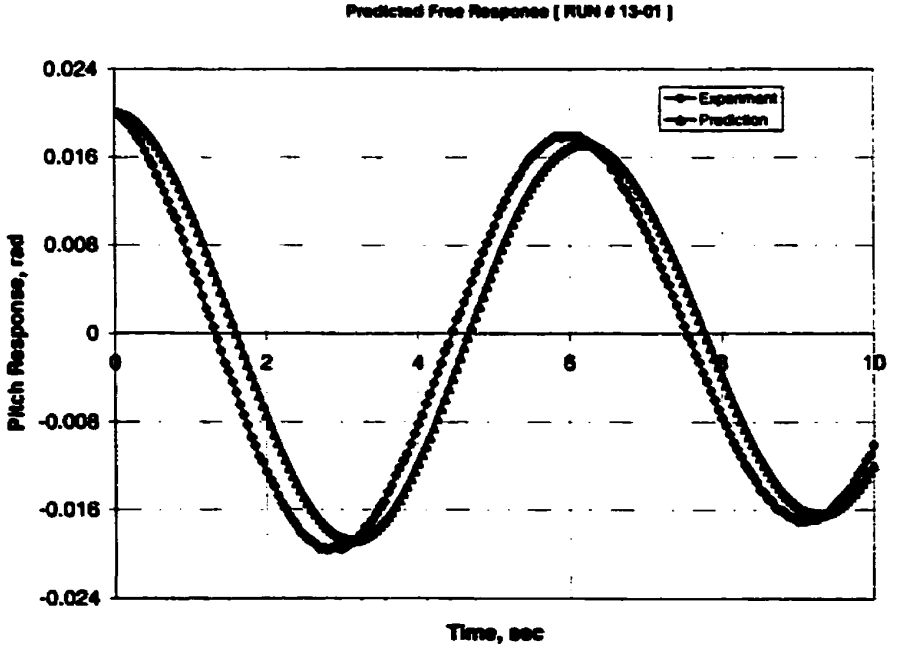

Figure 6.152 Comparison between the measured and the predicted free responses for pitch motion [Run # 13-01]

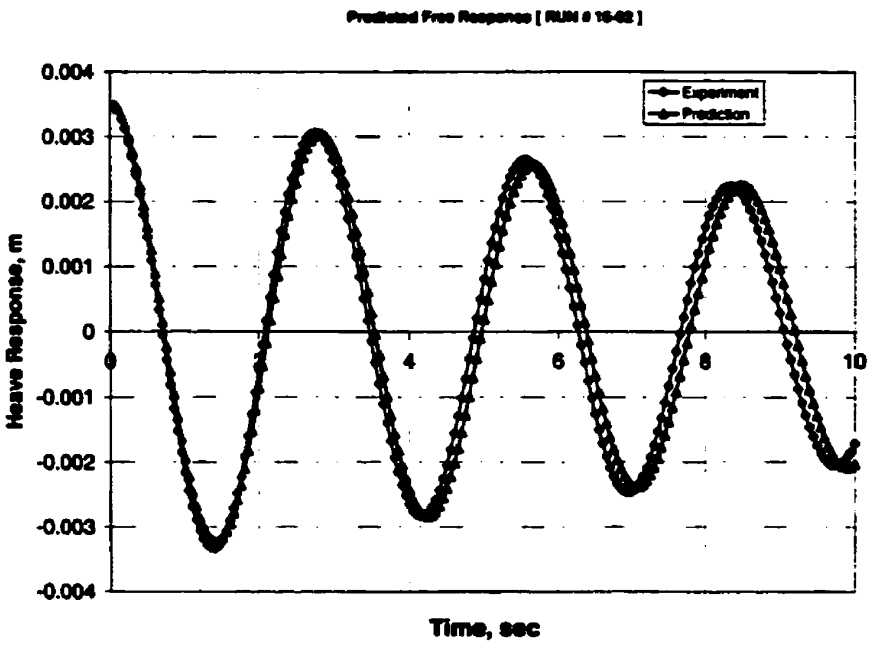

Figure 6.153 Comparison between the measured and the predicted free responses for heave motion [Run # 16-02]

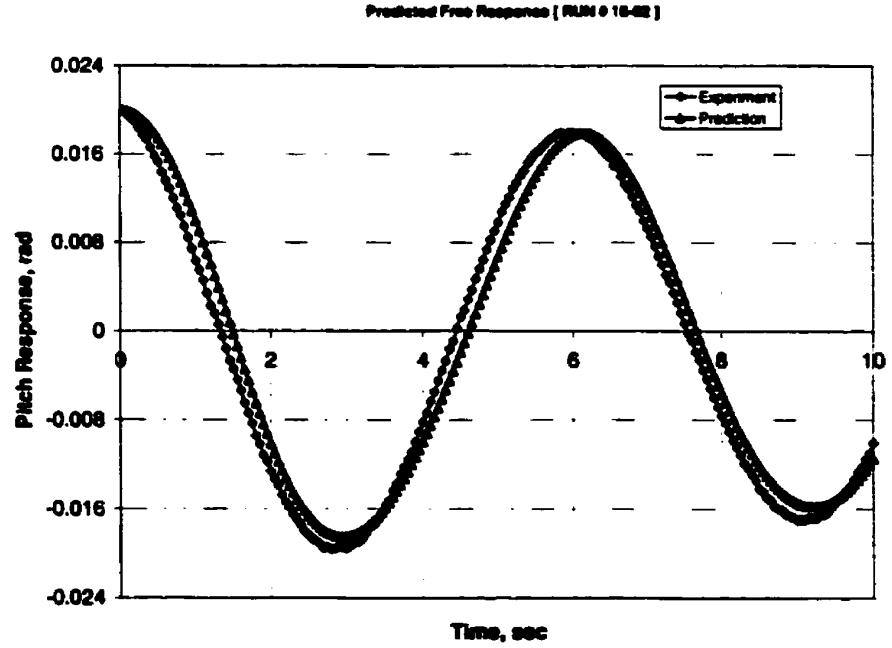

Figure 6.154 Comparison between the measured and the predicted free responses for pitch motion [Run # 16-02]

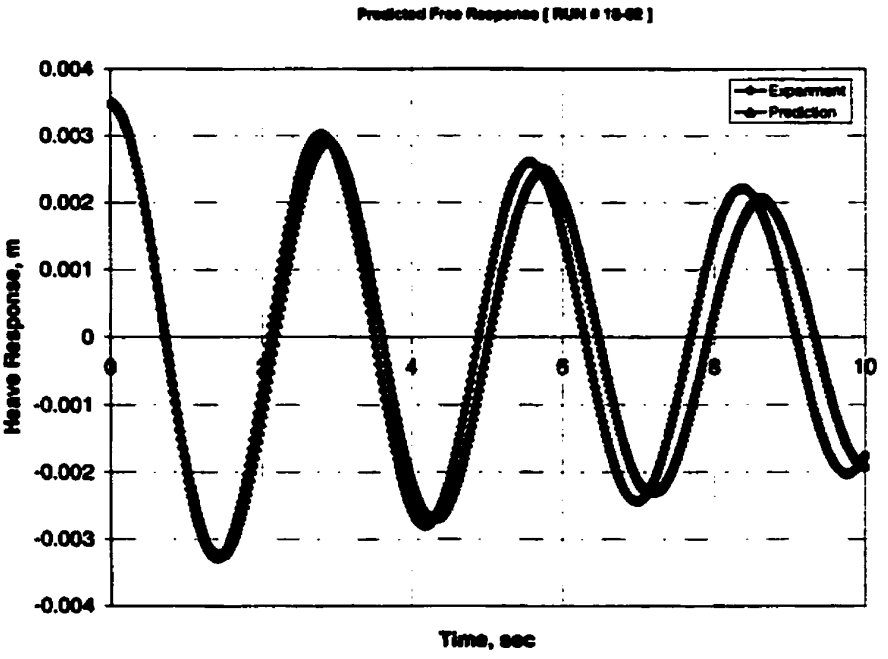

Figure 6.155 Comparison between the measured and the predicted free responses for heave motion [Run # 18-02]

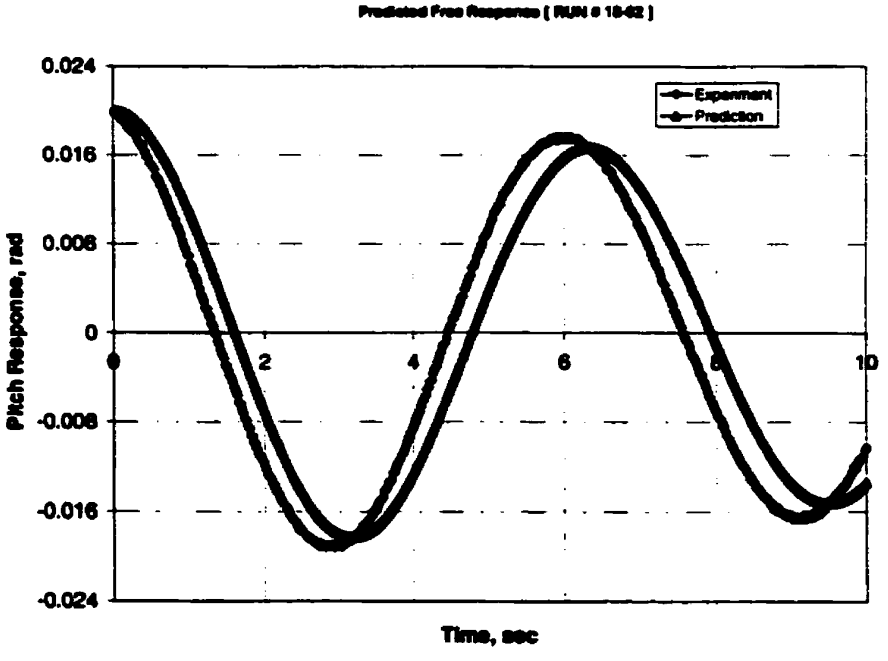

Figure 6.156 Comparison between the measured and the predicted free responses for pitch motion [Run # 18-02]

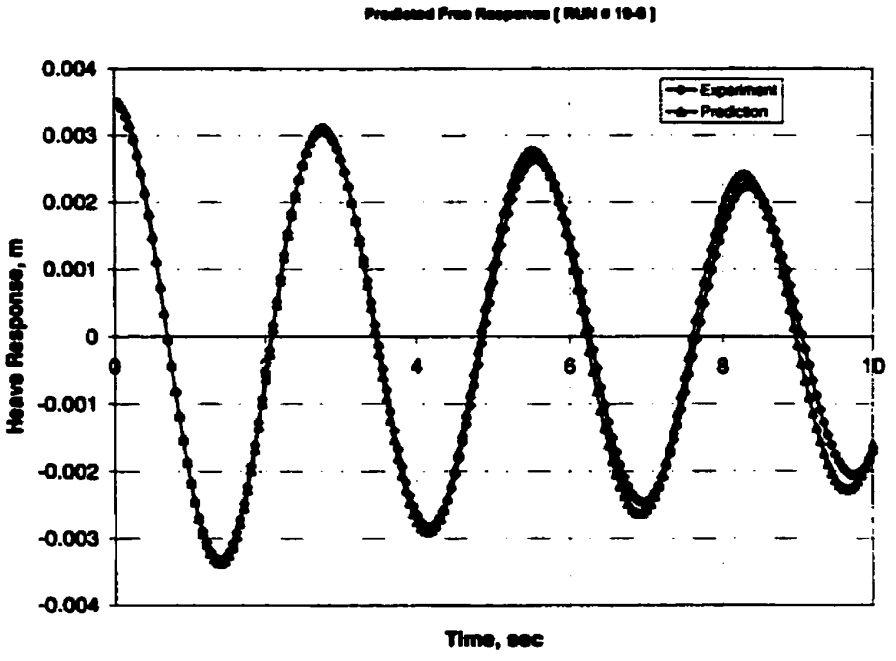

Figure 6.157 Comparison between the measured and the predicted free responses for heave motion [Run # 19-0]

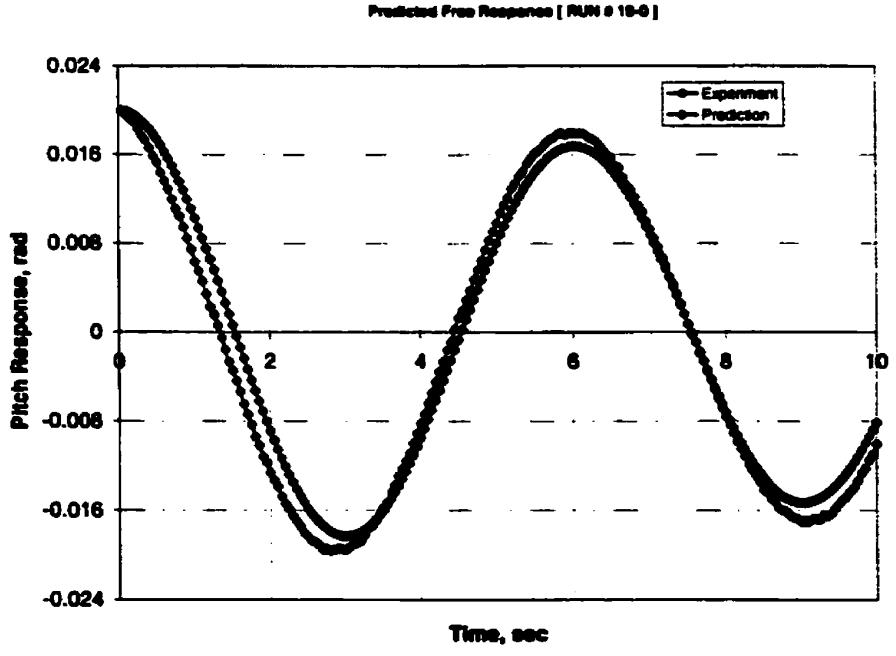

Figure 6.158 Comparison between the measured and the predicted free responses for pitch motion [Run # 19-0]

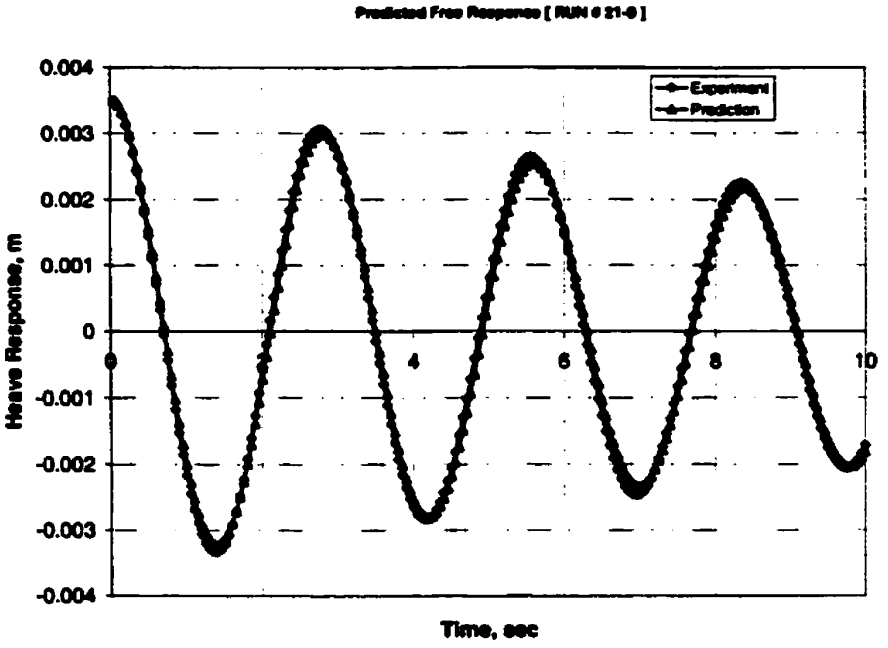

Figure 6.159 Comparison between the measured and the predicted free responses for heave motion [Run # 21-0]

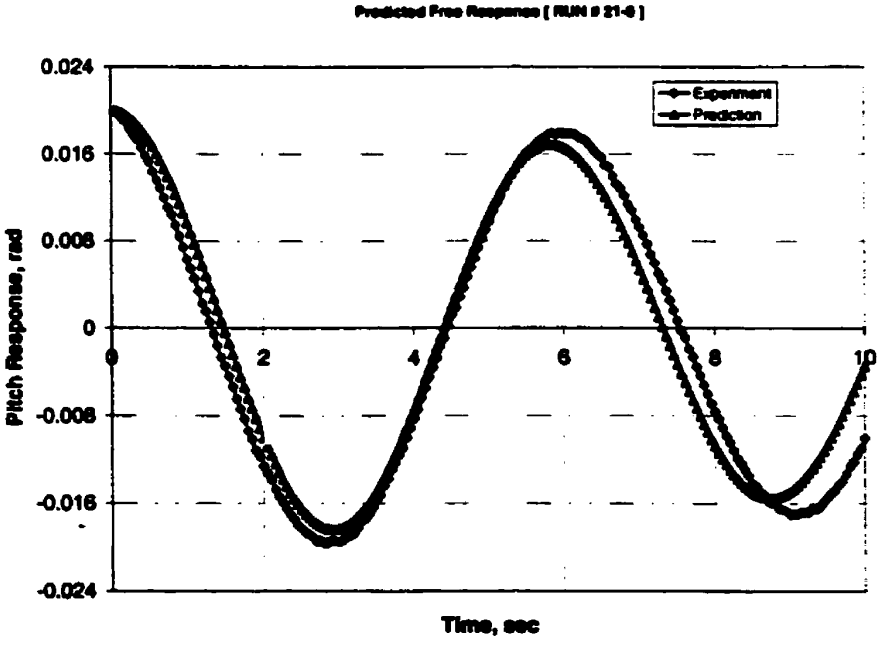

Figure 6.160 Comparison between the measured and the predicted free responses for pitch motion [Run # 21-0]

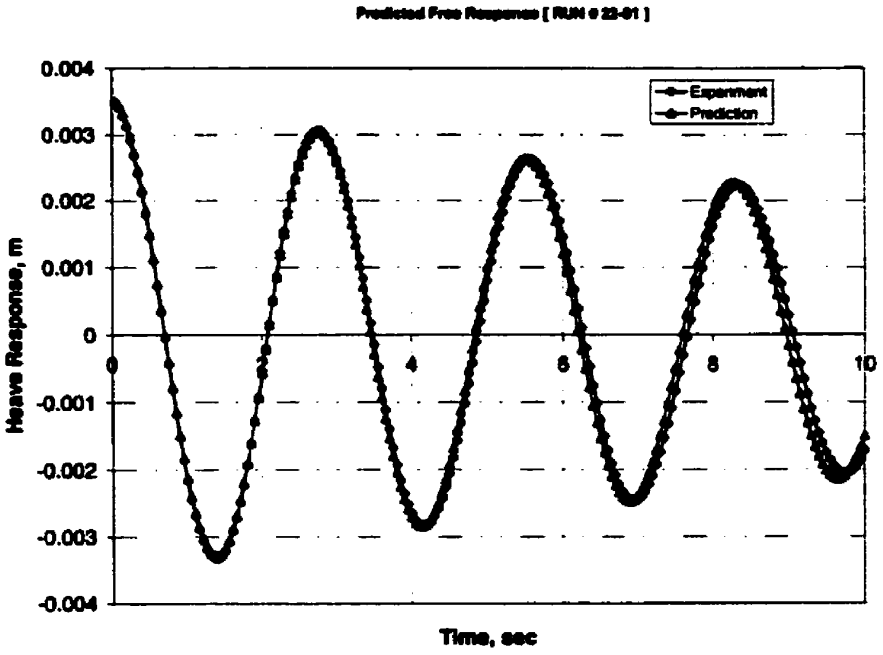

Figure 6.161 Comparison between the measured and the predicted free responses for heave motion [Run # 22-01]

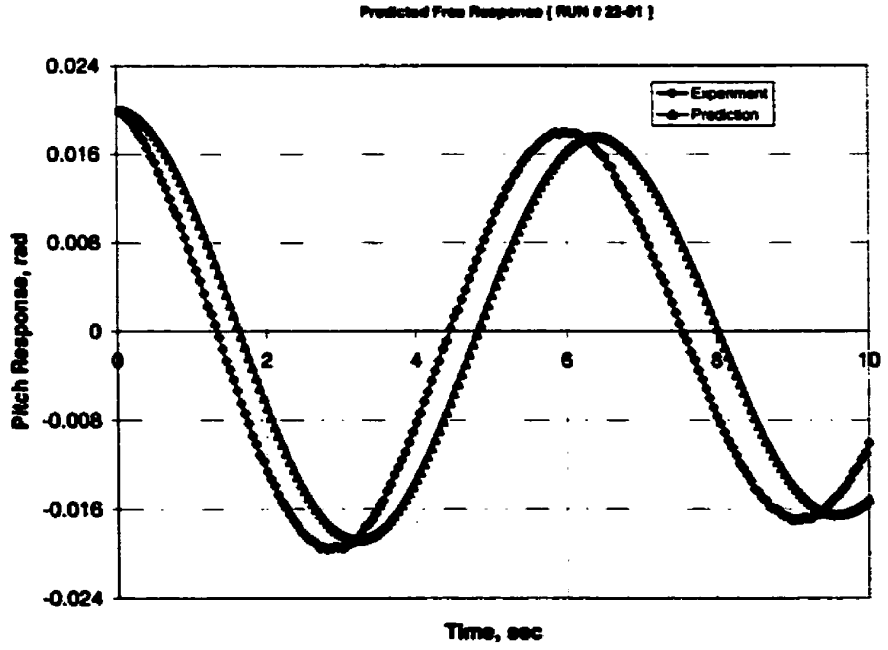

Figure 6.162 Comparison between the measured and the predicted free responses for pitch motion [Run # 22-01]

6.2.1 Effect of the Significant Wave Height, Wave Modal Frequency, and the Towing Speed

The experimental program for the random wave experiments covered ranges of three parameters: the significant wave height, H_S, the wave modal frequency, Ω, and the towing speed, U as shown in Appendix L. The main purpose of varying these parameters was to investigate the effect of different forms of the wave excitations on the utility of the developed identification technique for use in different wave environments.

The experimental runs given in Table (6.2) are chosen from the experimental program in order to show the effect of varying the three parameters on the utility of the developed technique in the identification of the hydrodynamic parameters for an URV sailing near the sea surface in random waves.

Two experimental runs: 1-0 and 10-0 are presented to investigate the effect of varying the significant wave height on the utility of the developed technique. These runs are carried out with different values of significant wave height: 0.07 m and 0.1 m, at constant wave modal frequency of 0.5 Hz in a stationary state case (U = 0 m/sec) as given in Table (6.2).

The results for the identified parameters for runs: 1-0, 10-0, and 19-0 from the experimental measurements are given in Tables (6.3) and (6.4). It is clear from these tables that changes in the significant wave height do not affect the predicted parameters. The damped natural frequencies in heave and pitch motions are not affected as well. Moreover, the agreement between the random decrement signature and the predicted free response is good and does not change as the significant wave height varies.

The effect of varying of the wave modal frequency on the utility of the developed technique can be investigated using runs 10-0 and 12-0 or runs 16-02 and 18-02 or runs 19-0 and 21-0. These runs are carried out with different wave modal frequencies at constant significant wave height and constant towing speed as given in Table (6.2).

The results of the identified parameters for these runs from using both the experimental measurements are given in Tables (6.3) and (6.4). It is clear from these tables that as the wave modal frequency varies, the damping and the restoring parameters are almost constant. Moreover, the random decrement signatures agree well with the measured free responses.

The effect of varying of the towing speed, U on the suitability of the developed technique can be ascertained using runs 1-0 and 5-02 or runs 10-0 and 13-01 or runs 19-0 and 22-01. These runs are conducted with different speeds and constant wave modal frequencies and constant significant wave height as given in Table (6.2). The results show that as the towing speed varies, the identified damping and restoring parameters are almost constant.

I can conclude from the above results that the developed identification technique provides values of the parameters, which are independent of the wave environment (significant wave height, wave modal frequency, and towing speed). It was shown above that the proposed identification technique is a suitable tool that can be used to identify the hydrodynamic parameters using the measured random coupled heave and pitch time series for an URV sailing near the sea surface in random waves.

The filtered data corresponds to narrow-band excitations was used to determine the random decrement signatures using the numerically generated data and experimentally measured data. The results obtained from the numerically generated data for the six case studies. It is clear that while the agreement between the random decrement signature and the free response is good for the first two cases, this agreement starts to deteriorate for Case (3').

The agreement between the random decrement signature and the free response obtained from the experimental data is excellent. So, it is clear that for highly damped systems the random decrement signature cannot be used to represent the free response of the system. However, the method developed in this work is successful with moderately damped systems. As can be seen from Tables (5.1), (5.2), (5.5), (5.6), (5.10), and (5.11), the damping level used in Case (2) is almost four times the values found for the physical model from the experimental data.

The random decrement signatures were used to identify the parameters in heave and pitch equations of motion using the developed technique. The parameters used in generating the numerical data as well as those predicted using the identification are shown in Tables (5.1), (5.2), (5.5), (5.6), (5.10), and (5.11). It is clear that there is variation in the values of the parameters while there is good agreement between the original and the predicted values for the direct parameters (d_{31}, d_{33}, d_{42}, and d_{44}). The agreement is poor for the coupling parameters (d_{32}, d_{34}, d_{41}, and d_{43}). This may be attributed to errors associated with the application of the regression analysis to the functions G_1 and G_2.

In the actual application of this technique we suggest that the functions G_1 and G_2 be used directly to estimate the motion response. The reason we used the regression technique at this point is to try to find how successful the regression technique would be in estimating these parameters. If instead, we use the predicted G_1 and G_2 functions in the equations of motion and integrate the equations to estimate the response, we find that the predicted response agrees well with the response calculated from the original model. The same comparison was made for the results obtained using the experimental data.

Chapter 7
Conclusions and Future Work

7.1 Conclusions

In this work I have developed an identification technique that can be applied to determine estimates for the damping, restoring, and coupling parameters in the coupled equations of heave and pitch motions for an underwater robotic vehicle sailing near the sea surface. The technique uses the response of the vehicle to random waves; however, it does not require prior knowledge of the excitation. This makes the technique a candidate for the continuous monitoring tool for the hydrodynamic parameters of these vehicles.

One of the main features of this technique is to apply a band-pass filter, centered around the damped natural frequency of heave and pitch, to the random response of the vehicle. This way, I was able to obtained accurate estimates for the free motion of the vehicle using the random decrement signature and the correlation functions technique.

To the best of the author's knowledge this approach has not been used before and represents a new methodology, which extends the applicability of the random decrement and the correlation function techniques to moderately damped motions.

The following conclusions have been arrived

1. Numerical simulations show that the level of damping and the difference between the natural frequencies and the wave modal frequency affects the accuracy of the

predictions of the hydrodynamic parameters in the equations of heave and pitch motions.

2. The developed technique can accurately predict the hydrodynamic model of an URV for both wide-band and narrow-band excitations.
3. Using numerically generated data, we have shown that the method is valid for a damping level about four times that measured experimentally. The method does not apply for a damping level higher than this. However, these results indicate that the technique will be valid for realistic vehicles.
4. The developed model was able to predict the hydrodynamic model of the vehicle in a range of different situations. The predictions are not affected by the significant wave height, the wave modal frequency, or the towing speed.

The developed identification technique was shown to provide models, which can accurately predict the free and regular responses of the vehicle. The fact that this technique provides results in a very short processing time and that it only requires the knowledge of the measured responses of the vehicle makes it a strong candidate for a system to be used onboard to provide an up-to date model for the heave-pitch motion of the vehicle. Better control of the vehicle's motion can be achieved if such a system is included in the control loop of the vehicle. This will be subject of a future study.

7.2 Future Work

Although the developed identification technique has been validated using numerically generated data as well as experimental data, I still need to investigate the reliability of the technique using full-scale measurements.

The experimental work in this dissertation is conducted for an URV-model, which was not equipped with foreword planes, after planes, rudder, vertical stabilizer, and propeller. It is not expected that these appendages will affect the ability of the developed technique. However, this needs to be ascertained.

Another way for the validation of the new technique is to use the Marine Dynamic Test Facility (MDTF) where the input and the output can be measured. The developed identification technique can be extended to the coupled sway and yaw motions for a URV sailing near the sea surface.

References

1 Committee on Undersea Vehicles, Marine Board, Undersea Vehicles and National Needs, National Research Council (U.S.), National Academy Press, 1996.

2 A Group of Authorities, *Submersible Vehicle Systems Design*, ed. E.E. Allmendinger, SNAME, pp. 18-25, 1990.

3 J. Yuh, "Development in Underwater Robotics," *in Proceedings, of the IEEE International Conference on Robotics and Automation*, Piscataway, N.J., U.S.A., pp. 1862-1867, 1995.

4 J. Yuh, "Control of Underwater Robotic Vehicles," *in Proceedings of the International Conference on Intelligent Robots and Systems*, Yokohama, Japan, July 26-30, pp. 517-521, 1993.

5 J. Yuh, "Issues on Control of the Underwater Robotic Vehicles," *in Proceedings, IEEE International Conference on Systems, Man, and Cybernetics*, Part 3 (of 5), Le Touquet, France, pp. 313-315, 1993.

6 G. Conte and A. Serrani, "Modeling and Simulation of Underwater Vehicles," *in Proceedings of the IEEE International Symposium on Computer-Aided Control System Design*, Dearborn, MI, pp. 62-67, 1996.

7 S. B. Cihen, and R. F. Beck, "Experimental and Theoretical Hydrodynamic Forces on a Mathematical Model in Confined Waters," *Journal of Ship Research*, vol. 27, no. 2, pp. 75-89, June 1983.

8 J. O. De kat and J. R. Paulling, "The Simulation of Ship Motions and Capsizing in Severe Seas," *SNAME Transactions*, vol. 97, pp. 139-168, 1989.

9 P. Baiardi, G. Casalino, R. Bono, G. Cannata, and G. Veruggio, "Dynamic Simulation Tools for the Analysis and Design of AUV's," *IEEE Symposium on Autonomous Underwater Vehicle Technology*, pp. 105-108, 1992.

10 M. A. Abkowitz, "Stability and Control of Ocean Vehicles," *the MIT Press*, Cambridage, Massachusetts, U.S.A., 1969.

11 H. A. Jr. Cole, "On-Line Failure Detection and Damping Measurement of Aerospace Structures by Random Decrement Signatures," *NASA CR-2205*, 1973.

12 H. A. Cole, "On-the Line Analysis of Random Vibrations," *AIAA/ASME 9th Structural Dynamics, and Materials Conference*, Palm Springs, CA, AIAA paper no. 68-288, 1968.

13 M. R. Haddara and Y. Wang, "Parametric Identification of Coupled Sway and Yaw Motions," *in Proceedings of 15th International Conference on Offshore Mechanics and Arctic Engineering*, vol. 1, Offshore Technology, pp. 267-273, 1996.

14 M. R. Haddara, "On the Random Decrement for Nonlinear Rolling Motion," *in Proceedings of the 12th International Conference on Offshore Mechanics and Arctic Engineering*, Calgary, Canada, pp. 283-288, 1992.

15 M. R. Haddara and J. Xu, "On the Use of Random Decrement in the Identification of Two Degrees of Freedom Systems," *in Proceedings of CSME FORUM*, Ryerson Polytechnic University. Toronto, vol. 4, pp. 499-507, May 19-22, 1998.

16 M. Nahon, "A Simplified Dynamics Model for Autonomous Underwater Vehicles," *in Proceedings, of the Symposium on Autonomous Underwater Vehicle Technology*, Monterey, California, U.S.A., pp. 373-379, June 2-6, 1996.

17 R. Battacharyya, *Dynamics of Marine Vehicles*, published by John Wiley and Sons Inc., New York, N.Y., U.S.A., pp.308, 1978.

18 Y. K. Alekseev, V. V. Kostenko, and A. Y. Shumsky, "Use of Identification and Fault Diagnostic Methods for Underwater Robotics," *in Proceedings of the IEEE*, Part 2 (of 3), Brest, France, pp. II-489 - II-494, 1994.

19 T. C. Smith, "Survey of Hydrodynamic Interaction Theories and Implementations," *National Defense Research and Development Branch*, Technical Memoradum 92/204, February 1992.

20 H. Bingham, F. Korsmeyer, and J. Newman, "Prediction of the Seakeeping Characteristics of Ships," *20th Symposium on Naval Hydrodynamics*, Santa Barbara, California, U.S.A., 1994, pp. 27-47.

21 H. L. Wong, "A Numerical Procedure for Slender Bodies at Leeway," *in Proceedings of the 3rd Canadian Marine Hydrodynamics and Structures Conference*, Halifax/Dartmouth, Nova Scotia, Canada, pp. 83-62,1995.

22 Y. Wu, J. Xia, and S. Du, " Two Engineering Approaches to Hydroelastic Analysis of Slender Ships," *in Proceedings of the International Union of Theoretical and Applied Mechanics Memorial Symposium on the Dynamics of Marine Vehicles and Structures in Waves*, Brunel University, Uxbridge, U.K., pp. 157-165, June 24-27, 1990.

23 S. K. Choi, G. Y. Takashige, and J. Yuh, "Experimental Study on an Underwater Robotic Vehicle: ODIN," *in Proceedings, of the Symposium on Autonomous Underwater Vehicle Technology*, Cambridge, Massachusetts, U.S.A, pp. 79-84, July 19-20, 1994.

24 M. A. Abkowitz and G. Liu, "Measurement of Ship Resistance, Powering and Maneuvering Coefficients from Simple Trials During a Regular Voyage," *Transactions of the Society of Naval Architects and Marine Engineers*, vol. 96, pp.97-128, 1988.

25 J. B. Robert, J. F. Dunne, and A. Debonos, "Estimation of Ship Roll Parameters in Random Waves," *in Proceedings of the 10th International Conference On Offshore Mechanics and Arctic Engineering*, vol. II, Safety and Reliability, pp. 97-106, 1991.

26 A. J. Healey, "Towards an Automatic Health Monitor for Autonomous Underwater Vehicles Using Parameter Identification," *in Proceedings of the 12th American Control Conference*, San Francisco, California, U.S.A., pp. 585-589, June 2-4,1993.

27 J. B. Roberts, J. F. Dunne, and A. Debonos, "Stochastic Estimation Methods for Non-linear Ship Roll Motion," *Probabilistic Engineering Mechanics 9*, pp. 83-93, 1994.

28 S. R. Ibrahim and E. C. Mikulcik, "A Method for the Direct Identification of Vibration Parameters from the Free Responses," *Shock and Vibration Bulletin*, Bulletin 47, pp. 183-198, 1997.

29 J. K. Vandiver, A. B. Dunwoody, R. B. Campbell, and M. F. Cook, "A Mathematical Basis for Random Decrement Vibration Signature Analysis Technique," *Journal of Mechanical Design*, vol. 104, pp. 307-313, April 1982.

30 M. R. Haddara, M. Wishahy, and X. Wu, "Assessment of Ship's Transverse Stability at Sea," *Ocean Engineering*, vol. 21, no. 8, pp. 781-800,1994.

31 M. Wishahy and M. R. Haddara, "Continuous Assessment of Stability at Sea," *4th Canadian Marine Hydrodynamics and Structures Conference*, Ottawa, Canada, 1997.

32 M. R. Haddara, "On the Use of Neural Network Techniques for the Identification of Ship Stability Parameters at Sea," *in Proceedings of th 14th International Conference on Offshore Mechanics and Arctic Engineering*, vol. II, Safety and Reliability, pp. 127-135, 1995.

33 C. Y. Liaw, H. F. Cheong, and Q. Xie, "Genetic Algorithms in Parameter Estimation of Nonlinear Models for Ship Motions," *in Proceedings of the 6th International Offshore and Polar Engineering Conference*, Los Angeles, U.S.A., vol. III, pp. 387-392, May 26-31, 1996.

34 R. P. Lippmann, "An Introduction to Computing with Neural Nets", IEEE ASSP Magazine, vol. 4, no.2, April 1987, pp. 4-22.

35 M. R. Haddara, and M. Hinchey, "On the Use of Neural Network Techniques in the Analysis of Free Roll Decay Curves," *International Shipbuilding Progress*, vol. 42, no. 430, pp. 166-178, 1995.

36 I. Flood and N. Kartam, "Neural Network in Civil Engineering I: Principles and Understanding," *Journal of Computing in Civil Engineering*, vol. 8, no. 2, pp.131-148, 1994.

37 S. F. Masri, A. G. Chassiakos, and T. K. Caughey, "Identification of Nonlinear Dynamic Systems Using Neural Networks," *Journal of Applied Mechanics*, vol. 60, pp. 123-133, 1993.

38 V. S. Kodogiannis, P. J. G. Lisboa, and J. Lucas, "Neural Network Based Predictive Control Systems for Underwater Robotic Vehicles," *Electro'94 International Conference*, Boston, Mass. U.S.A., pp.369-376, 1994.

39 M. R. Haddara and G. C. W. Sabin, "Parametric Identification of Hydrodynamic Characteristics from Ship Manoeuvring Trials Using Neural Networks," *in Proceedings of the Twenty-Fourth American Towing Tank Conference*, Texas A&M University, Texas, U.S.A., November 1995.

40 D. G. Lainiotis, K. N. Plataniotis, D. Menon, and C. J. Charalampous, "Neural Network Application to Ship Position Estimation," *in Proceedings Conference Oceans'93*, Piscataway, N.J., U.S.A., Part 1 (of 3), pp. I-384-I-388, 1993.

41 D. G. Lainiotis, and K. N. Plataniotis, "Neural Network Estimators: Application to Ship Position Estimation," *IEEE International Conference on Neural Network*, vol. 7, pp. 4710-4717, June 27-29, 1994.

42 J. Korbicz, and A. Janczak, "A Neural Network Approach to Identification of Structure Systems," *in Proceedings of the IEEE International Symposium on*

Industrial Electronics, Piscataway, NJ, U.S.A., vol.1, pp.98-103, June 17-20, 1996.

43 A. R. J. M. Lloyd, SEAKEEPING: Ship Behaviour in Rough Weather, Ellis Horwood Limited, 1989.

44 S. L. Dingman and K. P. Sharma, "Statistical Development and Validation of Discharge Equations for Natural Channels," *Journal of Hydrology*, vol. 199, pp. 13-35, 1997.

45 D. Montgomery, Design and Analysis of Experiments, John Wiley & Sons, New York, NY, 1997.

46 A. Dean and D. Voss, Design and Analysis of Experiments, Springer Text in Statistics, New York, NY, 1999.

47 Y. Wang, "Ship Maneuverability Prediction Using Neural Networks," M. Eng., Faculty of Engineering and Applied Science, Memorial University of Newfoundland, 1996.

48 T. Sarpkaya, and M. Isaacson, Mechanics of Wave Forces on Offshore Structures, Van Nostrand Reinhold Co., New York, NY, 1981.

49 S. R. Singiresu, Mechanical Vibrations, Published by Addison-Wesley Publishing Company, U.S.A., pp. 656-664, 1990.

50 R. G. Dean and R. A. Dalrymple, Water Wave Mechanics for Engineers and Scientists, World Scientific Publishing Co. Pte. Ltd, Advanced Series on Ocean Engineering, vol. 2, 1991.

51 Written by a group of authorities, Principles of Naval Architecture, ed. J. P. Comstock, SNAME, 1967.

52 I. Field, P. M. Ostafichuk, D. Cherchas, and S. Calisal, "Feedback Control Methods for an Underwater Vehicle," *5th Canadian Marine Hydrodynamics and Structures Conference*, St. John's, Newfoundland, Canada, July 8-9, 1999.

53 J. A. Keuning, "Nonlinear Heave and Pitch Motions for Fast Ships in Irregular Head Seas," *in Proceedings of the Intersociety High Performance Marine Vehicles, American Society of Naval Engineers*, pp. S&T13-S&T25, 1992.

54 N. Fonseca and C. Guedes Soares, " Nonlinear Wave Induced Responses of Ships in Irregular Seas," *17th International Conference on Offshore mechanics and Arctic Engineering, ASME*, 1998.

Appendix A

Expressions of the Hydrodynamic Parameters in the Mathematical Model

$$d_{31} = \frac{-c_{33}}{(m+a_{33})} - \frac{B}{A}\left[\frac{a_{53}\times c_{33}}{(m+a_{33})} - c_{53}\right] \tag{A.1}$$

$$d_{32} = \frac{-c_{35}}{(m+a_{33})} - \frac{B}{A}\left[\frac{a_{53}\times c_{35}}{(m+a_{33})} - c_{55}\right] \tag{A.2}$$

$$d_{33} = \frac{-b_{33}}{(m+a_{33})} - \frac{B}{A}\left[\frac{a_{53}\times b_{33}}{(m+a_{33})} - b_{53}\right] \tag{A.3}$$

$$d_{34} = \frac{-b_{35}}{(m+a_{33})} - \frac{B}{A}\left[\frac{a_{53}\times b_{35}}{(m+a_{33})} - b_{55}\right] \tag{A.4}$$

$$\varepsilon_1 = \frac{1}{(m+a_{33})}\left[\frac{B}{A}a_{53} + 1\right] \tag{A.5}$$

$$\varepsilon_2 = \frac{B}{A} \tag{A.6}$$

$$d_{41} = \frac{1}{A}\left[\frac{a_{53}\times c_{33}}{(m+a_{33})} - c_{53}\right] \tag{A.7}$$

$$d_{42} = \frac{1}{A}\left[\frac{a_{53}\times c_{35}}{(m+a_{33})} - c_{55}\right] \tag{A.8}$$

$$d_{43} = \frac{1}{A}\left[\frac{a_{53}\times b_{33}}{(m+a_{33})} - b_{53}\right] \tag{A.9}$$

$$d_{44} = \frac{1}{A}\left[\frac{a_{53}\times b_{35}}{(m+a_{33})} - b_{55}\right] \tag{A.10}$$

$$\sigma_1 = -\frac{1}{A}\left[\frac{a_{53}}{(m+a_{33})}\right] \tag{A.11}$$

$$\sigma_2 = -\frac{1}{A} \tag{A.12}$$

$$A = \left[(I+a_{55}) - \frac{a_{53}\times a_{35}}{(m+a_{33})}\right] \tag{A.13}$$

$$B = \frac{a_{35}}{a_{33}} \tag{A.14}$$

Appendix B

Design of the URV-Model

1. Introduction

A ¼ scale model of the main body of a well-known vehicle, DOLPHIN (Deep Ocean Logging Platform with Hydrographic Instrumentation for Navigation), has been designed and built for the purpose of this work. I called the designed model URV-model. Before building the model, a numerical simulation has been conducted to estimate the motion of the model for regular harmonic waves.

The model consists of four main parts: a hemispherical nose, cylindrical hull, conical tail, and a hydrofoil connection as shown in Figure (B.1), see Figure (5.8). The model is attached to the dynamometer flange using a vertical strut element, which is located inside a hydrofoil connection.

I investigate two major calculations for the model in calm water: the weight calculation and buoyancy calculation. In the former the total weight distribution of the model and its center of gravity (KG and LCG) are calculated. In the latter the total buoyancy distribution and its center of buoyancy (KB and LCB) are calculated. These calculations are based on the premise that the main body of the URV-model and the hydrofoil connection are designed to constitute one neutrally buoyant body taking into account the effect of the dynamometer flange. The main dimensions of the different parts of the model are given in the following sections.

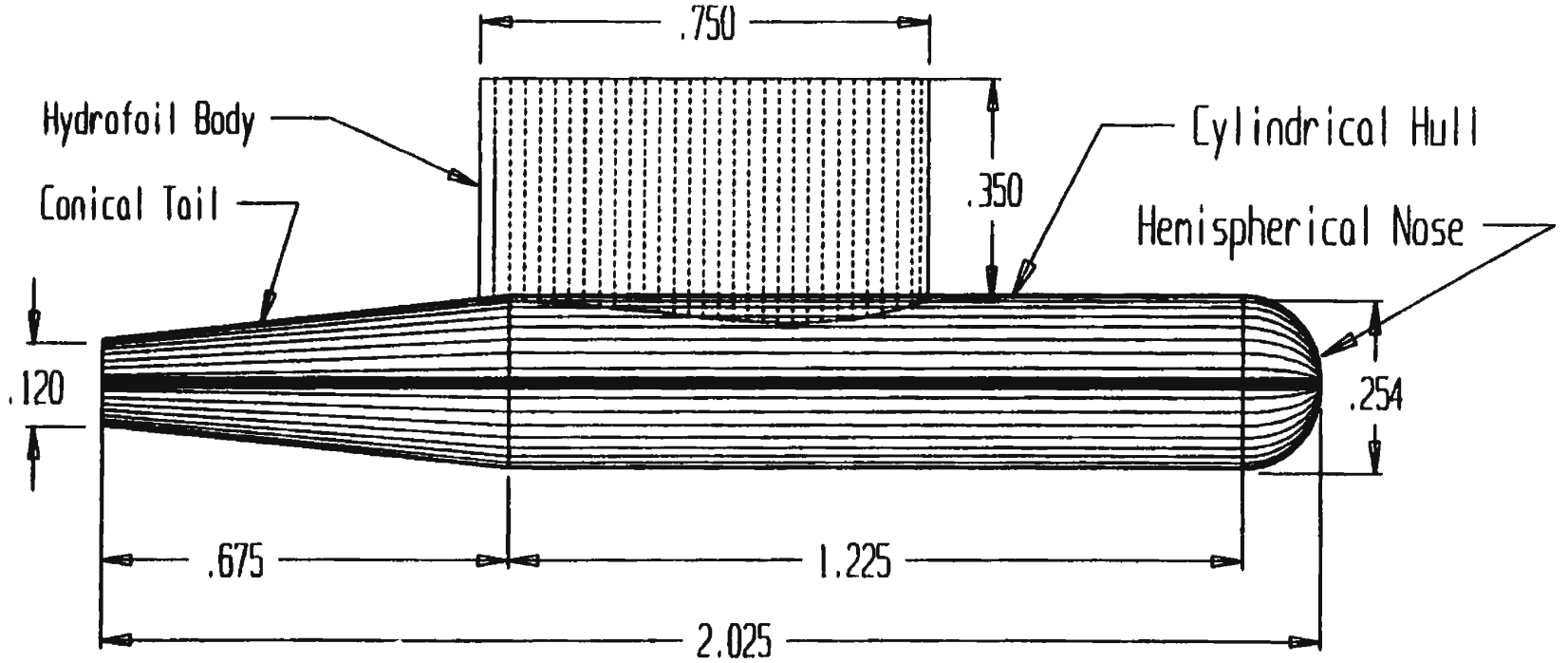

Figure B.1: URV-Model General Arrangment

The ballast calculation has been conducted based on the buoyancy and the weight calculations. Stability calculation is essentially needed to make sure that the attachment of the hydrofoil connection, the vertical dynamometer flange, and the main body of the URV-model, are statically stable in calm water.

2. Weight Calculations

The total weight of the URV-model consists of four weights: the hemispherical nose, cylindrical hull, conical tail, and the hydrofoil connection. According to the geometrical shape of each part, the corresponding weight per unit length and its longitudinal center of gravity are calculated. Furthermore, the weight distribution of the model can be estimated. Finally the total weight of the model and its LCG are calculated.

Aluminum alloys have many advantages compared to other materials. Some of these advantages are higher density, higher strength and good weldability. Therefore, it was suggested that the model be built from aluminum alloy which has the following properties:

Mass per unit volume $= 2640\ kg/m^3$

Weight per unit volume $= 24.9\ kN/m^3$

2.1 Hydrofoil Connection Weight

The installed dynamometer on the carriage of the wave tank measures the coupled heave and the pitch motions for a towed model. The dynamometer is attached to the model's

strut using a flange. The weight of this flange is nearly 73.6 N and is assumed to act as a concentrated load at the center of gravity of the model.

The model is attached to the dynamometer flange through a vertical aluminum strut inside the hydrofoil connection. The dimensions of the strut are 0.63 m × 0.105 m × 0.0254 m. The weight of the strut plate is approximately 38.6 N. This weight is assumed to be a concentrated load acting at the center of gravity of the model. The weight of the inner horizontal stiffener and top flange of the strut is 9.8 N. In addition, the weight of the *Styrofoam* material that has been used in the fabrication of the hydrofoil part is 54 N.

2.2 Nose, Tube, and Tail Weight

The hull weight of the model consists of three main parts: hemispherical nose, cylindrical hull, and conical tail. Assuming that the thickness of the shell plating of the model is 0.0032 m, a hemispherical nose of diameter 0.244 m will be built as shown in Figure (B.1). The corresponding weight of this nose is 13 N, which has been assumed linearly distributed on a length of 0.125 m from the forward perpendicular (FP).

The cylindrical hull of the model has dimensions of 1.225 m length, 0.251 m diameter, and 0.0032 m wall thickness, as shown in Figure (B.1). The weight of this tube is 75 N and is assumed to be a uniformly distributed over its entire length. In order to attach the strut to the main tube at the location of the LCG, another horizontal tube is inserted at that location. This tube has dimensions of 0.52 m length, 0.245 m diameter, and 0.0032 m wall thickness, and is assumed to be a uniformly distributed over its entire length. The corresponding weight of this tube is 34.3 N.

The conical tail of the URV-model has dimensions of small and large bases of 0.12 m and 0.244 m, respectively. The length of this part is 0.675 m as shown in Figure (B.1). The weight of the tail is 34.3 N, and is assumed to be a linearly distributed over its entire length.

Therefore, based on the above information, it can be determined that the total hull weight of the model is 206.14 N.

3. Buoyancy Calculations

The buoyancy forces for the main body of the vehicle and the submerged part of the hydrofoil connection are calculated as given in the following sections. In addition, the longitudinal center of buoyancy for the neutral buoyant body is calculated.

3.1 Hydrofoil Buoyancy

An aluminum strut is located inside the hydrofoil body at its center of gravity. The cross section of the hydrofoil body is NACA0024 with a chord length of 0.75 m. The offsets of this section are shown in Table (B.1). The hydrofoil connection is submerged to a draft of 0.20 m from its base line. The total buoyancy force corresponding to that draft for the hydrofoil connection is 189.7 N. Consequently, the assembly of dynamometer flange, the hydrofoil connection, and the main body of the URV-model constitutes one neutrally buoyant body.

3.2 Nose, Tube, and Tail Buoyancy

The buoyancy forces resulting from the submerged volume of the nose, tube, and tail parts are 42.1 N, 609.2 N, and 189.7 N, respectively. Therefore, the total buoyancy force for the main body of the model is 841 N. The LCB is 0.109 m forward of amidships which has been calculated using equation (B.1) as

$$LCB = \frac{\sum Moment\ of\ volumes}{\sum Volumes} \tag{B.1}$$

where ρ and g are the water density in kg/m^3 and the acceleration due to gravity in m/sec^2, respectively.

Then, the total buoyancy for the main body of the model and the hydrofoil connection is 1017.5 N and is acting upward at vertical center (KB) of 0.166 m from the base line and at longitudinal center 0.109 m forward amidships.

4. Ballast Calculations

Since the resulting buoyancy force from the submerged volume of the model is greater than its hull weight, a ballast weight is required. This weight is equal to the difference between the total buoyancy force and the hull weight of the model. Therefore, the required ballast mass for this model is 69.5 kg. Different materials can be used to ballast the model. One is lead, which has the following properties:

Mass per unit volume = 11 400 kg/m^3

Weight per unit volume =112 kN/m^3

Since the available weight of a lead block at the towing tank is 117.6 N, six blocks are required to provide the ballast weight. The total weight distribution of the model is shown in Figure (B.2). The area under the weight distribution represents the total weight of the model and the hydrofoil connection. The LCG for the model is 0.117 m forward amidships which has been calculated using equation (B.2).

$$LCG = \frac{\sum Moment\ of\ weights}{\sum Weights} \tag{B.2}$$

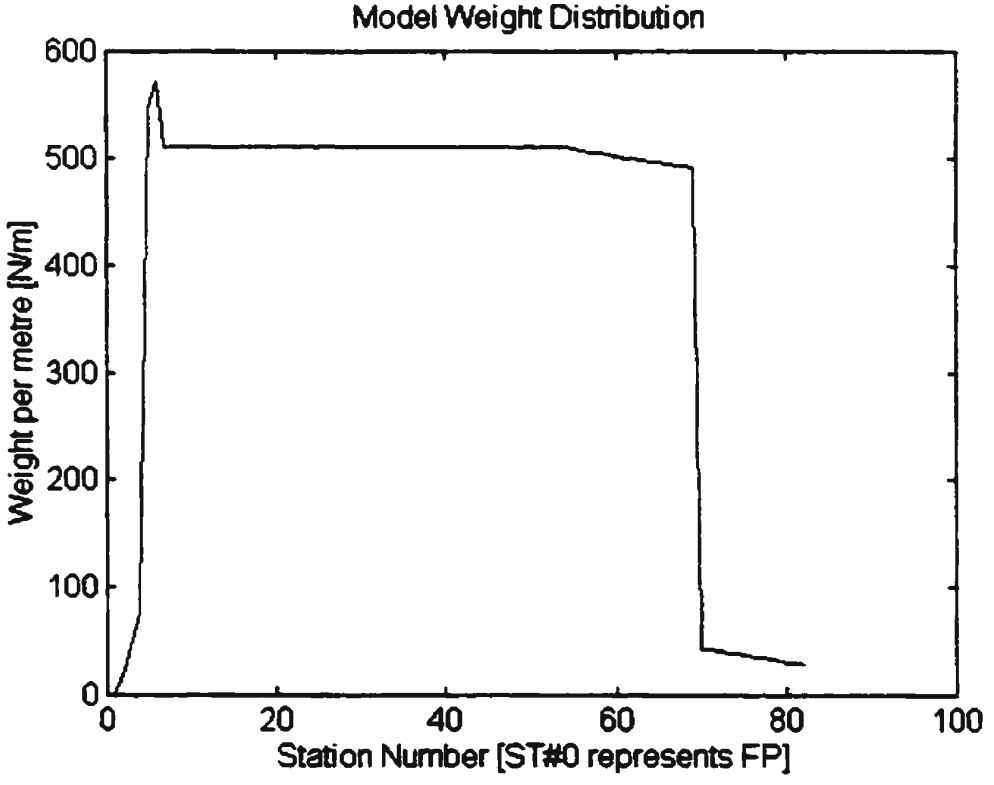

Figure B.2: Weight distribution for the URV-Model

5. Stability Calculations

Since the hydrofoil connection and the vertical dynamometer flange are acting with the main body of the URV-model, stability calculations are essential to make sure that the whole system is statically stable in calm water. In addition, the designed URV-model is considered as a semi-submersible vehicle in this work. The stability calculations are carried out for the neutrally buoyant body taking into account the effect of the vertical dynamometer flange.

Two main approaches are used in the assessment of the ship's survivability in a seaway: a static approach (quasi – static) and a dynamic one. The static approach is based on the minimum value that the longitudinal metacentric height (GM_L) should have and the shape of the static stability curve (GZ-θ). This approach is still being applied in the assessment of ship's stability criterion. I am going to use the static approach to assess the longitudinal stability of the neutral buoyant body with the vertical dynamometer flange.

The water plane sectional area (A_H) and its center (X_H) as well as the longitudinal moment of the waterplane area about the center of area (I_L) for the hydrofoil section NACA 0024, are calculated with the aim of Table (B.1) as

$$A_H = \frac{2}{3} \times S \times SUM_1 \tag{B.3}$$

$$X_H = \frac{SUM_2}{SUM_1 \times S} \tag{B.4}$$

$$I_L = \frac{2}{3} \times S^3 \times SUM_3 - A_H \times X_H{}^2 \tag{B.5}$$

where S is the longitudinal spacing for the stations and is equal to 0.025 m. X and Y_U are the longitudinal distance of the stations from the leading edge of the section and the half-breadth ordinate of hydrofoil section, respectively. L and SM are the lever distance from the mid-length of the section's chord (Station #15) and the Simpson's multiplier, respectively.

The values of A_H, X_H, and I_L are calculated as 0.09229 m^2, 0.059 m from Station #15, and 0.00285 m^4, respectively. The total buoyancy of the submerged body of the URV-model corresponding to the designed draft as well as its vertical and longitudinal centers (KB and LCB) are calculated as 1022.94 N, 0.1666 m from the base line and 0.109 m forward of amidships, respectively as shown in Table (B.2).

$$LCB = \frac{SUM_2}{SUM_1} \tag{B.6}$$

$$KB = \frac{SUM_3}{SUM_1} \tag{B.7}$$

where B_i is the total buoyancy force of part i^{th} in N. X_i and Y_i are the longitudinal and the vertical centers of buoyancy of part i^{th} from the after perpendicular (AP) and from the base line of the URV-model, respectively.

The total weight of the URV-model as well as its vertical and longitudinal centers (KG and LCG) are calculated as 1013.58 N, 0.1494 m from the base line and 0.116 m forward of amidships, respectively as shown in Table (B.3).

$$LCG = \frac{SUM_3}{SUM_2} \tag{B.8}$$

$$KG = \frac{SUM_4}{SUM_1} \tag{B.9}$$

where W_i and M_i are the weight magnitude of part i^{th} and its mass, respectively. X_i and Y_i are the longitudinal and the vertical centers of gravity of part i^{th} from the after perpendicular (AP) and from the base line of the URV-model, respectively.

It is obvious that the total buoyancy force obtained from Table (B.2) is not equal to the total weight of the model obtained from Table (B.3). This difference was expected since the measuring equipments for weights at the laboratory have some errors. When I measure the weight of a heavy object, the errors can be neglected. However, for a light object the error is significant. In our case, the individual weights are considered light objects. Therefore, when I measure the total weight of the URV-model with the effect of the dynamometer flange, the weight was found as 104 kg, which is almost the same as obtained from the buoyancy calculations. Then, the values of the BM_L and the GM_L are calculated as 0.0274 m and +0.0446 m, respectively as

$$BM_L = \frac{I_L}{\nabla} \tag{B.10}$$

$$GM_L = KB + BM_L - KG \tag{B.11}$$

where ∇ is the volume of the submerged body of the URV-model at the designed draft. It is obvious that the value of GM_L is positive which means that the main body of the URV-model, the hydrofoil connection and the dynamometer flange constitute a stable system.

Table B.1: NACA 0024 properties

ST.	X	Yu	SM	$Y_U \times SM$	L	$Y_U \times SM \times L$	$Y_U \times SM \times L^2$
0	0.000	0.000	1	0.000	15	0.000	0.000
1	0.025	0.045	4	0.179	14	2.501	35.016
2	0.050	0.060	2	0.120	13	1.563	20.314
3	0.075	0.070	4	0.281	12	3.372	40.459
4	0.100	0.077	2	0.155	11	1.703	18.732
5	0.125	0.083	4	0.330	10	3.300	33.005
6	0.150	0.086	2	0.172	9	1.549	13.942
7	0.175	0.088	4	0.353	8	2.828	22.622
8	0.200	0.090	2	0.179	7	1.255	8.784
9	0.225	0.090	4	0.360	6	2.161	12.964
10	0.250	0.090	2	0.179	5	0.897	4.483
11	0.275	0.089	4	0.355	4	1.418	5.673
12	0.300	0.087	2	0.174	3	0.522	1.567
13	0.325	0.085	4	0.340	2	0.680	1.359
14	0.350	0.082	2	0.165	1	0.165	0.165
15	**0.375**	**0.079**	**4**	**0.318**	**0**	**23.913**	**0.000**
16	0.400	0.076	2	0.152	1	0.152	0.152
17	0.425	0.072	4	0.290	2	0.579	1.159
18	0.450	0.068	2	0.137	3	0.411	1.232
19	0.475	0.064	4	0.257	4	1.027	4.109
20	0.500	0.060	2	0.119	5	0.597	2.985
21	0.525	0.055	4	0.220	6	1.319	7.914
22	0.550	0.050	2	0.100	7	0.700	4.898
23	0.575	0.045	4	0.179	8	1.433	11.462
24	0.600	0.039	2	0.079	9	0.708	6.374
25	0.625	0.034	4	0.135	10	1.348	13.479
26	0.650	0.028	2	0.056	11	0.612	6.733
27	0.675	0.022	4	0.087	12	1.042	12.508
28	0.700	0.015	2	0.031	13	0.400	5.194
29	0.725	0.009	4	0.035	14	0.491	6.871
30	0.750	0.002	1	0.002	15	0.028	0.425
				5.54	**Net**	**10.847**	**304.581**
				SUM_1	**SUM_2**	**13.065**	**SUM_3**

Table B.2: Buoyancy details for the URV-Model

Item #	Item Name	Bi (N)	Xi (m)	Yi (m)	Bi ×Xi (N.m)	Bi ×Yi (N.m)
1	Nose	42.08	1.947	0.127	81.92	5.34
2	Main Tube	608.91	1.288	0.127	783.97	77.33
3	Conical Tail	189.63	0.405	0.127	76.80	24.08
4	Hydrofoil	182.32	1.122	0.349	204.47	63.63
		1022.94			**1147.16**	**170.39**
		SUM_1			**SUM_2**	**SUM_3**

Table B.3: Weight details for the URV-Model

Item #	Item Name	M_i (kg)	W_i (N)	X_i (m)	Y_i (m)	$W_i \times X_i$ (N.m)	$W_i \times Y_i$ (N.m)
1	Conical Tail	3.79	37.20	0.405	0.127	15.07	4.72
2	Nose	1.40	13.73	1.947	0.127	26.74	1.74
3	Main Tube	8.06	79.04	1.288	0.127	101.76	10.04
4	Inner Tube	3.34	32.75	1.122	0.127	36.73	4.16
5	Horizontal Stiffener	0.67	6.59	1.122	0.127	7.39	0.84
6	Vertical Strut	4.74	46.49	1.122	0.275	52.14	12.78
7	Upper Flange	0.32	3.10	1.122	1.000	3.48	3.10
8	Hydrofoil	4.50	44.15	1.122	0.604	49.51	26.66
9	Ballast (1)	1.05	10.33	1.900	0.065	19.63	0.67
10	Ballast (2)	56.40	553.28	1.125	0.050	622.44	27.66
11	Ballast (3)	9.98	97.95	1.122	0.130	109.85	12.73
12	Ballast (4)	1.77	17.35	1.122	0.070	19.46	1.21
13	Dynamometer Flange	7.30	71.61	1.122	0.630	80.31	45.12
		103.32	**1013.58**			**1144.51**	**151.45**
		SUM_1	**SUM_2**			**SUM_3**	**SUM_4**

Appendix C

Numerical Simulation for Regular Motions

1. Introduction

Since both the main body of the URV-model and the hydrofoil connection constitute a neutral body which is considered as a semi-submersible vehicle in this work, the regular coupled heave and pitch motions for that body is investigated using linear two-dimensional strip theory as given in [17,43]. Korvin-Kroukovsk's and Jacobs developed this theory in 1957 [17] (The original reference of this work can be found in reference [17] pp. 487 'no. 121'). They studied the coupled heave and pitch motions for a ship in regular head seas. Several assumptions and limitations are considered in the numerical simulation in order to simplify the complex motion of the model. These assumptions can be classified into two main categories: assumptions related to the theory and others related to the problem [18,43,49]. The first category includes that the excitation is considered as regular harmonic waves, there is no interaction of the flows at the adjacent strips, the Froude-Krylov hypothesis is valid, other degrees of freedom are neglected, slender hull forms (i.e. the length is much greater than the beam or the draft and the beam is much less than the wavelength) are only considered, and the flow is irrotational and inviscid. The second category includes that a vehicle is assumed be studied in a head sea condition ($\mu = 180^{o}$) and moderate forward speeds are assumed.

Based on the above assumptions, the approach of the linear strip theory has been implemented in this work by assuming that the model's hull consists of an infinite cylinder having a series of infinite transverse strips. The flow around each strip has been treated as 2D flow. However, in our case, the calculations of the hydrodynamic parameters are obtained for the neutrally buoyant body that constitutes the main body of the URV-model and the hydrofoil connection. The relative vertical motion of each strip is calculated based on the coupled heave and pitch motions. After calculating the response for each strip, the total motion response of the vehicle in coupled heave and pitch directions can be obtained from numerical integration of the different component reactions of all strips along the vehicle length.

2. Hydrodynamic Parameters Calculation

The total vertical motion of each strip is assumed to consist of two components: the heave motion and the pitch motion. The hydrostatic, hydrodynamic, and inertial forces acting on each strip are described using equations (3.1) and (3.2). All other coefficients in equations (3.1) and (3.2) are defined in Appendix E, and they are calculated using the MATLAB program "*URV-MOTION*" as given in Appendix D. The hydrodynamic parameters are functions of the towing speed and the wave encounter frequency.

Then, equations (3.1) and (3.2) can be solved using a MATLAB toolbox or any other numerical integration algorithm such as the Runge-Kutta if the time series of the exciting forces time series are known. These forces depend on the hull geometry, towing speed, the encounter wave frequency, and the pressure distribution on the submerged

body of the model. Using 2D strip theory, these forces can be calculated for regular harmonic wave excitation [17].

3. Exciting Forces Calculation

All floating vehicles near the water surface are subjected to wave exciting forces and moments. The determination of these forces and moments has a significant importance at the design stage for such vehicles. At present there is no reliable procedure for calculating the interaction between the wave and the vehicle [49]. Numerous studies have been conducted in this area. Some of them are based on linear wave theory and Morison's equation where the wave forces are described as comprised of inertia and drag force component, and others are based on the strip theory [17,43,50,51]. Several methods to estimate the inertia and the drag coefficients have been developed.

For the purpose of the numerical simulation in the design stage for the URV-model, the regular wave forces acting on the model are calculated using linear 2D strip theory. The exciting forces consist of two main components: a Froude-Krylov component and a diffraction one [8,52]. The Froude-Krylov component can be obtained by integrating the pressure field acting on the submerged body of the model along the vehicle's length. The diffraction component, which is related to the scattering of the incident wave field, is associated with the disturbance introduced to the wave field by the presence of the vehicle [8,52,53]. In addition, the diffraction component is of minor importance compared with the Froude-Krylov one in the case of small structures [52]. However, for large structures such as Hibernia GBS, the diffraction component is significant. The Froude-Krylov component can be calculated in regular waves.

Regular waves are theoretical constructs, which never occur in the real ocean environment. An understanding of their nature is one of the helpful tools in the study of seakeeping. A train of regular waves can be produced in wave towing tanks and form the basis of many seakeeping model experiments. The theory of irregular waves that occur in nature, is based on the assumption that superimposing a large number of regular waves can represent them [43].

The assumption that the encountered wave is regular and harmonic allows us to express the instantaneous depression of the water surface below the mean level, ζ_w as follows:

$$\zeta_w = \zeta_a \sin(kL - \omega_e t) \tag{C.1}$$

where ζ_a and ω_e are the wave amplitude in metres, and the encountered wave frequency in rad /sec, respectively. L, k, and t are the lever of a particular strip from LCG in metre, wave number, and time in sec, respectively. Since L is equal to zero at the LCG of the model, the depression of the sea surface at the LCG becomes:

$$\zeta_w = -\zeta_a \sin(\omega_e t) \tag{C.2}$$

Equations (3.1) and (3.2) can be rewritten in a complex form as follows [17]:

$$P\bar{Z} + Q\bar{\Theta} = \bar{F} \tag{C.3}$$

$$S\bar{\Theta} + R\bar{Z} = \bar{M} \tag{C.4}$$

where

$$P = -(m + a_{33})\omega_e^{\,2} + b_{33}\,\omega_e\, i + c_{33};$$

$$Q = -a_{35}\,\omega_e^{\,2} + b_{35}\,\omega_e\, i + c_{35};$$

$$S = -(I_{yy} + a_{55})\omega_e^{\,2} + b_{55}\,\omega_e\, i + c_{55};$$

$$R = -a_{53}\,\omega_e^{\,2} + b_{53}\,\omega_e\, i + c_{53};$$

$$\overline{F} = F_O\, e^{i\sigma} = F_O \cos(\omega_e t + \sigma);$$

$$\overline{M} = M_O e^{iv} = M_O \cos(\omega_e t + v);$$

$$i = \sqrt{-1}$$

By manipulating equations (C.3) and (C.4), the heave and pitch motion responses can be calculated as follows:

$$\overline{Z} = \frac{\overline{M}Q - \overline{F}S}{QR - PS} \tag{C.5}$$

$$\overline{\Theta} = \frac{\overline{F}R - \overline{M}P}{QR - PS} \tag{C.6}$$

Substituting the above complex forms into equations (C.5) and (C.6), the final solution of the second order diffrential equations of motion can be obtained as follows:

$$\overline{Z} = Z_O \cos\,(\omega_e t + \delta) \tag{C.7}$$

$$\overline{\Theta} = \Theta_O \cos\,(\omega_e t + \varepsilon) \tag{C.8}$$

where Z_o and Θ_o are the heave, and the pitch amplitudes, respectively. δ and ε are the heave and pitch phase angles, respectively. The wave profile, the coupled heave and pitch responses, the exciting force and the exciting moment acting on the model are calculated and shown in Figures (C.1) to (C.5) as

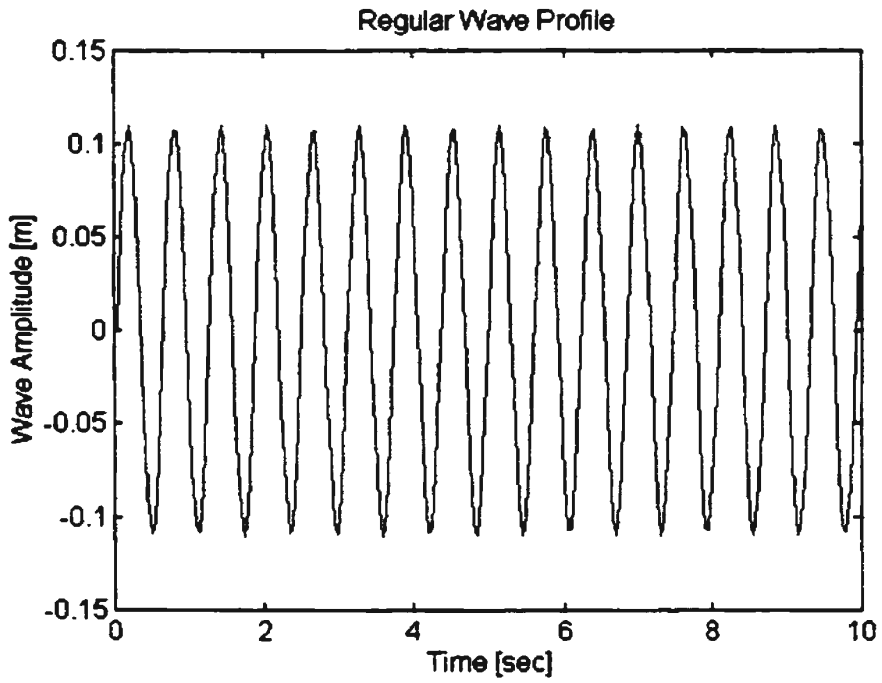

Figure C.1: Regular wave profile

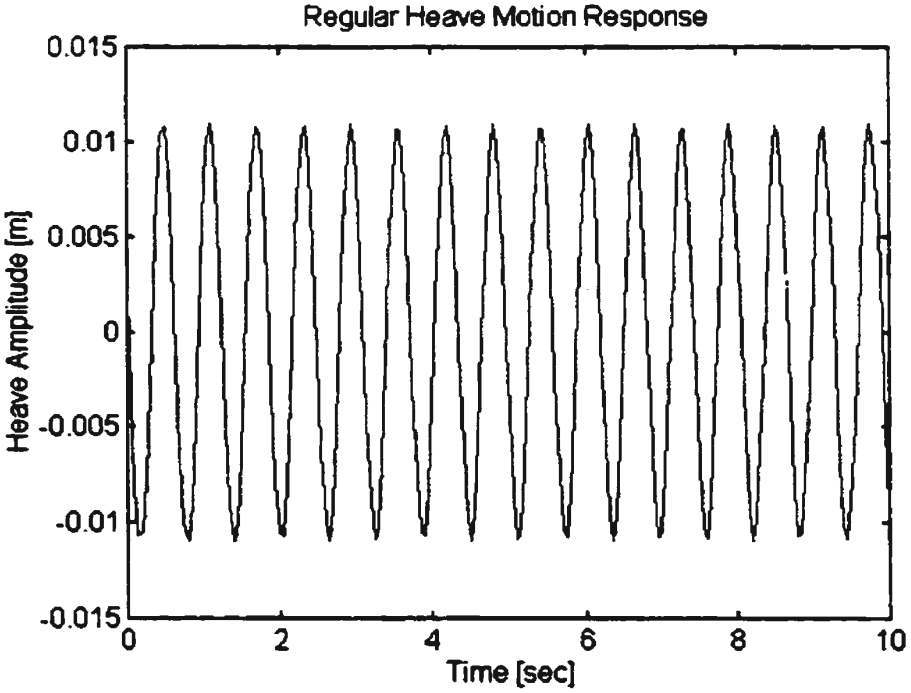

Figure C.2: Heave motion in regular waves

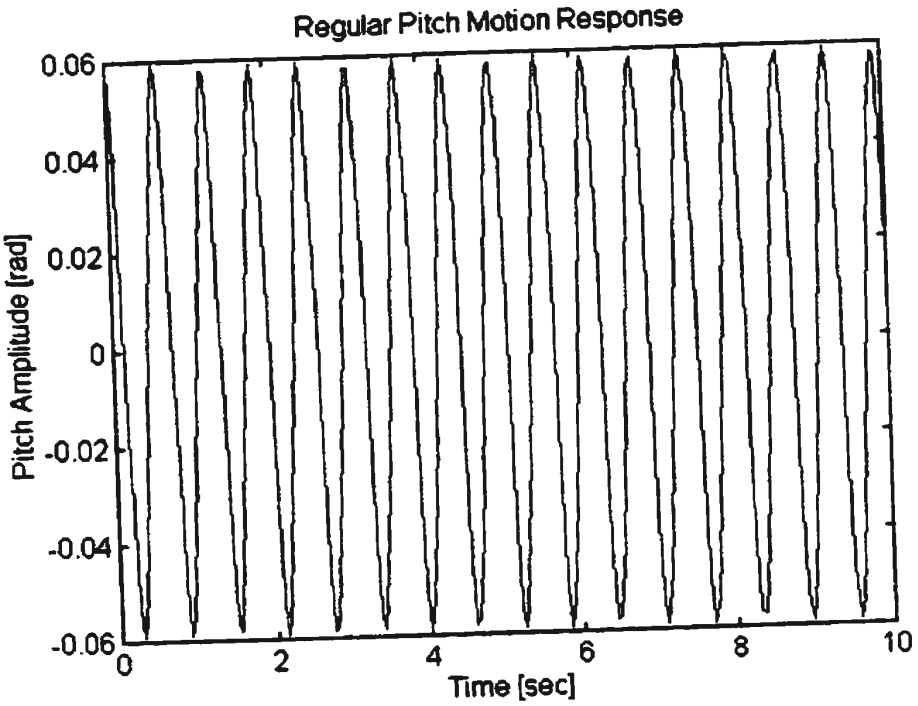

Figure C.3: Pitch motion in regular waves

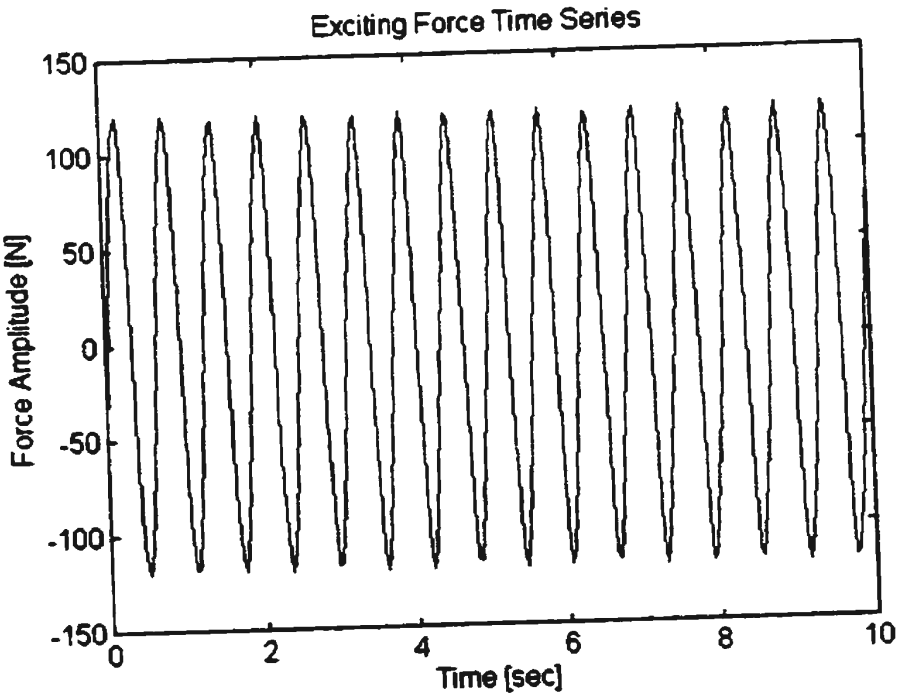

Figure C.4: Exciting force in regular waves

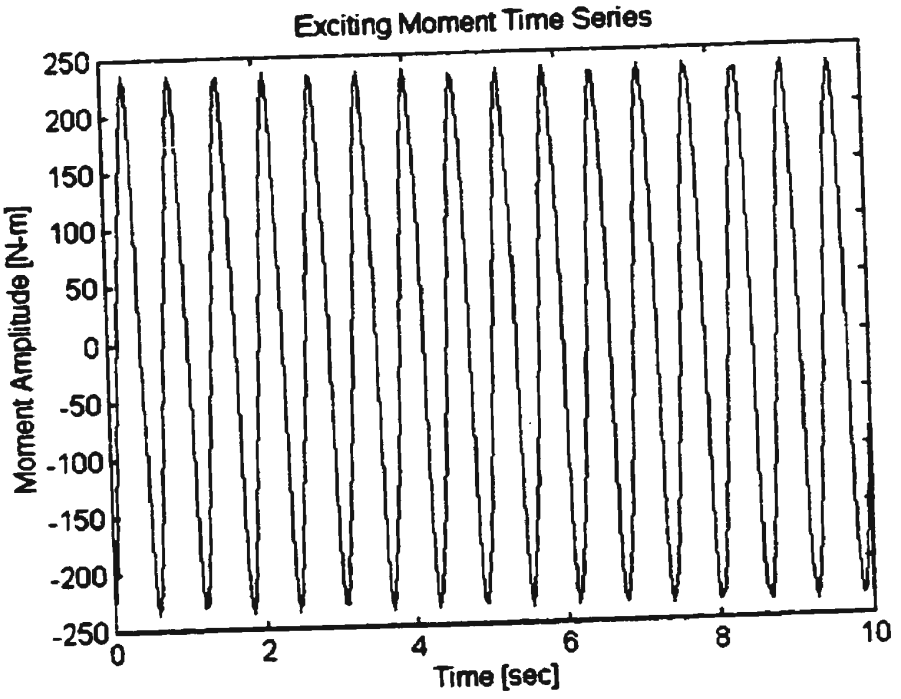

Figure C.5: Exciting moment in regular waves

Appendix D

MATLAB Program: *URV-Motion*

```
clear;
tf=300.0;
to=0.0;
dt=0.02;
nt=(tf-to)/dt;
fo=0.7;
H13=0.13;
ff=2.0*fo;
nf=70;
df=ff/nf;
nss=82;
pi=4*atan(1);
u=0.2;
g=9.81;
meu=pi;

for k=1:nf+1
   fw(k)=(k-1)*df;
   ww(k)=2*pi*fw(k);
   we(k)=ww(k)*(1-ww(k)*u*cos(meu)/g);
   fe(k)=we(k)/2/pi;
end
ssw=fw(2)-fw(1);
sse=fe(2)-fe(1);

sega=0.07;
segb=0.09;
gama=3.3;

for k=1:nf+1
   if fw(k) <= fo
     seg=sega;
   else
     seg=segb;
   end
   A1=5*H13^2*fo^4/(16*gama^(1/3));
   B1=5*fo^4/4;
   a2=exp(-1*(fw(k)-fo)^2/2/seg^2/fo^2);
   if fw(k)==0
     sw(k)=0;
     se(k)=0;
   else
     sw(k)=(A1/(fw(k))^5)*exp(-B1/(fw(k))^4)*gama^a2;
     se(k)=sw(k)/sqrt(1-4*fe(k)*u*cos(meu)/g);
   end
   a1w(k)=sqrt(2*sw(k)*ssw);
   a1e(k)=sqrt(2*se(k)*sse);
```

```
end

for k=1:nf+1
   aw(k,1)=fw(k);
   aw(k,2)=a1w(k);
end

for k=1:nf+1
   ae(k,1)=fe(k);
   ae(k,2)=a1e(k);
end

oddd=1:2:nf-1;
even=0:2:nf+1;

for k=1:nf+1
   if k==1
      sms(k)=1;
   elseif k==nf+1
      sms(k)=1;
   elseif k==even((k-1)/2+1)
      sms(k)=4;
   elseif k==oddd(k/2)
      sms(k)=2;
   end
end

ro=1000;
s1=0.025;

load brd;
load sm;
load l;
load tn;
l=l';
sm=sm';

for k=1:nf+1

   prod1=0.0;
   prod2=0.0;
   for k2=1:nss
      snb(k2)=(brd(k2))^2*pi/4;
      anb(k2)=ro*snb(k2);
      prod1=prod1+anb(k2)*sm(k2);
      prod2=prod2+(l(k2))^2*anb(k2)*sm(k2);
   end

   Az(k)=3*s1*prod1/8;
   Ayy(k)=3*s1*prod2/8;
end

load brdh;

for k2=1:nss
   tnh(k2)=0.25;
```

```
   snh(k2)=brdh(k2)*tnh(k2);
end

xw1=[0 0.2 0.4 0.6 0.8 1.0 1.2 1.4 1.6 2.0];
zw1=[0 0.4 0.8 1.2 1.6 2.0 2.4 2.8 3.6 4.4];
zw11=[0 0.4 0.8 1.2 1.4 2.0 2.4 2.8 3.6 4.4];

for k=1:nf+1
   prod1=0.0;
   prod2=0.0;
   prodt1=0.0;
   prodt2=0.0;
   for k2=1:nss
      term1h(k2,k)=(we(k))^2*brdh(k2)/2/g;
      r1h(k2,k)=brdh(k2)/tnh(k2);
      if brdh(k2)==0
         sach(k2)=0.0;
      else
         sach(k2)=snh(k2)/(brdh(k2)*tnh(k2));
      end

      if sach(k2)>= 1.0
         sach(k2)=1.0;
      elseif sach(k2)< 0.5
         sach(k2)=0.5;
      end


      xi=term1h(k2,k);
      yi=r1h(k2,k);
      if xi==0.0 & yi==0.0
         Cx(k2,k)=0.0;
      elseif sach(k2)>=0.5 & sach(k2)<=0.6
         load ch5a;
         load ch6a;
         ch5a=ch5a';
         ch6a=ch6a';

         zi1a(k2)=interp2(xw1,zw1,ch5a,xi,yi);
         zi2a(k2)=interp2(xw1,zw1,ch6a,xi,yi);
         zia(k2)=zi1a(k2)+((zi2a(k2)-zi1a(k2))/0.1)*(sach(k2)-0.5);
         Cx(k2,k)=zia(k2);
      elseif sach(k2)>=0.6 & sach(k2)<=0.7
         load ch6a;
         load ch7a;
         ch6a=ch6a';
         ch7a=ch7a';

         zi1a(k2)=interp2(xw1,zw1,ch6a,xi,yi);
         zi2a(k2)=interp2(xw1,zw1,ch7a,xi,yi);
         zia(k2)=zi1a(k2)+((zi2a(k2)-zi1a(k2))/0.1)*(sach(k2)-0.6);
         Cx(k2,k)=zia(k2);
      elseif sach(k2)>=0.7 & sach(k2)<=0.8
         load ch7a;
         load ch8a;
         ch7a=ch7a';
         ch8a=ch8a';
```

```
            zi1a(k2)=interp2(xw1,zw1,ch7a,xi,yi);
            zi2a(k2)=interp2(xw1,zw1,ch8a,xi,yi);
            zia(k2)=zi1a(k2)+((zi2a(k2)-zi1a(k2))/0.1)*(sach(k2)-0.7);
            Cx(k2,k)=zia(k2);
         elseif sach(k2)>=0.8 & sach(k2)<=0.9
            load ch8a;
            load ch9a;
            ch8a=ch8a';
            ch9a=ch9a';

            zi1a(k2)=interp2(xw1,zw1,ch8a,xi,yi);
            zi2a(k2)=interp2(xw1,zw1,ch9a,xi,yi);
            zia(k2)=zi1a(k2)+((zi2a(k2)-zi1a(k2))/0.1)*(sach(k2)-0.8);
            Cx(k2,k)=zia(k2);
         elseif sach(k2)>=0.9 & sach(k2)<=1.0
            load ch9a;
            load ch10a;
            ch9a=ch9a';
            ch10a=ch10a';

            zi1a(k2)=interp2(xw1,zw1,ch9a,xi,yi);
            zi2a(k2)=interp2(xw1,zw11,ch10a,xi,yi);
            zia(k2)=zi1a(k2)+((zi2a(k2)-zi1a(k2))/0.1)*(sach(k2)-0.9);
            Cx(k2,k)=zia(k2);
         end

         anh(k2,k)=Cx(k2,k)*ro*pi*(brdh(k2))^2/8;
         prod1=prod1+anh(k2,k)*sm(k2);
         prod2=prod2+anh(k2,k)*(l(k2))^2*sm(k2);
         ant(k2,k)=anb(k2)+anh(k2,k);
         prodt1=prodt1+ant(k2,k)*sm(k2);
         prodt2=prodt2+ant(k2,k)*(l(k2))^2*sm(k2);

      end
      Azh(k)=3*s1*prod1/8;
      Ayyh(k)=3*s1*prod2/8;
      Azt(k)=3*s1*prodt1/8;
      Ayyt(k)=3*s1*prodt2/8;

   end

   xw2=[0 0.2 0.4 0.6 0.8 1.0 1.2 1.4 1.6 2.0];
   zw2=[0 0.4 0.8 1.2 1.6 2.0 2.4 2.8 3.6 4.4];

   for k=1:nf+1
      prod3=0.0;
      prod4=0.0;
      for k2=1:nss
         term2b(k2,k)=(we(k))^2*brd(k2)/2/g;
         r2b(k2,k)=brd(k2)/tn(k2);
         if brd(k2)==0
            sacb(k2)=0.0;
         else
            sacb(k2)=snb(k2)/(brd(k2))^2;
         end
```

```
if sacb(k2)>= 1.0
   sacb(k2)=1.0;
elseif sacb(k2)< 0.5
   sacb(k2)=0.5;
end

xi=term2b(k2,k);
yi=r2b(k2,k);
if xi==0.0 & yi==0.0
   A1(k2,k)=0.0;
elseif sacb(k2)>=0.5 & sacb(k2)<=0.6
   load ch5b;
   load ch6b;
   ch5b=ch5b';
   ch6b=ch6b';

   zi1(k2)=interp2(xw2,zw2,ch5b,xi,yi);
   zi2(k2)=interp2(xw2,zw2,ch6b,xi,yi);
   zi(k2)=zi1(k2)+((zi2(k2)-zi1(k2))/0.1)*(sacb(k2)-0.5);
   A1(k2,k)=zi(k2);
elseif sacb(k2)>=0.6 & sacb(k2)<=0.7
   load ch6b;
   load ch7b;
   ch6b=ch6b';
   ch7b=ch7b';

   zi1(k2)=interp2(xw2,zw2,ch6b,xi,yi);
   zi2(k2)=interp2(xw2,zw2,ch7b,xi,yi);
   zi(k2)=zi1(k2)+((zi2(k2)-zi1(k2))/0.1)*(sacb(k2)-0.6);
   A1(k2,k)=zi(k2);
elseif sacb(k2)>=0.7 & sacb(k2)<=0.8
   load ch7b;
   load ch8b;
   ch7b=ch7b';
   ch8b=ch8b';

   zi1(k2)=interp2(xw2,zw2,ch7b,xi,yi);
   zi2(k2)=interp2(xw2,zw2,ch8b,xi,yi);
   zi(k2)=zi1(k2)+((zi2(k2)-zi1(k2))/0.1)*(sacb(k2)-0.7);
   A1(k2,k)=zi(k2);
elseif sacb(k2)>=0.8 & sacb(k2)<=0.9
   load ch8b;
   load ch9b;
   ch8b=ch8b';
   ch9b=ch9b';

   zi1(k2)=interp2(xw2,zw2,ch8b,xi,yi);
   zi2(k2)=interp2(xw2,zw2,ch9b,xi,yi);
   zi(k2)=zi1(k2)+((zi2(k2)-zi1(k2))/0.1)*(sacb(k2)-0.8);
   A1(k2,k)=zi(k2);
elseif sacb(k2)>=0.9 & sacb(k2)<=1.0
   load ch9b;
   load ch10b;
   ch9b=ch9b';
   ch10b=ch10b';

   zi1(k2)=interp2(xw2,zw2,ch9b,xi,yi);
```

```
            zi2(k2)=interp2(xw2,zw2,ch10b,xi,yi);
            zi(k2)=zi1(k2)+((zi2(k2)-zi1(k2))/0.1)*(sacb(k2)-0.9);
            A1(k2,k)=zi(k2);
         end

         if we(k)==0
            bn1(k2,k)=0;
         else
            bn1(k2,k)=ro*g^2*(A1(k2,k))^2/(we(k))^3;
            prod3=prod3+bn1(k2,k)*sm(k2);
            prod4=prod4+bn1(k2,k)*(l(k2))^2*sm(k2);
         end

      end
      b1(k)=3*s1*prod3/8;
      B1(k)=3*s1*prod4/8;
   end

   xw2=[0 0.2 0.4 0.6 0.8 1.0 1.2 1.4 1.6 2.0];
   zw2=[0 0.4 0.8 1.2 1.6 2.0 2.4 2.8 3.6 4.4];

   for k=1:nf+1
      prod3=0.0;
      prod4=0.0;
      prodt3=0.0;
      prodt4=0.0;

      for k2=1:nss
         term2h(k2,k)=(we(k))^2*brdh(k2)/2/g;
         r2h(k2,k)=brdh(k2)/tnh(k2);
         if brdh(k2)==0
            sach(k2)=0.0;
         else
            sach(k2)=snh(k2)/(brdh(k2)*tnh(k2));
         end

         if sach(k2)>= 1.0
            sach(k2)=1.0;
         elseif sach(k2)< 0.5
            sach(k2)=0.5;
         end

         xih=term2h(k2,k);
         yih=r2h(k2,k);
         if xih==0.0 & yih==0.0
            A2(k2,k)=0.0;
         elseif sach(k2)>=0.5 & sach(k2)<=0.6
            load ch5b;
            load ch6b;
            ch5b=ch5b';
            ch6b=ch6b';

            zi1(k2)=interp2(xw2,zw2,ch5b,xih,yih);
            zi2(k2)=interp2(xw2,zw2,ch6b,xih,yih);
            zi(k2)=zi1(k2)+((zi2(k2)-zi1(k2))/0.1)*(sach(k2)-0.5);
            A2(k2,k)=zi(k2);
         elseif sach(k2)>=0.6 & sach(k2)<=0.7
```

```
        load ch6b;
        load ch7b;
        ch6b=ch6b';
        ch7b=ch7b';

        zi1(k2)=interp2(xw2,zw2,ch6b,xih,yih);
        zi2(k2)=interp2(xw2,zw2,ch7b,xih,yih);
        zi(k2)=zi1(k2)+((zi2(k2)-zi1(k2))/0.1)*(sach(k2)-0.6);
        A2(k2,k)=zi(k2);
    elseif sach(k2)>=0.7 & sach(k2)<=0.8
        load ch7b;
        load ch8b;
        ch7b=ch7b';
        ch8b=ch8b';

        zi1(k2)=interp2(xw2,zw2,ch7b,xih,yih);
        zi2(k2)=interp2(xw2,zw2,ch8b,xih,yih);
        zi(k2)=zi1(k2)+((zi2(k2)-zi1(k2))/0.1)*(sach(k2)-0.7);
        A2(k2,k)=zi(k2);
    elseif sach(k2)>=0.8 & sach(k2)<=0.9
        load ch8b;
        load ch9b;
        ch8b=ch8b';
        ch9b=ch9b';

        zi1(k2)=interp2(xw2,zw2,ch8b,xih,yih);
        zi2(k2)=interp2(xw2,zw2,ch9b,xih,yih);
        zi(k2)=zi1(k2)+((zi2(k2)-zi1(k2))/0.1)*(sach(k2)-0.8);
        A2(k2,k)=zi(k2);
    elseif sach(k2)>=0.9 & sach(k2)<=1.0
        load ch9b;
        load ch10b;
        ch9b=ch9b';
        ch10b=ch10b';

        zi1(k2)=interp2(xw2,zw2,ch9b,xih,yih);
        zi2(k2)=interp2(xw2,zw2,ch10b,xih,yih);
        zi(k2)=zi1(k2)+((zi2(k2)-zi1(k2))/0.1)*(sach(k2)-0.9);
        A2(k2,k)=zi(k2);
    end

        if we(k)==0
        bn2(k2,k)=0;
    else
        bn2(k2,k)=ro*g^2*(A2(k2,k))^2/(we(k))^3;
        prod3=prod3+bn2(k2,k)*sm(k2);
        prod4=prod4+bn2(k2,k)*(l(k2))^2*sm(k2);
        bn(k2,k)=bn1(k2,k)+bn2(k2,k);
        prodt3=prodt3+bn(k2,k)*sm(k2);
        prodt4=prodt4+bn(k2,k)*(l(k2))^2*sm(k2);

    end

end
b2(k)=3*s1*prod3/8;
B2(k)=3*s1*prod4/8;
```

```
   b(k)=3*s1*prodt3/8;
   B(k)=3*s1*prodt4/8;

end

prod5=0.0;
prod6=0.0;
for k2=1:nss
   cn(k2)=ro*g*brdh(k2);
   prod5=prod5+cn(k2)*sm(k2);
   prod6=prod6+cn(k2)*(l(k2))^2*sm(k2);
end

c=3*s1*prod5/8;
for k=1:nf+1
   prod7=0.0;
   for k2=1:nss
      prod7=prod7+bn(k2,k)*l(k2)*sm(k2);
   end
  e(k)=-3*s1*prod7/8+u*Azt(k);
  E(k)=-3*s1*prod7/8-u*Azt(k);
  C(k)=3*s1*prod6/8-u*E(k);
end

prod9=0.0;
for k2=1:nss
   prod9=prod9+cn(k2)*l(k2)*sm(k2);
end

H=-3*s1*prod9/8;

for k=1:nf+1
   prod8=0.0;
      for k2=1:nss
         prod8=prod8+ant(k2)*l(k2)*sm(k2);
      end
      %d=dd1
   %D=dd2
   dd1(k)=-3*s1*prod8/8;
   dd2(k)=-3*s1*prod8/8;
   h(k)=-3*s1*prod9/8+u*b(k);
end

load wet;
prod10=0.0;
prod11=0.0;
for k2=1:nss
   mn(k2)=wet(k2)/g;
   prod10=prod10+mn(k2)*sm(k2);
   prod11=prod11+mn(k2)*(l(k2))^2*sm(k2);
end
m=3*s1*prod10/8;
Iyy=3*s1*prod11/8;

for k=1:nf+1
   wnh(k)=sqrt(c/(m+Azt(k)));
   wnp(k)=sqrt(C(k)/(Iyy+Ayy(k)));
```

```
end

for k2=1:nss
   sn(k2)=snb(k2)+snh(k2);
   if brd(k2)==0.0
      tm(k2)=0.0;
   else
      tm(k2)=sn(k2)/brd(k2);
   end

end

for k=1:nf+1
    for k2=1:nss
      if k2>1 & k2< nss
         DAN(k2)=0.5*((ant(k2+1)-ant(k2))/(l(k2+1)-l(k2))+(ant(k2)-
ant(k2-1))/(l(k2)-l(k2-1)));
      elseif k2==1
         DAN(k2)=(ant(k2+1)-ant(k2))/(l(k2+1)-l(k2));
      elseif k2==nss
         DAN(k2)=(ant(k2)-ant(k2-1))/(l(k2)-l(k2-1));
      end
   end
end

for k=1:nf+1
       al(k)=ae(k,2);
       tk(k)=(ww(k))^2/g;
       PROD1=0.0;
       PROD2=0.0;
       PROD3=0.0;
       PROD4=0.0;

       for J=1:nss

          EXPP(J,k)=exp(-tk(k)*tm(J));
          TERM0(J,k)=-(we(k))^2*ant(J)*al(k);
          CNETA(J,k)=cn(J)*al(k);
          TERM00(J,k)=TERM0(J,k)+CNETA(J,k);
          TERM1(J,k)=u*al(k)*we(k)*DAN(J);
          TERM2(J,k)=al(k)*we(k)*bn(J,k);
          TERM3(J,k)=TERM2(J,k)-TERM1(J,k);
          TERM4(J,k)=TERM00(J,k)*sin(tk(k)*l(J));
          TERM5(J,k)=TERM3(J,k)*cos(tk(k)*l(J));

          TERM6(J,k)=TERM4(J,k)+TERM5(J,k);

          TERM10(J,k)=TERM6(J,k)*EXPP(J,k);

          PROD1=PROD1+TERM10(J,k)*sm(J);

          TERM7(J,k)=TERM00(J,k)*cos(tk(k)*l(J));
          TERM8(J,k)=TERM3(J,k)*sin(tk(k)*l(J));
          TERM9(J,k)=TERM7(J,k)-TERM8(J,k);
          TERM11(J,k)=TERM9(J,k)*EXPP(J,k);
          PROD2=PROD2+TERM11(J,k)*sm(J);
          TERM12(J,k)=TERM10(J)*l(J);
```

```
            PROD3=PROD3+TERM12(J,k)*sm(J);
            TERM13(J,k)=TERM11(J,k)*l(J);
            PROD4=PROD4+TERM13(J,k)*sm(J);
        end

        F1(k)=3*s1*PROD1/8;
        F2(k)=3*s1*PROD2/8;
        M1(k)=3*s1*PROD3/8;
        M2(k)=3*s1*PROD4/8;

        Fo(k)=sqrt((F1(k))^2+(F2(k))^2);
        Mo(k)=sqrt((M1(k))^2+(M2(k))^2);
        [ANG1]=subr1(F1(k),F2(k));
        [ANG2]=subr1(M1(k),M2(k));
        ANGF(k)=ANG1;
        ANGM(k)=ANG2;

        sfor(k)=(Fo(k))^2/2/sse;
        smom(k)=(Mo(k))^2/2/sse;

end

for k=1:nf+1
    i=0 + 1.0000i;
    P1(k)=(-(m+Azt(k))*(we(k))^2+c);
    P2(k)=(b(k)*we(k));
    Po(k)=sqrt((P1(k))^2+(P2(k))^2);
    [ANG11]=subr1(P1(k),P2(k));
    angp(k)=ANG11;
    P(k)=Po(k)*exp(angp(k)*i);

    S1(k)=(-(Iyy+Ayyt(k))*(we(k))^2+C(k));
    S2(k)=(B(k)*we(k));
    So(k)=sqrt((S1(k))^2+(S2(k))^2);
    [ANG12]=subr1(S1(k),S2(k));
          angs(k)=ANG12;
    %angs(k)=atan(S2(k)/S1(k));
    S(k)=So(k)*exp(angs(k)*i);


    Q1(k)=(-dd1(k)*(we(k))^2+h(k));
    Q2(k)=(e(k)*we(k));
    Qo(k)=sqrt((Q1(k))^2+(Q2(k))^2);
    [ANG13]=subr1(Q1(k),Q2(k));
          angq(k)=ANG13;
    Q(k)=Qo(k)*exp(angq(k)*i);

    XRR1(k)=(dd2(k)*(we(k))^2+H);
    XRR2(k)=(E(k)*we(k));
    XRRo(k)=sqrt((XRR1(k))^2+(XRR2(k))^2);
    [ANG14]=subr1(XRR1(k),XRR2(k));
          angr(k)=ANG14;
    XRR(k)=XRRo(k)*exp(angr(k)*i);

    PS=P(k)*S(k);
    QR=Q(k)*XRR(k);
    PSQR1=PS-QR;
```

```
PSQR2=conj(PSQR1);
AAA=PSQR1*PSQR2;

Fx1(k)=F1(k);
Fx2(k)=F2(k);
Fxo(k)=sqrt((Fx1(k))^2+(Fx2(k))^2);
[ANG15]=subr1(Fx1(k),Fx2(k));
angf(k)=ANG15;
Fx(k)=Fxo(k)*exp(angf(k)*i);
Mx1(k)=M1(k);
Mx2(k)=M2(k);
Mxo(k)=sqrt((Mx1(k))^2+(Mx2(k))^2);
[ANG16]=subr1(Mx1(k),Mx2(k));
      angm(k)=ANG16;

Mx(k)=Mxo(k)*exp(angm(k)*i);


FS=Fx(k)*S(k);
MQ=Mx(k)*Q(k);
FSMQ=FS-MQ;

BBB=FSMQ*PSQR2;

MP=Mx(k)*P(k);
FR=Fx(k)*XRR(k);
MPFR=MP-FR;

CCCC=MPFR*PSQR2;

ZH(k)=BBB/AAA;
ZHa(k)=sqrt((real(ZH(k)))^2+(imag(ZH(k)))^2);
ZP(k)=CCCC/AAA;
ZPa(k)=sqrt((real(ZP(k)))^2+(imag(ZP(k)))^2);

[ANG18]=subr1(real(ZH(k)),imag(ZH(k)));
[ANG19]=subr1(real(ZP(k)),imag(ZP(k)));
    angzh(k)=ANG18;
    angzp(k)=ANG19;

if a1(k)==0
   ZHtf(k)=0.0;
   ZPtf(k)=0.0;
   Ftf(k)=0.0;
   Mtf(k)=0.0;

   RAOH(k)=0.0;
   RAOP(k)=0.0;
   RAOF(k)=0.0;
   RAOM(k)=0.0;
else
   ZHtf(k)=ZHa(k)/a1(k);
   ZPtf(k)=ZPa(k)/tk(k)/a1(k);
   Ftf(k)=Fo(k)/a1(k);
   Mtf(k)=Mo(k)/a1(k);
   RAOH(k)=(ZHa(k)/a1(k))^2;
   RAOP(k)=(ZPa(k)/a1(k))^2;
```

```
      RAOF(k)=(Fo(k)/a1(k))^2;
      RAOM(k)=(Mo(k)/a1(k))^2;
      SHH(k)=RAOH(k)*se(k);
      SPP(k)=RAOP(k)*se(k);
      SFF(k)=RAOF(k)*se(k);
      SMM(k)=RAOM(k)*se(k);
      r1h(k)=ZHa(k)/a1(k);
      r1p(k)= ZPa(k)/a1(k);

   end

   sz(k)=(ZHa(k))^2/2/sse;
   sp(k)=(ZPa(k))^2/2/sse;

   for J=1:nt+1

      ZH(J,k)=ZHa(k)*cos(we(k)*(J-1)*dt+angzh(k));
      ZHV(J,k)=-ZHa(k)*we(k)*sin(we(k)*(J-1)*dt+angzh(k));
      ZP(J,k)=ZPa(k)*cos(we(k)*(J-1)*dt+angzp(k));
      ZPV(J,k)=-ZPa(k)*we(k)*sin(we(k)*(J-1)*dt+angzp(k));
      Fxx(J,k)=Fxo(k)*cos(we(k)*(J-1)*dt+angf(k));
      Mxx(J,k)=Mxo(k)*cos(we(k)*(J-1)*dt+angm(k));

   end
end

prodww=0.0;
prodse=0.0;
prodSHH=0.0;
prodSPP=0.0;
prodsz=0.0;
prodsp=0.0;
prodSFF=0.0;
prodSMM=0.0;
prodsfor=0.0;
prodsmom=0.0;
for k=1:nf+1
   prodww=prodww+sw(k)*sms(k);
   prodse=prodse+se(k)*sms(k);
   prodSHH=prodSHH+SHH(k)*sms(k);
   prodSPP=prodSPP+SPP(k)*sms(k);
   prodsz=prodsz+sz(k)*sms(k);
   prodsp=prodsp+sp(k)*sms(k);
   prodSFF=prodSFF+SFF(k)*sms(k);
   prodSMM=prodSMM+SMM(k)*sms(k);
   prodsfor=prodsfor+sfor(k)*sms(k);
   prodsmom=prodsmom+smom(k)*sms(k);

end

mosw=ssw*prodww/3;
mose=sse*prodse/3;
moSHH=sse*prodSHH/3;
moSPP=sse*prodSPP/3;
mosz=sse*prodsz/3;
mosp=sse*prodsp/3;
moSFF=sse*prodSFF/3;
```

```
moSMM=sse*prodSMM/3;
mosfor=sse*prodsfor/3;
mosmom=sse*prodsmom/3;


Wsav=1.25*sqrt(mosw);
Wsav13=2.0*sqrt(mosw);
Wsav110=2.55*sqrt(mosw);
Wsav1100=3.34*sqrt(mosw);

Esav=1.25*sqrt(mose);
Esav13=2.0*sqrt(mose);
Esav110=2.55*sqrt(mose);
Esav1100=3.34*sqrt(mose);

Hav=1.25*sqrt(moSHH);
Hav13=2.0*sqrt(moSHH);
Hav110=2.55*sqrt(moSHH);
Hav1100=3.34*sqrt(moSHH);

Pav=1.25*sqrt(moSPP);
Pav13=2.0*sqrt(moSPP);
Pav110=2.55*sqrt(moSPP);
Pav1100=3.34*sqrt(moSPP);

Fav=1.25*sqrt(moSFF);
Fav13=2.0*sqrt(moSFF);
Fav110=2.55*sqrt(moSFF);
Fav1100=3.34*sqrt(moSFF);

Mav=1.25*sqrt(moSMM);
Mav13=2.0*sqrt(moSMM);
Mav110=2.55*sqrt(moSMM);
Mav1100=3.34*sqrt(moSMM);

t=0.0:dt:nt*dt;


for k=1:nf+1
    x=rand(1);
    xr(k)=x*2*pi;
end

for J=1:nt+1
    eta(J)=0.0;
    Fz(J)=0.0;
    Mp(J)=0.0;
    ZH1(J)=0.0;
    ZP1(J)=0.0;
    ZH1V(J)=0.0;
    ZP1V(J)=0.0;
    for k=1:nf+1

        eta(J)=eta(J)+a1(k)*cos(2*pi*fw(k)*(J-1)*dt+xr(k));
        Fz(J)=Fz(J)+Fxo(k)*cos(we(k)*(J-1)*dt+angf(k)+ xr(k));
        Mp(J)=Mp(J)+Mxo(k)*cos(we(k)*(J-1)*dt+angm(k)+ xr(k));
        ZH1(J)=ZH1(J)+ZHa(k)*cos(we(k)*(J-1)*dt+angzh(k)+ xr(k));
```

```
        ZP1(J)=ZP1(J)+ZPa(k)*cos(we(k)*(J-1)*dt+angzp(k)+ xr(k));
        ZH1V(J)=ZH1V(J)-ZHa(k)*we(k)*sin(we(k)*(J-1)*dt+angzh(k)+
xr(k));
        ZP1V(J)=ZP1V(J)-ZPa(k)*we(k)*cos(we(k)*(J-1)*dt+angzp(k)+
xr(k));

    end

end

nh=length(ZH1);
np=length(ZP1);
ns=500;
TRIGGER=0.003;
M=0;
N=0;

   yh=ZH1;
   yp=ZP1;
   for I=1:nh-ns
      if (yh(I) <= TRIGGER & yh(I+1) > TRIGGER)
         M=M+1;
         SP(M)=I;
         if (abs(yh(I)-TRIGGER) > abs(yh(I+1)-TRIGGER))
            SP(M)=I+1;
            I=I+1;
         end
      end
   end

   for I=1:nh-ns
      if (yh(I) >= TRIGGER & yh(I+1) < TRIGGER)
         N=N+1;
         SN(N)=I;
         if(abs(yh(I)-TRIGGER) > abs(yh(I+1)-TRIGGER))
            SN(N)=I+1;
            I=I+1;
         end
      end
   end

   K=M;
   if M > N
      K=N;
   end

   for J=1:ns+1
      RD1(J)=0.0;
      RD2(J)=0.0;

      for I=1:K
         RD1(J)=RD1(J)+yh(SP(I)+J-1);
         RD1(J)=RD1(J)+yh(SN(I)+J-1);
         RD2(J)=RD2(J)+yp(SP(I)+J-1);
         RD2(J)=RD2(J)+yp(SN(I)+J-1);
      end
      RD1(J)=RD1(J)/(2.0*K);
```

```
      RD2(J)=RD2(J)/(2.0*K);

end

   tr=0:dt:ns*dt;
   y1=xcorr(yh);
   y2=xcorr(yp);

   xx1=max(y1)/RD1(1);
   xx2=max(y2)/RD2(1);
   j1=1;
   n1=length(y1);
   n2=length(y2);
 for i1=1:n1

    if i1 >= floor(n1/2)
       x1(j1)=y1(i1)/xx1;
       if j1 >= ns+1,break
       else
         j1=j1+1;
       end
    end

 end

  j2=1;
 for i1=1:n2

     if i1 >= floor(n2/2)
        x2(j2)=y2(i1)/xx2;
        if j2 >= ns+1,break
        else
           j2=j2+1;
        end
     end

 end

for k1=1:nf+1
   for J=1:nt+1
      k(J,1)=Fxx(J,k1);
      k(J,2)=Mxx(J,k1);
   end

   xa1=b(k1)/(m+Azt(k1));
   xa2=c/(m+Azt(k1));
   xa3=dd1(k1)/(m+Azt(k1));
   xa4=e(k1)/(m+Azt(k1));
   xa5=h(k1)/(m+Azt(k1));
   xa6=1/(m+Azt(k1));

   xb1=B(k1)/(Iyy+Ayyt(k1));
   xb2=C(k1)/(Iyy+Ayyt(k1));
   xb3=dd2(k1)/(Iyy+Ayyt(k1));
   xb4=E(k1)/(Iyy+Ayyt(k1));
   xb5=H/(Iyy+Ayyt(k1));
   xb6=1/(Iyy+Ayyt(k1));
```

```
   xa31=-(xa2-xa3*(xb5-xb3*xa2)/(1-xa3*xb3));
   xa32=-(xa5-xa3*(xb2-xb3*xa5)/(1-xa3*xb3));
   xa33=-(xa1-xa3*(xb4-xb3*xa1)/(1-xa3*xb3));
   xa34=-(xa4-xa3*(xb1-xb3*xa4)/(1-xa3*xb3));

   xa41=-(xb5-xb3*xa2)/(1-xa3*xb3);
   xa42=-(xb2-xb3*xa5)/(1-xa3*xb3);
   xa43=-(xb4-xb3*xa1)/(1-xa3*xb3);
   xa44=-(xb1-xb3*xa4)/(1-xa3*xb3);

   AA=[0 0 1 0;0 0 0 1;xa31 xa32 xa33 xa34;xa41 xa42 xa43 xa44];

   xb31=xa6+xa3*xb3*xa6/(1-xa3*xb3);
   xb32=-xa3*xb6/(1-xa3*xb3);
   xb41=-xb3*xa6/(1-xa3*xb3);
   xb42=xa6/(1-xa3*xb3);

   BB=[0 0;0 0;xb31 xb32;xb41 xb42];
   U=k;
   CC=[0 0 0 0];
   D=[0 0];
   T=0:dt:nt*dt ;
   [Y,XX] = lsim(AA,BB,CC,D,U,T);

   for kk=1:nt+1
      X1(kk,k1)=XX(kk,1);
      X2(kk,k1)=XX(kk,2);
      X3(kk,k1)=XX(kk,3);
      X4(kk,k1)=XX(kk,4);
   end

end


for J=1:nt+1
   XZ(J)=0.0;
   XP(J)=0.0;
   for k=1:nf+1
      XZ(J)=XZ(J)+X1(J,k)*cos(we(k)*(J-1)*dt+xr(k));
      XP(J)=XP(J)+X2(J,k)*cos(we(k)*(J-1)*dt+xr(k));
   end
end

YH=fft(ZH1,512);
YP=fft(ZP1,512);
YF=fft(Fz,512);
YM=fft(Mp,512);

Phh=YH.*conj(YH)/512;
Ppp=YP.*conj(YP)/512;
Pff=YF.*conj(YF)/512;
Pmm=YM.*conj(YM)/512;

f=50*(0:51)/512;
```

Appendix E

Hydrodynamic Parameters Using Strip Theory

The definitions of the hydrodynamic coefficients in equations (3.1) and (3.2) are as follows [16]:

$$I_{yy} = \int (m_n \times x)\, dx \tag{E.1}$$

$$m = \int m_n \, dx \text{, vehicle mass, kg} \tag{E.2}$$

where m_n and x are the mass distribution of each strip, weight per metre / g and the distance of each strip from the longitudinal center of gravity (LCG).

$$a_{33} = \int a_n \, dx \text{, Added mass for heaving, kg-sec}^2\text{/m} \tag{E.3}$$

where a_n is the added mass for each strip is obtained as follows:

$$a_n = \frac{1}{4} \rho \pi B_n^{\,2} \tag{E.4}$$

where ρ and B_n are the water density in kg/m^3 and the diameter of each strip, in metre.

$$b_{33} = \int b_n \, dx \text{, Damping coefficient for heaving, kg-sec/rad} \tag{E.5}$$

where b_n is the damping coefficient per unit length for each strip is obtained as

$$b_n = \frac{\rho g^2 \overline{A}^2}{\omega_e^{\,3}} \tag{E.6}$$

where $\overline{A}$ is the ratio of the amplitude of the radiated waves to the amplitude of the heaving motion. This ratio is obtained from Figure (4.6) as shown on page 44 in refrence

[17]. As shown in this figure, the value of $\overline{A}$ depends on the sectional area coefficient of each strip, the ratio of the diameter of each strip to the local draft, and $\omega_e^2 B_n/2g$.

$c_{33} = \int c_n \, dx$, Restoring force coefficent for heaving, kg/m (E.7)

where c_n is the restoring force coefficient for each strip and is equal to $\rho g B_n$.

$a_{35} = -\int a_n \, x \, dx$, Coupling term, kg-sec^2 (E.8)

$b_{35} = -\int b_n \, x \, dx + u \, x \, a_{33}$, Coupling term, kg-sec^2/sec (E.9)

where u is forward speed of the towed model in m/sec.

$c_{35} = -\int c_n \, x \, dx + u \, x \, b_{33}$, Coupling term, kg (E.10)

$a_{55} = \int a_n \, x^2 \, dx$, Added mass moment of inertia for pitching, , kg-sec^2/m (E.11)

$b_{55} = \int b_n \, x^2 \, dx$, Damping coefficent for pitching, kg-m-sec/rad (E.12)

$c_{55} = \int c_n \, x^2 \, dx - u \, x \, b_{53}$, Restoring moment coefficient for pitching, kg-m/rad (E.13)

$a_{53} = a_{35} = -\int a_n \, x \, dx$, Coupling term, kg-sec^2 (E.14)

$b_{53} = -\int b_n \, x \, dx - u \, x \, a_{33}$, Coupling term, kg-sec^2/sec (E.15)

$c_{53} = -\int c_n \, x \, dx$, coupling term, kg (E.16)

Exciting force, F(t):

$$F = F_1 \cos(\omega_e t) + F_2 \sin(\omega_e t) = F_O \cos(\omega_e t + \sigma) \quad \text{(E.17)}$$

$$F_O = \sqrt{F_1^2 + F_2^2} \quad \sigma = -\tan^{-1}(F_2 / F_1) \quad \text{(E.18)}$$

where F_O and σ are the amplitude of the exciting force and the its phase lag relative to the wave propagation.

$$F_1 = \int \frac{dF_1}{dx} dx \quad \text{and} \quad F_2 = \int \frac{dF_2}{dx} dx \tag{E.19}$$

where

$$\frac{dF_1}{dx} = \zeta_a e^{-kz}(\omega_e^{\,2} a_n + c_n)\sin(kx) + \zeta_a e^{-kz}\omega_e(b_n - u\frac{da_n}{dx})\cos(kx) \tag{E.20}$$

$$\frac{dF_2}{dx} = \zeta_a e^{-kz}(-\omega_e^{\,2} a_n + c_n)\cos(kx) - \zeta_a e^{-kz}\omega_e(b_n - u\frac{da_n}{dx})\sin(kx) \tag{E.21}$$

where z is the mean draft for each strip, T_m, and is equal to strip sectional area/ maximum breadth. The wave number is represented by k and is equal ω_e^2/g.

Exiciting moment, M(t):

$$M = M_1 \cos(\omega_e t) + M_2 \sin(\omega_e t) = M_O \cos(\omega_e t + \tau) \tag{E.22}$$

$$M_O = \sqrt{M_1^{\,2} + M_2^{\,2}} \quad \text{and} \quad \tau = -\tan^{-1}(M_2 / M_1) \tag{E.23}$$

where M_O and τ are the amplitude of the exciting moment and the its phase lag relative to the wave motion.

$$M_1 = \int \frac{dM_1}{dx} dx \quad \text{and} \quad M_2 = \int \frac{dM_2}{dx} dx \tag{E.24}$$

Appendix F

MATLAB Program: *D.E.Solver*

```
      clear;
      load meu2
      dt=0.02;
      pi=4.0*atan(1.0);
      N1=70;
      N2=4;
      y(1)=2.71*0.01;
      y(2)=0.017;
      y(3)=0.0;
      [A,S,W]=pspect2(N1);
      kx=2;
      TI=0.0;TLAST=400.0;
      H=dt;
      N=(TLAST-TI)/H;
      T=TI;
      TY1(1)=y(1);
      TY2(1)=y(2);
      TY3(1)=y(3);
      TY4(1)=y(4);
      TY11(1)=y(1);
      TY22(2)=y(2);
      TY33(1)=y(3);
      TY44(1)=y(4);

      tr=H:H:N*H;

for J=1:N

          for I=1:N1
              R1=rand(1);
              ran1(I)=2*pi*R1;
          end

          SUMF=0;
          SUMM=0;
          for  I=1:N1
          SUMF=SUMF+ 0.07*sin(W(I)*T+ran1(I));
          SUMM=SUMM+ 0.15*sin(W(I)*T+ran1(I));
          end
          F(J)=SUMF;
          M(J)=SUMM;

      [yout]=rk42(SUMF,SUMM,ran1,y,N2,A,W,T,H);

      TY1(J)=yout(1);
      TY2(J)=yout(2);
      TY3(J)=yout(3);
      TY4(J)=yout(4);
```

```
        TY11(J)=TY1(J);
        TY22(J)=TY2(J);
        TY33(J)=TY3(J);
        TY44(J)=TY4(J);

        y(1)=yout(1);
        y(2)=yout(2);
        y(3)=yout(3);
        y(4)=yout(4);

        T=T+H;
end
```

Appendix G

MATLAB Program: *RD&AC_Sim*

```
clear;
M=0;
N=0;
ns=499;
TRIGGER=0.03;
load heaved
load pitchd
yh=heaved;
yp=pitchd;
nh=length(yh);
np=length(yp);
dt=0.02;
fs=1/dt;

zh=fft(yh,512);
zp=fft(yp,512);

Phh=zh.*conj(zh)/512;
Ppp=zp.*conj(zp)/512;

f=fs*(0:51)/512;
t1=(1:nh)/fs;
t2=(1:np)/fs;

[b1,a1]=butter(4,[0.07 0.9]*2/fs);
[h1,w1]=freqz(b1,a1,512);
sf1=filter(b1,a1,yh);

[b2,a2]=butter(4,[0.07 0.65]*2/fs);
[h2,w2]=freqz(b2,a2,512);
sf2=filter(b2,a2,yp);

for I=1:nh-ns
   if (yh(I) <= TRIGGER & yh(I+1) > TRIGGER)
      M=M+1;
      SP(M)=I;
      if (abs(yh(I)-TRIGGER) > abs(yh(I+1)-TRIGGER))
         SP(M)=I+1;
         I=I+1;
      end
   end
end

for I=1:nh-ns
   if (yh(I) >= TRIGGER & yh(I+1) < TRIGGER)
      N=N+1;
      SN(N)=I;
      if(abs(yh(I)-TRIGGER) > abs(yh(I+1)-TRIGGER))
```

```
            SN(N)=I+1;
            I=I+1;
         end
      end
   end

   K=M;
   if M > N
      K=N;
   end

   for J=1:ns+1
      RD1(J)=0.0;
      RD2(J)=0.0;

      for I=1:K
         RD1(J)=RD1(J)+yh(SP(I)+J-1);
         RD1(J)=RD1(J)+yh(SN(I)+J-1);
         RD2(J)=RD2(J)+yp(SP(I)+J-1);
         RD2(J)=RD2(J)+yp(SN(I)+J-1);
      end
      RD1(J)=RD1(J)/(2.0*K);
      RD2(J)=RD2(J)/(2.0*K);

end

[x1]=correlx(nh,ns,RD1,yh);
[x2]=correlx(np,ns,RD2,yp);

[Drd1]= firstderv (RD1,ns,dt);
[Drd2]= firstderv (RD2,ns,dt);

[DDrd1]= firstderv (Drd1,ns,dt);
[DDrd2]= firstderv (Drd2,ns,dt);

for i=1:ns-4
   trx(i)=tr(i);
   RD1x(i)=RD1(i);
   RD2x(i)=RD2(i);
   Drd1x(i)=Drd1(i);
   Drd2x(i)=Drd2(i);
   DDrd1x(i)=DDrd1(i);
   DDrd2x(i)=DDrd2(i);
   x1x(i)=x1(i);
   x2x(i)=x2(i);
end

x1x=x1x'
x2x=x2x';
Drd1x=Drd1x';
Drd2x=Drd2x';
DDrd1x=DDrd1x';
DDrd2x=DDrd2x';
RD1x=RD1x';
RD2x=RD2x';
trx=trx';
xh1=[trx RD1x Drd1x];
```

```
xp1=[trx RD2x Drd2x];
yhaut=[trx RD1x x1x]
ypaut=[trx RD2x x2x]

RH=RD1;
Haut1=x1;
RP=RD2;
Paut1=x2;
H1=dt;

K11=1;
for I=1:ns-1

   if (RH(I)>= 0.0 & RH(I+1) < 0.0)
      if abs(RH(I))==0.0
         ZP1(K11)=I;
         K11=K11+1;
      elseif abs(RH(I+1))==0.0
         ZP1(K11)=I+1;
         K11=K11+1;

      elseif (abs(RH(I)) < abs(RH(I+1)))
         ZP1(K11)=I;
         K11=K11+1;
      elseif abs(RH(I)) > abs(RH(I+1))
         ZP1(K11)=I+1;
         K11=K11+1;
      end
   end

end


K22=1;
for I=1:ns-1

   if (Haut1(I)>= 0.0 & Haut1(I+1) < 0.0)
      if abs(Haut1(I))==0.0
         ZP2(K22)=I;
         K22=K22+1;
      elseif abs(Haut1(I+1))==0.0
         ZP2(K22)=I+1;
         K22=K22+1;

      elseif (abs(Haut1(I)) < abs(Haut1(I+1)))
         ZP2(K22)=I;
         K22=K22+1;
      elseif abs(Haut1(I)) > abs(Haut1(I+1))
         ZP2(K22)=I+1;
         K22=K22+1;
      end
   end

end

if RD2(1) < 0
   TRIGGERP=min(RD2);KK=2;
```

```
elseif RD2(1)> 0
   TRIGGERP=max(RD2);KK=1;
end

if KK == 2
   for i=1:ns
      RP(i)=-RP(i);
      Paut1(i)=-Paut1(I
   end
end

K33=1;
for I=1:ns-1

   if (RP(I)>= 0.0 & RP(I+1) < 0.0)
      if abs(RP(I))==0.0
         ZP3(K33)=I;
         K33=K33+1;
      elseif abs(RP(I+1))==0.0
         ZP3(K33)=I+1;
         K33=K33+1;

      elseif (abs(RP(I)) < abs(RP(I+1)))
         ZP3(K33)=I;
         K33=K33+1;
      elseif abs(RP(I)) > abs(RP(I+1))
         ZP3(K33)=I+1;
         K33=K33+1;
      end
   end

end

K44=1;

for I=1:ns-1

   if (Paut1(I)>= 0.0 & Paut1(I+1) < 0.0)
      if abs(Paut1(I))==0.0
         ZP4(K44)=I;
         K44=K44+1;
      elseif abs(Paut1(I+1))==0.0
         ZP4(K44)=I+1;
         K44=K44+1;
      elseif (abs(Paut1(I)) < abs(Paut1(I+1)))
         ZP4(K44)=I;
         K44=K44+1;
      elseif abs(Paut1(I)) > abs(Paut1(I+1))
         ZP4(K44)=I+1;
         K44=K44+1;
      end
   end

end
```

Appendix H

Random Decrement and Free Response: Simulation

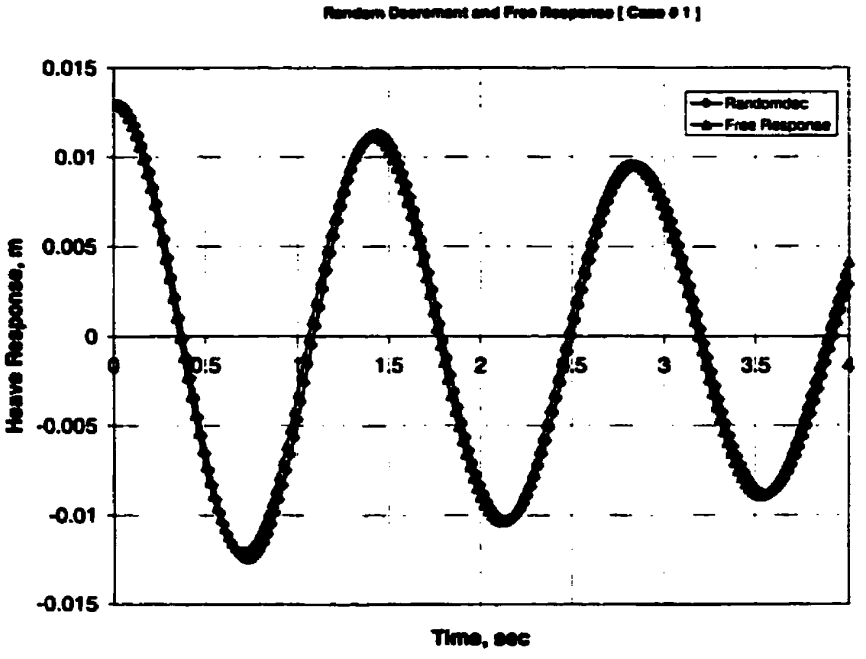

Figure H.1: Comparison between the random decrement and the free response for heave motion [Case # 1]

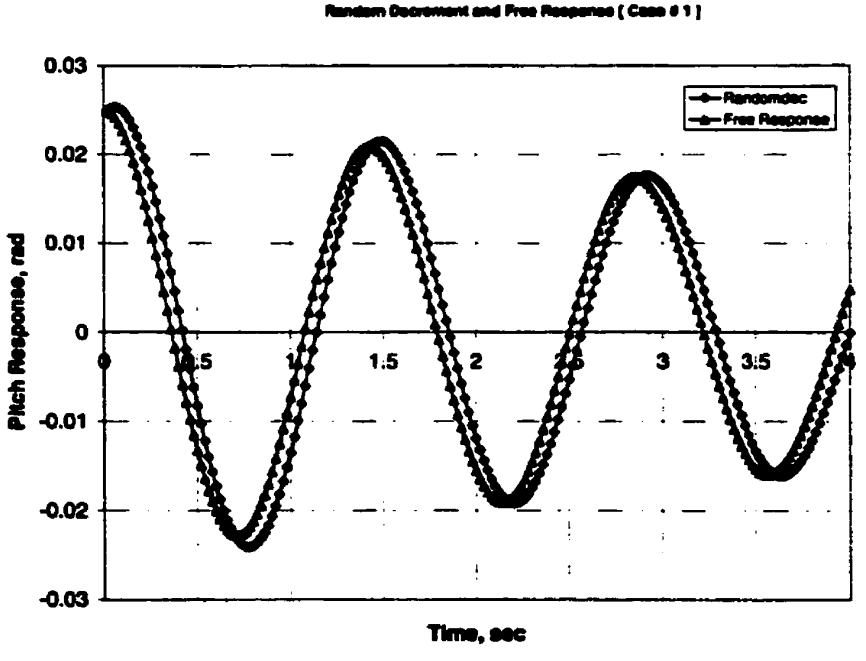

Figure H.2: Comparison between the random decrement and the free response for pitch motion [Case # 1]

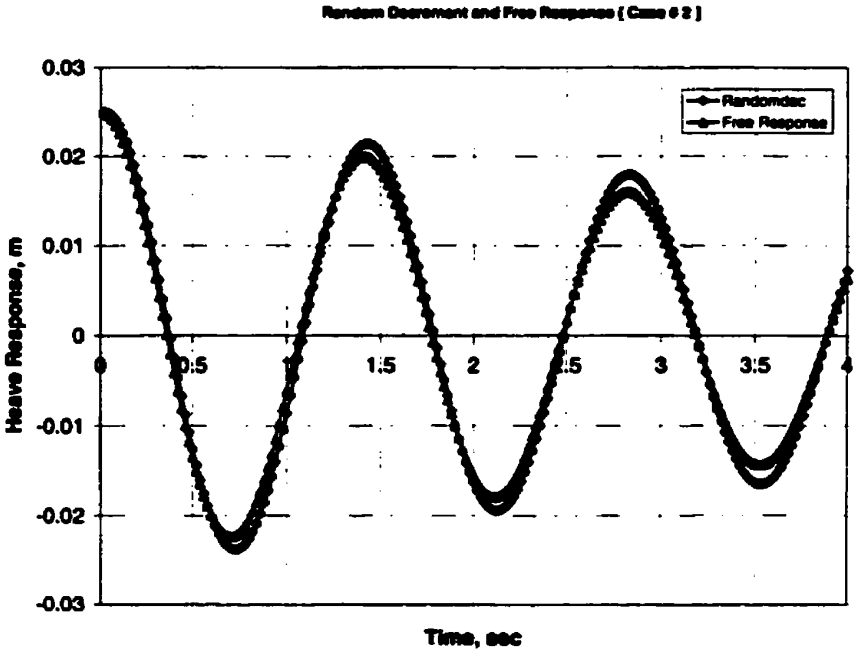

Figure H.3: Comparison between the random decrement and the free response for heave motion [Case # 2]

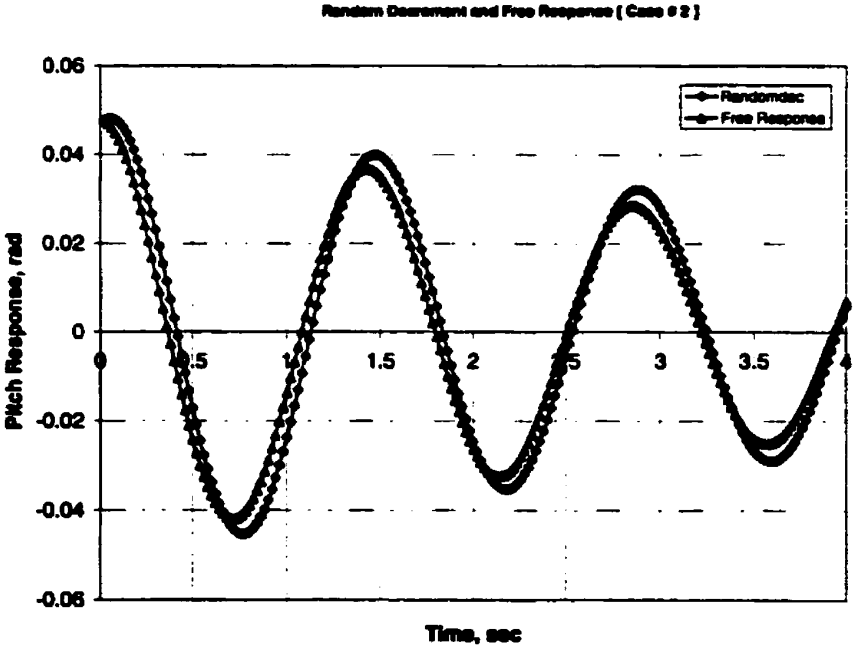

Figure H.4: Comparison between the random decrement and the free response for pitch motion [Case # 2]

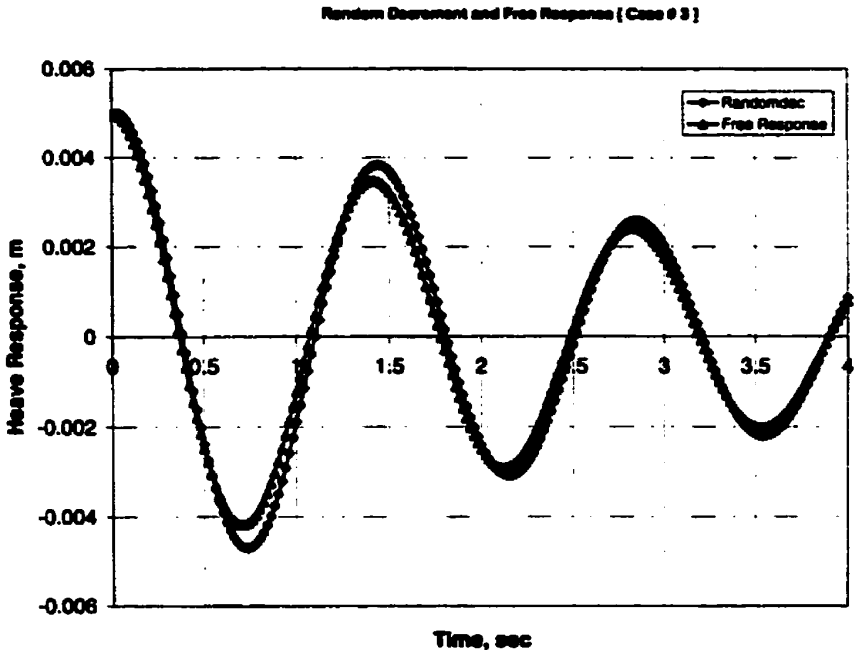

Figure H.5: Comparison between the random decrement and the free response for heave motion [Case # 3]

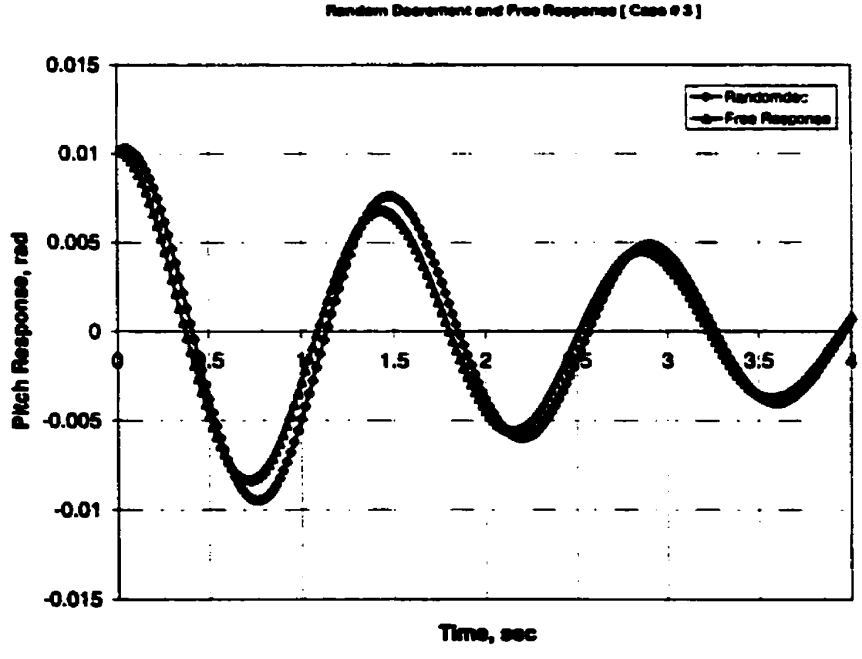

Figure H.6: Comparison between the random decrement and the free response for pitch motion [Case # 3]

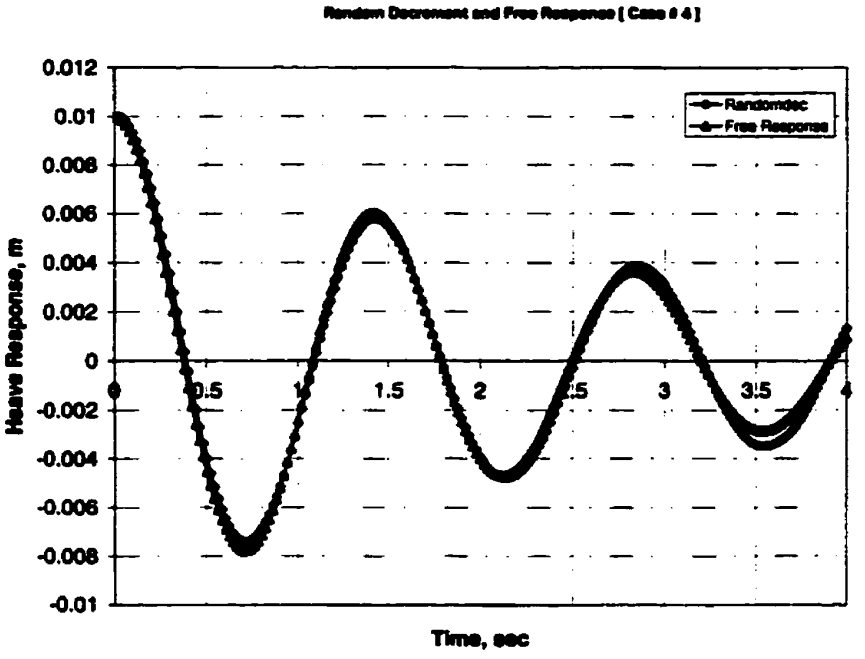

Figure H.7: Comparison between the random decrement and the free response for heave motion [Case # 4]

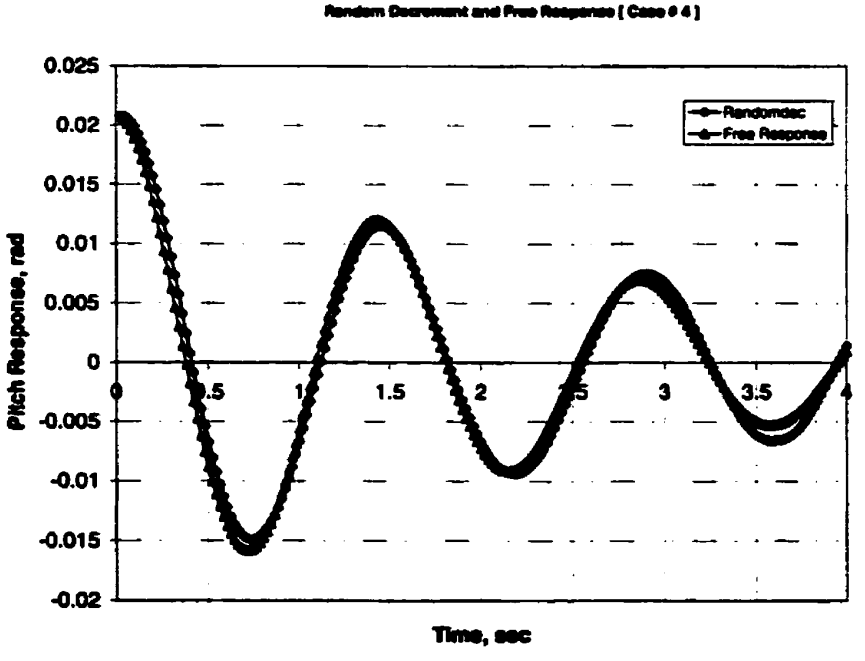

Figure H.8: Comparison between the random decrement and the free response for pitch motion [Case # 4]

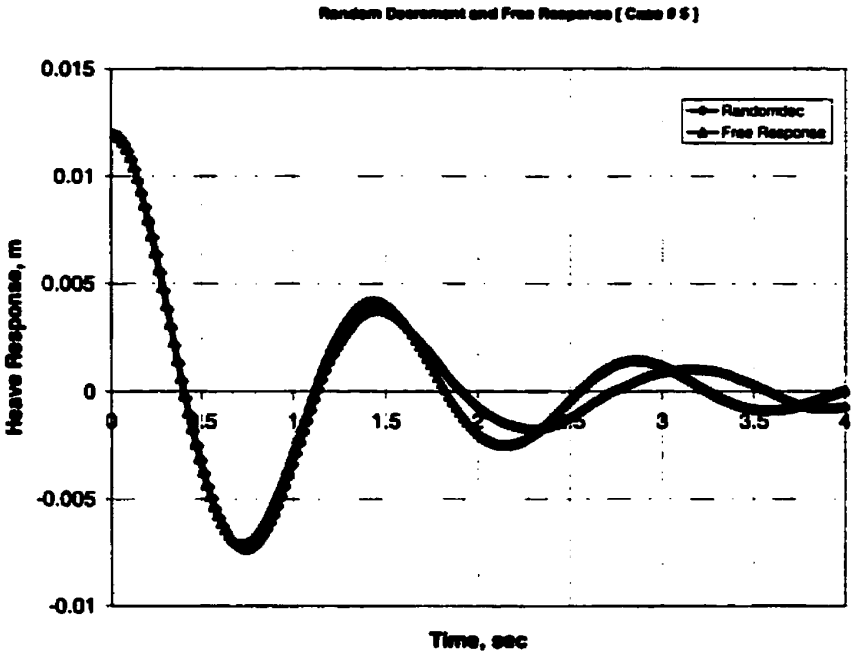

Figure H.9: Comparison between the random decrement and the free response for heave motion [Case # 5]

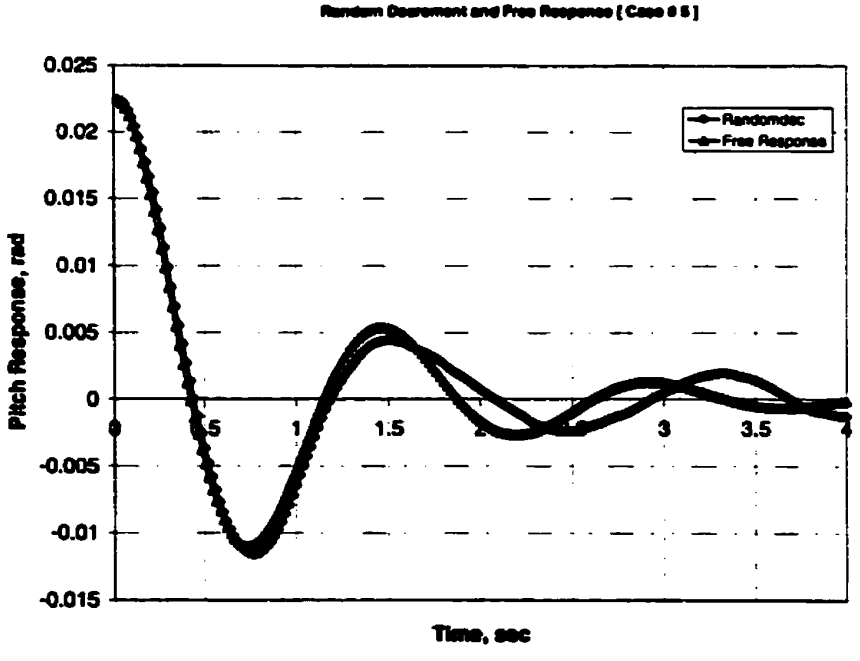

Figure H.10: Comparison between the random decrement and the free response for pitch motion [Case # 5]

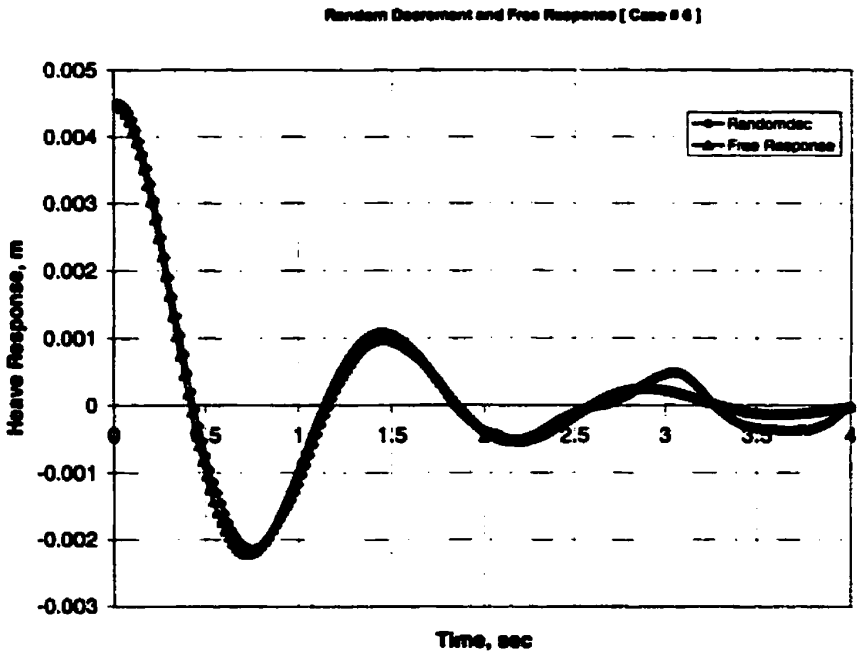

Figure H.11: Comparison between the random decrement and the free response for heave motion [Case # 6]

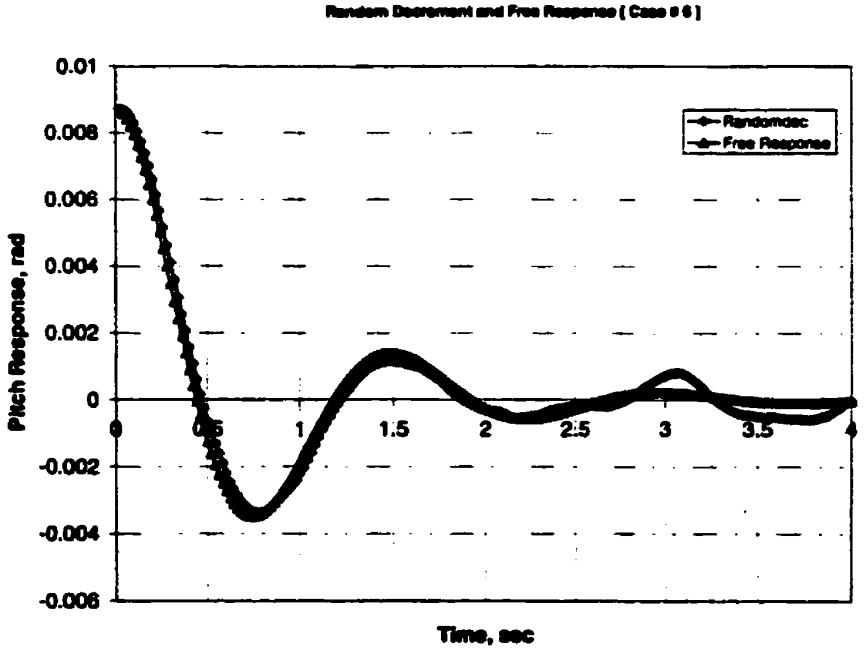

Figure H.12: Comparison between the random decrement and the free response for pitch motion [Case # 6]

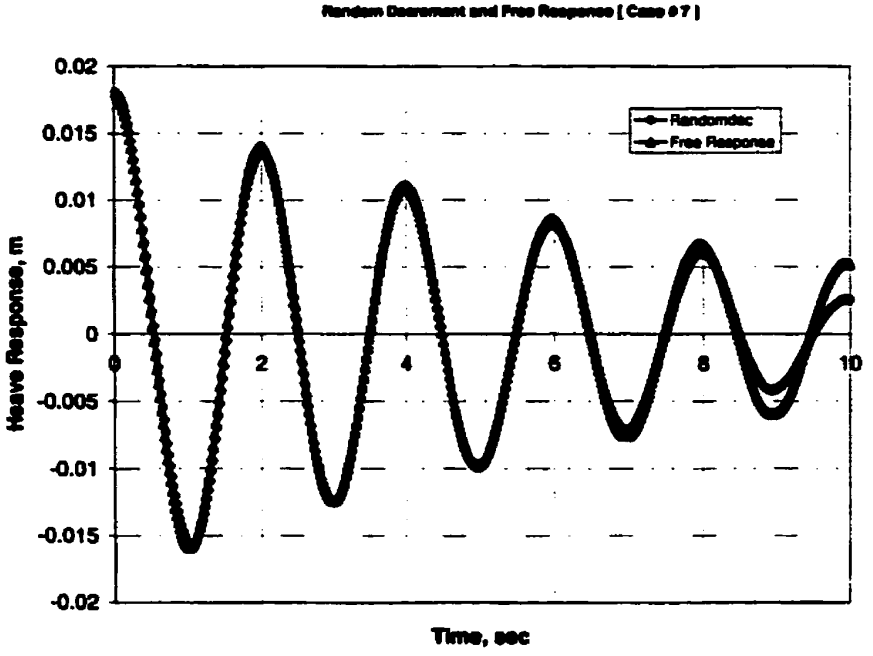

Figure H.13: Comparison between the random decrement and the free response for heave motion [Case # 7]

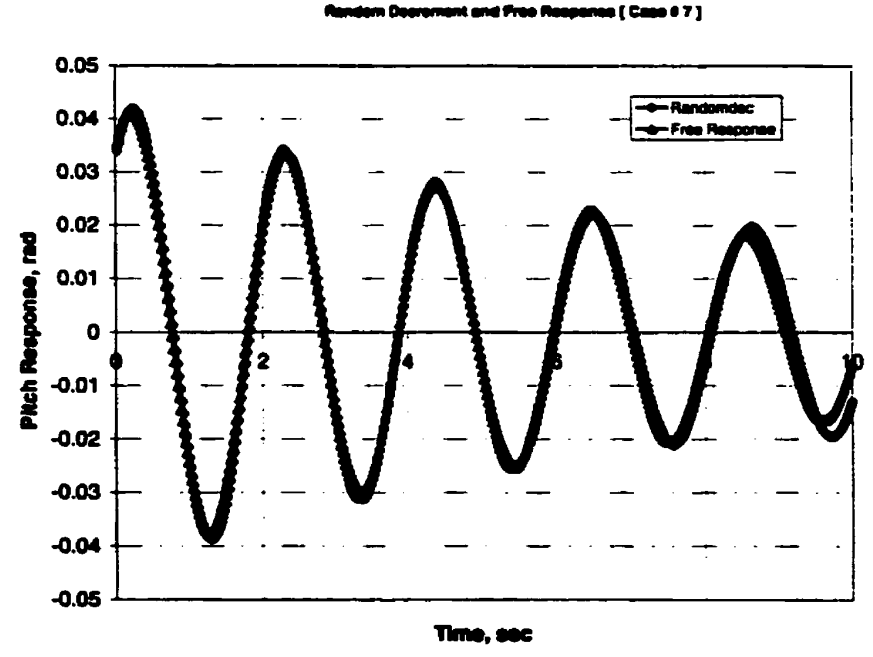

Figure H.14: Comparison between the random decrement and the free response for pitch motion [Case # 7]

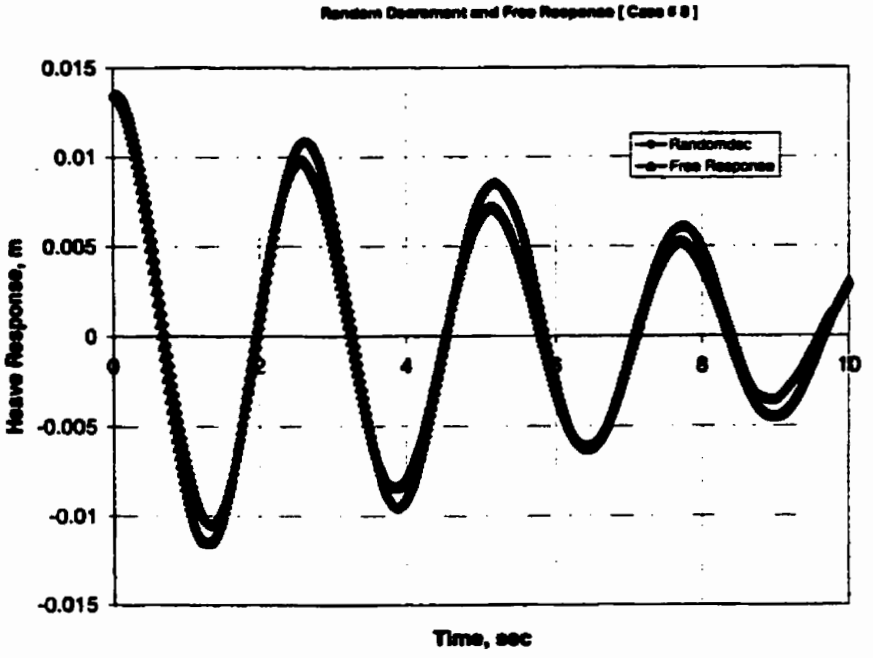

Figure H.15: Comparison between the random decrement and the free response for heave motion [Case # 8]

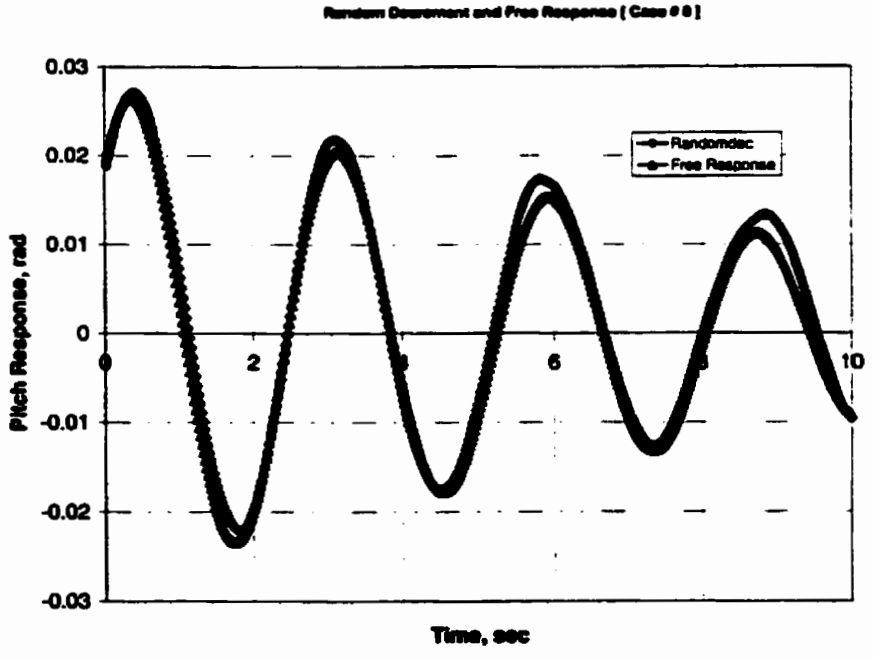

Figure H.16: Comparison between the random decrement and the free response for pitch motion [Case # 8]

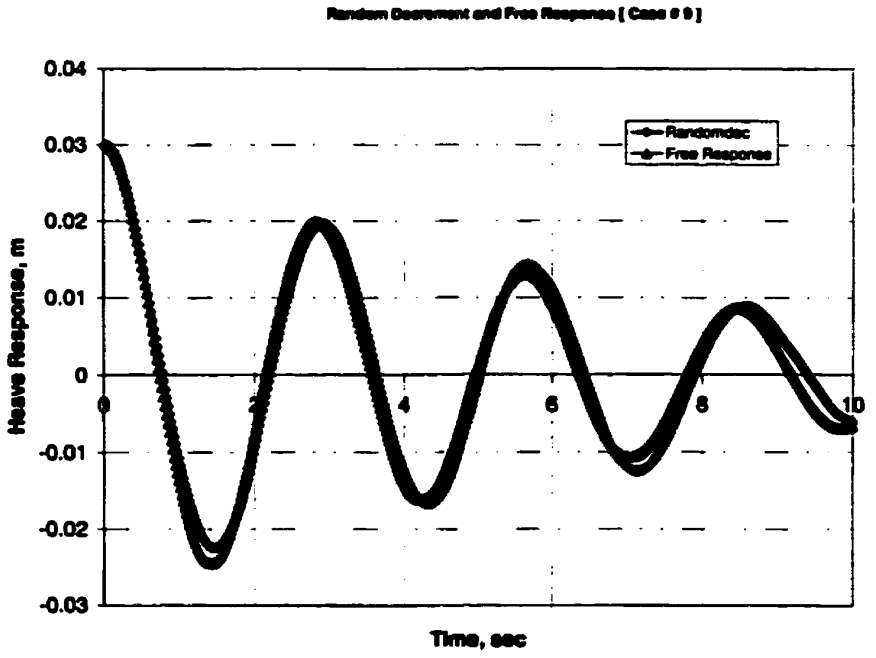

Figure H.17: Comparison between the random decrement and the free response for heave motion [Case # 9]

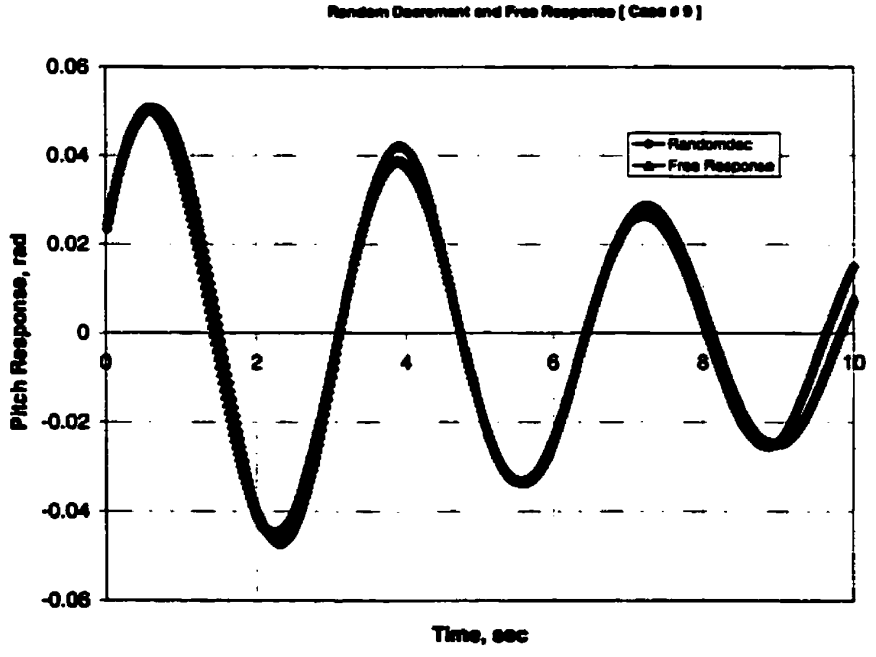

Figure H.18: Comparison between the random decrement and the free response for pitch motion [Case # 9]

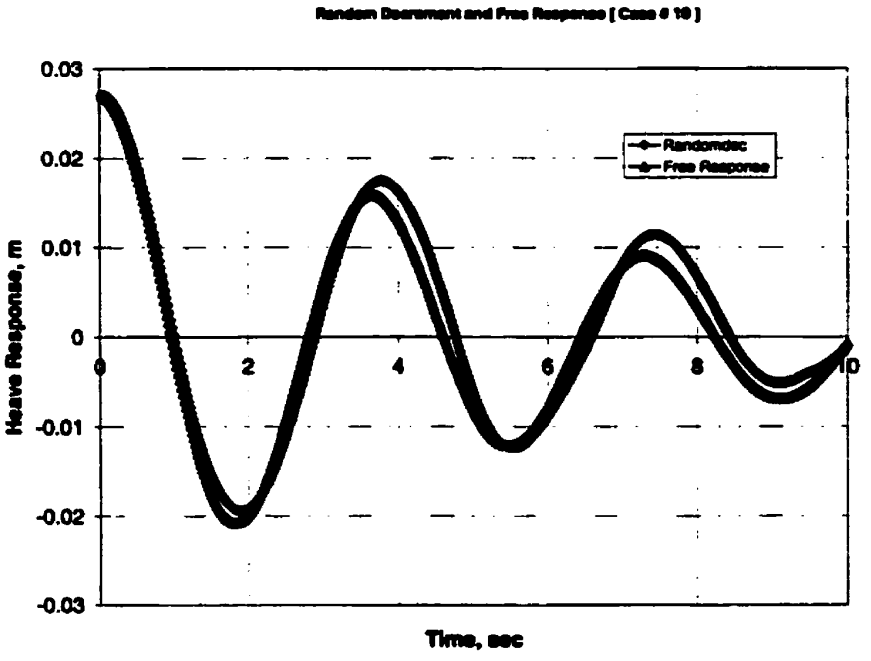

Figure H.19: Comparison between the random decrement and the free response for heave motion [Case # 10]

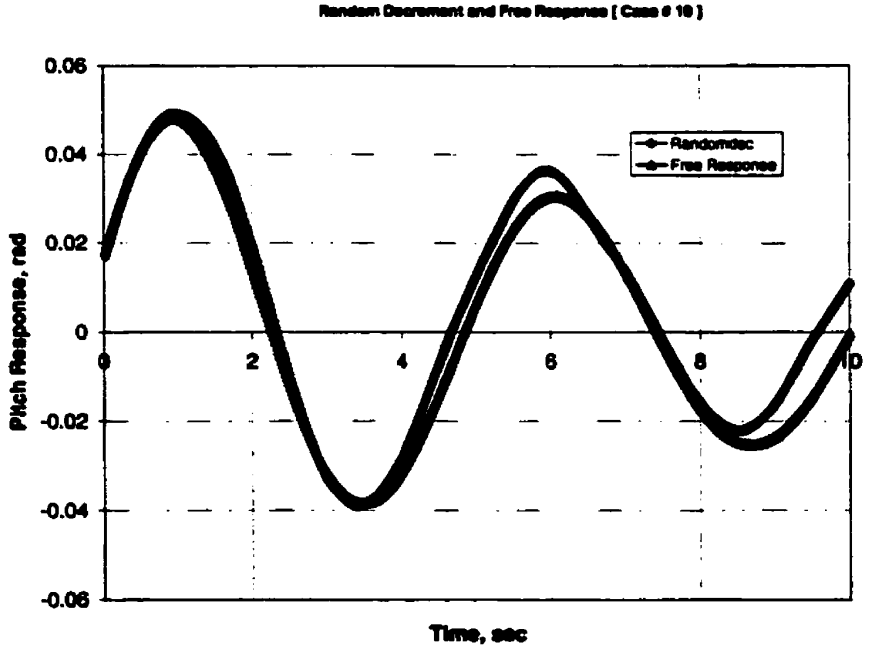

Figure H.20: Comparison between the random decrement and the free response for pitch motion [Case # 10]

Appendix I

Random Decrement and Auto-correlation Function: Simulation

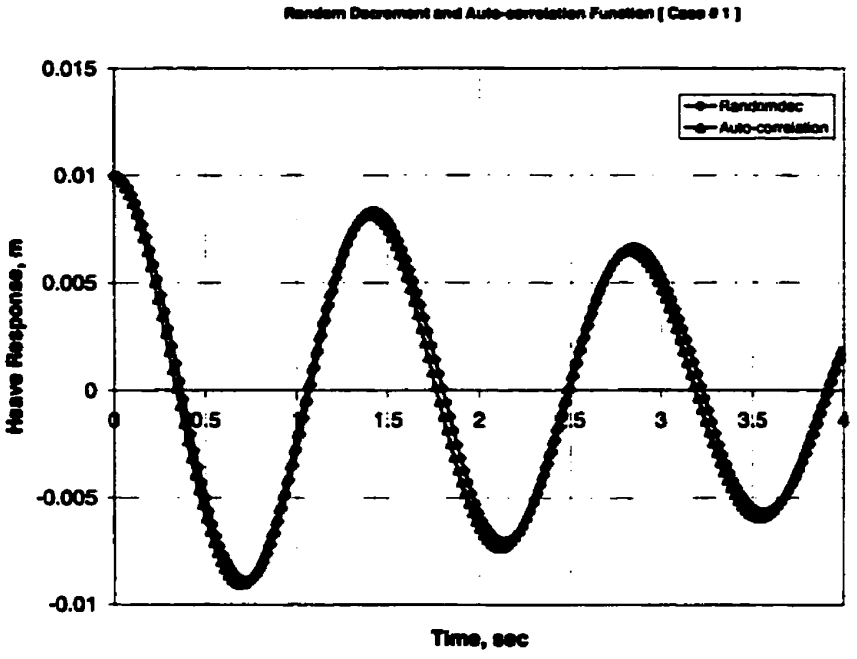

Figure I.1: Comparison between the random decrement and the auto-correlation function for heave motion [Case # 1]

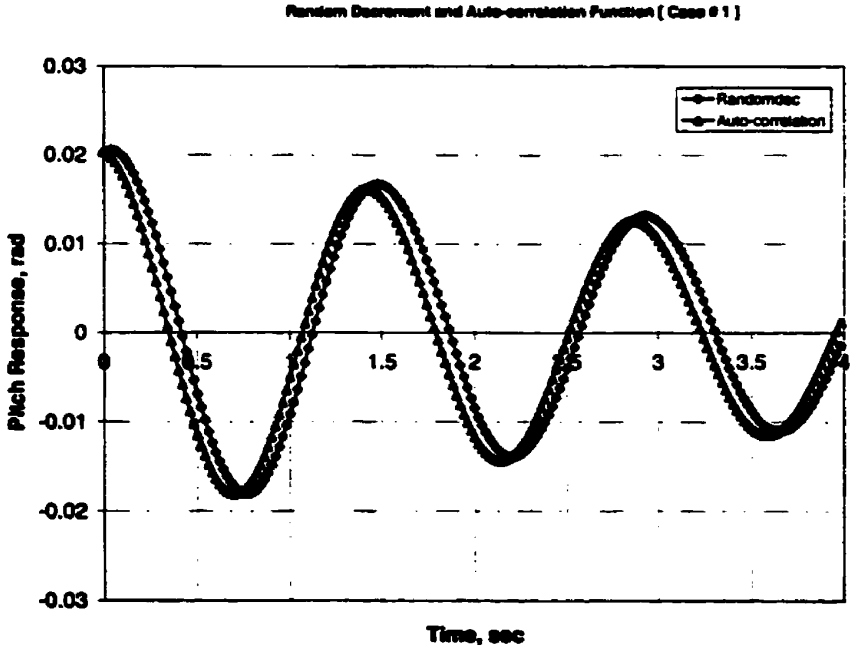

Figure I.2: Comparison between the random decrement and the auto-correlation function for pitch motion [Case # 1]

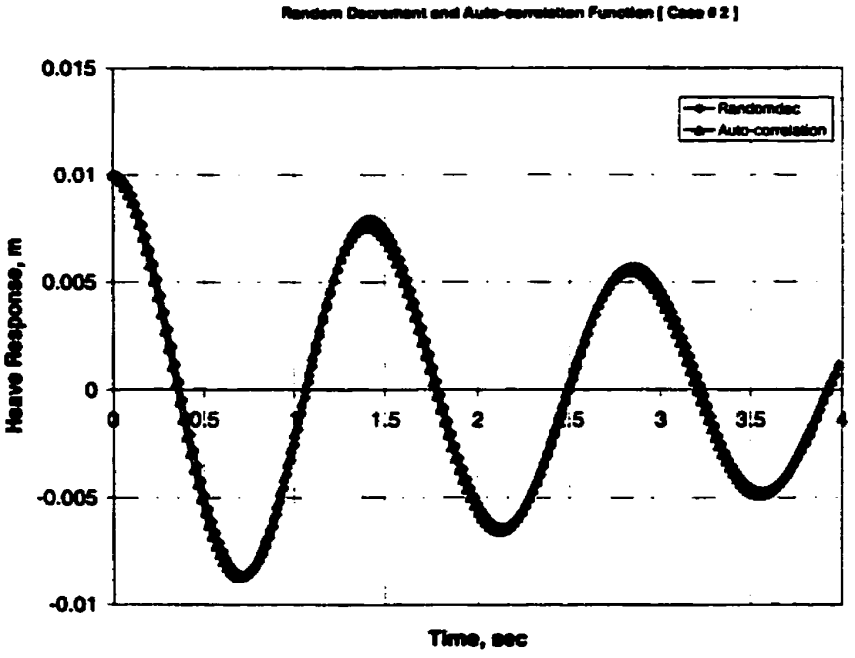

Figure I.3: Comparison between the random decrement and the auto-correlation function for heave motion [Case # 2]

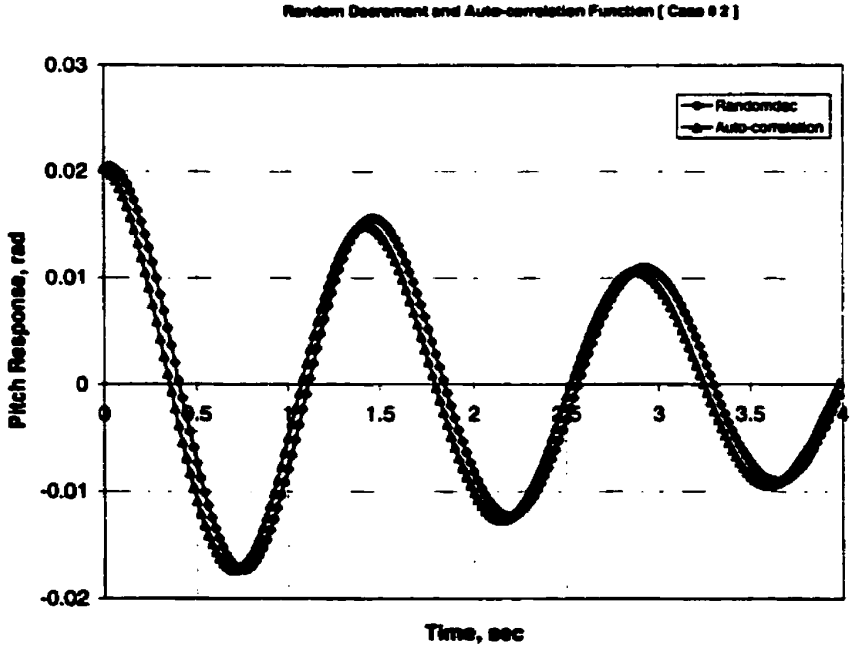

Figure I.4: Comparison between the random decrement and the auto-correlation function for pitch motion [Case # 2]

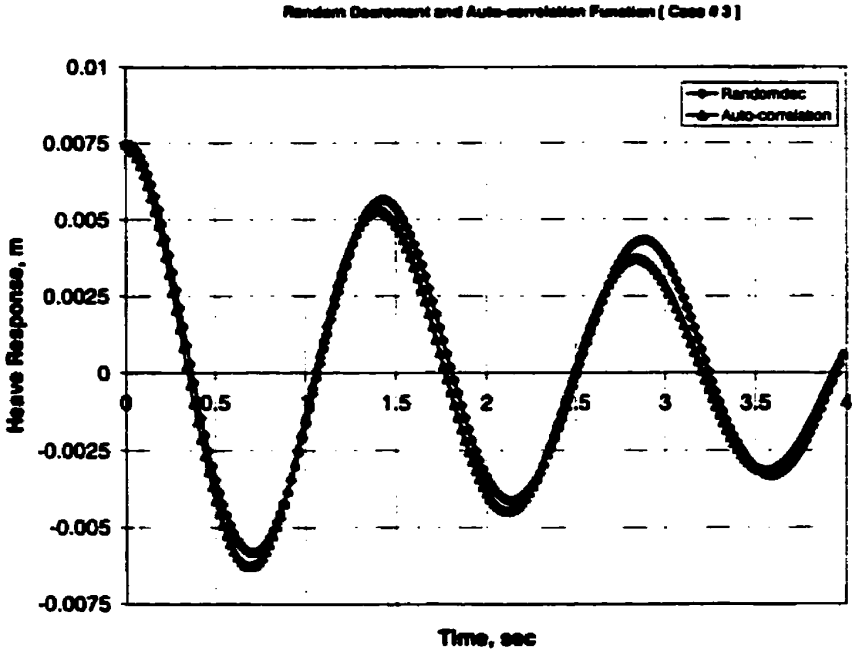

Figure I.5: Comparison between the random decrement and the auto-correlation function for heave motion [Case # 3]

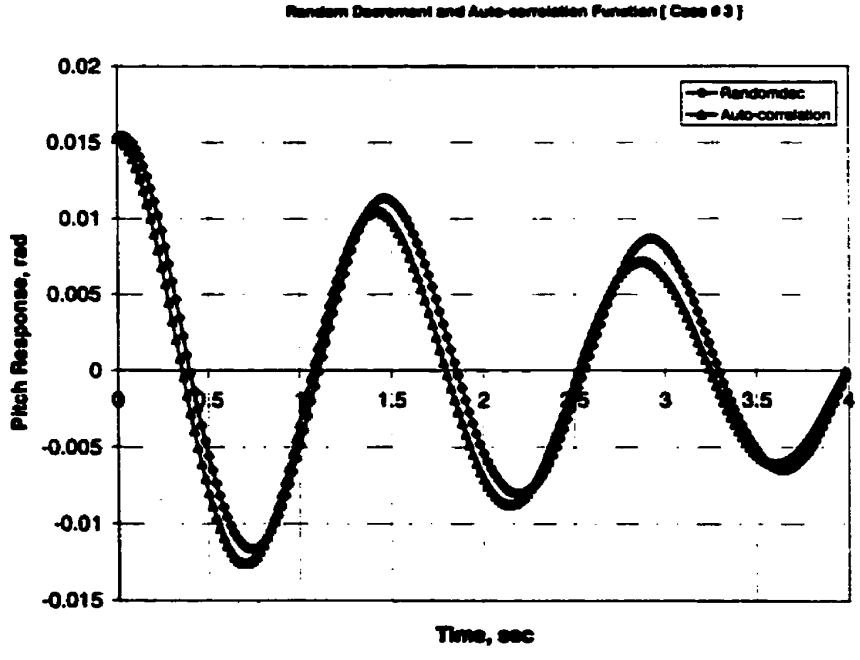

Figure I.6: Comparison between the random decrement and the auto-correlation function for pitch motion [Case # 3]

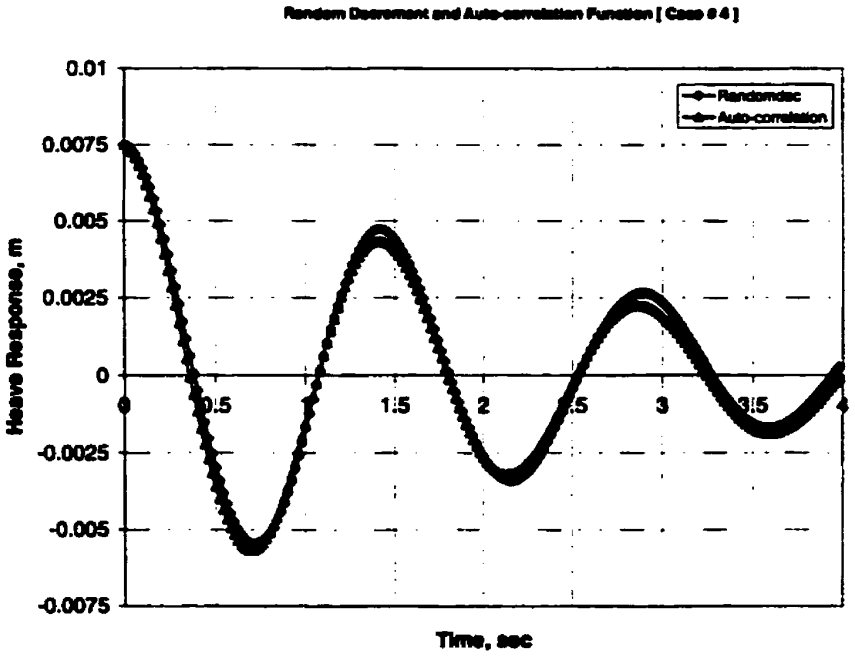

Figure I.7: Comparison between the random decrement and the auto-correlation function for heave motion [Case # 4]

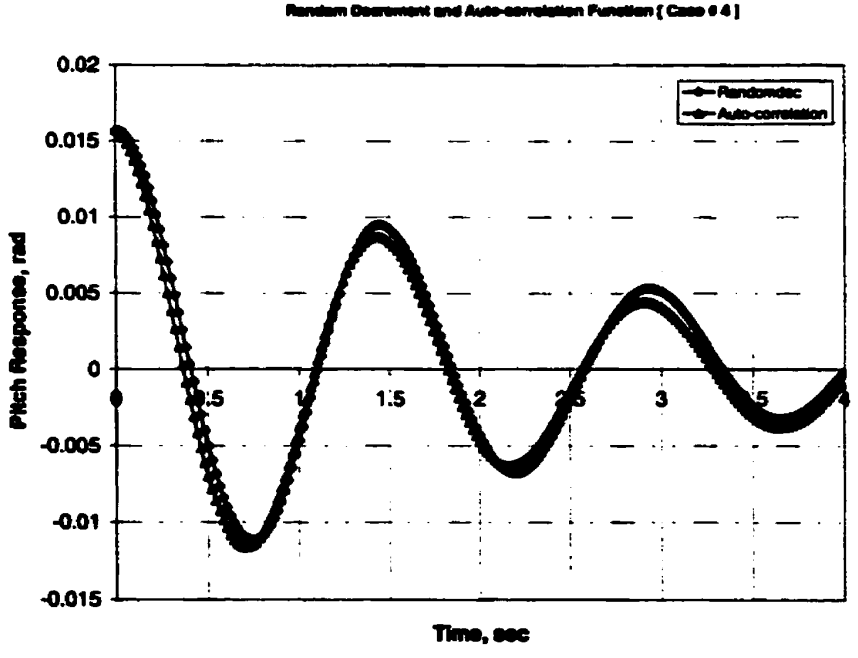

Figure I.8: Comparison between the random decrement and the auto-correlation function for pitch motion [Case # 4]

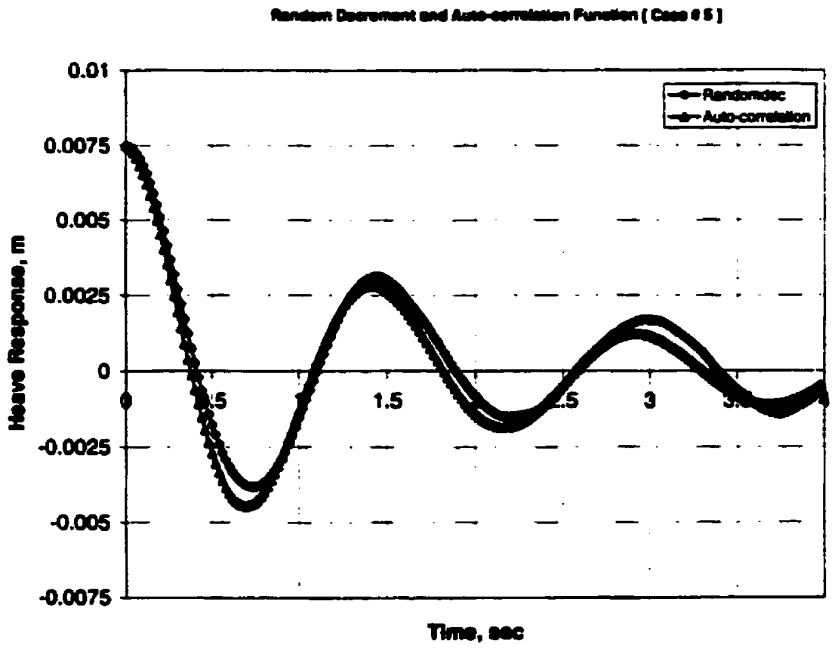

Figure I.9: Comparison between the random decrement and the auto-correlation function for heave motion [Case # 5]

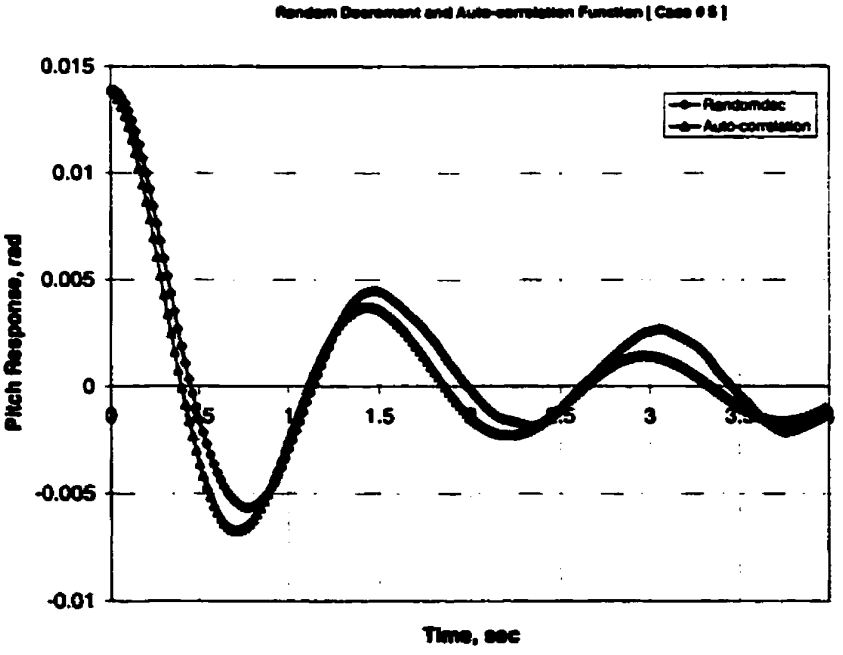

Figure I.10: Comparison between the random decrement and the auto-correlation function for pitch motion [Case # 5]

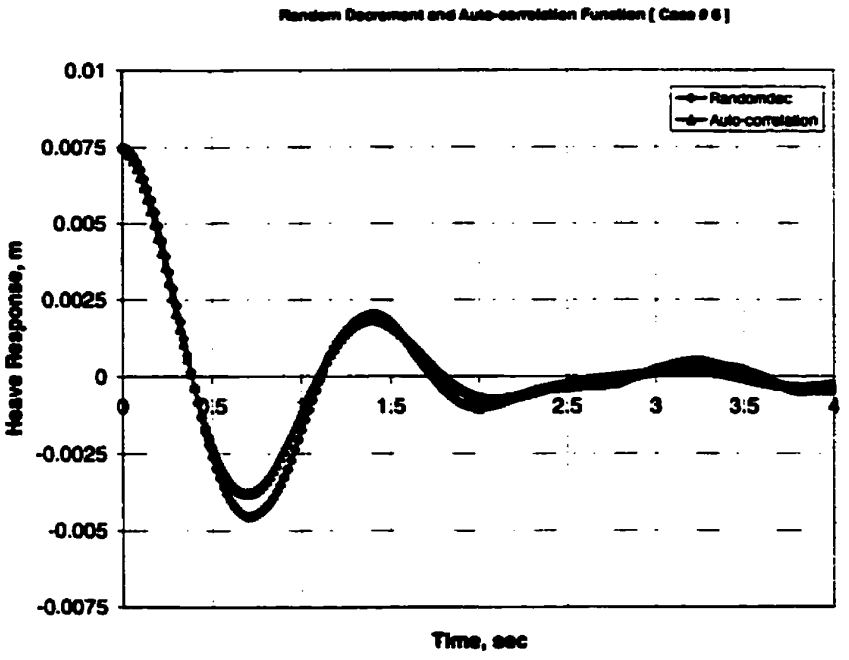

Figure I.11: Comparison between the random decrement and the auto-correlation function for heave motion [Case # 6]

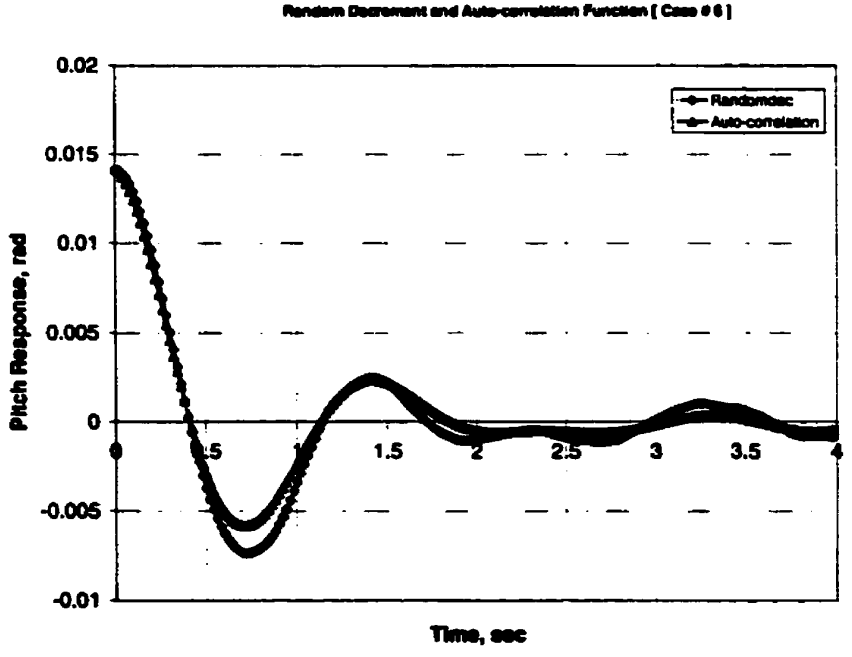

Figure I.12: Comparison between the random decrement and the auto-correlation function for pitch motion [Case # 6]

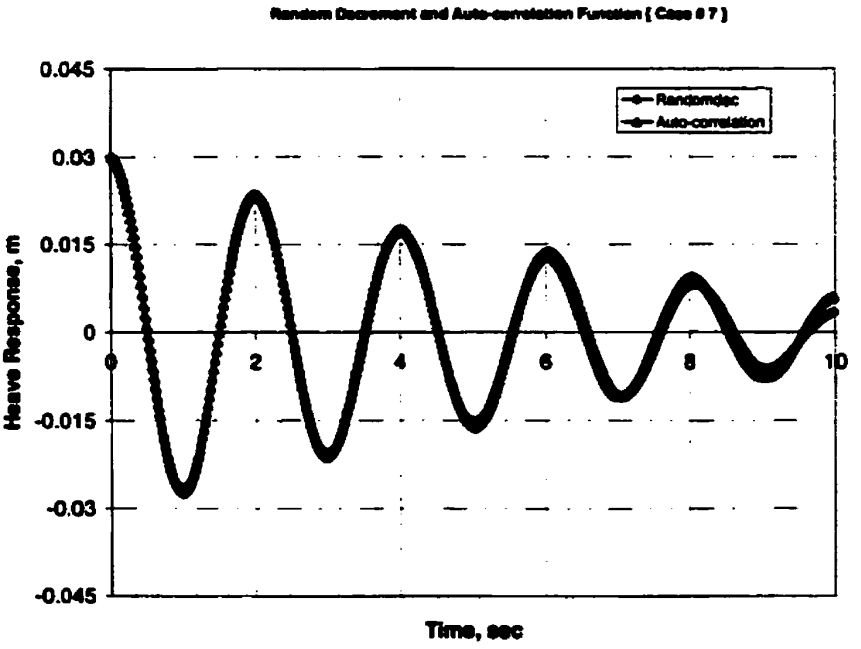

Figure I.13: Comparison between the random decrement and the auto-correlation function for heave motion [Case # 7]

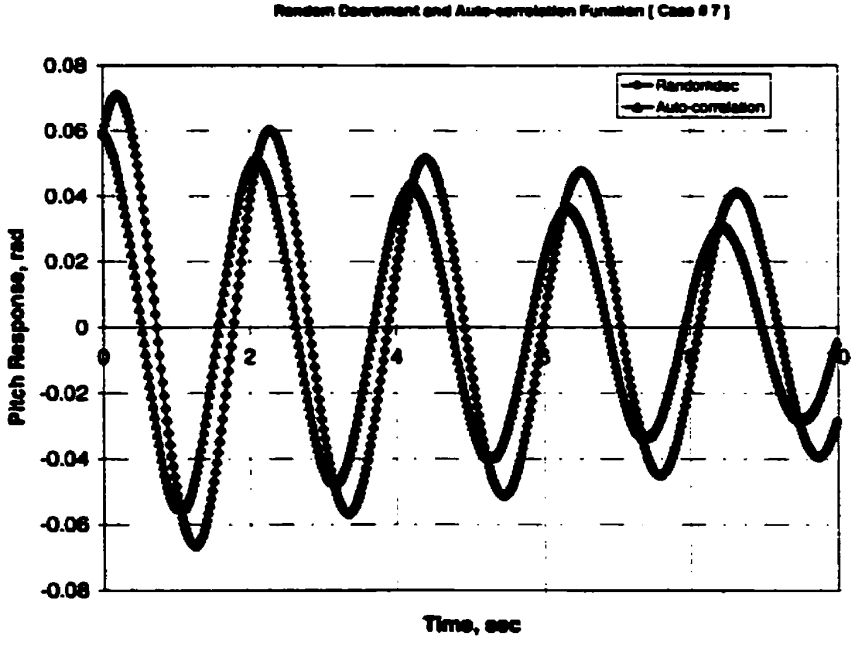

Figure I.14: Comparison between the random decrement and the auto-correlation function for pitch motion [Case # 7]

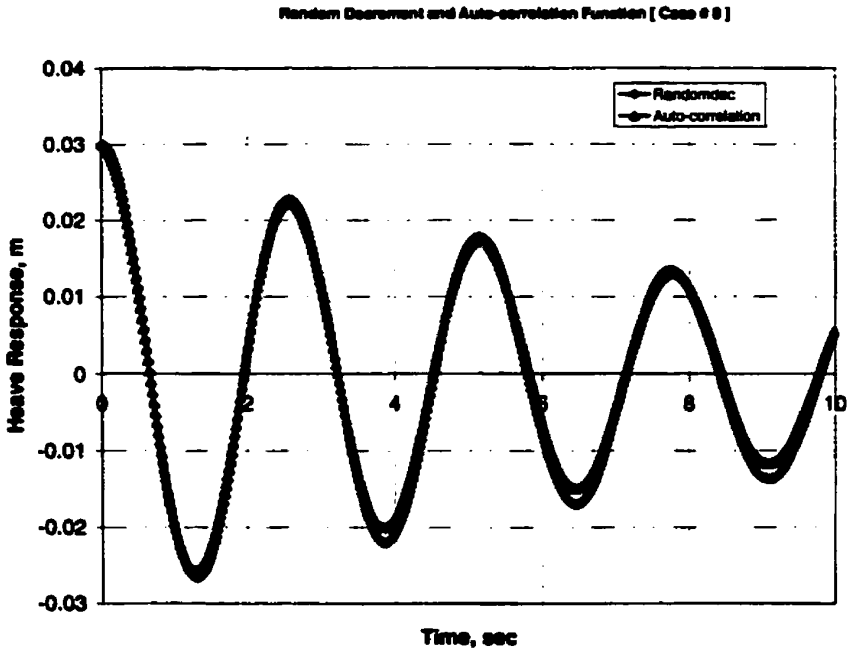

Figure I.15: Comparison between the random decrement and the auto-correlation function for heave motion [Case # 8]

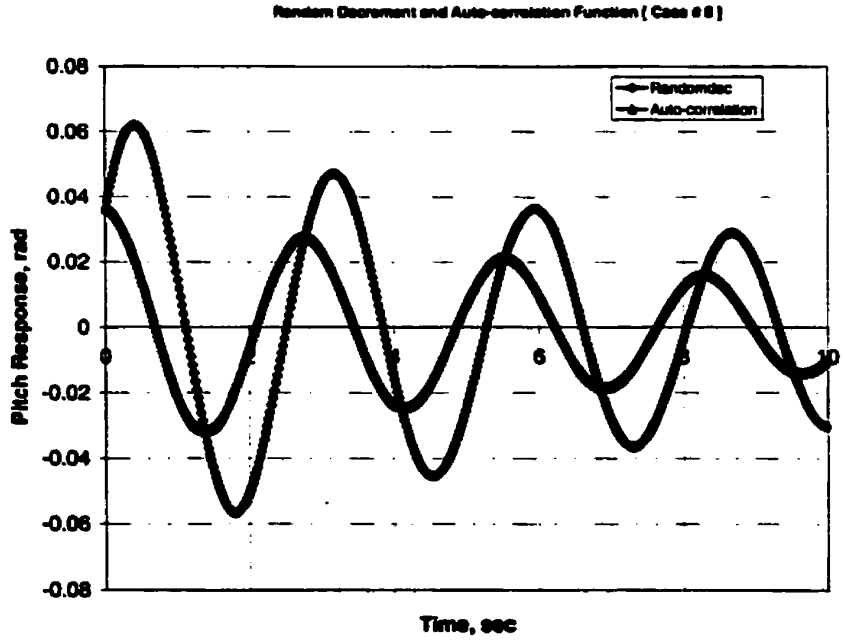

Figure I.16: Comparison between the random decrement and the auto-correlation function for pitch motion [Case # 8]

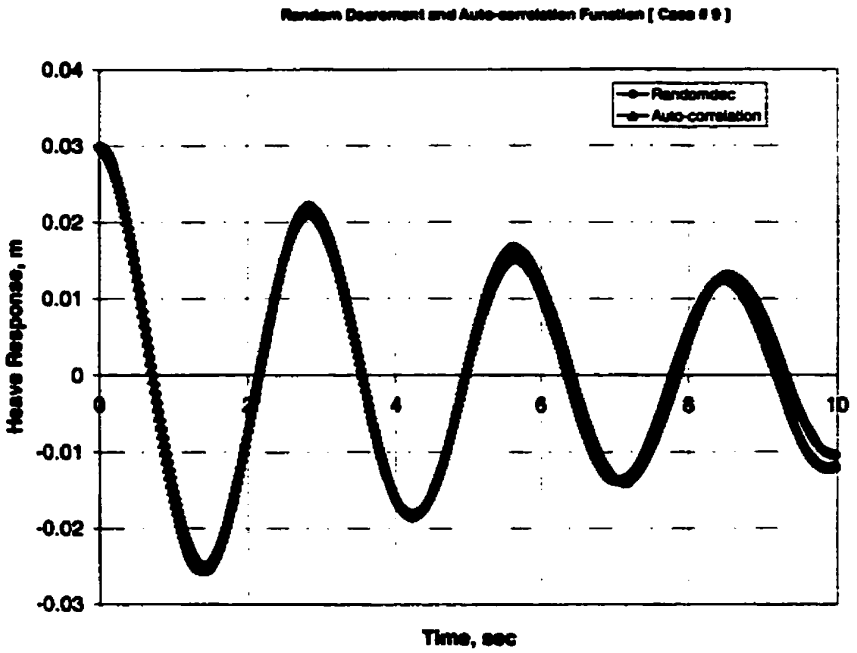

Figure I.17: Comparison between the random decrement and the auto-correlation function for heave motion [Case # 9]

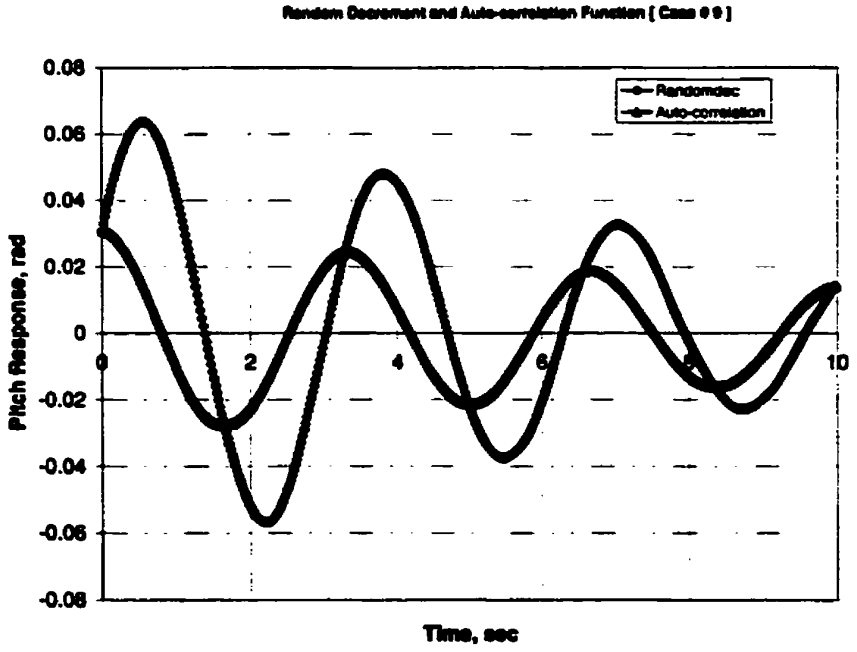

Figure I.18: Comparison between the random decrement and the auto-correlation function for pitch motion [Case # 9]

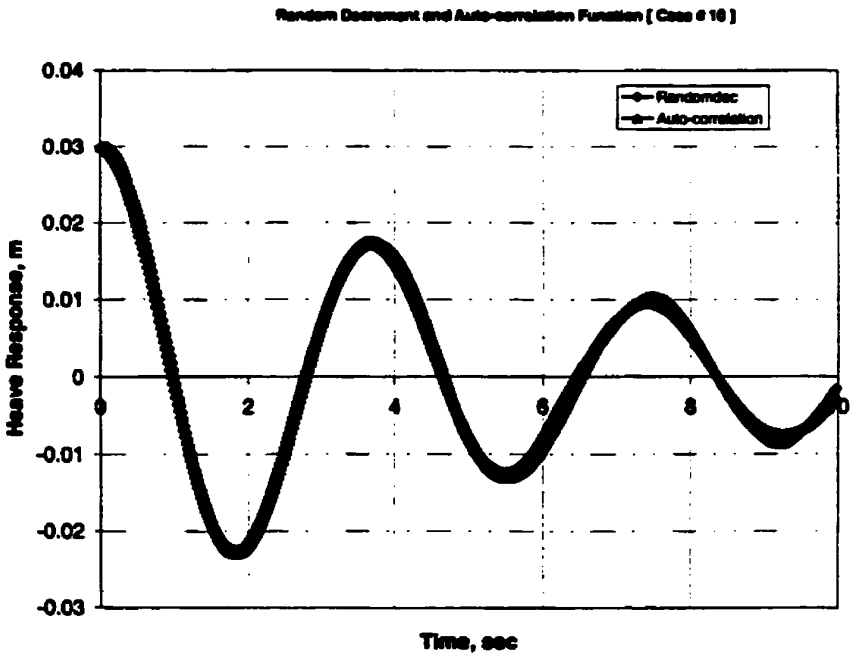

Figure I.19: Comparison between the random decrement and the auto-correlation function for heave motion [Case # 10]

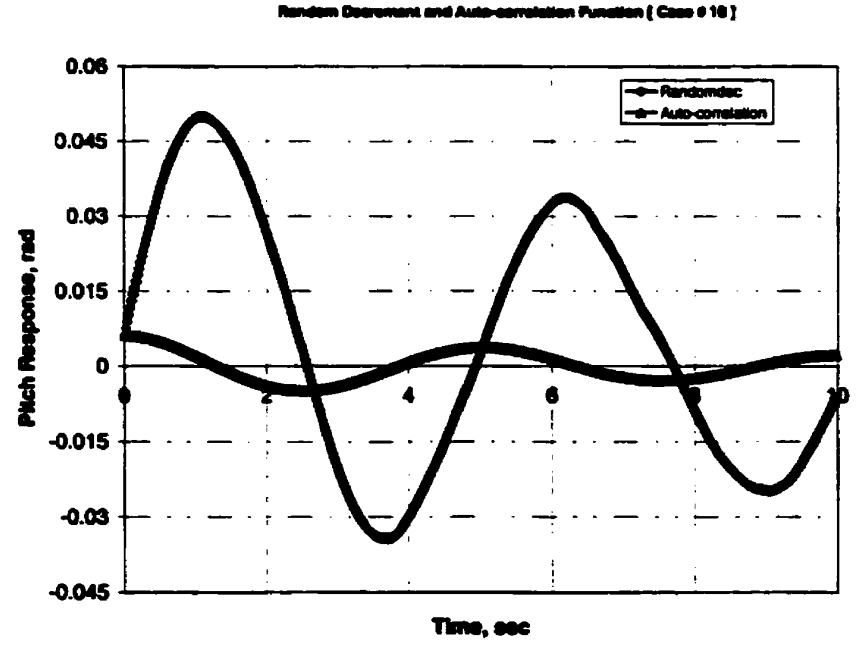

Figure I.20: Comparison between the random decrement and the auto-correlation function for pitch motion [Case # 10]

Appendix J

Predicted Free Responses: Simulation

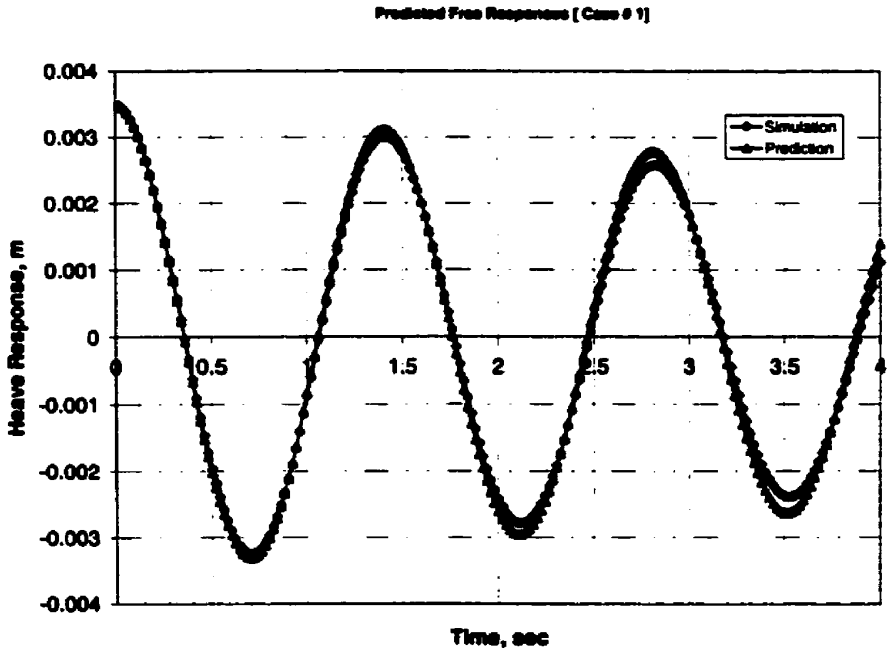

Figure J.1: Comparison between the simulated and the predicted free responses for heave motion [Case # 1]

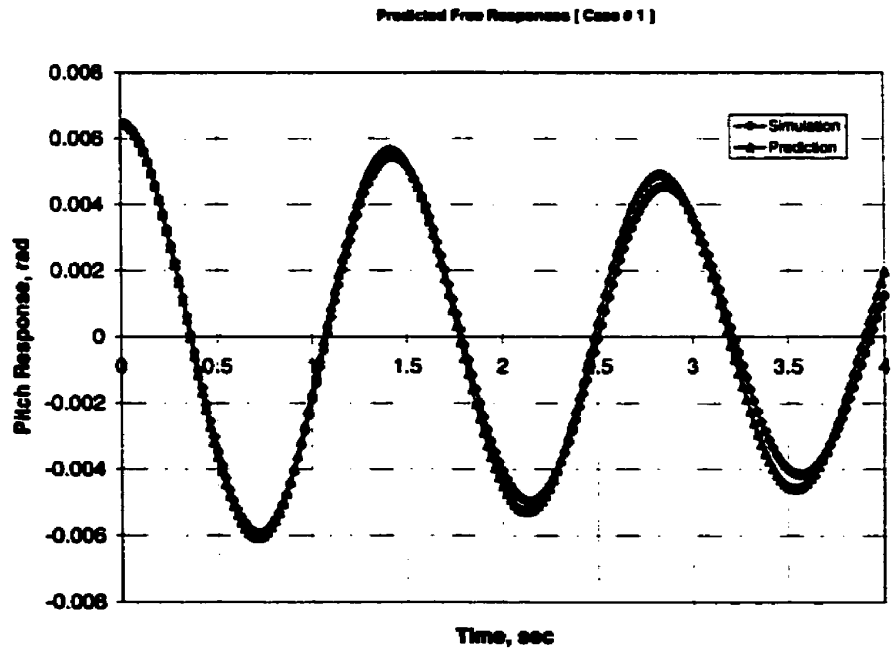

Figure J.2: Comparison between the simulated and the predicted free responses for pitch motion [Case # 1]

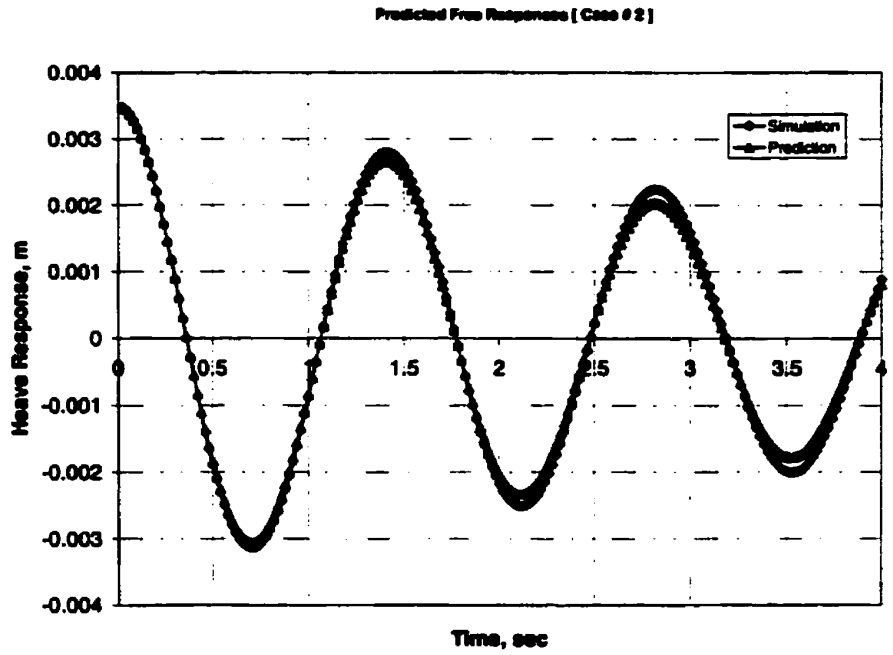

Figure J.3: Comparison between the simulated and the predicted free responses for heave motion [Case # 2]

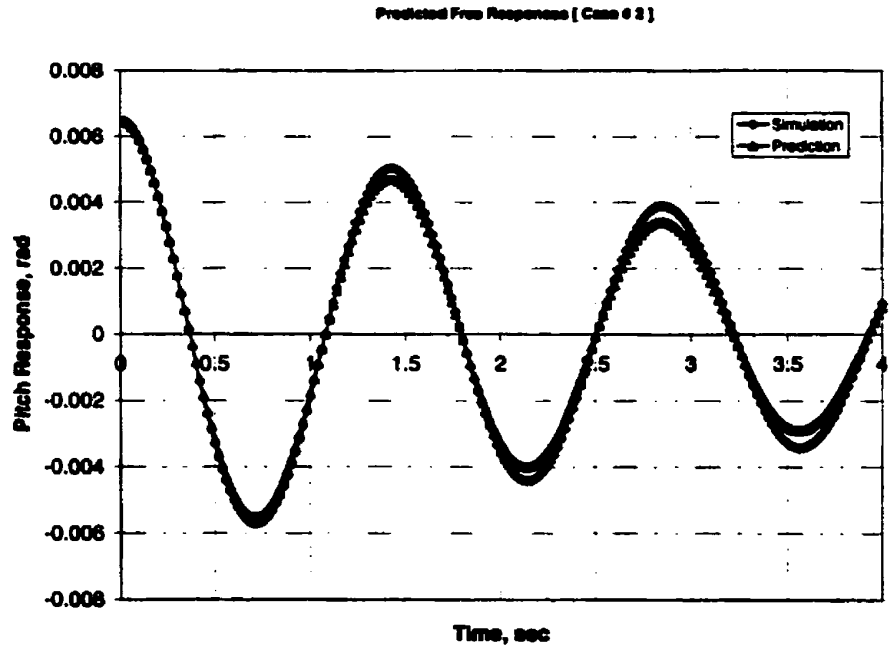

Figure J.4: Comparison between the simulated and the predicted free responses for pitch motion [Case # 2]

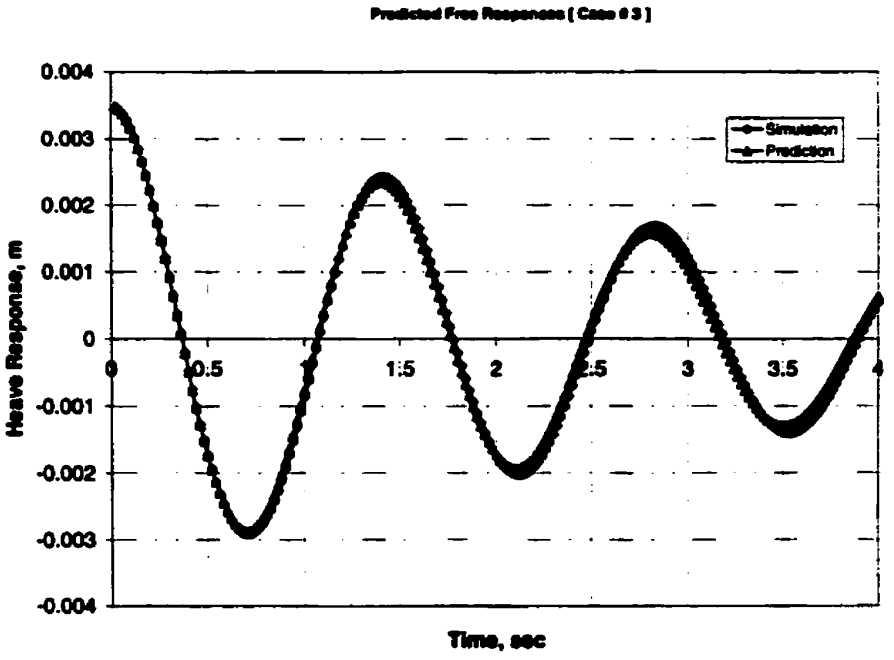

Figure J.5: Comparison between the simulated and the predicted free responses for heave motion [Case # 3]

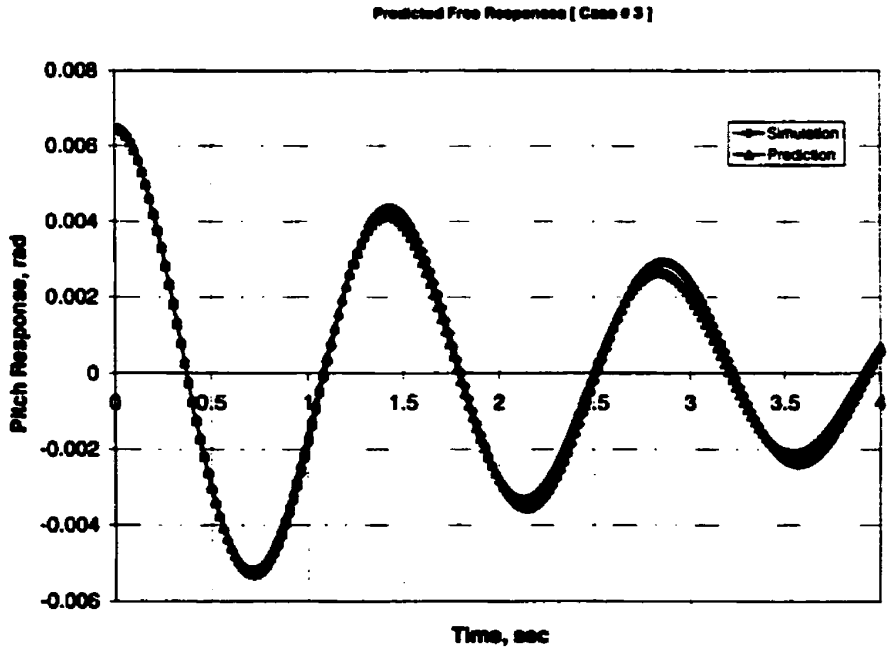

Figure J.6: Comparison between the simulated and the predicted free responses for pitch motion [Case # 3]

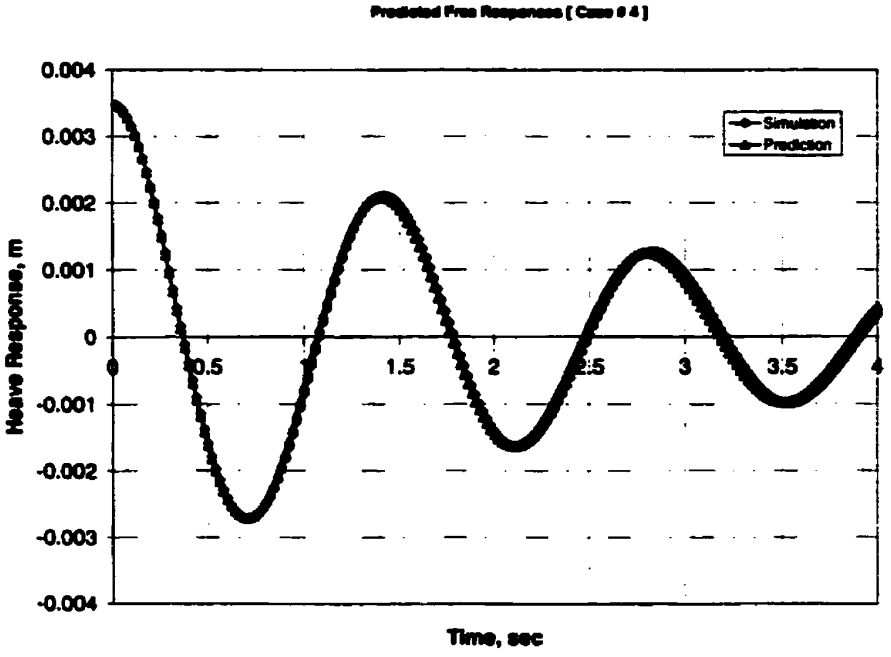

Figure J.7: Comparison between the simulated and the predicted free responses for heave motion [Case # 4]

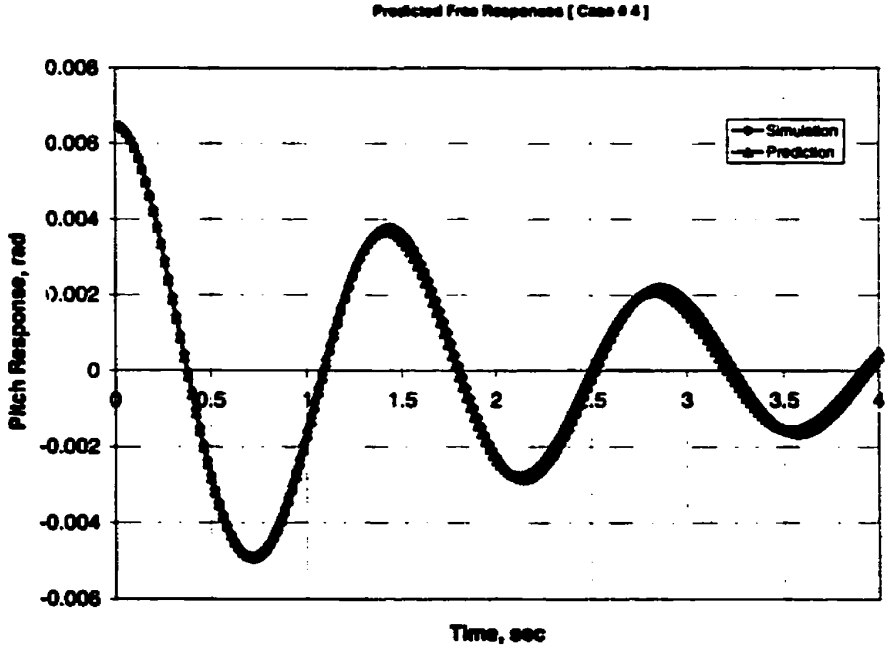

Figure J.8: Comparison between the simulated and the predicted free responses for pitch motion [Case # 4]

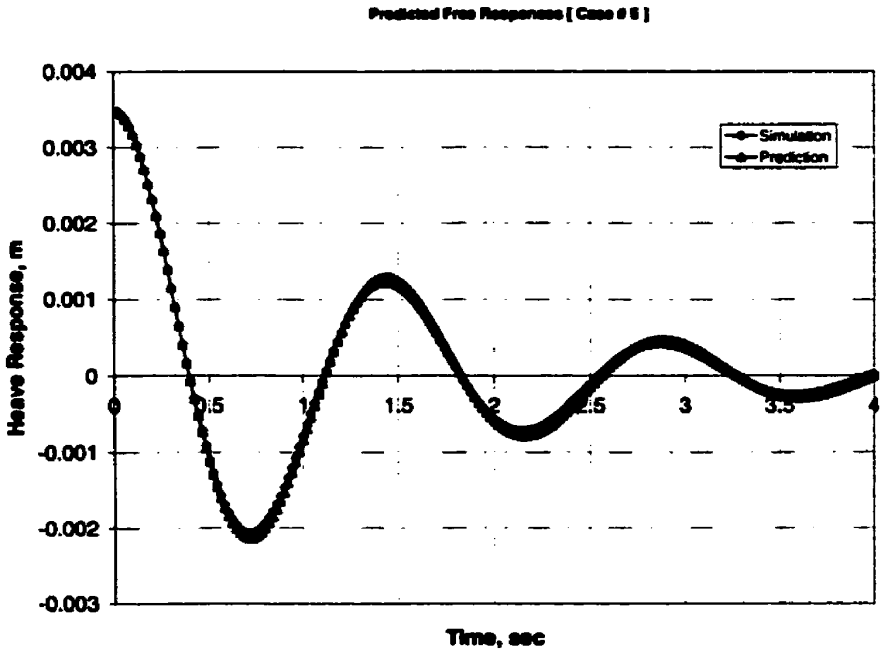

Figure J.9: Comparison between the simulated and the predicted free responses for heave motion [Case # 5]

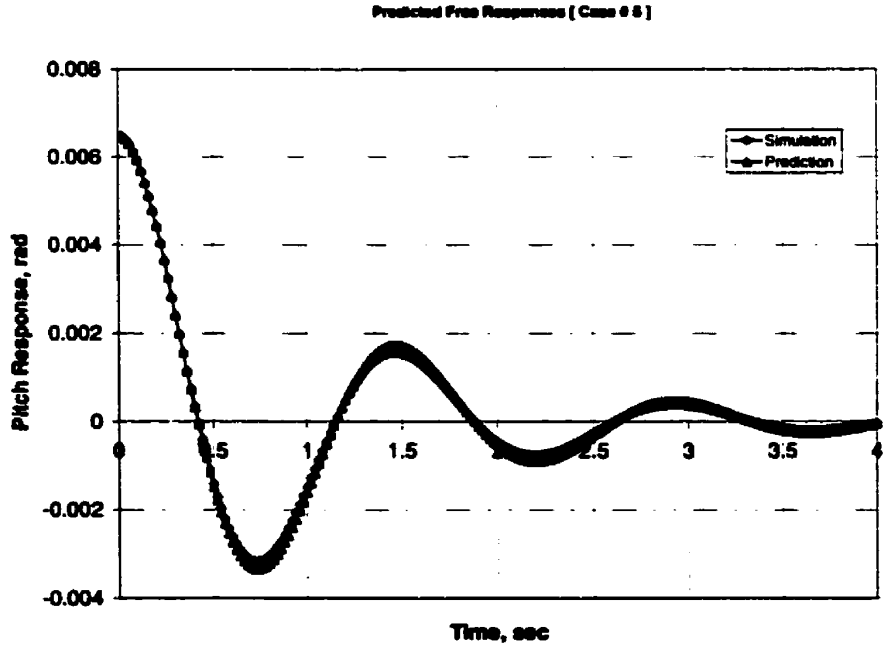

Figure J.10: Comparison between the simulated and the predicted free responses for pitch motion [Case # 5]

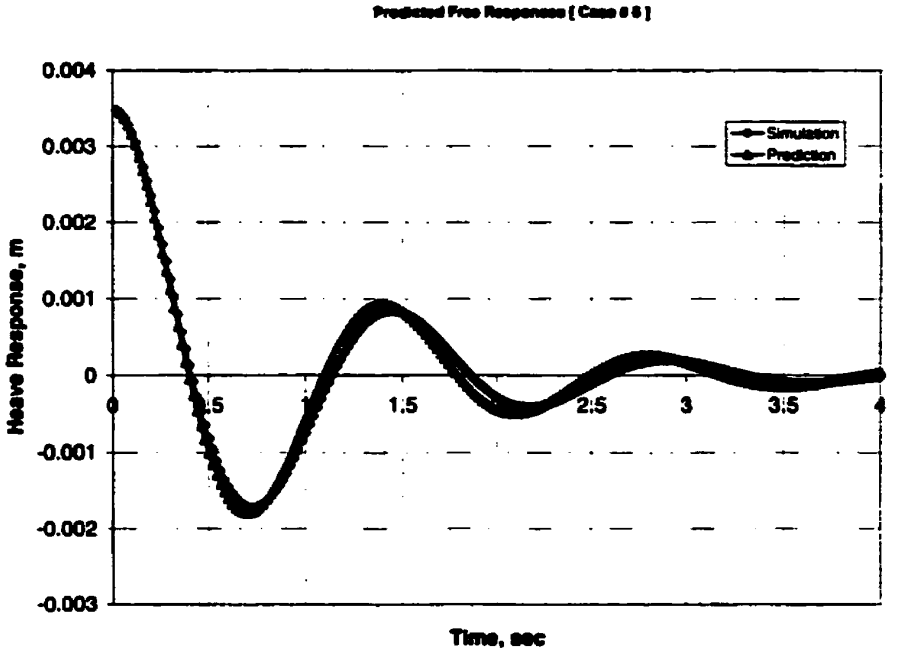

Figure J.11: Comparison between the simulated and the predicted free responses for heave motion [Case # 6]

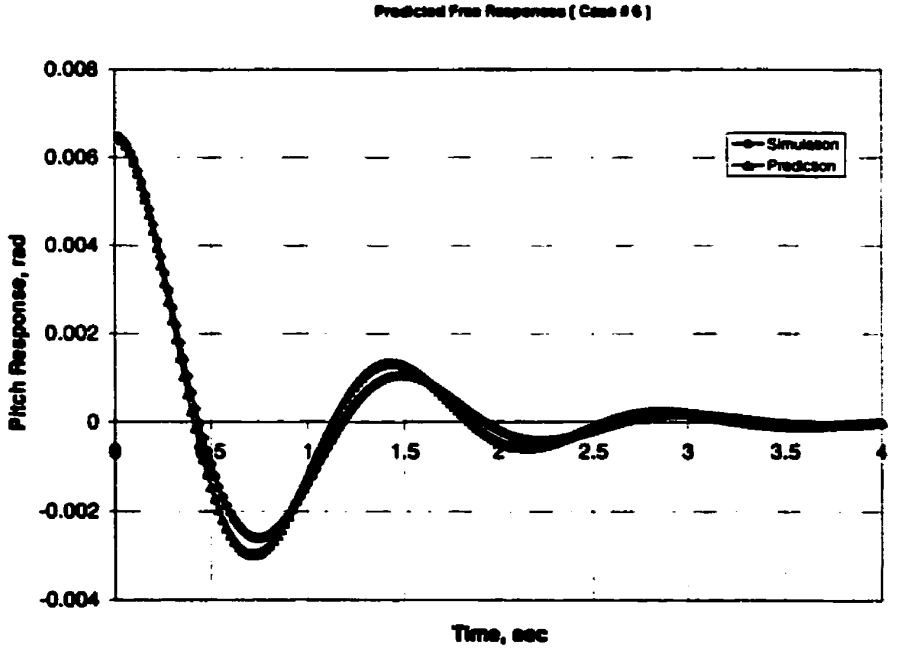

Figure J.12: Comparison between the simulated and the predicted free responses for pitch motion [Case # 6]

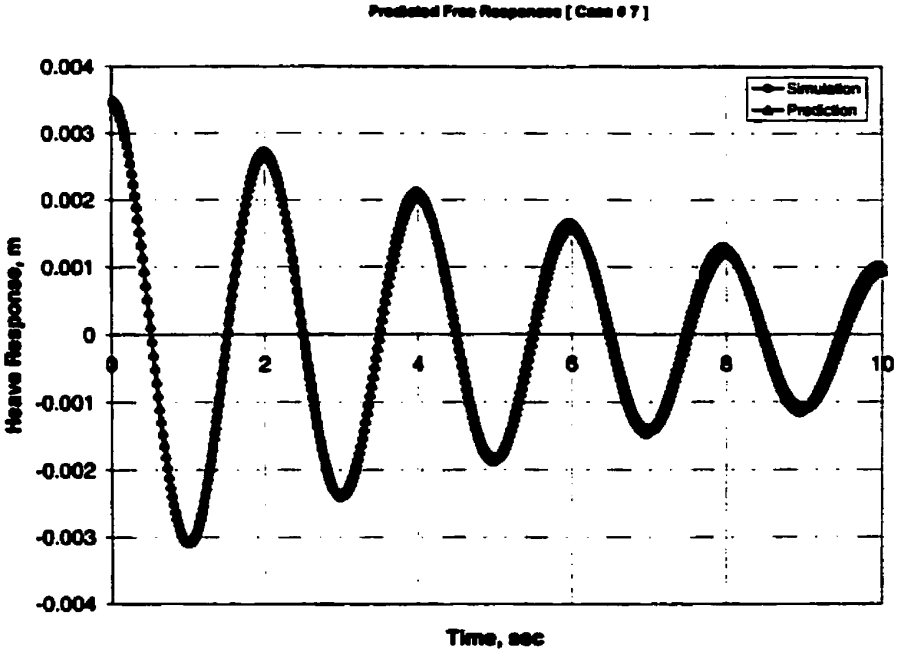

Figure J.13: Comparison between the simulated and the predicted free responses for heave motion [Case # 7]

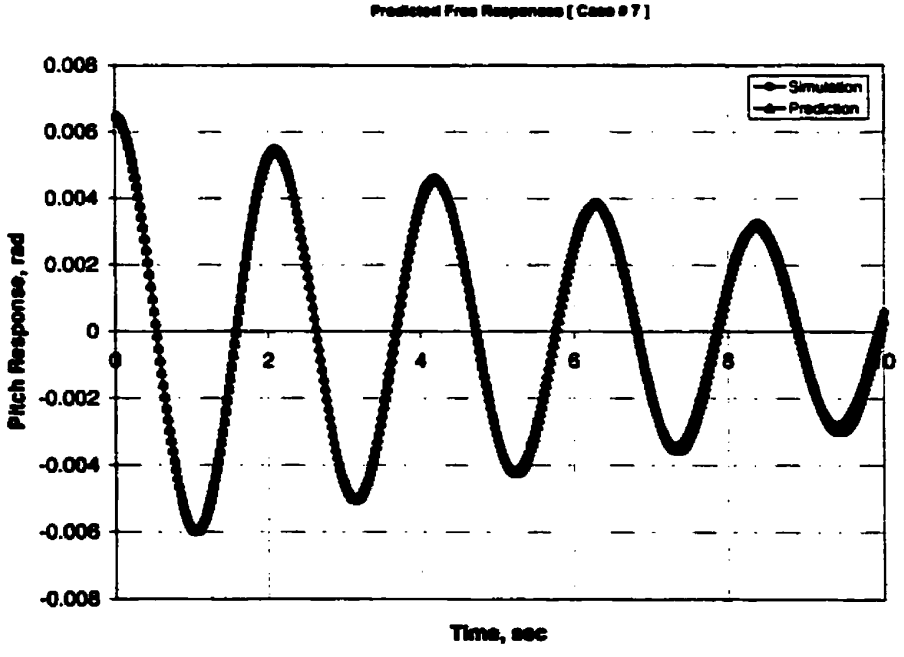

Figure J.14: Comparison between the simulated and the predicted free responses for pitch motion [Case # 7]

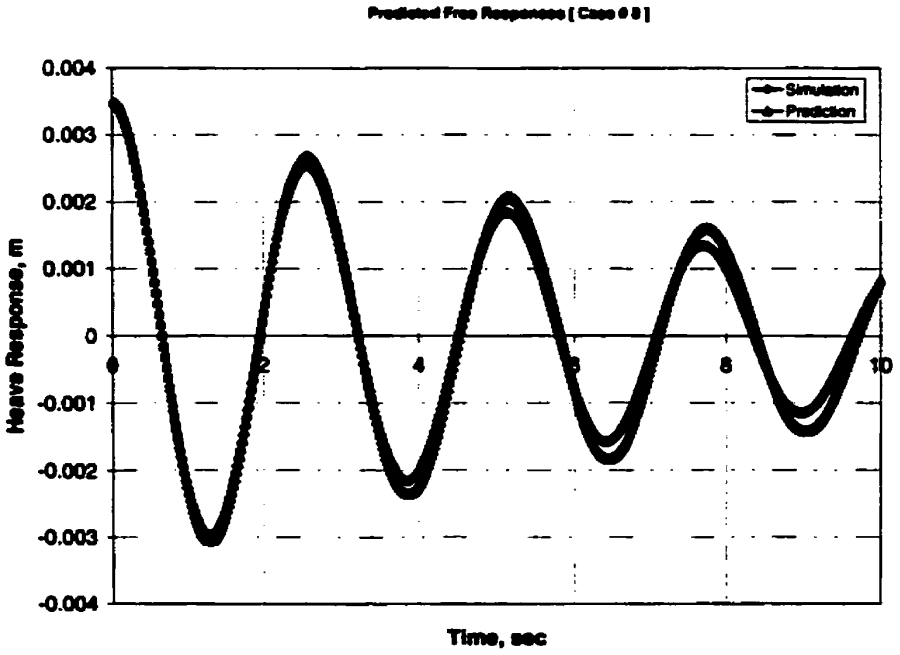

Figure J.15: Comparison between the simulated and the predicted free responses for heave motion [Case # 8]

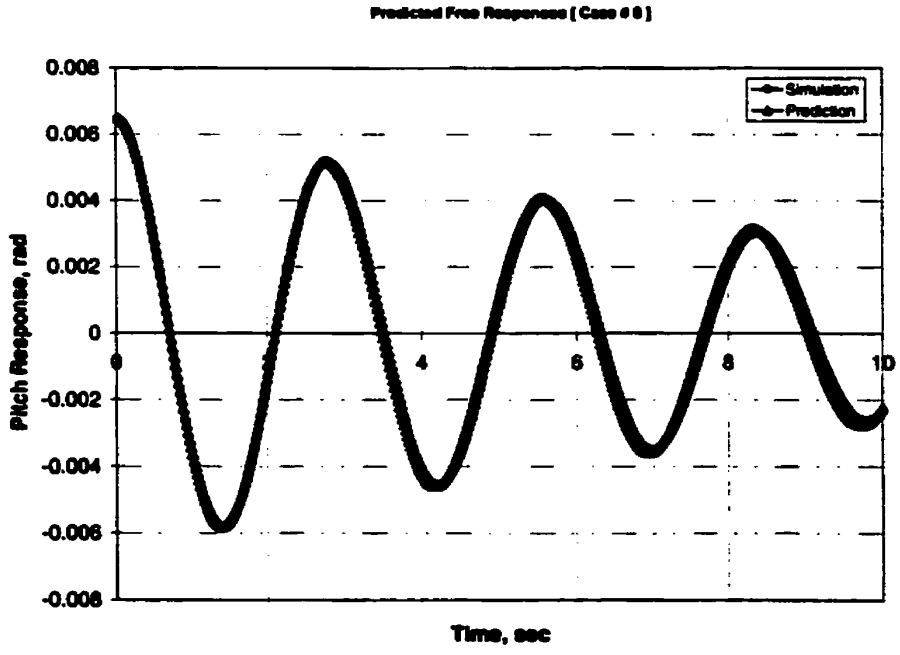

Figure J.16: Comparison between the simulated and the predicted free responses for pitch motion [Case # 8]

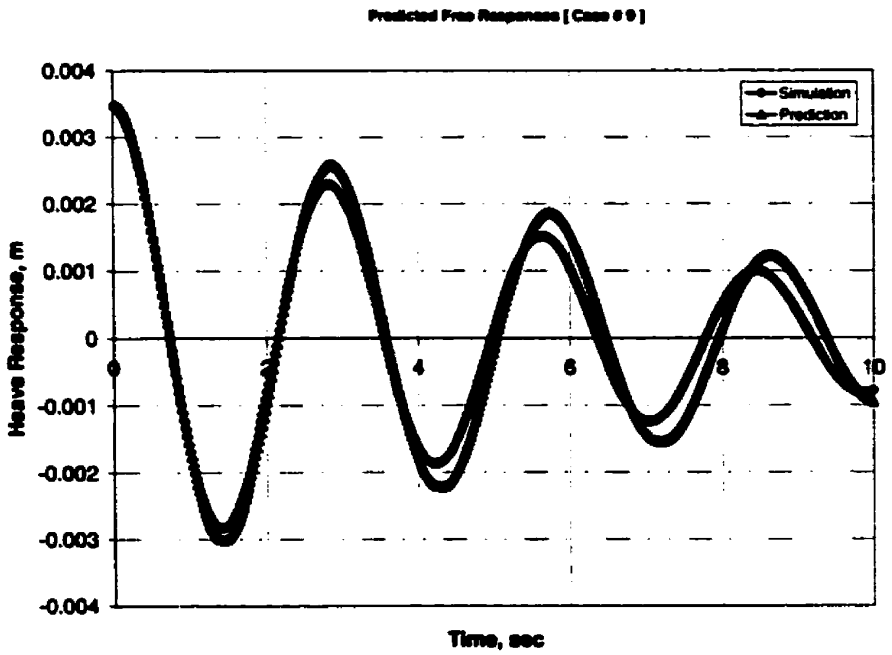

Figure J.17: Comparison between the simulated and the predicted free responses for heave motion [Case # 9]

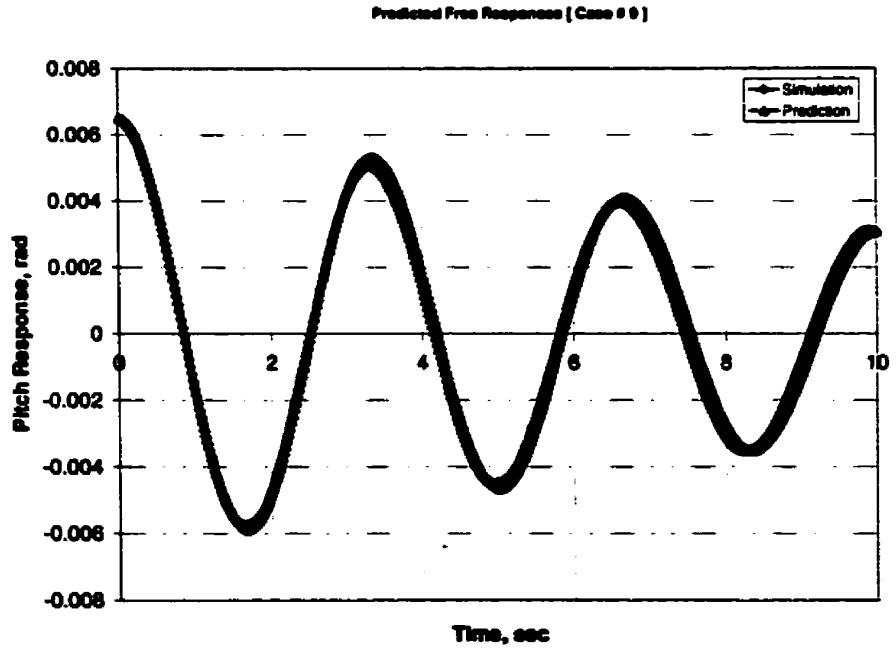

Figure J.18: Comparison between the simulated and the predicted free responses for pitch motion [Case # 9]

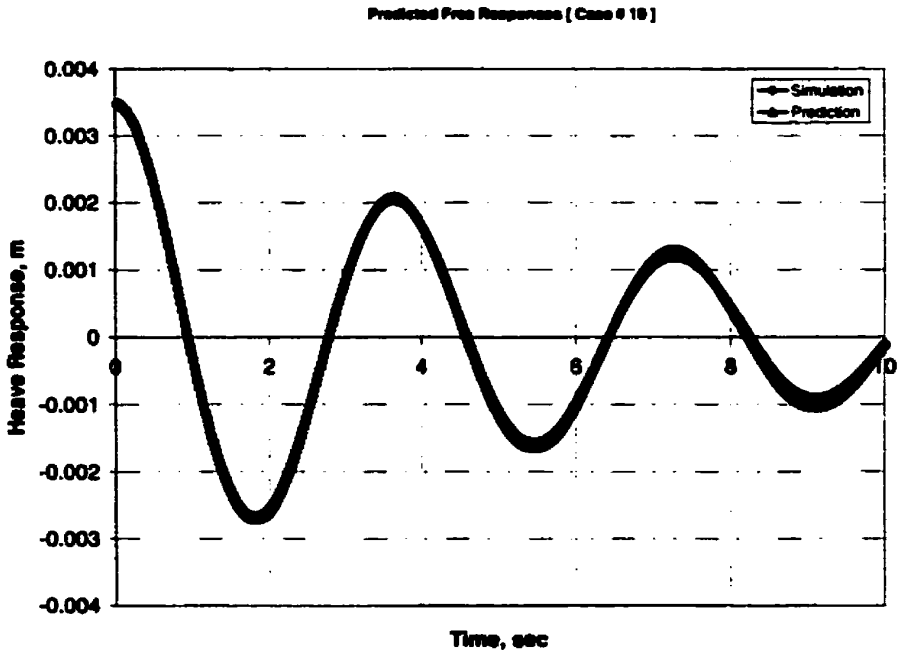

Figure J.19: Comparison between the simulated and the predicted free responses for heave motion [Case # 10]

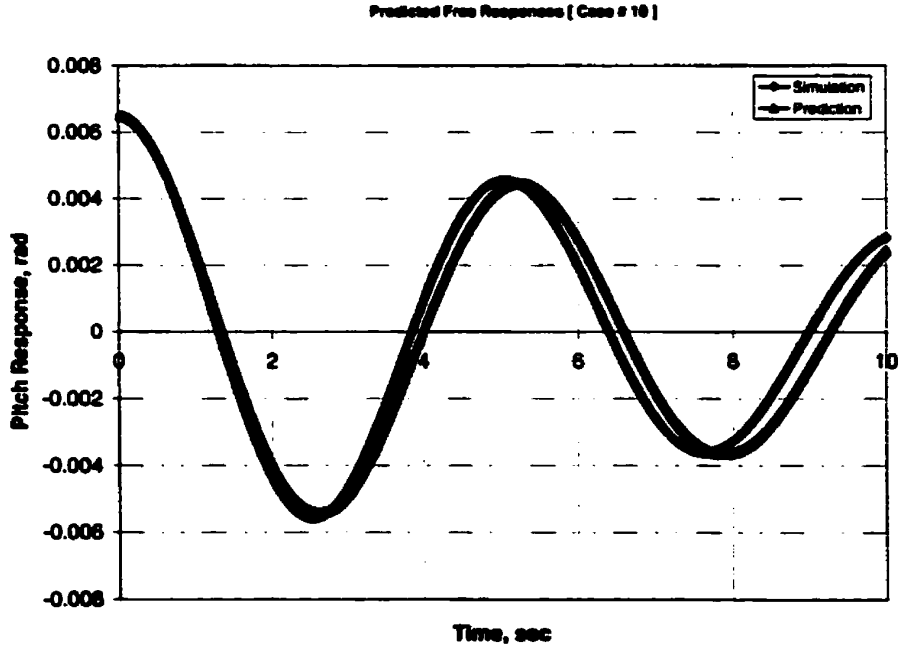

Figure J.20: Comparison between the simulated and the predicted free responses for pitch motion [Case # 10]

Appendix K

Predicted Regular Responses: Simulation

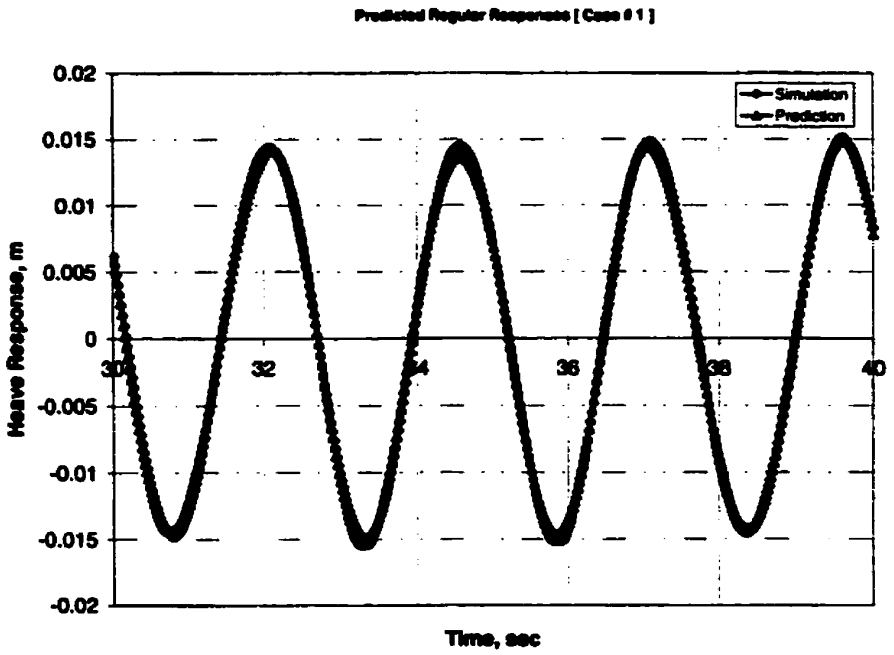

Figure K.1: Comparison between the simulated and the predicted regular responses for heave motion [Case # 1]

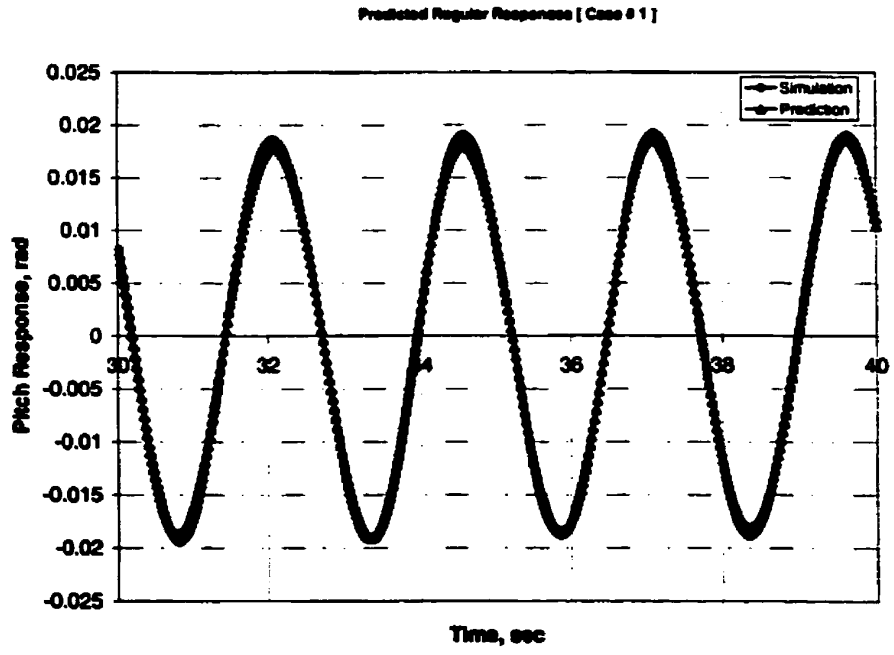

Figure K.2: Comparison between the simulated and the predicted regular responses for pitch motion [Case # 1]

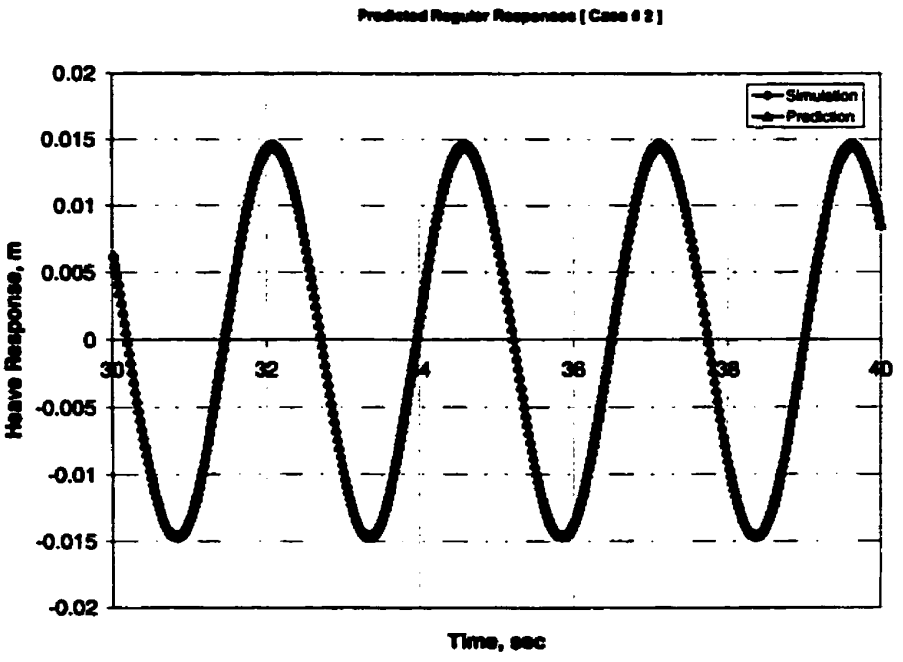

Figure K.3: Comparison between the simulated and the predicted regular responses for heave motion [Case # 2]

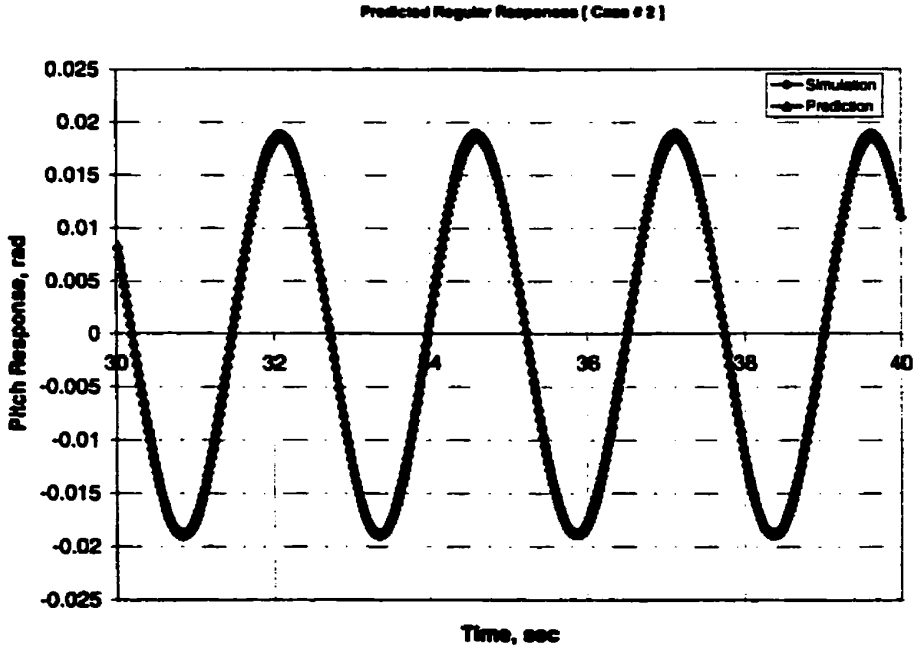

Figure K.4: Comparison between the simulated and the predicted regular responses for pitch motion [Case # 2]

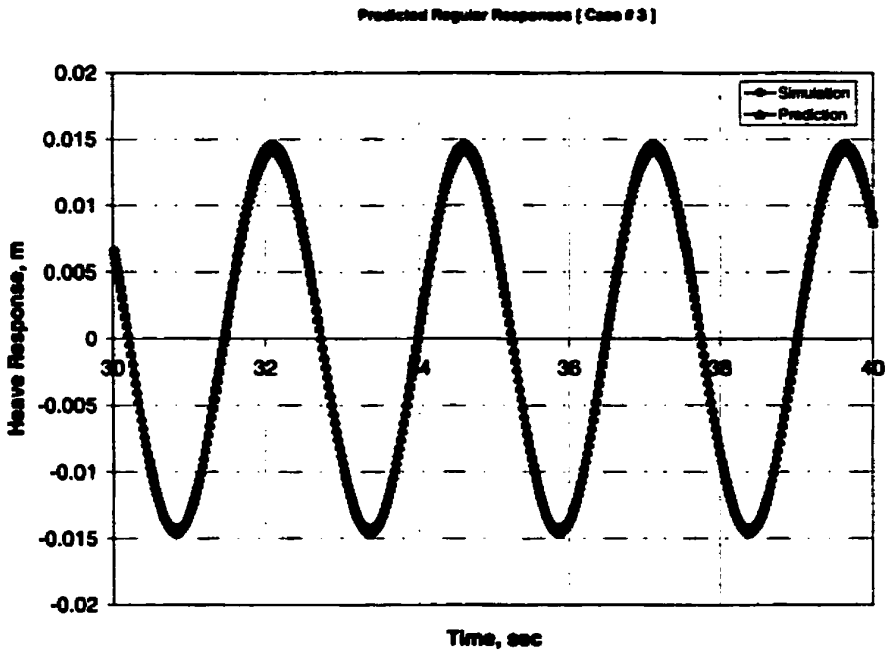

Figure K.5: Comparison between the simulated and the predicted regular responses for heave motion [Case # 3]

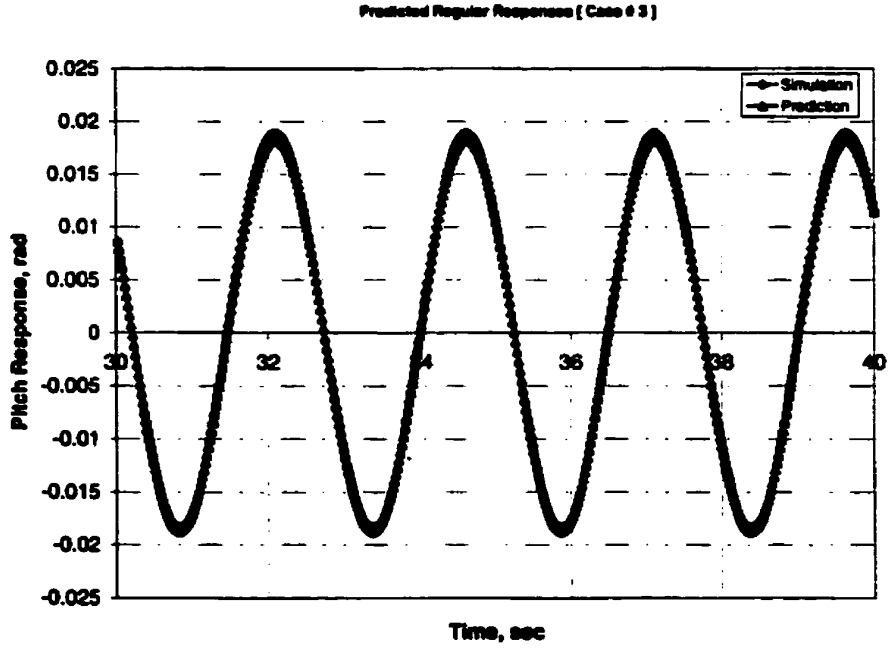

Figure K.6: Comparison between the simulated and the predicted regular responses for pitch [Case # 3]

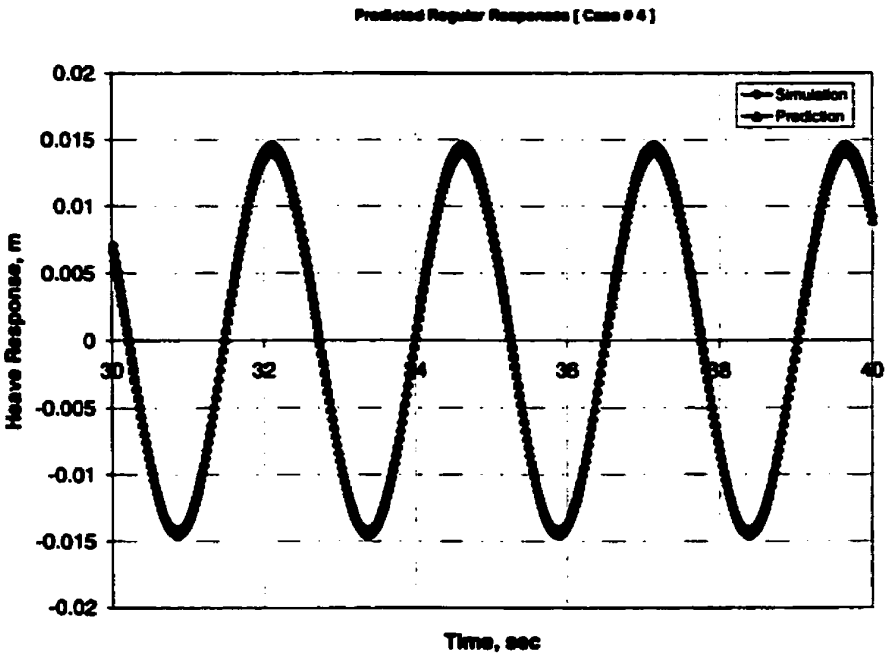

Figure K.7: Comparison between the simulated and the predicted regular responses for heave motion [Case # 4]

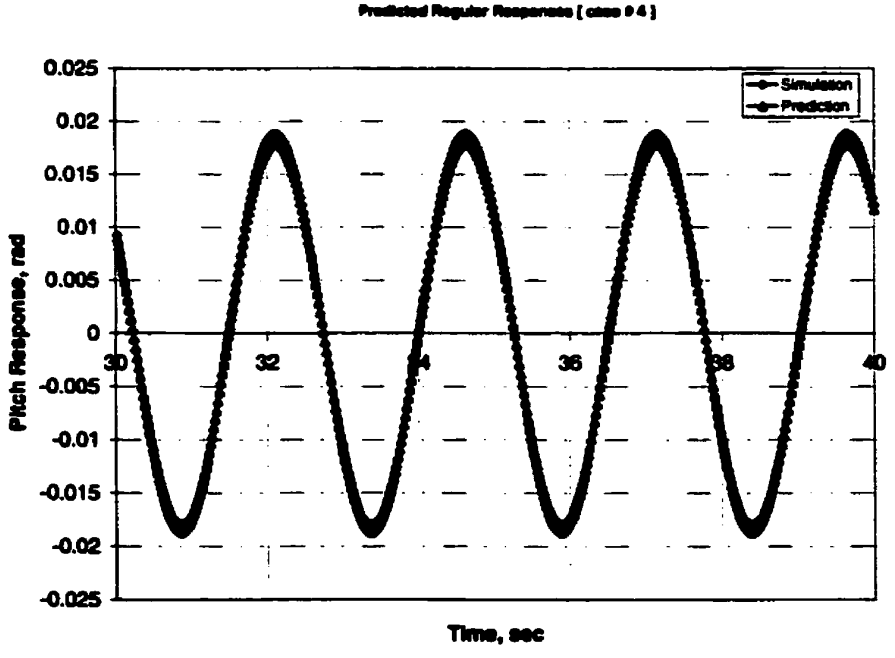

Figure K.8: Comparison between the simulated and the predicted regular responses for pitch motion [Case # 4]

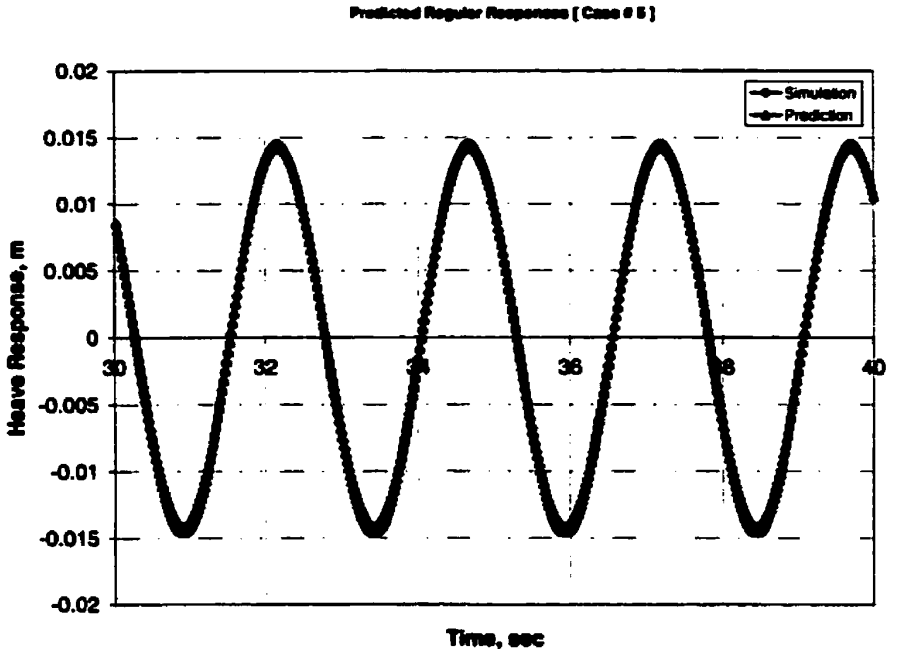

Figure K.9: Comparison between the simulated and the predicted regular responses for heave motion [Case # 5]

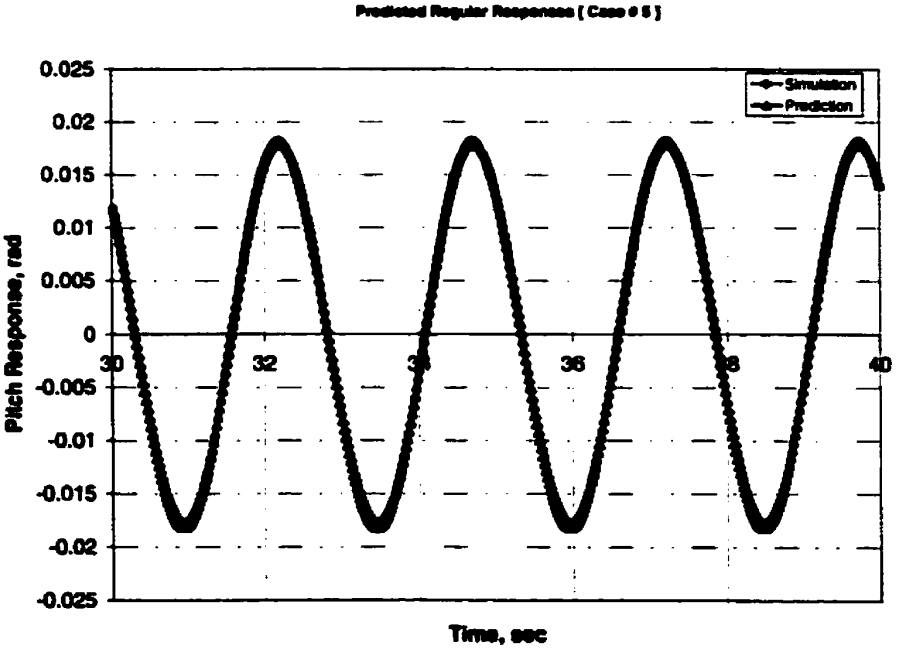

Figure K.10: Comparison between the simulated and the predicted regular responses for pitch motion [Case # 5]

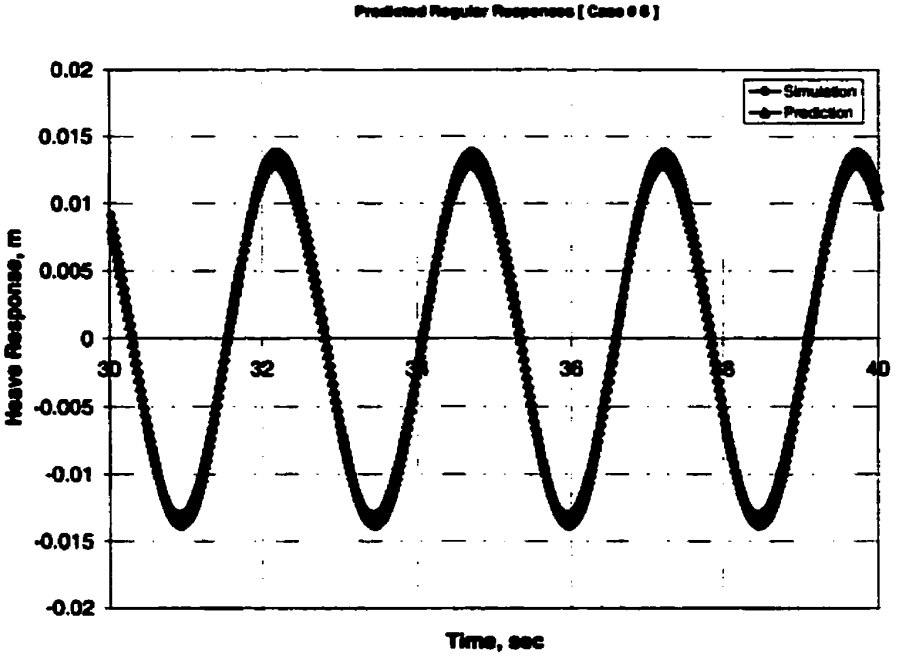

Figure K.11: Comparison between the simulated and the predicted regular responses for heave motion [Case # 6]

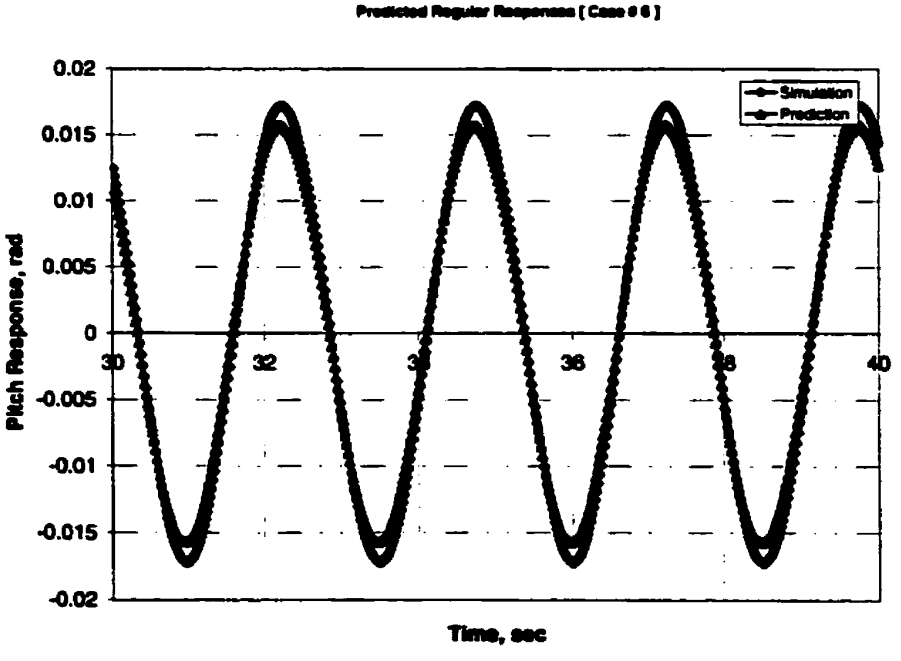

Figure K.12: Comparison between the simulated and the predicted regular responses for pitch motion [Case # 6]

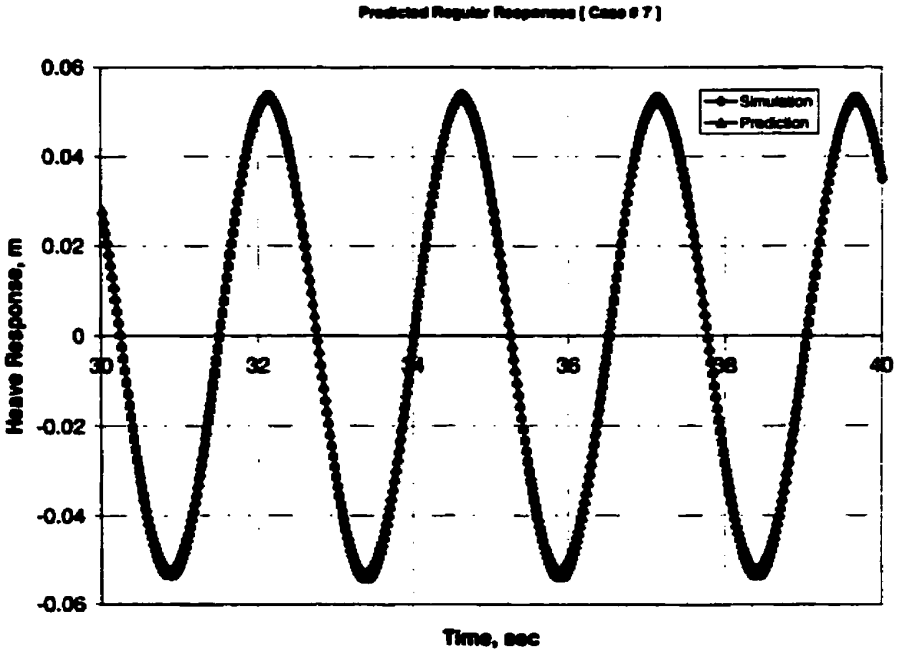

Figure K.13: Comparison between the simulated and the predicted regular responses for heave motion [Case # 7]

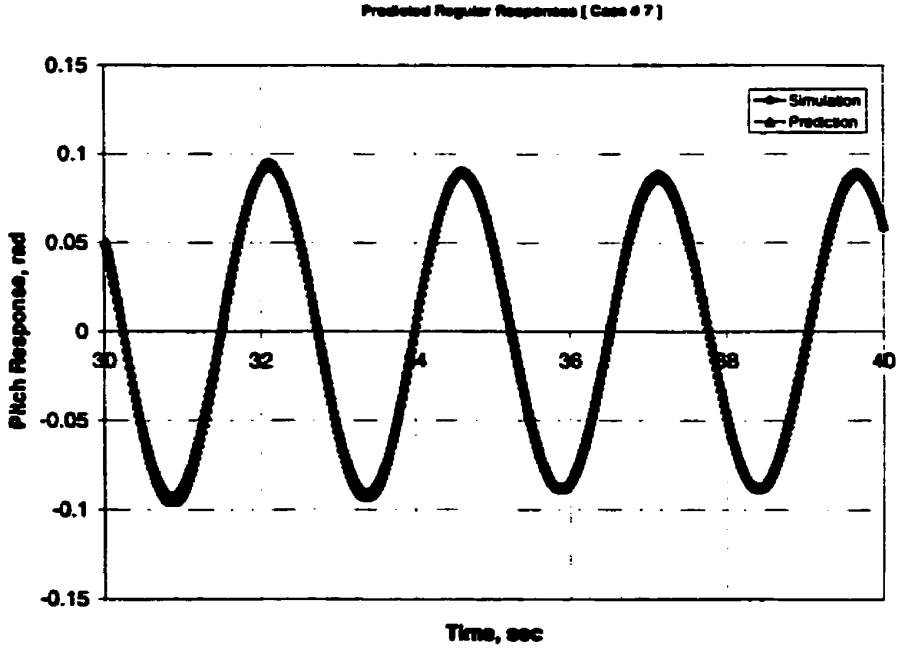

Figure K.14: Comparison between the simulated and the predicted regular responses for pitch motion [Case # 7]

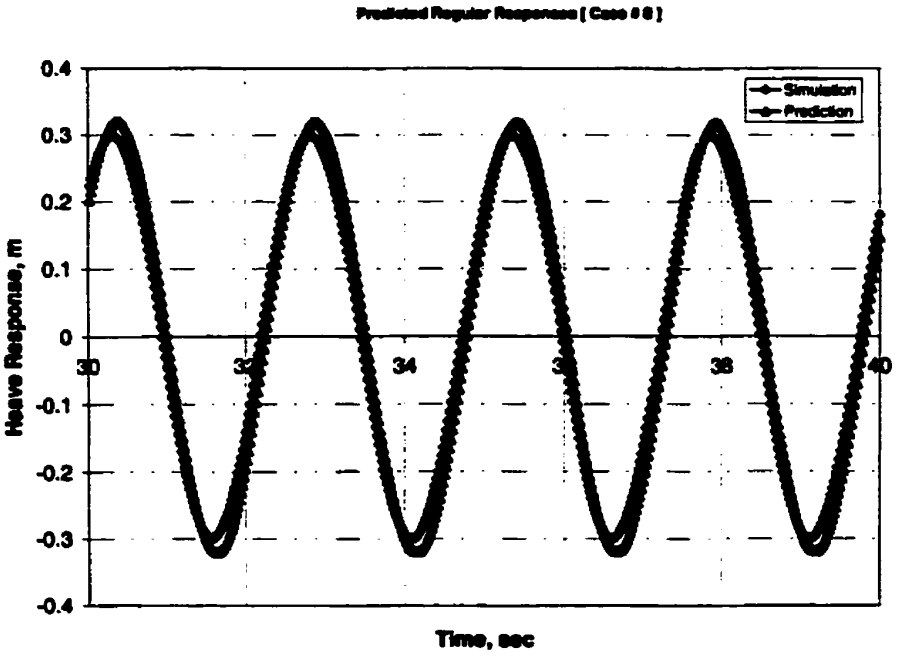

Figure K.15: Comparison between the simulated and the predicted regular responses for heave motion [Case # 8]

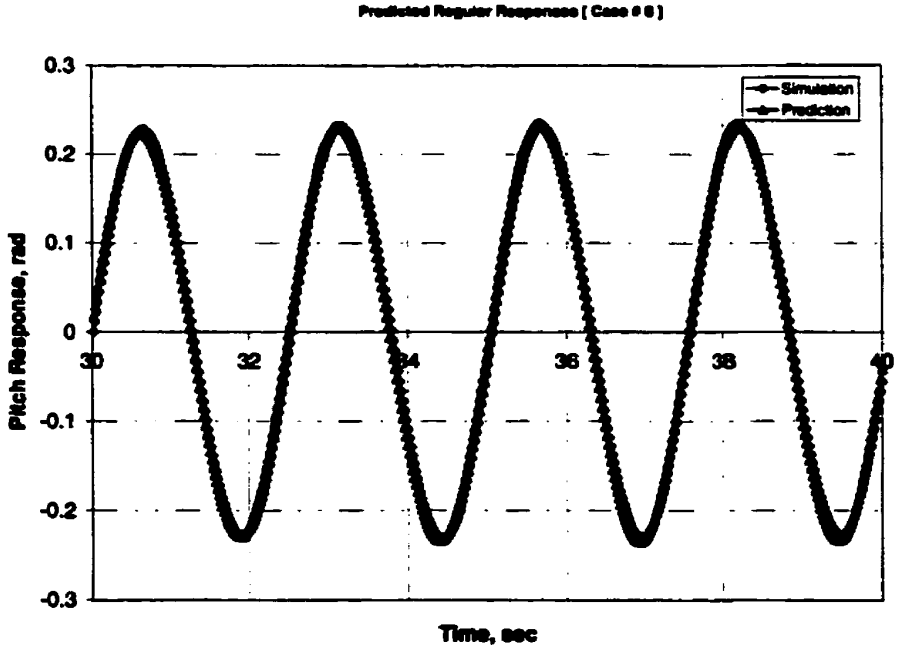

Figure K.16: Comparison between the simulated and the predicted regular responses for pitch motion [Case # 8]

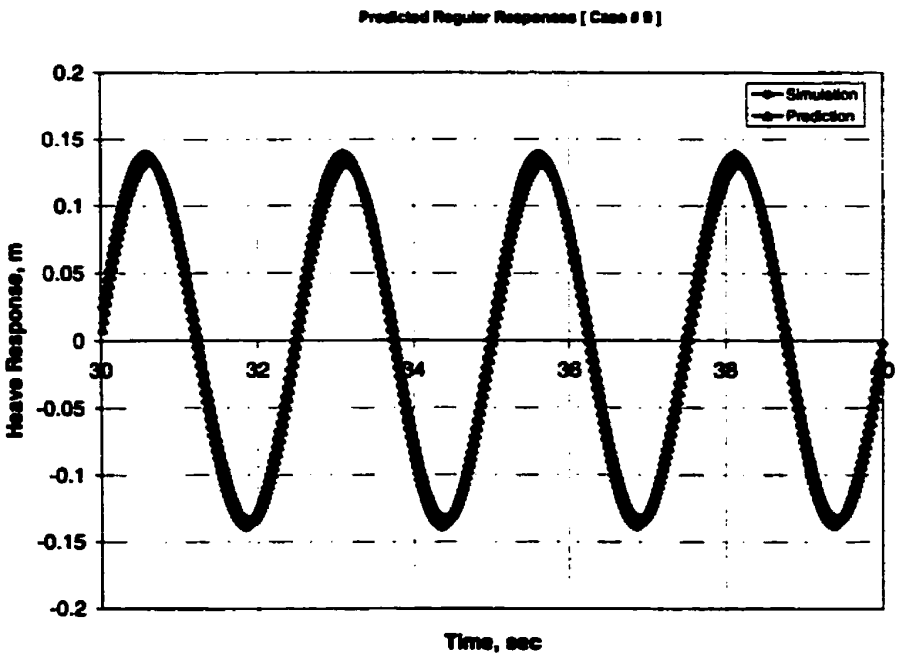

Figure K.17: Comparison between the simulated and the predicted regular responses for heave motion [Case # 9]

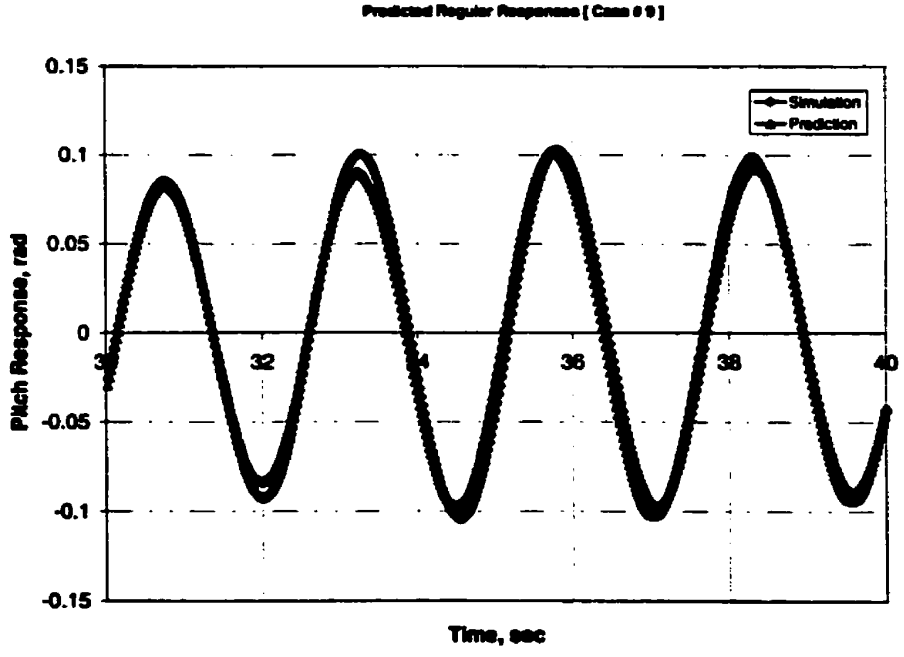

Figure K.18: Comparison between the simulated and the predicted regular responses for pitch motion [Case # 9]

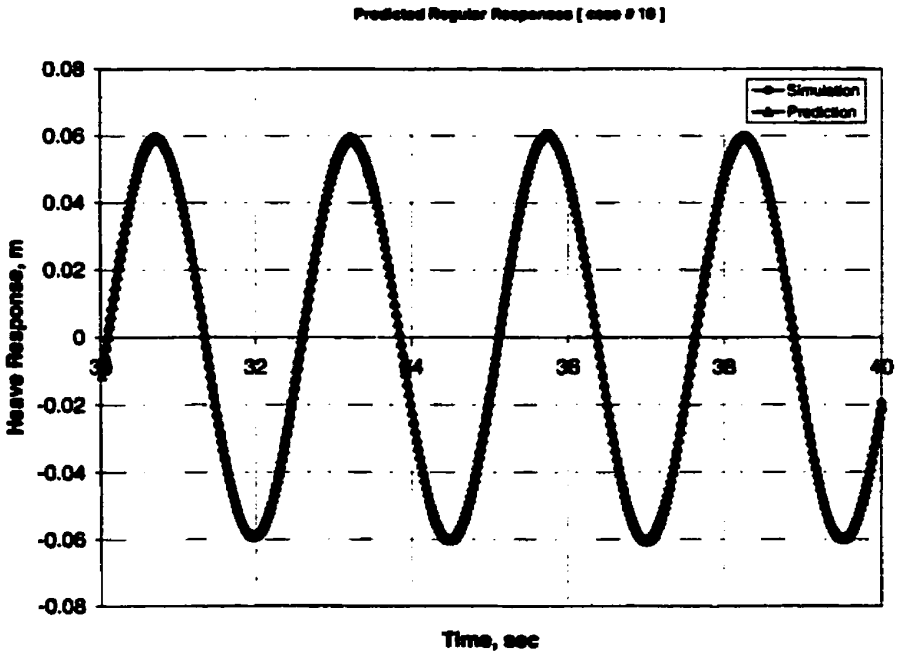

Figure K.19: Comparison between the simulated and the predicted regular responses for heave motion [Case # 10]

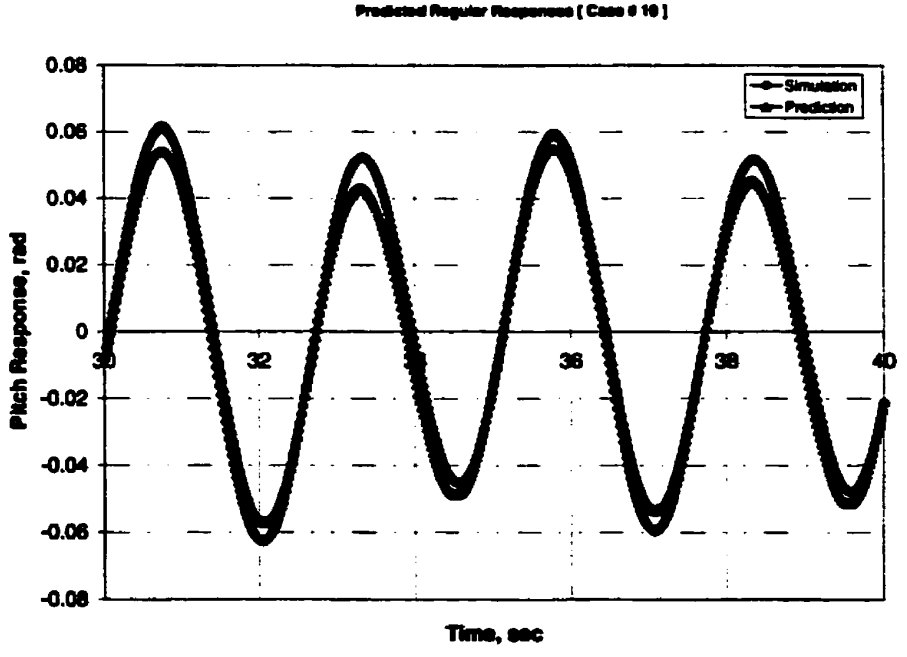

Figure K.20: Comparison between the simulated and the predicted regular responses for pitch motion [Case # 10]

Appendix L

Experimental Program

Table L.1: Random wave experiments: Group # 1

RUN #	File Name	Run Name	H_S (m)	Ω (Hz)	U (m/sec)	Time (sec)
1	RUN_1_0_HS7_F05_U00	RUN1_0	0.07	0.5	0.0	400
2	RUN_2_0_HS7_F06_U00	RUN2_0	0.07	0.6	0.0	400
3	RUN_3_0_HS7_F07_U00	RUN3_0	0.07	0.7	0.0	400
4	RUN_4_1_HS7_F05_U01	RUN4_01	0.07	0.5	0.1	200
5	RUN_4_2_HS7_F05_U01		0.07	0.5	0.1	200
6	RUN_5_1_HS7_F05_U02	RUN5_02	0.07	0.5	0.2	100
7	RUN_5_2_HS7_F05_U02		0.07	0.5	0.2	100
8	RUN_5_3_HS7_F05_U02		0.07	0.5	0.2	100
9	RUN_5_4_HS7_F05_U02		0.07	0.5	0.2	100
10	RUN_6_1_HS7_F06_U01	RUN6_01	0.07	0.6	0.1	200
11	RUN_6_2_HS7_F06_U01		0.07	0.6	0.1	200
12	RUN_7_1_HS7_F06_U02	RUN7_02	0.07	0.6	0.2	100
13	RUN_7_2_HS7_F06_U02		0.07	0.6	0.2	100
14	RUN_7_3_HS7_F06_U02		0.07	0.6	0.2	100
15	RUN_7_4_HS7_F06_U02		0.07	0.6	0.2	100
16	RUN_8_1_HS7_F07_U01	RUN8_01	0.07	0.7	0.1	200
17	RUN_8_2_HS7_F07_U01		0.07	0.7	0.1	200
18	RUN_9_1_HS7_F07_U02	RUN9_02	0.07	0.7	0.2	100
19	RUN_9_2_HS7_F07_U02		0.07	0.7	0.2	100
20	RUN_9_3_HS7_F07_U02		0.07	0.7	0.2	100
21	RUN_9_4_HS7_F07_U02		0.07	0.7	0.2	100

Table L.2: Random wave experiments: Group # 2

RUN #	File Name	Run Name	H_S (m)	Ω (Hz)	U (m/sec)	Time (sec)
22	RUN_10_0_HS10_F05_U00	RUN10_0	0.10	0.5	0.0	400
23	RUN_11_0_HS10_F06_U00	RUN11_0	0.10	0.6	0.0	400
24	RUN_12_0_HS10_F07_U00	RUN12_0	0.10	0.7	0.0	400
25	RUN_13_1_HS10_F05_U01	RUN13_01	0.10	0.5	0.1	200
26	RUN_13_2_HS10_F05_U01		0.10	0.5	0.1	200
27	RUN_14_1_HS10_F05_U02	RUN14_02	0.10	0.5	0.2	100
28	RUN_14_2_HS10_F05_U02		0.10	0.5	0.2	100
29	RUN_14_3_HS10_F05_U02		0.10	0.5	0.2	100
30	RUN_14_4_HS10_F05_U02		0.10	0.5	0.2	100
31	RUN_15_1_HS10_F06_U01	RUN15_01	0.10	0.6	0.1	200
32	RUN_15_2_HS10_F06_U01		0.10	0.6	0.1	200
33	RUN_16_1_HS10_F06_U02	RUN16_02	0.10	0.6	0.2	100
34	RUN_16_2_HS10_F06_U02		0.10	0.6	0.2	100
35	RUN_16_3_HS10_F06_U02		0.10	0.6	0.2	100
36	RUN_16_4_HS10_F06_U02		0.10	0.6	0.2	100
37	RUN_17_1_HS10_F07_U01	RUN17_01	0.10	0.7	0.1	200
38	RUN_17_2_HS10_F07_U01		0.10	0.7	0.1	200
39	RUN_18_1_HS10_F07_U02	RUN18_02	0.10	0.7	0.2	100
40	RUN_18_2_HS10_F07_U02		0.10	0.7	0.2	100
41	RUN_18_3_HS10_F07_U02		0.10	0.7	0.2	100
42	RUN_18_4_HS10_F07_U02		0.10	0.7	0.2	100

Table L.3: Random wave experiments: Group # 3

RUN #	File Name	Run Name	H_S (m)	Ω (Hz)	U (m/sec)	Time (sec)
43	RUN_19_0_HS15_F05_U00	RUN19_0	0.15	0.5	0.0	400
44	RUN_20_0_HS15_F06_U00	RUN20_0	0.15	0.6	0.0	400
45	RUN_21_0_HS13_F07_U00	RUN21_0	0.13	0.7	0.0	400
46	RUN_22_1_HS15_F05_U01	RUN22_01	0.15	0.5	0.1	200
47	RUN_22_2_HS15_F05_U01		0.15	0.5	0.1	200
48	RUN_23_1_HS15_F05_U02	RUN23_02	0.15	0.5	0.2	100
49	RUN_23_2_HS15_F05_U02		0.15	0.5	0.2	100
50	RUN_23_3_HS15_F05_U02		0.15	0.5	0.2	100
51	RUN_23_4_HS15_F05_U02		0.15	0.5	0.2	100
52	RUN_24_1_HS15_F06_U01	RUN24_01	0.15	0.6	0.1	200
53	RUN_24_2_HS15_F06_U01		0.15	0.6	0.1	200
54	RUN_25_1_HS15_F06_U02	RUN25_02	0.15	0.6	0.2	100
55	RUN_25_2_HS15_F06_U02		0.15	0.6	0.2	100
56	RUN_25_3_HS15_F06_U02		0.15	0.6	0.2	100
57	RUN_25_4_HS15_F06_U02		0.15	0.6	0.2	100
58	RUN_26_1_HS13_F07_U01	RUN26_01	0.13	0.7	0.1	200
59	RUN_26_2_HS13_F07_U01		0.13	0.7	0.1	200
60	RUN_27_1_HS13_F07_U02	RUN27_02	0.13	0.7	0.2	100
61	RUN_27_2_HS13_F07_U02		0.13	0.7	0.2	100
62	RUN_27_3_HS13_F07_U02		0.13	0.7	0.2	100
63	RUN_27_4_HS13_F07_U02		0.13	0.7	0.2	100

Appendix M

Wave Power Spectral Density Function: Experiment

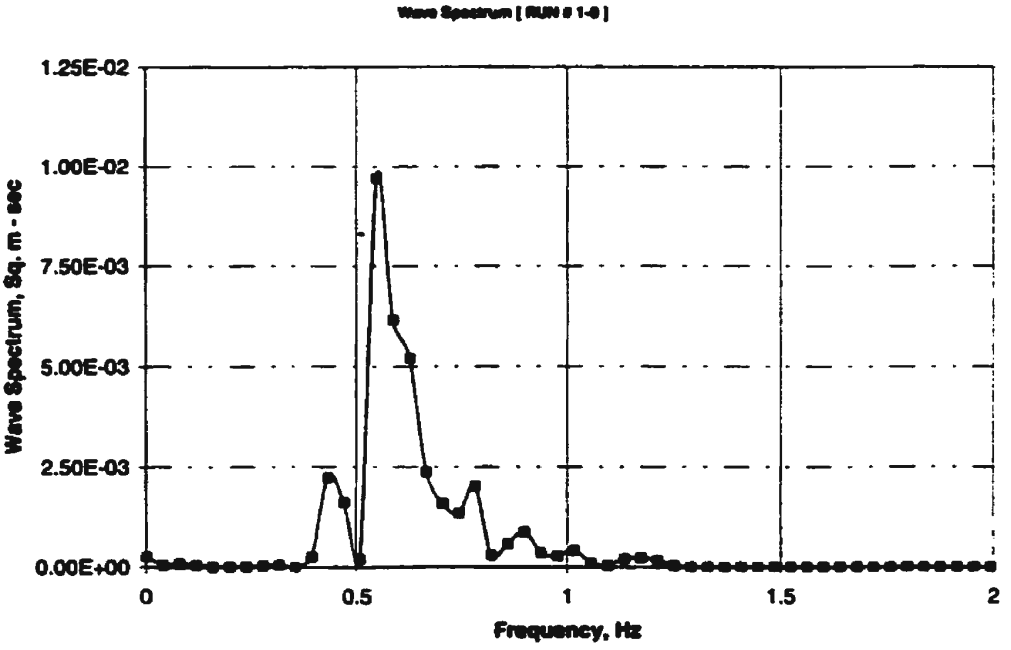

Figure M.1: Wave power spectral density function [Run # 1-0]

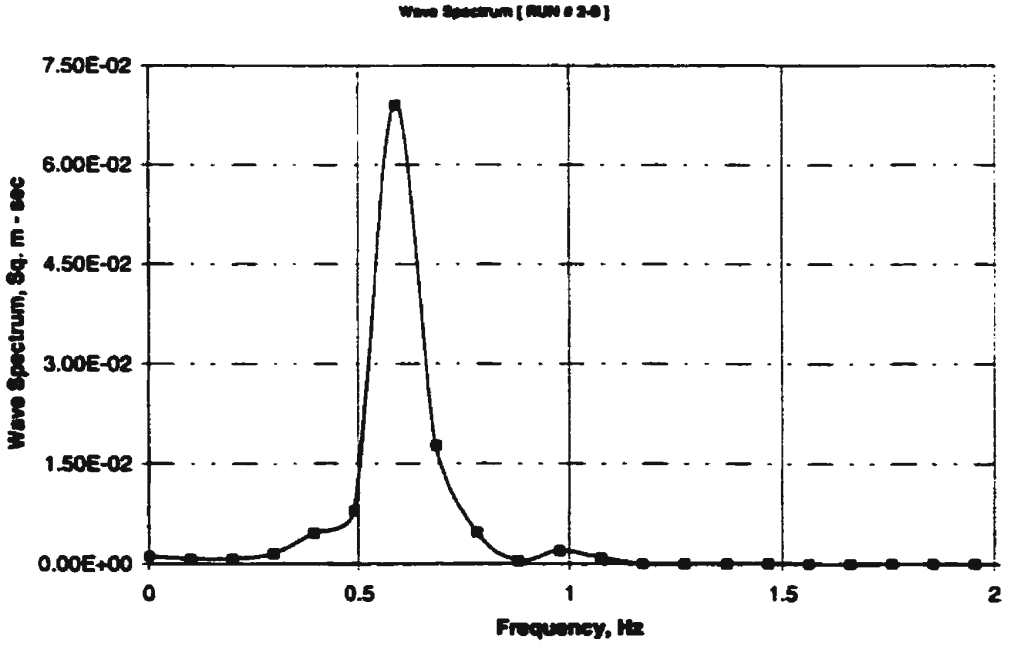

Figure M.2: Wave power spectral density function [Run # 2-0]

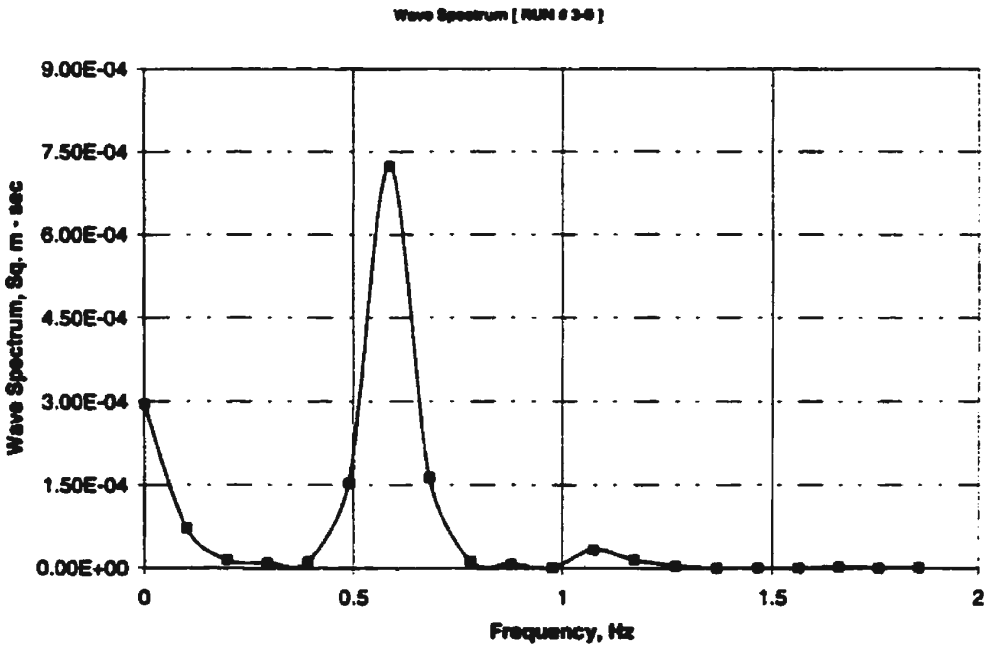

Figure M.3: Wave power spectral density function [Run # 3-0]

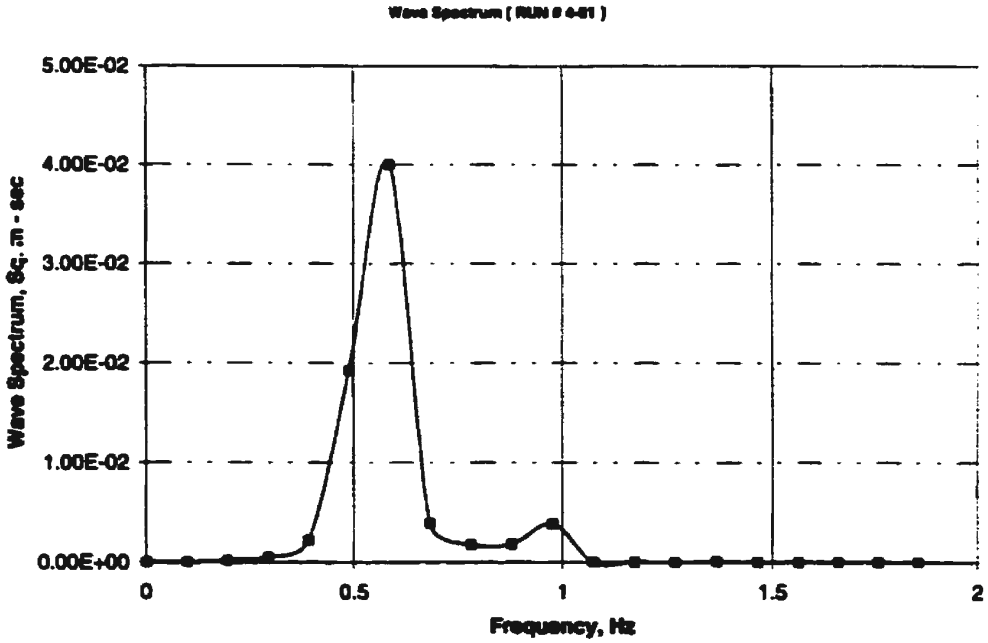

Figure M.4: Wave power spectral density function [Run # 4-01]

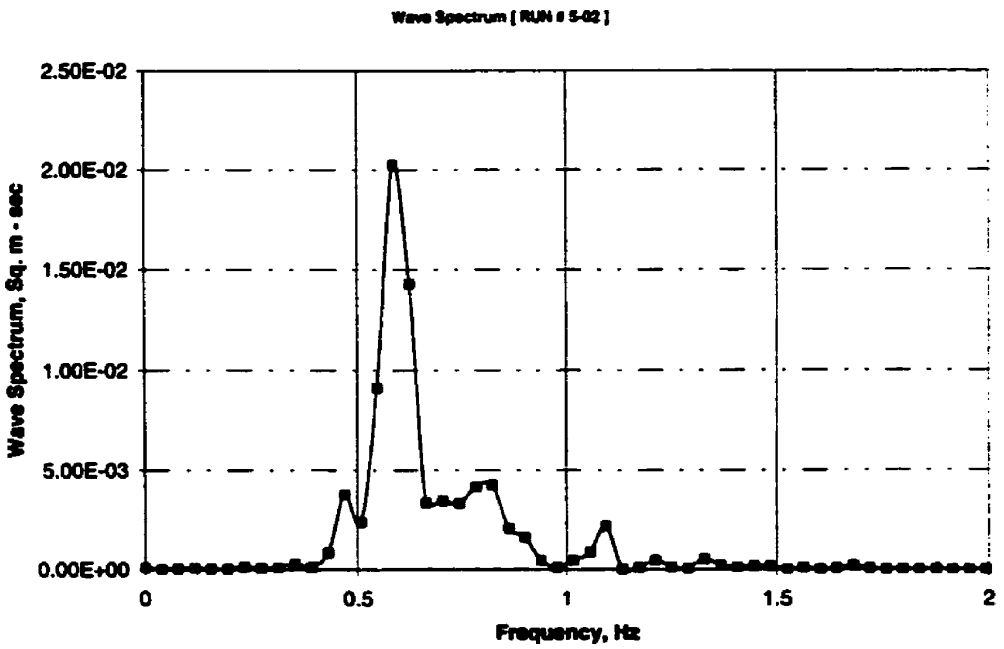

Figure M.5: Wave power spectral density function [Run # 5-02]

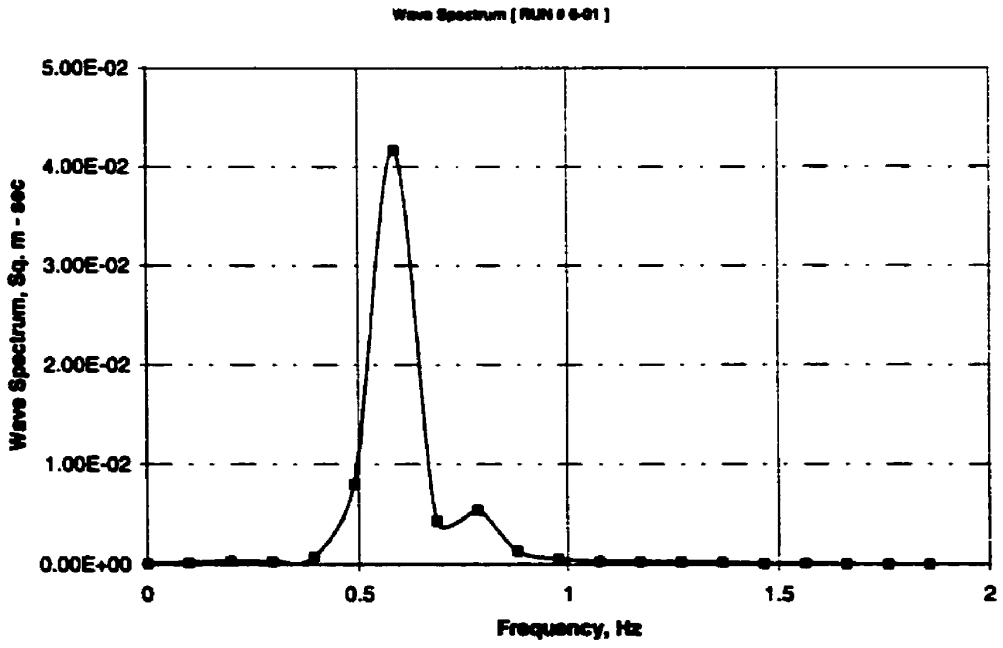

Figure M.6: Wave power spectral density function [Run # 6-01]

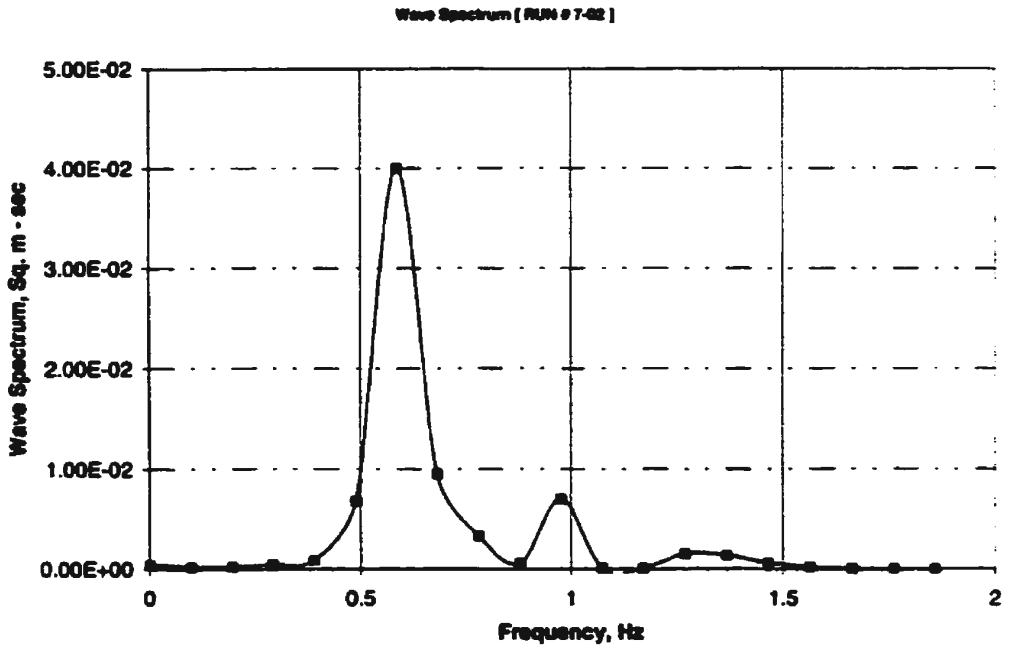

Figure M.7: Wave power spectral density function [Run # 7-02]

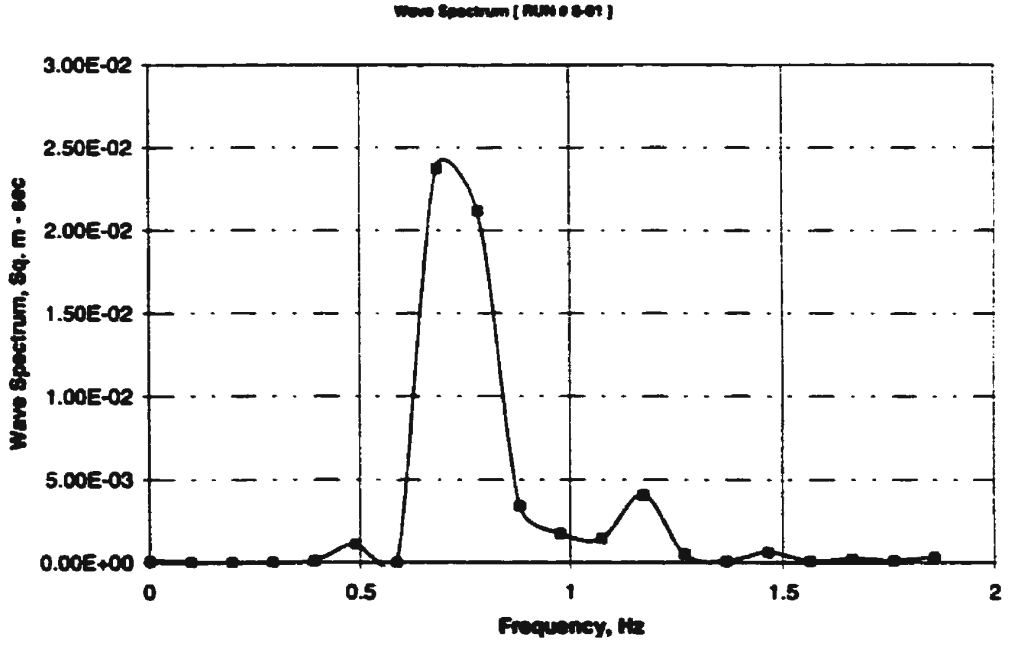

Figure M.8: Wave power spectral density function [Run # 8-01]

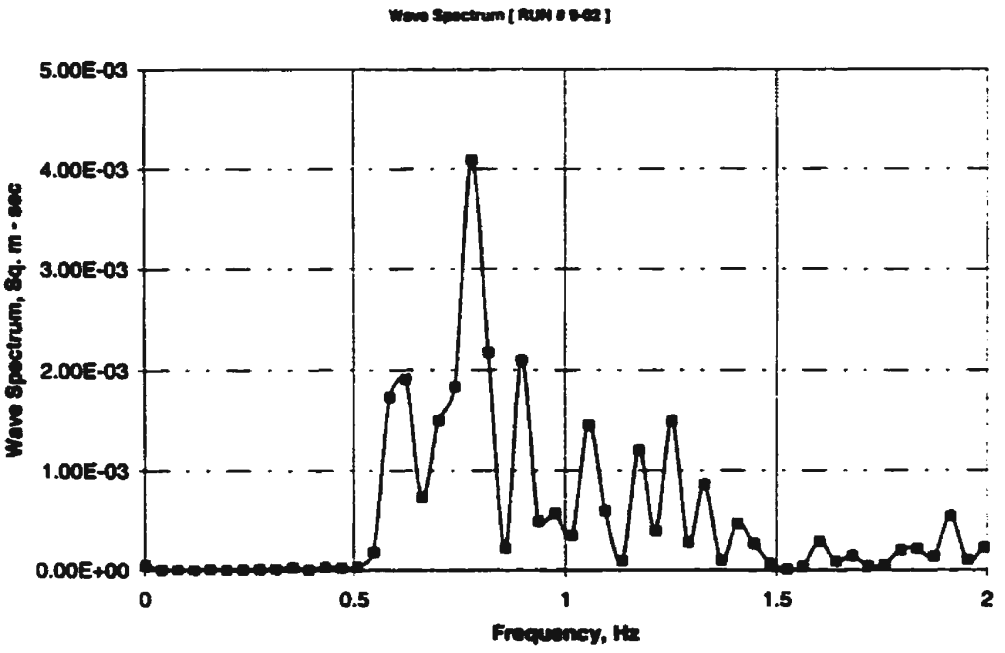

Figure M.9: Wave power spectral density function [Run # 9-02]

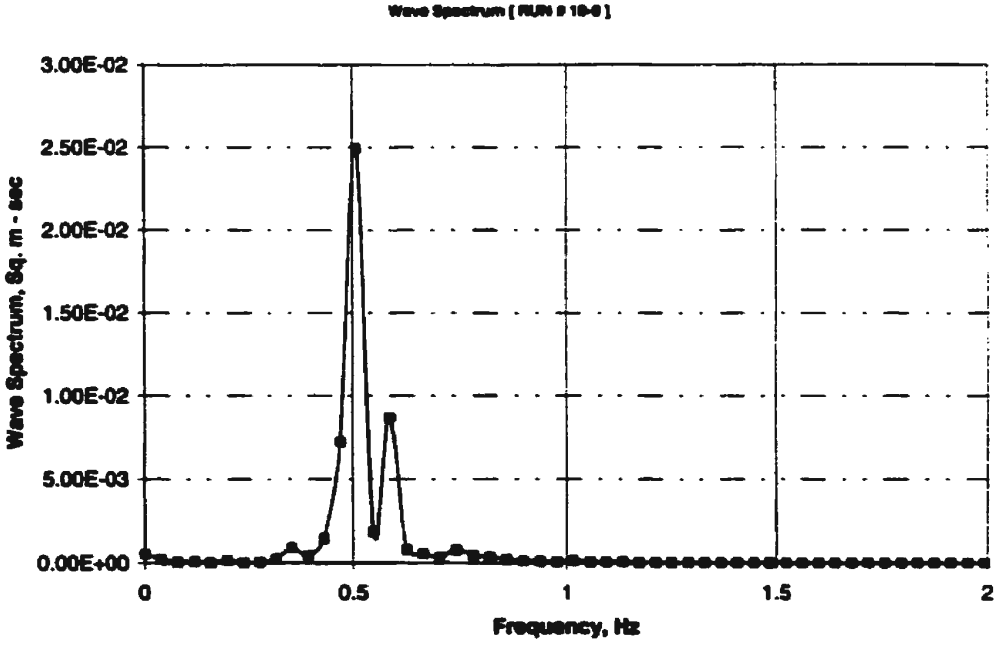

Figure M.10: Wave power spectral density function [Run # 10-0]

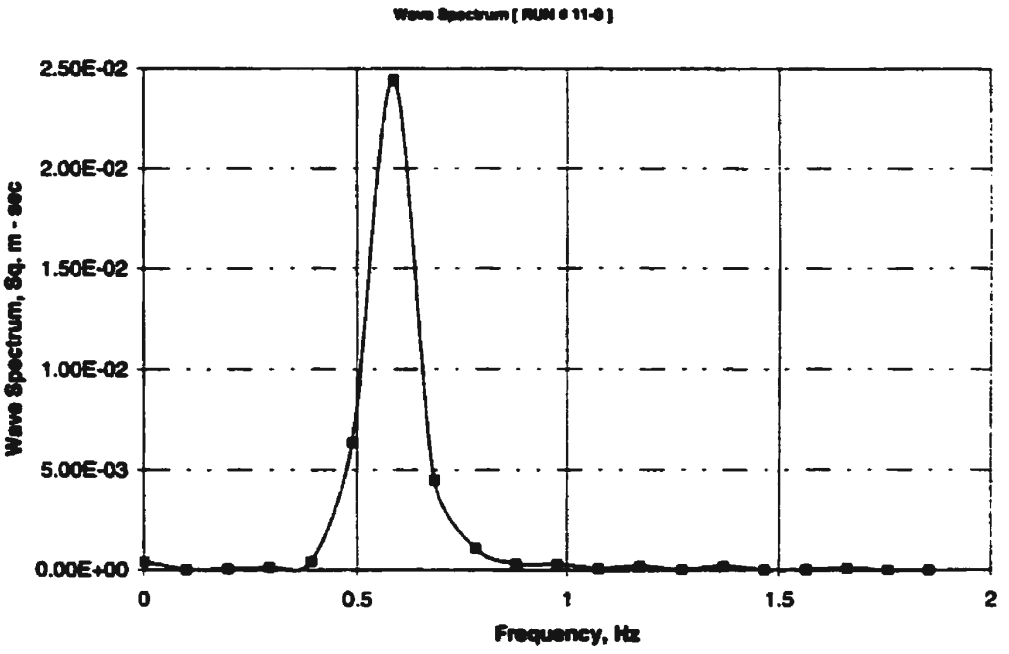

Figure M.11: Wave power spectral density function [Run # 11-0]

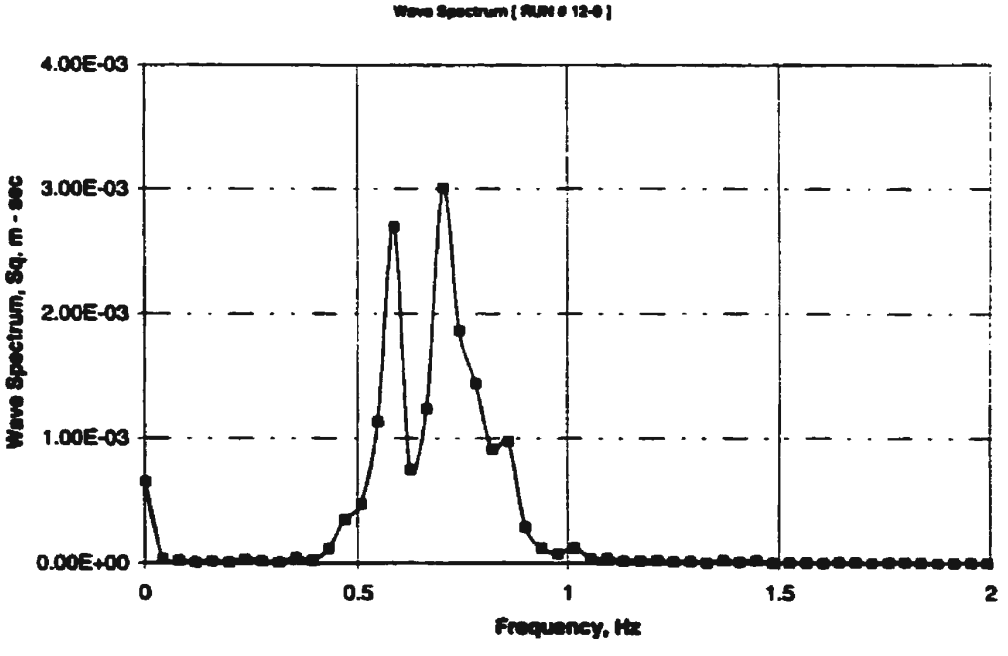

Figure M.12: Wave power spectral density function [Run # 12-0]

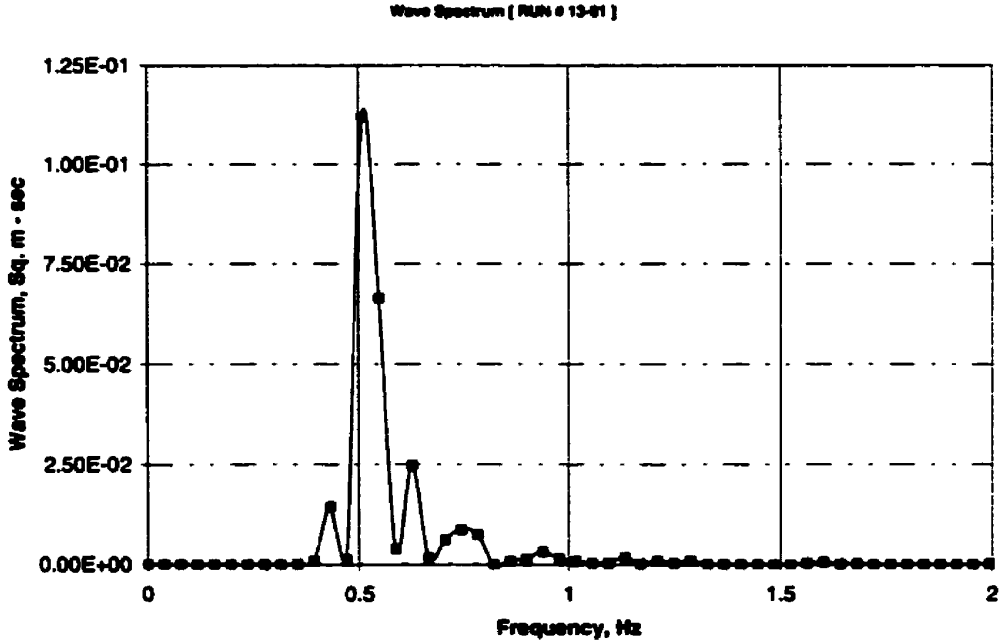

Figure M.13: Wave power spectral density function [Run # 13-01]

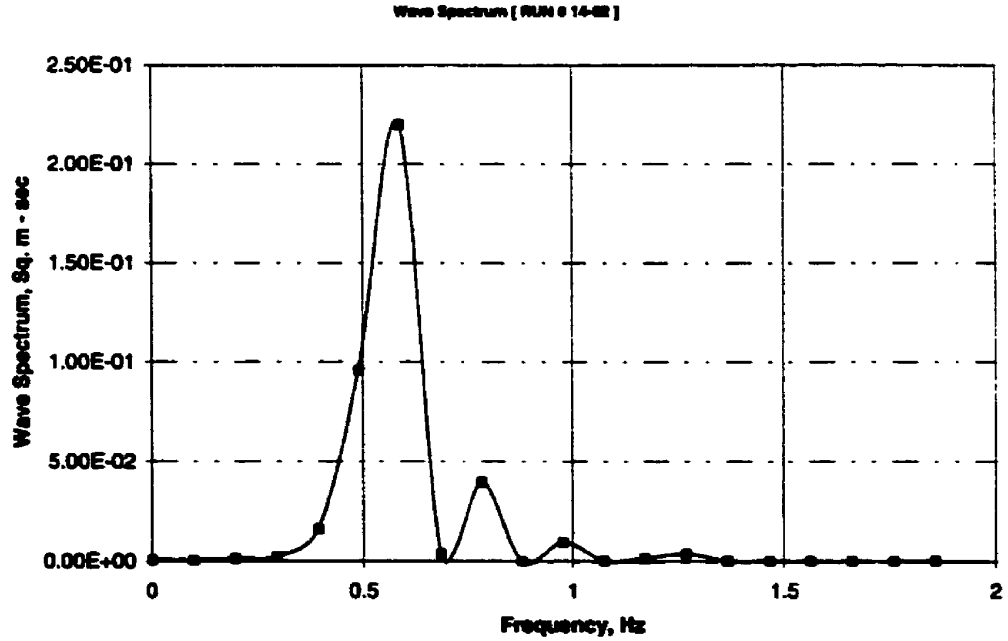

Figure M.14: Wave power spectral density function [Run # 14-02]

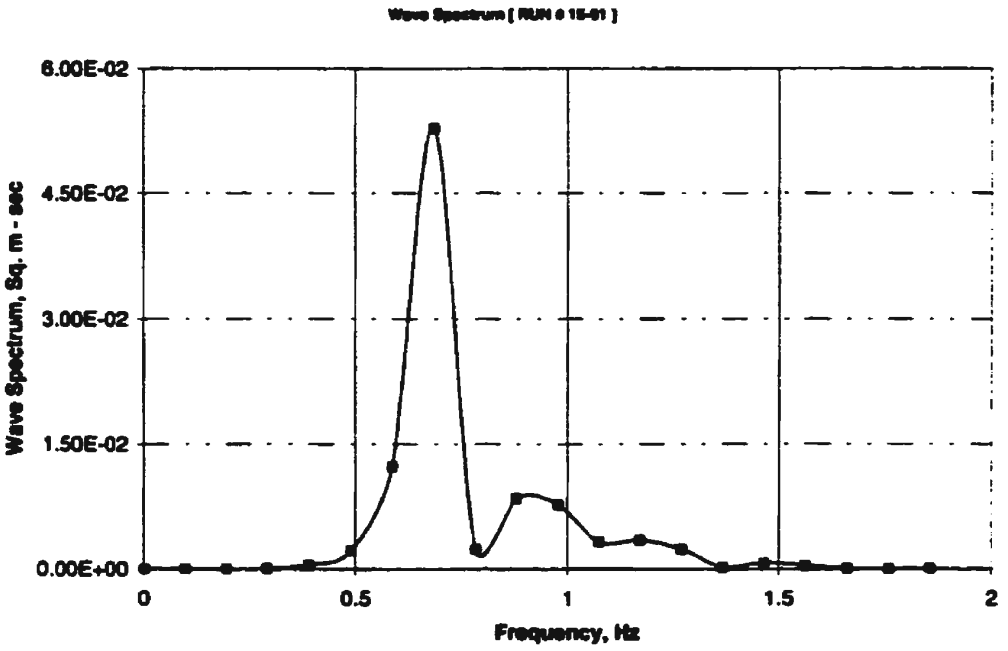

Figure M.15: Wave power spectral density function [Run # 15-01]

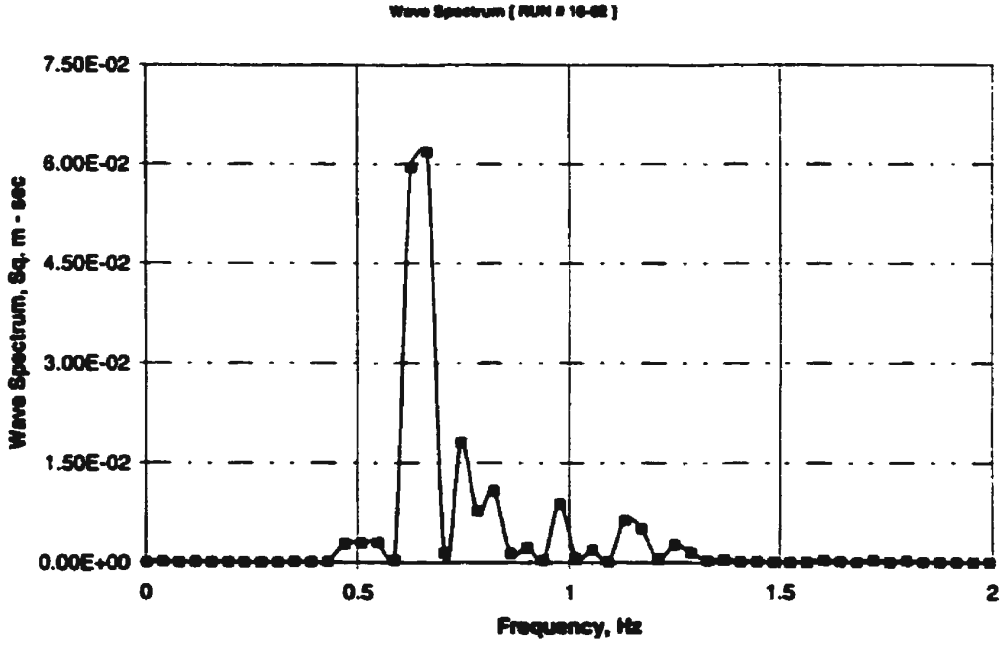

Figure M.16: Wave power spectral density function [Run # 16-02]

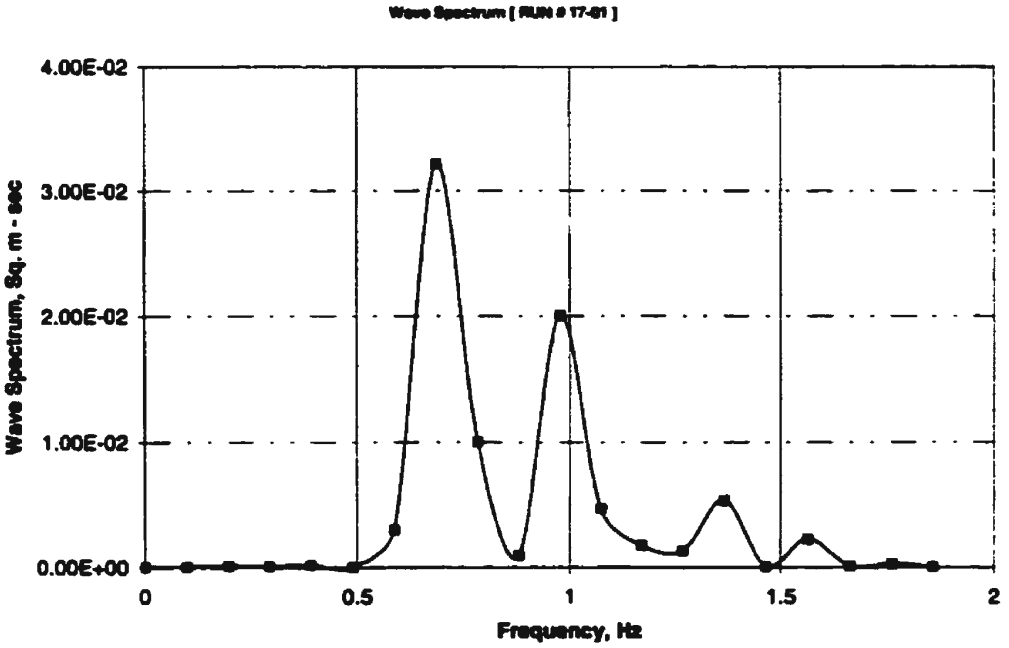

Figure M.17: Wave power spectral density function [Run # 17-01]

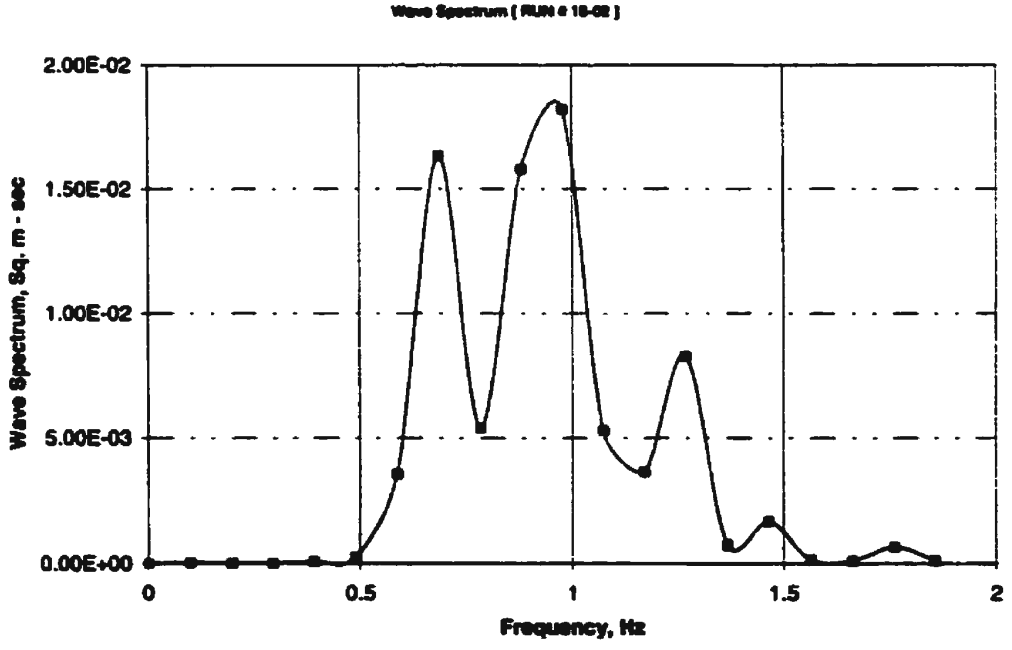

Figure M.18: Wave power spectral density function [Run # 18-02]

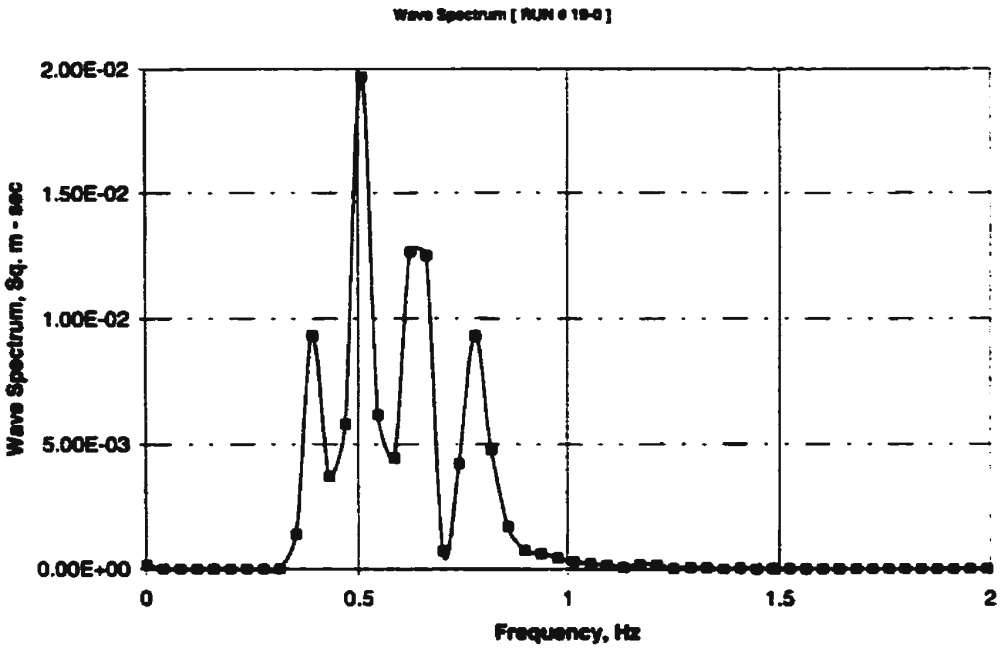

Figure M.19: Wave power spectral density function [Run # 19-0]

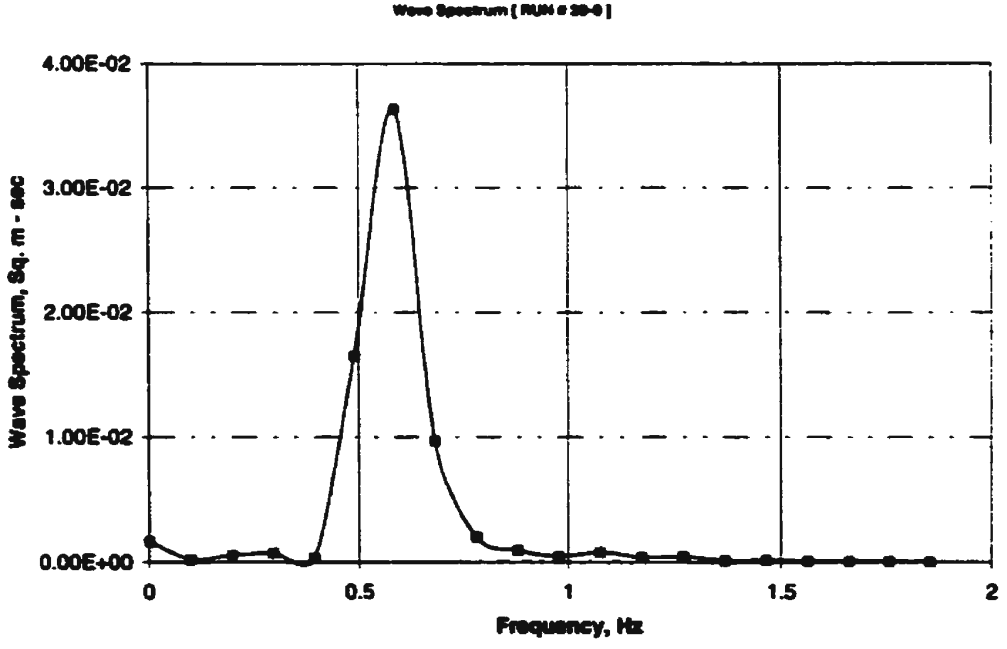

Figure M.20: Wave power spectral density function [Run # 20-0]

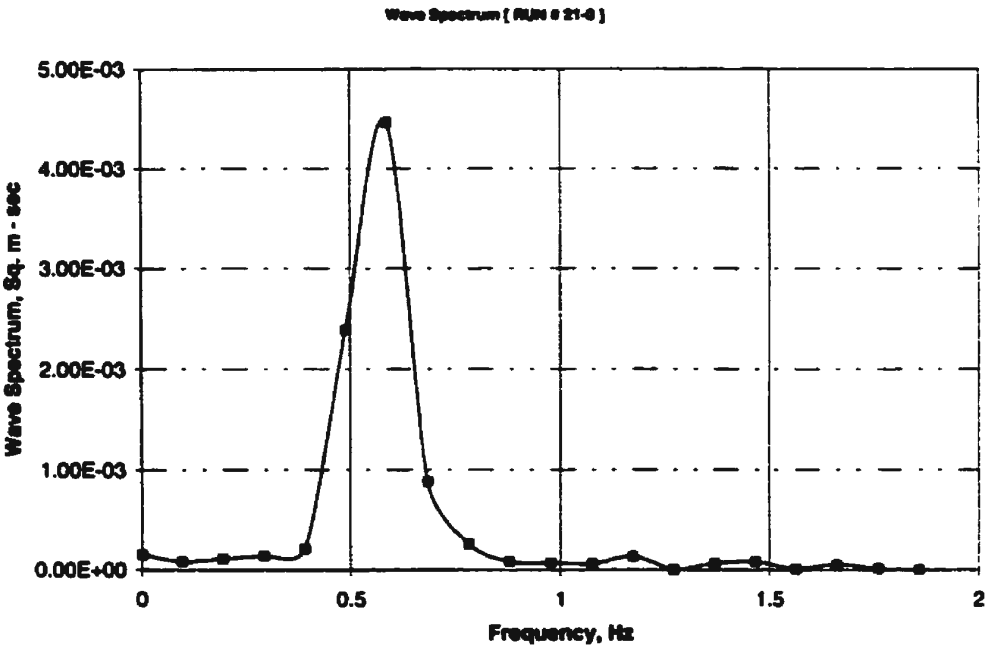

Figure M.21: Wave power spectral density function [Run # 21-0]

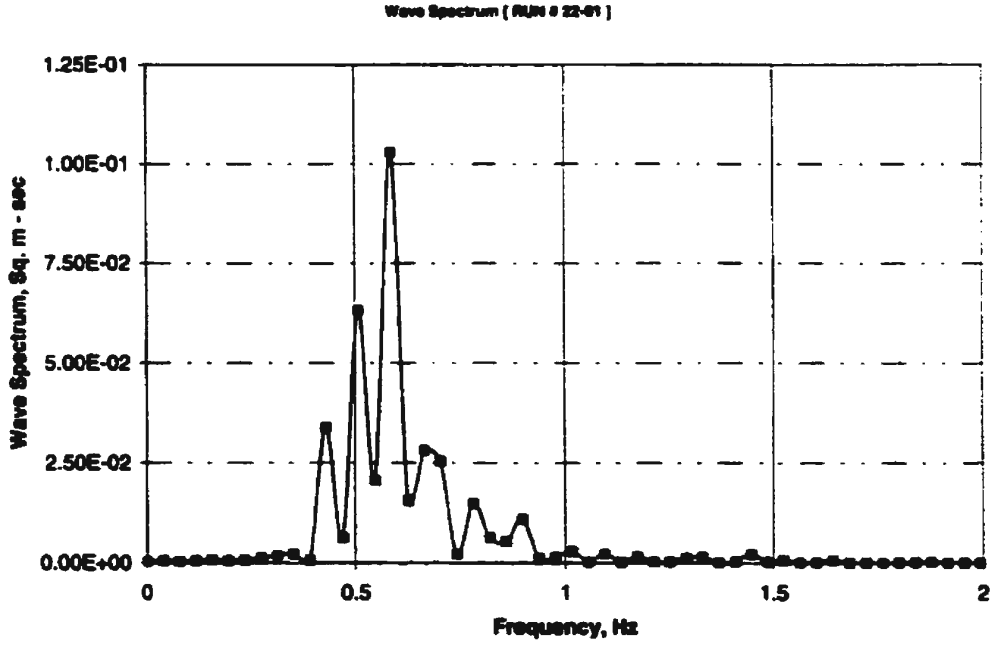

Figure M.22: Wave power spectral density function [Run # 22-0]

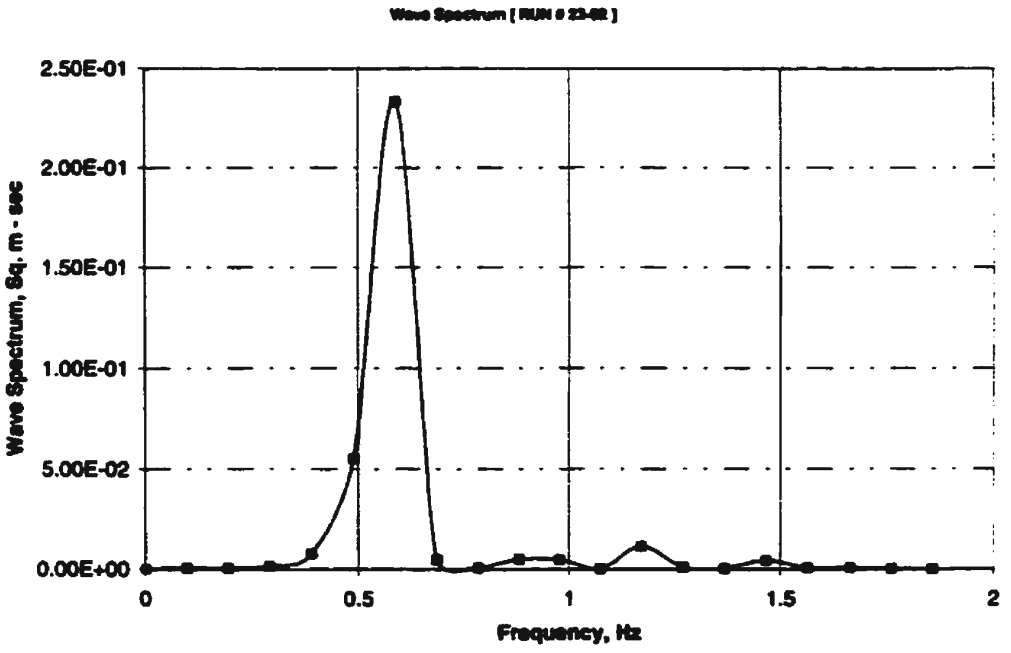

Figure M.23: Wave power spectral density function [Run # 23-02]

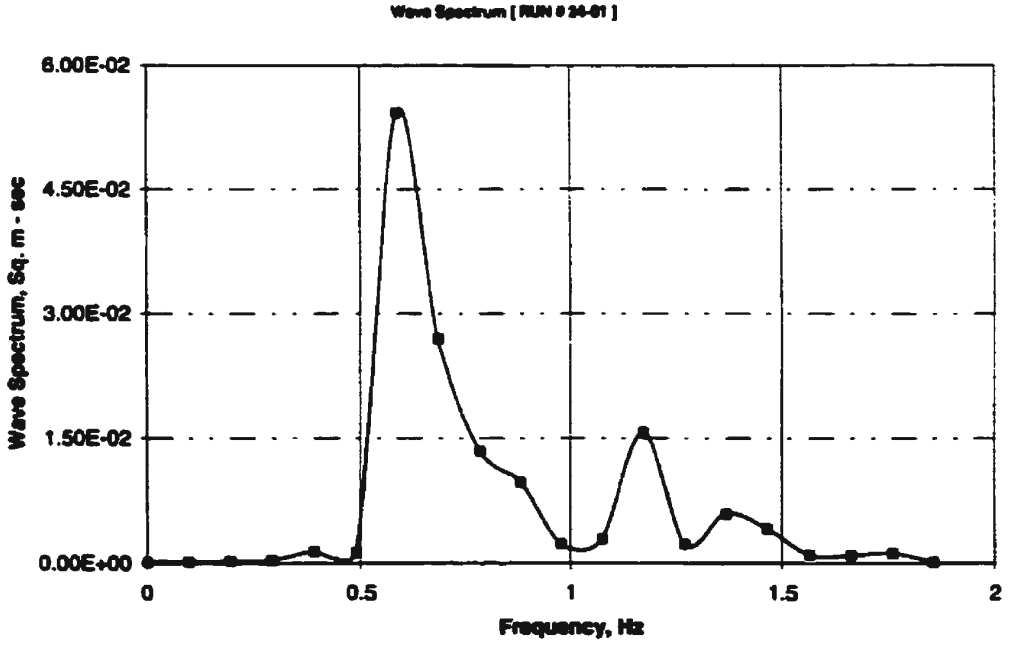

Figure M.24: Wave power spectral density function [Run # 24-01]

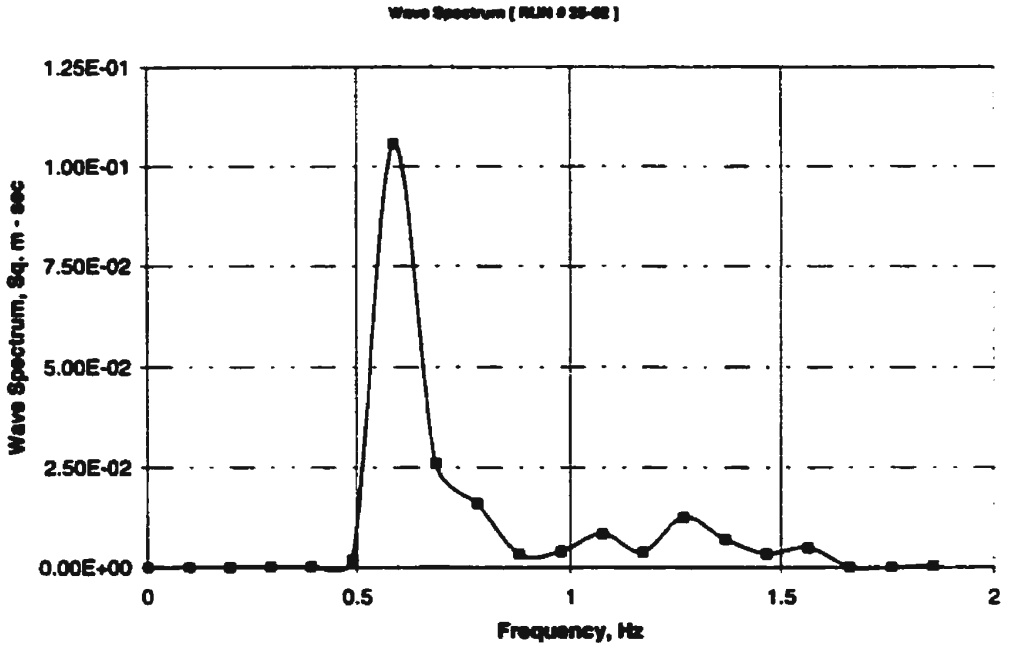

Figure M.25: Wave power spectral density function [Run # 25-02]

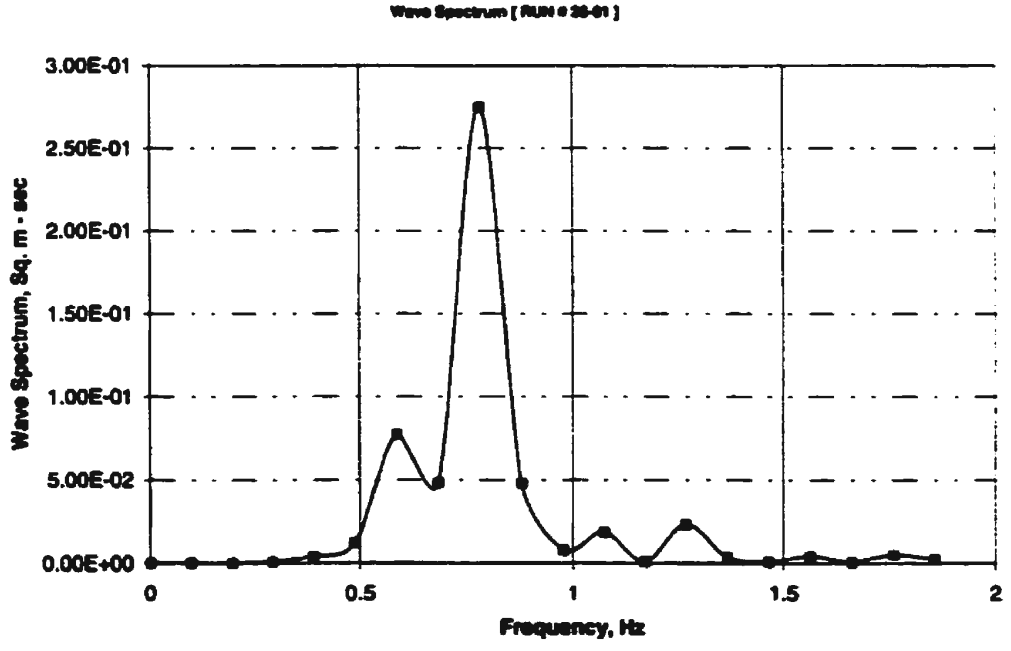

Figure M.26: Wave power spectral density function [Run # 26-01]

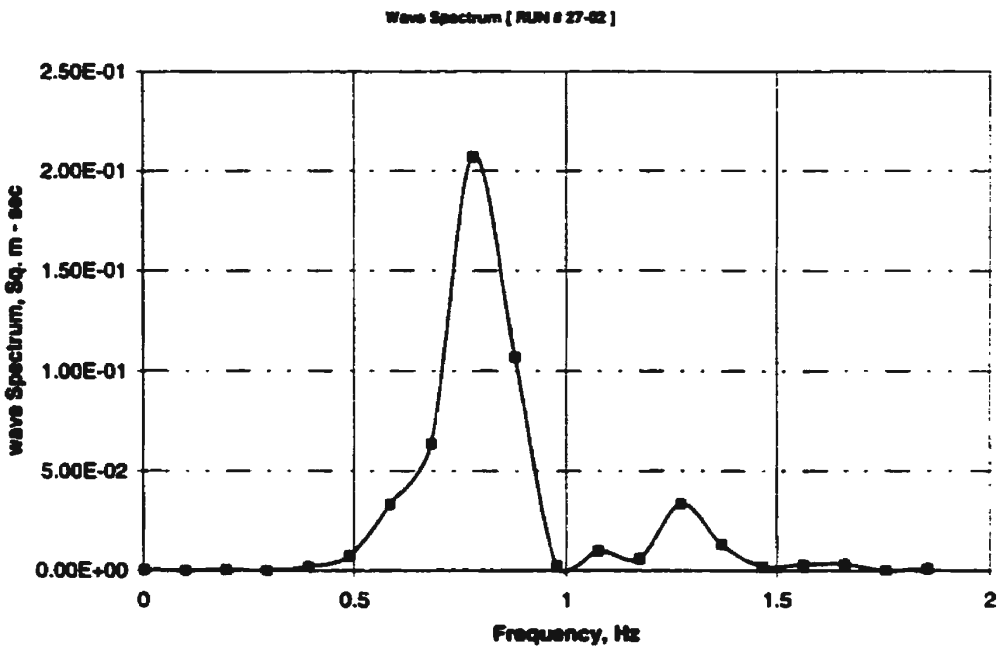

Figure M.27: Wave power spectral density function [Run # 27-02]

Appendix N

Heave Power Spectral Density Function: Experiment

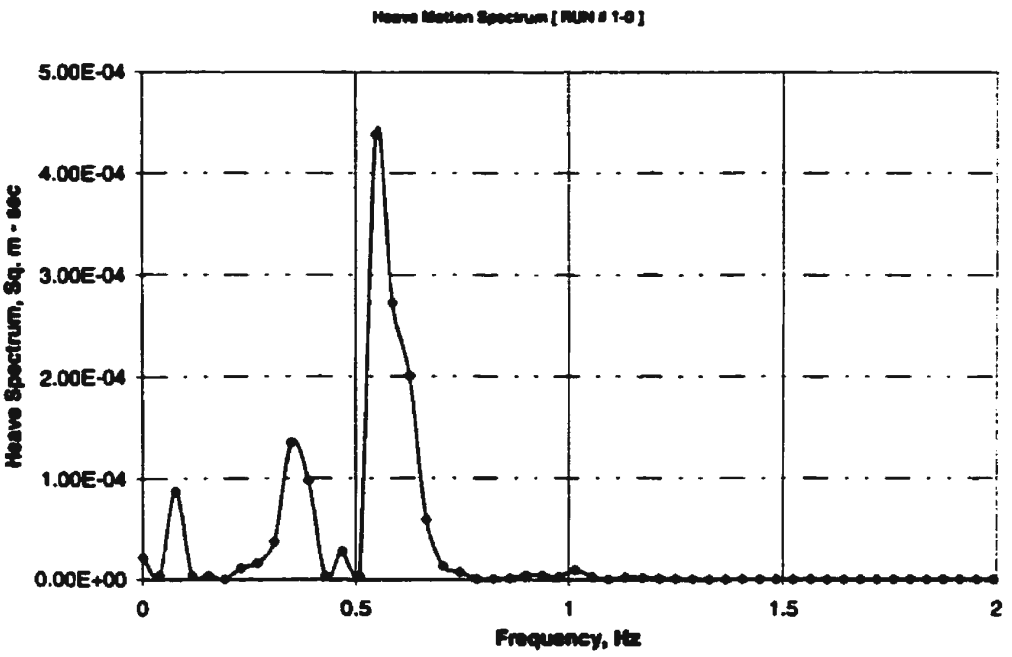

Figure N.1: Heave power spectral density function [Run # 1-0]

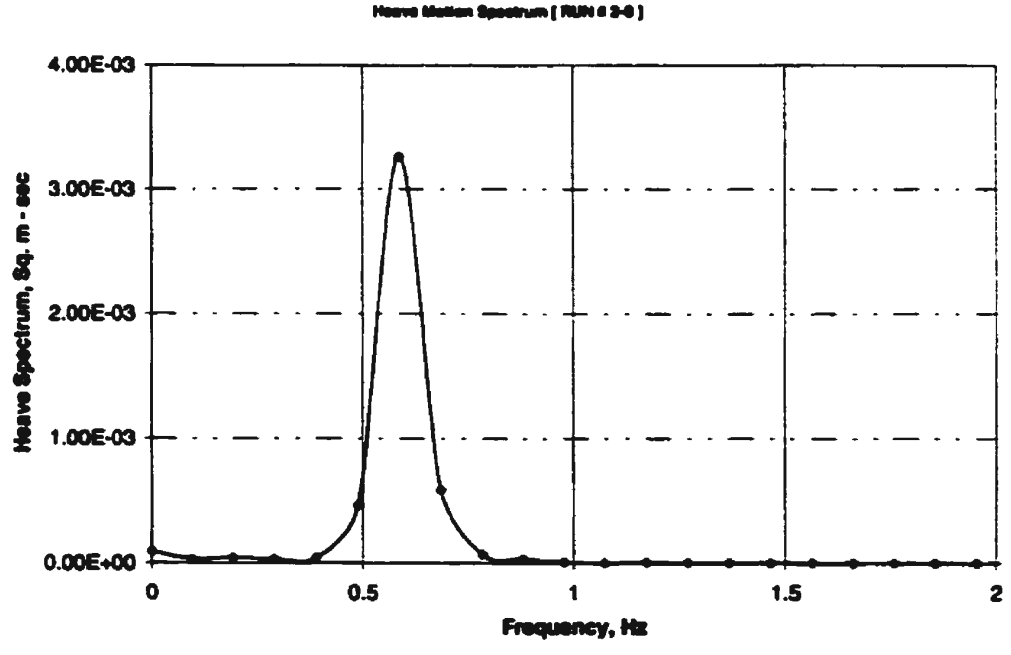

Figure N.2: Heave power spectral density function [Run # 2-0]

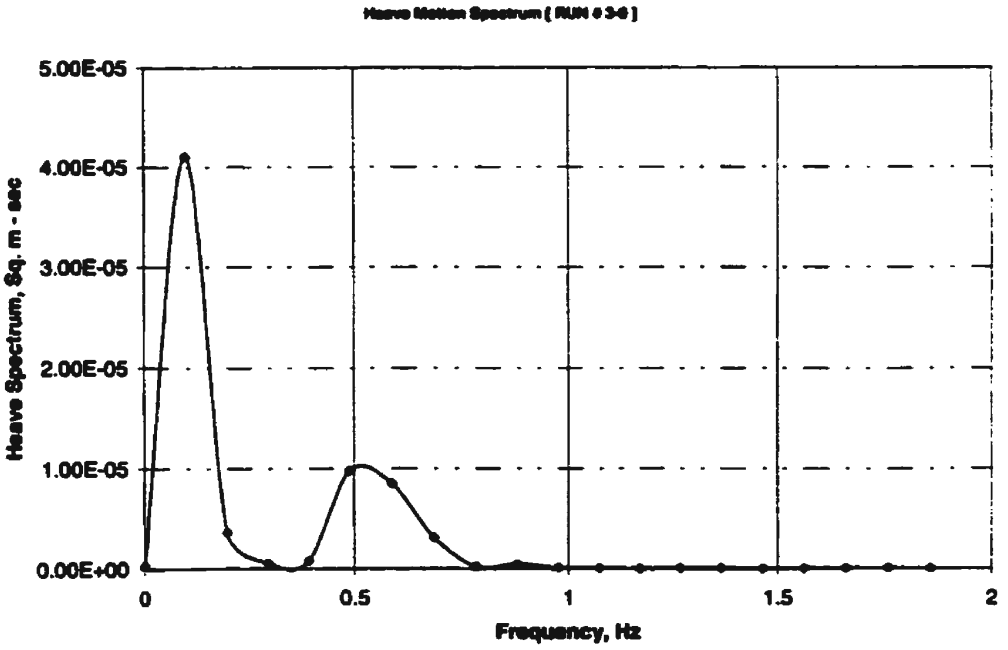

Figure N.3: Heave power spectral density function [Run # 3-0]

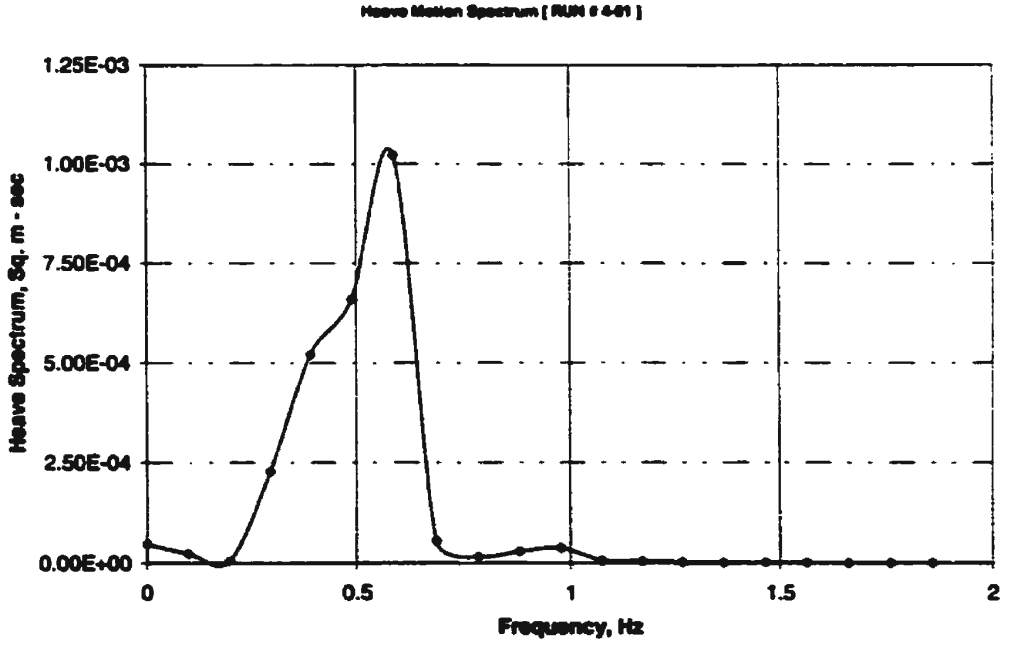

Figure N.4: Heave power spectral density function [Run # 4-01]

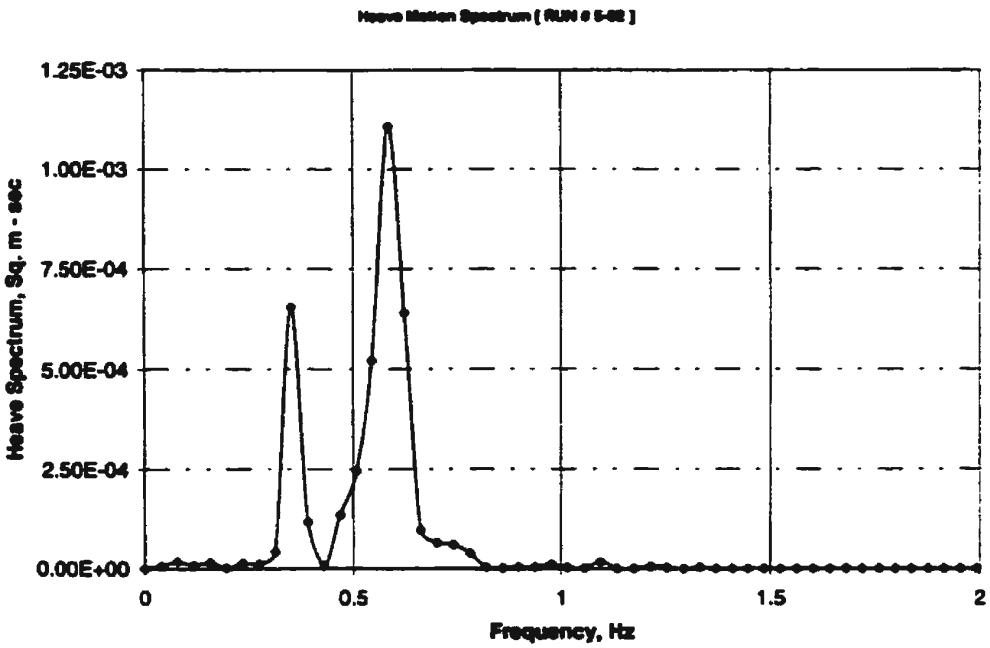

Figure N.5: Heave power spectral density function [Run # 5-02]

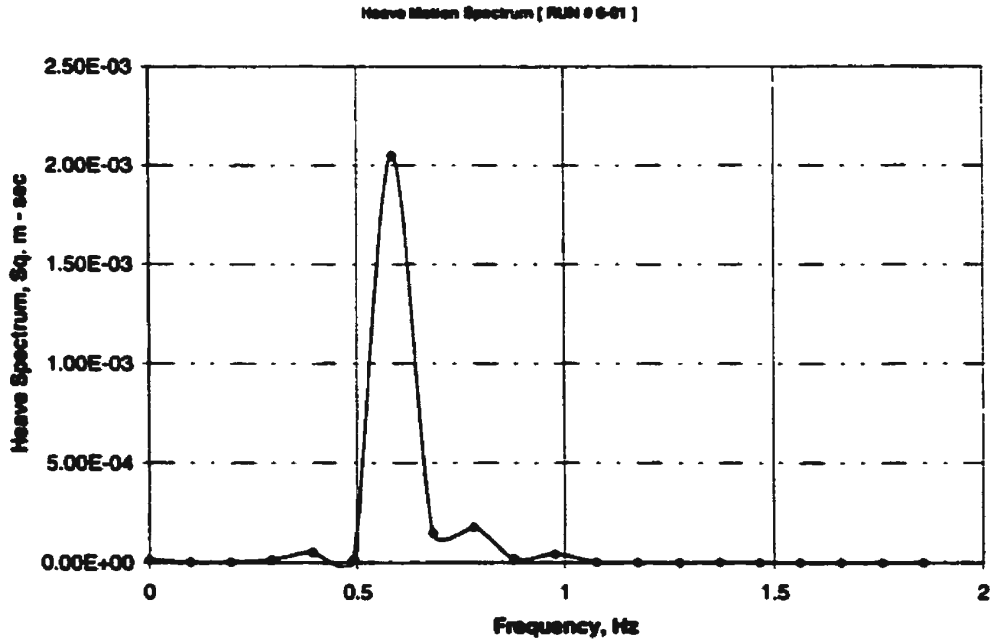

Figure N.6: Heave power spectral density function [Run # 6-01]

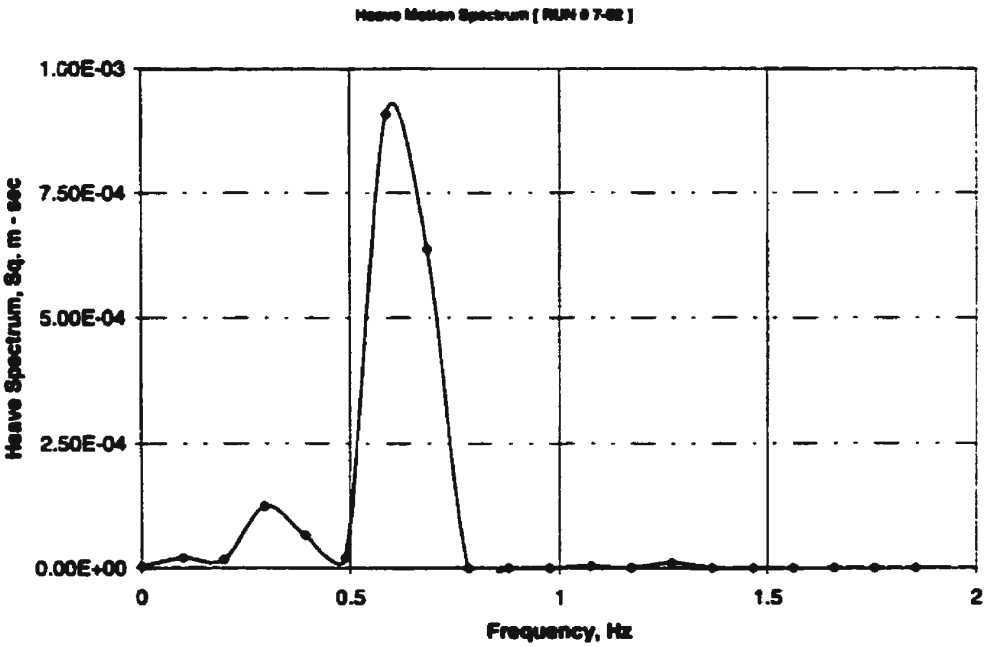

Figure N.7: Heave power spectral density function [Run # 7-02]

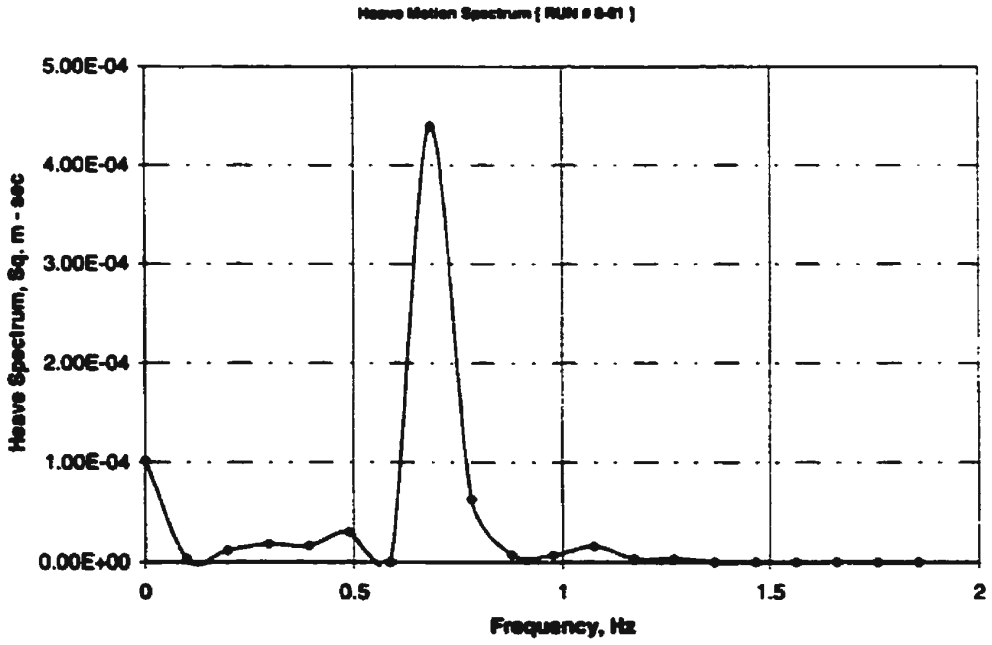

Figure N.8: Heave power spectral density function [Run # 8-01]

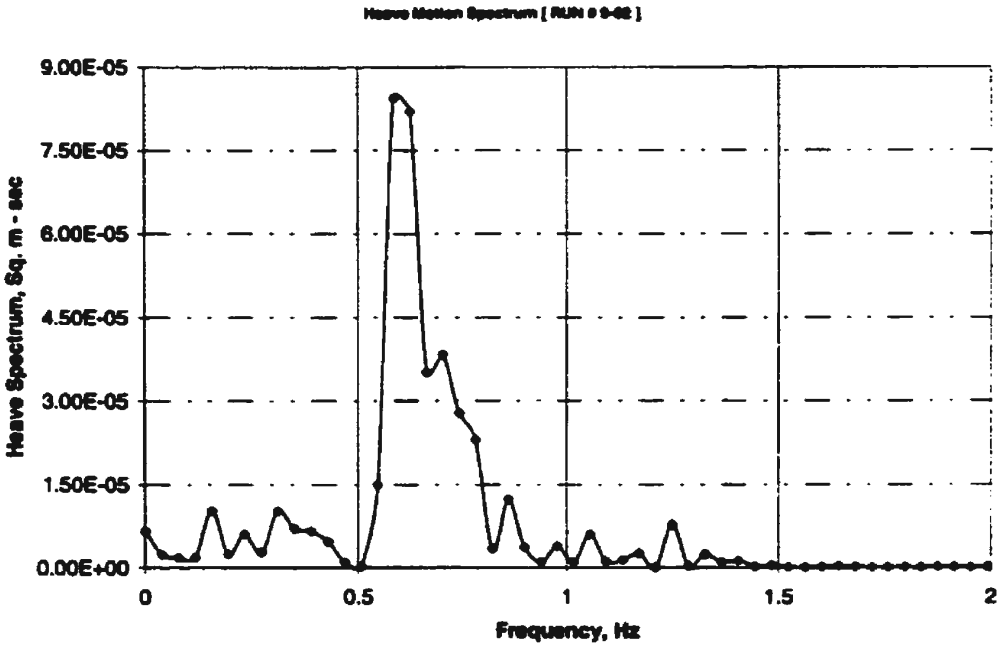

Figure N.9: Heave power spectral density function [Run # 9-02]

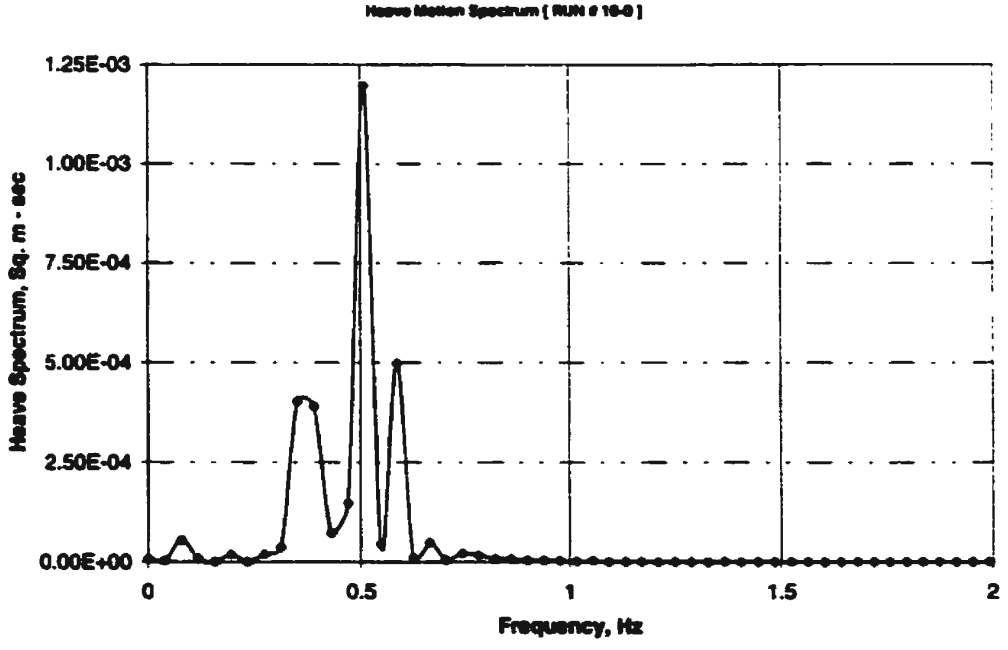

Figure N.10: Heave power spectral density function [Run # 10-0]

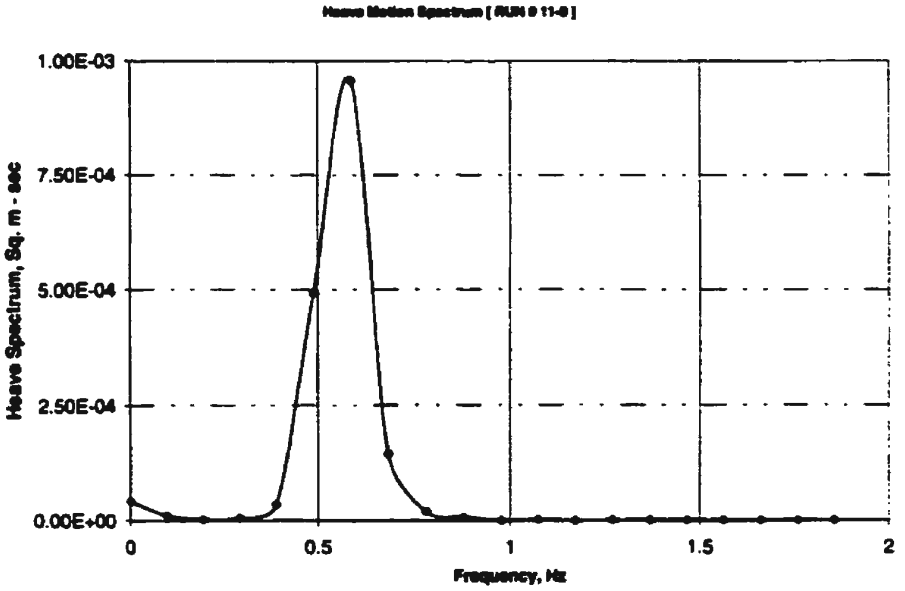

Figure N.11: Heave power spectral density function [Run # 11-0]

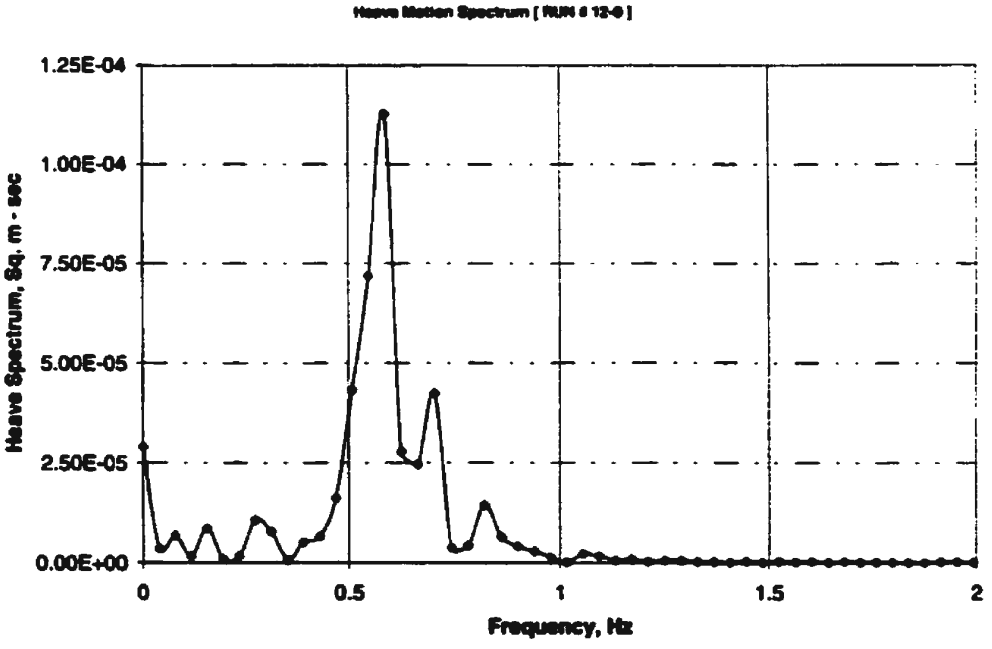

Figure N.12: Heave power spectral density function [Run # 12-0]

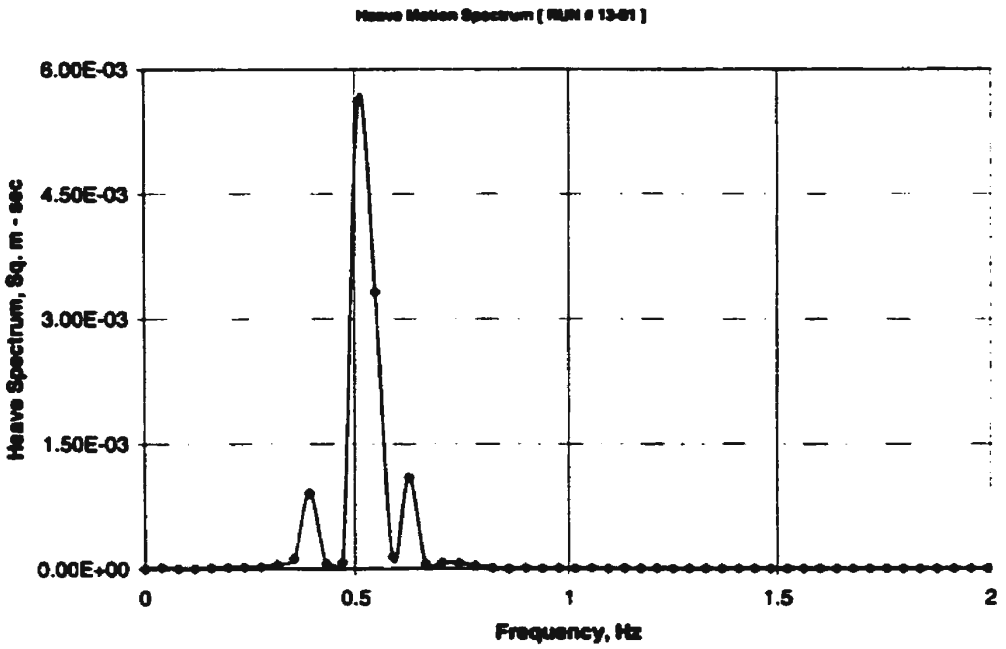

Figure N.13: Heave power spectral density function [Run # 13-01]

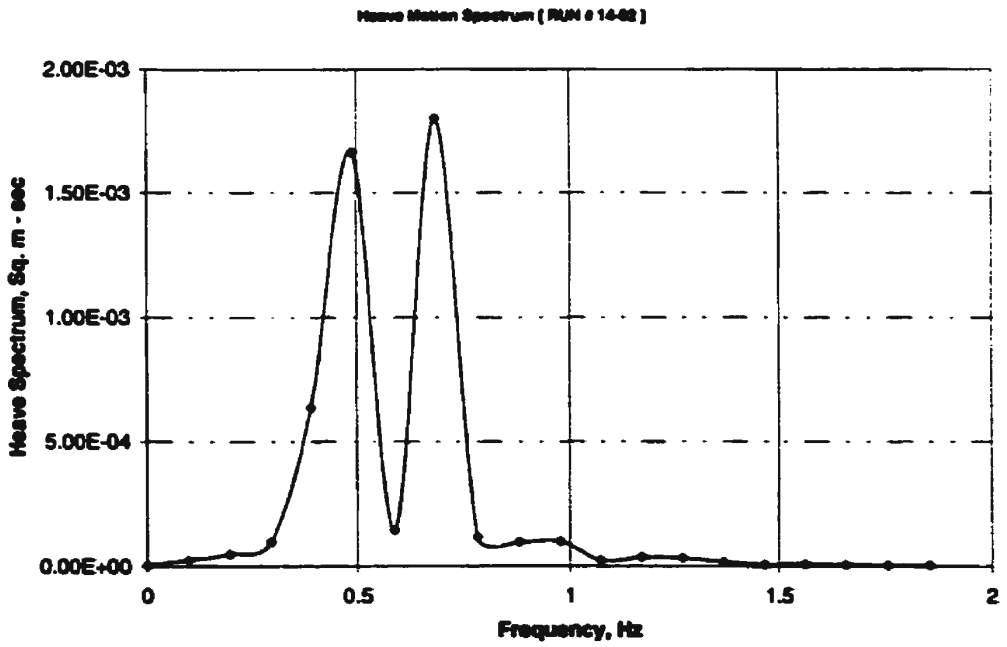

Figure N.14: Heave power spectral density function [Run # 14-02]

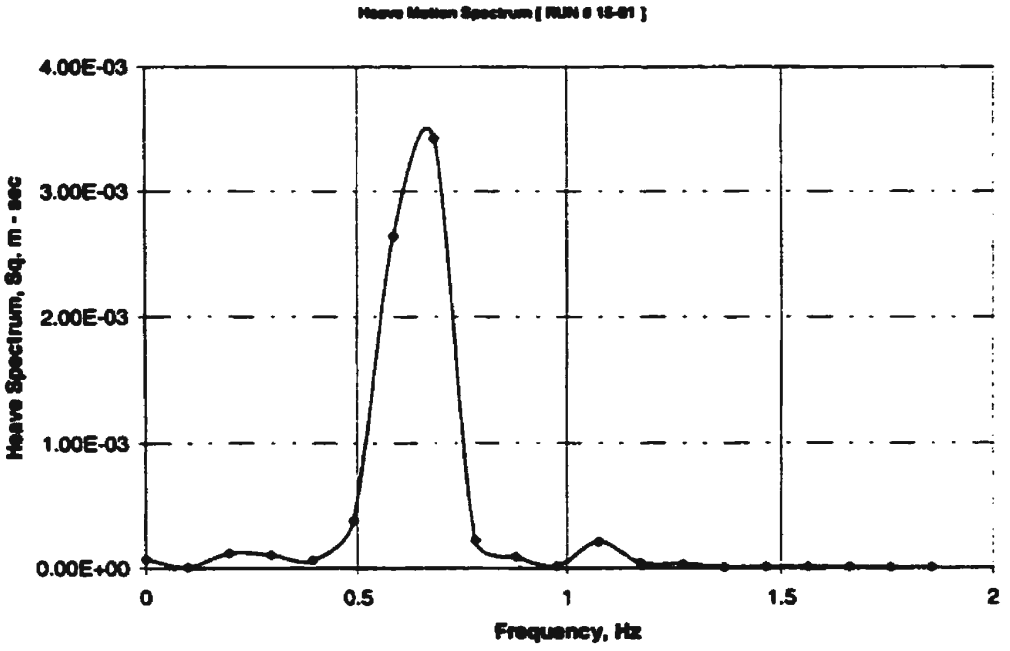

Figure N.15: Heave power spectral density function [Run # 15-01]

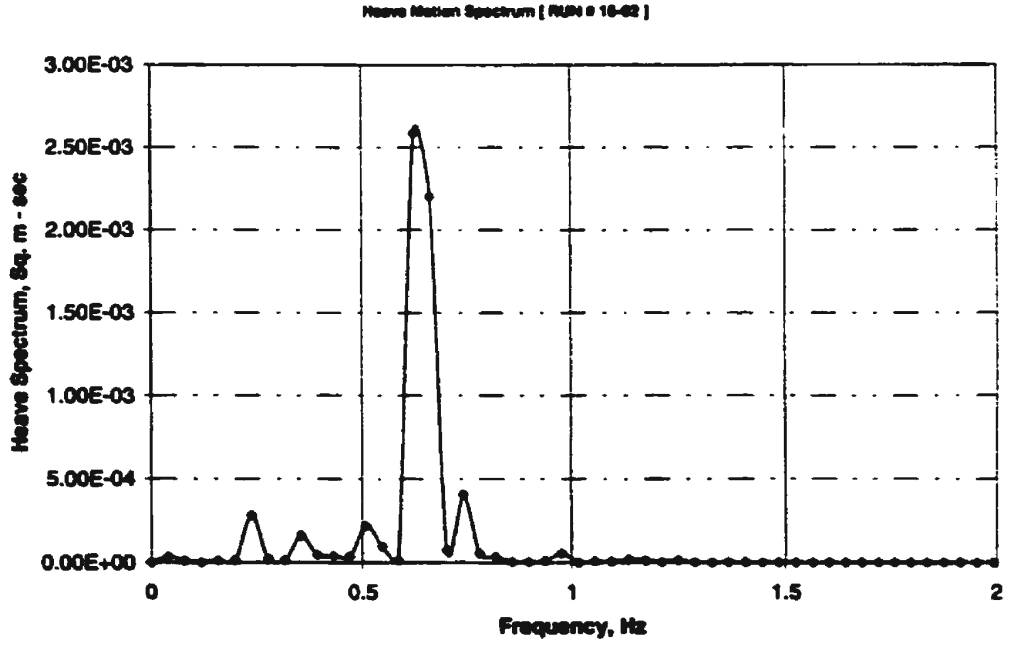

Figure N.16: Heave power spectral density function [Run # 16-02]

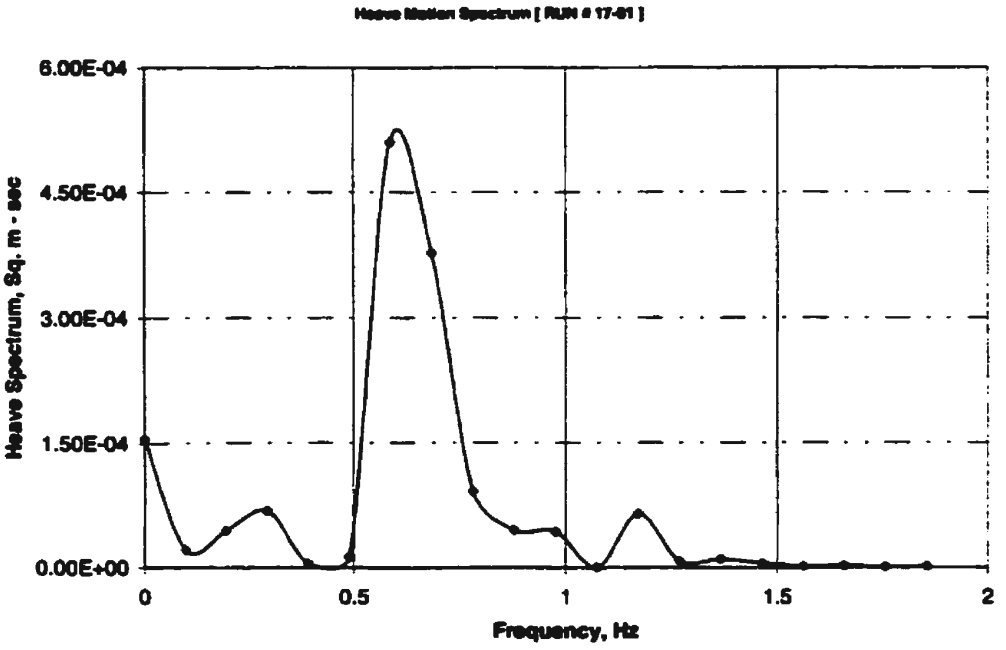

Figure N.17: Heave power spectral density function [Run # 17-01]

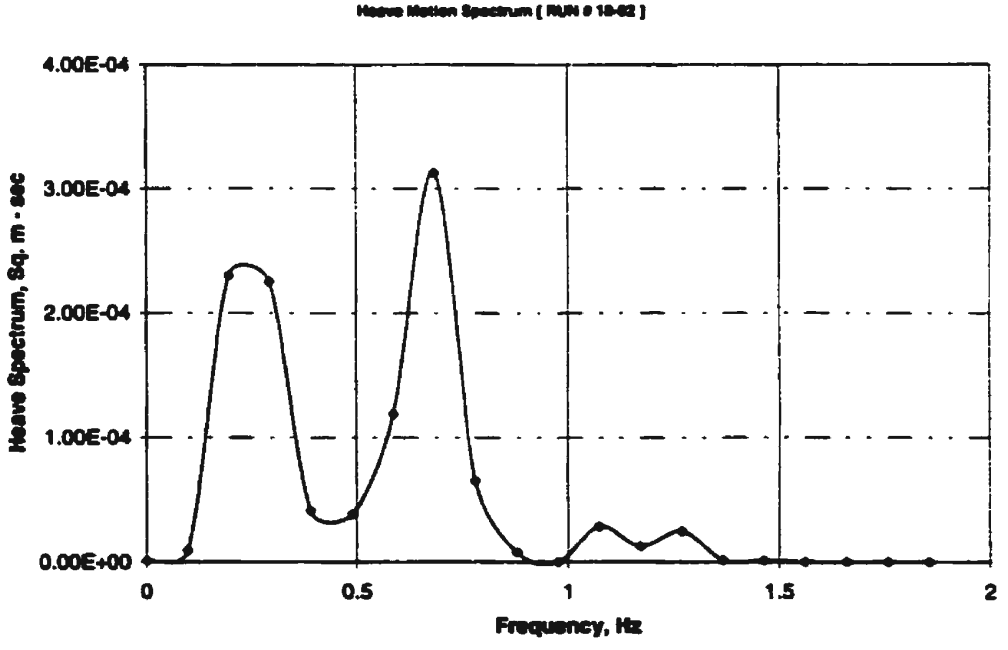

Figure N.18: Heave power spectral density function [Run # 18-02]

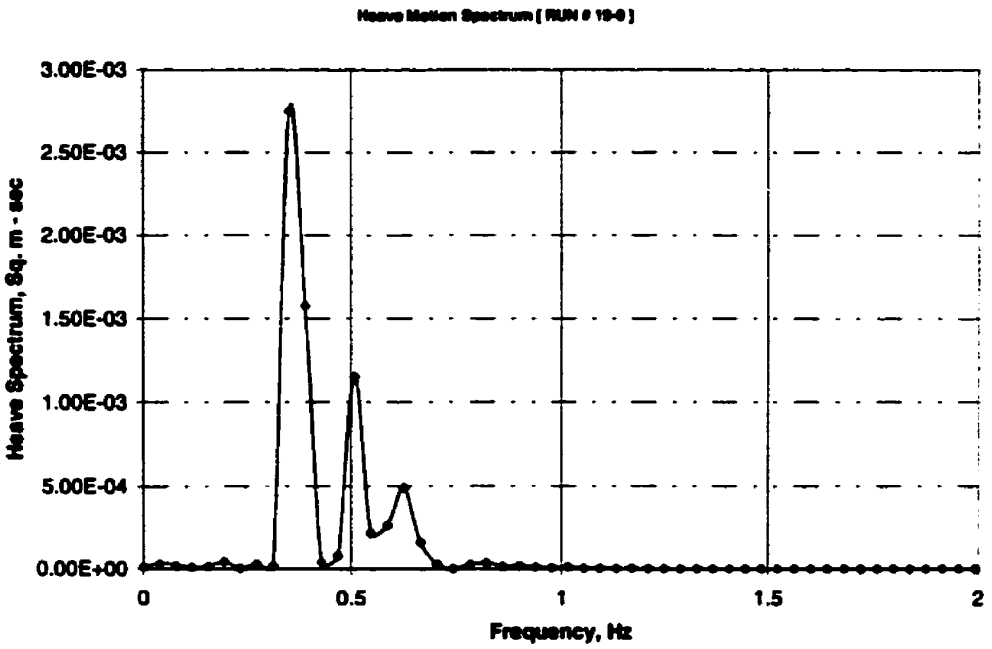

Figure N.19: Heave power spectral density function [Run # 19-01]

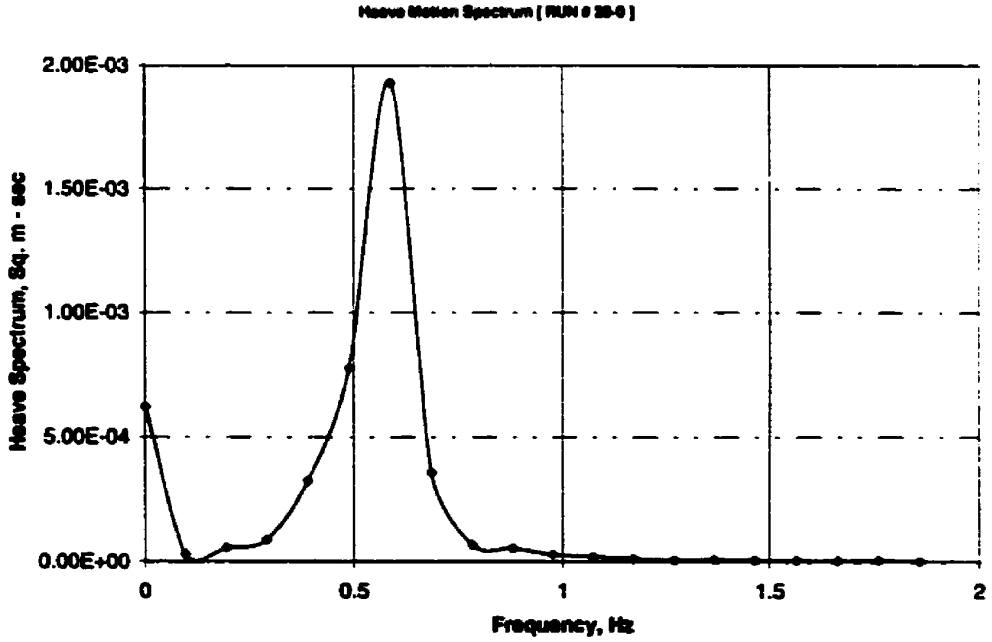

Figure N.20: Heave power spectral density function [Run # 20-0]

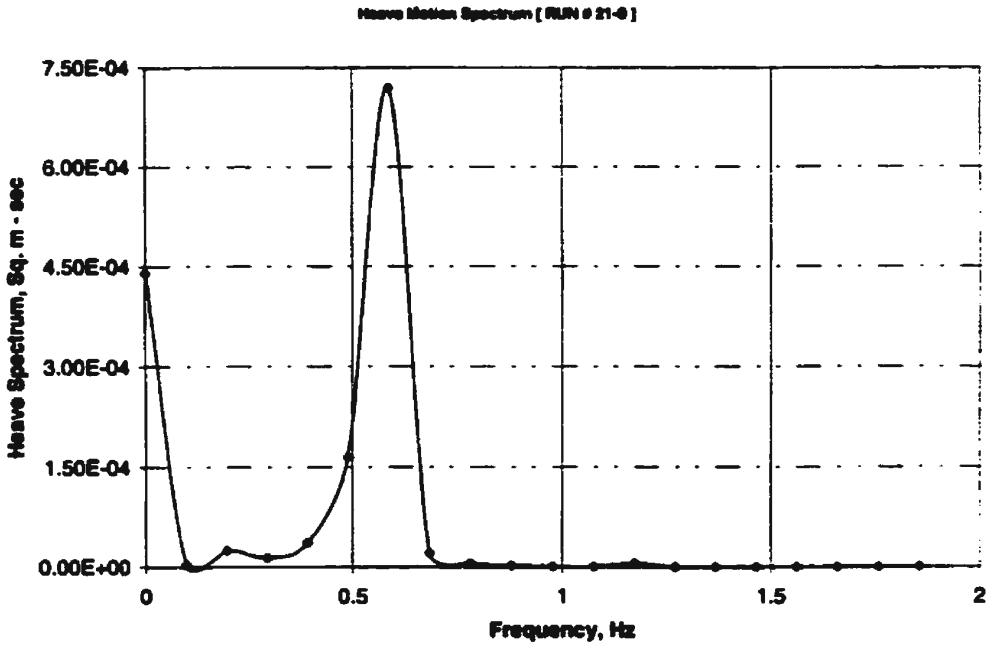

Figure N.21: Heave power spectral density function [Run # 21-0]

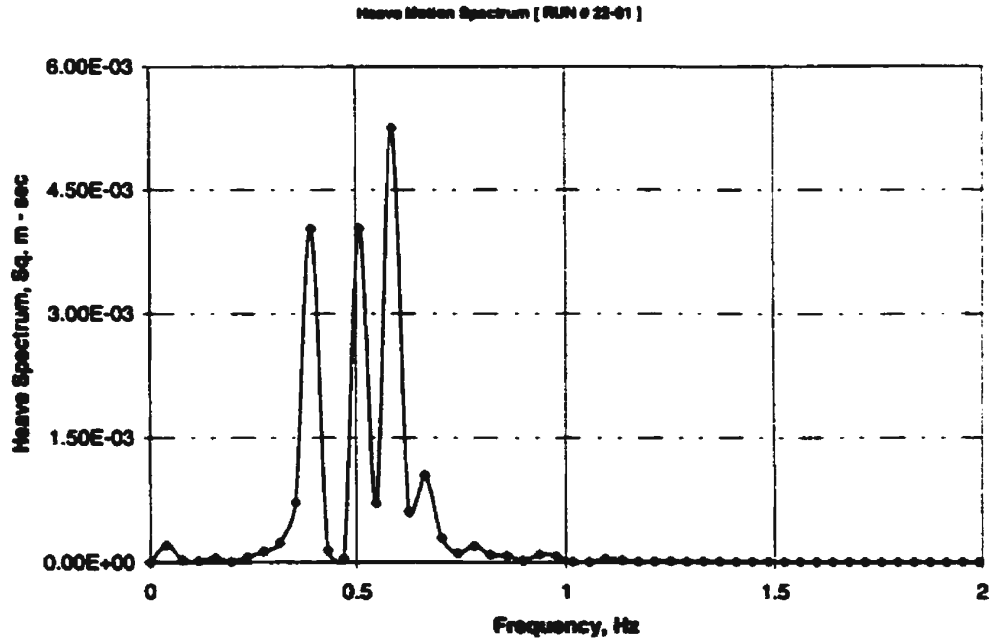

Figure N.22: Heave power spectral density function [Run # 22-01]

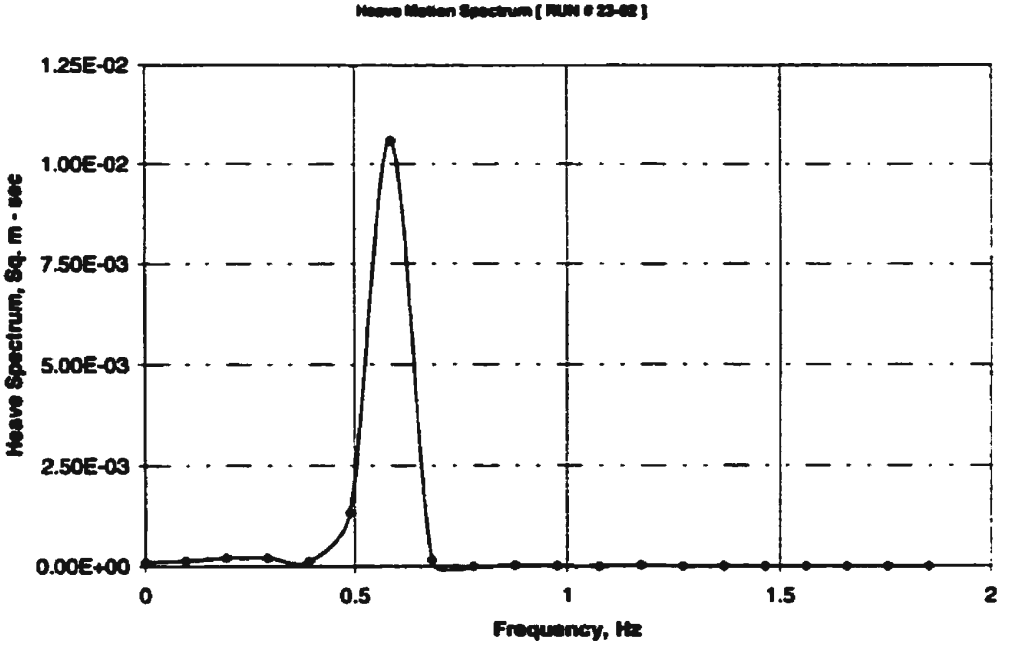

Figure N.23: Heave power spectral density function [Run # 23-02]

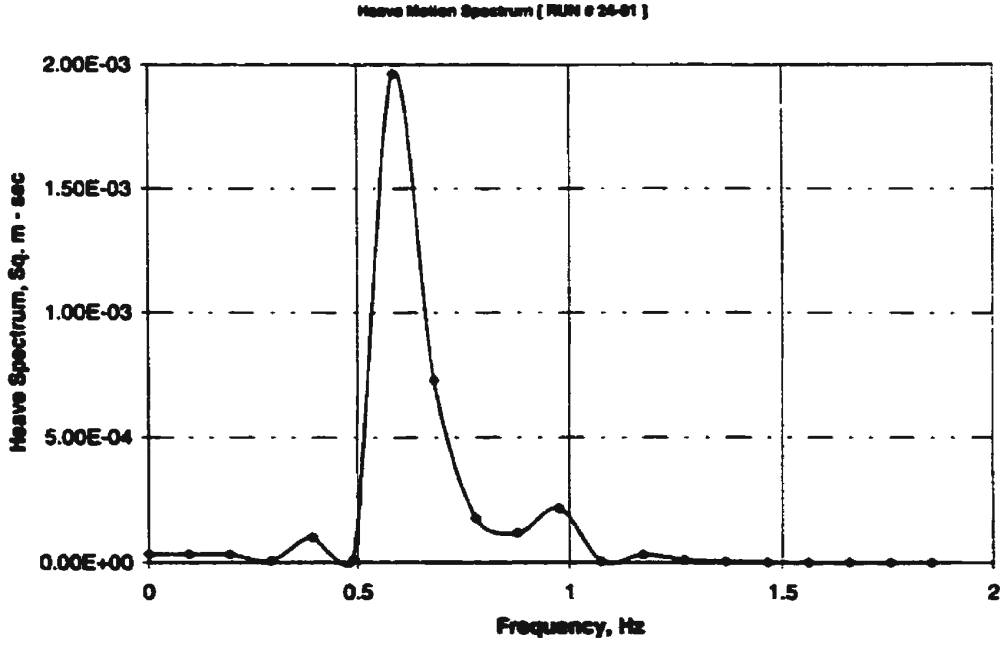

Figure N.24: Heave power spectral density function [Run # 24-01]

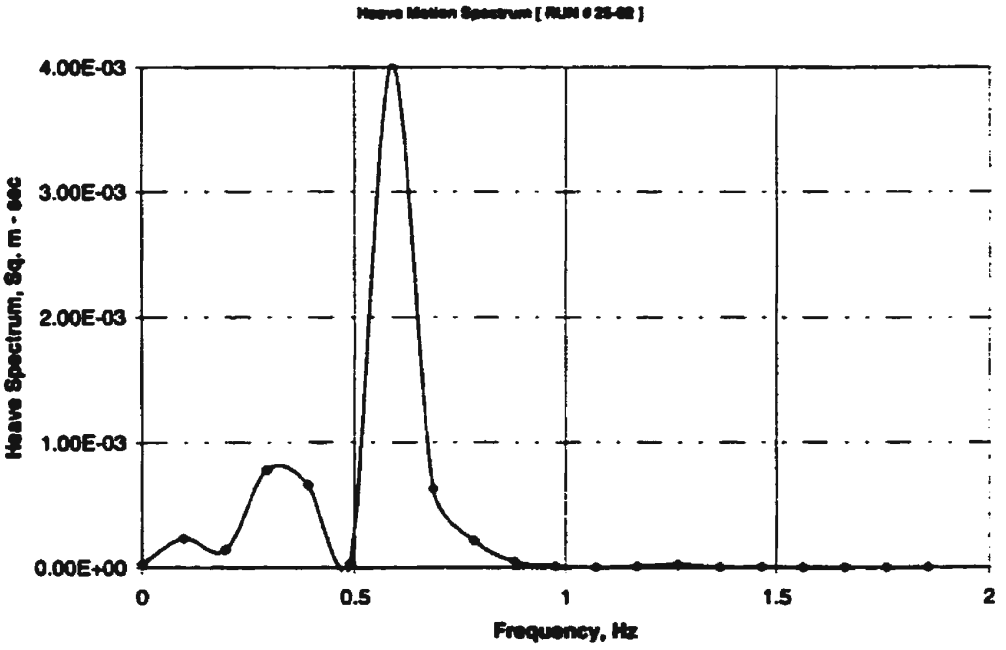

Figure N.25: Heave power spectral density function [Run # 25-02]

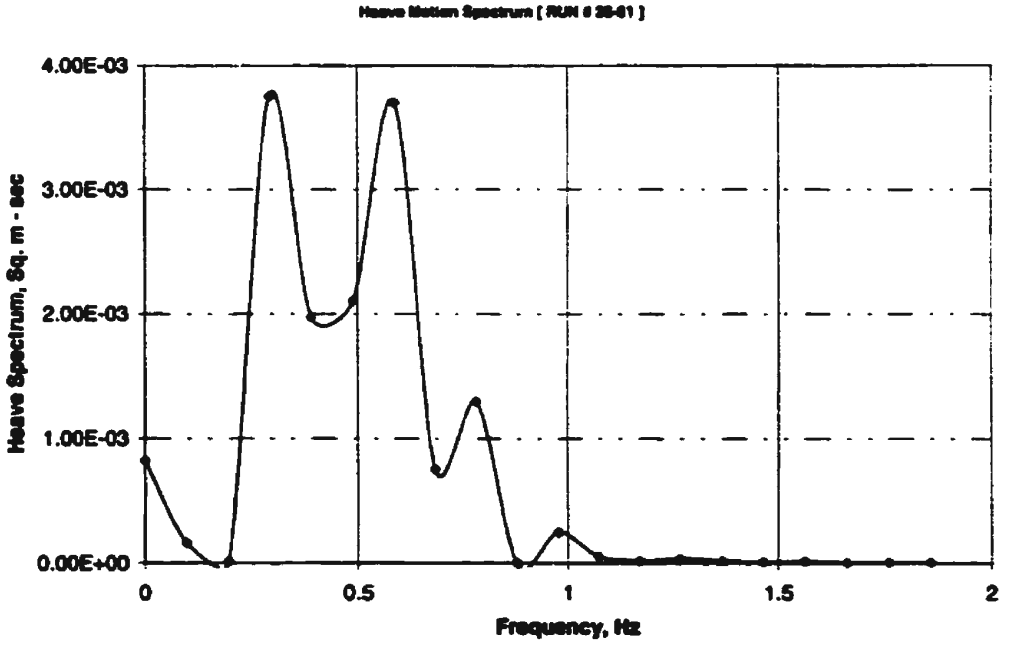

Figure N.26: Heave power spectral density function [Run # 26-01]

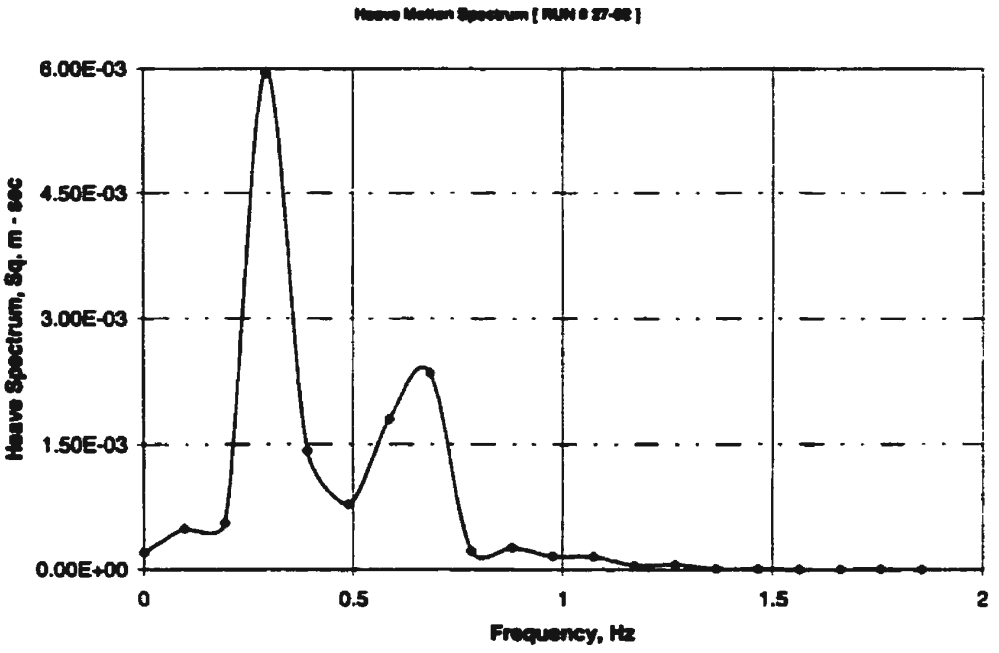

Figure N.27: Heave power spectral density function [Run # 27-02]

Appendix O

Pitch Power Spectral Density Function: Experiment

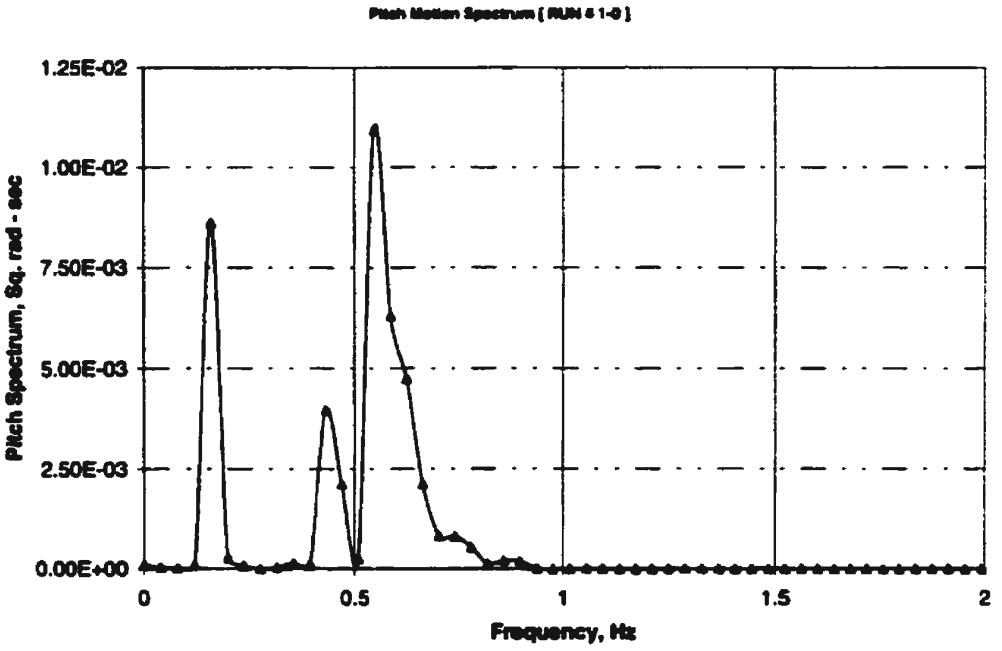

Figure O.1: Pitch power spectral density function [Run # 1-0]

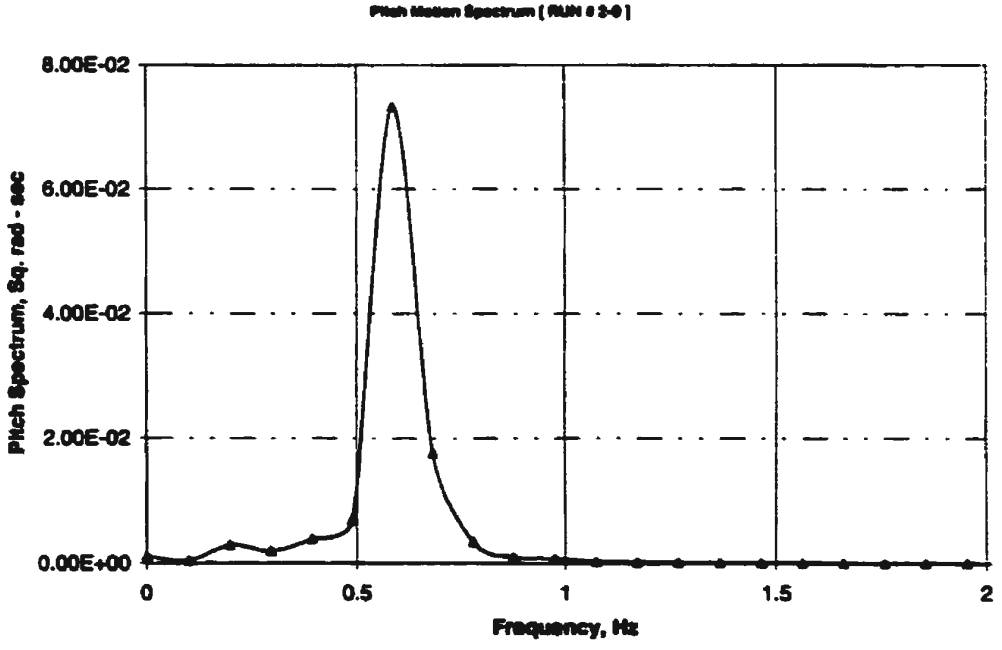

Figure O.2: Pitch power spectral density function [Run # 2-0]

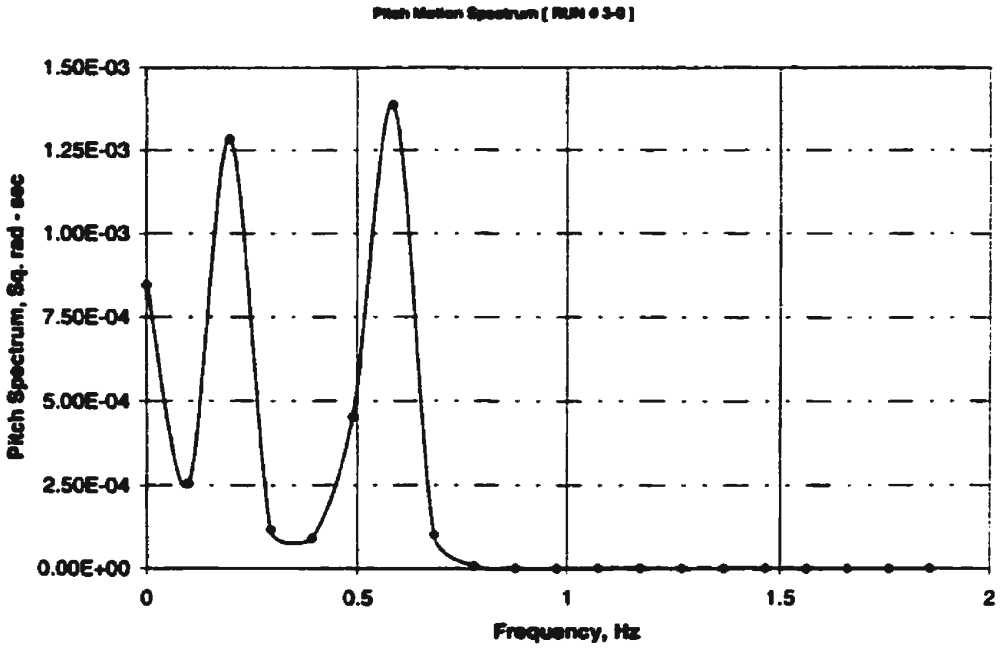

Figure O.3: Pitch power spectral density function [Run # 3-0]

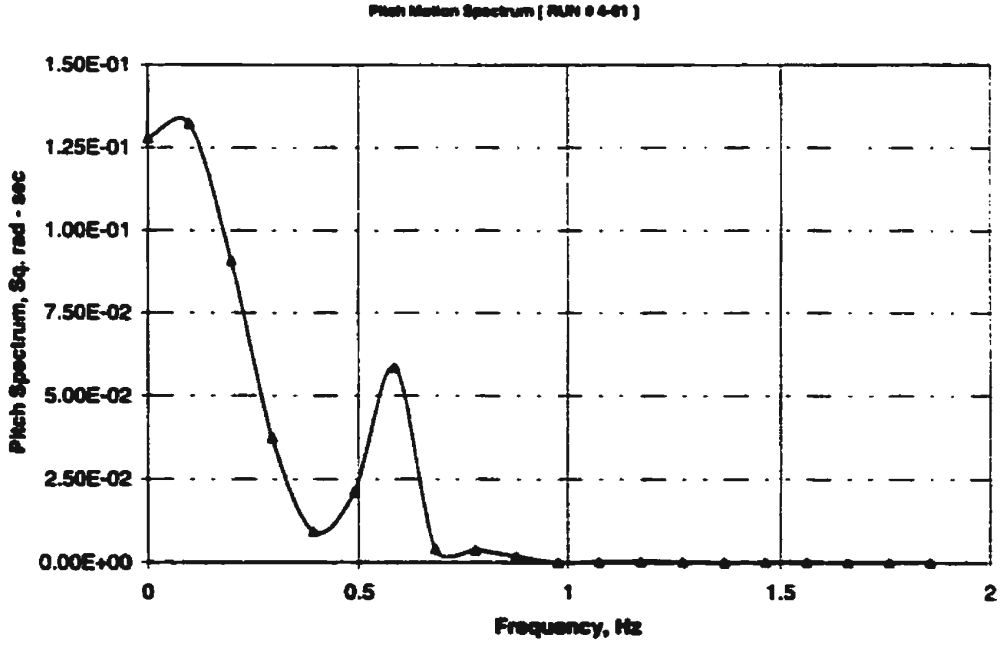

Figure O.4: Pitch power spectral density function [Run # 4-01]

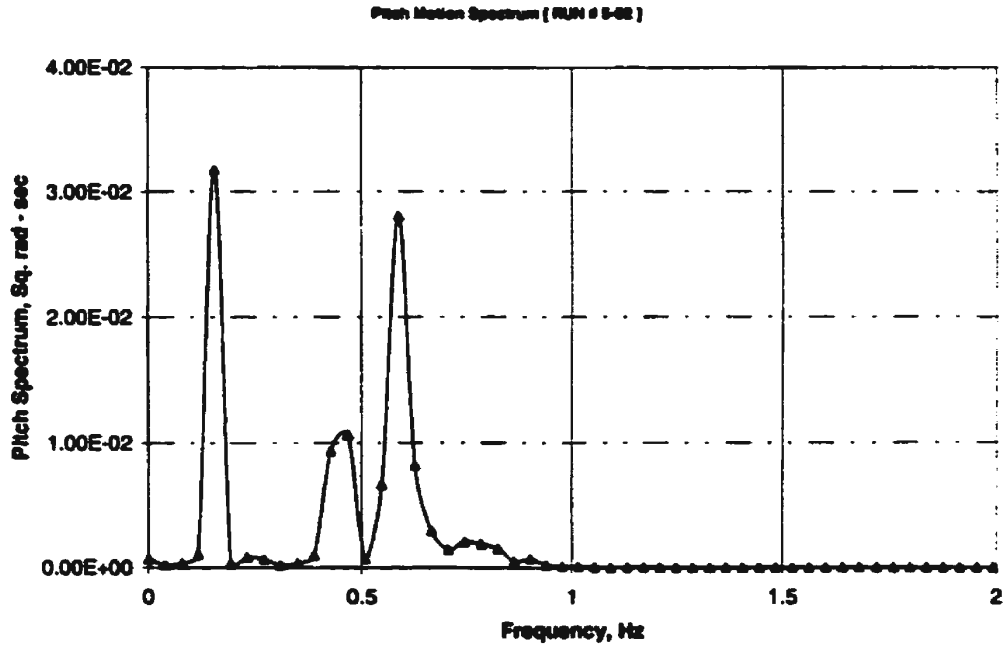

Figure O.5: Pitch power spectral density function [Run # 5-02]

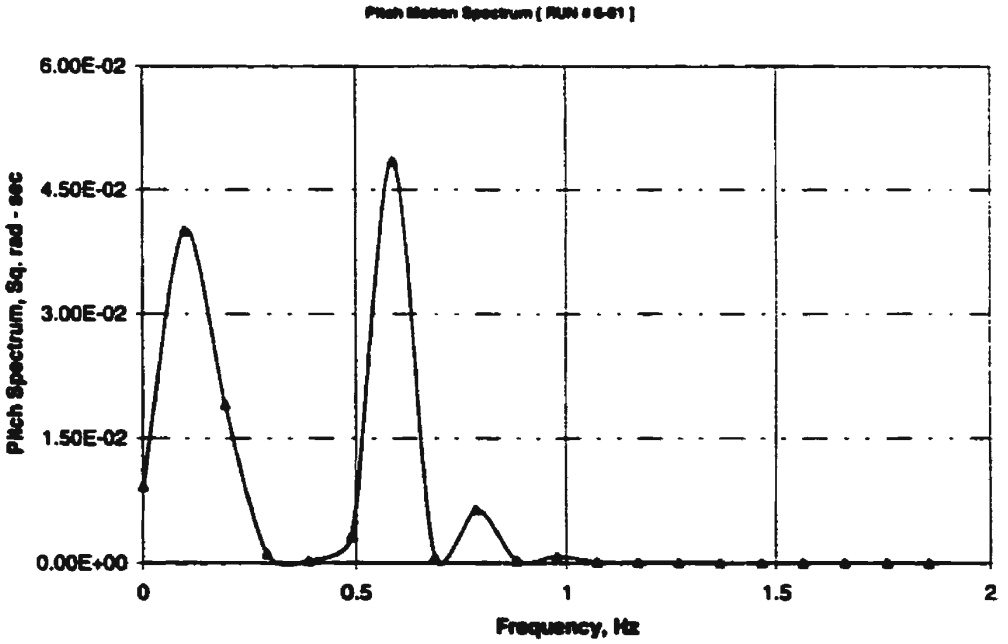

Figure O.6: Pitch power spectral density function [Run # 6-01]

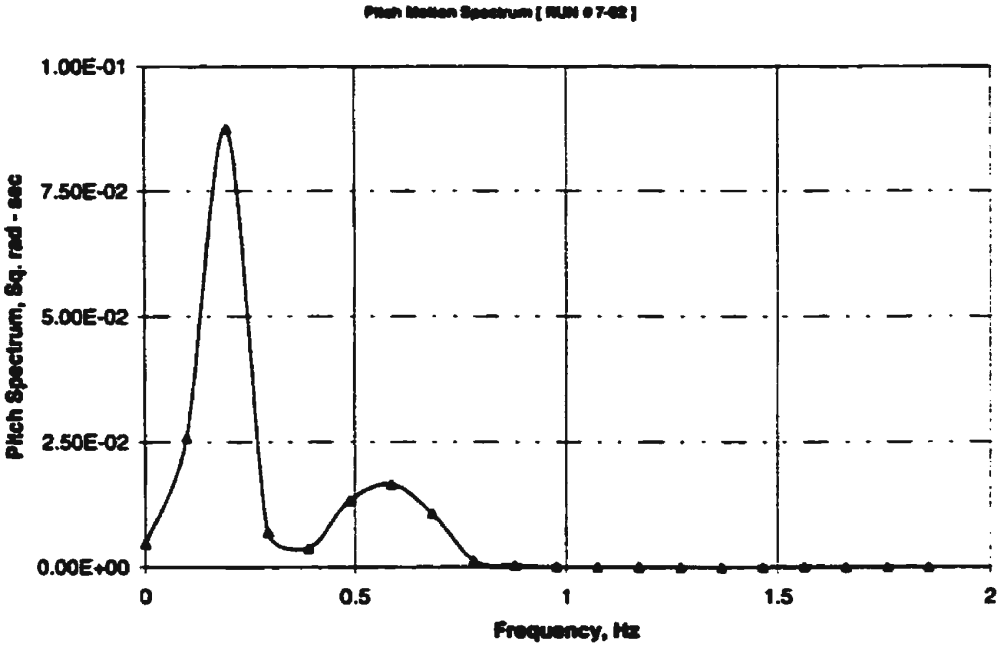

Figure O.7: Pitch power spectral density function [Run # 7-02]

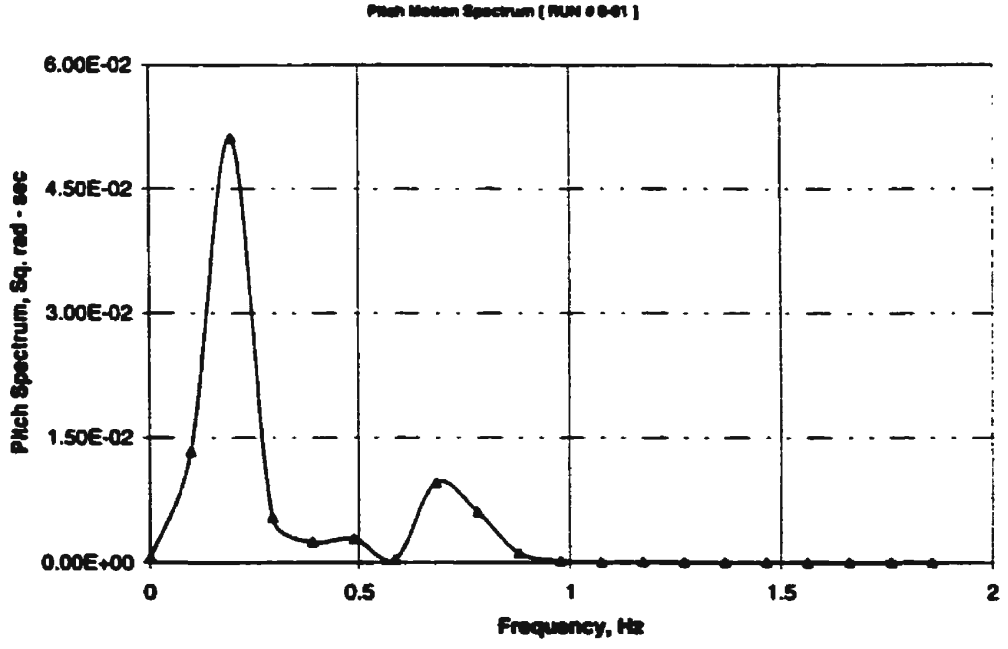

Figure O.8: Pitch power spectral density function [Run # 8-01]

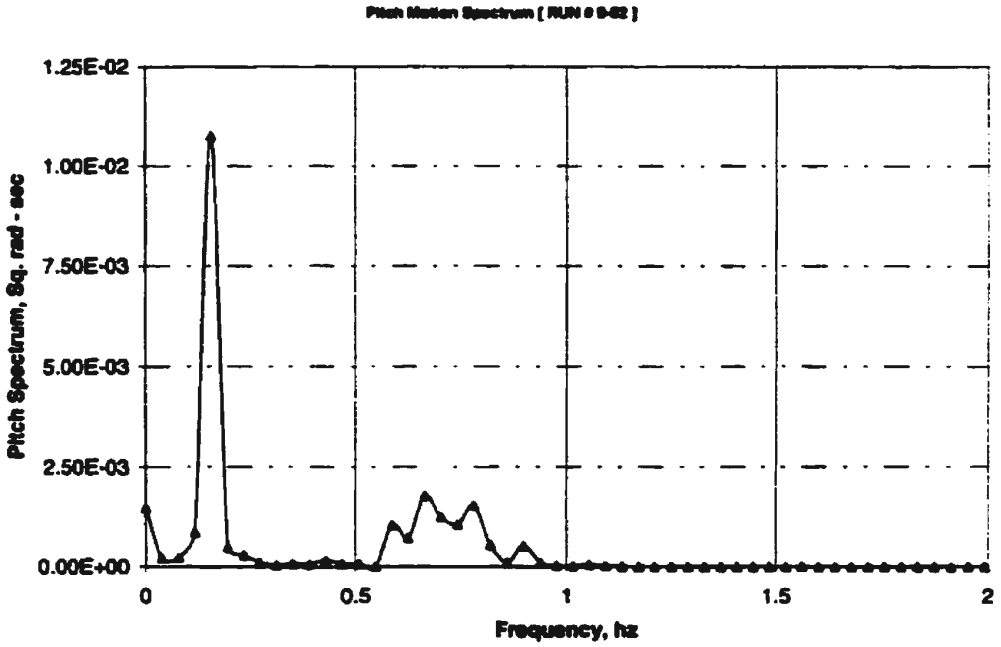

Figure O.9: Pitch power spectral density function [Run # 9-02]

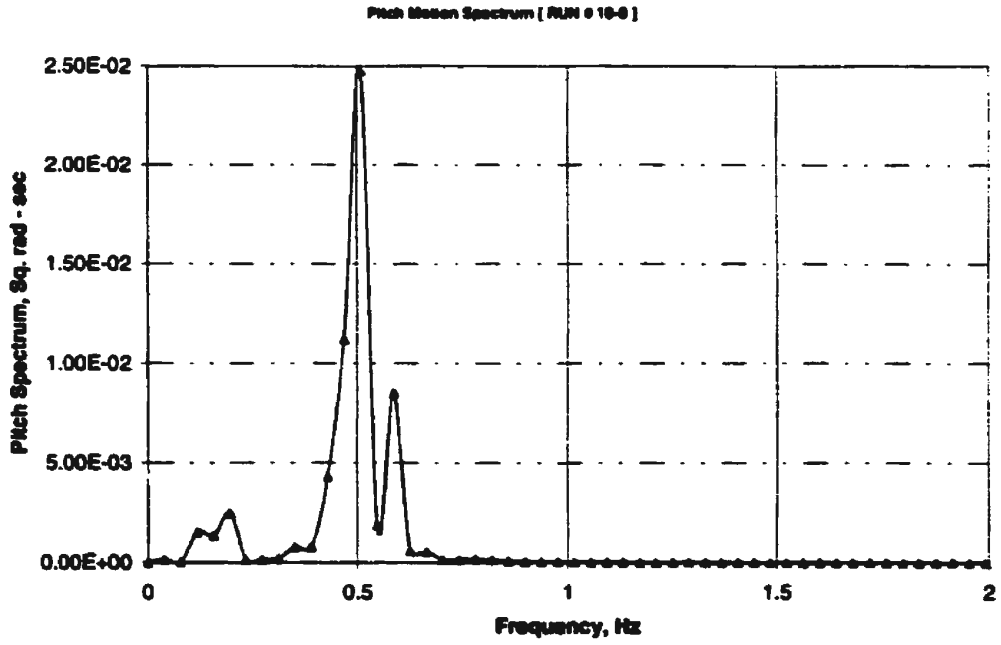

Figure O.10: Pitch power spectral density function [Run # 10-0]

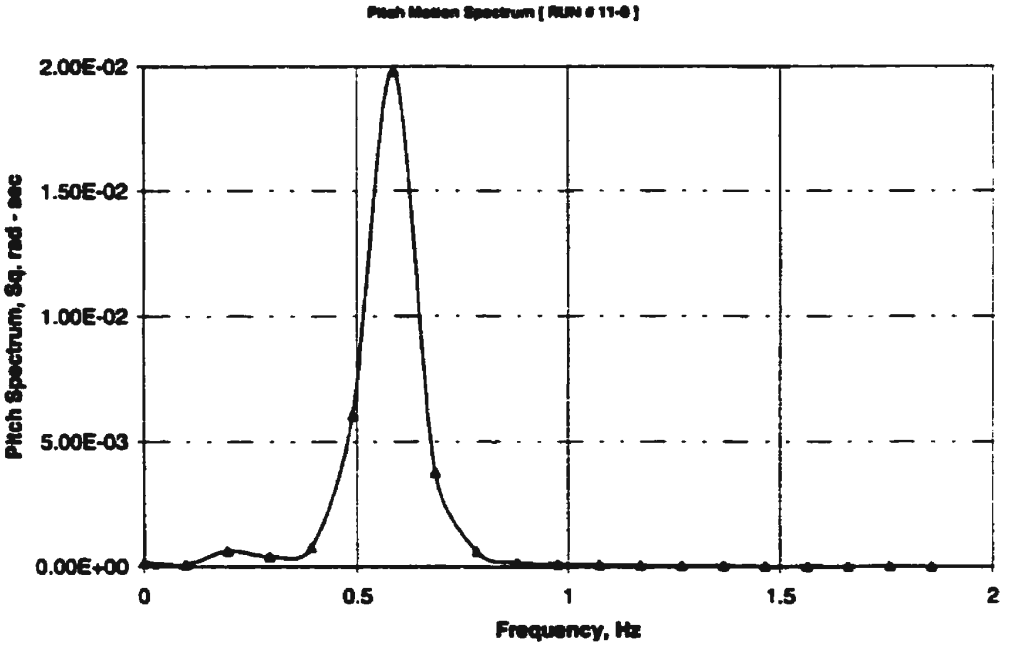

Figure O.11: Pitch power spectral density function [Run # 11-0]

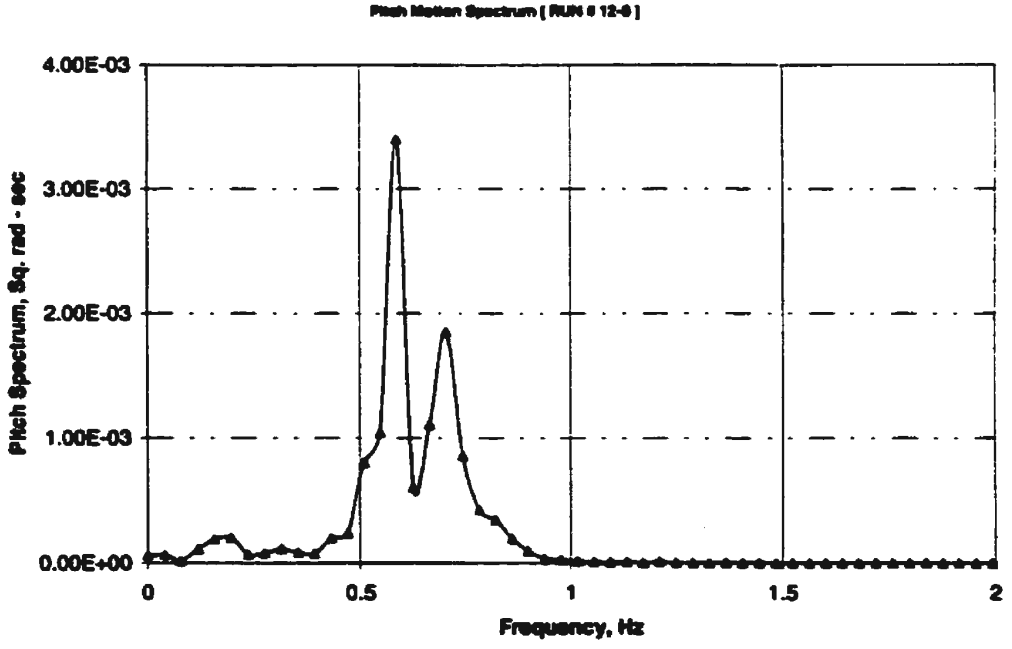

Figure O.12: Pitch power spectral density function [Run # 12-0]

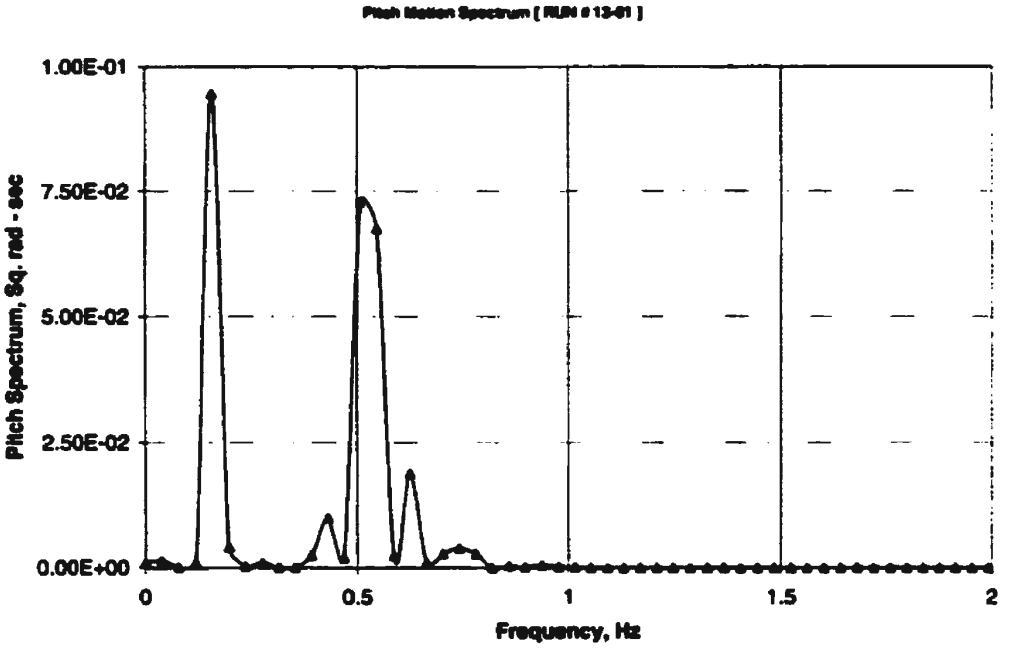

Figure O.13: Pitch power spectral density function [Run # 13-01]

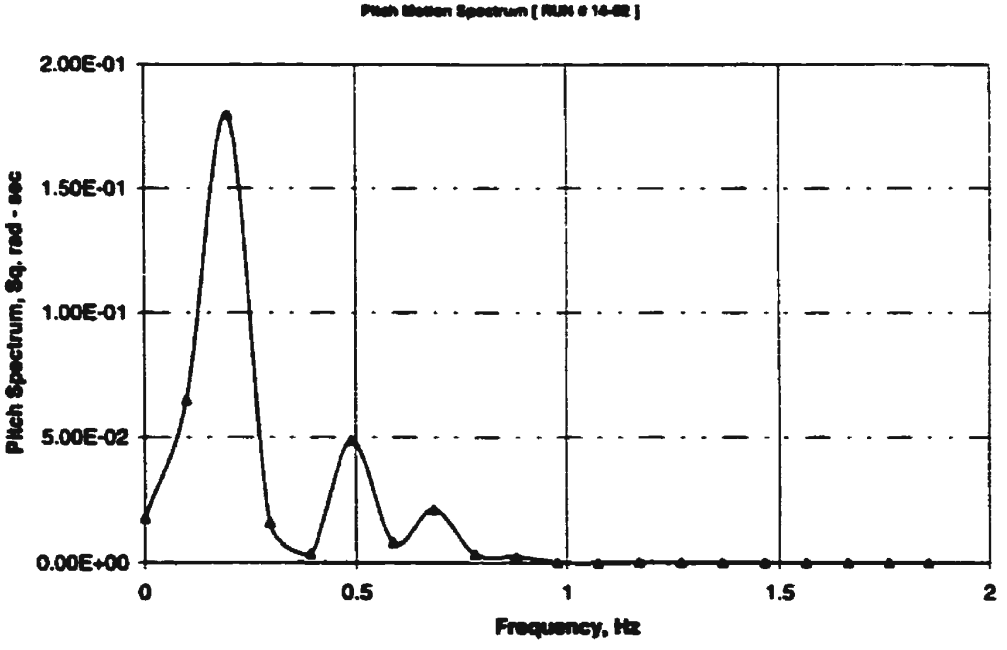

Figure O.14: Pitch power spectral density function [Run # 14-02]

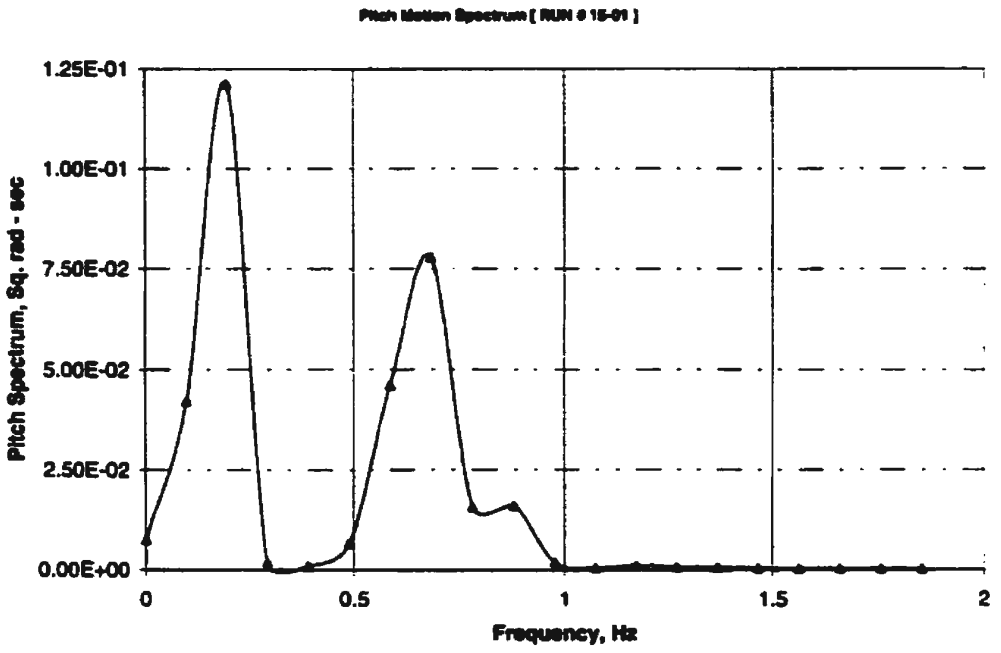

Figure O.15: Pitch power spectral density function [Run # 15-01]

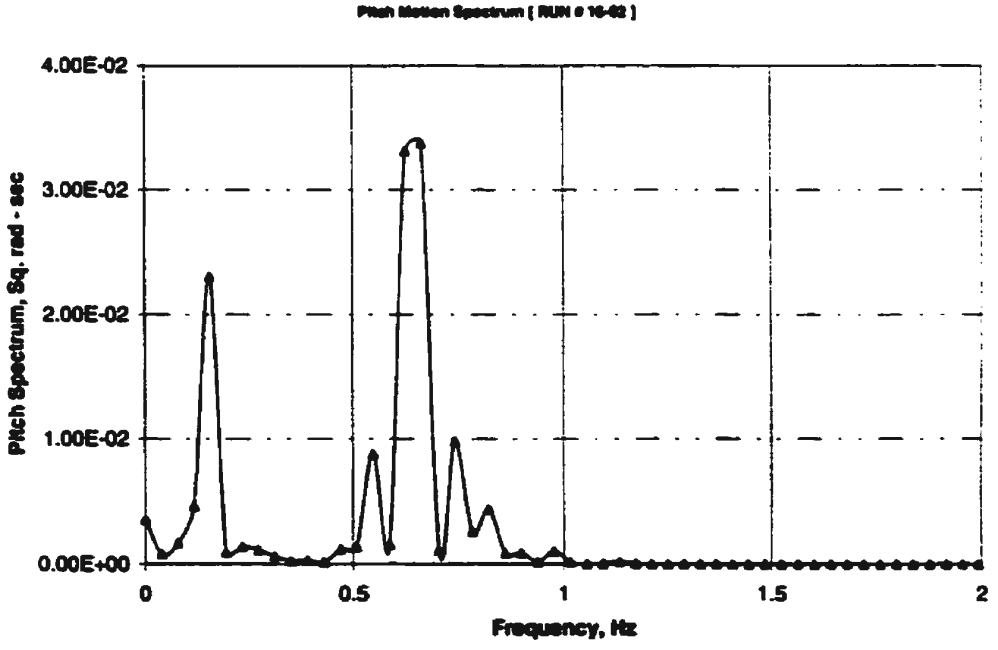

Figure O.16: Pitch power spectral density function [Run # 16-02]

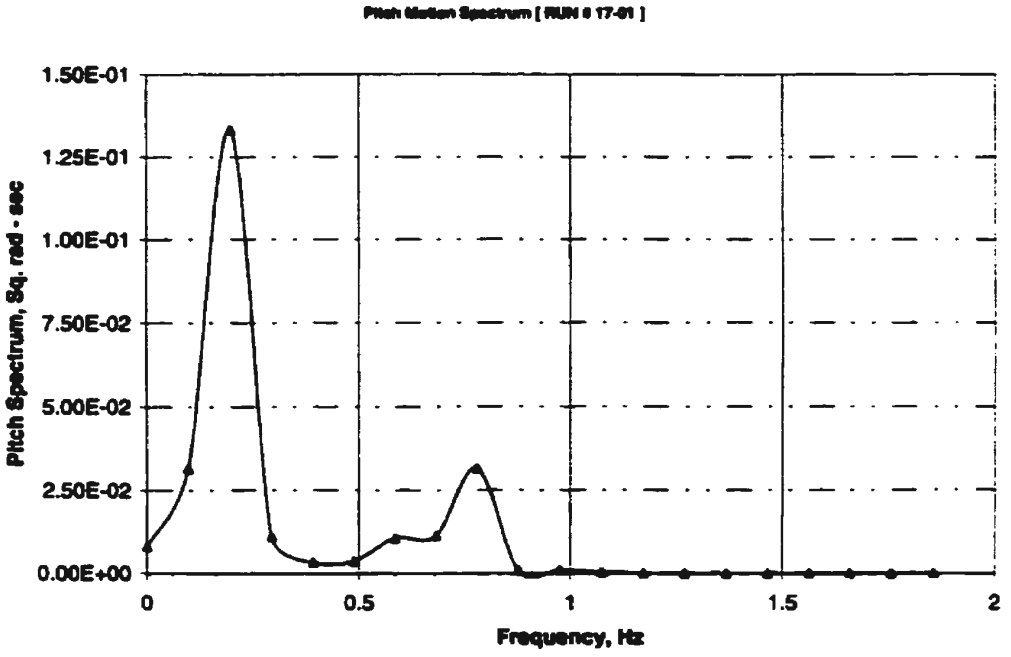

Figure O.17: Pitch power spectral density function [Run # 17-01]

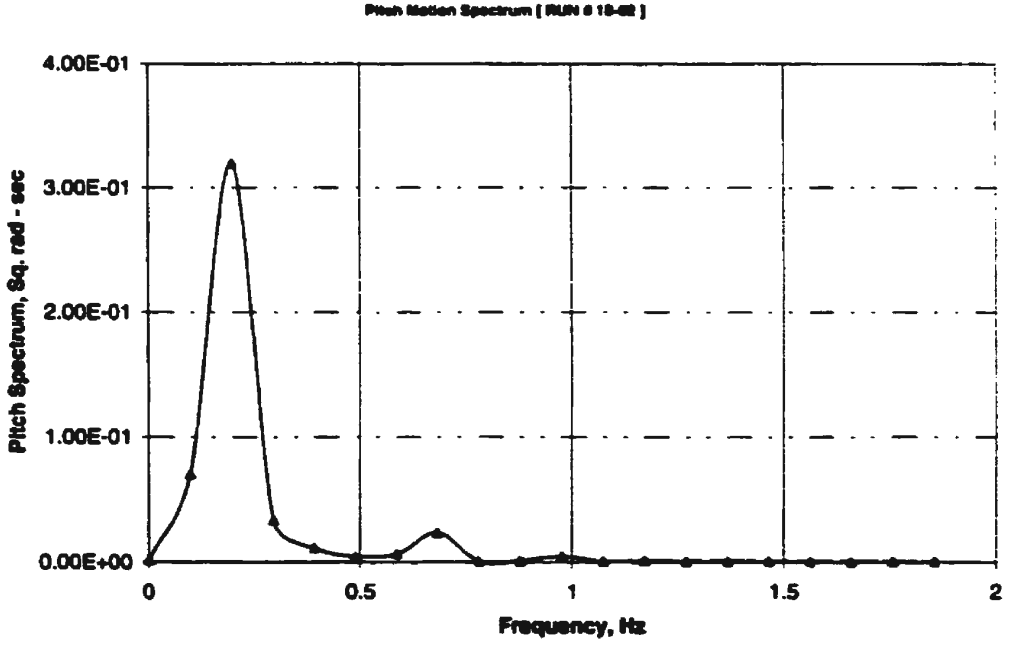

Figure O.18: Pitch power spectral density function [Run # 18-02]

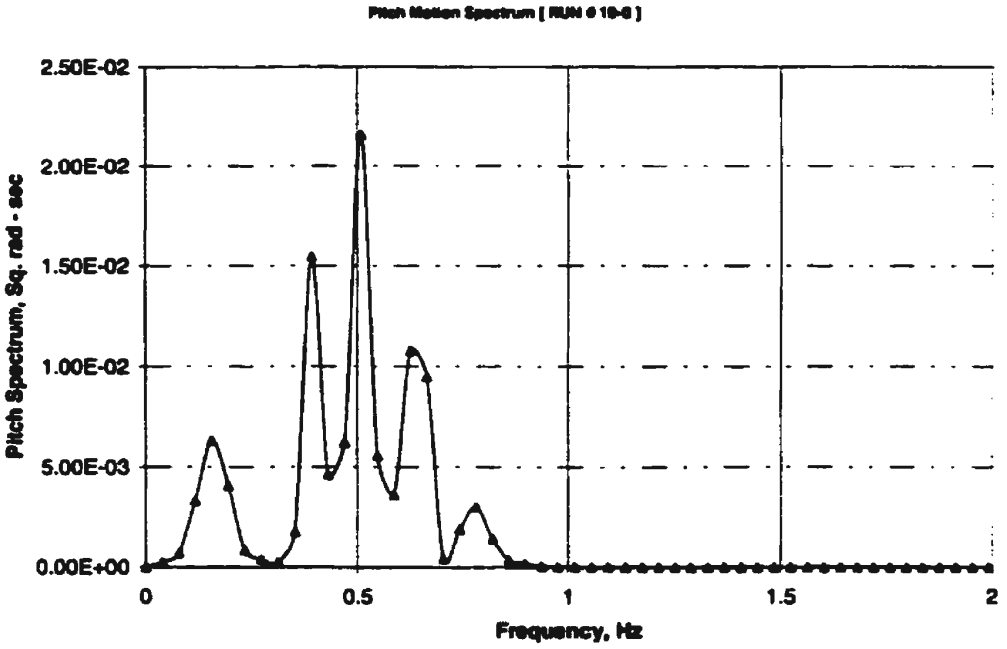

Figure O.19: Pitch power spectral density function [Run # 19-0]

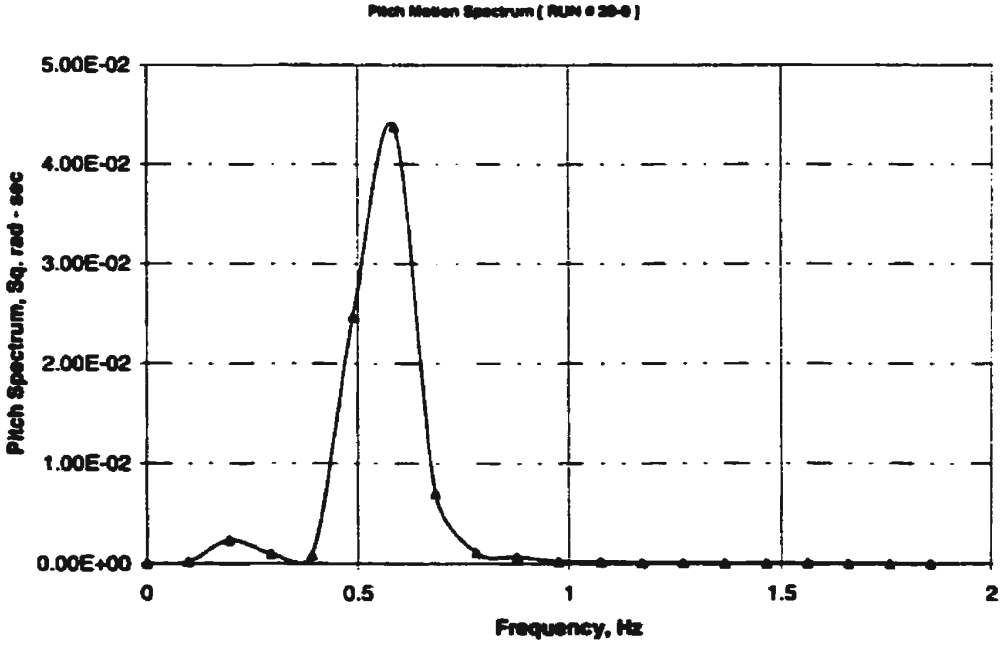

Figure O.20: Pitch power spectral density function [Run # 20-0]

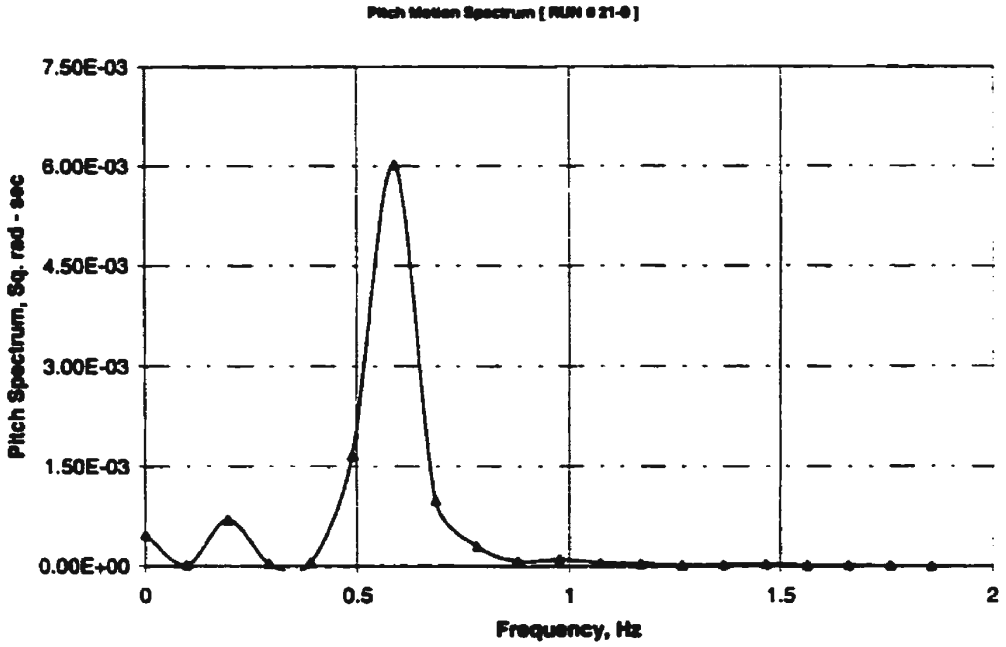

Figure O.21: Pitch power spectral density function [Run # 21-0]

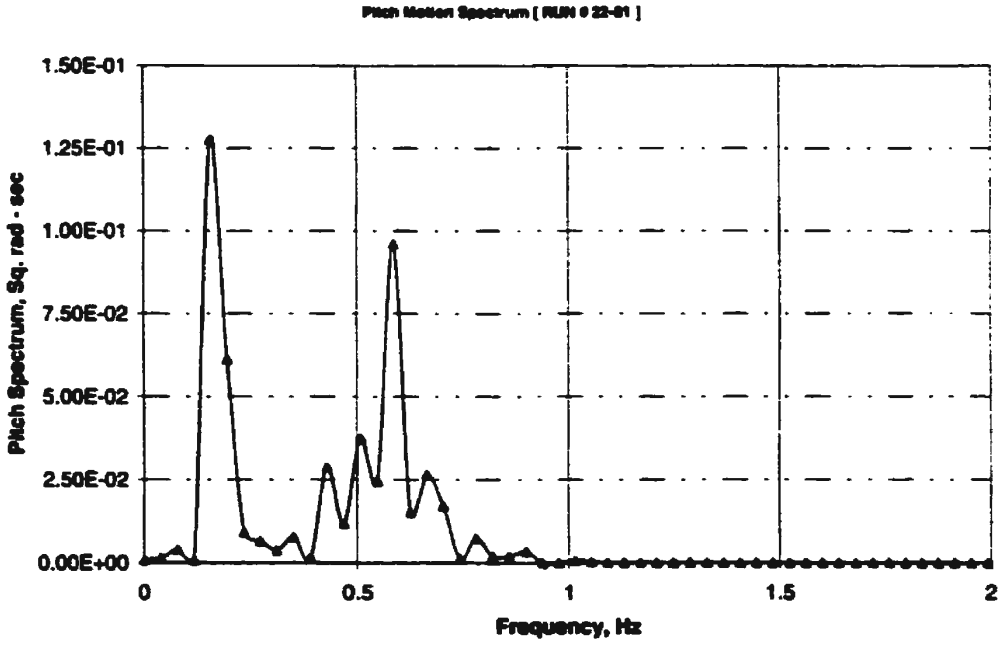

Figure O.22: Pitch power spectral density function [Run # 22-01]

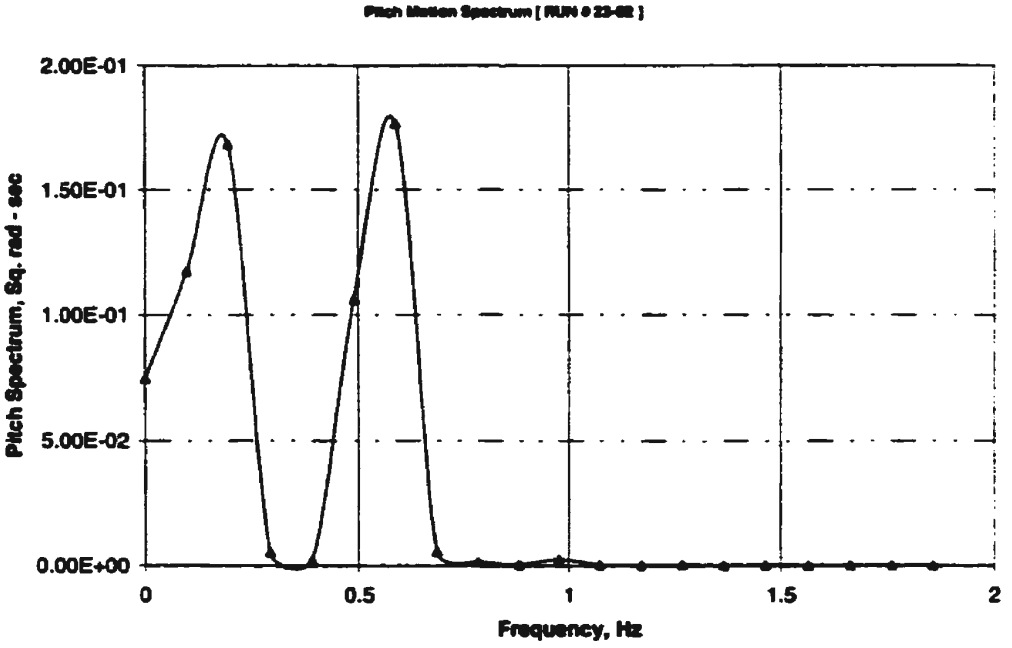

Figure O.23: Pitch power spectral density function [Run # 23-02]

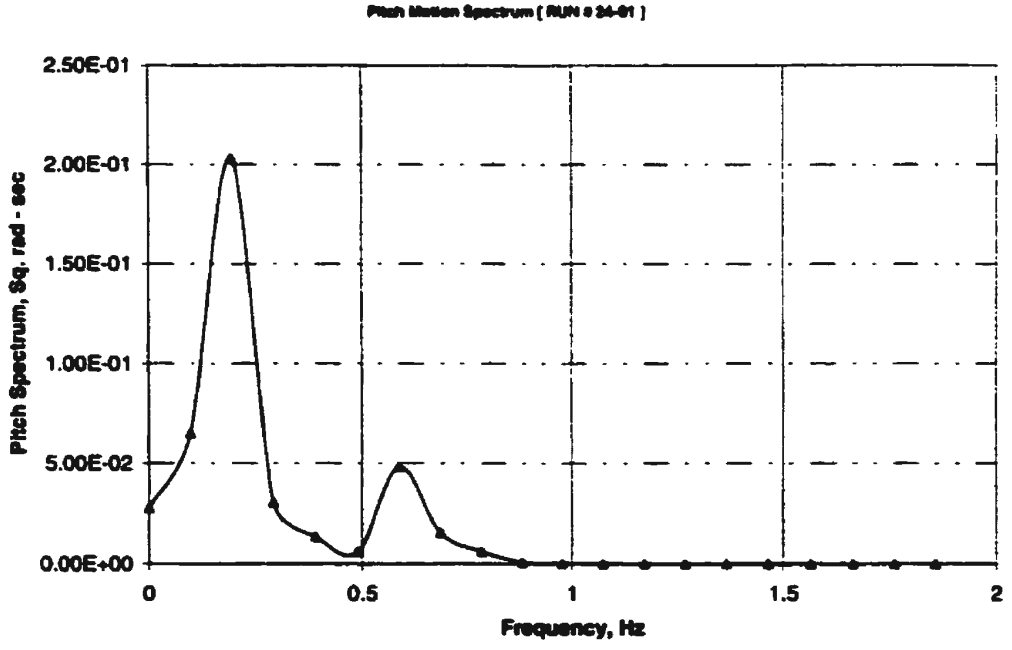

Figure O.24: Pitch power spectral density function [Run # 24-01]

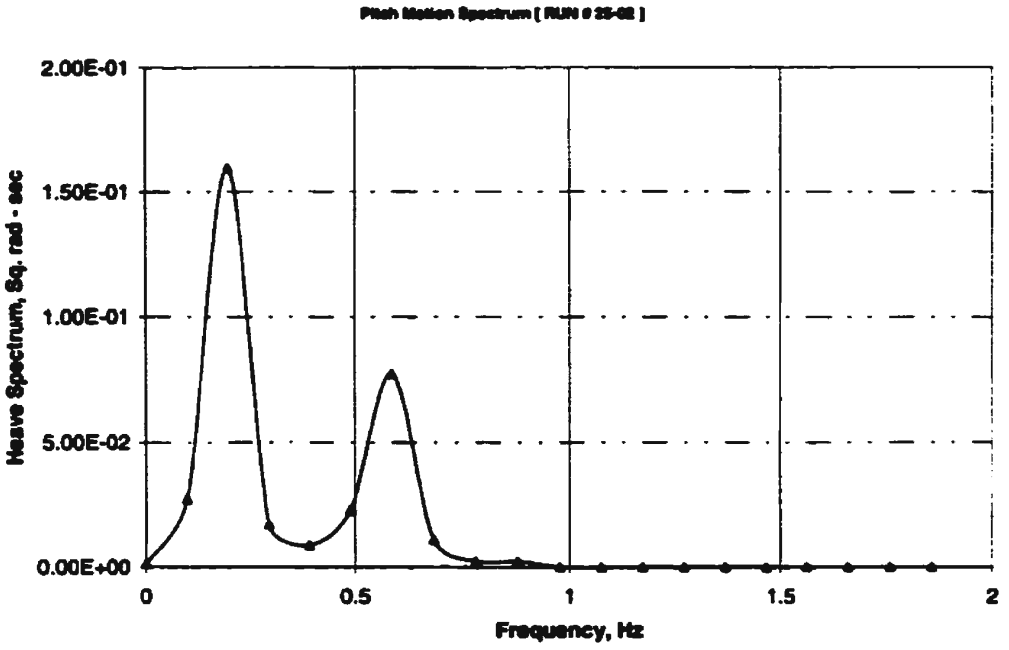

Figure O.25: Pitch power spectral density function [Run # 25-02]

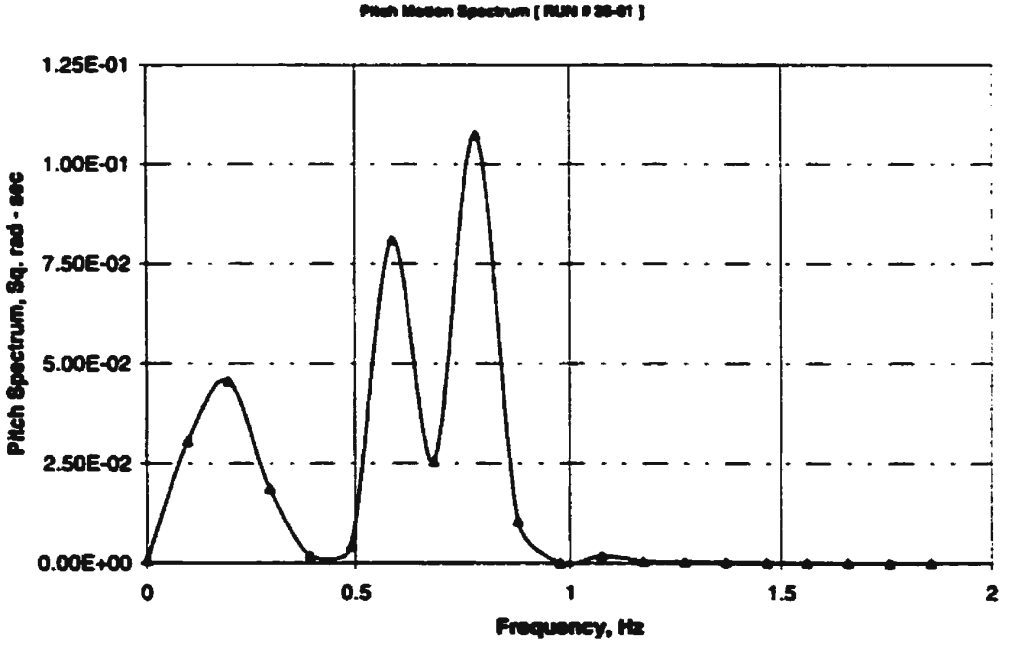

Figure O.26: Pitch power spectral density function [Run # 26-01]

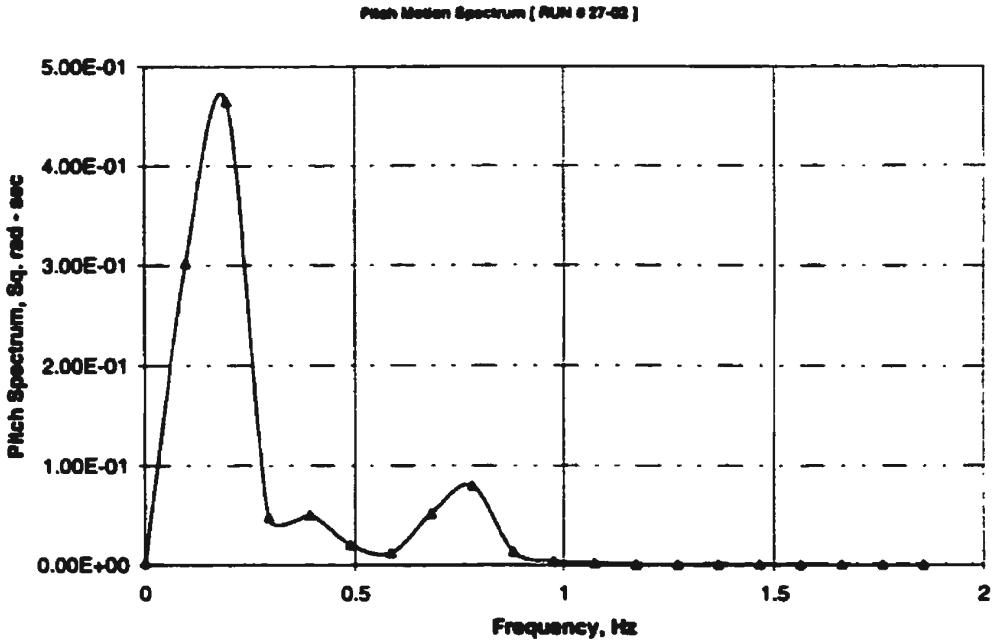

Figure O.27: Pitch power spectral density function [Run # 27-02]